UNIVERSITÉ DE STRASBOURG

École Doctorale des Sciences Chimiques

UMR CNRS 7509

THÈSE

Présentée par:

Peter ŠRAMEL

Soutenue le: 30 Novembre, 2017

Pour obtenir le grade de: **Docteur de l'université de Strasbourg**

Discipline: **Chimie organique et médicinale**

Synthèse et Screening Biologique d'Inhibiteurs de Tyrosine Kinase, KDR, conçus *in silico*

Directeur:	**Dr. Gilles HANQUET**, Université de Strasbourg, ECPM, UMR CNRS 7509, Strasbourg, France
Co-directeur :	**assoc. Prof. Andrej BOHÁČ**, Univerzita Komenského v Bratislave, Faculté des Sciences Naturelles, Bratislava, Slovaquie
Rapporteurs:	**Prof. Danijel KIKELJ**, Univerza v Ljubljani, Faculté de Pharmacie, Ljubljana, Slovénie **Prof. Stefano ALCARO**, Università degli Studi "Magna Graecia" di Catanzaro, Département des Sciences de la Santé, Catanzaro, Italie
Autres Membres:	**Prof. Line BOUREL**, Université de Strasbourg, Faculté de Pharmacie, UMR CNRS 7199, Strasbourg, France **Prof. Milan REMKO**, Univerzita Komenského v Bratislave, Faculté de Pharmacie, Bratislava, Slovaquie **Dr. Pavol KOIŠ**, Univerzita Komenského v Bratislave, Faculté des Sciences Naturelles, Bratislava, Slovaquie

Resume in English

Peter Šramel: A Synthesis and Biological Screening of Predicted Inhibitors of Tyrosine Kinases e.g. KDR
Université de Strasbourg, Ecole européene de Chimie, Polymères et Matériaux (ECPM), UMR CNRS 7509, Laboratoire SynCat , Strasbourg, France

Protein kinases represent a group of enzymes responsible for phosphorylation – transfer of a phosphate group from adenosine triphosphate (ATP) to tyrosine or serine / threonine residues. Protein phosphorylation is one of the most important tools regulating a cell activity. A cell "signalization" through an endothelial receptor tyrosine kinase VEGFR2 TK (KDR) is the important pathway influencing growth of a tumor. Small-molecule inhibitors of VEGFR2 TK (VEGFR2 TKIs) have become an important tool for the treatment of various types of cancer.

This dissertation thesis resulted in a discovery of 16 biologically active *N*,5-diaryloxazol-2-amines (IC_{50}, VEGFR2 TK). Very good results were achieved especially with compounds **189**, **191**, **211**, **214**, **220**, **221**, **223** and **4** exhibiting the activity under 500 nM. Within the first project a theory of Regioisomeric bioisostery (*RegBio*) was proposed and its evaluation is currently in progress. The second project brought a discovery of new interaction region – Salt bridge containing pocket (SBCP) in a specific intermediate conformation of the VEGFR2 TK. The third project resulted in the synthesis of aldehyde precursor **269** which was subsequently used for the preparation of *N*-aryloxazole-2-amine-based CLK1inhibitor **261**. Within the last project, bioactivities of quinoides **270** – **274** and VEGFR2 TKIs **275**, **2**, **191**, **15** were studied on hepatocellular cancer (HCC) and its cancer stem cells (HCSCs). An aggressiveness factor (AF) characteristic was proposed to estimate a quality of novel drug candidates for their ability to eradicate CSCs sub population.

Key words: tyrosine kinase inhibitors, VEGFR2 TK (KDR), bioisosterism, *N*-aryloxazol-2-amines.

Resume in French

Peter Šramel: Synthèse et Screening Biologique d'inhibiteurs de Tyrosine Kinase, KDR, conçus *in silico*
Université de Strasbourg, Ecole européene de Chimie, Polymères et Matériaux (ECPM), UMR CNRS 7509, Laboratoire SynCat, France

Les protéines kinases représentent le groupe d'enzymes qui servent d'intermédiaire pour la phosphorylation de protéines – le transfert d'un groupe phosphate de l'adénosine triphosphate (ATP) sur des chaînes latérales correspondantes de tyrosine, de serine ou de thréonine des acides aminées. La phosphorylation de protéines est un des outils les plus importants pour la régulation de l'activité cellulaire. La « signalisation » cellulaire par le récepteur de tyrosine kinase VEGFR2 (KDR) appartient aux réactions biochimiques clés influençant la croissance de tumeurs. L'inhibition thérapeutique de cette réaction à l'aide des composés de faible poids moléculaire spécifiques est devenue une stratégie utile dans le cadre des thérapies anticancéreuses.

Ce travail a amené à la découverte de 16 substances biologiquement actives sur la base *N*,5-diaryloxazol-2-amine (IC_{50}, VEGFR2 TK). D'excellents résultats ont été atteints notamment dans le cas des substances **189**, **191**, **211**, **214**, **220**, **221**, **223** et **4** qui montrent une activité inhibitrice inférieure à 500 nM. Dans le cadre du premier projet nous avons proposé la théorie de la Bioisostérie régioisomère (*RegBio*) dont l'évaluation est toujours en cours. Le résultat de notre deuxième projet a été la découverte d'une nouvelle zone d'interaction – SBCP (une poche contenant un pont salin) à l'intérieur de l'espace de liaison ATP du récepteur de tyrosine kinase VEGFR2. Dans le cadre du troisième projet nous avons proposé et réalisé la synthèse du précurseur aldéhyde **269** qui a été consommé durant la préparation d'un inhibiteur actif *N*-aryloxazol-2-amine de kinase CLK1 **261**. Dans le cadre du quatrième projet nous avons étudié l'impact des dérivées quinones **270 – 274** et des inhibiteurs VEGFR2 TK **275**, **2**, **191** et **15** sur le carcinome hépatocellulaire (HCC) et ses cellules souches (HCSCs). En se basant sur les résultats de notre recherche nous avons proposé le terme de facteur d'agressivité (AF) qui caractérise le pouvoir des inhibiteurs de tumeurs de diminuer la sous-population des cellules cancéreuses correspondantes.

Mots clés: inhibiteurs de tyrosine kinase, VEGFR2 (KDR), bioisostérisme, *N*-aryloxazol-2-amines.

Acknowledgement

Firstly, I would like to express my sincere gratitude to my both supervisors Dr. Gilles Hanquet and assoc. prof. RNDr. Andrej Boháč, PhD. for their continuous support of my PhD study and related research, for their patience, motivation and immense knowledge. Their guidance helped me in all the time of research and writing the thesis.

I thank to my fellow labmates and colleagues for stimulating discussions, useful advices and professional help but also for many great situations and experiences we enjoyed together.

Besides my supervisors and colleagues, I would like to thank Biomagi, Ltd. for the proposed structures of VEGFR2 TKIs, development of the *RegBio* hypothesis, discovery of the SBCP pocket and the intermediate VEGFR2 TK conformation.

I am very grateful also to the Institut Français de Slovaquie for an opportunity to complete my PhD study at the Université de Strasbourg in the frame of the "Cotutelle" program and to the organizations Campus France and Collège Doctoral Européen for the invaluable support during my stay in France.

Last but not least, I would like to thank my family: my great mom and dad for helping and encouraging me under every circumstance throughout writing the thesis and my whole life in general.

Abbreviations

Medicinal chemistry	
Aβ (Abeta)	Amyloid beta
ADME	Absorption, distribution, metabolism and excretion – describes the disposition and fate of a pharmaceutical compound within a living organism
ALK	Anaplastic lymphoma receptor tyrosine kinase
ALL	Acute lymphoid leukemia
AML	Acute myeloid leukemia
α_2AR (alpha2AR)	α_2 adrenoreceptor / alpha 2 adrenoreceptor
ATP	Adenosine triphosphate
BA (%)	Bioavailability – a subcategory of absorption and the fraction of administered dose of unchanged drug that reaches the systemic circulation
CAM	Chick chorioallantoic membrane assay – a model for studying neovascularization
CDK	Cyclin-dependent kinase
CLK1	Dual specificity protein kinase CLK1
CLL	Chronic lymphocytic leukemia
C_{max} (ng / ml)	Maximum serum concentration of a drug achieved in a specific compartment or test area of the body after the drug has been administrated
CMGC	A specific group of kinomically related kinases CDK, MAP, GSK and CLK
CML	Chronic myeloid leukemia
CNS	Central nervous system
COX-1 / 2	Cyclooxygenase-1 / 2
CYP19	Aromatase / Estrogen synthase

Abbreviations

DAPT	Inhibitor of Notch pathway (commercially available CSC inhibitor)
DDR	Discoidin domain receptor
DGAT	Diglyceride acetyltransferase
DLBCL	Diffused large B-cell lymphoma
DRD1-3	Dopamine receptor D1-3
dTMP	Deoxythymidine monophosphate
dUMP	Deoxyuridine monophosphate
ED_{50} (e.g., mg / kg, mmol / kg or mg / l, mmol / l when a tissue is perfused)	Half maximal effective dose – the dose of a drug that produces a specified *in vivo* response in 50 % of a test population
EGFR	Epidermal growth factor receptor
EPHA	Ephrin type-A receptor
EPHB	Ephrin type-B receptor
FDA (US FDA)	US Food and drug administration agency
FGFR	Fibroblast growth factor receptor
FLT3	Fms-like tyrosine kinase 3
G +	Gram-positive organism
G-	Gram-negative organism
HCC	Hepatocellular carcinoma
HCSC	Hepatocellular carcinoma stem cells
Hep3B	Liver cancer cell line (epithelial)
Hin	*Haemophilus influenzae*
HTS	High-throughput screening – a method for scientific (chemical, genetic, pharmaco-logical…) experimentation used in drug discovery
Huh7	Liver cancer cell line (epithelial)

IC_{50} (M)	Half maximal inhibitory concentration – the concentration of an agonist drug required for 50 % inhibition of particular biological target
IGFR	Insulin growth factor receptor
IMPDH	Inosine monophosphate dehydrogenase (IMP dehydrogenase)
INSR	Insulin receptor
IP	International patent
I_1R	I_1 imidazoline receptor
K_d (M)	Dissociation constant defining affinity between a drug and a protein, corresponding to the concentration of a drug at which the binding site of a protein is half-occupied
K_i (M)	Equilibrium dissociation constant for ligand receptor interactions determined in inhibition studies
5-LOX	5-Lipoxygenase
LTK	Leukocyte tyrosine kinase
Mahlavu	Liver cancer cell line (mesenchymal)
MED (e.g., mg / kg, mmol / kg or mg / l, mmol / l when a tissue is perfused)	Minimum effective dose – the lowest dose level of a pharmaceutical product that provides a clinically significant response in average efficiency
MAP kinase	Mitogen-activated protein kinase
MIC	Minimum inhibitory concentration – the lowest concentration of a tested compound that prevents visible growth of a bacteria
nAChR	Nicotinic acetylcholine receptor
NS3 (HCV)	Nonstructural protein 3
NSAI	Nonstereoidal aromatase inhibitor

Abbreviations

NSCLC	Non-small lung cancer carcinoma
NTRK	Neurotrophic tyrosine kinase
PDGFR	Platelet-derived growth factor receptor
PET	Positron emission tomography
PGI_2	Prostacyclin (prostaglandin I2)
PPAR-γ	Peroxisome prolifelator-activated receptor gamma
PTP1B	Protein-tyrosine phosphatase 1B
RCC	Renal cell carcinoma
ROR	Receptor tyrosine kinase-like orphan receptor
RTK	Receptor tyrosine kinase
SAR	Structure-activity relationship – the relationship between the molecule and its biological activity
Sau	*Staphylococcus aureus*
Spn	*Streptococcus pneumoniae*
SRC	Binding domain for proto-oncogene tyrosine protein kinase
TK	Tyrosine kinase
TKI	Tyrosine kinase inhibitor
T_{max} (h)	The time at which is C_{max} observed
TrpV1	Transient receptor potential cation channel subfamily V member 1 (Capsaicin receptor)
VEGF	Vascular endothelial growth factor
VEGFR2 TK (KDR)	Vascular endothelial growth factor receptor 2 (Kinase Inserted Domain Receptor)

Organic synthesis	
Ar	Argon atmosphere
Bn (protecting group)	Benzyl
Boc (protecting group)	*tert*-Butyloxycarbonyl
Brine	Saturated aq solution of NaCl
CataCXium A	Butyldi-1-adamantylphosphine
DES	Deep eutetic solvent
DMF	*N*,*N*-Dimethylformamide, $(CH_3)_2NCHO$
DMSO	Dimethyl sulfoxide, $(CH_3)_2SO$
EA	Ethyl acetate, $CH_3CO_2CH_2CH_3$
EDC . HCl	1-Ethyl-3-(3-dimethylaminopropyl) carbodiimide hydrochloride
ESI	Electrospray ionization
FLC	Flash liquid chromatography
Hex	Hexol (a mixture of hexanes)
HOBt hydrate	1-Hydroxybenzotriazole hydrate
HRMS	High resolution mass spectrometry
HV	High vacuum (< 0.1 Torr)
IR Spectroscopy	Infrared spectroscopy
LC-MS	Liquid chromatography – mass spectrometry
LiHDMS	Lithium hexamethyldisilazide, $LiN(SiMe_3)_2$
MIDA	*N*-methyliminodiacetic acid
MS	Mass spectrometry
MW	Microwave irradiation
NMP	*N*-Methyl-2-pyrrolidone
NMM	*N*-Methylmorpholine

Abbreviations

NMO . H_2O	4-Methylmorpholine *N*-oxide monohydrate
NMR	Nuclear magnetic resonance spectroscopy
–OMs	Mesylate / Methanesulfonate
–ONs	Nosylate / *para*-Nitrobenzenesulfonate
–OTf	Triflate / Trifluoromethanesulfonate
–OTs	Tosylate / *para*-Toluenesulfonate
PEG-400	Polyethylene glycol 400
PMB (protecting group)	*para*-Methoxybenzyl
RT	Room temperature
Rotavap, RVE	Rotary vacuum evaporator
SPhos	2-Dicyclohexylphosphino-2',6'-dimethoxybiphenyl
T3P	Propylphosphonic anhydride
TBAF	Tetrabutylammonium fluoride, $(CH_3CH_2CH_2CH_2)N^+F^-$
TBS / TBDMS (protecting group)	*tert*-Butyldimethylsilyl
TFA	Trifluoroacetic acid, CF_3CO_2H
THF	Tetrahydrofuran
TLC	Thin layer chromatography
TMS (protecting group)	Trimethylsilyl
TosMIC	Toluenesulfonylmethyl isocyanide, $CH_3C_6H_4SO_2CH_2NC$
Tr (protecting group)	Trityl / Triphenylmethyl
Ts (protecting group)	Tosyl / *para*-Toluenesulfonyl
US	Ultrasound irradiation
XPhos	2-Dicyclohexylphosphino-2',4',6'-triisopropylbiphenyl

Summary

Chapter 1. **Introduction**

1. Introduction

Cancer is the name given to a collection of related diseases. In all types of cancer, some of the body's cells begin to divide without stopping and spread into surrounding tissues. Cancer can start almost anywhere in the human body, which is made up of trillions of cells.

Normally, human cells grow and divide to form new cells as body needs them. When cells grow old or become damaged, they die, and new cells take their place. However, when cancer develops, this orderly process breaks down. As cells become more and more abnormal, old and damaged survive and new cells form when they are not needed. These extra cells can divide without stopping and may form growths called tumors.

Cancerous tumors are malignant, which means they can spread into or invade nearby tissues. In addition, as these tumors grow, some cancer cells can break off and travel to distant places in the body through the blood or the lymph system and form new tumors far from its place of origin.

Angiogenesis is the formation of new blood vessels. This process involves the migration, growth and differentiation of endothelial cells, which line the inside of the vascular wall. Angiogenesis plays a critical role in the growth and spread of cancer. A blood supply is necessary for tumors to grow beyond a few millimeters in size Tumors can induce a formation of this supplementary vascular system by giving off chemical signals that stimulate angiogenic growth. Tumors can also stimulate nearby normal cells to produce angiogenesis signaling molecules. The resulting new blood vessels supply growing tumors with oxygen and nutrients, allowing the cancer cells to invade nearby tissue, to move throughout the body and to form new colonies of cancer cells, called metastases.[1]

As it was mentioned above, the process of angiogenesis is controlled by chemical signals in the body. Vascular endothelial growth factors (VEGFs) and their endothelial tyrosine kinase receptors (VEGFRs) are central regulators of angiogenesis. VEGF signaling through VEGFR2 TK (KDR) is the major angiogenic pathway which blockage using small-molecule inhibitors represents perspective anti-angiogenic strategy for cancer therapy.[2]

[1] www.cancer.gov (accessed October 4th, 2017).
[2] Lohela, M.; Bry, M.; Tammela, T.; Alitalo, K. *Curr. Opin. Cell. Bio.* **2009**, *21*, 154 – 165.

Many of the **small-molecule inhibitors of VEGFR2 TK (KDR)** are competitive for ATP and exert their inhibitory activity by binding to the ATP pocket of the highly conserved kinase domain. In general, the ATP binding site of protein kinases lies at the cleft between the amino-terminal and carboxy-terminal lobes, which are joined by key residues capable of forming hydrogen bonds with ATP. As a result of the structural conservation of the ATP-binding pockets in protein kinases, small-molecule agents often display high affinity for additional members of the receptor tyrosine kinase (RTK) family. The multikinase inhibitor profile of some small-molecule inhibitors offers the possibility of disrupting several independent biological pathways that are vital for tumor proliferation and metastasis.[3]

The introduction of small-molecule VEGFR2 TK inhibitors has added another dimension in the treatment of several oncology indications as they offer a unique mechanism. The VEGFR2 TK inhibitors have demonstrated superior benefits in treating certain types of tumors, such as renal cell carcinoma and hepatocellular carcinoma, as a monotherapy option. Many of the approved VEGFR2 TK inhibitors have also shown synergy when used in combination with other anticancer agents.[4]

The optimization of ligands in a medicinal chemistry development into potential small-molecule therapeutics requires a number of key design principles. Through consideration of the synthetic possibilities in a compound with a desired physiological profile, it is possible for a medicinal chemistry project team to identify potential replacements that maintain or modulate certain desirable or undesirable properties. **Bioisosterism** is the concept of certain similarity between functional groups or scaffolds in molecules in terms of their biological interactions. Reasonable replacement of molecular groups is defined as bioisosteric replacement. A subset of bioisosteric replacement is referred to as scaffold hopping, where the core of a small-molecule is replaced. The core may be of direct functional importance in interacting with the protein target or it may provide the necessary scaffolding that allows substitution with functional groups in the appropriate geometric configuration.[5]

[3] Ivy, S. P.; Wick, J. Y.; Kaufman, B. M. *Nat. Rev. Clin. Oncol.* **2009**, *6*, 569 – 579.
[4] Sharma, K.; Suresh, P. S.; Mullangi, R.; Srinivas, N. R. *Biomed. Chromatogr.* **2015**, *29*, 803 – 834.
[5] Brown, N. *Mol. Inf.* **2014**, *33*, 458 – 462.

In 2005 Harris *et al.* (GlaxoSmithKline) published a scientific article where a series of *N*,5-diaryloxazol-2-amine (**1**) derivatives was identified as ATP-competitive inhibitors of VEGFR2 TK. The structure-activity relationship (SAR) study of the new *N*,5-diaryloxazol-2-amine scaffold was described. Optimization of the aryl rings led to the discovery of potent inhibitors which exhibited very good biological activities at the both enzymatic and cellular levels. Especially, a compound **2** (AAZ) showed also excellent solubility and good oral pharmacokinetics when dosed as its bis-mesylate salt. Because of these beneficial properties, the compound **2** (AAZ) was selected as a promising drug candidate.[6] (Figure 1)

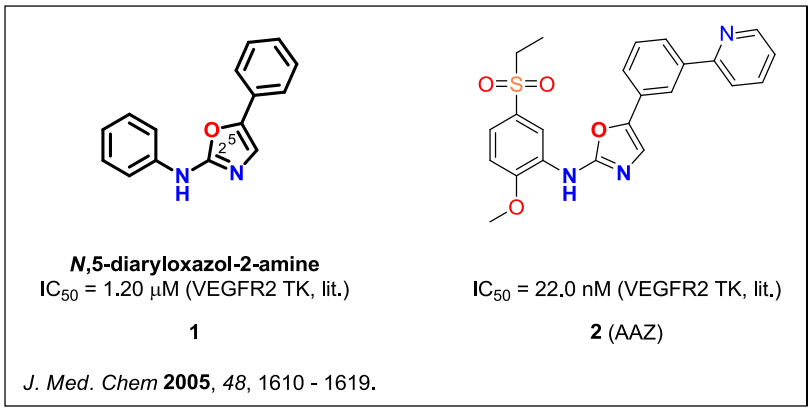

Figure 1. Chemical structures and determined biological activities of *N*,5-diaryloxazol-2-amine (**1**) and the drug candidate **2** (AAZ).

This dissertation thesis is primary devoted to the development of novel, *in silico* predicted AAZ-based inhibitors of VEGFR2 TK and the determination of their activity by *in vitro* enzymatic assays. Our goal is to broaden the knowledge about these compounds from chemical and also biological point of view and effectively apply it in the medicinal chemistry praxis. The utilization of small-molecule inhibitors may serve as a valuable tool for better understanding the molecular mechanisms of splicing and it may also lead to the discovery of a novel class of therapeutics.

Within the first main project – **Regioisomeric bioisostery (*RegBio*)** we aimed to synthesize and determine a biological activity of the predicted series of *N*,5-diaryloxazol-2-amines, e. g. **2** (AAZ) (AAZ-like compounds) and their regioisomeric *N*,4-diaryloxazol-

[6] Harris, P. A.; Cheung, M.; Hunter III, R. N.; Brown, M. L.; Veal, J. M.; Nolte, R. T.; Wang, L.; Liu, W.; Crosby, R. M.; Johnson, J. H.; Epperly, A. H.; Kumar, R.; Luttrell, D. K.; Stafford, J. A. *J. Med. Chem.* **2005**, *48*, 1610 – 1619.

2-amine analogues, e. g. **3** (AAZ-regio) (AAZ-regio-like compounds). These regioisomers are expected to have a similar binding position in the ATP-binding pocket of VEGFR2 TK possibly resulting in the similar inhibitory activities known for the AAZ-like compounds. For the proposed hypothesis we introduced the name Regioisomeric Bioisostery (*RegBio*). Based on obtained activity values (IC_{50}, VEGFR2 TK) of the predicted compounds and subsequent comparative study, we would like to evaluate our theory. (Figure 2)

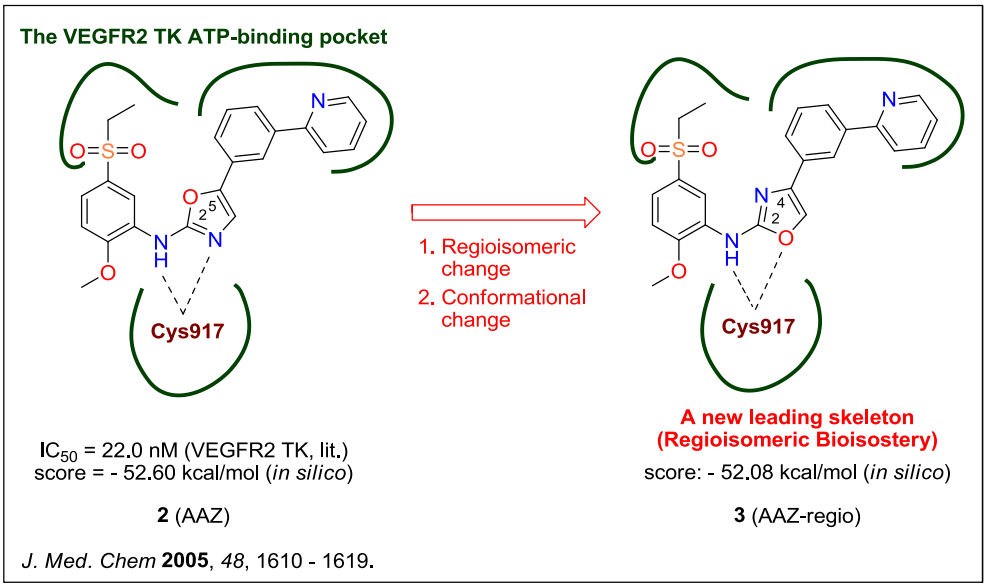

Figure 2. Regioisomeric Bioisostery (*RegBio*) – the suitable regioisomeric change in **2** (AAZ) followed by the induced conformational change leads to the bioisosteric candidate **3** (AAZ-regio).

Within the second main project – **Salt bridge containing pocket (SBCP)** we aimed to synthesize and determine a biological activity of the predicted series of specifically substituted *N*,5-diaryloxazol-2-amines, e. g. **4**. Based on obtained activity values (IC_{50}, VEGFR2 TK), we would like to evaluate our predictions concerning additional interactions inside the ATP-binding pocket of VEGFR2 TK. We are interested especially in the interactions within a novel binding region named Salt bridge containing pocket (SBCP), which was recently discovered in a unique DFG-IN / OUT conformation of VEGFR2 TK. No discussion about the possible interactions within this pocket and their influence on the activity of potential inhibitors was published in the literature. (Figure 3)

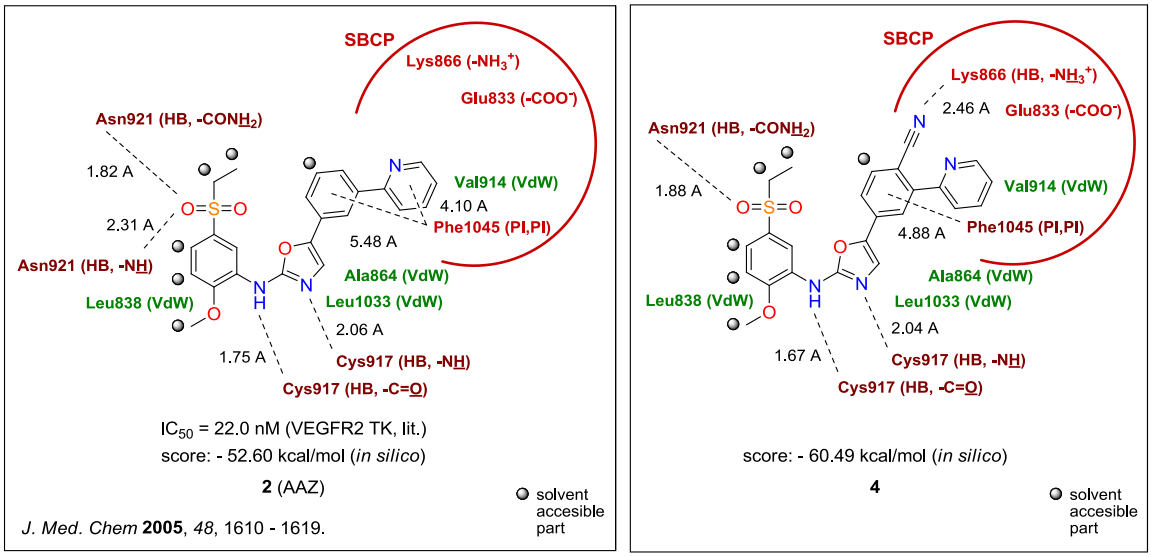

Figure 3. Interaction analysis, predicted docking score (*in silico*) and published biological activity (if available) of **2** (AAZ) and newly designed **4** in the VEGFR2 TK ATP-binding site with the highlighted SBCP region.

Within the third and fourth project, a broader exploitation of the influence of *N*,5-diaryloxazol-2-amines on different biological targets (kinase CLK1, cancer cells, etc.) was aimed to be carried out. Results of these projects were succesfuly published in the scientific literature. The complete manuscripts are attached in the corresponding chapter of this dissertation thesis. (Chapter 15)

Chapter 2. **Receptor tyrosine kinases (RTKs) and their inhibition**

2. Receptor tyrosine kinases (RTKs) and their inhibition

The concept of "**oncogenic addiction**" established by Weinstein described that tumor cells may exhibit addiction on an activated oncogenic signaling pathway to sustain their survival and proliferation. Several oncoproteins, including tyrosine kinases, are known to be essential for the oncogenic process.

Protein kinases are enzymes that are responsible for phosphorylation and transfer of a phosphate group from adenosine triphosphate (ATP) to tyrosine, serine or threonine residues. Protein phosphorylation is one of the most important tools regulating cell activities. Some oncoproteins need phosphorylation for regulation and activation.[7,8]

Among different protein kinases, RTKs have emerged as key pharmacological targets in oncology. Phosphorylation of other protein kinases, as well as intracellular intermediates by these RTKs is critical for signal transduction, regulation of cellular activity and function. Among 58 known RTKs, 30 of them have been shown to be necessary for oncogenesis in various tumors.

Similar to transmembrane proteins, RTK's structure consists of three different parts: **extracellular**, **transmembrane** and **cytoplasmic region**. The extracellular part is preceded by a cleavable signal sequence and holds the binding sites that interact with ligands. The extracellular domain is also involved in the dimerization of RTKs, a process that is critical for the activation of intrinsic tyrosine kinase. The cytoplasmic region contains tyrosine residues that are phosphorylated upon ligand binding and activation, regulate catalytic function, and also serve as docking sites for SRC Homology 2 (SH 2) domain-containing proteins.[9]

Deregulation of RTK activity is the major mechanism by which tumor cells escape from physiological constraints on survival and growth. Aberrant RTK activation due to receptor over-expression, chromosomal translocation, gene amplification, mutations, and impaired receptor downregulation contribute to the development of various forms of cancer in human. Some examples of RTKs that are under investigation are listed in the table below.[8,10,11] (Table 1)

[7] Weinstein, I. B. *Carcinogenesis* **2000**, *21*, 857 – 864.
[8] Tsai, C. J.; Nussinov, R. *Semin. Cancer. Biol.* **2013**, *23*, 235 – 242.
[9] Hojjat-Farsangi, M. *Int. J. Mol. Sci.* **2014**, *15*, 13768 – 13801.
[10] Haglund, K.; Rusten, T. E.; Stenmark, H. *Crit. Rev. Oncol.* **2007**, *13*, 39 – 74.
[11] Abella, J. V.; Park, M. *Am. J. Physiol. Endocrinol. Metab.* **2009**, *296*, 973 – 984.

Table 1. Oncogenic receptor tyrosine kinases identified in particular type of cancer.[9]

Oncogenic RTK (Examples)	**Cancer (Examples)**	**Approved Selective TKI for Treatment**
ALK	NSCLC, colorectal cancer, breast cancer	-
AXL	Lung, colon, breast, AML, CML	-
CCK4 (PTK7)	SCLC, breast cancer, gastric and colon cancer, AML	-
DDR1	NSCLC, breast cancer, AML, ovarian cancer	-
DDR2	NSCLS, lung cancer, CML, breast cancer	-
EGFR1 (ERBB1 / HER1)	Breast cancer, hepatocellular carcinoma	+
EGFR2 (ERBB2 / HER2)	Breast cancer, gastric adenocarcinomas	+
EGFR (ERBB3 / HER3)	Breast cancer, ovarian cancer, squamous cell lung cancer	+
EGFR4 (ERBB4 / HER4)	Breast cancer, melanoma	+
EPHA1	NSCLC, prostate cancer	-
EPHA2	Hepatocellular carcinoma, colorectal cancer, breast cancer	-
EPHA3	Glioblastoma, lung cancer, melanoma, ALL	-
EPHA4	NSCLC, gastric cancer	-
EPHA5	Breast cancer, hepatocellular carcinoma, ALL	-
EPHB1	NSCLC, cervical cancer, ovarian cancer	-
EPHB2	Cervical cancer, breast cancer	-
EPHB3	NSCLC, breast cancer, colorectal cancer	-
EPHB4	Breast cancer, melanoma, glioma	-
FGFR1	Squamous cell lung cancer, breast cancer	-
FGFR2	Squamous cell lung cancer, breast cancer, thyroid cancer	-
FGFR3	Bladder cancer, squamous cell carcinoma	-
FLT3	AML, acute promyelocytic leukemia	-
IGF1R	CLL, breast cancer, pancreatic cancer	-
IGF2R	Breast cancer, prostate cancer, colorectal carcinoma	-
INSR	Colorectal cancer, prostate cancer	-
INSRR	Neuroblastoma	-
KIT	AML, melanoma, ovarian carcinoma	-

LTK	Gastric cancer, lymphomas and leukemias	-
MER	Glioblastoma, hepatocellular carcinoma	-
MET	Hepatocellular carcinoma, CLL, breast cancer	-
MUSK	Ovarian cancer	-
NTRK1 (TrkA)	Colorectal cancer, breast cancer	-
NTRK2 (TrkB)	Neuroblastoma, astrocytoma	-
NTRK3 (TrkC)	Neuroblastoma, breast cancer	-
PDGFRA	Lung adenocarcinoma, gastrointestinal stromal tumors	-
PDGFRB	Gastrointestinal stromal tumors, glioblastoma	-
RET	NSCLC, medullary, thyroid carcinoma	-
RON (MST1R)	Pancreatic cancer, breast cancer, NSCLC	-
ROR1	CLL, ALL, AML, MCL, HCL, melanoma	-
ROR2	Melanoma, hepatocellular carcinoma, colon cancer	-
ROS1	NSCLC, ovarian cancer	-
RYK	CML, ovarian cancer	-
TIE	Glioblastoma, breast tumor	-
TEK	Bladder cancer, glioblastoma, AML	-
TYRO3	Colon cancer, melanoma, thyroid cancer, breast cancer	-
VEGFR1 (FLT1)	Ovarian cancer, NSCLC, colorectal carcinoma	+
VEGFR2 (KDR)	Renal cell carcinoma, breast cancer	+
VEGFR3 (FLT4)	Thyroid carcinoma, breast cancer	+

Identifying new oncogenic RTKs that are over-expressed by tumor cells and regulate the growth, survival, invasion and communication of these cells with their microenvironment have facilitated the development of new anti-cancer agents and have revolutionized treatment options. Therefore, due to the interesting biological features, RTKs are of the main focus for developing new **tyrosine kinase inhibitors (TKIs)** for therapeutic intervention in cancer patients.[9]

TKIs, as well as other small inhibitors, are low molecular weight organic compounds. A cut off at 500 D (Daltons) is recommended and based on the observation that clinical attrition rates are significantly reduced when the molecular weight falls below 500 D. On the other hand, the recommended upper weight is about 900 D.[12,13]

Proper TKIs hits are usually selected by high-throughput screening (HTS), alternatively by *in-silico* screening methods that detect the most proper TKI candidates among a large library of compounds. Absorption, distribution, metabolism, excretion and toxicity (ADMET) of a drug candidate are very important elements that should be optimized for *in vivo* use. Based on these properties, there are several challenges in front of the selection of effective inhibitors. Membrane permeability, inactivation due to metabolism of the drug, decreasing due to non-specific interactions with other cellular components or rapid excretion, toxicity and lack of distribution into appropriate cellular compartment represent the major problems behind the drug discovery.

For TKIs, there are two basic processes of inhibition RTKs signalization activity. TKIs can prevent and block vital pathways through targeting signaling molecules which interact with and activate RTKs. TKIs can also translocate through the cell membrane by interacting with the cytoplasmic domain of RTKs and inhibit the catalytic activity of the TK domain by interfering with the binding of ATP or its substrates.[14,15] (Figure 4)

[12] Lipinsky, C. A. *Drug Discov. Today* **2004**, *1*, 337 – 341.
[13] Veber, D. F.; Johnson, S. R.; Cheng, H. Y. ; Smith, B. R.; Ward, K. W.; Kopple, K. D. *J. Med. Chem.* **2002**, *45*, 2615 – 2623.
[14] Prueksaritanont, T.; Tang, C. *AAPS J.* **2012**, *14*, 410 – 419.
[15] Johnson, L. N. *Q. Rev. Biophys.* **2009**, *42*, 1 – 40.

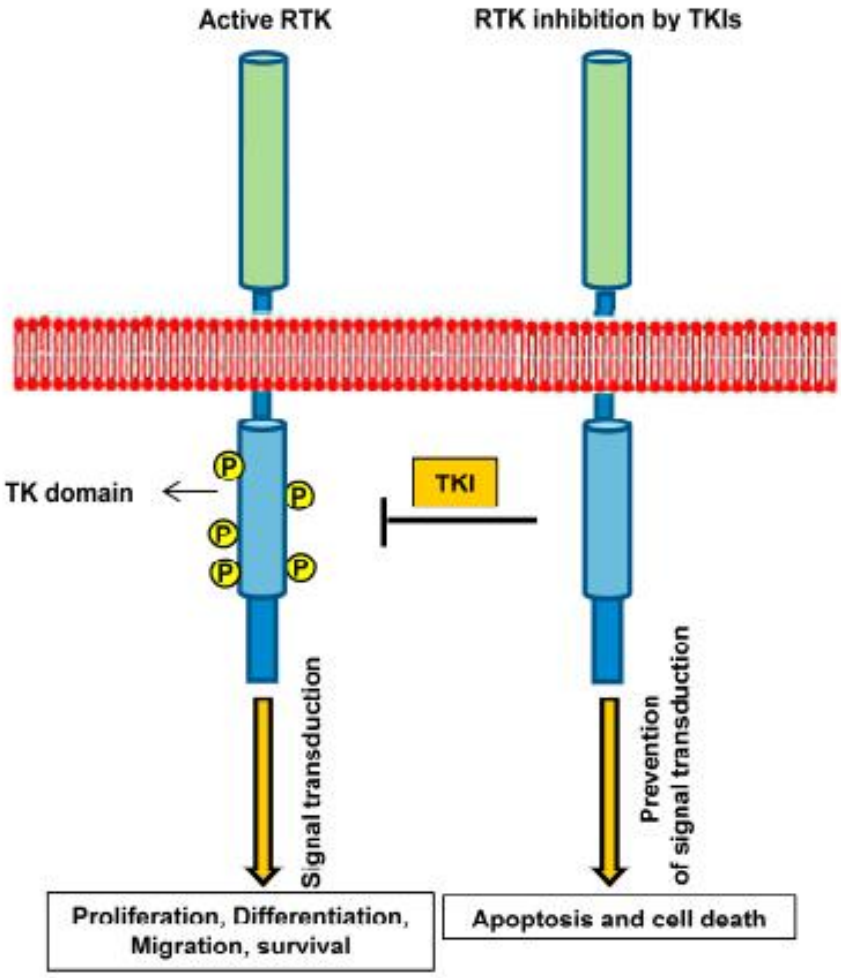

Figure 4. Targeting receptor tyrosine kinase by tyrosine kinase inhibitors (TKIs). Blocking small-molecule inhibitors of kinase domain prevents the phosphorylation of the receptor at TK domain and subsequently interferes with cell proliferation, differentiation, migration, and survival and induces cell apoptosis.[9]

2.1. VEGFR2 TK (KDR) inhibitors

Small-molecule multiple tyrosine kinase inhibitors belonging to the **VEGFR2 TK** (Vascular Endothelial Growth Factor Receptor 2), resp. **KDR** (Kinase Inserted Domain Receptor) class have become an important tool for the treatment of various types of cancer. Many of the compounds in this class have been approved for several cancer indications as a monotherapy option, while this includes renal cell carcinoma (RCC), gastrointestinal stromal tumor (GIST), hepatocellular carcinoma (HCC) and leukemia. In addition the usefulness of VEGFR2 TK inhibitors has also been confirmed in combination treatment with other well-established pharmacological treatments such as cytotoxic drugs and/or monoclonal antibodies.[4]

The overview of some current representatives of specific/selective RTK inhibitors and multi-target kinase inhibitors (TKIs) interacting with VEGFR2 TKs listed in the following tables. (Table 2 and 3) The corresponding chemical structures are shown on the figures below. (Figure 5 and 6)

Table 2. Current specific/selective RTK inhibitors interacting with VEGFR2 TK.[9,16,17]

Name	Trade / Code name	Mol. Mass (g/mol)	*IC_{50} (nM)	Cancer (examples)	Clinical phase / FDA approved
cediranib **5**	Recentin	450.50	<1.00	NSCLC, kidney and colorectal cancer	Phase 3
lenvatinib **6**	E7080	426.85	<4.00	Thyroid cancer	Since 2016
tivozanib **7**	AV-951	454.86	6.50	RCC, breast cancer	Phase 3
vatalanib **8**	PTK787 / PTK / ZK	346.81	37.0	NSCLC, DLBCL, colorectal adenocarcinoma	Phase 2

Table 3. Current multi-target tyrosine kinase inhibitors (TKIs) interacting with VEGFR2 TK.[9,16,17]

Name	Trade / Code name	Mol. Mass (g/mol)	*IC_{50} (nM)	Cancer (examples)	Clinical phase / FDA approved
axitinib **9**	Inlyta	386.50	0.20	RCC	Since 2012
foretinib **10**	EXEL-2880 / XL-880	632.65	0.90	NSCLC, breast, gastric, papillary renal cancer	Phase 2
golvatinib **11**	E7050	633.69	16.0	Gastric cancer, HCC, glioblastoma, melanoma	Phase 2
MGCD-265 **12**	-	517.60	3.00	NSCLC	Phase 2
pazopanib **13**	Votrient	437.51	30.0	Advanced renal cell carcinoma	Since 2009

[16] www.selleckchem.com (accessed February 12th, 2017).
[17] www.fda.gov (accessed February 12th, 2017).

ponatinib **14**	Iclusig	532.56	1.50	CML, philadelphia positive chromosome ALL	Since 2012
sorafenib **15**	Nexavar	464.80	90.0	Hepatocellular carcinoma	Since 2005
sunitinib **16**	Sutent	532.56	80.0	Gastrointestinal stromal tumor	Since 2006
vandetanib **17**	Caprelsa	475.35	40.0	Metastatic medullary thyroid cancer	Since 2011

*Half maximal inhibitory concentration (IC_{50}) represents the measure of the effectiveness of TKIs in inhibiting the VEGFR2 TK in biochemical assays. It is the concentration of an agonist drug required for 50 % inhibition of a particular biological target.[18]

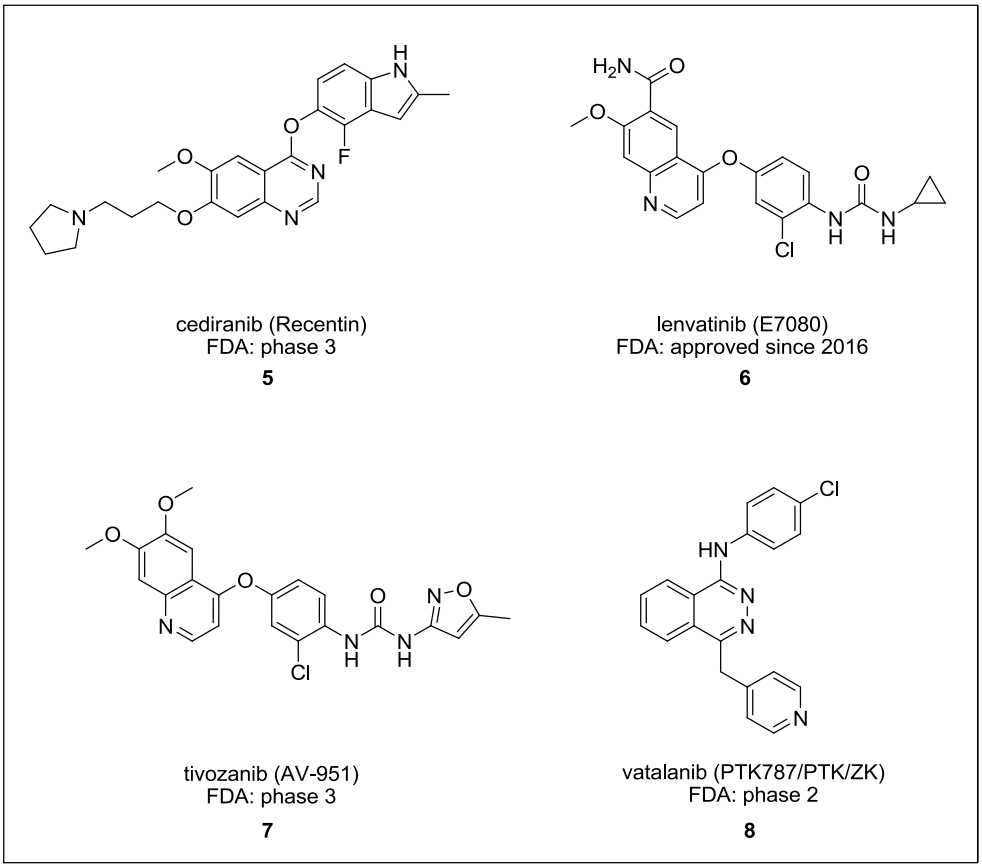

Figure 5. Chemical structures of the current specific/selective RTK inhibitors interacting with VEGFR2 TK.[9,16]

[18] Neubig, R. R.; Spedding, M.; Kenakin, T.; Christopoulos, A. *Pharmacol. Rev.* **2003**, *55*, 597 – 606.

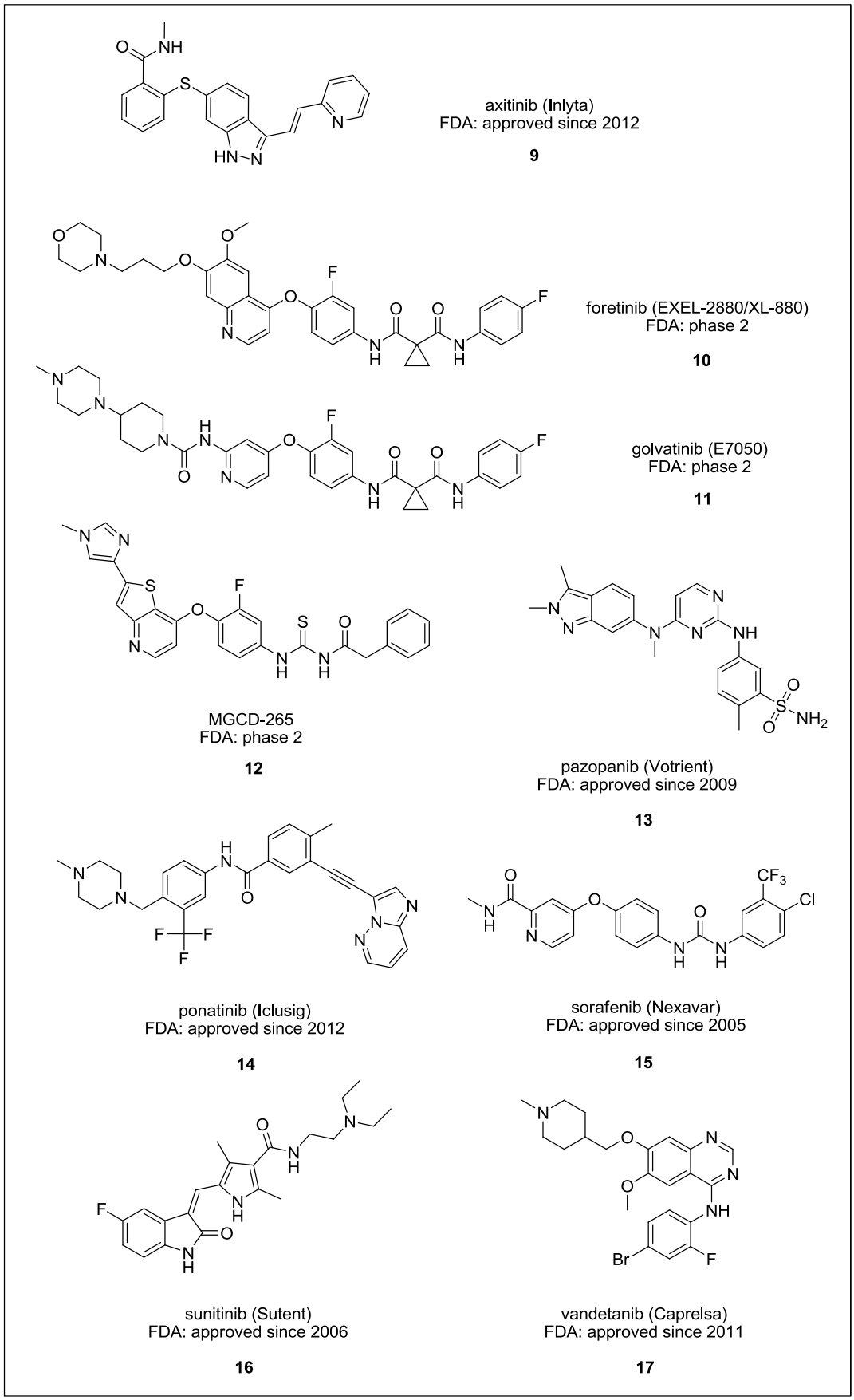

Figure 6. Chemical structures of the current multi-target TKIs interacting with VEGFR2 TK.[9,16]

2.2. VEGFR2 TK activity assay

The radioisotope filter binding assay is considered to be the standard for measuring the kinase activity of the VEGFR2 TK protein and it is the only format for the direct detection of a true enzymatic product. Analyzed compounds are incubated with a corresponding kinase, a substrate, cofactors, and a radioisotope-labelled ATP (^{32}P-ɣ-ATP or ^{33}P-ɣ-ATP). The reaction mixtures are then applied onto specific filter papers, which bind the radioisotope-labelled catalytic product, while the unreacted ATP is removed by washing of the papers.

The IC_{50} profile of the experimental compounds developed and discussed within this dissertation thesis was determined by testing at 10 concentrations (1×10^{-4} M to 3×10^{-9} M) for each compound. All positively tested compounds bound selectively to VEGFR2 TK by concentration dependent manner. The measurements were performed by Reaction Biology Corp.,USA.[19]

[19] Determination of enzymatic IC_{50} activity on VEGFR2 receptor has been performed by Reaction Biology Corp., Malvern, Pennsylvania, USA, www.reactionbiology.com/webapps/site/ (accessed May 13th, 2017).

Chapter 3. **Isosterism and bioisosterism in drug design**

3. Isosterism and bioisosterism in drug design

One of the key challenges for the medicinal chemists is the modulation and mediation of the potency of small-molecule therapeutics against their biological target. In addition, it is essential to ensure that the molecule reaches its target effectively while also satisfies necessary safety requirements. One of the most significant approaches for targeted modulation of molecular properties is bioisosteric replacement.

Because the bioisosteric replacement, resp. scaffold hopping represents the main idea of the Regioisomeric Bioisostery (*RegBio*) project, in the following chapter we will provide a theoretical background of this concept and an overview of possibly replacable groups together with corresponding practical examples.

3.1. Isosterism

The concept of **isosterism** was originally contemplated by James Moir in 1909. This notion was further refined by Irving Langmuir based on his experimental observations.[20] According to Langmuir's studies from 1919 isosteres were defined as **compounds or groups of atoms that have the same number and arrangement of electrons**. Such compounds should show remarkable similarity in physical properties. Using the octet rule and measured properties of a number of substances, Langmuir was able to identify particular isosteric groupings. The relationship was demonstrated to be true between nitrogen and carbon monoxide in terms of physical properties and the same similarities were also observed between nitrous oxide (N_2O) and carbon dioxide (CO_2). The list of isosteres defined by Langmuir is given in the table below.[21] (Table 4)

Table 4. Groups of isosteres identified by Langmuir.[21,22]

Groups	Isosteres
1	H^-, He, Li^+
2	O^{2-}, F^-, Ne, Na^+, Mg^{2+}, Al^{3+}
3	S^{2-}, Cl^-, Ar, K^+, Ca^{2+}

[20] Langmuir, I. *J. Am. Chem. Soc.* **1919**, *41*, 1543 – 1559.
[21] Meanwell, N. A. *J. Med. Chem.* **2011**, *54*, 2529 – 2591.
[22] Patani, G. A.; LaVoie, E. J.; *Chem. Rev.* **1996**, *96*, 3147 – 3176.

4	Cu^{+}, Zn^{2+}
	↓
8	N_2, CO, NC^{-}
9	CH_4, NH_4^{+}
10	CO_2, N_2O, N_3^{-}, $(NCO)^{-}$
	↓
20	MnO_4^{-}, CrO_4^{2-}
21	SeO_4^{2-}, AsO_4^{3-}

In 1925, H. G. Grimm extended the idea of isosterism, introduced by Langmuir, with Grimm's hydride displacement law. According to this law, **the addition of hydrogen atom will result in a pseudoatom with similar properties to the atom of the next highest atomic number**. E.g., –CH= is isosteric with –N= and –NH– is isosteric with –O– and so on.[23]

In 1932, Friedrich Erlenmeyer further broadened previous studies and redefined isosteres as **atoms, ions, and molecules in which the peripheral layers of electrons can be considered identical**. [24] In addition, Erlenmeyer also proposed the following three additions to the concept of isosteres:

1. All elements within the same group in the periodic table are isosteres to each other. Therefore, silicon and carbon are isosteres as well as oxygen and sulfur.
2. The term "pseudoatoms" is used to characterize atoms, resp. groups of atoms that appear superficially different but are actually very similar in physical properties. For example pseudohalogens represent the class, where –Cl is isosteric to –CN or –SCN and so on.
3. Finally, "ring equivalences" are used to permit isosteric matches between different ring systems. For example the similar isosteric properties of benzene and thiophene, where –CH=CH– from benzene is replaced by –S– in thiophene.

[23] Grimm, H. G. *Z. Electrochem* **1925**, *31*, 474 – 480.
[24] Erlenmeyer, H.; Berger, E.; Leo, M. *Helv. Chim. Acta* **1933**, *16*, 733 – 738.

3.2. Bioisosterism

The widespread application of the concept of isosterism to modify biological activity has given rise bioisosterism. The emergence of bioisosteres as structurally distinct compounds similarly recognized by biological systems has its origin in a series of later Erlenmeyer's studies. It was showed that particular antibodies were unable to discriminate between –O–, –NH– and $–CH_2–$ (**19**, **20**, **21**) or phenyl and thienyl rings (**22**, **23**) in the context of artificial antigens derived by reacting of diazonium ions with proteins.[21,25] (Scheme 1)

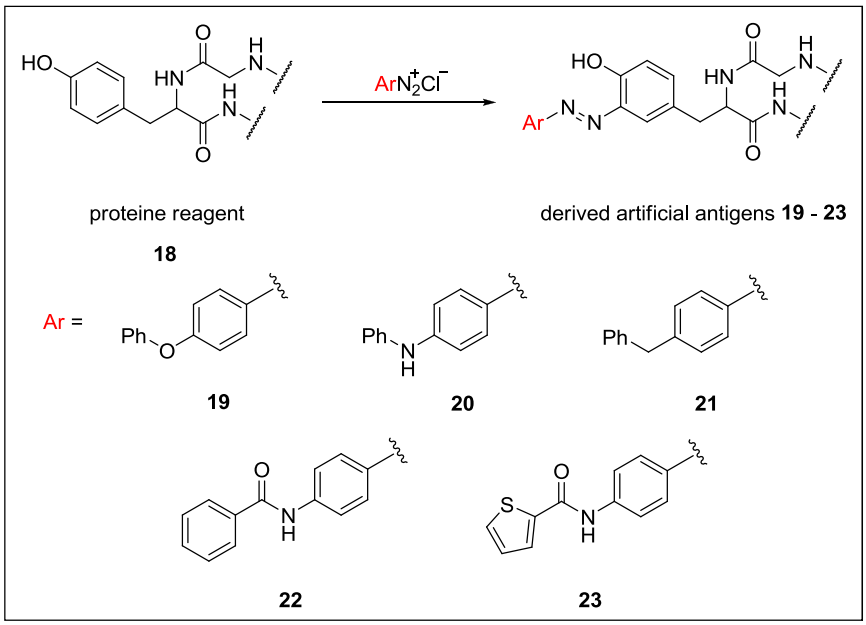

Scheme 1. The example of the bioisosteric antigens **19** – **23** tested by Erlenmeyer.

The term "**bioisostere**" was introduced by Harris Friedman in 1951. He defined bioisosteres as **structural moieties which fit the broadest definition of isosteres and have the same type of biological activity**. This definition really only considers the macromolecular recognition of bioisosteres, which is also highly important, but largely ignores the specifics of numerous other physicochemical properties that are optimized in a medicinal chemistry project.[25,26]

Friedman's definition was followed in 1979 with the definition from Thornber which says that **bioisosteres are groups or molecules which have chemical and physical**

[25] Brown, N. *Bioisosteres in Medicinal Chemistry* **2012** Wiley-VCH, Weinheim.
[26] Friedman, H. L. *Influence of Bioisosteric Replacements upon Biological Activity* **1951** NAS-NRS, Washington.

similarities producing broadly similar biological properties.[27] This notion suggests that bioisosteres are typically less than exact structural mimetics and are often more alike in biological rather than physical properties. Therefore, an effective bioisostere for one chemical application may not be usable in another setting, which necessitating the careful selection and tailoring of an isostere for a specific case. Consequently, the design of bioisosteres usually introduces structural changes that can be, depending on the context, favorable or unfavorable. These changes affecting mainly:

1. Size: molecular weight
2. Shape: bond angles and hybridization states
3. Electronic distribution: polarizability, inductive effects, charge and dipoles
4. Lipid solubility
5. Water solubility
6. pKa
7. Chemical reactivity, including likelihood of metabolism
8. Hydrogen bonding capacity

In the medicinal chemistry practice, the development and application of bioisosteres have become a fundamental approach influencing mainly four key parameters:

1. **Structural:** Structural moieties often have an important role in maintaining a preferred conformation of a molecule and influencing parameters such a molecular size or bond angles. This is relevant especially for moieties creating the basis of a particular chemical structure. Scaffold hopping can be seen as an example.
2. **Receptor interactions:** When the moiety that is being replaced interacts directly with a receptor or enzyme, then the most relevant parameters will be size, shape, electronic properties, pKa, chemical reactivity and hydrogen bonding.
3. **Pharmacokinetics:** Except of the direct biological response optimization, it is important also to optimize the absorption, transport, and excretion properties of the molecule. In these situations, the most important parameters to consider are lipophilicity, hydrophilicity, hydrogen bonding and pKa.

[27] Thornber, C. W. *Chem. Soc. Rev.* **1979**, *8*, 563 – 580.

4. **Metabolism:** A particular moiety can be involved in blocking or assisting with biological metabolism of the molecule. For example, –Cl and $–CH_3$ groups on benzene are potentially interchangeable for some situations. However, toluene derivative could be metabolized to a benzoic acid with the result being a short half-life and/or unexpected side effects.[25]

In 1991, Alfred Burger defined bioisosteres as **compounds or groups that possess near-equal molecular shapes and volumes, approximately the same distribution of electrons, and exhibiting similar physicochemical properties**. Burger's definition included all of the aforementioned extensions and resulted in the classification of bioisosteres into classical and nonclassical group.[28,29]

Classical bioisosteres represent the concept of structurally simple, mono-, di-, and trivalent atoms or groups and ring equivalents. In contrast, nonclassical bioisosteres extend the concept to structural elements offering more subtle and sophisticated form of biochemical equivalence.[21]

[28] Burger, A. *Prog. Drug Res.* **1991**, *37*, 288 – 362.
[29] Burger, A. *In Medicinal Chemistry* **1970** Wiley-Interscience, New York.

3.2.1. Classical bioisosteres

Monovalent atoms and groups replacements

Figure 7. Bioisosterically replaceable monovalent atoms and groups.

One of the most common monovalent isosteric replacements is the substitution of hydrogen with fluorine. These atoms have similar van der Waals radius but different electronic effects, whereas fluorine is the most electronegative element in the periodic table. Due to the high strength of the C-F bond, fluorine is often introduced to achieve metabolic stability. Moreover, due to its high electronegativity, fluorine can be introduced to reduce basicity of proximal amines or increase acidity of proximal acids and also to influence a conformation in molecules. One of the most well-known examples of effective replacement of hydrogen with fluorine is observed in the antineoplastic drug 5-fluorouracil (**25**). This compound is metabolized *in vivo* to 5-fluoro-2'-deoxyuridine monophosphate (5-fluoro-dUMP) (**26**), which is the active drug that forms a stable ternary complex with enzyme thymidilate synthase (TS), the enzyme providing the DNA replication *via* the conversion of deoxyuridine monophosphate (dUMP) to deoxythymidine monophosphate (dTMP).[25,30] (Scheme 2)

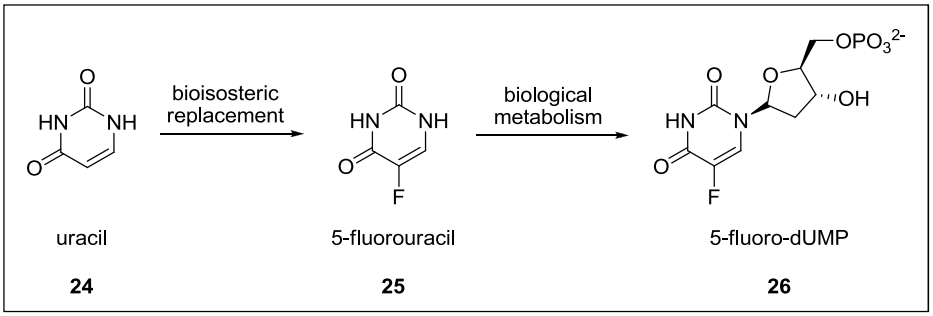

Scheme 2. Bioisosteric H / F replacement in the prodrug – 5-fluorouracil (**25**).

[30] Longley, D. B.; Harkin, D. P.; Johnston, P. G. *Nat. Rev. Cancer* **2003**, *5*, 330 – 338.

Although the $–CHF_2$ moiety has not been widely exploited by medicinal chemists, it is beginning to attract attention and several interesting applications have recently been examined. In one of the most successful demonstrations of utility, the $–CHF_2$ moiety was recognized as a potential isostere of a thiol in the context of inhibitors of NS3 (HCV) protease, an important antiviral target that cleaves the substrates at the carboxy terminal of cysteine. Difluoro-Abu analogue **29** of the hexapeptide NS3 inhibitor **27** proved to be equipotent and 20-fold more potent than simple Abu derivative **28**. An X-ray cocrystal of a related inhibitor revealed the key ligand-protein interactions, with the $–CHF_2$ moiety donating a H-bond to the carbonyl group of Lys136 and at the same time accepting a weak H-bond from the aromatic C4-hydrogen atom of Phe154.[31] (Figure 8)

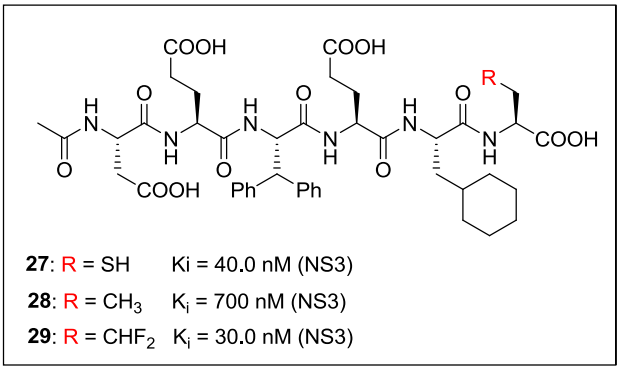

Figure 8. Hexapeptide HCV NS3 inhibitor **27** and its analogues, Abu **28** and difluoro-Abu **29**.

Hydroxamic acid moiety represents an important pharmacophoric fragment, widely used in medicinal chemistry. However, hydroxamic acids can express toxicity based on a metabolic activation, which manifests either as Lossen rearrangement to the corresponding isocyanate or as hydrolytic degradation to release the carboxylic acid and hydroxylamine.[32] The potential of $–CHF_2$ moiety to act as an isostere of the hydroxyl of hydroxamic acids has been evaluated in a series of dual inhibitors of cyclooxygenase-2 (COX-2) and 5-lipoxygenase (5-LOX). Hydroxamic acids are well-established inhibitors of 5-LOX, binding to the active site iron, and substitution of the toluene ring of **30** with a cyclic hydroxamic acid affords the dual COX-2 / 5-LOX inhibitor **31**. The $–CHF_2$ analogue **32** was explored as a non-hydroxamic acid isostere and appeared to be an effective mimetic,

[31] Narjes, F.; Koehler, K. F.; Koch, U.; Gerlach, B.; Colarusso, S.; Steinkühler, C.; Brunetti, M.; Altamura, S.; De Francesco, R.; Matassa, V. G. *Bioorg. Med. Chem. Lett.* **2002**, *12*, 701 – 704.
[32] Filipo, M.; Charton, J.; Hocine, A.; Dassonneville, S.; Deprez, B.; Deprez-Poulain, R. *J. Med. Chem.* **2009**, *52*, 6790 – 6802.

although the mechanism of action of this compound has not been fully clarified.[33] (Figure 9)

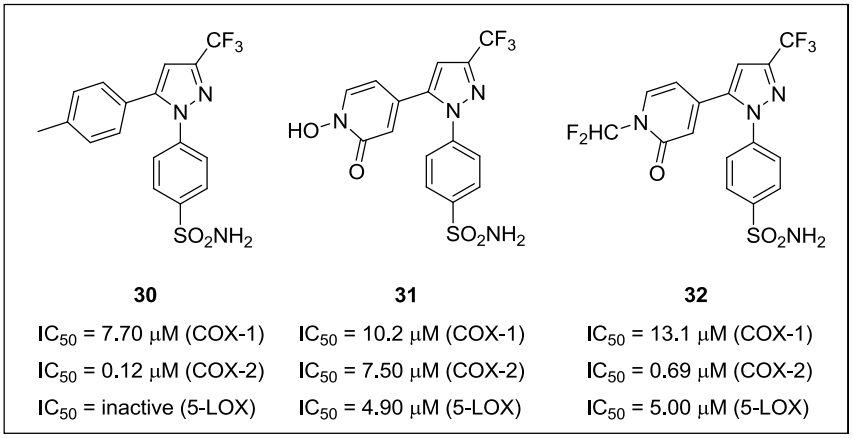

Figure 9. Cyclooxygenase and lipoxygenase inhibition associated with a series of pyrazole-based inhibitors **30**, **31** and **32**.

Bivalent atoms and groups replacements

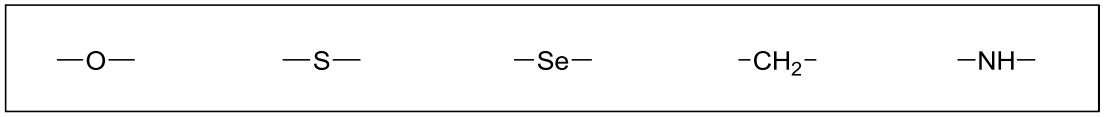

Figure 10. Bioisosterically replaceable bivalent atoms and groups.

A successful use of bivalent bioisosteres can be found in derivatives of the antihypertensive drug rilmenidine (**33**), where they were used as a way of finding similar compounds with reduced side effects. Rilmenidine (**33**) exerts its activity by binding to the I_1 imidazoline receptors (I_1Rs), but it also binds to the α_2-adrenoreceptors (α_2ARs), which are considered to be responsible for the side effects. As shown, several bivalent bioisosteres **34** – **40** of rilmenidine (**33**) were able to maintain I_1Rs binding, while losing affinity to the α_2ARs.[25,34] (Figure 11)

[33] Chowdhury, M. A.; Abdellatif, K. R. A.; Dong, Y.; Das, D.; Suresh, M. R.; Knaus, E. E. *J. Med. Chem.* **2009**, *52*, 1525 – 1529.
[34] Shann, S.; Bruban, V.; Pompermeyer, K.; Feldman, J.; Pfeiffer, J.; Renard, P.; Scalbert, E.; Bousquet, P.; Ehrhardt, J. D. *J. Med. Chem.* **2001**, *44*, 1588 – 1593.

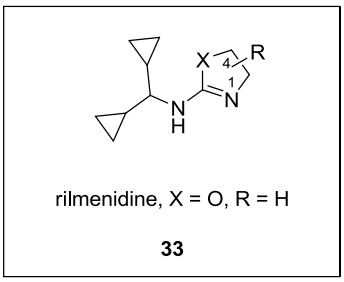

rilmenidine, X = O, R = H

33

Compound	R	X	*pK_i I_1Rs (M)	*pK_i α_2ARs (M)
33	H	O	7.13±0.10	7.25±0.08
34	H	CH_2	6.29±0.11	<5
35	5-CH_3	CH_2	5.80±0.08	<5
36	3-CH_3	CH_2	<5	<5
37	4-CH_3	CH_2	6.19±0.10	<5
38	*cis/trans*-4,5-diCH_3	CH_2	6.27±0.11	<5
39	5-Et	CH_2	6.77±0.09	<5
40	*cis*-4,5-$(CH_2)_4$	CH_2	<5	<5

Figure 11. Bivalent bioisosteric analogues of rilmenidine (**33**).

*K_i - equilibrium dissociation constant for ligand receptor interactions determined in inhibition studies. It has the dimension M (mol / l). The K_i for a given ligand is typically (but not necessarily) determined in a competitive radioligand binding study by measuring the inhibition of the binding of a reference radioligand by the competing ligand of interest under equilibrium conditions.[18] K_i is the concentration of a competitive inhibitor that is required to decrease the maximal rate of an enzymatic reaction by half.

pK_i - The negative logarithm to base 10 of the equilibrium dissociation constant (K_i) in molar concentration units (M). The major benefit to using the pK_i measures of pharmacological potency rather than the constant Ki is that pharmacological potency often ranges over many orders of magnitude (K_i values from 10^{-10} to > 10^{-3} M), it is easier to present and discuss these differences in pK_i form (i.e., values generally range from about 10 to 3).[18]

Trivalent atoms and groups replacements

Figure 12. Bioisosterically replaceable trivalent atoms and groups.

An application of trivalent bioisosterism can be found in the development of hypocholesterolemic agents, where two CH groups present in cholesterol (**41**) were replaced with two nitrogen atoms. This resulted in 20,25-diazacholesterol (**42**), which is potent inhibitor of cholesterol biosynthesis. An introduction of the nitrogen atom induced a loss of the stereogenic centre and improved the possibility of additional interactions in the enzymatic active site.[22,35] (Figure 13)

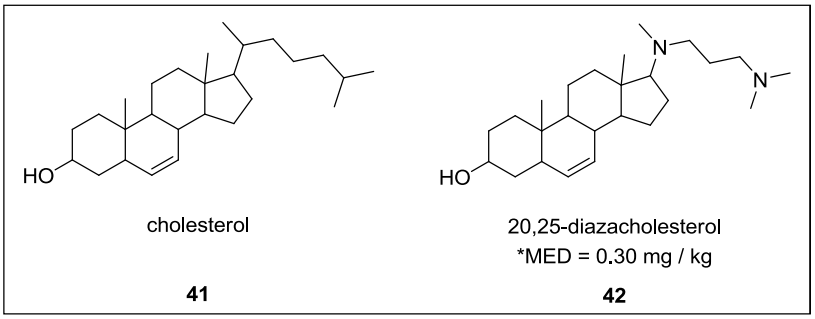

Figure 13. Cholesterol (**41**) and its bioisosteric analogue 20,25-diazacholesterol (**42**).

*Minimum effective dose (MED) – the lowest dose level of a drug that providing a clinically significant response in average efficiency, which is statistically superior to the response provided by the placebo.[36]

Tetravalent Atoms Replacements

Figure 14. Bioisosterically replaceable tetravalent atoms and groups.

A recent example of bioisosteric replacement of a carbon with silicon was reported by Warneck and colleagues, who synthesized the silicon derivative **44** of p38 MAP kinase inhibitor BIRB-796 (**43**), which is in clinical evaluation for several inflammatory diseases, such as rheumatoid arthritis, Crohn's disease and psoriasis. The silicon bioisostere **44** was found to be unusually less lipophilic than BIRB-796 (**43**), of comparable potency, and more metabolically stable in human liver microsomes.[25,37] (Figure 15)

[35] Counsell, R. E.; Klimstra, P. D.; Nysted, L. N.; Ranney, R. E. *J. Med. Chem.* **1965**, *8*, 45 – 48.
[36] Chow, S. C. *Encyclopedia of Pharmaceutical Statistics (3rd ed.)* **2010** Informa Healthcare, London.
[37] Barnes, M. J.; Conroy, R.; Miller, D. J.; Mills, J. S.; Montana, J. G.; Pooni, P. K.; Showell, G. A.; Walsh, L. M.; Warneck, J. B. H. *Bioorg. Med. Chem. Lett.* **2007**, *17*, 354 – 357.

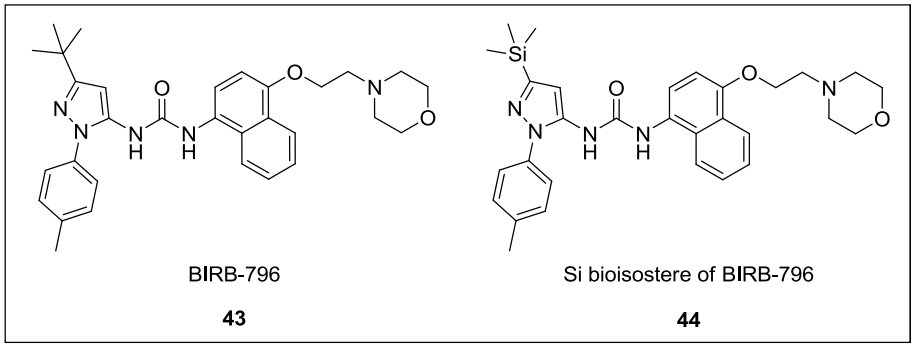

Figure 15. Example of carbon / silicon bioisosteric replacement.

Ring replacements

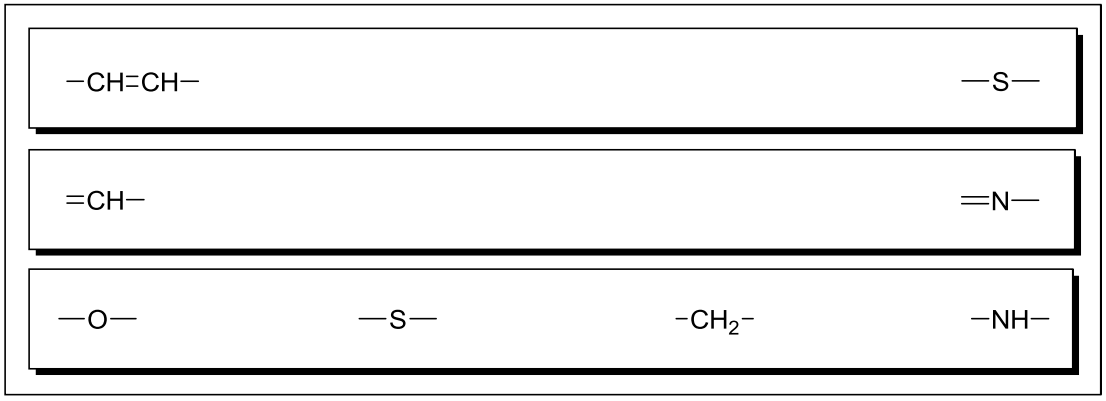

Figure 16. Bioisosterically replaceable atoms and groups in ring moieties.

The substitution of phenyl ring with pyridine is widely used to improve metabolic stability or pKa value. One efficient example of this can be recently found in a group of HIV-1 inhibitors **45**, **46** which are currently in clinical development. Compound **45** was identified as a lead in the discovery of HIV-inhibiting drugs, due to its fast metabolism and low solubility; bioisosteres of phenyl ring were evaluated. This led to the identification of BMS-488043 (**46**) – a potent HIV-inhibitor with better pharmacokinetic profile.[25, 38] (Figure 17)

[38] Wang, T.; Yin, Z.; Zhang, Z.; Bender, J. A.; Yang, Z.; Johnson, G.; Zadjura, L. M.; D'Arienzo, C. J.; Parker DiGiugno, D.; Gesenberg, C.; Yamanaka, G. A.; Gong, Y. F.; Ho, H. T.; Fang, H.; Zhou, N.; McAuliffe, B. V.; Eggers, B. J.; Fan, L.; Nowicka-Sans, B.; Dicker, I. B.; Gao, Q.; Colonno, R. J.; Lin, P. F.; Meanwell, N. A.; Kadow, J. F. *J. Med. Chem.* **2009**, *52*, 7778 – 7787.

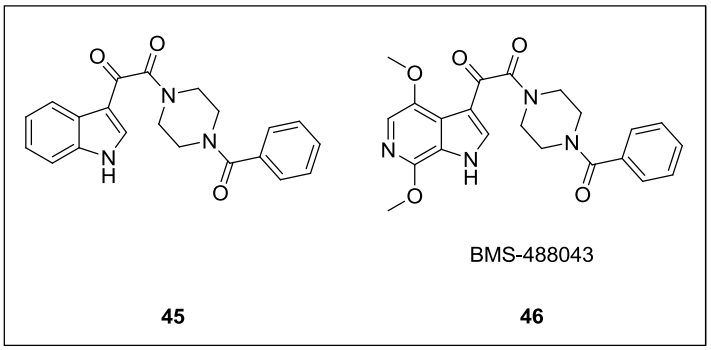

Figure 17. The example of phenyl / pyridine bioisosteric replacement.

S-4CPG (**47**) is a metabotropic glutamate receptor 1 (mGluR1) antagonist which activity is dependent on the distance between its ω-carboxylic acid and α-amino acid moieties and their linear topological relationship. The propellane (bicyclo[1.1.1]pentane) derivative **48** was explored as a bioisostere of **47** exhibiting good antagonist activity against mGluR1a. The propellane moiety, which serves as a spacer in this compound, has a different stereoelectronic profile to the phenyl ring but is able to keep the ω-carboxylate and α-amino acidic moieties in the coplanar position crucial for activity. [39,40] (Figure 18)

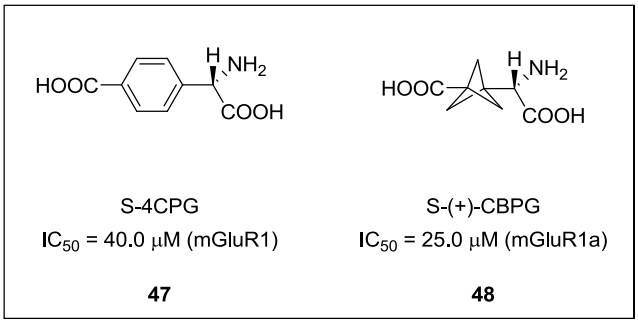

Figure 18. The example of unconventional phenyl / propellane bioisosteric replacement.

[39] Watkins, J.; Collingridge, G. *Trends Pharmacol. Sci.* **1994**, *15*, 333 – 342.
[40] Pellicciari, R.; Raimondo, M.; Marinozzi, M.; Natalini, B.; Costantino, G.; Thomsen, C. *J. Med. Chem.* **1996**, *39*, 2874 – 2876.

3.2.2. Nonclassical bioisosteres

Carbonyl group replacements

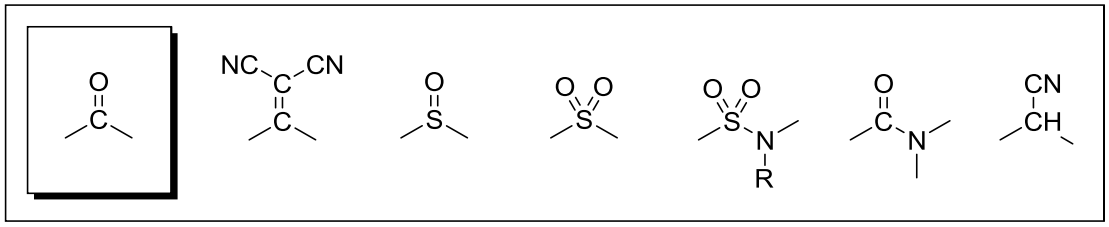

Figure 19. Bioisosterically replaceable carbonyl-like moieties.

Modafinil (**49**) is a widely used drug in the treatment of excessive sleepiness caused by narcolepsy, shift work sleep disorder, and obstructive sleep apnea. This compound has a stereogenic sulfoxide group, and it is currently marketed as racemate. De Risi *et al.* investigated the replacement of the sulfoxide group with a carbonyl to facilitate synthesis and to remove problems associated with chirality. Compound **50** showed a slight loss of activity compared to modafinil, but this was restored when the amide function was modified in compound **51**.[25,41] (Figure 20)

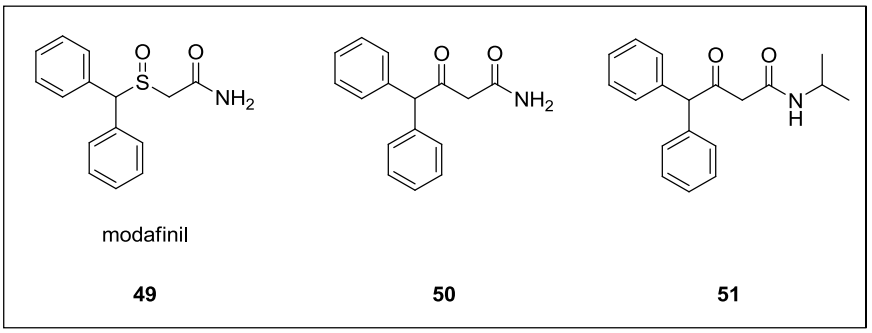

Figure 20. Bioisosteric analogues of modafinil (**50**, **51**).

[41] De Risi, C.; Ferraro, L.; Pollini, G. P.; Tanganelli, S.; Valente, F.; Veronese, A. C. *Bioorg. Med. Chem. Lett.* **2008**, *18*, 923 – 928.

Carboxylic acid replacements

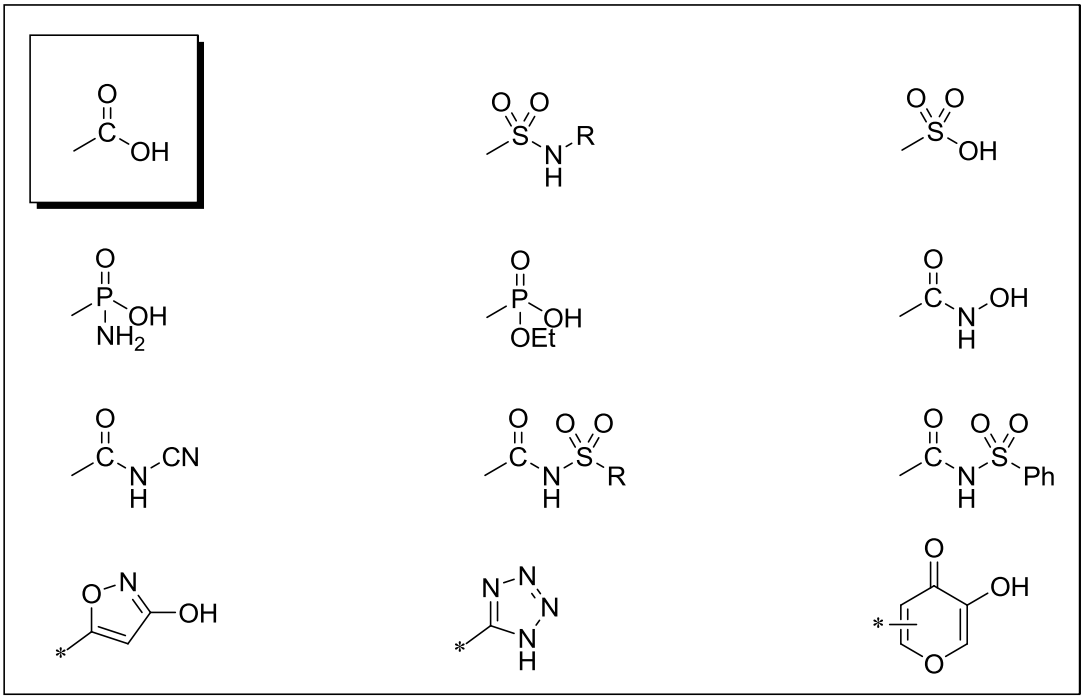

Figure 21. Bioisostericly replacable carboxylic acid-like moieties.

Angiotensin II receptor antagonists provide an instructive insight into carboxylic acid isostere design, since binding affinity to the receptor in a series of biphenyl acids is quite sensitive to the character of the acidic element. The tetrazole moiety in Losartan (**53**) causes a 10-fold increase in inhibitory potency compared to the carboxylic analogue **52**, a result explored through geometrical analysis that indicated the tetrazole projects the acidic –NH– group 1.5 Å further from the aryl ring than a –COOH group. The $–CONHSO_2Ph$ moiety incorporated into **54** exhibits the similar geometrical topology to –COOH in **52** and therefore offers a comparable potency.[21,42,43] (Figure 22)

[42] Li, C.; Benet, L. Z.; Grillo, M: P. *Chem. Res. Toxicol.* **2002**, *5*, 1309 – 1317.
[43] Carini, D. J.; Christ, D, D.; Duncia, J. V.; Pierce, M. E. *Pharm. Biotechnol.* **1998**, *11*, 29 – 56.

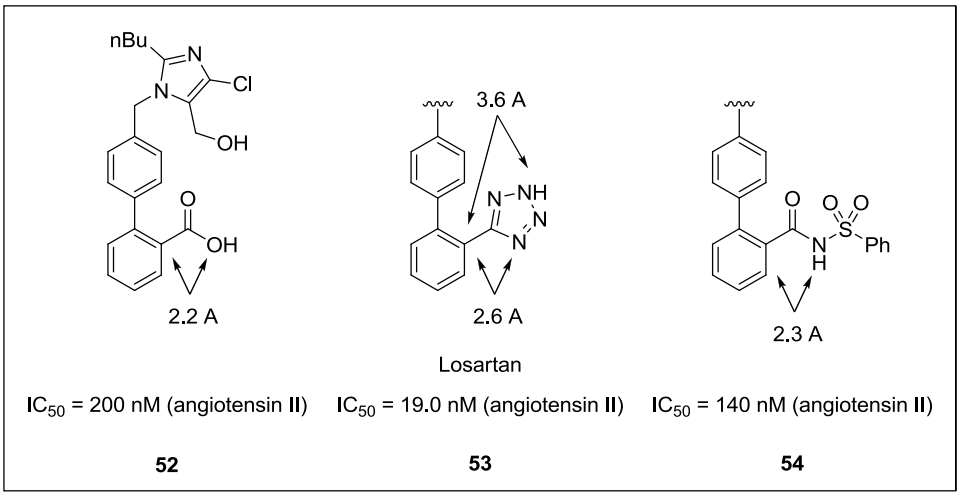

Figure 22. Geometrical arrangements associated with the carboxylic acid, tetrazole and acylsulfonamide moiety in angiotensin II antagonists **52** – **54** and their biological activities.

Hydroxyl group replacements

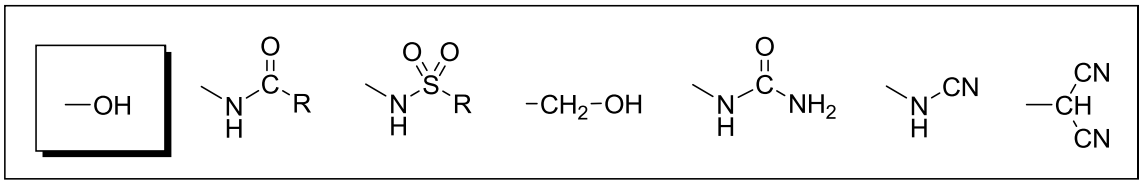

Figure 23. Bioisosterically replaceable hydroxyl-like moieties.

In 2005, the synthesis and biological evaluation of phenol bioisosteric analogues of benzazepine D_1 / D_5 antagonist were reported. The most promising compound **55** has undergone several clinical trials, including schizophrenia, cocaine addiction, and obesity. Expect of proved good antagonist activity, the compound **55** presented problematic pharmacokinetic issues. This liability was mainly caused by O-glucuronidation on phenolic –OH group and by demethylation of N-CH_3 group. Therefore several novel compounds **56** – **59** containing heterocyclic rings with N-H hydrogen bond donor as isosteres of the phenolic –OH group were investigated. The investigation resulted in improved pharmacokinetic profiles and maintained good antagonist activity.[25,44] (Figure 24)

[44] Wu, W. L.; Burnett, D. A.; Spring, R.; Greenlee, W. J.; Smith, M.; Favreau, L.; Fawzi, A.; Zhang, H.; Lachowicz, J. E. *J. Med. Chem.* **2005**, *48*, 680 – 693.

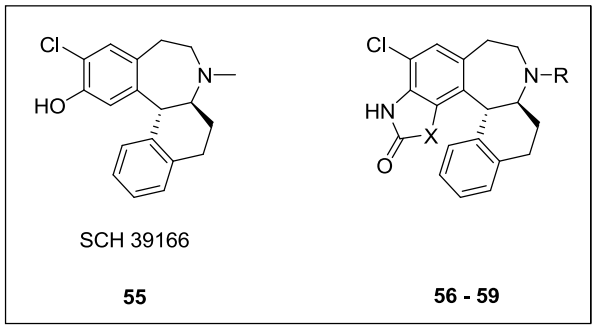

Compound	R	X	K_iD_1 (nM)	K_iD_5 (nM)	*C_{max} (ng/ml)	*T_{max} (h)	*BA (%)
55	-	-	1.20	2.00	72	0.5	0.6
56	Me	NH	7.00	4.20	1300	1.0	87
57	H	NH	16.5	2.40	1640	6.0	42
58	Me	S	2.10	2.80	462	2.0	-
59	H	S	6.50	1.70	5690	1.0	-

Figure 24. The compound **55** and its bioisosteres **56**, **57**, **58** and **59** showing good pharmacokinetic profiles, while maintaining good antagonist activity on the D_1 / D_5 receptors.

*C_{max} (ng / ml) is a term used in pharmacokinetics refers to the maximum serum concentration that a drug achieves in a specific compartment or test area of the body after the drug has been administrated. T_{max} (h) is the time at which the C_{max} is observed.[45] BA (%) is a bioavailability – a subcategory of absorption and the fraction of administered dose of unchanged drug that reaches the systemic circulation. By definition, when a medication is administered intravenously, its bioavailability is 100 %.[46]

Catechol

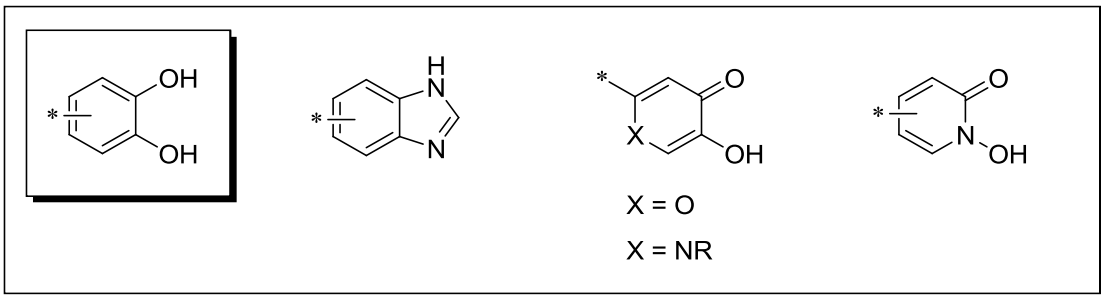

Figure 25. Bioisosterically replaceable catechol-like moieties.

[45] Craig, C. R.; Stitzel, R. E. *Modern Pharmacology with Clinical Applications(6th ed.)* **2004** Lippincot Williams & Wilkins.
[46] Griffin, J. P.; Posner, J.; Barker, G. R. *The Textbook of Pharmaceutical Medicine (7th ed.)* **2013** Wiley-Blackwell.

Catechol bioisosteres are often utilized to overcome pharmacokinetic and toxicological issues linked to this moiety. Successful examples of bioisosteric replacement of catechols can be found in catecholamines. Benzimidazole analogues **62** and **63** of the adrenergic agonist norepinephrine (**60**) and isoproterenol (**61**) were synthesized to evaluate their activity in adrenergic systems and also to improve their biological stability.[25,47] (Figure 26)

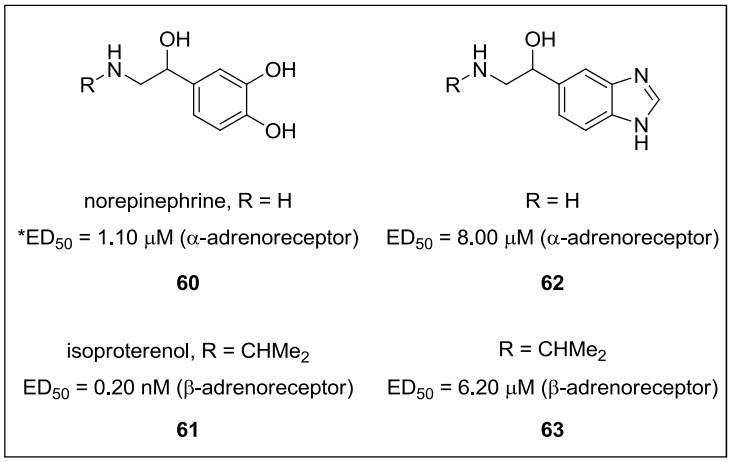

Figure 26. Catecholamines **60**, **61** and their benzimidazole bioisosteres **62**, **63**.

*Half maximal effective dose (ED_{50}) represents the amount of a drug that produces a specified response in 50 % of a test population.[18]

Halogen replacements

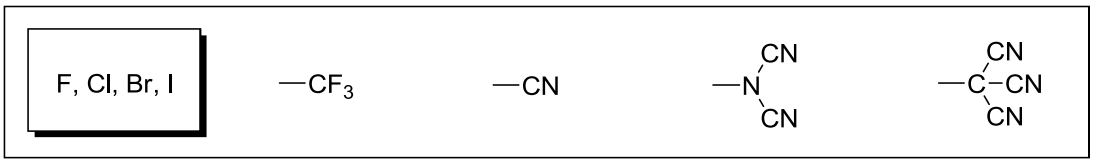

Figure 27. Bioisosterically replacable halogen-like moieties.

One of the approaches in the development of drug targeting breast cancer is the inhibition of estrogen biosynthesis with aromatase (CYP19) inhibitors. Nonsteroidal aromatase inhibitors (NSAI) such as vorozole (**64**) and liarozole (**65**) have shown several advantages over steroidal drugs in adjuvant treatment. A new class of NSAI based 2-,3-,5-, and 7-[(aryl)(azoyl)methyl]-1*H*-indoles as more potent and selective inhibitors was developed.

[47] Arnett, C. D.; Wright, J.; Zenker, N. *J. Med. Chem.* **1978**, *21*, 72 – 78.

Compounds **66** and **67** were modified on the indolic nitrogen and on the phenyl ring. The compound **66** with X = Cl and the compound **67** with X = CN proved to be equipotent on CYP19 and selective toward CYP17.[25,48] (Figure 28)

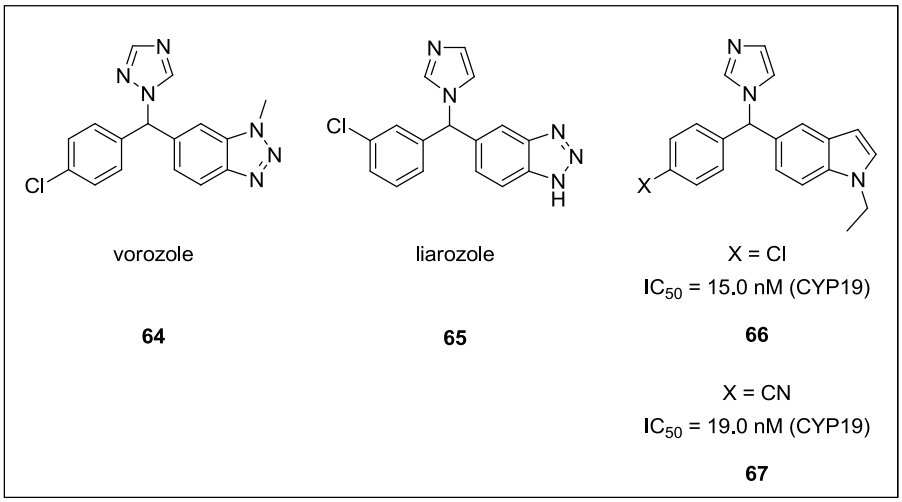

Figure 28. Bioisosteric replacement in nonsteroidal aromatase inhibitors **64** – **67**.

Amide and ester bioisosteres

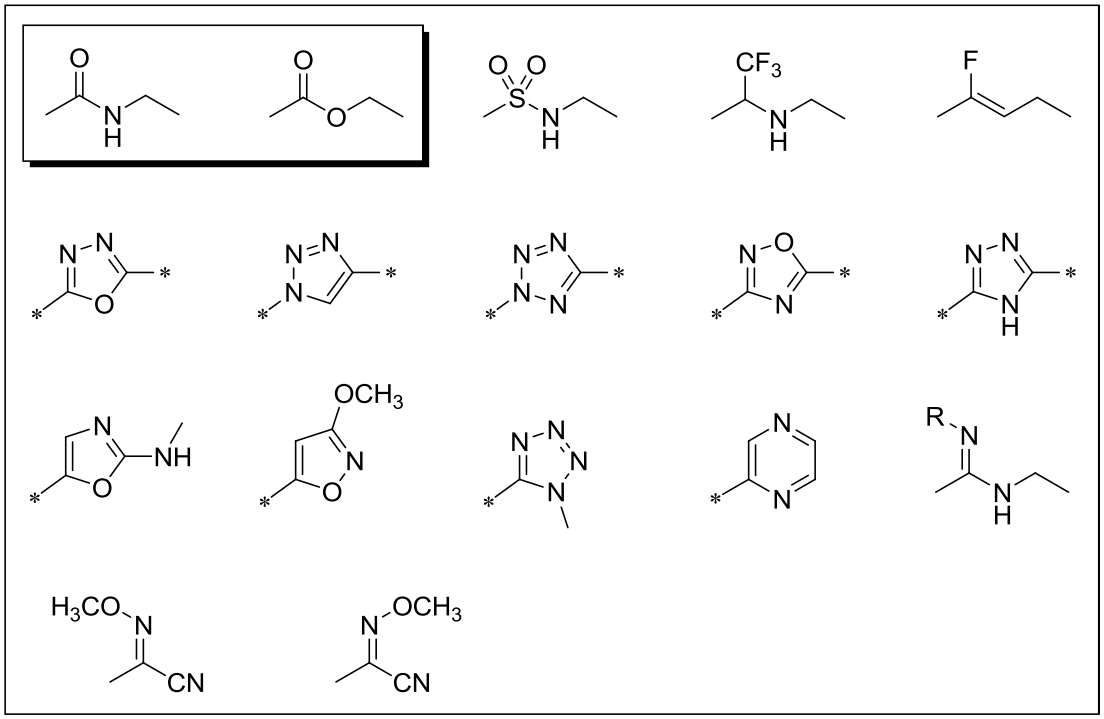

Figure 29. Bioisosterically replaceable amide-like and ester-like moieties.

[48] Leze, M. P.; Le Borgne, M.; Pinson, P.; Palusczak, A.; Duflos, M.; Le Baut, G.; Hartmann, R. W. *Bioorg. Med. Chem. Lett.* **2006**, *16*, 1134 – 1137.

Bioisosteres of amides are generally introduced to modulate polarity and bioavailability, while ester bioisosteres are used to improve metabolism.

A recent successful example of amide bioisosterism can be found in the development of inhibitors of the enzyme cathepsin K, which is involved in osteoclastic bone resorption and is a target for the treatment of osteoporosis. Compound **68** was identified as a potent inhibitor of cathepsin K, but it was not selective over other cathepsines in cell-based assays. Modifications led to **69**, a highly selective cathepsin K inhibitor, which presented metabolic liabilities. The metabolic problems of the compound **69** led to the identification of odanacatib (**70**), which is currently under clinical evaluation.[25,49] (Figure 30)

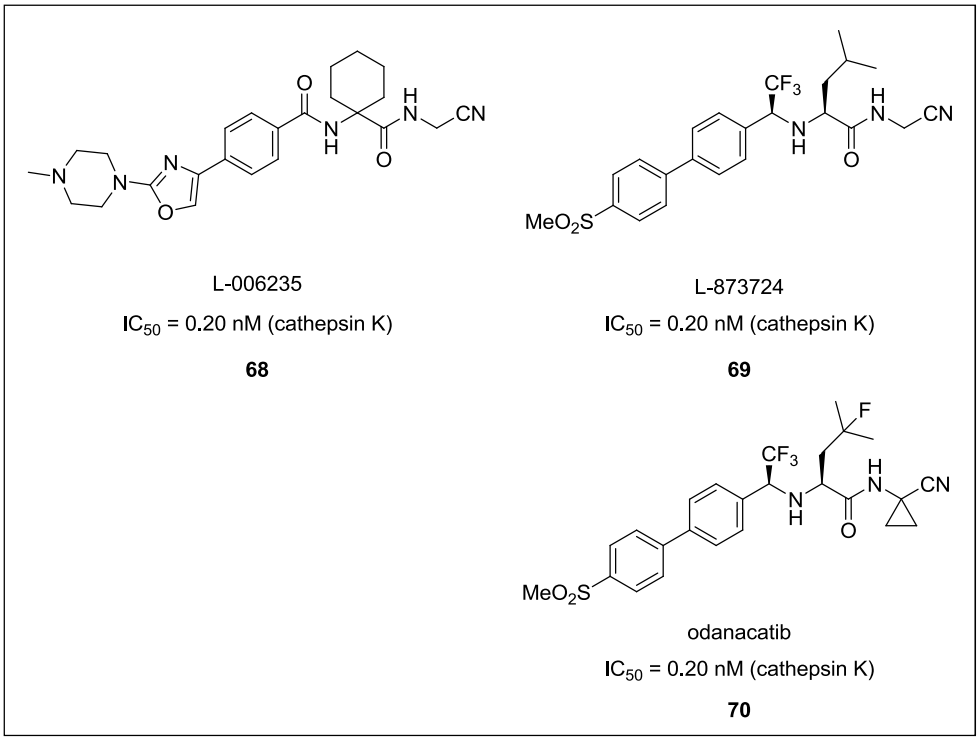

Figure 30. An example of bioisosteric replacement of amide moiety in **68** leading to the clinical candidate odanacatib (**70**).

[49] Gauthier, J. Y.; Chauret, N.; Cromlish, W.; Desmarais, S.; Duong, L. T.; Falgueyret, J. P.; Kimmel, D. B.; Lamontagne, S.; Leger, S.; LeRichte, T.; Li, C. S.; Massé, F. ; McKay, D. J.; Nicoll-Griffith, D. A.; Oballa, R. M.; Palmer, J. T.; Percival, D. J.; Riendeau, D.; Robichaud, J.; Rodan, G. A.; Rodan, S. B.; Seto, C.; Therien, M.; Truong, V. L.; Venuti, M. C.; Wesolowski, G.; Young, R. N.; Zamboni, R.; Black, W. C. *Bioorg. Med. Chem. Lett.* **2008**, *18*, 923 – 928.

Thiourea replacements

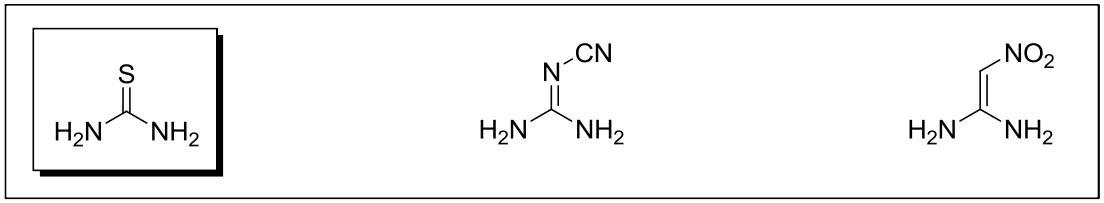

Figure 31. Bioisosterically replaceable thiourea-like moieties.

Metiamide (**71)** is an antiulcer drug acting as antagonist of the histamine H_2 receptor. Its high-dosage chronic toxicity tests revealed kidney damage and agranulocytosis, which was attributed to presence of thiourea fragment in the molecule. For this reason, the bioisosteric replacement of the sulfur in metiamide (**71**) was investigated. A cyanoguanidine analogue cimetidine (**72**) retained the same activity as metiamide (**71**), without toxic effects at high doses.[25,50] (Figure 32)

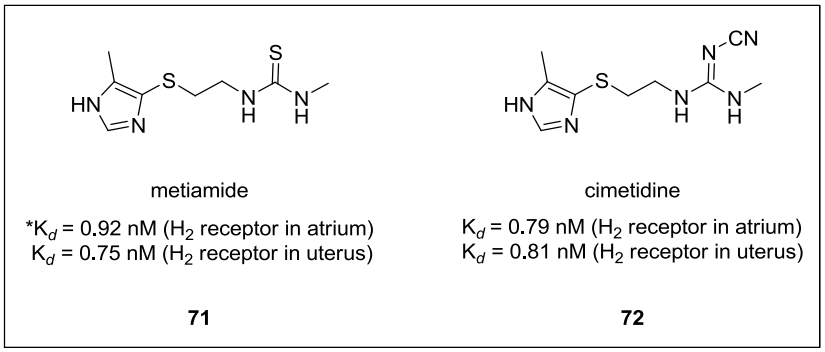

Figure 32. Thiourea bioisosteric replacement in antiulcer drugs **71** and **72**.

*The dissociation constant K_d reffers to the equilibrium dissociation constant for ligand-receptor interactions determined directly in a binding assay using a labeled form of the ligand.[18] It is commonly used to describe the affinity between a ligand (a drug) and a protein, i. e. how tightly a ligand binds to a particular protein. The dissociation constant has molar units (M), which corresponds to the concentration of a ligand at which the binding site on a particular protein is half-occupied.

[50] Durant, G. J.; Emmett, J. C.; Ganellin, C. R.; Miles, P. D.; Parsons, M. E.; Prain, H. D.; White, G. R. *J. Med. Chem.* **1977**, *7*, 901 – 906.

Pyridine replacements

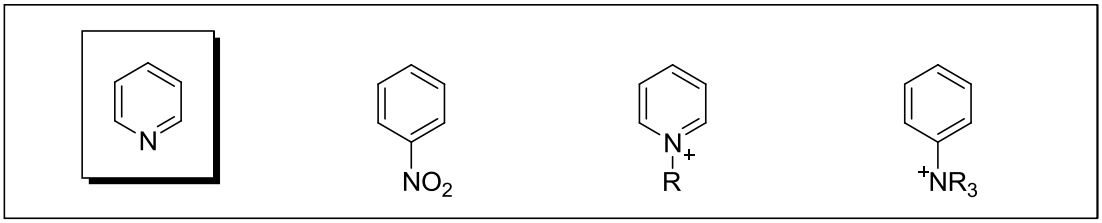

Figure 33. Bioisosterically replaceable pyridine-like moieties.

(+)-Anatoxin-a (**73**) is an alkaloid from algae, which binds a variety of nicotinic acetylcholine receptor (nAChR) subtypes. PHT (**74**) was the first bioisosteric and conformationally constrained modification of **73** retaining similar activity. In 2001, the synthesis and biological evaluation of some pyridine bioisosteres of PHT (**74**) was published. These compounds were designed and synthesized as new ligands selective for certain nAChR subtypes to be used in the treatment of several CNS disorders or as analgesics. The pyridine in **74** was replaced by other nitrogen-containing rings such as 1,2- or 1,3-diazines and compound **75** was found to be the most potent among all synthesized compounds.[25,51] (Figure 34)

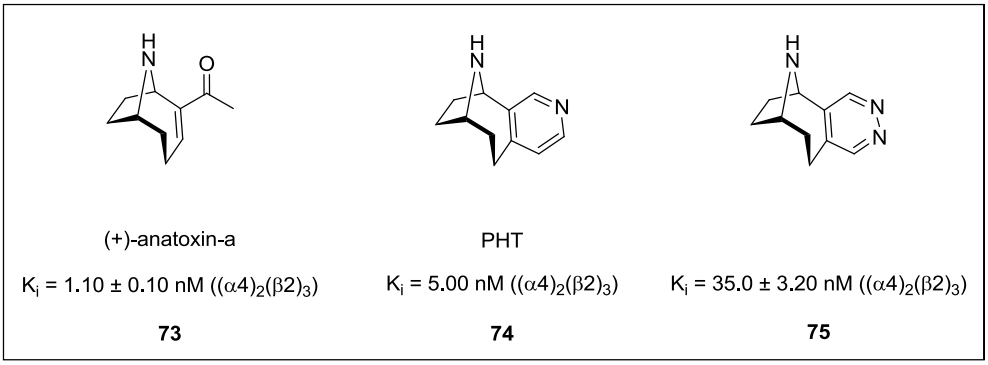

Figure 34. Pyridine bioisosteric replacement in **73** leading to selective inhibitor **75** of nicotinic acetylcholine receptor $(\alpha4)_2(\beta2)_3$.

[51] Gundisch, D.; Kampchen, T.; Schwarz, S.; Seitz, G.; Siegl, J.; Wegge, T. *Bioorg. Med. Chem.* **2002**, *10*, 1 – 9.

Cyclic *versus* noncyclic system replacements

A classical example of the replacement of a cyclic system with an acyclic analogue can be found in the nonsteroidal estrogen *trans*-diethylstilbestrol (**77**). This compound was designed by opening of rings A and B of estradiol (**76**) and only *E*-isomer **77** showed significant estrogen activity.[25,52] (Figure 35)

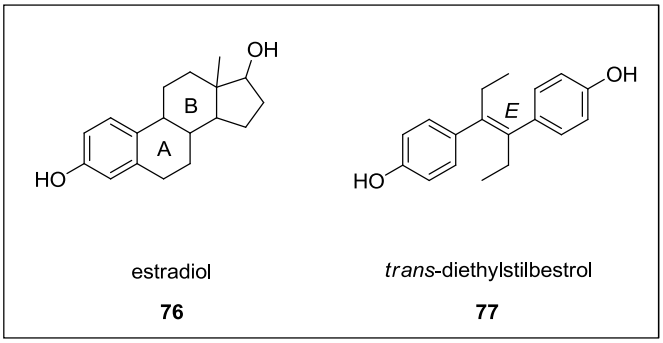

Figure 35. Example of bioisosteric replacement of estradiol (**76**) by *trans*- diethylstilbestrol (**77**).

3.2.3. Heterocyclic bioisosterism in drug design

Five- and six-membered heterocycles play a prominent role in drug design, especially because of their application as drug scaffolds or important structural elements. The versatility of heterocycles based on their size and shape allows them to be projected along a range of vectors, while their natural electronic and physical properties are important for mediating drug-target interactions. By rational selection and disposition of substituents, their electronic and physical properties as well as acidity and basicity can be easily modulated. The most important features of heterocycles utilizable in drug design and bioisosteric mimicry are their ability to act as H-bond donor (N-H, O-H, C-H) or acceptor, their electron withdrawing or donating effects, and their potential to be engaged in π-π interactions. In addition, their ability of tautomerisation offers an additional possibility to optimize the spatial location of interacting groups or substituents.[21]

[52] Dodds, E. C.; Goldberg, L.; Lawson, W.; Robinson, R. *Nature* **1938**, *141*, 247 – 248.

Heteroatoms as H-bond acceptors

Two approaches have been taken to address the question of which atom, O or N, interacts with H-bond donor when both are available in molecules containing, for example alkoxypyridine (**78**), alkoxime (**79**), oxazole (**80**) or isooxazole moiety (**81**). An *ab initio* study (computational chemistry methodology) of functional groups interacting with water provided theoretical insight, while the analysis of H-bonding interactions in molecules deposited in the CSD (Cambridge Structural Database) provided practical examples. The *ab initio* calculated data about H-bond lengths and interaction energies indicated that N is a much stronger H-bond acceptor than O when these atoms are integrated to, resp. conjugated with sp^2 π-conjugated systems. This result is supported also by the prevalence of N acting as the H-bond acceptor in the CSD. For methoxypyridine (**78**) and oxazole (**80**), the difference in the energy of H-bond provided by O and N acting as acceptors varies from 6 to 12 kJ/mol.[53] (Figure 36)

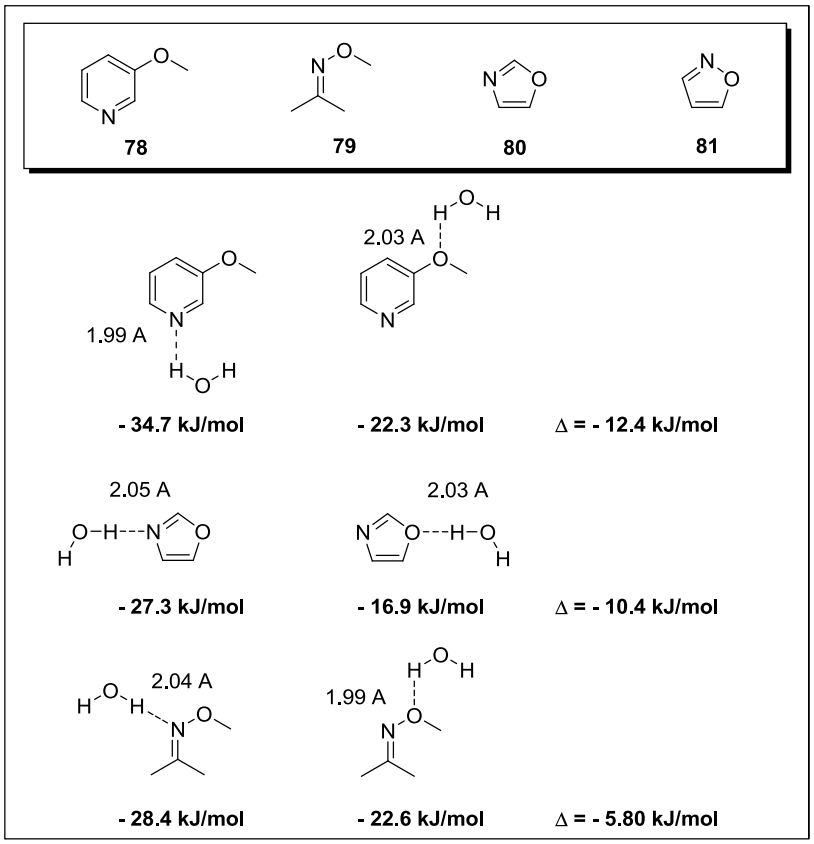

Figure 36. Examples of molecules containing two potentional H-bond acceptors **78 – 81** and comparison of the calculated H-bond interaction energies of H_2O with N and O atoms in some of the given molecules.

[53] Böhm, H. J.; Klebe, G.; Brode, S.; Hesse, U. *Chem. Eur. J.* **1996**, *2*, 1509 – 1513.

A practical example of the consequences of different H-bond interactions associated with oxazole rings is provided by series of prostacyclin (PGI_2) mimetics **82**, **83** and **84** inhibiting blood platelet aggregation. Their activity is sensitive to the topology of the central oxazole ring causing a 5-fold difference in EC_{50} between the isomers **82** and **83**. The decreased activity of the inhibitor **83**, comparable to the *cis*-olefin **84**, suggests that the differently orientated oxazole ring does not contribute to binding and acts simply as a scaffolding element providing the optimal geometry of the ligand to complement the PGI_2 receptor. The obtained analytical data led to the conclusion that the N atom of the "central" oxazole ring in **82** participates on the important H-bond interaction in PGI_2 receptor active site while the similarly positioned oxazole O atom in **83** is not able to interact in the same manner.[54,55] (Figure 37)

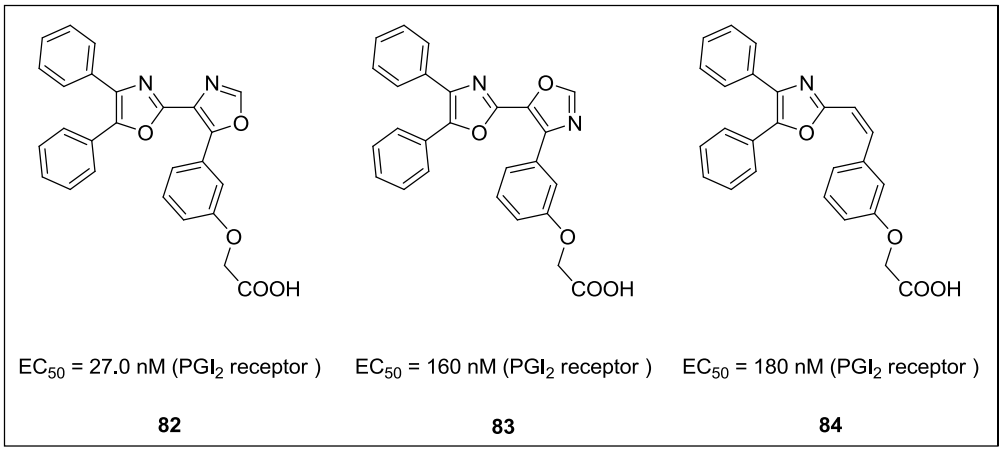

Figure 37. Series of prostacylin (PGI_2) mimetics **82** – **84** and their corresponding activities.

An interesting example of regioisomeric 2-aminooxazoles possibly providing different H-bond interactions was published by Perner *et al.* Compounds **85** and **86** were designed as inhibitors of the transient receptor potential vanilloid 1 (TRPV1) which plays the significant role as a principle integrator of multiple pain-producing stimuli. The compound **85** containing 5-phenyloxazol-2-amine moiety exhibited comparable inhibition potency (IC_{50} = 0.20 μM) against TRPV1 as its 4-phenyloxazol-2-amine analogue **86** (IC_{50} = 0.90 μM). Unfortunately no ligand-receptor analysis was published in the study, so the direct

[54] Meanwell, N. A.; Romine, J. L.; Rosenfeld, M. J.; Martin, S. W.; Trehan, A. K.; Wright, J. J. K.; Malley, M. F.; Gougoutas, J. Z.; Brassard, C. L.; Buchanan, J. O.; Federici, M. E.; Fleming, J. S.; Gamberdella, M.; Hartl, K. S.; Zavoico, G. B.; Seiler, S. M. *J. Med. Chem.* **1992**, *36*, 3884 – 3903.

[55] Meanwell, N. A.; Rosenfeld, M. J.; Wright, J. J. K.; Brassard, C. L.; Buchanan, J. O.; Federici, M. E.; Fleming, J. S.; Gamberdella, M.; Hartl, K. S.; Zavoico, G. B.; Seiler, S. M. *J. Med. Chem.* **1993**, *36*, 3871 – 3883.

influence of the differently substituted oxazole core on the interaction pattern of the given inhibitors is debatable.[56] The 4-phenyloxazol-2-amine moiety could also influence the pharmacokinetic properties of **86** and in this way change the overall activity. (Figure 38)

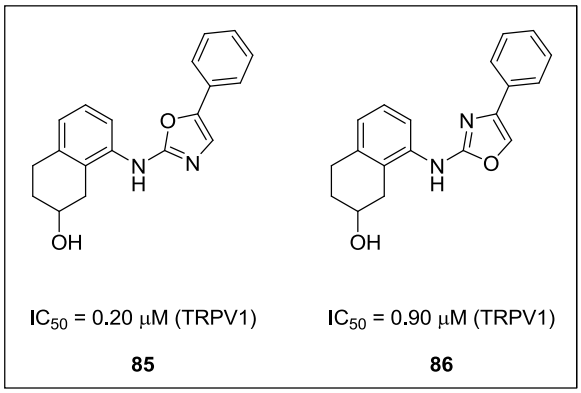

Figure 38. Example of the regioisomeric 2-aminooxazole analogues **85** and **86** and their biological activities.

3.3. Scaffold hopping

Bioisosterism is the concept of similarity between functional groups or scaffolds in molecules that exhibit a similar shape and electronic distribution (stereocompatibility) in terms of their potential biological interactions. A rational replacement of molecular groups (or fragments) is defined as a bioisosteric replacement.[5]

A subset of bioisosteric replacement is referred to as **scaffold hopping**, where the core structure of a small-molecule ligand is replaced. The core may be of direct functional importance in interacting with the protein target or it may provide the necessary scaffolding that allows substitution with functional groups in the appropriate geometric configuration.[57]

Bioisosteric replacement and scaffold replacement is commonly integrated to modern medicinal chemistry and drug design. (Figure 39)

[56] Perner, R. J.; Koenig, J. R.; DiDomenico, S.; Gomtsyan, A.; Schmidt, R. G.; Lee, C. H.; Hsu, M. C.; McDonald, H. A.; Gauvin, D. M.; Joshi, S.; Turner, T. M.; Reilly, R. M.; Kym, P. R.; Kort, M. E. *Bioorg. Med. Chem.* **2010**, *18*, 4821 – 4829.

[57] Brown, N. *Scaffold Hopping in Medicinal Chemistry* **2013** Wiley-VCH, Weinheim.

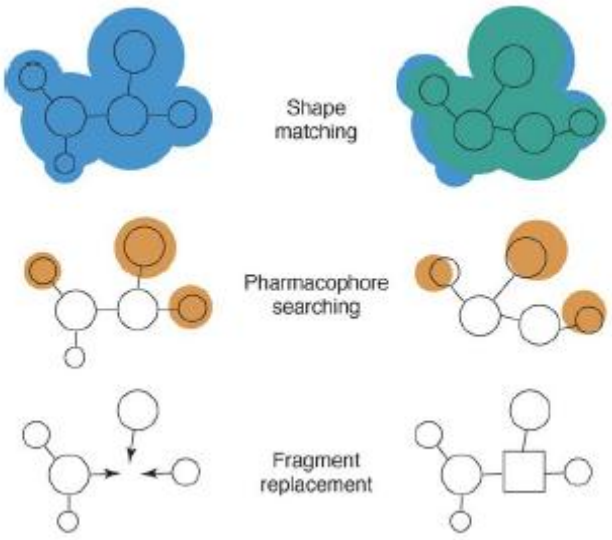

Figure 39. Schematic representation of the principal spproaches to scaffold hopping.[58]

3.3.1. Examples of successful scaffold hopping

One of the early examples of successful scaffold hopping is the discovery of GABA-receptor modulators originating from the benzodiazepine core, e. g. diazepam (**87**). After the discovery of **87** in 1950s, many attempts were undertaken to enhance its pharmacokinetic and pharmacodynamic properties by changing substituents, but also by moving to a completely new structures. Examples of compounds with a novel scaffold are zopiclone (**88**), zolpidem (**89**) and zaleplon (**90**).[59] (Scheme 3)

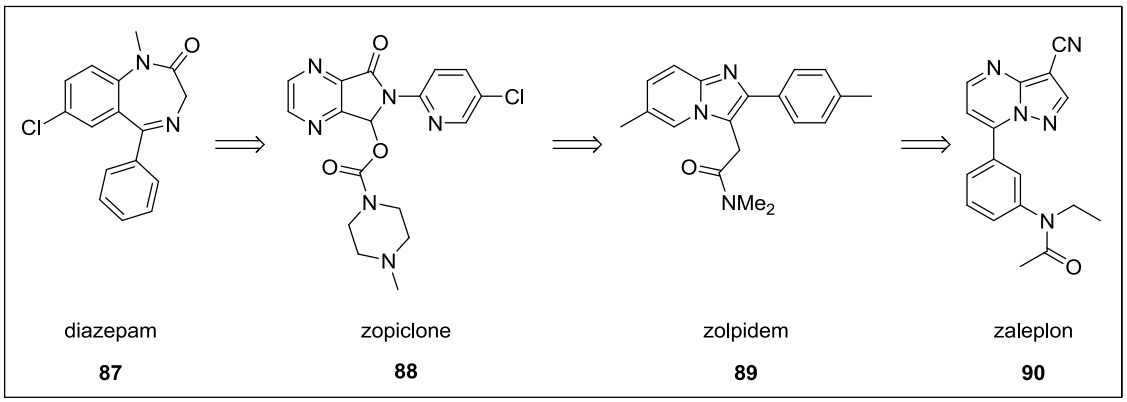

Scheme 3. Literature example for scaffold hopping – novel GABA ligands **87** – **90**.

[58] Böhm, H. J.; Flohr, A.; Stahl, M. *Drug Discov. Today Technol.* **2004**, *1*, 217 – 224.
[59] Teuber, L.; Wätjens, F.; Jensen, L. H. *Curr. Pharm. Des.* **1999**, *5*, 317 – 343.

Another example is represented by the set of dopamine agonists **91** – **94**. These molecules nicely demonstrate that the scaffold hopping strategy originating from the natural ligand – dopamine (**91**) can lead to the discovery of ligands with high structural similarity to **91**, e. g. fenoldopam (**93**) but also to completely novel structures, e. g. quinpyrrole (**94**).[60,61] (Scheme 4)

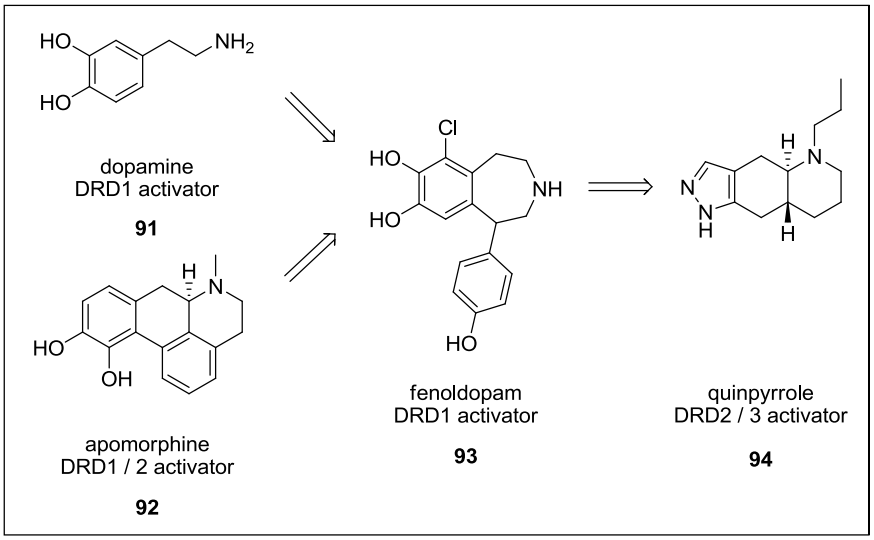

Scheme 4. Literature example for scaffold hopping – novel dopamine agonists **93** and **94**.

[60] Andersen, P. H. *Eur. J. Pharm.* **1990**, *2*, 335 – 347.
[61] Kebabian, J. W. *Drug Discov. Today* **1990**, *2*, 333 – 340.

Chapter 4. **2-Aminooxazoles in medicinal chemistry**

4. 2-Aminooxazoles in medicinal chemistry

Oxazoles are a class of heterocyclic compounds that are believed to occur in the nature from post-translational modification of serine and threonine residues in peptides. These structural motifs represent very important building blocks of natural products, pharmaceuticals and synthetic intermediates. Among numerous heterocyclic moieties of the biological or pharmacological interest, the oxazole ring is endowed with various biological activities, such as hypoglycemic, anti-inflammatory, and antibacterial activities.[62]

One of the most important pharmacophoric elements of inhibitors designed in our research group is *N*,5-diaryloxazol-2-amine moiety (**1**) respectively its regioisomeric form – *N*,4-diaryloxazol-2-amine (**95**). (Figure 40) Harris *et al.* identified structure **1** as a promising initial hit during the development of a new series of VEGFR2 inhibitors. Oxazole **1** represented an attractive starting point, exhibiting moderate VEGFR2 enzyme potency (IC_{50} = 1.20 μM) and inhibiting VEGF-induced proliferation of human umbilical vein endothelial cells (HUVEC) with an IC_{50} of 3.00 μM. Based on the SAR studies a several improved derivatives of *N*,5-diaryloxazol-2-amine (**1**) were discovered.[6] Nowadays, there is no known comparative study dealing with biological activities of the regioisomeric *N*,5-diphenyloxazol-2-amine (**1**) and *N*,4-diaryloxazol-2-amine (**95**) or their derivatives.

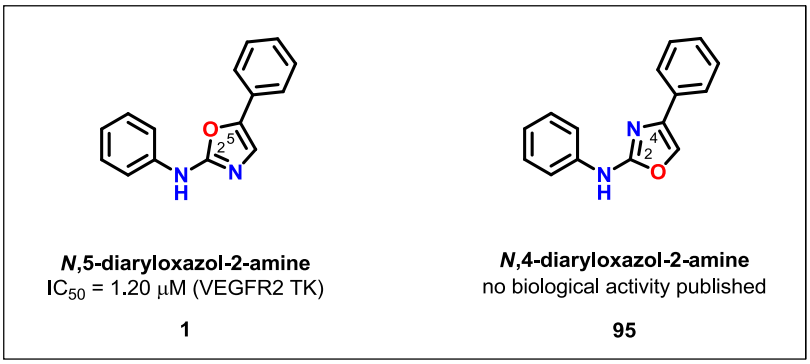

Figure 40. Chemical structure of the 2-aminooxazole regioisomers **1** and **95**.

[62] Rauf, A.; Farshori, N. N. *Microwave-Induced Synthesis of Aromatic Heterocycles* **2012** Springer, Dordrecht, Heidelberg, London, New York.

4.1. *N*,5-Diaryloxazol-2-amines – their synthesis and activity

The scientific database Reaxys describes 1110 chemical compounds containing ***N*,5-diaryloxazol-2-amine moiety** (**1**). 907 of the described compounds possess various biological activities.[63] These compounds are mostly antineoplastic species influencing the following therapeutic targets: vascular endothelial growth factor receptors (VEGFRs),[6] inosine monophosphate dehydrogenase (IMPDH II),[64] epidermal growth factor receptors (EGFRs), cyclin-dependent kinases (CDKs 2 and 4), platelet-derived growth factor receptors (PDGFRs),[65] capsaicin receptors (TrpV1),[66] protein tyrosine phosphatase (PTP 1B),[67] blood-coagulation factor VII A,[68] diglyceride acetyltranferase (DGAT),[69] cKit tyrosine kinase,[70,71] Flt 1 and Flt3 receptor kinases,[72] BCR-ABL tyrosine kinase,[73] tubulins,[74] fibroblast growth factor receptors (FGFRs),[75] sphingosine kinases (SK 1 and 2), dihydroceramide desaturase (Des 1),[76] protein kinase CLK 1[77] and virus HIV-1.[78]

[63] Reaxys Database, Elsevier Information Systems GmbH.www.reaxys.com/reaxys/secured/start.do (accessed February 19th, 2017).
[64] Machrouhi, F.; Ouhamou, N.; Laderoute, K.; Calaogan, J.; Bukhtiyarova, M.; Ehrlich, P. J.; Klon, A. E. *Bioorg. Med. Chem. Lett.* **2010**, *20*, 6394 – 6399.
[65] Brown, M. L.; Cheung, M.; Dickerson, S. H.; Gauthier, C.; Harris, P. A.; Hunter III, R. N.; Pacofsky, G.; Peel, M. R.; Stafford, J. A. *SmithKline Beecham Corp.* **2004**, WO2004/032882, A3.
[66] Dhar, T. G. M.; Shen, Z.; Guo, J.; Liu, C.; Watterson, S. H.; Gu, H. H.; Pitts, W.; Fleener, C. A.; Rouleau, K. A.; Sherbina, N. Z.; McIntyre, K. W.; Witmer, M. R.; Tredup, J. A.; Chen, B. C.; Yhao, R.; Bednarz, M. S.; Cheney, D. L.; MacMaster, J. F.; Miller, L. M.; Berry, K. K.; Harper, T. W.; Barrish, J. C.; Hollenbaugh, D. L.; Iwanowicz, E. J. *J. Med. Chem.* **2002**, *45*, 2127 – 2130.
[67] Petry, S.; Tennagels, N.; Kirsch, R.; Baringhaus, K. H. *Sanofi-Aventis Deutschland GMBH* **2005**, WO2005/116003, (A3).
[68] Herpin, T.; Bisacchi, G. S.; Pi, Z.; Prietsley, E. S.; Dhar, T. G. *Bristol-Meyers Squibb Comp.* **2004**, WO2004/000214, (A1).
[69] Serrano-Wu, M. H.; Kwak, Y. S.; Liu, W. *Novartis AG / Novartis Pharma GmbH* **2007**, WO2007/126957, (A2).
[70] Grierson, D.; Benjahad, A.; Moussy, A. *AB Science / CNRS / Institut Curie* **2006**, WO2006/106437, (A3).
[71] Benjahad, A.; Moussy, A.; Chevenier, E.; Picoul, W.; Lermet, A.; Pez, D.; Martin, J.; Sandrinelli, F. *AB Science* **2013**, WO2013/014170, (A1).
[72] Perner, R. J.; Koenig, R. J.; DiDomenico, S.; Gomtsyan, A.; Schmidt, R. G.; Lee, C. H.; Hsu, M. C.; McDonald, H. A.; Gauvin, D, M.; Joshi, S.; Turner, T. M.; Reilly, R. M.; Kym, P. R.; Kort, M. E. *Bioorg. Med. Chem.* **2010**, *18*, 4821 – 4829.
[73] Ouyang, X.; Piatkinski, E. L.; Pattaropong, V.; Chen, X.; He, H. Y.; Kiselyov, A. S.; Velankar, A.; Kawakami, J.; Labelle, M.; Smith II, L.; Lohman, J.; Ping Lee, S.; Malikzay, A.; Fleming, J.; Gerlak, J.; Wang, Y.; Rosler, R. L.; Zhou, K.; Mitelman, S.; Camara, M.; Surguladze, D.; Doody, J. F.; Tuma, M. C. *Bioorg. Med. Chem. Lett.* **2006**, *16*, 1191 – 1196.
[74] Remko, M.; Boháč, A.; Kováčiková, L. *Struc. Chem.* **2011**, *22*, 635 – 648.
[75] Moussy, A.; Wermuth, C.; Grierson, D.; Benjahad, A.; Croisy, M.; Ciufolini, M.; Giethlen, B. *AB Science / CNRS / Institut Curie* **2005**, WO2005/040139, (A3).
[76] Aurelio, L.; Scullino, C. V.; Pitman, M. R.; Sexton, A.; Oliver, V.; Davies, L.; Rebello, R. J.; Furic, L.; Creek, D. J.; Pitson, S. M.; Flynn, B. L. *J. Med. Chem.* **2016**, *59*, 965 – 984.
[77] Murár, M.; Dobiaš, J.; Šramel, P.; Addová, G.; Hanquet, G.; Boháč, A. *Euro. J. Med. Chem.* **2017**, *126*, 754 – 761.
[78] Kim, S. H.; Markowitz, B.; Trovato, R.; Murphy, B. R.; Austin, H.; Willardsen, A. J.; Baichwal, V.; Morham, S.; Bajji, A. *Bioorg. Med. Chem. Lett.* **2013**, *23*, 2888 – 2892.

Derivatives of *N*,5-diaryloxazol-2-amine (**1**) are described as anti-angiogenic and anti-tumor agents,[6,64,76] antibiotics, immunosuppressants, anti-inflammatory compounds,[68,77] antiviral compounds, fungicides, platelet aggregation inhibitors,[64,78] antirheumatics, anti-arteriosklerotics,[70] anti-diabetics,[67] anti-obesity agents[68] and allergy inhibitors.[69] Some examples of the structuraly related bioactive compounds are given below. (Figure 41)

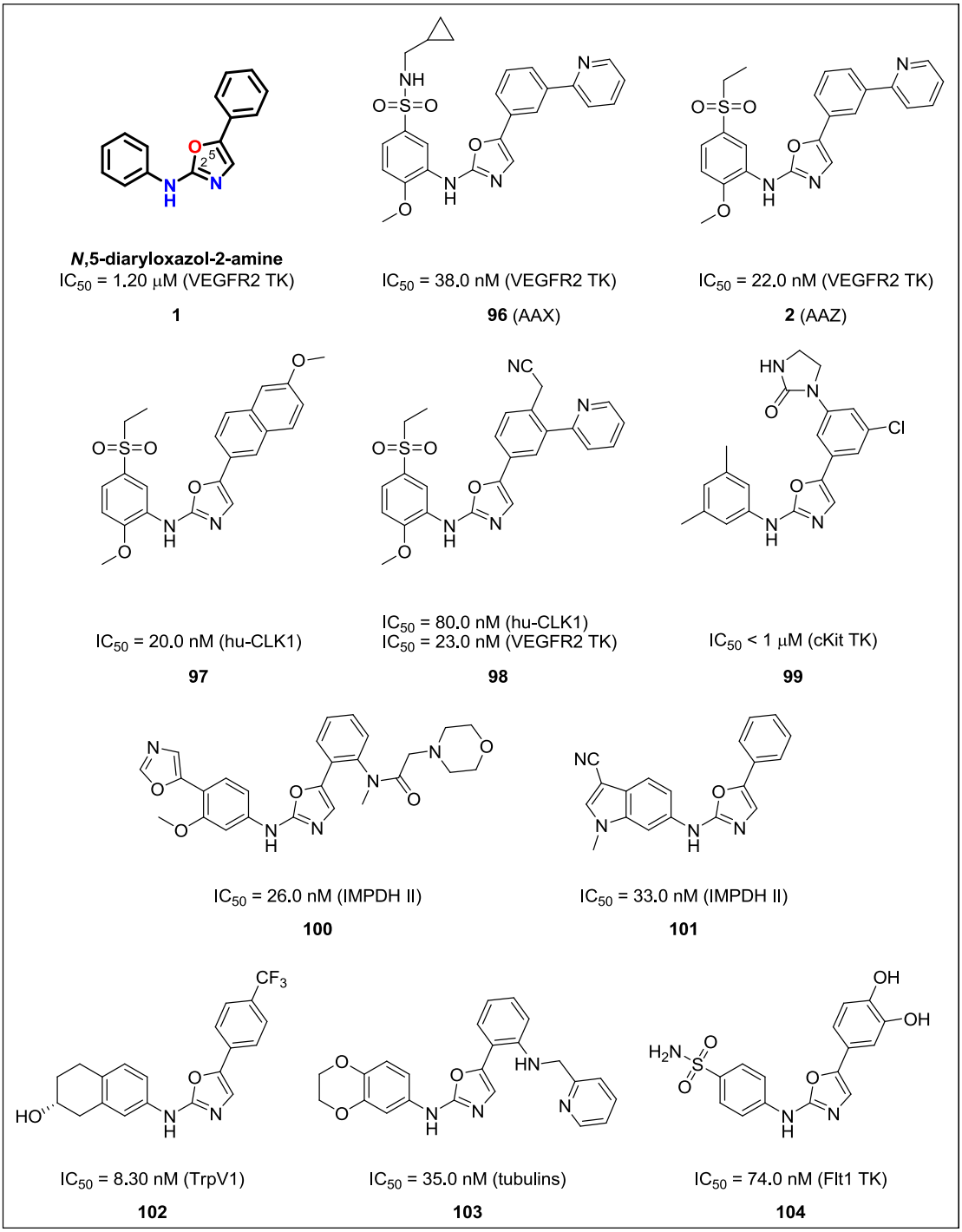

Figure 41. The structures of *N*,5-diaryloxazol-2-amine (**1**) and some bioactive structuraly related compounds with their corresponding activities.

Despite a broad biological exploitation, synthesis of *N*,5-diaryloxazol-2-amine (**1**) based compounds is still not optimally developed. Preparation of the specifically substituted oxazole-2-amine moiety is a relatively complex topic, and often low yields are observed.

The most common and efficient methodology for the preparation of *N*,5-diaryloxazol-2-amine (**1**) containing compounds was described in literature as a reaction of arylisothiocyanates, resp. arylisocyanates with α-azidoacetophenones. This reaction requires the presence of PPh_3 or $pPPh_3$ (a polymer resin-bound PPh_3) and it is usually performed under two possible types of conditions: in dioxane (80 to 95 °C, 30 min to 4 h) [78,79,80,81] or in CH_2Cl_2 (0 °C to RT, 1 to 12 h).[82,6,83] Yields of the aminooxazoles obtained by this methodology are described in the range from 1 to 95 %. The reactions performed in dioxane (80 to 95 °C, 30 min to 4 h) using arylisothiocyanates have usually higher yields compared to reactions performed with arylisocyanates in CH_2Cl_2 (0 °C to RT, 1 to 12 h). The yield of the reaction also seems to be dependent on the structure of used substrates.[82]

The chosen examples of previously published cyclizations between arylisothiocyanates, resp. arylisocyanates with α-azidoacetophenones leading to the formation of *N*,5-diaryloxazol-2-amine (**1**) based products are depicted on the schemes below. (Scheme 5 and 6)

[79] Kahraman, D. C.; Hanquet, G.; Jeanmart, L.; Lanners, S.; Šramel, P.; Boháč, A.; Cetin-Atalay, R. *Med. Chemm. Commun.* **2017**, *8*, 81 – 87.
[80] Suh, J. H.; Yum, E. K.; Cho, Y. S. *Chem. Phar. Bull.* **2015**, *63*, 573 – 578.
[81] Bursavich, M. G.; Parker, D. P.; Willardsen, J. A.; Gao, Z. H.; Davis, T.; Ostanin, K.; Robinson, R.; Peterson, A.; Cimbora, D. M.; Zhu, J. F.; Richards, B. *Bioorg. Med. Chem. Lett.* **2010**, *20*, 1677 – 1679.
[82] Lintnerová, L.; Kováčiková, L.; Hanquet, G.; Boháč, A. *J. Heterocyclic. Chem.* **2015**, *52*, 425 – 439.
[83] Lintnerová, L.; Garcia-Caballero, M.; Gregáň, F.; Melicherčík, M.; Quesada, A. R.; Dobiaš, J.; Lác, J.; Sališová, M.; Boháč, A. *Euro. J. Med. Chem.* **2014**, *72*, 146 – 159.

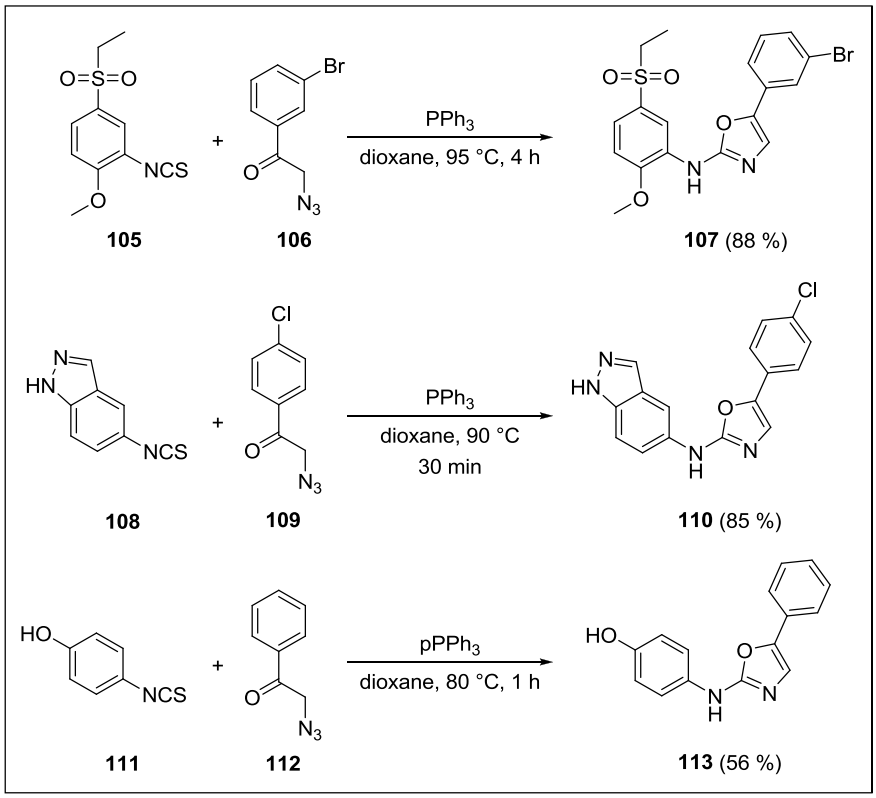

Scheme 5. Examples of the cyclization reactions leading to *N*,5-diaryloxazol-2-amine derivatives **107**, **110** and **113** (reaction conditions: PPh_3, dioxane, 80 to 95 °C, 30 min to 4 h).

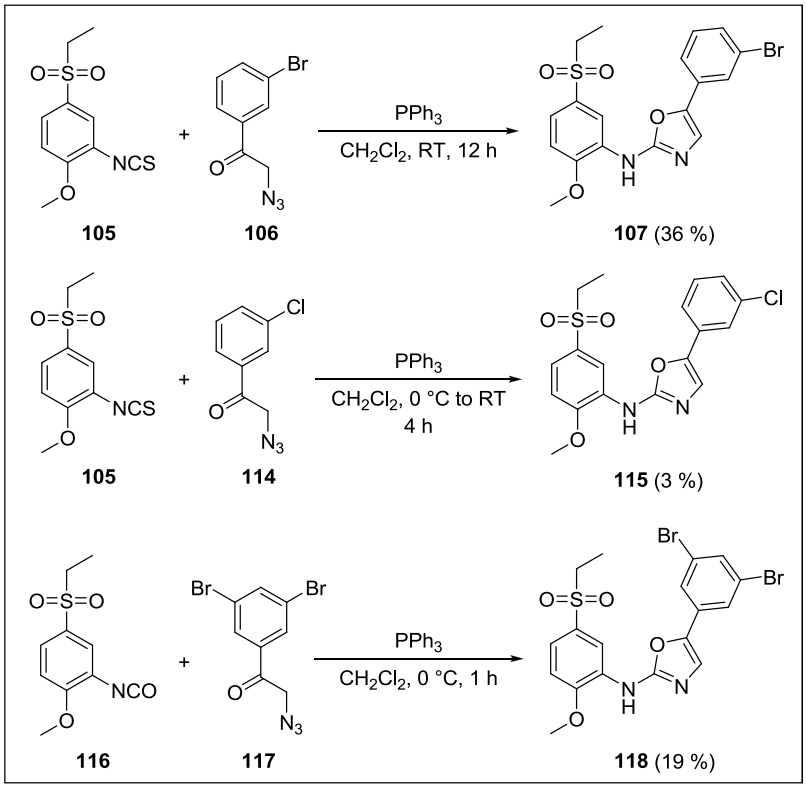

Scheme 6. Examples of the cyclization reactions leading to *N*,5-diaryloxazol-2-amine derivatives **107**, **115** and **118** (reaction conditions: PPh_3, CH_2Cl_2, 0 °C or RT, 1 h to 12 h).

The addition-elimination reaction between variously substituted anilines and derivatives of 2-chloro-5-phenyl oxazole represents another useful synthetic methodology leading to the preparation of *N*,5-diaryloxazol-2-amine (**1**) containing compounds.

The first synthesis from literature began with a transformation of 2-amino-1-phenylethanone (**119**) to 5-phenyloxazole-2-thiol (**120**) using CS_2 and Na_2CO_3 in a mixture of EtOH and H_2O. 2-Chloro-5-phenyl oxazole (**121**) was subsequently prepared by the reaction of **120** with $POCl_3$ in Et_3N. The final addition-elimination reaction between the 2-chlorooxazole **121** and aniline **122** was performed in ^{i}PrOH at 80 °C and provided *N*,5-diaryloxazol-2-amine derivative **123** with the yield of 26 %.[6] (Scheme 7)

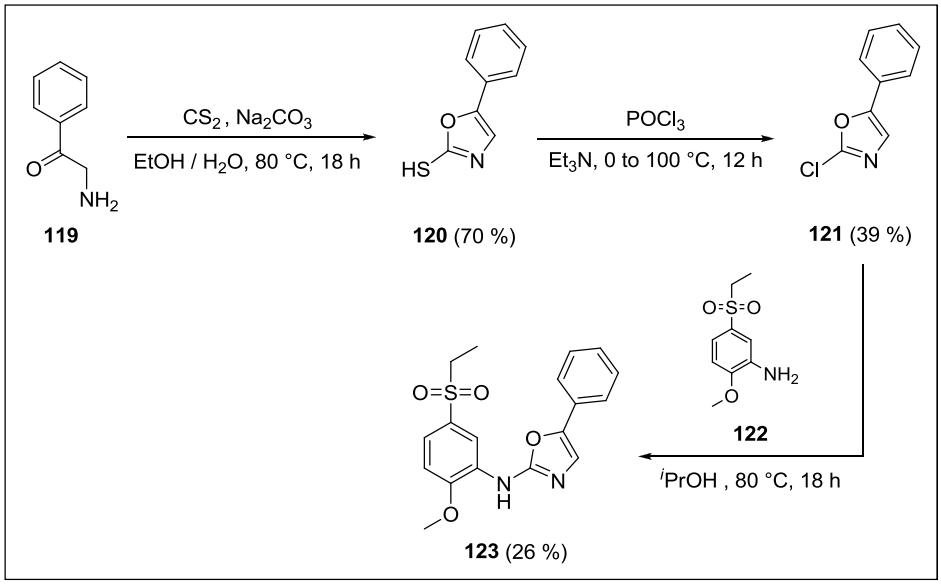

Scheme 7. Preparation of *N*,5-diaryloxazol-2-amine derivative **123** using the addition-elimination reaction of 2-chlorooxazole **121** with aniline **122**.

Another example represents the synthesis starting with a transformation of 4-formylbenzonitrile (**124**) to 4-(oxazol-5-yl)benzonitrile (**125**) using toluenesulfonylmethyl isocyanide (TosMIC) and K_2CO_3 in refluxing MeOH. The subsequent preparation of 2-chlorooxazole derivative **126** was performed by treating the oxazole **125** with LiHDMS and Cl_3CCCl_3 in THF. The final addition-elimination reaction between the 2-chlorooxazole **126** and aniline **127** in ^{i}PrOH at 80 °C provided *N*,5-diaryloxazol-2-amine derivative **128** in 78 % yield.[84] (Scheme 8)

[84] Laxman, D. S.; Srinivas, C. *Neosome Life Sciences, LLC* **2013**, US2012/0302578, (A1).

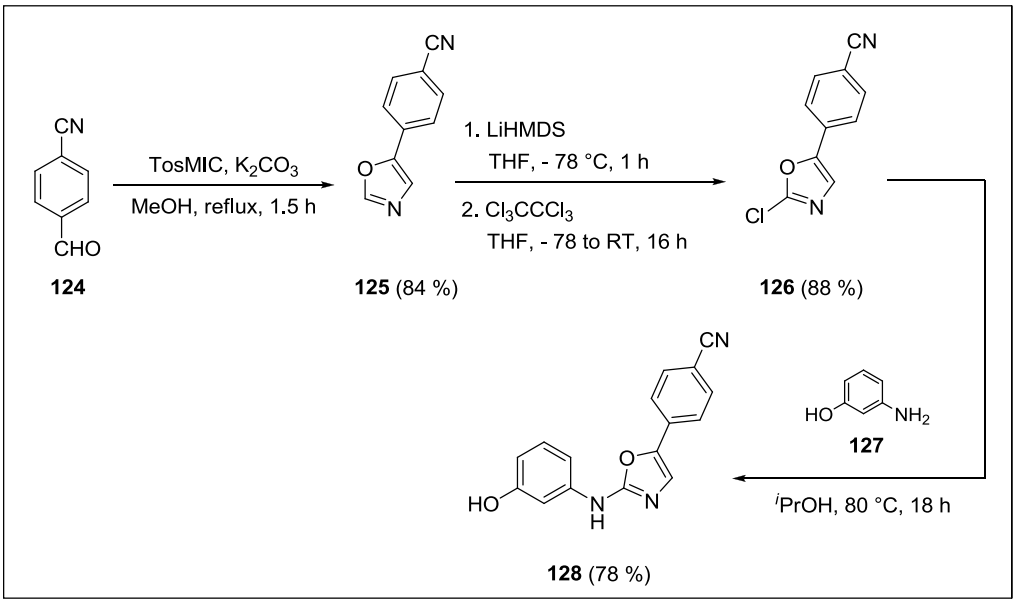

Scheme 8. Preparation of *N*,5-diaryloxazol-2-amine derivative **128** using the addition-elimination reaction of 2-chlorooxazole **126** with aniline **127**.

The similar synthetic methodology was used for the preparation of 2-chlorooxazole derivative **129**. However, the preparation of *N*,5-diaryloxazol-2-amine derivative **131** was described as a reaction of the 2-chlorooxazole **129** with acetanilide **130** in the presence of NaH in DMF. The product **131** was isolated with the yield of 44 %.[71] (Scheme 9)

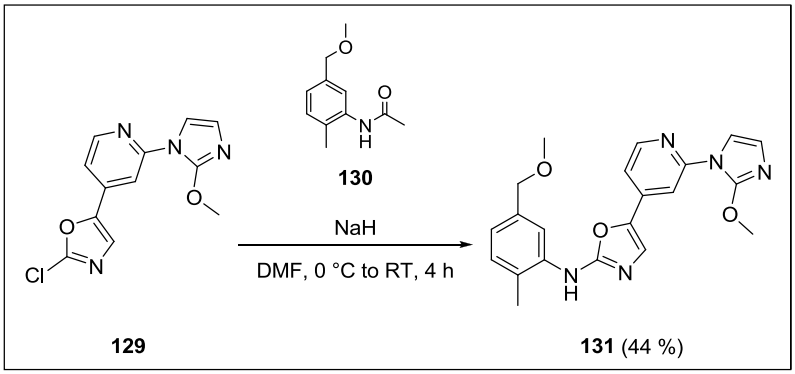

Scheme 9. Preparation of *N*,5-diaryloxazol-2-amine derivative **131** using the addition-elimination reaction of 2-chlorooxazole **129** with aniline **130**.

An interesting synthetic strategy for the preparation of *N*,5-diaryloxazol-2-amine (**1**) derivatives uses specific reactions based on the transition-metal catalysis.

For example, the $Rh_2(OAc)_4$ catalyzed reaction of *N*,*N*-disubstituted cyanamides with α-diazoacetophenones providing the corresponding *N*,*N*-disubstituted derivatives of 5-phenyloxazole-2-amines in high yields (**134**, 84 %). Unfortunately the same reaction using

N-monosubstituted, resp. unsubstituted cyanamides provided the corresponding derivatives of 5-aryloxazole-2-amine in relatively low yields (**136**, 33 %).[85]

Another synthtetic example is the gold-catalyzed heterocyclization of various arylacetylenes with *N*,*N*-disubstituted resp. *N*-monosubstituted cyanamides in the presence of an oxidation agent 2-methylpyridine *N*-oxide (**139**). In the most described cases, 2-aminooxazoles functionalized at the nitrogen atom as well as at the fifth position of the heterocyclic ring were prepared and isolated in good to moderate yields (**1**, 78 %).[86] (Scheme 10)

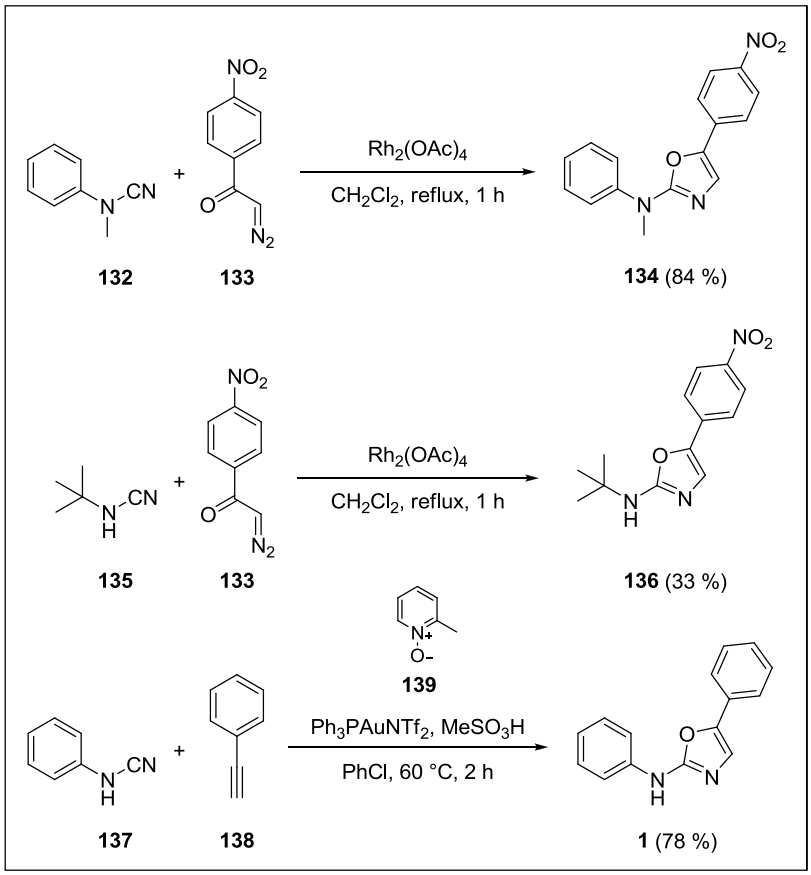

Scheme 10. The synthesis of *N*,5-diaryloxazol-2-amines **134**, **136** and **1** *via* transition-metals catalyzed cyclization.

[85] Fukushima, K.; Ibata, T. *Heterocycles* **1995**, *40*, 149 – 154.
[86] Rassadin, V. A.; Boyarskiy, V. P.; Kukushkin, V. Y. *Org. Lett.* **2015**, *17*, 3502 – 3505.

4.2. *N*,4-Diaryloxazol-2-amines – their synthesis and activity

In contrast with previously discussed derivatives of *N*,5-diaryloxazol-2-amine (**1**), the synthesis and practical utilization of ***N*,4-diaryloxazol-2-amine** (**95**) based compounds are far less fequently described in the literature. The database Reaxys describes 41 chemical compounds containing *N*,4-diaryloxazol-2-amine moiety (**95**) while only 6 of the described compounds possess biological activity. These compounds are known to be used as modulators of amyloid β (Aβ) aggregation levels[87,88] and antagonists of the vanilloid 1 receptor (TrpV1).[56] Derivatives of *N*,4-diaryloxazol-2-amine (**95**) are described as agents for the Alzheimer disease treatment,[87,88] analgesics (painkillers) and agents for the inflammatory hyperalgesia treatment (hypersensitivity to pain).[56] An overview of some *N*,4-diaryloxazol-2-amine (**95**) based compounds together with their biological activities is given below. (Figure 42)

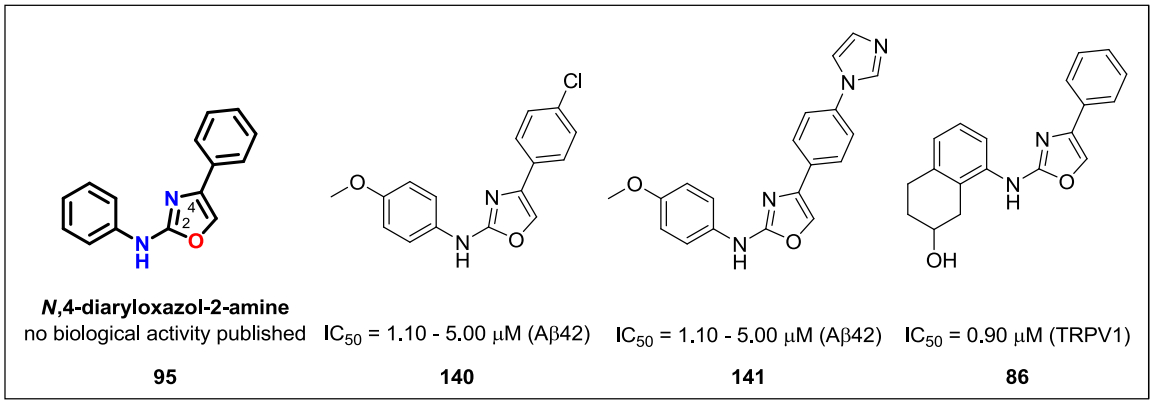

Figure 42. Structure of *N*,4-diphenyloxazole-2-amine (**95**) and some examples of bioactive compounds possessing this moiety.

Regarding the published procedures for the preparation of *N*,4-diaryloxazol-2-amine (**95**) derivatives, the most used is a cyclization reaction of arylureas with α-bromoacetophenones. The reaction was described under various conditions with relatively broad range of yields. For example, Pathak *et al.* performed the first reaction scope in refluxing EtOH. The final 2-aminooxazole products were isolated in good yields (42 to 55 %).[89] An interesting possibility is represented by the reaction in the deep eutetic solvent

[87] Cheng, S.; Comer, D. D.; Mao, L.; Balow, G. P.; Pleynet, D. **2005**, US2005/0070538, (A1).
[88] Cheng, S.; Comer, D. D.; Mao, L.; Balow, G. P.; Pleynet, D. *NeuroGenetic Pharmaceuticals, Inc.* **2015**, EP1628666, (B1).
[89] Pathak, V. N.; Goyal, M. K.; Jain, M.; Joshi, K. C. *J . Indian. Chem. Soc.* **1993**, *70*, 539 – 542.

(DES) consisting of melted choline chloride and urea in molar ratio of 1 / 2. The reaction was described to be carried out by sonication or heating at 65 °C. According to the published results ultrasound driven reactions provided the desired products with higher yield and in shorter time (82 to 90 % in 15 min) compared to the reactions driven by heating (45 to 60 % in 4 h).[90] Another oxazolation examples were published using glycerine or PEG-400 (RT) as a solvent with suprisingly high yields (76 to 90 %).[91,92] The newest published synthesis of *N*,4-diaryloxazol-2-amine (**95**) derivatives was performed in DMF at 95 °C with the yield of 56 %.[88] (Scheme 11)

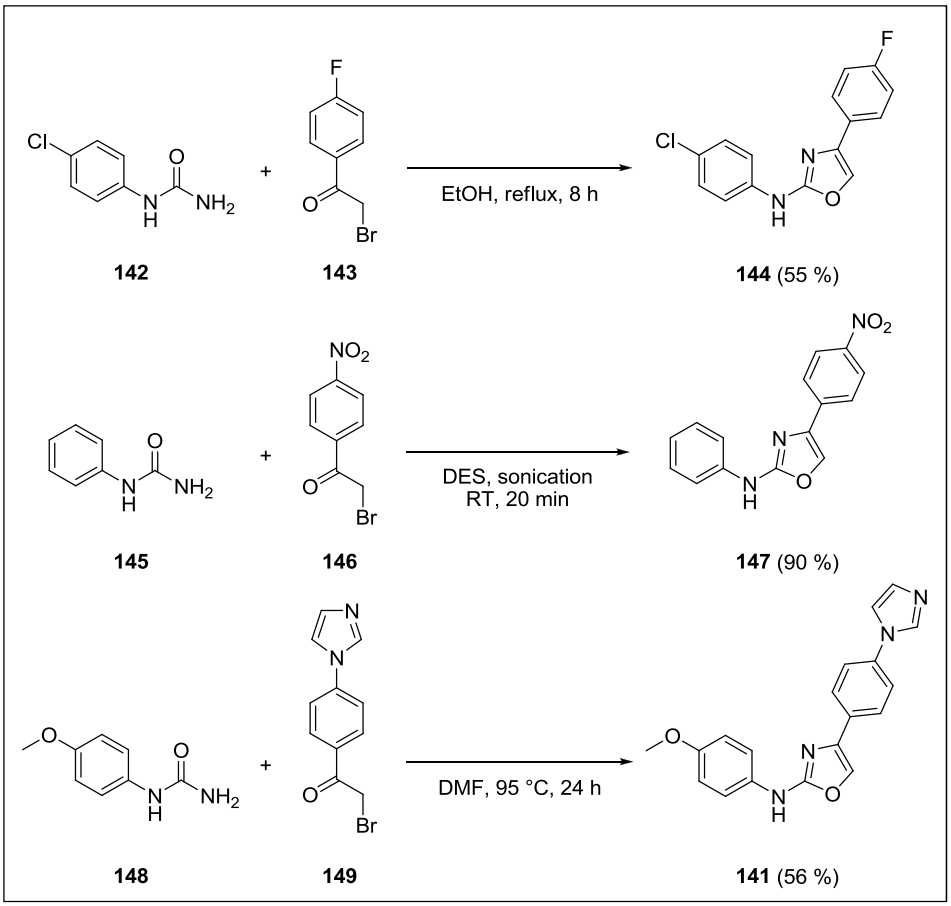

142 143 **144** (55 %)

145 146 **147** (90 %)

148 149 **141** (56 %)

Scheme 11. Examples of the cyclization reaction leading to the *N*,4-diaryloxazol-2-amine derivatives **144**, **147** and **141**.

[90] Singh, B. S.; Lobo, H. R.; Pinjari, D. V.; Jarag, K. J.; Pandit, A. B.; Shankarling, G. S. *Ultrason. Sonochem.* **2013**, *20*, 287 – 293.
[91] Narsaiah, A. V.; Ghogare, R. S.; Biradar, D. O. *Org. Commun.* **2011**, *4*, 75 – 81.
[92] Gokhale, K. M.; Wagal, O.; Kanitkar, A. *Int. J. Pharm. Phytopharmacol. Res.* **2012**, *1*, 156 – 160.

Different synthesis leading to *N*,4-diarylloxazol-2-amine (**86**) was performed *via* cyclization reaction of α-bromoacetophenone (**150**) with formamide.[93] The reaction provided 4-phenyloxazole (**151**) which was subsequently transformed to 2-chloro-4-phenyloxazole (**152**) using lithium hexamethyldisilazide (LiHMDS) and Cl_3CCCl_3 in THF. The final product **86** was preparated by microvawe driven addition-elimination reaction of **152** with aniline **153** in CH_3CN in 5 % yield.[56] (Scheme 12)

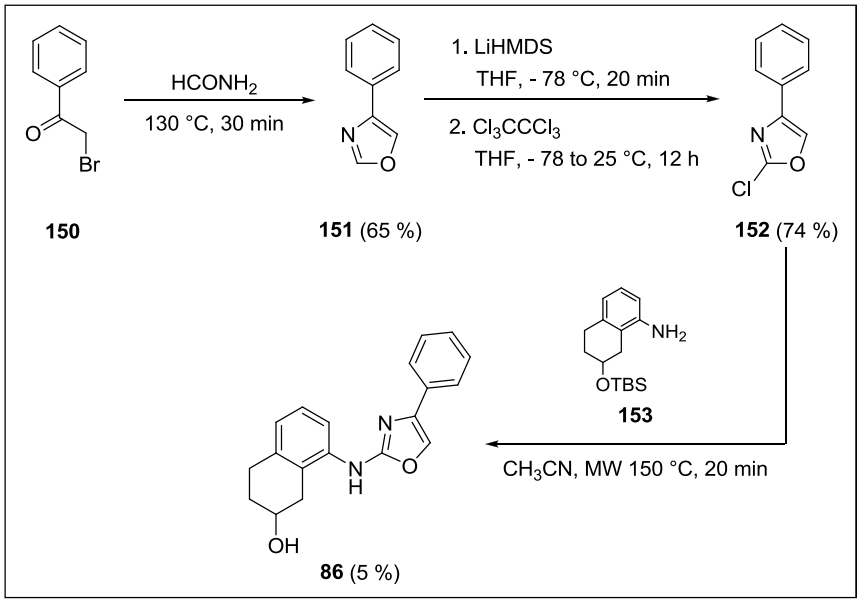

Scheme 12. Synthesis of *N*,4-diaryloxazol-2-amine (**86**) using the addition-elimination reaction 2-chlorooxazole **152** with aniline **153**.

[93] Yamamuro, D.; Uchida, R.; Ohtawa, M.; Arima, S.; Futamura, Y.; Katane, M.; Homma, H.; Nagamitsu, T.; Osada, H.; Tomoda, H. *Bioorg. Med. Chem. Lett.* **2015**, *25*, 313 – 316.

Chapter 5. **Transition-metal catalyzed coupling reactions in medicinal chemistry**

5. Transition-metal catalyzed coupling reactions in medicinal chemistry

Coupling reactions represent an important synthetic procedure, without which the preparation of many compounds, designed within this dissertation thesis, would not be possible. The coupling reactions were utilized for the preparation of the potential VEGFR2 TK inhibitors across most of the thesis projects. In the following chapter we will provide general information about the chemistry behind the coupling reactions and also a brief overview of the particular reaction methodologies that were utilized within our projects together with some practical examples of their successful application in medicinal chemistry.

C-C bond-forming reactions play a decisive and important role in modern organic synthesis. In the last quarter of the 20th century, a family of C-C bond-forming reactions evolved as a new powerful tool in synthesis. Based on transition-metal catalysis, this newly acquired ability to forge C-C bonds between or within functionalized and sensitive substrates provided new opportunities, particularly in total synthesis but also in medicinal and process chemistry as well as in chemical biology and nanotechnology. Among these processes, **the palladium-catalyzed cross-coupling reactions** are the most prominent.[94]
From a medicinal chemistry point of view, the ability to create C-C bonds under mild conditions opens many new possibilities for designing novel compounds, further enhanced when it is combined with combinatorial approaches.[95,96] Since some of the palladium-catalyzed cross-coupling reactions are rapid and mild, even ^{11}C ($t_{1/2}$ = 20.4 min) or ^{18}F ($t_{1/2}$ = 110 min) labeled compounds can be successfully prepared for the Positron Emission Tomography (PET) studies using these methods.[97] From a process chemistry viewpoint, the cross-coupling reactions allow us to develop more convergent processes and provide more flexibility in the process designs.[98]
Most palladium catalyzed reactions are believed to have quite similar catalytic cycle. The mechanism has been widely accepted to involve an initial oxidative addition of an

[94] Nicolaou, K. C.; Bulger, P. G.; Sarlah, D. *Angew. Chem. Int. Ed.* **2005**, *44*, 4442 – 4489.
[95] Hermkens, P. H. H.; Ottenheijm, H. C. J.; Rees, D. *Tetrahedron* **1996**, *52*, 4527 – 4554.
[96] Franzén, J. *Can. J. Chem.* **2000**, *78*, 957 – 962.
[97] Piarraud, A.; Lasne, M. C.; Barré, L.; Vaugeois, J. M.; Lancelot, J. C. *J. Labelled Compd. Radiopharm.* **1993**, *32*, 253 – 254.
[98] King, A. O.; Yasuda, N. *Topics Organomet. Chem.* **2004**, *6*, 205 – 245.

electrophile R^1-X (where X represents a leaving group) to an electron-rich Pd(0)-species producing an organo-Pd(II) complex. Transmetalation of an organometallic reagent R^2-M (where M represents a metal atom) results in the formation of a mixed diorgano-Pd(II) complex. Subsequent *trans-cis* isomerization in the ligand sphere of Pd(II) and C-C bond formation upon reductive elimination regenerate the initial Pd(0) catalyst and release the coupling product R^1-R^2.[99] (Scheme 13)

It should be kept in mind that also unwanted homocoupling by-products can be formed, mostly by oxidative dimerization of the organometallic species (with air or by the electrophile being the oxidant) or by reductive (Wurtz-type) dimerization of the organohalide (by the Pd(0) complex or *via* metal residues from the formation of the organometallic species). Under ligand-free conditions or when the ligand-Pd coordination is labile, homo-coupling can be significant.[100]

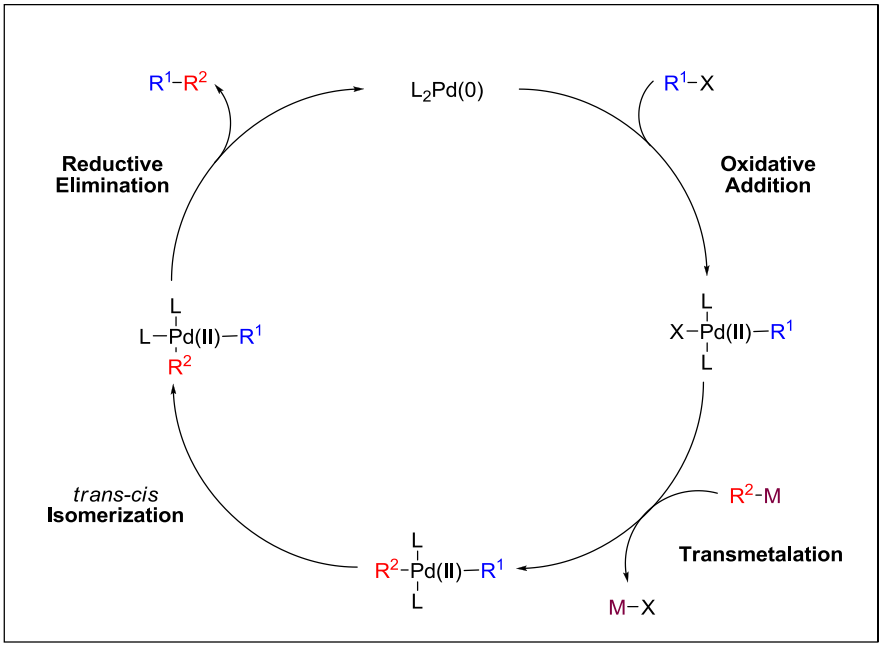

Scheme 13. Catalytic cycle of palladium catalyzed cross-coupling reaction. $L_2Pd(0)$ represents an initial Pd(0)-catalyst, R^1-X represents an electrophile (where X is a leaving group), R^2-M represents an organometallic reagent (where M is a metal atom) and R^1-R^2 represents a final coupling product.

Careful choice of a ligand can influence two steps of the catalytic cycle. The use of strong σ-donating ligands, such as trialkylphosphines, increases electron density around the metal, accelerating the oxidative addition of the catalyst to the substrate. This is commonly

[99] Geissler, H. *Transition Metals-Catalyzed Cross Coupling Reaction* in *Transition Metals for Organic Synthesis, vol. 1*. **1998** Wiley-VCH, Weinheim.
[100] Knappke, C. E. I.; Wangelin von, A. J. *Chem. Soc. Rev.* **2011**, *40*, 4948 – 4962.

believed to be the rate determining step. Choice of the ligand also determines the mechanism by which the oxidative addition occurs.[101] The elimination step is accelerated by the use of bulky ligand, in particular the phosphine ligand exhibiting a large cone angle (also known as Tolman's angle - θ).[102] (Figure 43)

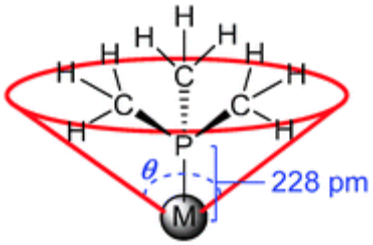

Figure 43. Tolman's cone angle - θ of the monodentate $P(CH_3)_3$ ligand attached to a metal atom (M).[103]

5.1. Stille coupling

The palladium-catalyzed cross-coupling of organic electrophiles with organotin compounds (containing Sn-C bond) is known as the Stille reaction (developed in 1978). This reaction is one of the most widely applied palladium-catalyzed C-C bond-forming procedures, in large part due to typically mild reaction conditions, the ease of preparation of coupling partners, and the tolerance of a variety of sensitive functionalities in this transformation.[104,105] (Scheme 14)

The Sn-C represents one of the most covalent bond as compared to other possible cross-coupling partners containing Li-C, Mg-C, Al-C, Zn-C, or B-C bond. This suggests that Sn-C compounds are the least nucleophilic coupling partners among the group and therefore the least reactive for a transmetalation step. On the transmetalation of organotin compounds can participate not only sp and sp^2 hybridized carbons but in many cases also carbons with sp^3 hybridization. Organostannanes can be prepared by transmetalation of C-Li or C-MgX with R_3SnX, nucleophilic substitution of R_3SnLi, hydrostannation of olefins with R_3SnH, or palladium-catalyzed coupling of Ar-X with R_3SnSnR_3.[106] Organostannanes

[101] Galardon, E.; Ramdeehul, S.; Brown, J. M.; Cowley, A.; Hii, K. K.; Jutand, A. *Angew. Chem. Int. Ed.* **2002**, *41*, 1760 – 1763.
[102] Tolman, C. A. *Chem. Rev.* **1977**, *77*, 313 – 348.
[103] Fleckenstein, C. A.; Plenio, H. *Chem. Soc. Rev.* **2010**, *39*, 694 – 711.
[104] Farina, V.; Krishnamurthy, V.; Scott, W. J. *Org. React.* **1997**, *50*, 1 – 652.
[105] Milstein, D.; Stille, J. K. *J. Am. Chem. Soc.* **1979**, *101*, 4992 – 4998.
[106] Kosugi, M.; Ohya, T.; Migita, T. *Bull. Chem. Soc. Jap.* **1983**, *56*, 3855 – 3856.

are air and water stable and isolable by standard laboratory techniques. This makes from the Stille coupling a versatile reaction suitable for the medicinal chemistry use where quick assembly of building blocks is one of the most important aspects.

There are some problems associated with the Stille coupling reaction. The biggest issue is the toxicity of organostannanes which could make it undesirable especially on a process scale. Removal of organostannane by-products (typically R_3SnOH) from a coupled product can be difficult.[98]

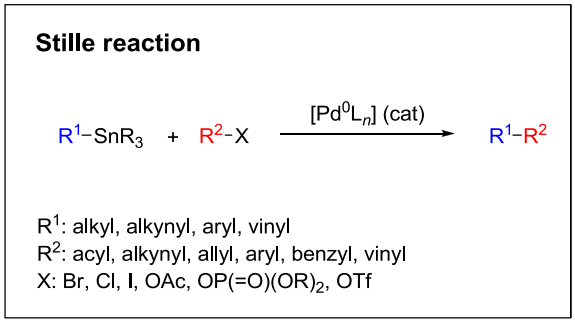

Scheme 14. General scheme of the Stille cross-coupling reaction.[94]

On the following scheme there is an example of the Stille coupling reaction successfully used for the preparation of the *N*,5-diaryloxazol-2-amine **2** (AAZ) developed by GlaxoSmithKline as an inhibitor of VEGFR2 TK. According to its good *in vitro* as well as *in vivo* activity, the compound **2** was chosen as the promising drug candidate.[6] (Scheme 15)

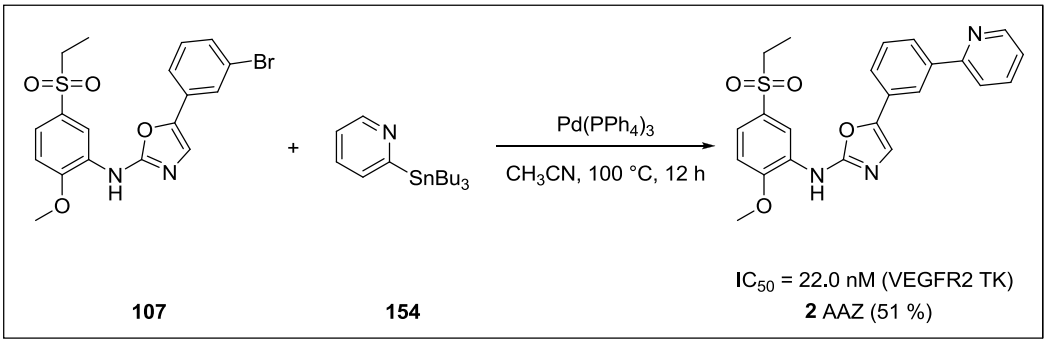

Scheme 15. Stille coupling reaction used for the preparation of VEGFR2 TK inhibitor **2** (AAZ).

Another example of the effective Stille reaction applied in a medicinal chemistry represents the synthesis of *cis*-cefprozil (**158**) - an orally active antibiotics launched by Bristol-Meyers Squibb. The first known preparation of this drug based on the Wittig

reaction had a serious *E*/*Z* selectivity problem.[107] Later, Farina and his co-workers applied the Stille coupling reaction, which took advantage of the retention of *cis* configuration of the organostannane reagent **156**.[108] (Scheme 16) Farina's pioneering work led to the discovery of tris-(2-furyl)phosphine as a ligand and his kinetic studies with Liebeskind became the gold standard in cross-coupling reactions.[98,109]

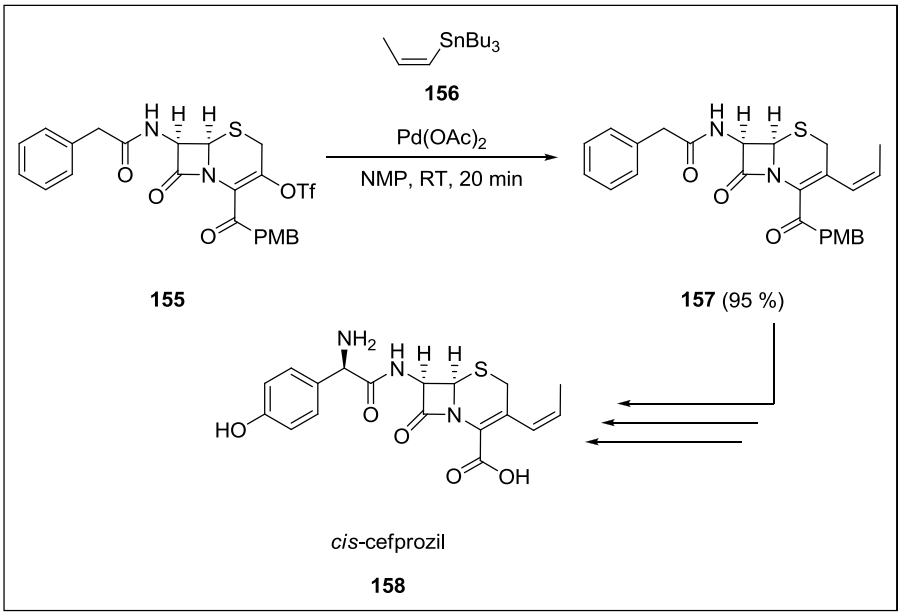

Scheme 16. Stille coupling reaction used for the preparation of the antibiotic *cis*-cefprozil (**158**).

5.2. Suzuki-Miyaura

Another palladium-catalyzed C-C bond-forming reaction involves the palladium-mediated coupling of organic electrophiles, such as aryl or alkenyl halides and triflates, with organoboron compounds in the presence of base. This chemical process is called Suzuki-Miyaura coupling reaction and for the first time it was reported by the Suzuki group in 1979.[110,111] The Suzuki-Miyaura reaction is particularly useful method for the construction of conjugated dienes and higher polyene systems of high stereoisomeric purity, as well as of biaryl and related systems. Furthermore, tremendous progress has been made in the

[107] Naito, T.; Hoshi, H.; Aburaki, S.; Abe, Y.; Okumura, J.; Tomatsu, K.; Kawaguchi, H. *J. Antibiot.* **1987**, *40*, 991 – 1005.
[108] Farina, V.; Baker, S. R.; Jr Sapino, C. *Tetrahedron Lett.* **1988**, *29*, 6043 – 6046.
[109] Farina, V.; Krishnamurthy, V.; Scott, W. J. *The Stille Reaction.* **1998** Wiley, New York.
[110] Suzuki, A. *Acc. Chem. Res.* **1982**, *15*, 178 – 184.
[111] Miyaura, N.; Yamada, K.; Suzuki, A. *Tetrahedron Lett.* **1979**, *20*, 3437 – 3440.

development of Suzuki coupling reactions of unactivated alkyl halides, enabling sp^2-sp^3 carbon bond and even sp^3-sp^3 carbon bond formation. The ease of preparation of organoboron compounds and their relative stability to air and water, combined with the relatively mild conditions as well as the formation of nontoxic byproducts, makes the Suzuki-Miyaura reaction a valuable tool in organic synthesis.[112,113,114] (Scheme 17)

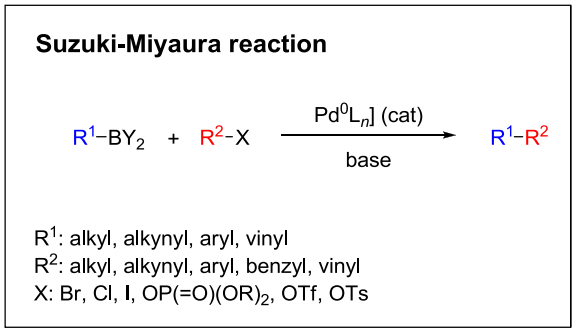

Scheme 17. General scheme of the Suzuki-Miyaura cross-coupling reaction.[94]

The boron reagents initially employed for the Suzuki-Miyaura coupling were alkenylboranes and catechol boronic esters **159**, both conveniently obtained through the hydroboration of terminal alkynes. However, by the 1990s boronic acids **160** had become the reagents of choice, especially for aryl couplings, primarily due to their enhanced reactivity and high atom-economy. Pinacol boronic esters **161** also became popular, particularly in the context of Miyaura-borylation.[115] Over the last two decades, a wide range of new reagents for the Suzuki-Miyaura coupling have been developed, with stabilities that allow distal manipulation and expansion of substrate scope. Organotrifluoroborate salts **162** and MIDA (*N*-methyliminodiacetic acid) boronates **163** are two of the most developed systems, but several other alternatives have also been well advanced (**164**, **165** and **166**). For Suzuki-Miyaura coupling with sp^3 carbon bearing boronic species, 9-BBN (9-borabicyclo[3.3.1]nonane) derivatives **167** are used in order to increase electron density at the boron atom.[116,117] (Figure 44)

[112] Ishiyama, T.; Abe, S.; Miyaura, N.; Suzuki, A. *Chem. Lett.* **1992**, 691 – 694.
[113] Zhou, J.; Fu, G. C. *J. Am. Chem. Soc.* **2004**, *126*, 1340 – 1341.
[114] Frisch, A. C.; Beller, M. *Angew. Chem.* **2005**, *117*, 680 – 695.
[115] www.organic-chemistry.org/namedreactions/miyaura-borylation-reaction.shtm (accessed March 13th, 2017).
[116] Suzuki, A. *J. Organomet. Chem.* **1999**, *576*, 147 – 168.
[117] Lennox, A. J. J.; Lloyd-Jones, G. C. *Chem. Soc. Rev.* **2013**, *43*, 412 – 443.

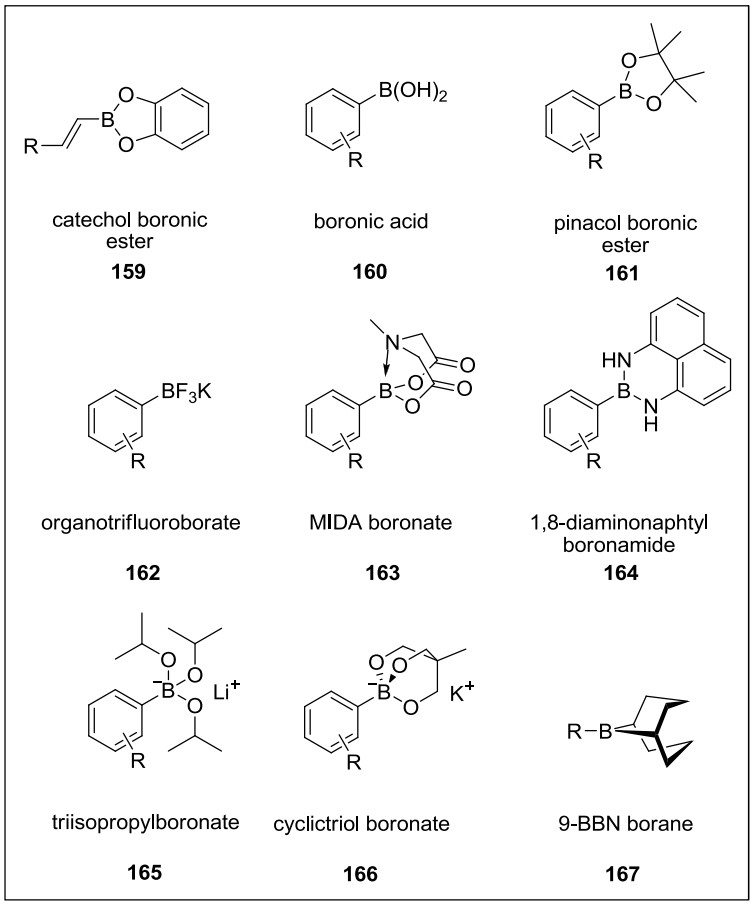

Figure 44. The most common boron reagents used for the Suzuki-Miyaura coupling reaction.[117]

The synthesis of the first generation of cyclooxygenase-2 (COX-2) inhibitor – rofecoxib (Merck) (**171**) using the Suzuki-Miyaura coupling reaction as the key step is depicted on the following scheme.[118] (Scheme 18)

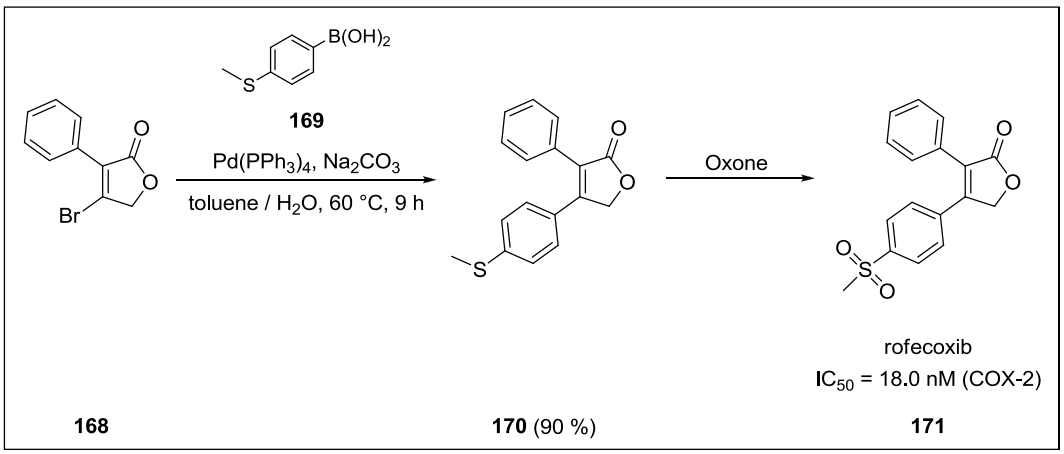

Scheme 18. Synthesis of the first generation COX-2 inhibitor – rofecoxib (**171**).

[118] Desmond, R.; Dolling, U.; Marcune, B.; Tillyer, R.; Tschaen, D. *Merck and Co., Inc.* **1996**, WO1996/008482, (A1).

The synthesis of the second generation of (COX-2) inhibitor – etoricoxib (Merck) (**177**) utilizes the Suzuki-Miyaura coupling reaction twice. The first cross-coupling of 3-bromo-5-chloro-2-aminopyridine (**172**) with boronic acid **169** takes place at the bromide carbon. The amino group of product **174** is afterwards transformed to a bromine group under Sandmeyer conditions. The resulting 2-bromo-5-chlroro-3-(4-(methylsulfonyl)phenyl) pyridine (**175**) is coupled with boronate **176** to provide the final product **177**. [98,119] (Scheme 19)

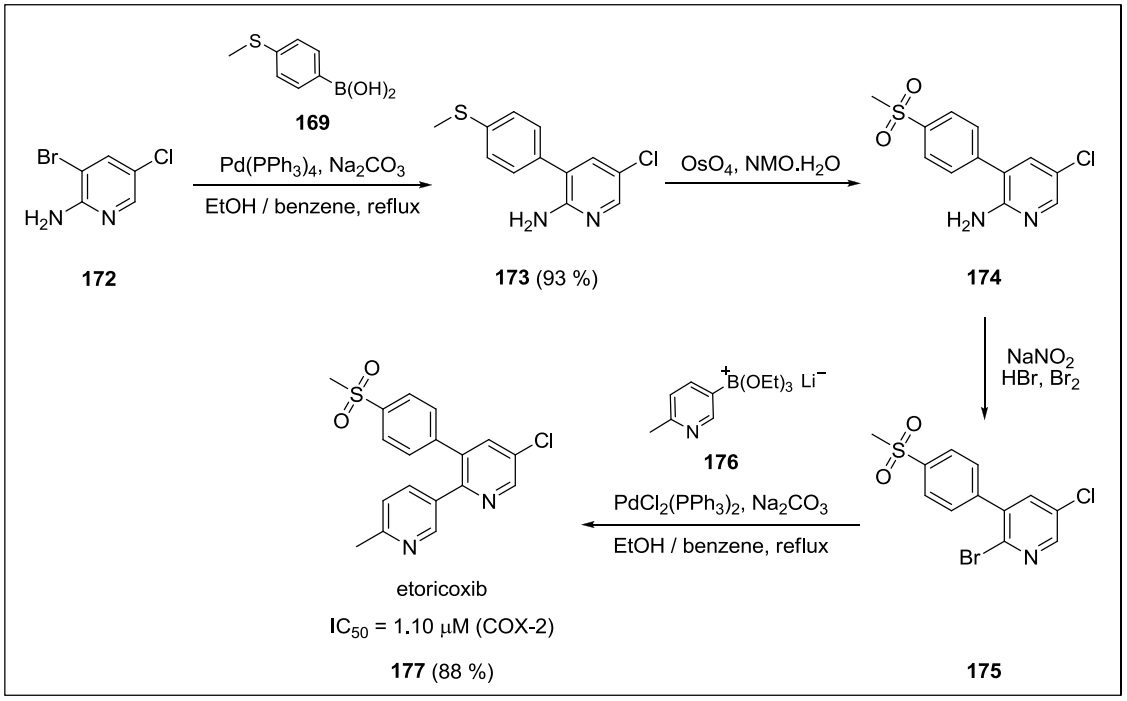

Scheme 19. Synthesis of the second generation COX-2 inhibitor – etoricoxib (**177**).

5.3. Sonogashira coupling

Currently, the cross-coupling reaction for forming a sp^2-sp carbon bond is one of the mildest and most successful methods in this field. The palladium-catalyzed coupling of terminal alkynes with vinyl or aryl halides was reported independently by the groups of Cassar and Heck in 1975. [120 , 121] A few months later, Sonogashira and coworkers

[119] Friesen, D. W.; Brideau, C.; Chan, C. C.; Charleson, S.; Deschenes, D.; Dubé, D.; Ethier, D.; Fortin, R.; Gauthier, J. Y.; Girard, Y.; Gordon, R.; Greig, G. M.; Riendeau, D.; Savoie, C.; Wang, Z.; Wong, E.; Visco, D.; Xu, L. J.; Young, R. N. *Bioorg. Med. Chem. Lett.* **1998**, *8*, 2777 – 2782.
[120] Cassar, L. *J. Organomet. Chem.* **1975**, *93*, 253 – 259.
[121] Dieck, H. A.; Heck, F. R. *J. Organomet. Chem.* **1975**, *93*, 259 – 263.

demonstrated that this cross-coupling reaction can be accelerated by the addition of catalytic amount of Cu(I) salts. The success of reaction relies on the acidity of the terminal alkynyl hydrogen. Therefore, unlike other methods, there is no need to activate the nucleophile cross-coupling partner. For instance, Negishi, Suzuki-Miyaura, and Stille reactions require preparing C-Zn, C-B, C-Sn bond-containing reagents, respectively, prior to their coupling reactions.

The Sonogashira reaction provides a valuable method for the synthesis of conjugated acetylenic systems with broad range of applications from natural products and pharmaceuticals to specifically designed molecules in biotechnology and nanotechnology. Practically, this is the easiest methodology to create C-C bonds, while the resulting triple bond can be easily transformed to other functional moieties. [98,122,123] (Scheme 20)

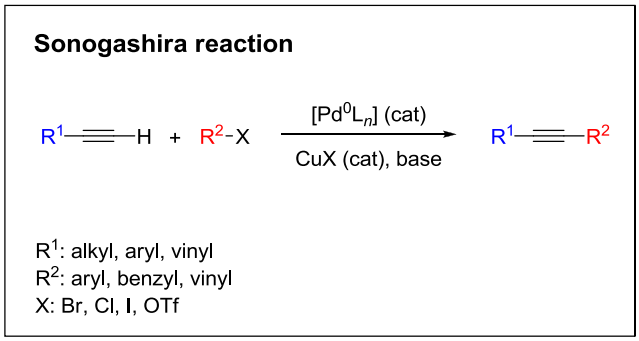

Scheme 20. General scheme of the Sonogashira cross-coupling reaction.[94]

On the following scheme there is shown the synthesis of an HIV-1 protease inhibitor candidate **183** which key building block, chlorinated furopyridine (**182**), was effectively prepared *via* the Sonogashira reaction. [124] The reaction resembled the Larock indole synthesis.[125] The structure of **183** is very similar to that of Crixivan (Merck) (**184**) – the powerful inhibitor of HIV-1 protease. (Scheme 21)

[122] Sonogashira, K.; Tohda, Y.; Hagihara, N. *Tetrahedron. Lett.* **1975**, *16*, 4467 – 4470.
[123] Sonogashira, K. *J. Organomet. Chem.* **2002**, *653*, 46 – 49.
[124] Houpis, I. N.; Choi, W. B.; Reider, P. J.; Molina, A.; Churchill, H.; Lynch, J.; Volante, R. P. *Tetrahedron Lett.* **1994**, *35*, 9355 – 9358.
[125] Larock, R. C.; Yum, E. K. *J. Am. Chem. Soc.* **1991**, *113*, 6689 – 6690.

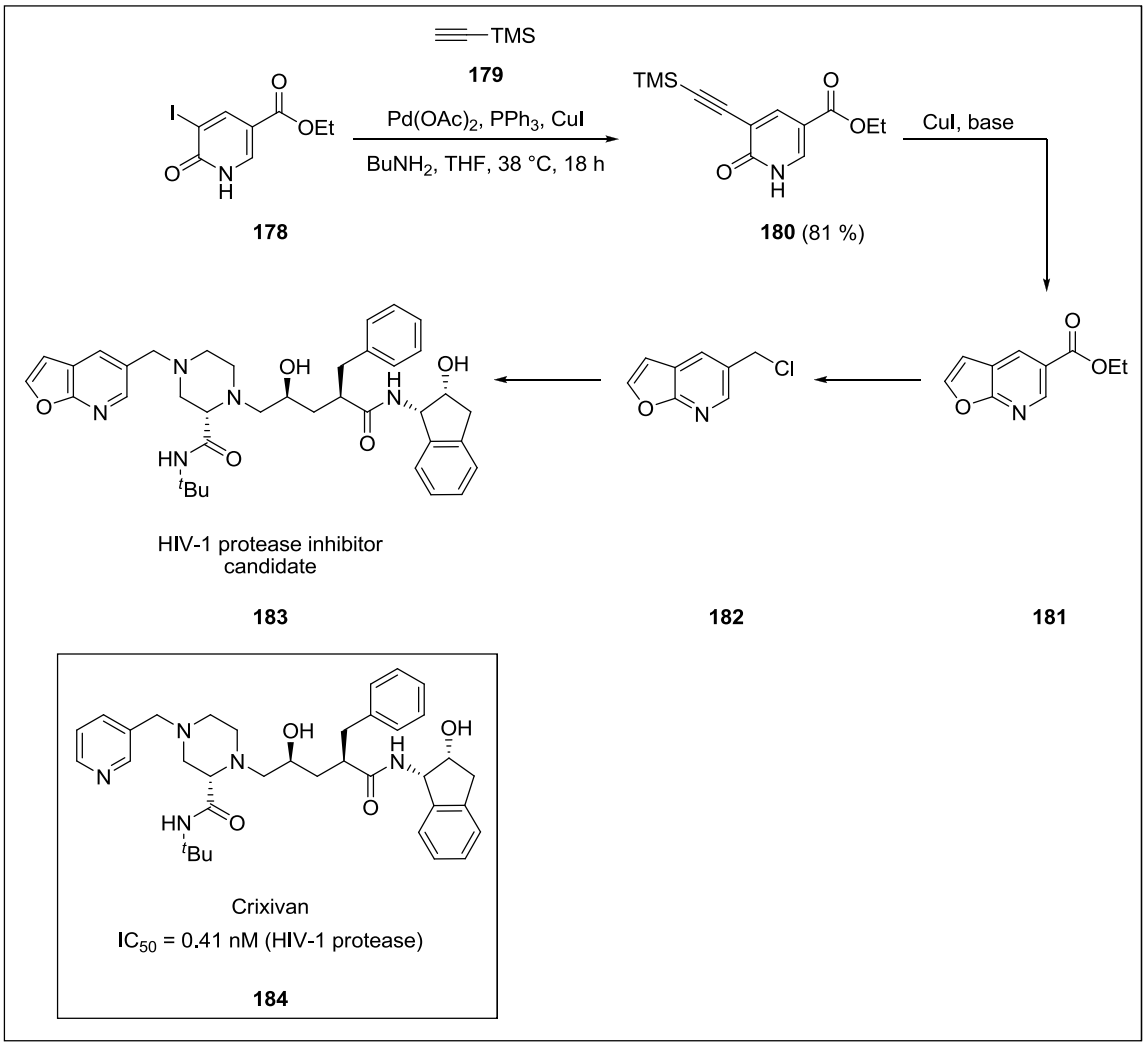

Scheme 21. Synthesis of the HIV-1 protease inhibitor candidate **183**.

Another example for the utilization of Sonogashira reaction in medicinal chemistry represents the synthesis of an oxazolidinone derivative **188** which was designed as the antibacterial agent against Gram-positive and Gram-negative microorganisms, including multi-drug resistant strains. The synthesis begins with the Sonogashira coupling between trimethylsilylacetylene (**179**) and iodophenyloxazolidinone **185** followed by removal of the silyl group, the click cycloaddition reaction with *p*-methoxybenzyl azide (**187**) and deprotection with trifluoroacetic acid leading to the final triazole-containing oxazolidinone **188**.[126] (Scheme 22)

[126] Hauck, S. I.; Cederberg, C.; Doucette, A.; Grosser, L.; Hales, N. J.; Poon, G.; Gravestock, M. B. *Bioorg. Med. Chem. Lett.* **2007**, *17*, 337 – 340.

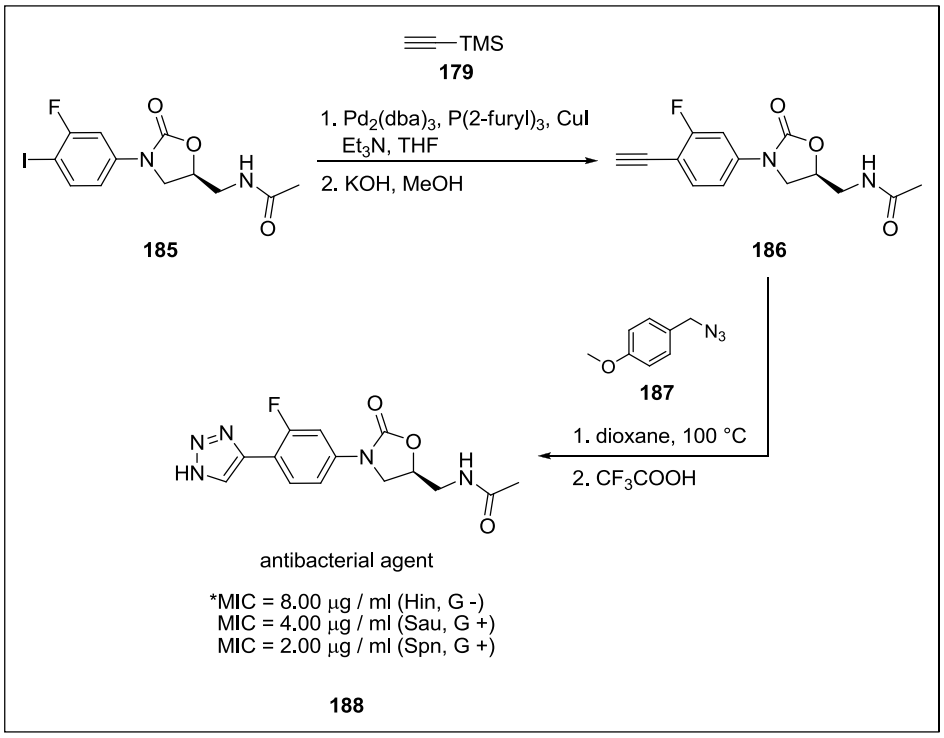

Scheme 22. Synthesis of the antibacterial agent **188**.

*In microbiology, the minimum inhibitory concentration (MIC) is the lowest concentration of a chemical that prevents visible growth of a bacteria (the concentration of a chemical with bacteriostatic activity).[127]

[127] Tripathi, K. D. *Essentials of Medicinal Pharmacology (7th ed.)* **2013** Jaypee Brothers Medical Publishers, New Delhi.

Chapter 6. **Project – Regioisomeric bioisostery (*RegBio*)**

6. Project – Regioisomeric bioisostery (*RegBio*)

An oxazole compound **2** (AAZ) was initially developed by GlaxoSmithKline[128] as a powerful VEGFR2 TK ATP-competitive inhibitor. Because **2** showed good pharmacokinetic properties and strong VEGFR2 TK inhibitory activity (lit. IC_{50} = 22.0 nM (VEGFR2 TK)), the compound was selected as a promising drug candidate.[6]

The **2** (AAZ) represents the *N*,5-diaryloxazol-2-amine derivative containing 2,5-disubstitued oxazole ring as one of the key pharmacophoric fragments. A compound **3** (AAZ-regio), *N*,4-diaryloxazol-2-amine derivative, contains 2,4-disubstituted oxazole ring and represents the regioisomeric compound to **2**. We expect that the compound **3** takes a very similar binding position in the ATP-binding site of the VEGFR2 TK preserving the essential H-bond with Cys917 possibly leading to the similar inhibition properties as known for the inhibitor **2**.

The oxazole compound **3** (AAZ-regio) represents a new type of chemical structure. Oxygen atom from the oxazole ring is the isosteric atom to oxazole nitrogen. The appropriate conformer of **3** (AAZ-regio) is a bioisosteric candidate of the inhibitor **2** (AAZ). For the proposed hypothesis we introduced the name Regioisomeric bioisostery (*RegBio*). (Figure 45 and 46)

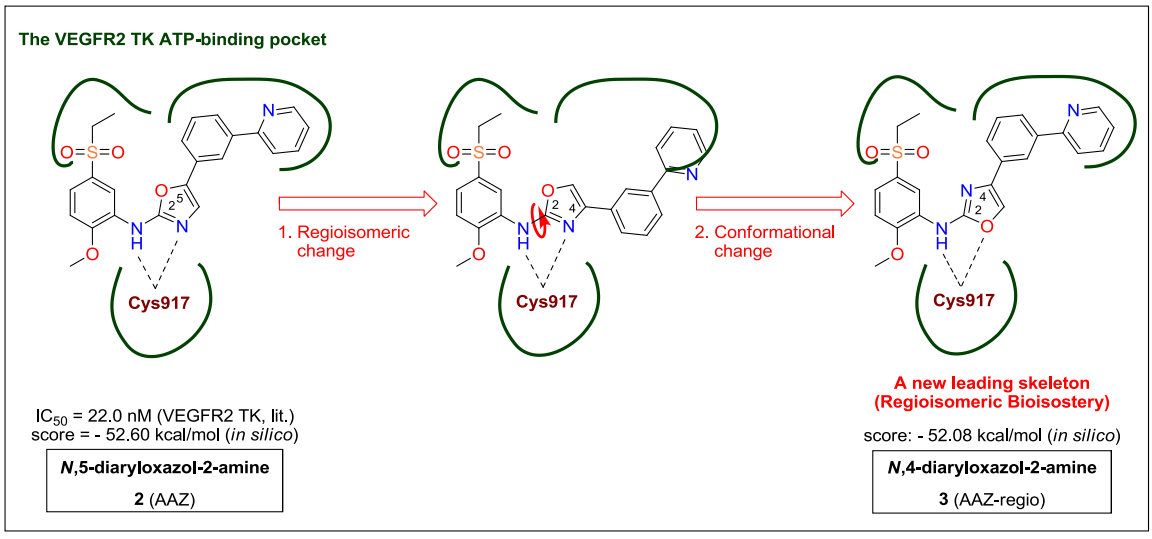

Figure 45. Regioisomeric bioisostery – the suitable regioisomeric change in **2** (AAZ) followed by the induced conformational change leads to the bioisosteric candidate **3** (AAZ-regio).

[128] GlaxoSmithKline, Five Moore Drive, Research Triangle Park, North Carolina 27709, USA.

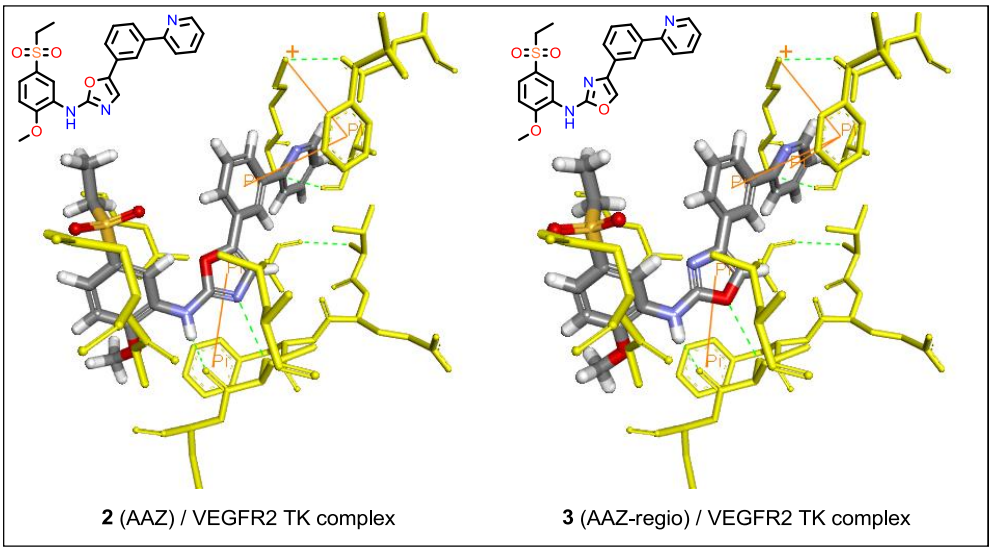

Figure 46. Binding positions of inhibitor **2** (AAZ) and its regioisomeric analogue **3** (AAZ-regio) in the VEGFR2 TK ATP-binding pocket obtained by docking.

The *RegBio* project is focused on the development of novel AAZ-like and corresponding AAZ-regioisomeric compounds with VEGFR2 TK inhibiting activity. According to the results of *in silico* screening we aimed to prepare five predicted regioisomeric pairs, a series of *N*,5-diaryloxazol-2-amine derivatives with pyridin-2-yl **2** (AAZ), pyrimidin-2-yl **189**, pyrimidin-5-yl **190**, pyrrol-3-yl **191**, tiophen-3-yl **192** substituent and a corresponding series of regioisomeric *N*,4-diaryloxazol-2-amines **3** (AAZ-regio), **193**, **194**, **195**, **196**, and determine their biological activity (IC_{50}, VEGFR2 TK). (Figure 47 and 48)

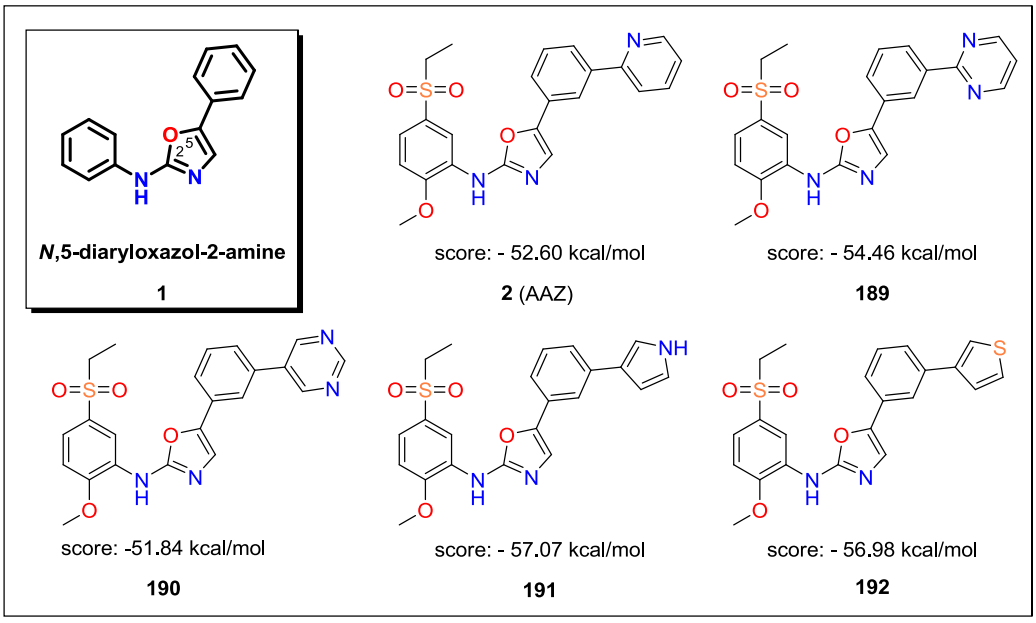

Figure 47. Series of predicted *N*,5-diaryloxazol-2-amine (**1**) derivatives **2** (AAZ), **189**, **190**, **191** and **192** with their *in silico* docking score.

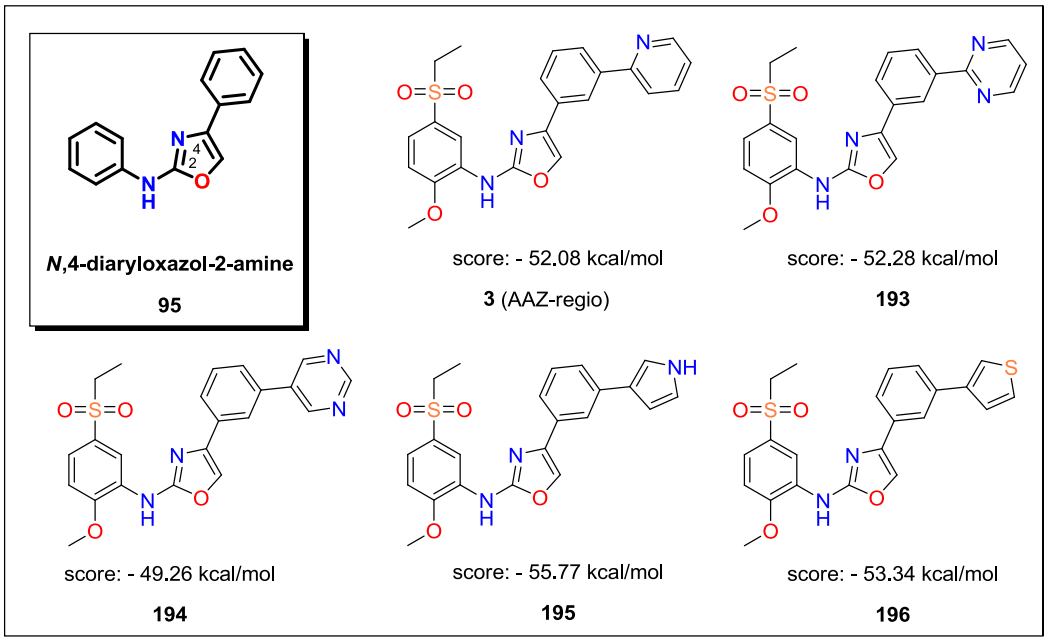

Figure 48. Series of predicted *N*,4-diaryloxazol-2-amine (**95**) derivatives **3** (AAZ-regio), **193**, **194**, **195** and **196** with their *in silico* docking score.

6.1. Synthesis of *N*,5-diaryloxazol-2-amines 2, 189, 190, 191, 192

Based on information from the databases (Reaxys, SciFinder) and primary scientific literature we designed synthetic procedures of *N*,5-diaryloxazol-2-amines **2**, **189**, **190**, **191** and **192**.

In the first part of the synthesis an important oxazole precursor **107** was prepared. Its preparation originated from aniline **122** which was developed in our scientific group.[140] The compound **122** was transformed to isothiocyanate **105** by $CSCl_2$ and subsequently used in a PPh_3-mediated thermic cyclization reaction with α-azidoacetophenone **106** providing the target oxazole precursor **107** in a good overall yield (48 %). (Scheme 23)

The utilized cyclization reaction was optimized in our group and effectively used for the synthesis of many different *N*,5-diaryloxazol-2-amine derivatives. The proposed reaction mechanism was already published and it is depicted on the scheme below.[82] (Scheme 24)

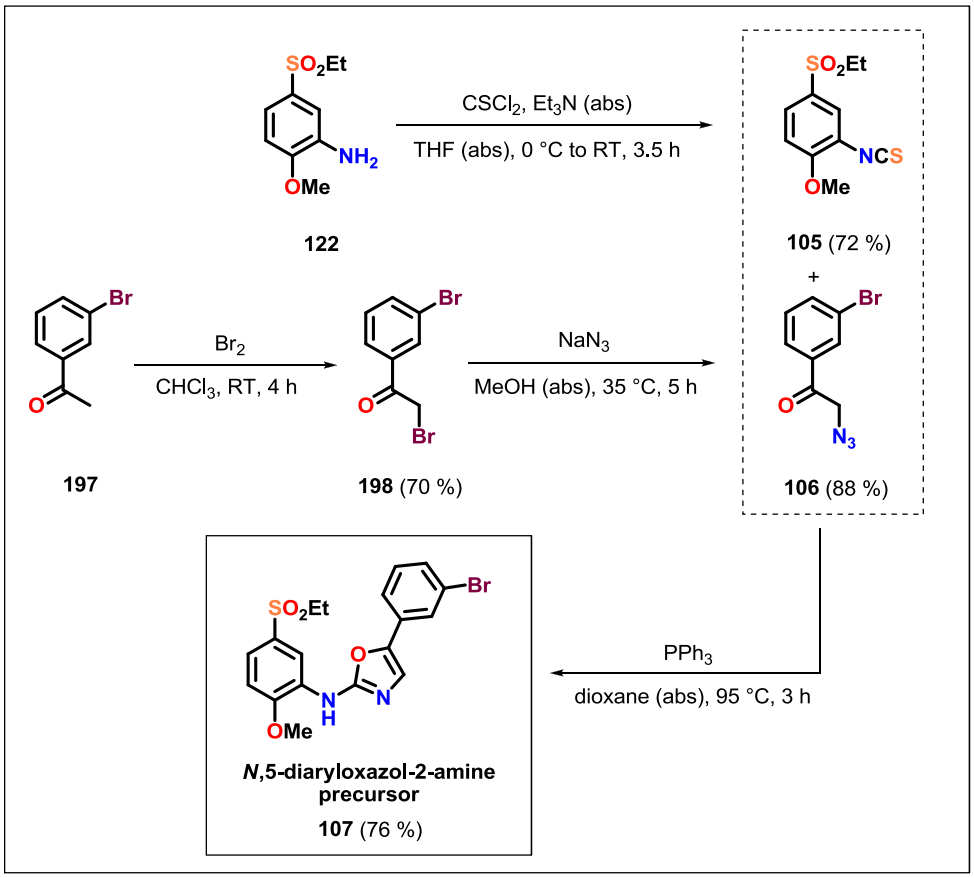

Scheme 23. Synthesis of *N*,5-diaryloxazol-2-amine precursor **107**.

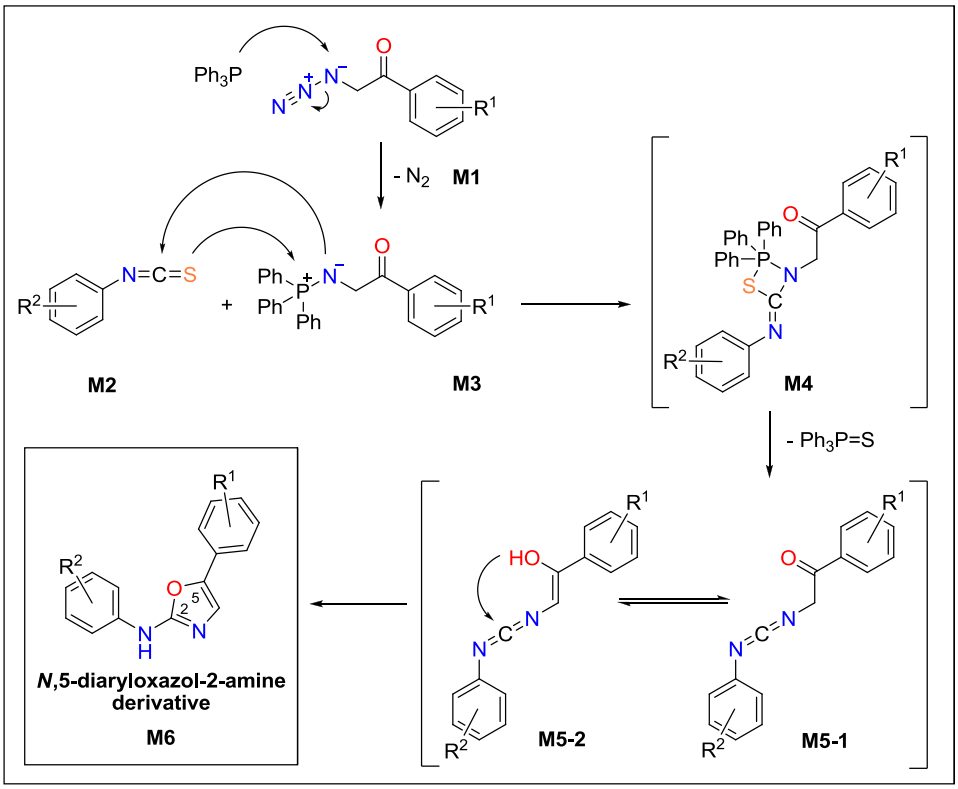

Scheme 24. Proposed mechanism of the reaction leading to *N*,5-diaryloxazol-2-amine derivative **M6**.

The second part of the synthesis leading to *N*,5-diaryloxazol-2-amines **2**, **189**, **190**, **191** and **192** was successfully carried out by a coupling reaction of the precursor **107** with an appropriate heterocyclic coupling reagent. The compounds **2**, **189** and **190** were prepared by the Stille coupling reaction of **107** with organostannanes **154**, **199** and **200** respectively, in the presence of $Pd(PPh_3)_4$ and Bu_4NBr in CH_3CN (abs). A yield of the reactions varied from moderate (**189**, 33 %) to good (**2**, 50 % and **190**, 60 %). (Scheme 25) Because of avoiding the further utilization of highly toxic organostannanes, a good commercial availability of suitable boronic coupling reagents and our attempt to finalize the synthesis in as short time as possible, we decided to use Suzuki coupling reaction for the preparation of **191** and **192**. The compound **191** was prepared in 78 % yield by the coupling reaction of **107** with pinacol boronate **201** in presence of $Pd(PPh_3)_4$ and Na_2CO_3 in a mixture of DMF / H_2O. The compound **192** was prepared in 54 % yield by the coupling reaction of **107** with MIDA boronate **202** in presence of $Pd(OAc)_2$, SPhos and K_3PO_4 in a mixture of THF / H_2O. (Scheme 25 cont.)

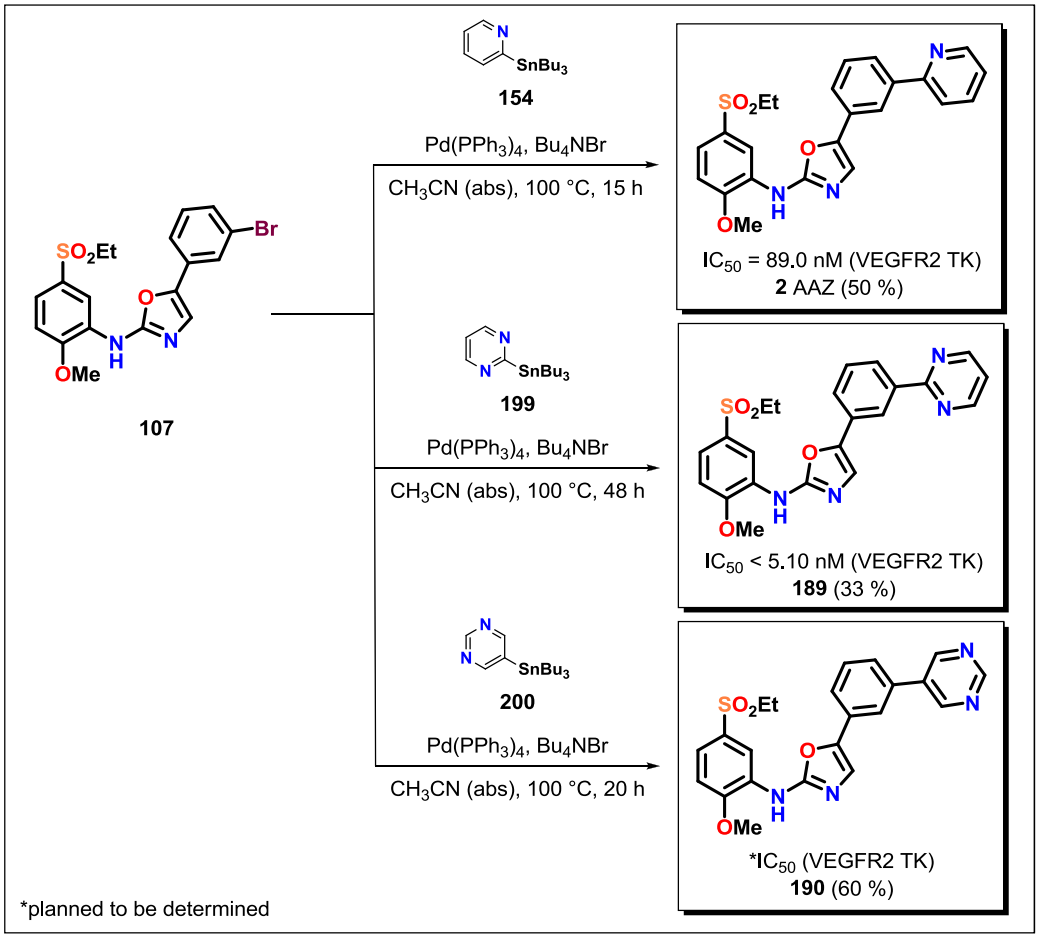

Scheme 25. Synthesis of *N*,5-diaryloxazol-2-amines **2**, **189** and **190**.

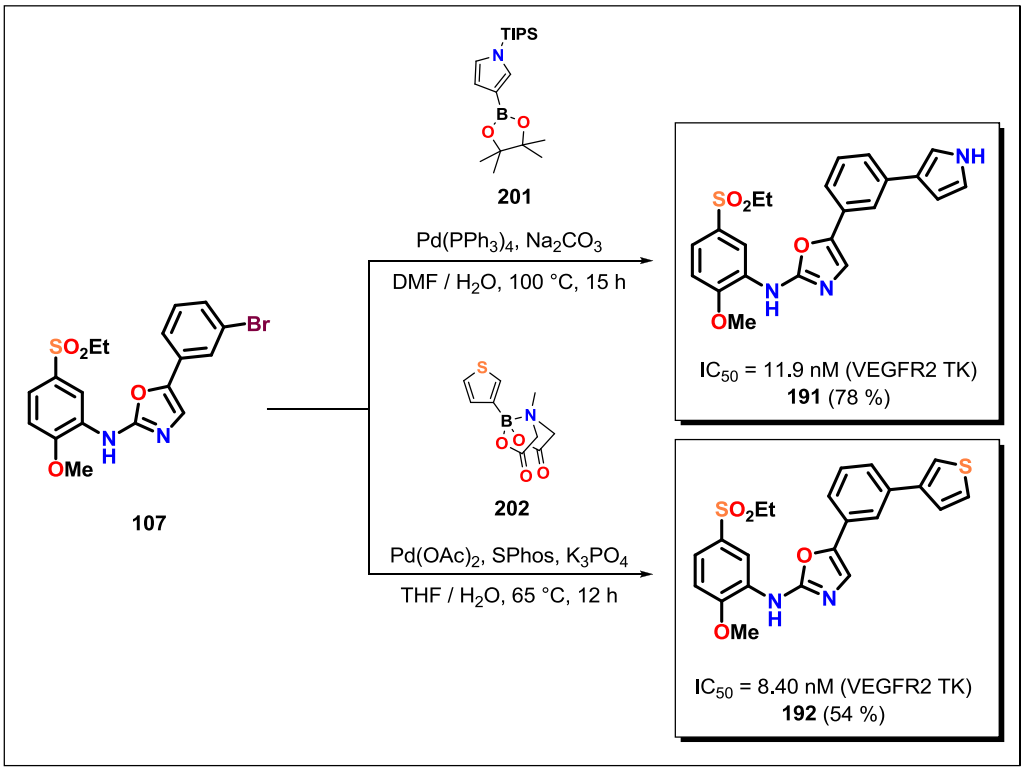

Scheme 25 cont. Synthesis of *N*,5-diaryloxazol-2-amines **191** and **192**.

6.2. Described synthesis of *N*,4-diaryloxazol-2-amines and unexpected synthesis of 1,5-diarylimidazolidine-2,4-dione 204

According to available information from the scientific databases (Reaxys, SciFinder) and primary literature the most common procedure for the preparation of *N*,4-diaryloxazol-2-amine (**95**) derivatives is a cyclization reaction between arylureas and α-bromoacetophenones carried out under various conditions. The more detailed overview of the published synthetic procedures could be found in the theoretical part of this dissertation thesis. (Chapter 4.2)

With the aim to synthesize the desired *N*,4-diaryloxazol-2-amine precursor **205**, we prepared appropriate starting compounds **203** and **198** and tested several published cyclization procedures. After analyzing the performed reactions we observed either the unreacted starting material (**203** and **198**) or a formation of many different mostly unknown products. More interestingly, the reaction performed in refluxing EtOH in the presence of catalytic amount of HCl within 5 days provided a formation of dominant 1,5-

diarylimidazoline-2,4-dione **204** (41 % yield). (Scheme 26) The structure of **204** was supported by the standard analytical methodologies (^{1}H-NMR, ^{13}C-NMR, IR, MS, elemental analysis) and confirmed also by the X-ray spectroscopy. The X-ray analysis proved the presence of **204-syn** product which was created as a racemic compound (both enantiomeres were packed in the crystal cell in the ratio of 1 / 1). (Figure 49)

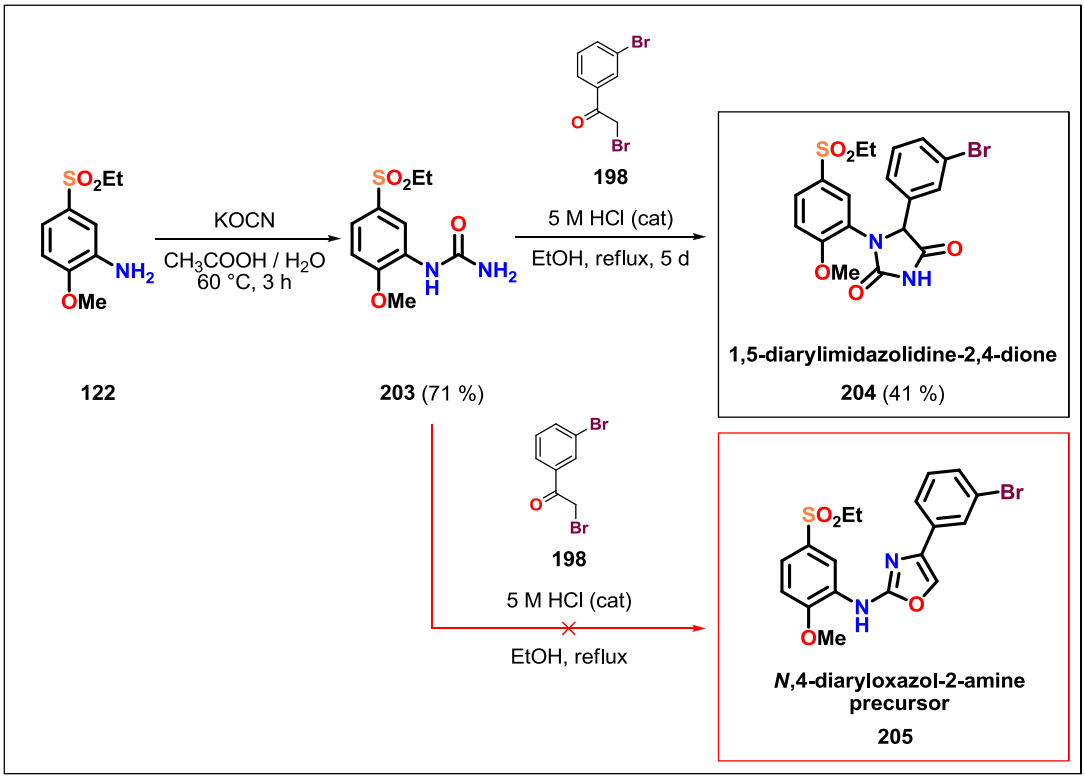

Scheme 26. Unexpected synthesis of 1,5-diarylimidazolidine-2,4-dione **204**.

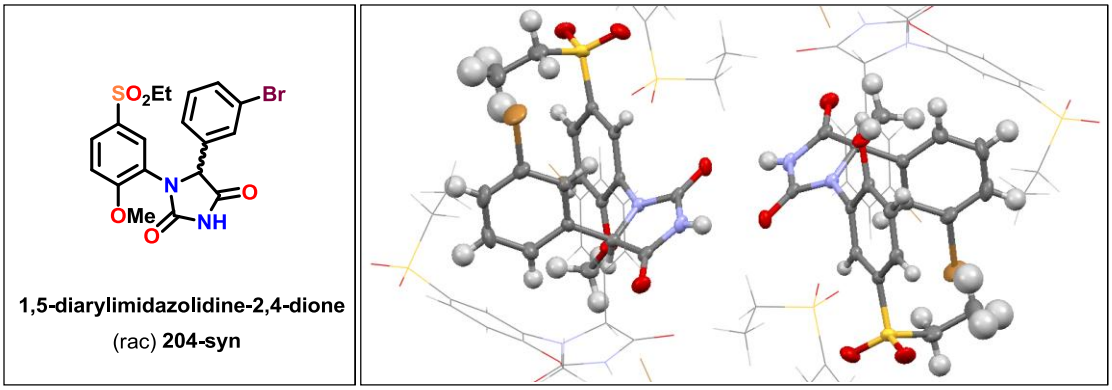

Figure 49. Structure and molecular arrangement of (rac) **204-syn** proved by the X-Ray spectroscopy. In the crystal of **204-syn** are highlighted both enantiomeres; (*R*)-**204-syn** is depicted on the left side and (*S*)-**204-syn** on the right side.

The proposed mechanism of the cyclization leading to 1,5-diarylimidazolidine-2,4-dione derivatives is depicted on the scheme below. (Scheme 27) α-Bromoacetophenone **M7** is in the thermic, HCl catalyzed disproportionation reaction transformed to acetophenone **M8** and α,α-dibromoacetophenone **M9**. A significant presence of the both **M8** and **M9** in a reaction mixture after several hours of heating was proved by TLC and ^{1}H-NMR analyses. The compound **M9** subsequently reacts with urea derivative **M10** providing an intermediate **M12** which undergoes the cyclization reaction leading to the formation of 1,5-diarylimidazolidine-2,4-dione derivative (rac) **M15-syn**.

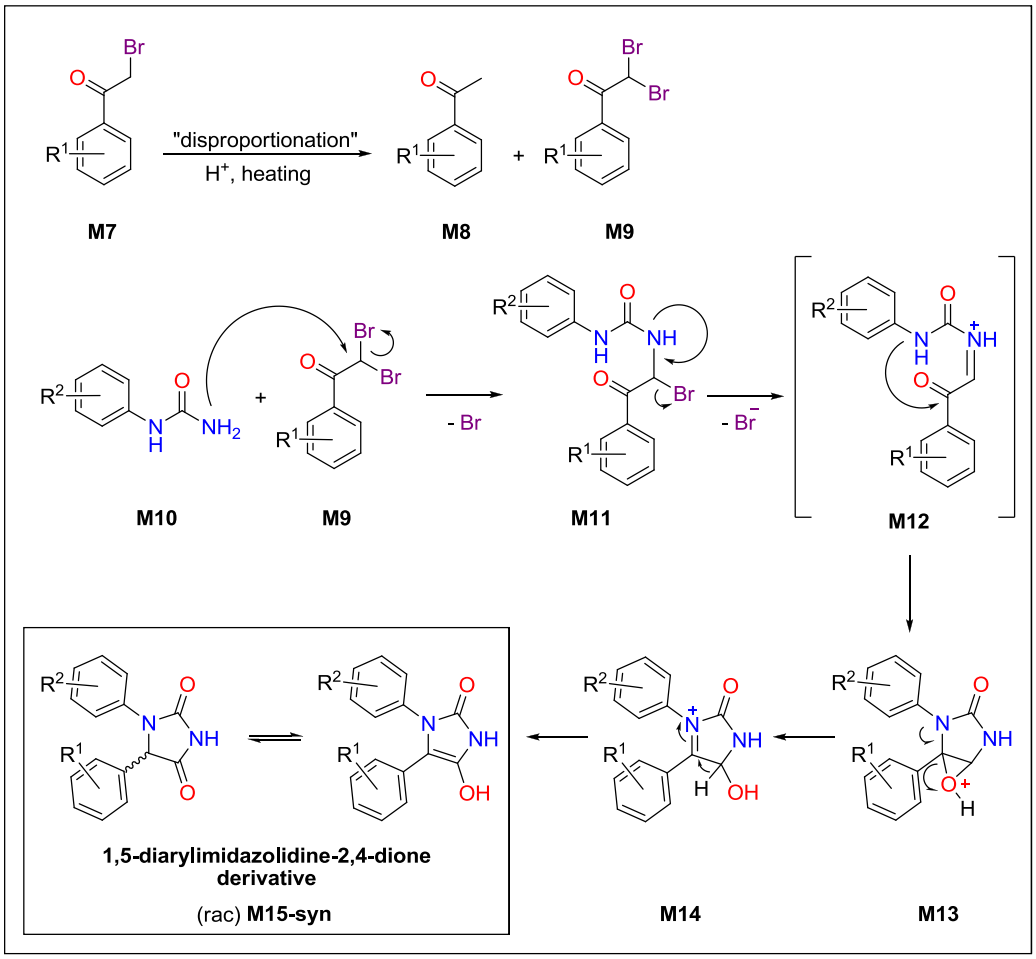

Scheme 27. Proposed mechanism of the reaction leading to 1,5-diarylimidazolidine-2,4-dione derivative (rac) **M15-syn**.

According to the interesting chemical structure of **204** and its potential of a biological activity, derivatives **206** and **207** were synthesized by a coupling reaction of **204** with the heterocyclic reagents **154** and **201**. The compound **206** was prepared in 40 % yield under conditions of the Stille coupling reaction of **204** with stannane **154** and the compound **207**

was prepared in 53 % yield using the Suzuki coupling of **204** with pinacol boronate **201**. (Scheme 26 cont.)

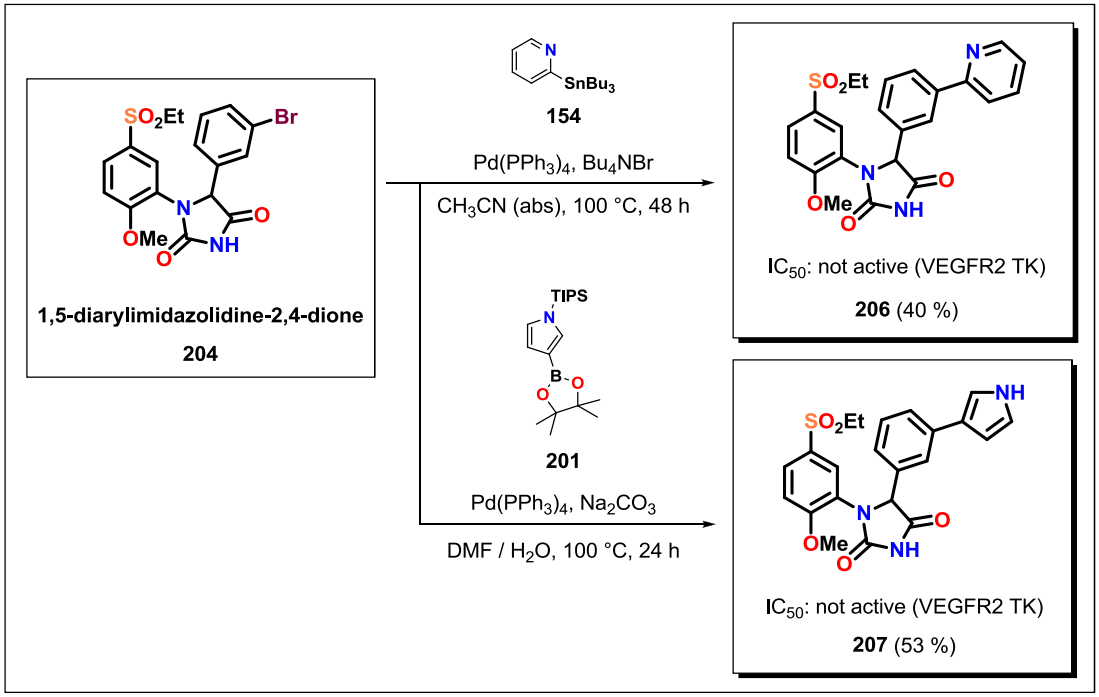

Scheme 26 cont. Synthesis of 1,5-diarylimidazolidine-2,4-diones **206** and **207**.

6.3. Novel synthesis of *N*,4-diaryloxazol-2-amine precursor 205

After our unsuccessful attempts to follow the literature procedures and synthetize *N*,4-diaryloxazol-2-amine precursor **205** for the preparation of the predicted derivatives **3**, **193**, **194**, **195** and **196**, we had to rethink our synthetic approach and develop our own synthesis. In 2014 Bailey and Sudini published the effective synthesis of various 2,4-disubstituted oxazoles by AgOTf-mediated reaction of amides with α-bromoketones in EA (50 °C).[129] We applied the publication-inspired reaction conditions on the cyclization of arylurea **203** and α-bromoacetophenone **198**. The reaction preformed in refluxing EA (abs) in the presence of AgOTf provided the desired product **205** in ca 10 % yield (^{1}H-NMR, crude). (Scheme 28) In the crude mixture we observed the compound **205** and aniline **122** in a ratio of 1 / 1, the unreacted starting material **203** and many unidentified impurities. The

[129] Bailey, J. L.; Sudini, R. R. *Tetrahedron Lett.* **2014**, *55*, 3674 – 3677.

influence of AgOTf is essential for the formation of **205** because it improves a leaving group ability of the α-bromine atom in **198**. Unfortunately the presence of AgOTf is also responsible for the degradation of urea **203** to aniline **122** which was proved by a simple reaction of **203** with the silver salt in refluxing EA. This fact together with the commonly known low thermal stability of α-haloacetophenones could cause the low yield of the desired product **205**.

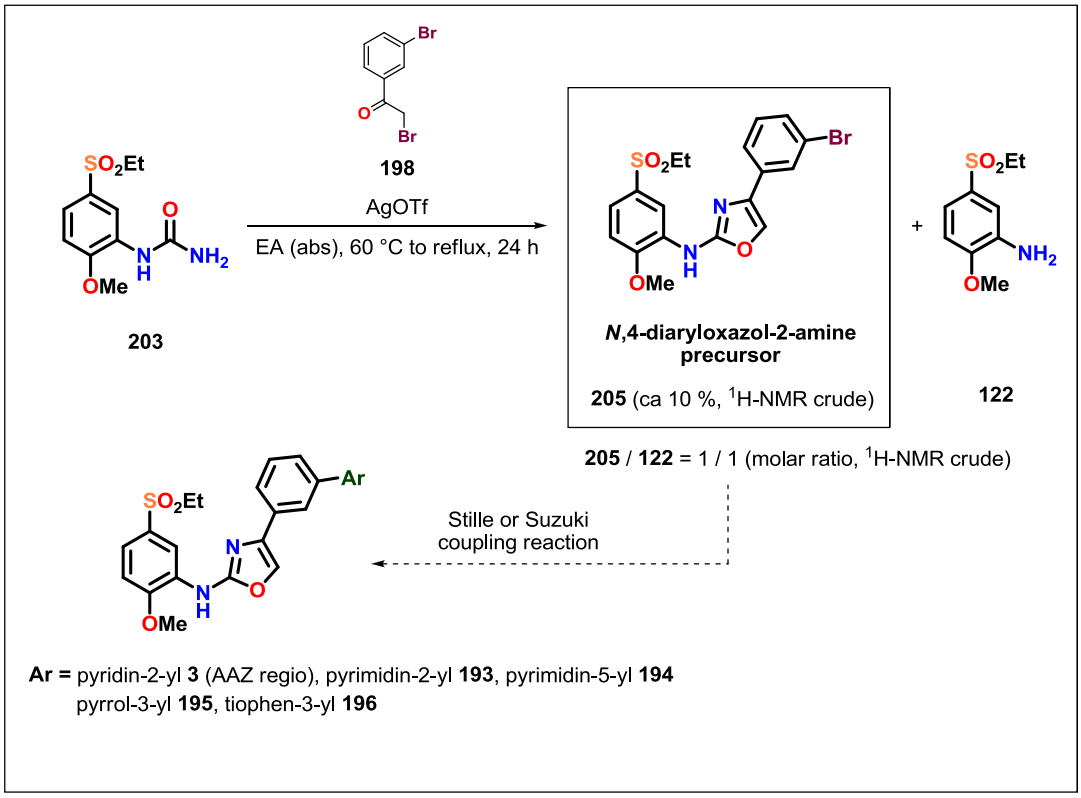

Scheme 28. Synthesis of *N*,4-diaryloxazol-2-amine precursor **205**.

The proposed mechanism of the cyclization leading to *N*,4-diaryloxazol-2-amine derivatives is depicted on the scheme below. (Scheme 29) Urea derivative **M10** nucleophilically attacks the carbonyl group of α-bromoacetophenone **M7** which leads to the formation of an intermediate **M16**. After the Ag-mediated thermal cyclization and subsequent water elimination, the final *N*,4-diaryloxazol-2-amine derivative **M18** is formed.

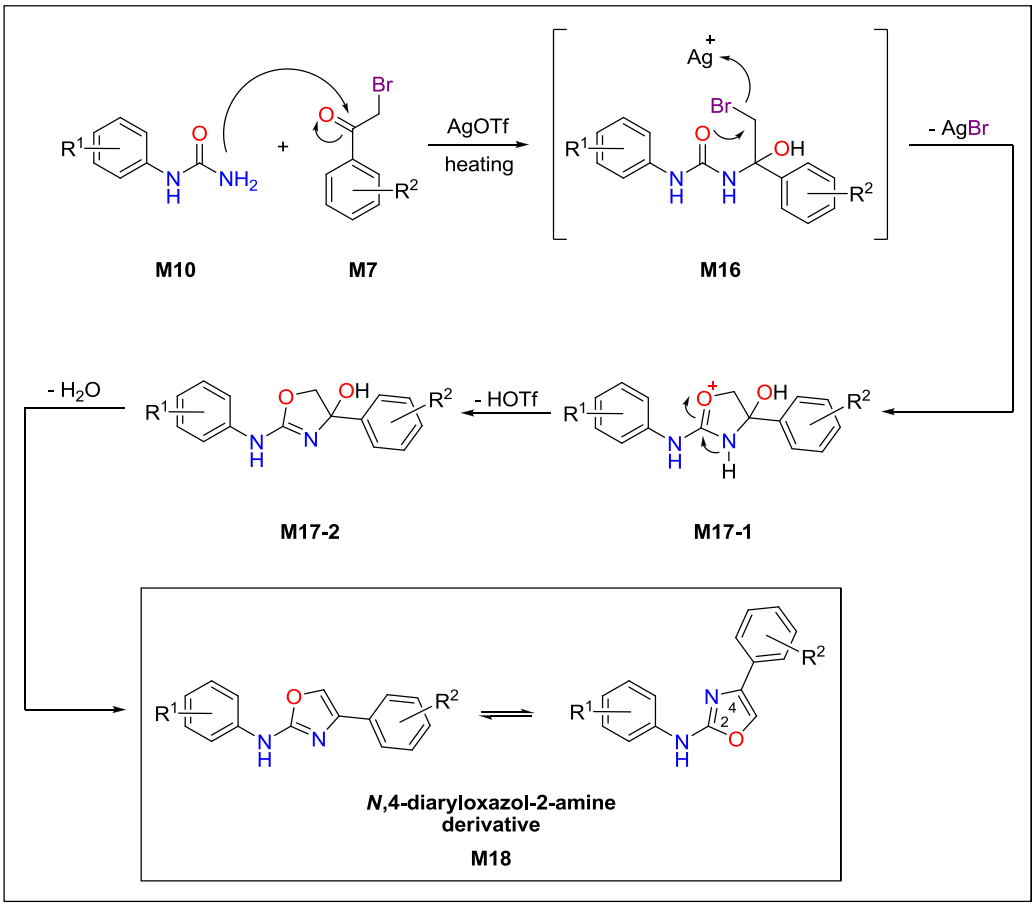

Scheme 29. Proposed mechanism of the reaction leading to *N*,4-diaryloxazol-2-amine derivative **M18**.

Despite we managed to prepare the desired product **205** only in a low yield, we gained a lot of important knowledge about the starting material properties and also about the reaction itself. We plan to improve the product yield and optimize the reaction by the utilization of starting acetophenones substituted with a better leaving group on the α-carbon (–OTs, –OMs, –ONs etc.) without the addition of the silver salts damaging starting urea derivatives. We also plan to do a solvent scope possibly resulting in improvement of the reaction rate allowing us to perform the reaction at lower temperatures. After the successful synthesis of the precursor molecule **205** we will be able to prepare and biologically screen the predicted *N*,4-diaryloxazole-2-amine derivatives **3**, **193**, **194**, **195**, **196** and finalize the project.

6.4. Biological activity of the prepared compounds and evaluation of the *RegBio* project

Within the *RegBio* project we successfully prepared the series of the predicted *N*,5-diaryloxazol-2-amine derivatives **2**, **189**, **190**, **191**, and **192**. We also determined *in vitro* inhibitory activities (IC_{50}, VEGFR2 TK) of **2**, **189**, **191** and **192**. An activity of the compound **190** is planned to be determined soon. (Figure 50) All biological assays were done by Reaction Biology Corp., USA.[19] (Chapter 2.2)

The synthesis and inhibitory potency (IC_{50}, VEGFR2 TK) of the pyridin-2-yl and tiophen-3-yl derivatives (**2**, **192**) were already published by Harris *et al.*[6] We prepared and analyzed these compounds as comparative standards for the utilized biological assay verification. Our determined IC_{50} activity values were mostly lower but comparable to the originally published values. The IC_{50} value from functional studies is not a constant and it is dependent on the condition of the experiment (tissue, receptor expression, type of measurement, etc.). Thus, IC_{50} should only be used for comparison of drugs under the specific conditions.[18] According to the different experimental methodology used by Harris *et al.*, the small differences in the published and our obtained IC_{50} values were not surprising.

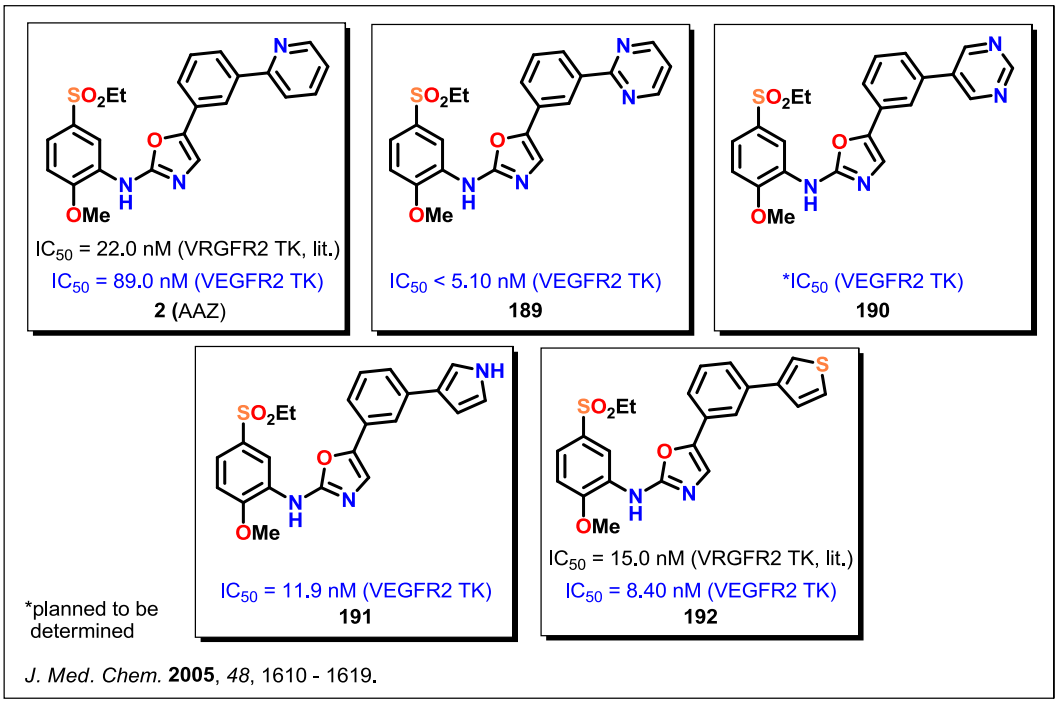

Figure 50. Overview of the prepared *N*,5-diaryloxazol-2-amines **2**, **189**, **190**, **191** and **192** together with their determined inhibitory activities (if available).

The pyrimidin-2-yl, pyrimidin-5-yl and pyrrol-3-yl derivatives (**189**, **190** and **191**) were prepared as new compounds and fully characterized. Moreover, **189** and **191** showed high inhibitory activities against VEGFR2 TK, especially the activity of **189** reached nearly a sub-nanomolar inhibitor level. The higher activities of **189**, **191** and also **192** compared to the activity of **2** (AAZ) are probably caused by lower polarity of the corresponding heterocyclic substituents (according to their dipole moments) interacting in a hydrophobic pocket of the VEGFR2 TK active site. The higher activity of **191** could be caused also by the additional H-bond of the pyrrol –NH– group with Val912. A binding visualization of the inhibitors **189** and **191** in the ATP-binding site of VEGFR2 TK is depicted on the following figure. (Figure 51)

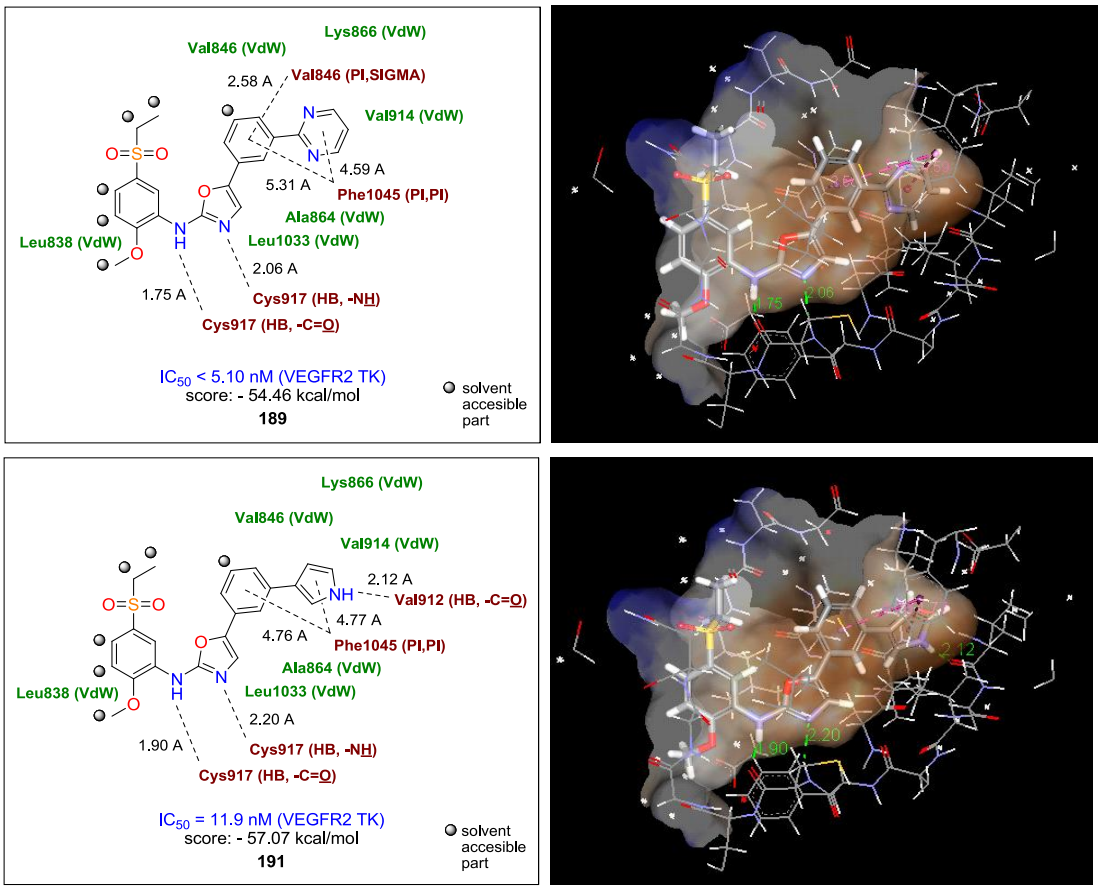

Figure 51. Interaction analysis and binding positions of the pyrimidin-2-yl inhibitor **189** and its pyrrol-3-yl analogue **191** in the ATP-binding site of VEGFR2 TK obtained by docking.

Within the synthesis of the key *N*,4-diaryloxazol-2-amine precursor **205**, we found out the commonly published synthetic procedures are not suitable for its preparation. The HCl-catalyzed cyclization reaction of arylurea **203** with α-bromoacetophenone **198** in refluxing EtOH led to the formation of 1,5-diarylimidazolidine-2,4-dione product **204** instead of the

expected precursor **205**. It have to be mentioned that the preparation of 1,5-diarylimidazolidine-2,4-diones under the conditions discussed above has not been described in the literature. The compound **204** was later transformed to the pyridin-2-yl and pyrrol-3-yl derivatives **206** and **207**. A biological activity (IC_{50}, VEGFR2 TK) of these compounds was examined by Reaction Biology Corp., USA providing a negative result. An activity of **206** and **207** is planned to be predicted and tested also on different appropriate biological targets. An overview of the prepared 1,5-diarylimidazolidine-2,4-dione derivatives is depicted below. (Figure 52)

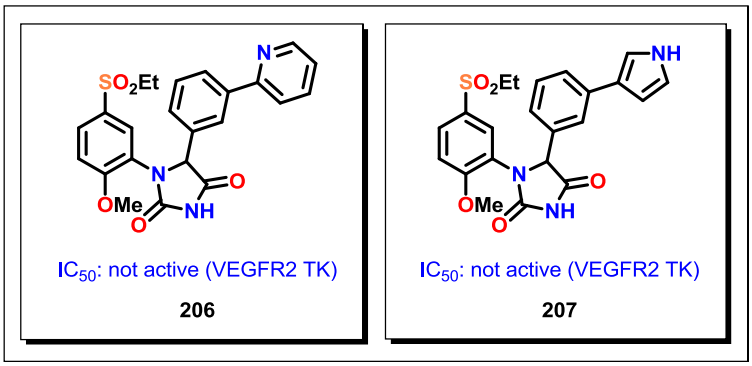

Figure 52. Overview of the prepared 1,5-diarylimidazolidine-2,4-dione derivatives **206** and **207**.

With regard to the unsuccessful synthesis of the *N*,4-diaryloxazol-2-amine precursor **205** using published procedures, we applied the reaction conditions developed for the preparation of 1,4-disubstitued oxazoles from amides and α-bromoketones. Using the AgOTf-mediated reaction of arylurea **203** with α-bromoacetophenone **198** in refluxing EA (abs), we prepared the required compound **205** in ca 10 % yield (^{1}H-NMR, crude). Currently, we are working on the further optimization of the reaction.

Summing-up the *RegBio* project, the proposed *N*,5-diaryloxzole-2-amine derivatives **2**, **189**, **190**, **191** and **192** were prepared and biologically screened with very good results while the synthesis of their regioisomeric *N*,4-diaryoxazole-2-amine analogues **3**, **193**, **194**, **195** and **196** is still in progress. Because of the missing biological data, we are currently not able to make the final activity comparison between the proposed regioisomeric pairs and evaluate our theory of Regioisomeric bioisostery. However, the obtained synthetic achievements and the outstanding assay results encourage us for the project finalization.

Chapter 7. **Project – Salt bridge containig pocket (SBCP)**

7. Project – Salt bridge containing pocket (SBCP)

Twenty-two derivates of *N*,5-diaryloxazol-2-amine (**1**) (included **2** (AAZ)) with determined enzymatic (IC_{50}, VEGFR2 TK) and cellular (IC_{50}, hu-HUVEC / VEGF) activities were described.[6] Five of them were substituted on the oxazole attached phenyl ring on its *p*-position (4-Cl, 4-CN, 4-$CONH_2$, 4-OMe and 4-F). The derivatives containing an ionizable substituent, resp. a substituent able to form an H-bond interaction showed noticeable increase in the inhibitory activity. All the mentioned *p*-substituents were projected towards a small **Salt bridge containing pocket (SBCP)** that we discovered recently in a unique DFG-IN / OUT conformation of VEGFR2 TK induced by the *N*,5-diaryloxazol-2-amine-type of ligands. The SBCP pocket (consisting of Lys866, Glu883 and Phe1045 amino acid residues) represents an important interaction region over the ATP-binding site of the kinase. No discussion about the interactions within this pocket and their influence on the activity of potential inhibitors was noted in the literature. (Figure 53)

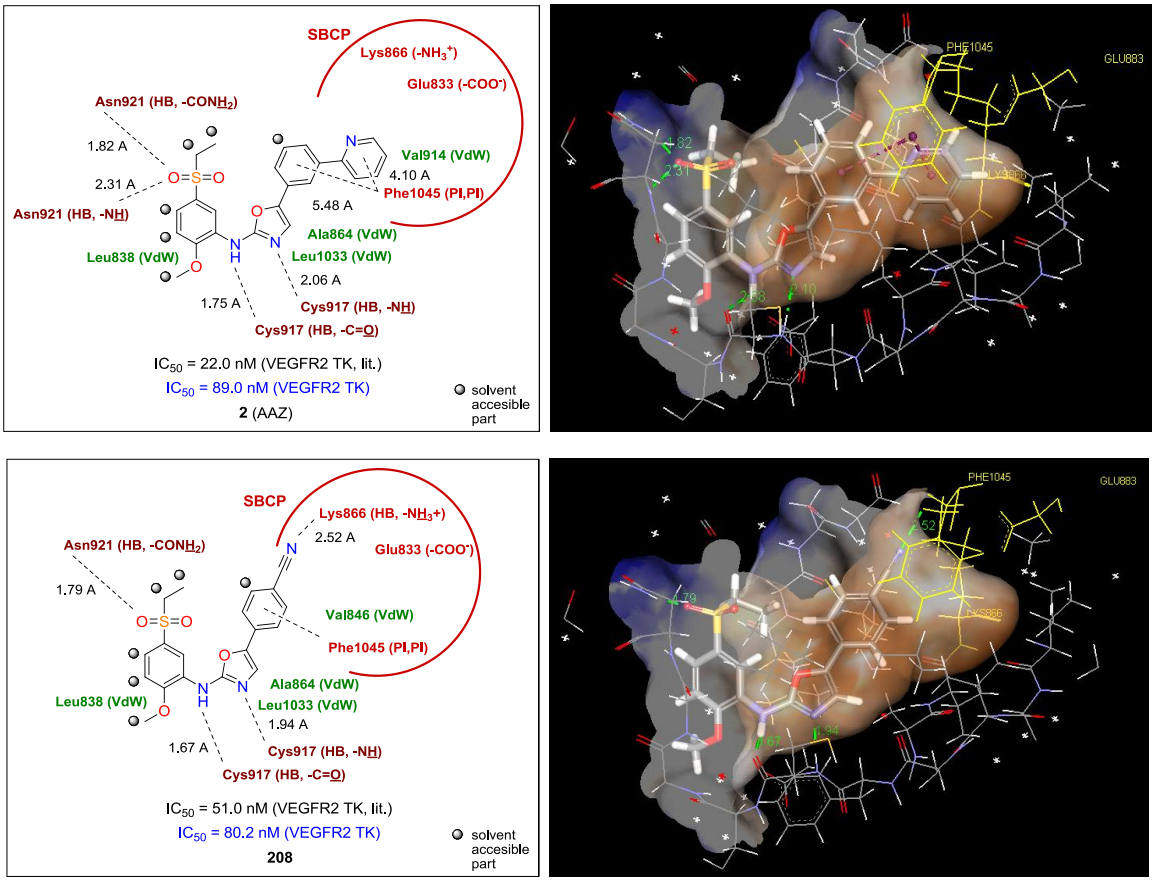

Figure 53. Interaction analyses, activities and predicted binding positions of **2** (AAZ) and **208** in the VEGFR2 TK ATP-binding site with highlighted SBCP region.

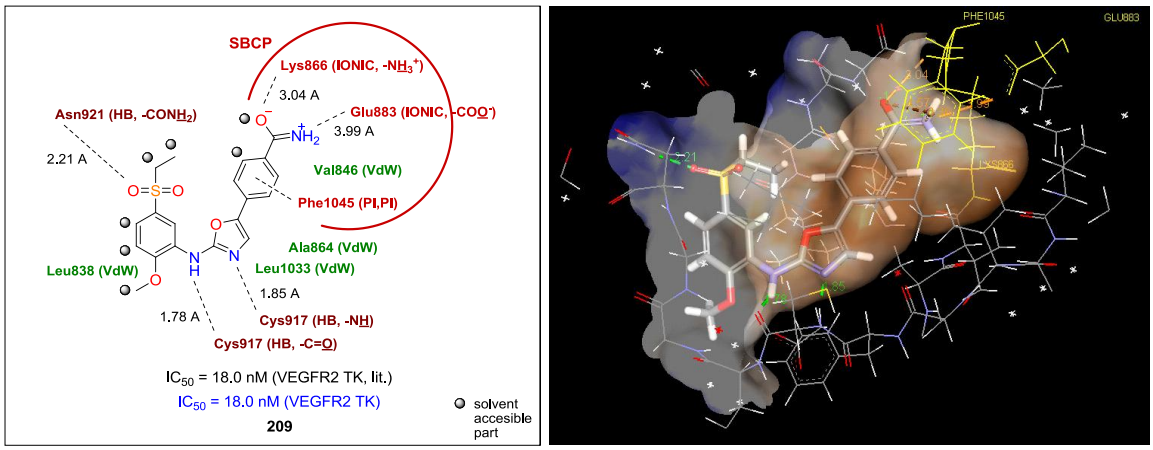

Figure 53 cont. Interaction analysis, activity and predicted binding position of **209** in the VEGFR2 TK ATP-binding site with highlighted SBCP region.

The SBCP project is focused on the development of a novel series of *p*-substituted *N*,5-diaryloxazol-2-amine compounds **208**, **209**, **210**, **211**, **212**, a series of their *m*-substituted analogues **213**, **214**, **215**, **216**, **217** (Figure 54) and subsequent comparative analysis of their binding interactions and determined inhibitory activities (IC_{50}, VEGFR2 TK).

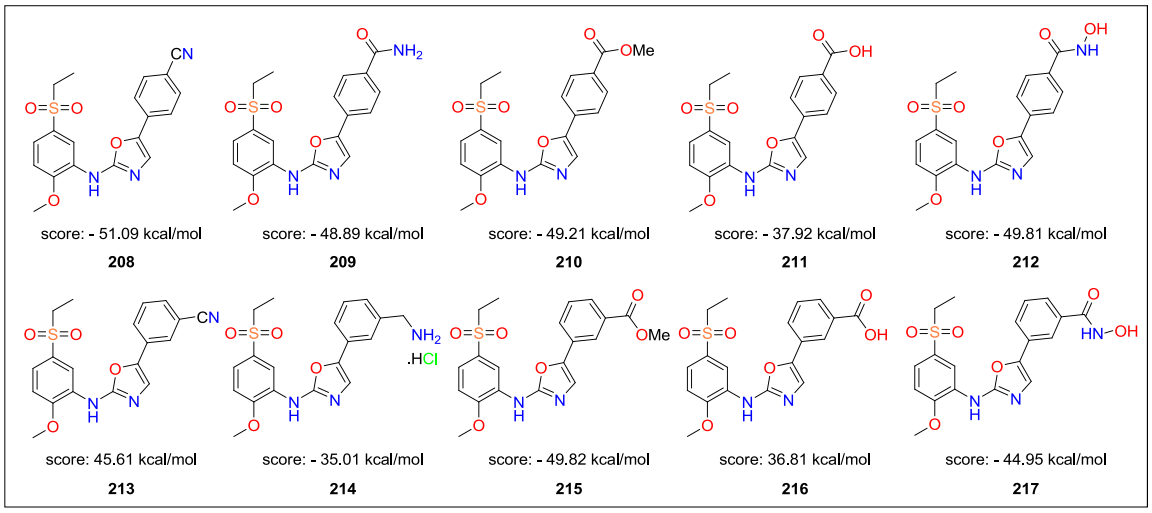

Figure 54. Series of predicted *N*,5-diaryloxazol-2-amines substituted in *p*-position **208**, **209**, **210**, **211**, **212** and their *m*-substituted analogues **213**, **214**, **215**, **216** and **217**.

Besides that we aimed to develop a series of predicted structurally related compounds **218**, **219**, **220**, **221**, **222** and **223** containing a suitable heterocyclic substituent in the *m*-position allowing to get besides the beneficial hydrophobic interactions known for **2** (AAZ) also additional H-bond, resp. ionic interactions in the SBCP. With the same intention we aimed

to prepare a pair of *N*,5-diaryloxazol-2-amines **4**, **224** containing both suitable *p*- and *m*-substituents possibly resulting in the synergic binding. (Figure 55)

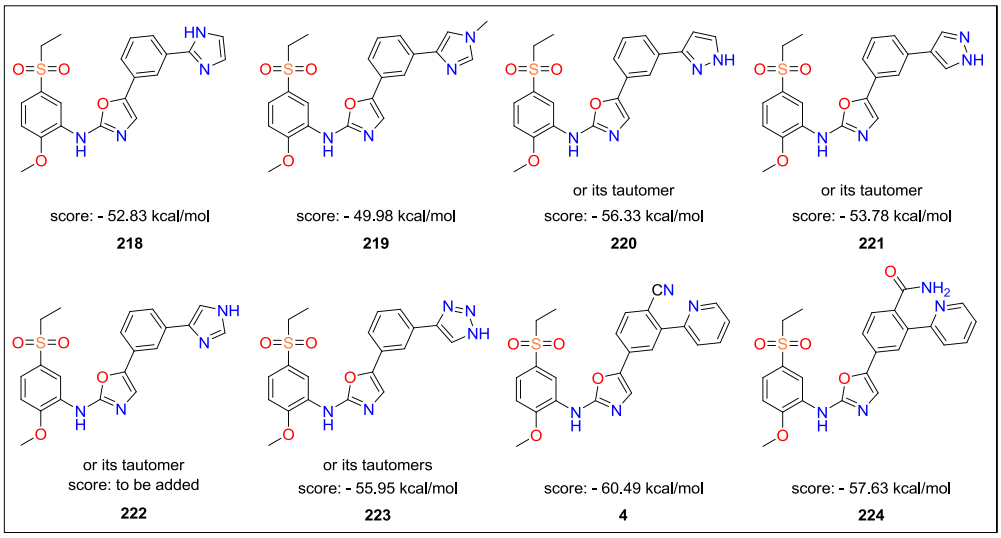

Figure 55. Series of predicted *N*,5-diaryloxazol-2-amines substituted in *m*-position **218**, **219**, **220**, **221**, **222**, **223** or *p*- and *m*-position **4**, **224** together with their docking score.

7.1. Synthesis of *p*-substituted *N*,5-diaryloxazol-2-amines 208, 209, 210, 211, 212

Based on information from the databases (Reaxys, SciFinder) and primary scientific literature we designed a preparation of the predicted *p*-substituted *N*,5-diaryloxazol-2-amines **208** – **212**.

The synthesis of **208** and **209** originated from a commercially available 4-(2-bromoacetyl)benzonitrile (**225**) which was transformed to its azide derivative **226** using NaN_3 in a mixture of acetone / H_2O in 84 % yield. A PPh_3-mediated thermal cyclization of **226** with isothiocyanate **105** in dioxane (abs) provided the target oxazol derivative **208** in 54 % yield. The similar preparation of **208** in CH_2Cl_2 (abs) at RT has been previously published with only 6 % yield.[6] The proposed mechanism of the cyclization is depicted in the chapter 6.1. A procedure for the preparation of the oxazole **209** started from the nitrile **225** which was transformed to amide **227** by a thermal acid hydrolysis in a mixture of TFA / H_2SO_4 (4 / 1) in 92 % yield. A reaction of **227** with NaN_3 in a mixture of acetone / H_2O yielded 91 % of azide **228** which was then used in the oxazolation reaction with the isothiocyanate **105** providing the target oxazole **209** in 31 % yield. (Scheme 30) The

compound **209** can be prepared also directly from **208** by the thermal hydrolysis in TFA / H_2SO_4 (4 / 1) in ca 90 % yield.

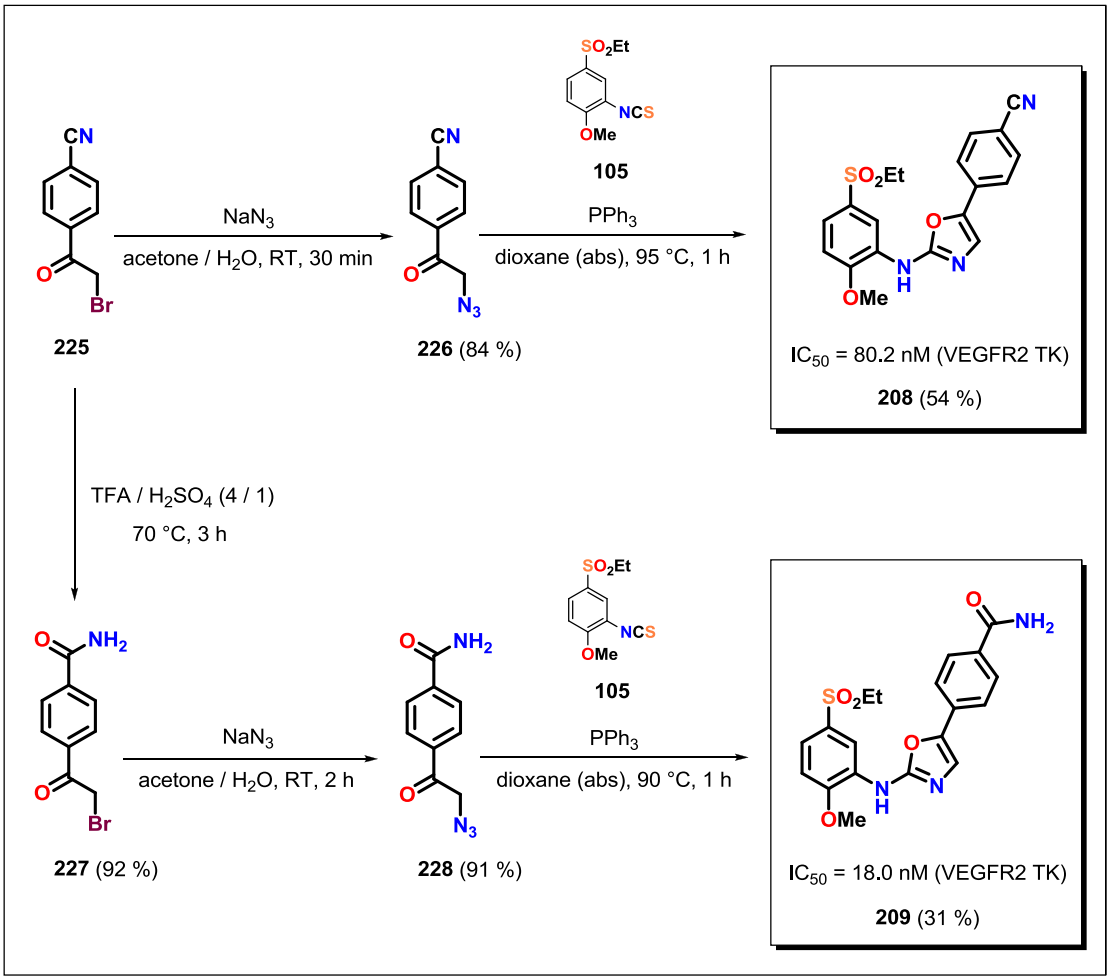

Scheme 30. Synthesis of *p*-substituted *N*,5-diaryloxazol-2-amines **208** and **209**.

The synthesis of **210**, **211** and **212** started from a commercially available methyl 4-acetylbenzoate (**229**) which was transformed to its bromo derivative **230** by trimethylphenylammonium tribromide in THF (abs) in 66 % yield. The compound **230** was then used in a reaction with NaN_3 in a mixture of acetone / H_2O yielding 87 % of azide **231**. The target oxazolester **210** was prepared by the thermic PPh_3-mediated oxazolation reaction of **231** with the isothiocyanate **105** in 67 % yield. The oxazolester **210** was transformed to the target oxazolecarboxylic acid **211** by a thermal hydrolysis with $LiOH.H_2O$ in a mixture of THF / H_2O in 80 % yield. Our original attempts to prepare the oxazolehydroxamic acid derivative **212** were through a direct reaction of the oxazole ester

210 with $NH_2OH.HCl$ in the presence of KOH in MeOH (abs)[130] or by a reaction of oxazolecarboxylic acid **211** with $NH_2OH.HCl$ in the presence of NMM and T3P (50 % w/w in EA) in CH_3CN (abs).[131] Both of the above reactions provided a mixture of **211** and **212** which was very difficult to purify by FLC or by crystallization. Finally we decided to perform an amide coupling reaction of the oxazolecarboxylic acid **211** with $BnONH_2.HCl$, HOBt, EDC.HCl and Et_3N in CH_2Cl_2 (abs) providing benzyl-protected oxazolehydroxamic acid **232** in 79 % yield. The intermediate **232** was purified by FLC and the isolated product was deprotected by hydrogenolysis in the presence of 10 % Pd / C in MeOH (abs) yielding 60 % of the target oxazolehydroxamic acid **212**. (Scheme 31)

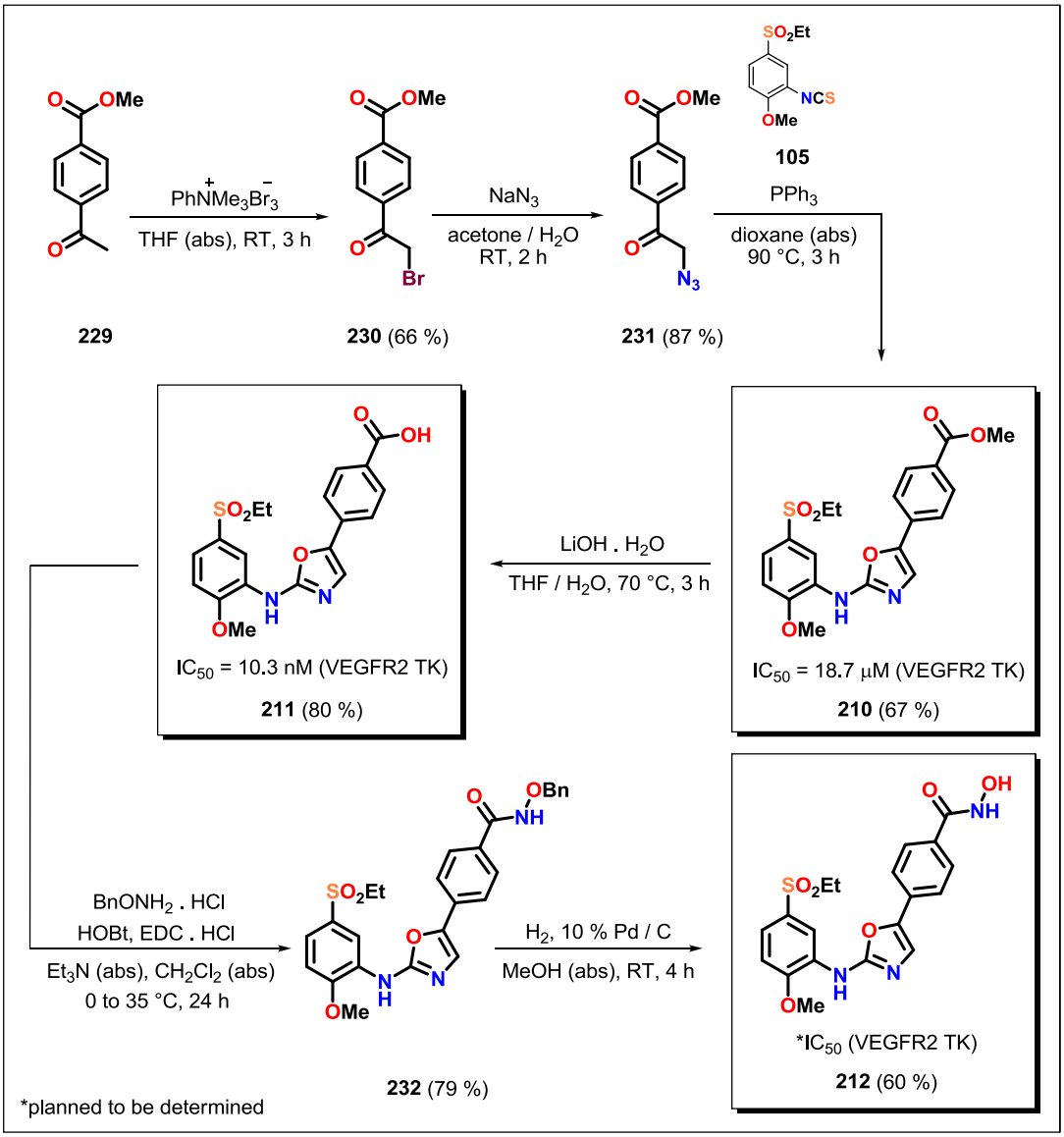

Scheme 31. Synthesis of *p*-substituted *N*,5-diaryloxazol-2-amines **210**, **211** and **212**.

[130] Rakshit, S.; Grohmann, C.; Besset, T.; Glorius, F. *J. Am. Chem. Soc.* **2011**, *133*, 2350 – 2353.
[131] Vasantha, B.; Hemantha, H. P.; Sureshbabu, V. V. *Synthesis* **2010**, *17*, 2990 – 2996.

7.2. Synthesis of *m*-substituted *N*,5-diaryloxazol-2-amines 213, 214, 215, 216, 217

A synthetic approach leading to the preparation of *m*-substituted *N*,5-diaryloxazol-2-amines **213**, **215**, **216** and **217** was inspired by the synthesis of their *p*-substituted analogues. A synthesis of the derivative **214** was more specific and required further literature research.

The synthesis of **213** started from a commercially available 1-(3-bromophenyl)ethanone (**197**) which was transformed to benzonitrile **233** using a Pd-catalyzed cyanation with $Zn(CN)_2$ in DMF (abs) in 96 % yield. The compound **233** was treated with trimethylphenyl ammonium tribromide in THF (abs) providing its bromo derivative **234** in 90 % yield. The compound **234** was then used in a reaction with NaN_3 in a mixture of acetone / H_2O yielding 75 % of azide **235**. The target oxazole benzonitrile **213** was prepared by the thermic PPh_3-mediated heterocyclization of **235** with the isothiocyanate **105** in 38 % yield. The similar synthesis of **213** in CH_2Cl_2 (abs) at RT has been previously published in the literature with in only 1 % yield.[6] The reduction of **213** to the oxazoleamine **214** was carried out using a standard catalytic hydrogenation in the presence of 10 % Pd / C and HCl in MeOH (abs)[132] or by a non-catalytic reaction with $LiAlH_4$ in THF (abs).[133] After performing these reactions we observed serious problems with the reactivity of **213** and low stability of the oxazoleamine **214** (as free amine) resulting in the formation of mixtures containing many unidentified products with only a very small content of **214**. The successful synthesis of the oxazoleamine hydrochloride **214** was done in 72 % yield by a fluoride activated hydrosilylation of **213** with $PhSiH_3$ and TBAF in toluene (abs) followed by a hydrolysis with 1 M HCl in MeOH. (Scheme 32)

[132] Vidal Juan, B.; Forns Berenguel, M. P.; Castillo Mcquade, M.; Erra Sola, M.; Mir Cepeda, M. *Almirall, S.A.* **2012**, WO2012/41476, A1.

[133] Beesu, M.; Caruso, G.; Salyer, A. C. D.; Khetani, K. K.; Sil, D.; Weerasinghe, M.; Tanji, H.; Ohto, U.; Shimizu, T.; David, S. A. *J. Med. Chem.* **2015**, *58*, 7833 – 7849.

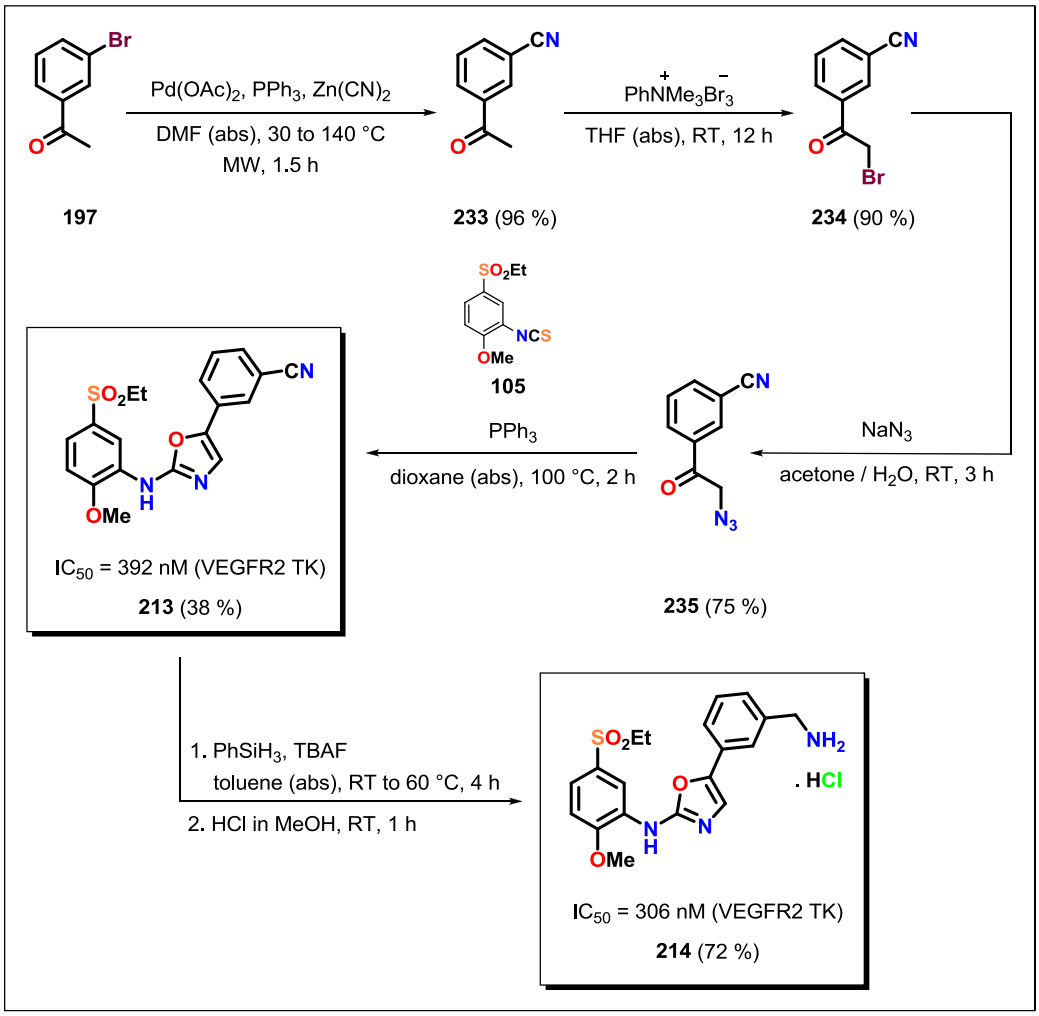

Scheme 32. Synthesis of *m*-substituted *N*,5-diaryloxazol-2-amines **213**, **214**.

The synthesis of **215** – **217** started from a commercially available methyl 3-acetylbenzoate (**236**) which was transformed to its bromo derivative **237** by trimethylphenylammonium tribromide in THF (abs) in 76 % yield. The compound **237** was then used in a reaction with NaN_3 in a mixture of acetone / H_2O yielding 58 % of azide **238**. The target oxazolester **215** was prepared by the thermic PPh_3-mediated heterocyclization of **238** with the isothiocyanate **105** in 58 % yield. The oxazolester **215** was then transformed to the target oxazolecarboxylic acid **216** by a thermal hydrolysis with $LiOH.H_2O$ in a mixture of THF / H_2O in 97 % yield.

The compound **216** was converted in the amide coupling reaction with $BnONH_2.HCl$, HOBt, EDC.HCl and Et_3N in CH_2Cl_2 (abs) to benzyl-protected oxazolehydroxamic acid **239** in 67 % yield. The intermediate **239** was purified by FLC and the isolated product was deprotected by hydrogenolysis in the presence of 10 % Pd / C in MeOH (abs) yielding 67 % of the pure target oxazolehydroxamic acid **217**. (Scheme 33)

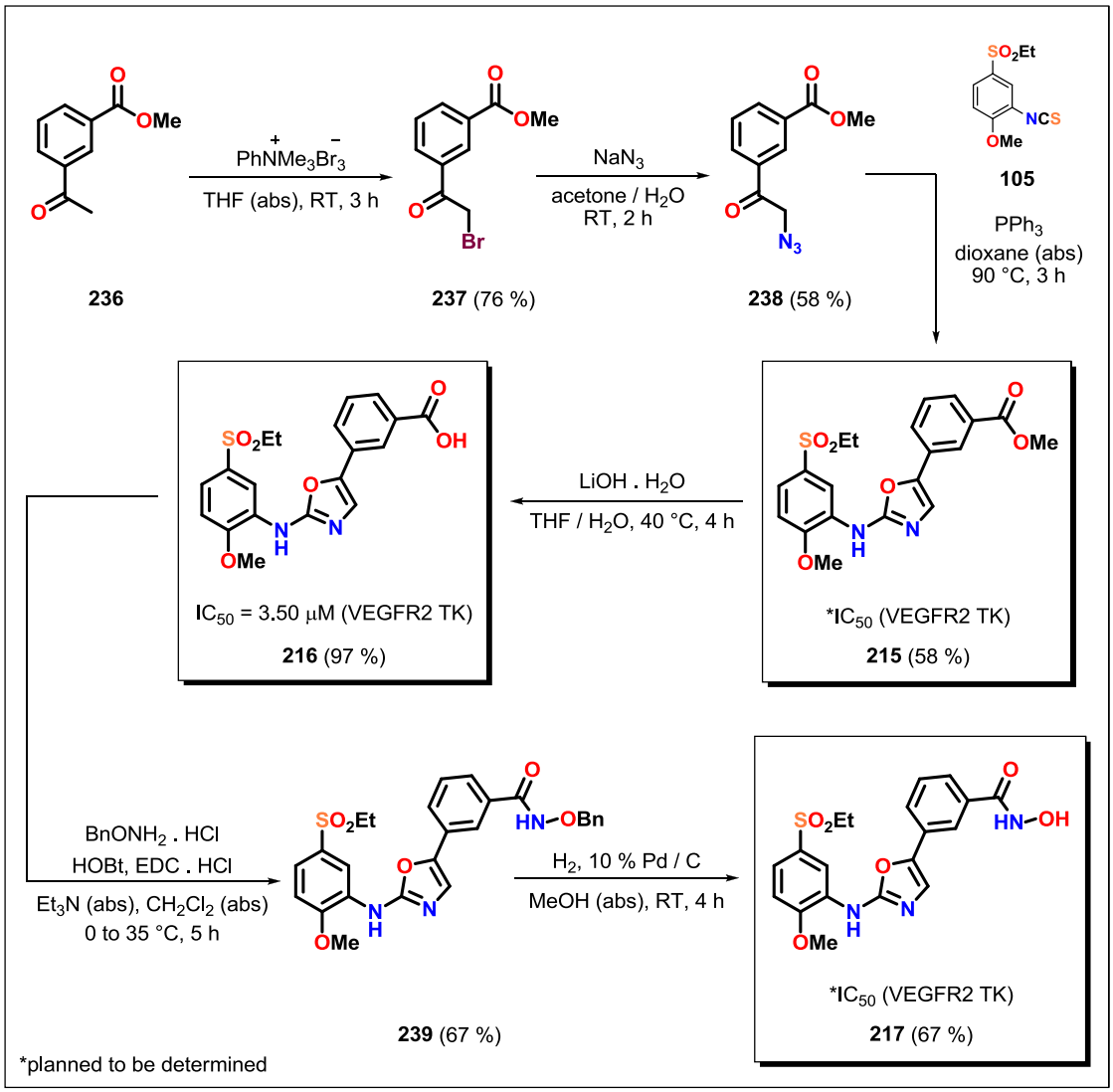

Scheme 33. Synthesis of *m*-substituted *N*,5-diaryloxazol-2-amines **215**, **216** and **217**.

7.3. Synthesis of *m*-substituted heterocyclic *N*,5-diaryl oxazol-2-amines 218, 219, 220, 221, 222, 223

A preparation of the *m*-substituted heterocyclic *N*,5-diaryloxazol-2-amines **218** – **221** started from the coupling precursor **107** successfully used also for the preparation of the compounds **2**, **189**, **190**, **191** and **192** within the project *RegBio*. (Scheme 25)

The compound **218** was prepared in 50 % yield by quite unconventional direct coupling reaction of **107** with imidazole (**240**). The reaction was performed in the presence of $Pd(OAc)_2$ and CuI in DMF (abs) at 150 °C. The mechanism of this reaction is probably very similar to the Sonogashira coupling. The compound **219** was prepared in 80 % yield

by the Stille coupling reaction of **107** with organostannane **241** in the presence of $Pd(PPh_3)_4$ and Bu_4NBr in CH_3CN (abs). The compounds **220** and **221** were prepared by the Suzuki coupling reaction of **107** with boronic acid **242**, resp. boronic acid pinacol boronate **243** in the presence of $Pd(PPh_3)_4$ and Na_2CO_3 in a mixture of DMF / H_2O in 90 %, resp. 83 % yield. All the utilized heterocyclic coupling reagents were obtained from commercial sources. (Scheme 34)

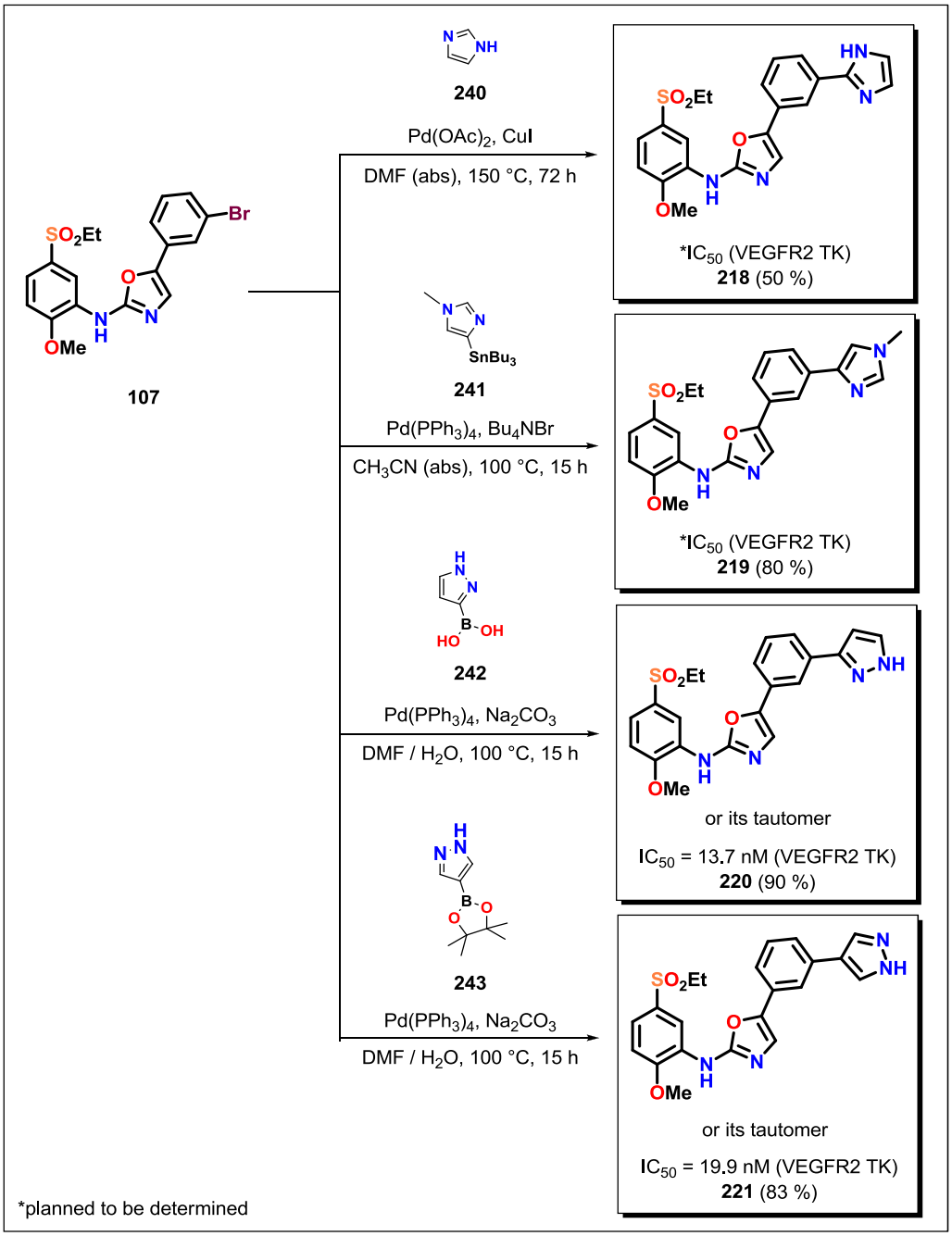

Scheme 34. Synthesis of *m*-substituted *N*,5-diaryloxazol-2-amines **218**, **219**, **220** and **221**.

Because of a limited availability of any 1*H*-imidazol-4-yl containing Stille or Suzuki coupling reagents and our unsuccessful attempts to perform the Miyaura borylation on 4-bromo-1*H*-imidazole (**246**) or its Boc-protected derivative **247** (only starting material was isolated), we decided to choose an opposite approach. We prepared a Suzuki coupling precursor **245** by the reaction of **107** with bis-(pinacolato)diboron (**244**) in the presence of $PdCl_2$(dppf) and KOAc in toluene (abs) in 84 % yield. Then we performed several test coupling reactions of **245** with 4-bromo-1*H*-imidazole (**246**) or with its Boc-protected derivative **247**. The reactions were examined under either specific conditions developed for Suzuki couplings of halo imidazoles ($Pd(OAc)_2$, CataCXiumA, K_2CO_3, dioxane / H_2O, 90 °C, 15 h)[134] or under the standard conditions we previously used for Suzuki couplings ($Pd(PPh_3)_4$, Na_2CO_3, DMF / H_2O, 100 °C, 15 h). Despite we detected the desired product **222** (always without the Boc-group) in the crude mixture; a homocoupling product of **245** was formed in the reaction prevailingly. Moreover because of the high polarity of **222** and relatively high basicity of imidazole derivatives in general (pK_a of the conjugated acid of imidazole is approximately 6.95), we have not managed to perform an effective purification by FLC (SiO_2). The preparation of **222** is currently under optimization. (Scheme 35)

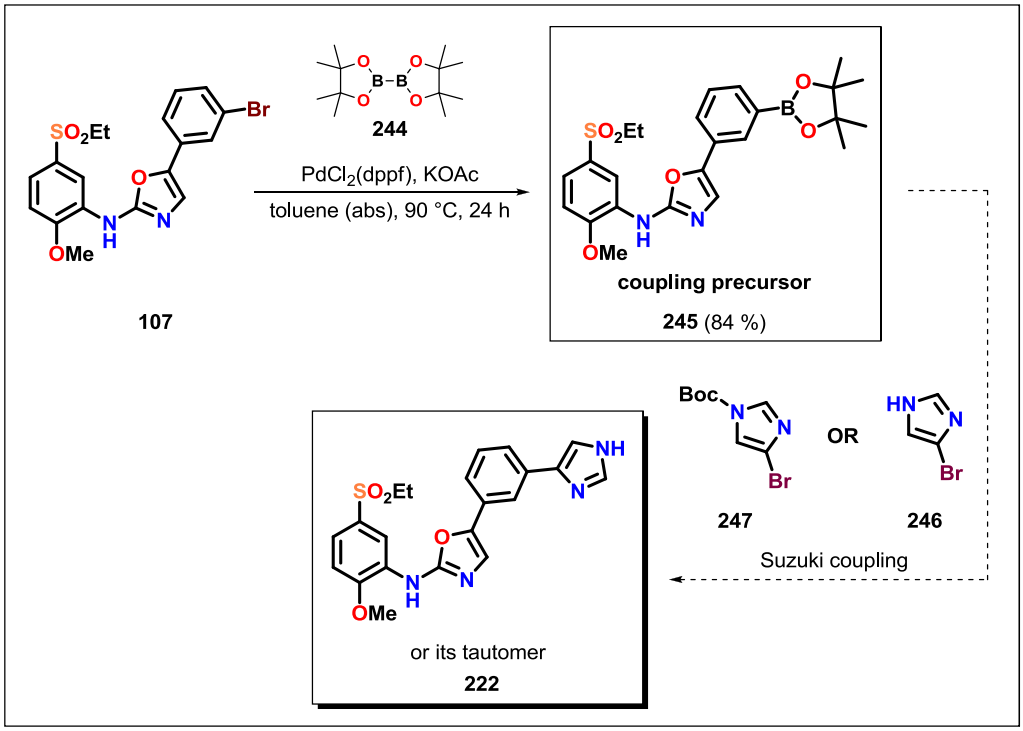

Scheme 35. Synthesis of *m*-substituted *N*,5-diaryloxazol-2-amine coupling precursor **245**.

[134] Tan, J.; Chen, Y.; Li, H.; Yasuda, N. *J. Org. Chem.* **2014**, *79*, 8871 – 8876.

An originally designed synthesis for the preparation of the triazole **223** originated from the compound **107** subsequently transformed by the Sonogashira coupling to its acetylene derivative which was meant to be transformed to the final product **223** by CuI-mediated click reaction with trimethylsilyl azide at 100 °C.[135] The synthesis failed in the last step because of low thermic stability of the acetylene derivative.

According to information from the literature, we designed a new synthetic procedure starting from the bromoacetophenone **197** which was transformed to acetylene derivative **248** in 61 % by the Sonogashira coupling reaction followed by a TMS deprotection. A click reaction of **248** with previously prepared azide derivative **187** in the presence of $CuSO_4.5H_2O$ and sodium L-ascorbate in a mixture of CH_2Cl_2 / H_2O provided *p*-methoxybenzyl-protected triazole **251** in 82 % yield. (Scheme 36) α-Brominated product **252** was then synthesized by a reaction of **251** with trimethylphenylammonium tribromide in THF (abs) in 71 % yield. The compound **252** was used in a reaction with NaN_3 in a mixture of acetone / H_2O yielding 77 % of azide **253**. The target triazole **223** was prepared by the thermic PPh_3-mediated heterocyclization of **253** with the isothiocyanate **105** (64 % yield) followed by a *p*-methoxybenzyl deprotection in refluxing TFA (51 % yield). (Scheme 36 cont.)

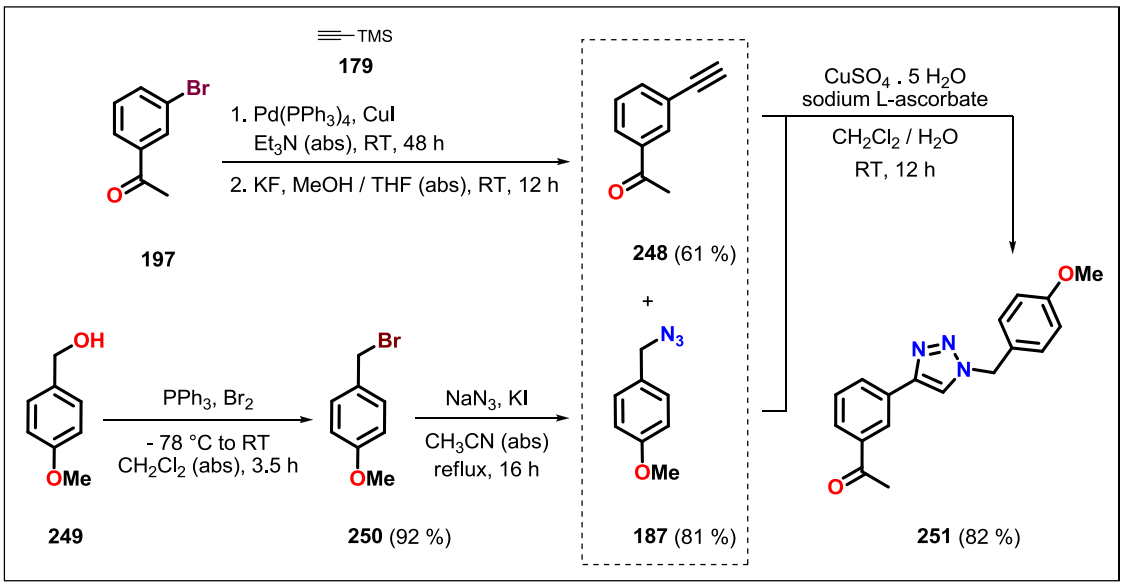

Scheme 36. Synthesis of *p*-methoxybenzyl-protected triazole **251**.

[135] Jin, T.; Kamijo, S.; Yamamoto, Y. *Eur. J. Org. Chem.* **2004**, 3789 – 3791.

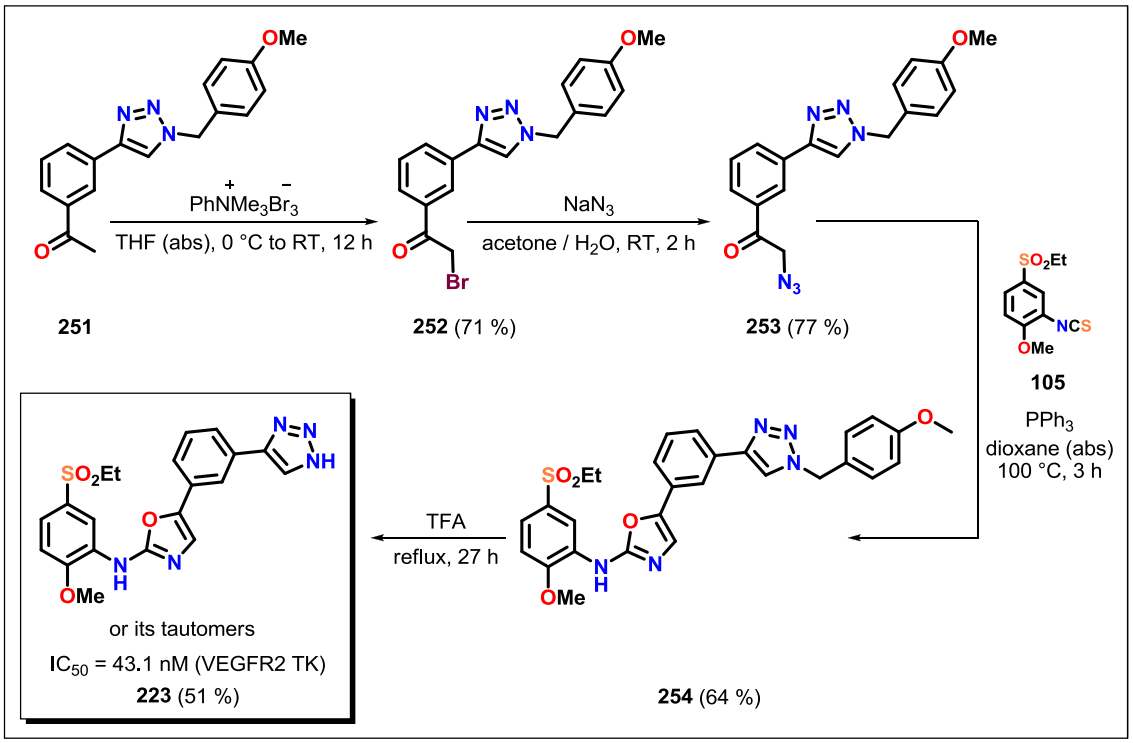

Scheme 36 cont. Synthesis of *m*-substituted *N*,5-diaryloxazol-2-amine **223**.

7.4. Synthesis of *p,m*-disubstituted heterocyclic *N*,5-diaryl oxazol-2-amines 4, 224

A synthesis of *p,m*-disubstituted heterocyclic *N*,5-diaryloxazol-2-amines **4** and **224** was performed only in a small scale due to the problems with stability, purification and characterization of some intermediates and therefore it has to be further optimized. This is the reason why this synthesis is not regularly presented in the experimental part of the thesis.

The synthetic procedure started with a transformation of aminoethanone **255** to benzonitrile **256** by a two-stage diazotation reaction in the presence of ^{t}BuONO, $BF_3.Et_2O$ in CH_2Cl_2 and CuCN, NaCN in H_2O. The compound **256** was isolated in 65 % yield. A following bromination of **256** was performed by Br_2 in $CHCl_3$ yielding 81 % of compound **257**. Azide derivative **258** was prepared from **257** treated with NaN_3 in MeOH. Because of a low stability of **258** resulting into very problematic FLC purification, a yield of this reaction was only estimated to 70 % by ^{1}H-NMR analysis of the crude product. Oxazole intermediate **259** was prepared by the thermic PPh_3-mediated heterocyclization of **258** with the isothiocyanate **105**. A yield of the reaction was estimated to 60 % by ^{1}H-NMR analysis

of the crude product for the same reasons mentioned above. A Stille coupling reaction of **259** with organostannane **154** in the presence of $Pd(PPh_3)_4$ and LiCl in dioxane (abs) provided the target oxazole **4** in 40 % yield. The target oxazole **224** was then prepared by an acid hydrolysis of **4** in a mixture of TFA / H_2SO_4 in 80 % yield. The target products **4** and **224** were prepared only in a small amount (ca 10 mg each). They were characterized by ^{1}H-NMR and MS analyses and used directly in the biological assay (IC_{50}, VEGFR2 TK). (Scheme 37)

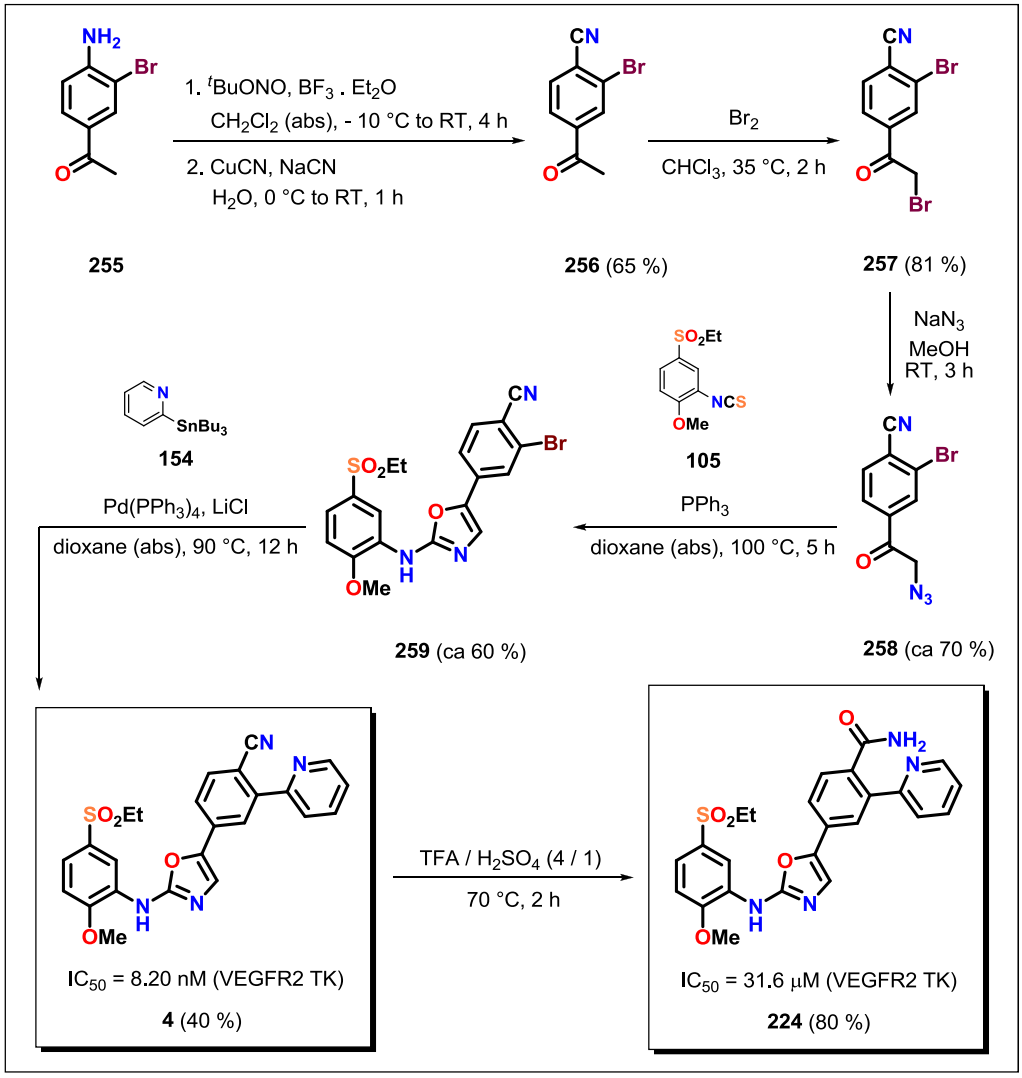

Scheme 37. Synthesis of *p*,*m*-disubstituted *N*,5-diaryloxazol-2-amines **4** and **224**.

7.5. Biological activity of the prepared compounds and evaluation of the SBCP project

Within the SBCP project we successfully prepared the series of the *p*-substituted *N*,5-diaryloxazol-2-amine derivatives **208** – **212** and their *m*-substituted analogues **213** – **217**. We also determined the *in vitro* inhibitory activity IC_{50} (VEGFR2 TK) of **208**, **209**, **210**, **211**, **213**, **214** and **216**. All biological assays were done by Reaction Biology Corp., USA.[19] (Chapter 2.2) An activity determination of the *m*-substituted ester **215** and the pair of hydroxamic acids **212**, **217** is planned to be carried out soon. (Figure 56 and 57)

The synthesis and inhibitory activity (IC_{50}, VEGFR2 TK) of the derivatives **208**, **209** and **213** were already published by Harris *et al.*[6] We prepared and analyzed these compounds as comparative standards for the biological assay verification. The same approach was chosen when the *RegBio* project was evaluated. The *p*-substituted derivatives **210**, **211**, **212** and *m*-substituted derivatives **214**, **215**, **216**, **217** were prepared as new compounds and fully characterized.

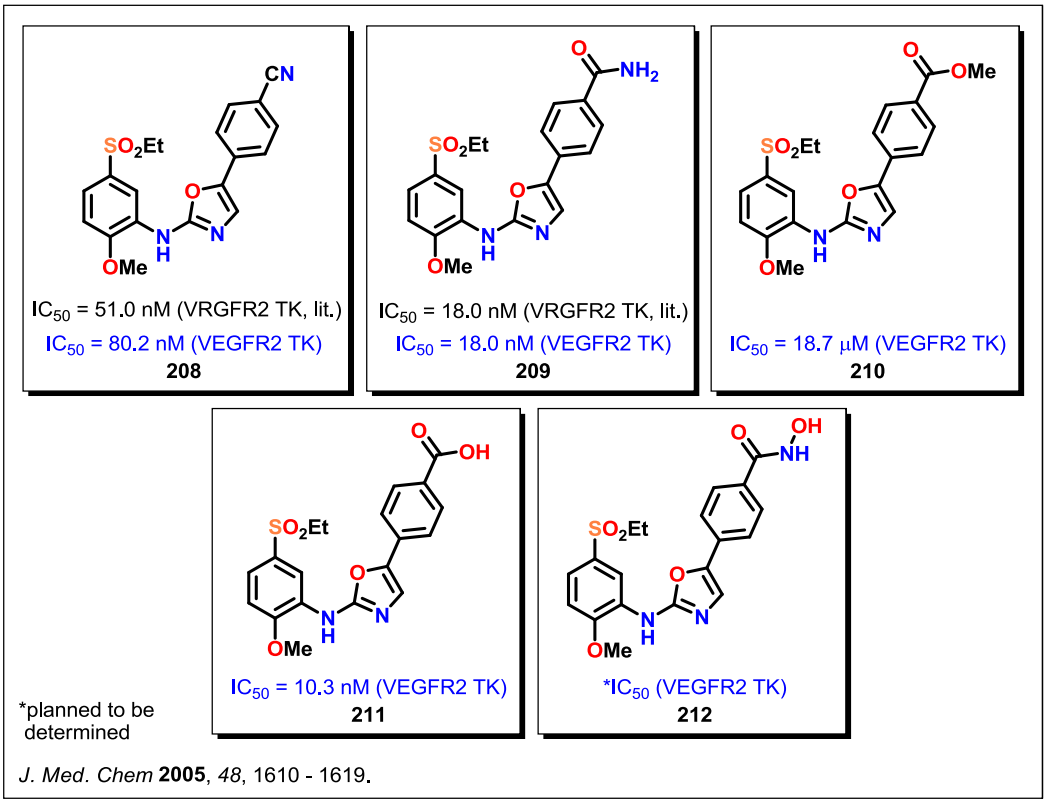

Figure 56. Overview of the prepared *p*-substituted *N*,5-diaryloxazol-2-amines **208**, **209**, **210**, **111** and **212** together with their inhibitory activities (if available).

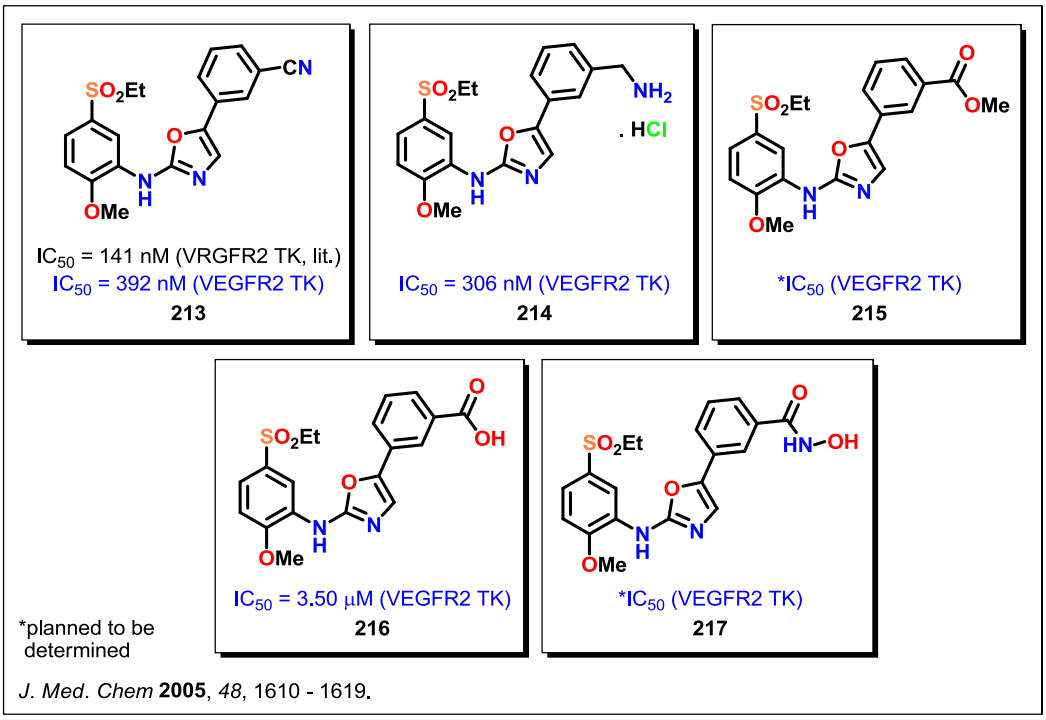

Figure 57. Overview of the prepared *m*-substituted *N*,5-diaryloxazol-2-amines **213**, **214**, **215**, **216** and **217** together with their inhibitory activities (if available).

We proposed the theory that suitably *p*-substituted *N*,5-diaryloxazol-2-amines interacting in the SBCP binding region of VEGFR2 TK active site should exhibit an increased inhibitory activity. The results obtained from the performed biological assays and subsequent comparative study confirmed this suggestion. The tested *p*-substituted benzonitrile **208** and carboxylic acid **211** showed noticeable higher activities than their *m*-substituted analogues **213** and **216**. Especially the carboxylic acid **211** showed very good inhibitory potency. (Figure 58)

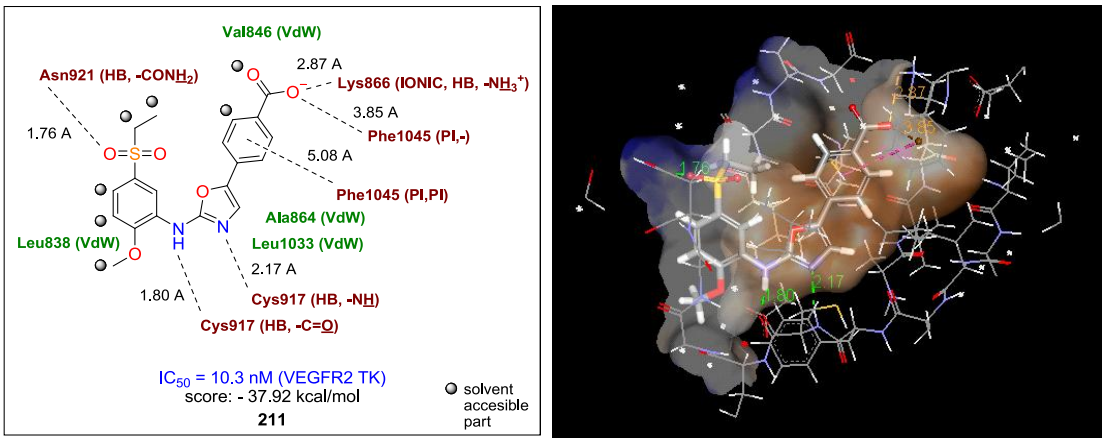

Figure 58. Interaction analysis, activity and predicted binding position of **211** in the VEGFR2 TK ATP-binding site.

The high inhibitory activity was detected also for the *p*-substituted amide **209**. The *m*-substituted derivative **214** containing a terminal amine group showed lower activity that was expected. The terminal amine group was chosen because the assumed ability to form a cation, π-interaction with Phe1045 in its protonised form. Unfortunately, the low activity value of **214** together with its *in silico* predicted interaction map suggest the protonised amine interacts more likely with a polar cytosolic fluid. (Figure 59)

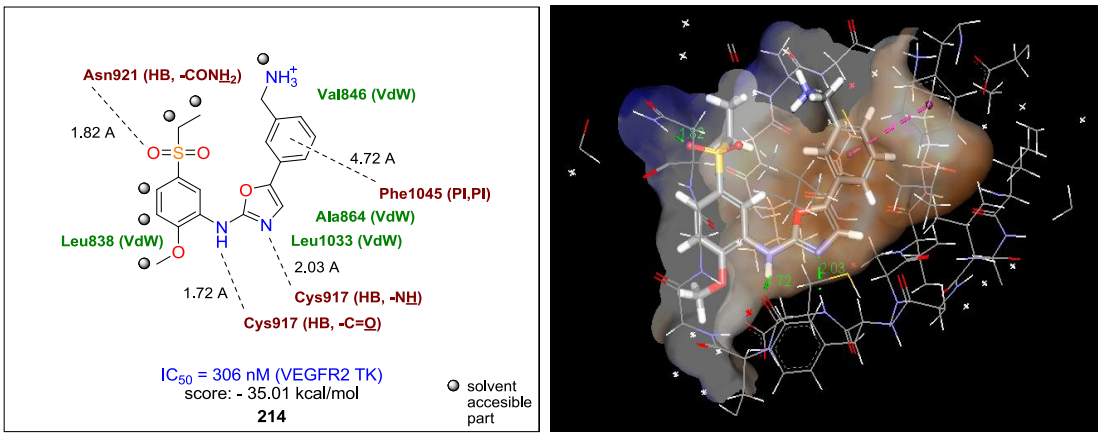

Figure 59. Interaction analysis, activity and predicted binding position of **214** in the VEGFR2 TK ATP-binding site.

Despite of the promising prediction, only *p*-substituted derivative showing quite low activity was the ester **210** (probably because of its lower polarity or adverse steric effect). (Figure 60)

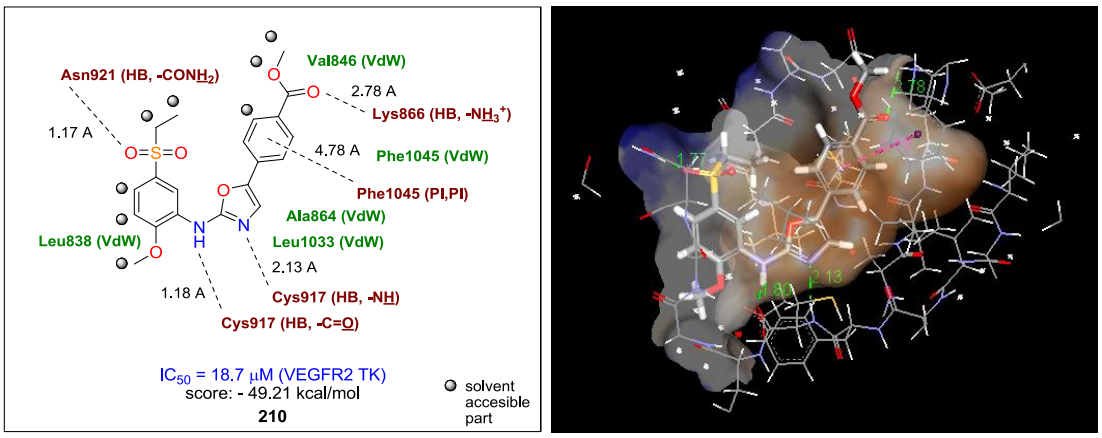

Figure 60. Interaction analysis, activity and predicted binding position of **210** in the VEGFR2 TK ATP-binding site.

With the aim of better binding examination within the SBCP and the synthesis of wider range of VEGFR2 TKIs, we predicted and prepared the series of *m*-substituted heterocyclic *N*,5-diaryloxazol-2-amines **218**, **219**, **220**, **221**, **223** and *p*,*m*-disubstituted heterocyclic derivatives **4**, **224**. (Figure 61) We also sucesfully determined a biological activity of the derivatives **220**, **221**, **223**, **4** and **224**. All biological assays were done by Reaction Biology Corp., USA.[19] (Chapter 2.2) An activity determination of **218** and **219** is planned to be carried out soon.

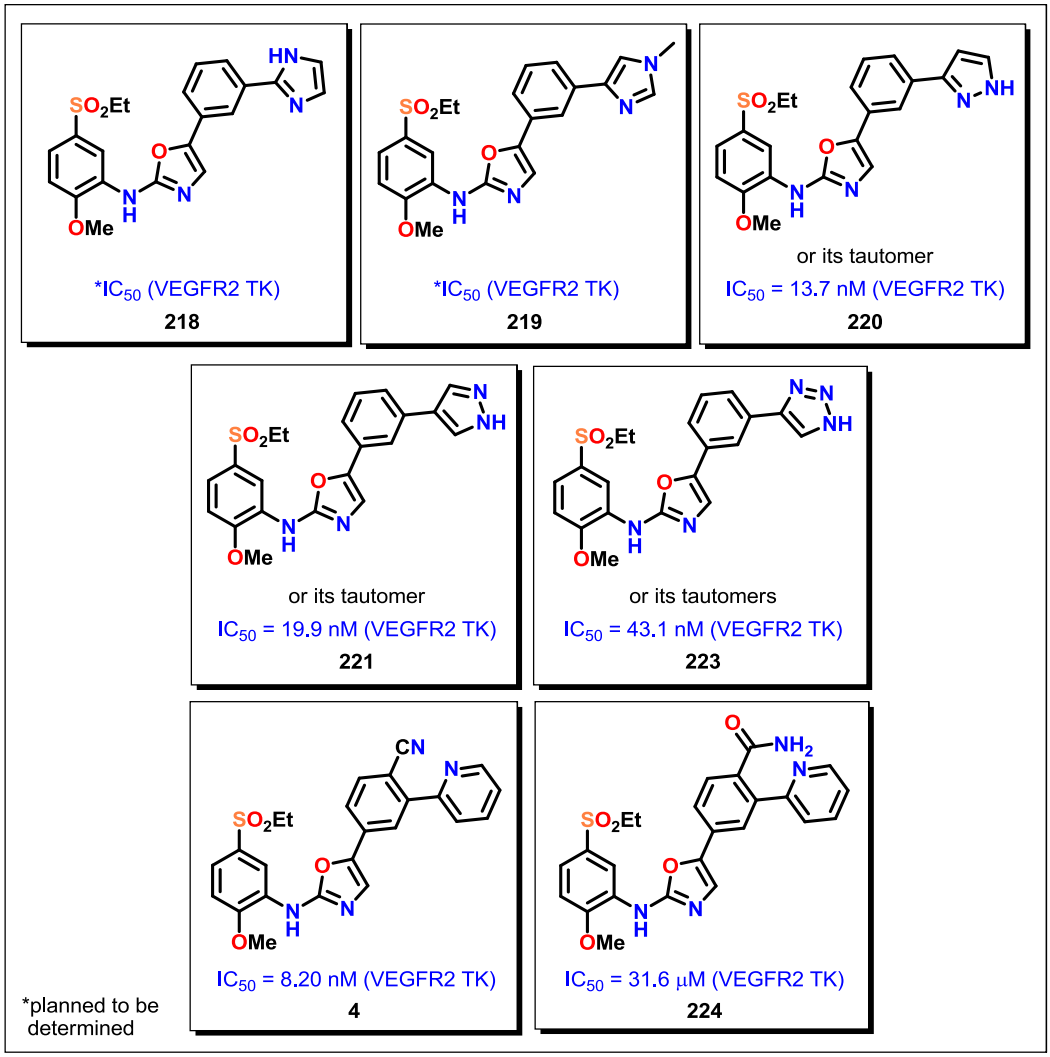

Figure 61. Overview of the prepared *m*-substituted and *p*,*m*-disubstituted heterocyclic *N*,5-diaryloxazol-2-amines **218**, **219**, **220**, **221**, **223**, **4** and **224** together with their inhibitory activities (if available).

The compounds **218**, **219** and **222** containing the imidazole *m*-substituent were designed as bioisosteres of the *m*-pyridine derivate **2** (AAZ) discussed within the *RegBio* project. (Chapter 6) Besides of the beneficial interactions in the hydrophobic pocket of VEGFR2

TK ATP-binding site known for **2** (AAZ), we expected also an additional induced dipole interaction between possibly protonised imidazole nitrogen in position 3 (pK_a of the conjugated acid is approximately 6.95) and Phe1045. Unfortunately, because the biological activities of **218** and **219** are still unknown and the synthesis of **222** is in progress, we are not able to confirm this theory.

The *m*-substituted pyrazole derivatives **220**, **221** and triazole **223** were designed as bioisosteres of the *m*-pyrrole derivative **191** from the *RegBio* project. (Chapter 6) Besides of the previously mentioned interactions in the hydrophobic pocket, we expected also an additional H-bond interaction of the heterocyclic –NH– group with Glu833, resp. Val912. According to the good inhibitory activities obtained for all three derivatives, our expectations could be evaluated positively. We can also assume that the observed slight activity decrease is probably caused by higher polarities of **220**, **221** and especially **223** in comparison with **191**. (Figure 62 and 63)

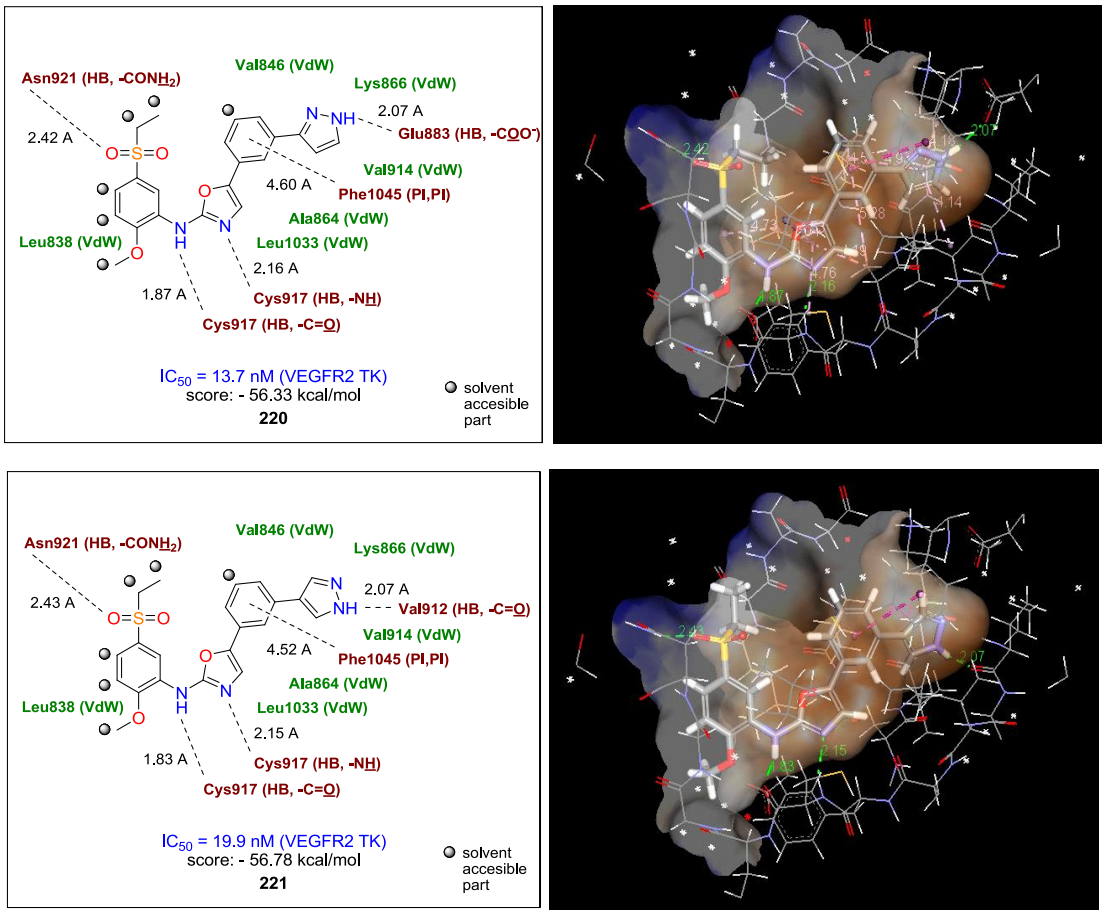

Figure 62. Interaction analyses, activities and predicted binding positions of **220** and **221** in the VEGFR2 TK ATP-binding site.

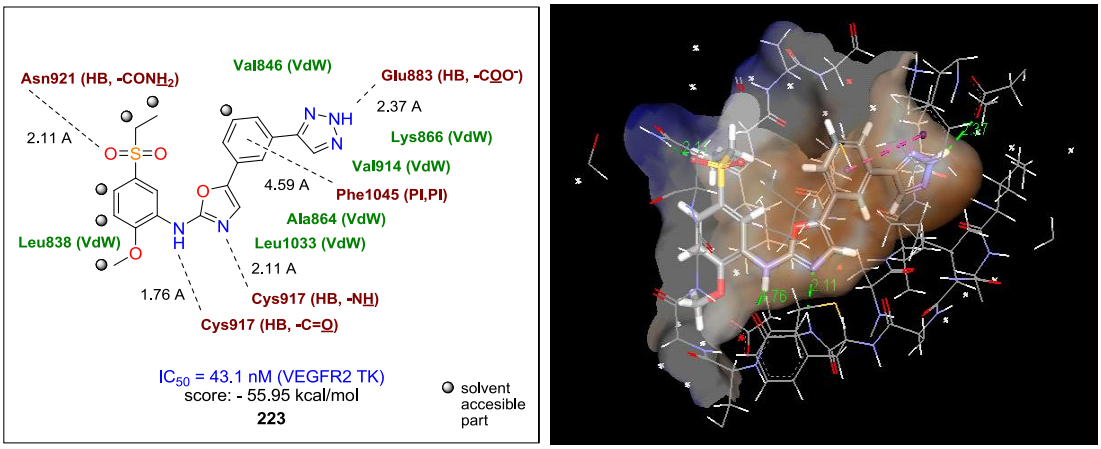

Figure 63. Interaction analysis, activity and predicted binding position of **223** in the VEGFR2 TK ATP-binding site.

Finally the *p*,*m*-disubstituted derivatives **4** and **224** were designed to have a synergic interaction pattern combining the hydrophobic interactions of the pyridine substituent in *m*-position (known for **2** (AAZ)) and the H-bond, resp. ionic interactions provided by the suitable substituent in *p*-position (known for **208**, **209** etc.). After we obtained the biological activity results, the proposed synergic effect was confirmed in the nitrile derivative **4**. An increase of the inhibitory activity of **4** compared to **2** and **208** was approximately tenfold. Surprisingly, the activity of the amide derivative **224** was in comparison to **2** and **209** significantly decreased. We assume that this activity decrease is caused by unfavorable interactions between the amide and pyridine substituent of **224** (intramolecular H-bond, steric hindrance…) disrupting an ideal active conformation in the VEGFR2 TK ATP-binding site. (Figure 64 and 65)

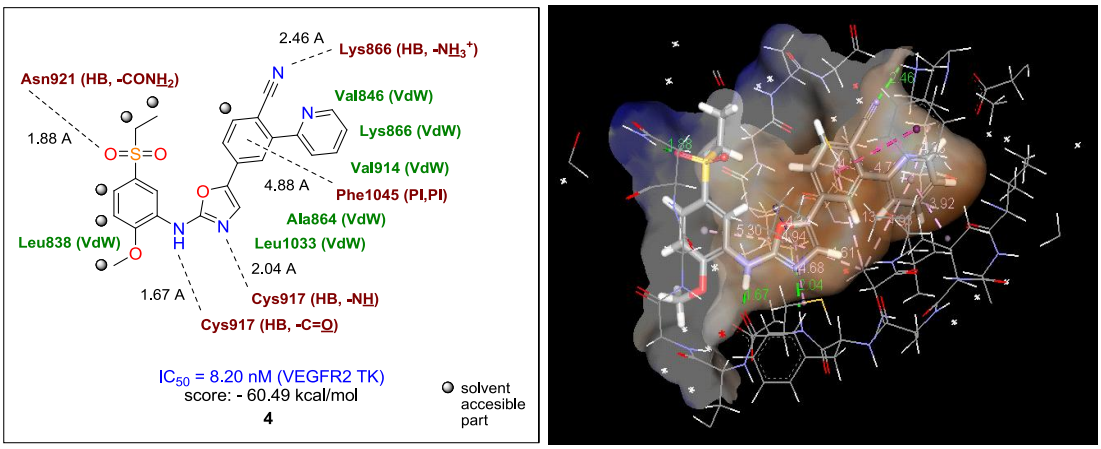

Figure 64. Interaction analysis, activity and predicted binding position of **4** in the VEGFR2 TK ATP-binding site.

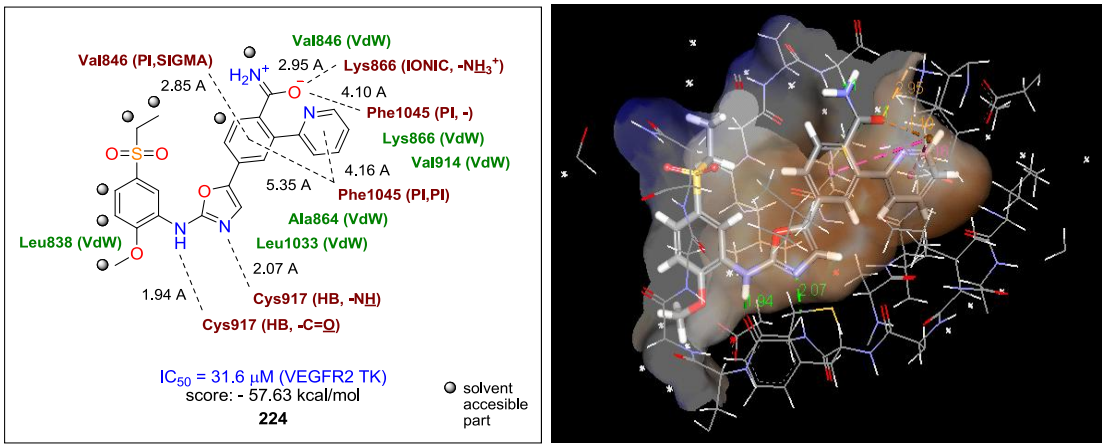

Figure 65. Interaction analysis, activity and predicted binding position of **224** in the VEGFR2 TK ATP-binding site.

Summing-up the SBCP project, the proposed series of *p*- and *m*-substituted *N*,5-diaryloxzole-2-amine derivatives **208** – **217** were prepared and most of them were biologically screened with very good results. We also prepared the series of *m*-substituted and *p*,*m*-disubstituted heterocyclic derivates **218**, **219**, **220**, **221**, **223**, **4**, **224** and successfully determined the biological activity in the most cases. An optimization of syntheses of the imidazole **222** and *p*,*m*-disubstituted derivatives **4**, **224** is currently in progress. As we achieved the good results from the performed biological assays, made the interaction analyses and predictions supporting our hypothesis, the SBCP project is going to be finalized and published in a short time.

Chapter 8. **Project – CLK1 inhibition**

8. Project – CLK1 inhibition

Inhibitors of CLK protein kinases suppress cell growth and induce apoptosis by modulating pre-mRNA splicing in cancer. CLK family kinases are also involved in alternative splicing and RNA processing in Duchenne muscular dystrophy, Alzheimer's disease, HIV-1, and influenza virus.

Our research within the CLK1 inhibition project resulted in a discovery of four novel CLK1 inhibitors **97**, **260**, **261** and **98** possessing the *N*,5-diaryloxazol-2-amine scaffold. (Figure 66) The discovery included a determination of the corresponding inhibitory activities against CLK1 and some other CMGC kinases, a prediction of CLK binding poses, together with synthesis and complete physico-chemical characterization of the developed inhibitors. Additionally, analysis of all PDB available CLK structures and their ligand interactions were performed.

As we determined by searching Reaxys / SciFinder database, there are only few powerful dual CLK / VEGFR TK inhibitors known in the literature. We proposed that our inhibitors have similar binding poses and interactions in CLK1, 3 and VEGFR2 TK mostly due to the *N*,5-diaryloxazol-2-amine pharmacophoric fragment. One of our developed inhibitors (**98**) already proved a good activity against both VEGFR2 and CLK1 enzymes. The research and obtained results have been already published in the literature.[77] The manuscript is attached in the corresponding chapter. (Chapter 15)

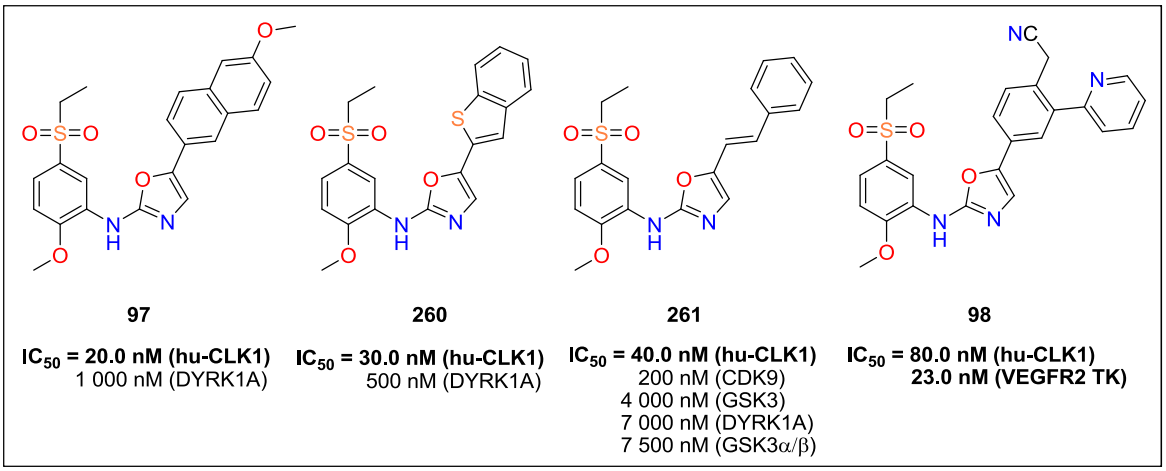

Figure 66. Developed CLK1 inhibitors **97**, **260**, **261** and **98** together with their biological activities determined against some CMGC protein kinases or VEGFR2 TK.

Within this dissertation thesis, we developed a methodology for the preparation of an important aldehyde precursor **269** which was used in the synthesis of the highly active CLK1 inhibitor **261**. The synthesis started by a reaction of commercially available ethyl 2-chloroacetate (**262**) with ethyl formate (**263**) in the presence of ^{t}BuOK in THF (abs) which provided (*E*)-ethyl 2-chloro-3-hydroxyacrylate (**264**) in 73 % yield. The compound **264** was subsequently transformed to 2-aminooxazole **265** by the cyclization reaction with urea in H_2O in 51 % yield. A diazotation reaction of **265** in the presence of ^{t}BuONO, $CuCl_2$ (abs) in CH_3CN yielded 83 % of 2-chlorooxazole **266**. An addition-elimination reaction of **266** with the aniline **122** in ^{i}PrOH (abs) provided *N*-aryloxazol-2-amine derivative **267** in 65 % yield. An ester group of **267** was then reduced by $LiAlH_4$ in THF (abs) yielding 82 % of alcohol derivative **268**. The final aldehyde precursor **269** was prepared by an oxidation of **268** by MnO_2 in CH_2Cl_2 (abs) in 56 % yield. (Scheme 38)

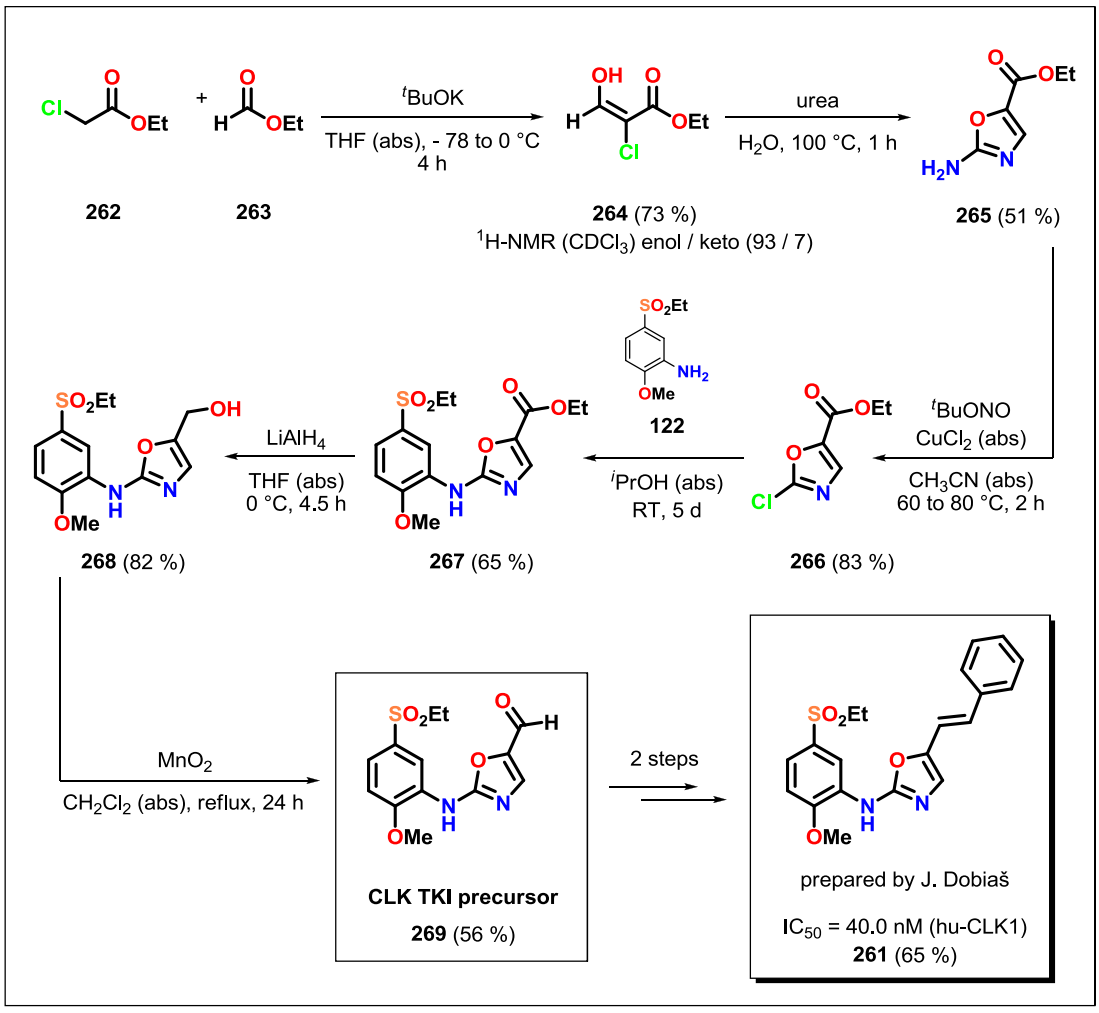

Scheme 38. Synthesis of CLK1 inhibitor precursor **269**.

Chapter 9. **Project – HCC and HCSCs influencing TKIs**

9. Project – HCC and HCSCs influencing TKIs

The Hepatocellular Carcinoma (HCC) is the sixth most frequent and second most deadly cancer worldwide. HCC patients are resistant to chemotherapy and radiotherapy, because conventional therapies can only reduce the bulk of the tumor mass but are unable to restrain tumor regrowth and relapse. HCC is a highly heterogeneous tumor in terms of morphology and as well as in clinical outcome.

Bioactivities of quinoides **270** – **274** (Figure 67) and VEGFR2 TKIs **275**, **2** (AAZ), **191** and **15** (Figure 68) were studied on hepatocellular cancer (HCC) and its cancer stem cells (HCSCs). The compounds exhibited IC_{50} values in μM concentrations in HCC cells. The quinoid **272** was able to eradicate cancer stem cells, similar to the action of HCSCs killer standard - DAPT. However more cytotoxic VEFGR TKIs including sorafenib **15**, which is the only FDA approved drug for the treatment of HCC, enriched the hepatocellular cancer stem cell population 2-3 fold after treatment. An aggressiveness factor (AF) characteristic was proposed to estimate a quality of drug candidates for their ability to eradicate CSCs sub population. Considering the tumor heterogeneity and HCSCs subpopulation enrichment upon TKIs treatment in patients, this study emphasized an importance of the chemotherapeutic agent choice synergistically acting on all the tumor subpopulations including its CSCs. The research and obtained results have been already published in the literature.[79] The manuscript is attached in the corresponding chapter. (Chapter 15)

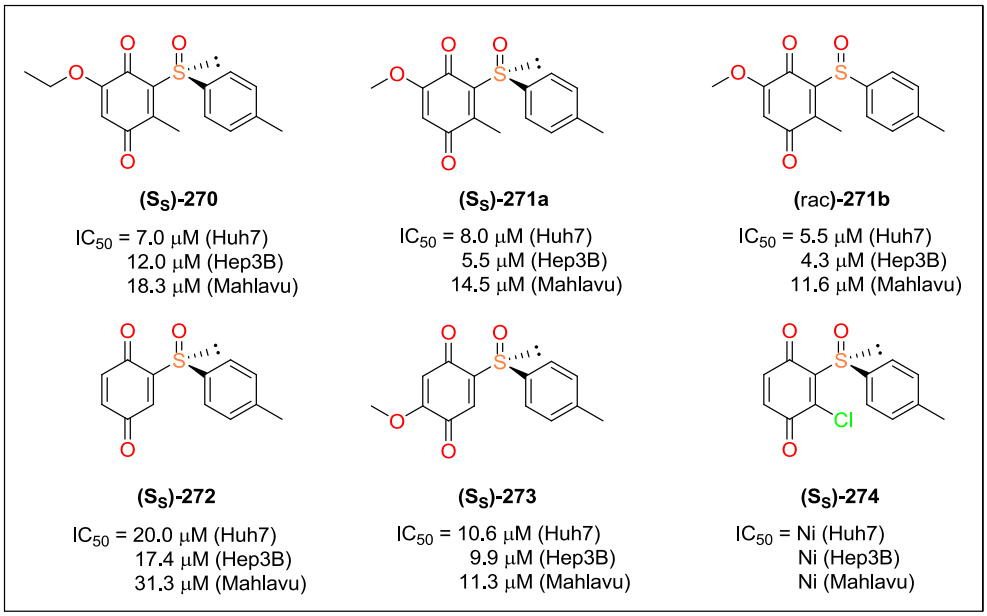

Figure 67. Chemical structures of the quinoides **270** – **274** together with their inhibitory activities.

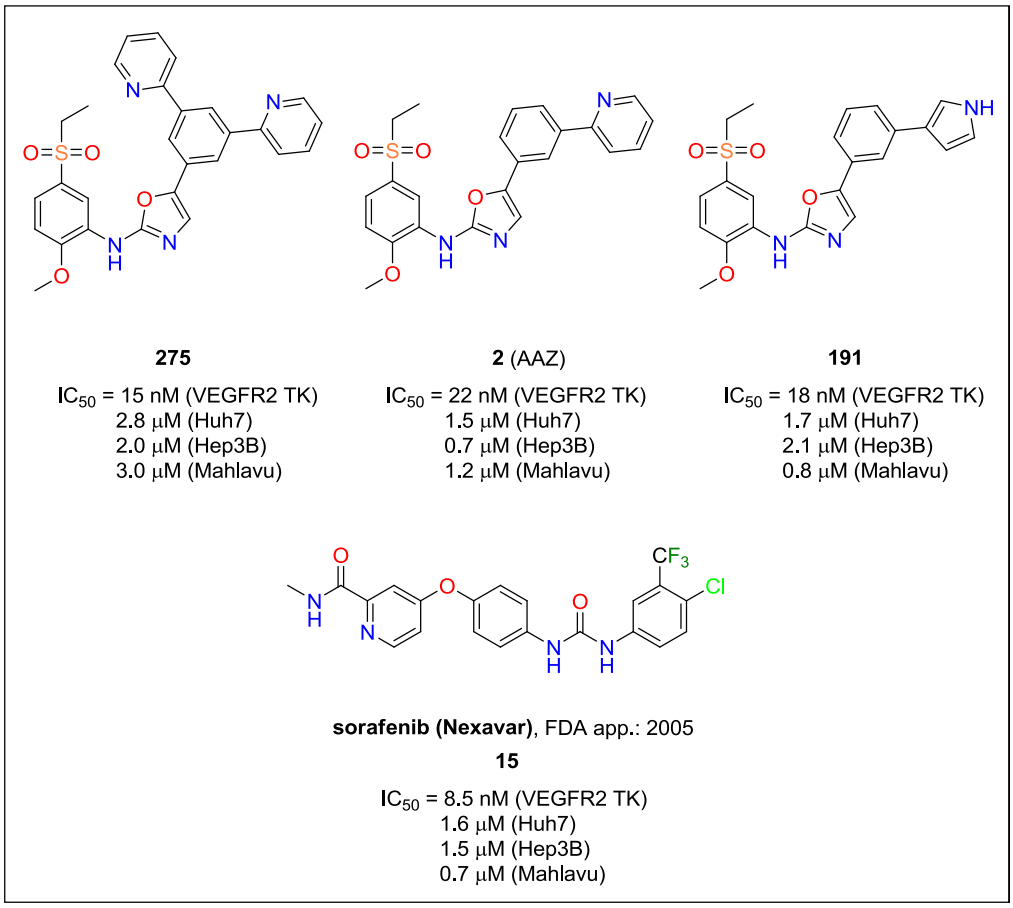

Figure 68. Chemical structures of the VEGFR2 TKIs **275**, **2** (AAZ), **191** and **15** together with their inhibitory activities.

Within this dissertation thesis, we prepared the examined series of VEGFR2 TKIs **275**, **2** and **191** (expect of the commercially available sorafenib **15**) and proposed the aggressiveness factor as the novel drug characteristic.

Chapter 10. **Conclusions**

10. Conclusions

Within the project Regioisomeric bioisostery (*RegBio*) we proposed that the regioisomeric *N*,4-diaryloxazol-2-amine **3** (AAZ-regio) is able to maintain the VEGFR2 TK inhibition properties known for the biologically active *N*,5-diaryloxazol-2-amine **2** (AAZ) (IC_{50} = 22.0 nM, VEGFR2 TK, lit.).[6] Compounds possessing the *N*,4-diaryloxazole-2-amine scaffold represent the novel chemical species and possibly a new class of VEGFR2 TKIs. With the goal of proving our theory, we designed a series of variously substituted *N*,5-diaryloxazol-2-amines **2** (AAZ), **189**, **190**, **191**, **192** and their *N*,4-diaryloxazol-2-amine analogues **3** (AAZ-regio), **193**, **194**, **195** and **196**. After completion of the synthesis, we intended to determine and evaluate their biological activities (IC_{50}, VEGFR2 TK).

We successfully prepared the series of *N*,5-diaryloxazol-2-amine derivatives **2**, **189**, **190**, **191** and **192**. We also determined the *in vitro* inhibitory activity (IC_{50}, VEGFR2 TK) of **2**, **189**, **191** and **192**. An activity evaluation of the compound **190** is planned to be determined soon. The compounds **189** and **191** showed high inhibitory activities against VEGFR2 TK, especially the activity of **189** reached nearly a sub-nanomolar inhibitor level.

We discovered that the published heterocyclizations for the preparation of *N*,4-diaryloxazol-2-amine derivatives from arylureas and α-bromoacetophenones provided 1,5-diarylimidazolidine-2,4-dione **204** when applied on our starting material. According to the interesting structure of **204**, we prepared and biologically screened the derivatives **206** and **207**. Unfortunately, no inhibitory activity against VEGFR2 TK was detected.

The *N*,4-diaryloxazol-2-amine precursor **205** was finally prepared by the AgOTf-mediated reaction of arylurea **203** and α-bromoacetophenone **198** in ca 10 % yield (^{1}H-NMR, crude). Analysis and further optimization of the reaction are currently in progress.

Because the synthesis of predicted *N*,4-diaryloxazol-2-amines **3**, **193**, **194**, **195** and **196** is not finished, we were not able to make the final comparison of the biological activities and evaluate the *RegBio* theory. However, based on the positive synthetic and biological results, the project is going to be finished in a short time.

Within the project Salt bridge containing pocket (SBCP) we discovered the specific intermediate conformation DFG-IN / OUT of VEGFR2 TK which can be stabilized by the interaction with *N*,5-diaryloxazol-2-amine ligands. In this conformation a new binding region in the VEGFR2 TK is created. We named this domain the Salt bridge containing

pocket (SBCP) because the present Lys866 and Glu833 residues are able to participate on the additional salt bridge, resp. H-bond interaction. According to our observations and information form the available literature, we proposed that suitably *p*-substituted derivatives of *N*,5-diaryloxazol-2-amine should posses an increased inhibitory activity.

With the aim of the further exploitation of the VEGFR2 TK and evaluation of the SBCP hypothesis, we focused on the development of *p*-substituted derivatives of *N*,5-diaryloxazol-2-amine **208** – **212**, their *m*-substituted analogues **213** – **217** and subsequent comparative analysis of their inhibitory activities. We also developed a series of *m*-substituted heterocyclic *N*,5-diaryloxazol-2-amine derivatives **218** – **223** possibly showing the hydrophobic interactions known for **2** (AAZ) and also the H-bond, resp. ionic interactions in the SBCP. With the same intention, we aimed to prepare a pair of *N*,5-diaryloxazol-2-amines **4**, **224** containing both a suitable *p*-substituent and a heterocyclic *m*-substituent hopefully resulting in the synergic kinase binding.

The both series of *p*-substituted derivatives **208** – **212** and their *m*-substituted equivalents **213** – **217** were successfully prepared. Inhibitory activities (IC_{50}, VEGFR2 TK) of **208**, **209**, **210**, **211**, **213**, **214** and **216** were determined. An activity determination of the *m*-substituted ester **215** and the pair of hydroxamic acids **212**, **217** is planned to be carried out soon. The results obtained from the biological assays and subsequent comparative studies suggest that our hypothesis was right. The tested *p*-substituted benzonitrile **208** and carboxylic acid **211** showed noticeable higher activities than their *m*-substituted analogues **213** and **216**. Especially the carboxylic acid **211** showed very good inhibitory potency. The high inhibitory activity was detected also for the *p*-substituted amide **209**.

We prepared the series of *m*-substituted heterocyclic *N*,5-diaryloxazol-2-amines **218**, **219**, **220**, **221**, **223** and *p*,*m*-disubstituted heterocyclic derivatives **4**, **224**. We determined a biological activity of the derivatives **220**, **221**, **223**, **4** and **224**. An activity determination of **218** and **219** will be carried out soon. The *m*-substituted pyrazole derivatives **220**, **221** and triazole **223** were expected to interact in the hydrophobic pocket and to exhibit an additional H-bond with Glu833 from the SBCP, resp. Val912. According to the good inhibitory activities obtained for all three derivatives, our expectations could be evaluated positively. Finally the *p*,*m*-disubstituted derivatives **4** and **224** were designed to have a synergic interaction pattern combining the hydrophobic interactions of the pyridine substituent in *m*-position and the H-bond, resp. ionic interactions in the SBCP provided by the substituent in *p*-position. After we obtained the biological activity values, we observed the proposed synergic effect on the nitrile derivative **4** resulting in the high inhibitory

activity. Surprisingly, the activity of the amide derivative **224** was significantly low. We assumed that this activity decrease is caused by unfavorable interactions between the amide and pyridine substituent of **224** (intramolecular H-bond, steric hindrance…) disrupting an ideal active conformation in the VEGFR2 TK ATP-binding site.

The CLK1 inhibition project resulted in a discovery of four novel CLK1 inhibitors **97**, **260**, **261** and **98** possessing *N*,5-diaryloxazol-2-amine skeleton. Moreover one of our developed inhibitors (**98**) proved a good activity against both CLK1 and VEGFR2 TK enzymes. Within this dissertation thesis, we developed a methodology for the preparation of an important aldehyde precursor **269** which was used in the synthesis of the highly active CLK1 inhibitor **261**. These research results have been already published in the literature.[77]

Within our last project, bioactivities of quinoides **270** – **274** and VEGFR2 TKIs **275**, **2** (AAZ), **191** and **15** were studied on hepatocellular cancer (HCC) and its cancer stem cells (HCSC). The compounds exhibited IC_{50} values in μM concentrations in HCC cells. Quinoid **272** was able to eradicate cancer stem cells, similar to the action of HCSCs killer standard - DAPT. However more cytotoxic VEFGR TKIs including sorafenib **15**, which is the only FDA approved drug for the treatment of HCC, enriched the hepatocellular cancer stem cell population 2-3 fold after treatment. An aggressiveness factor (AF) characteristic was proposed to estimate a quality of novel drug candidates for their ability to eradicate CSCs sub population. Within this dissertation thesis, we prepared the examined series of VEGFR2 TKIs **275**, **2** and **191** (expect of the commercially available sorafenib **15**) and proposed the aggressiveness factor characteristic. These research results have been already published in the literature.[79]

Summing up the dissertation thesis, we prepared 61 compounds (including the synthesis of **4** and **224**) from which 36 were new. From 28 predicted final compounds, we prepared 22 while 16 of them were biologically examined (IC_{50}, VEGFR2 TK) with outstanding results. The compounds **189**, **191**, **211**, **214**, **220**, **221**, **223** and **4** exhibited the activity under 500 nM.

Chapter 11. **Discussion and conclusions in French**

11. Discussion and conclusions in French

Ce travail de thèse s'articule autour du squelette diaryloxazole-2-amine qui a été utilisé comme « core central » des dérivés possédant une activité VEGFR2 TKIs. Ces composés ont été synthétisés dans le cadre de quatre projets : *RegBio*, SBCP, CLK1 et HCC.

11.1. Projet – Regioisomeric bioisostery (*RegBio*)

Dans le cadre du premier projet « bioisostérie régioisomérique » (*RegBio*) nous avons proposé que le composé *N*,4-diaryloxazol-2-amine **3** (AAZ-regio), régioisomère du composé biologiquement actif connu *N*,5-diaryloxazol-2-amine **2** (AAZ)[128] (IC_{50} = 22.0 nM, VEGFR2 TK, lit.)[6] soit capable de conserver les propriétés inhibitrices du VEGFR2 TK de ce dernier. Les composés possédant le squelette *N*,4-diaryloxazole-2-amine représentent de nouvelles espèces chimiques non protégées et potentiellement une nouvelle classe d'inhibiteurs de VEGFR2 TKs. (Figure 45 et 46)

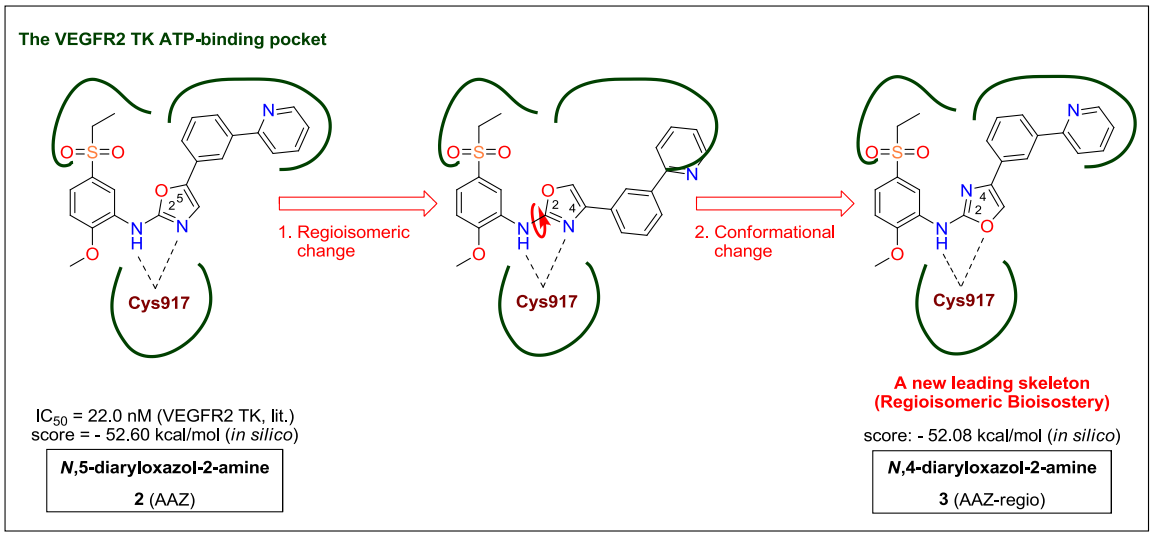

Figure 45. Bioisostérie régioisomérique - le changement régioisomérique approprié dans **2** (AAZ) suivi par le changement de conformation conduit au bioisostère **3** (AAZ-regio).

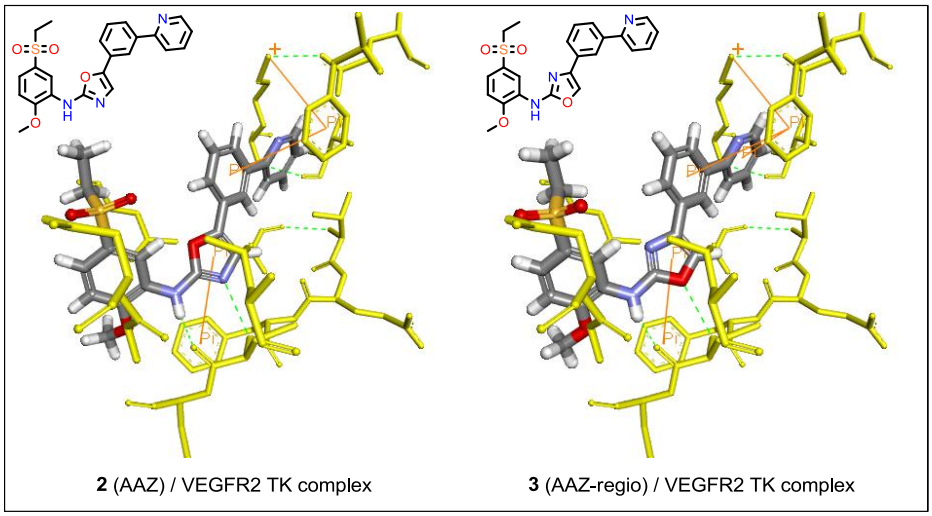

Figure 46. Les positions de liaison de l'inhibiteur **2** (AAZ) et de son analogue régioisomère **3** (AAZ-regio) dans le site actif de VEGFR2 TK.

Afin de prouver notre hypothèse, nous avons fait le design *in silico* d'une série de *N*,5-diaryloxazol-2-amines **2** (AAZ), **189** – **192** et de *N*,4-diaryloxazol-2-amines **3** (AAZ-regio), **193** – **196** différemment substituées. Après complétion de leur synthèse, nous avons évalué leur activité biologique (IC_{50}, VEGFR2 TK). Nous avons préparé avec succès une série de cinq dérivés *N*,5-diaryloxazol-2-amines **2** (AAZ), **189**, **190**, **191**, **192** et déterminé l'activité inhibitrice *in vitro* (IC_{50}, VEGFR2 TK) de quatre d'entre eux **2** (AAZ), **189**, **191** et **192**. L'activité du dérivé **190** est en cours d'évaluation. (Figure 69)

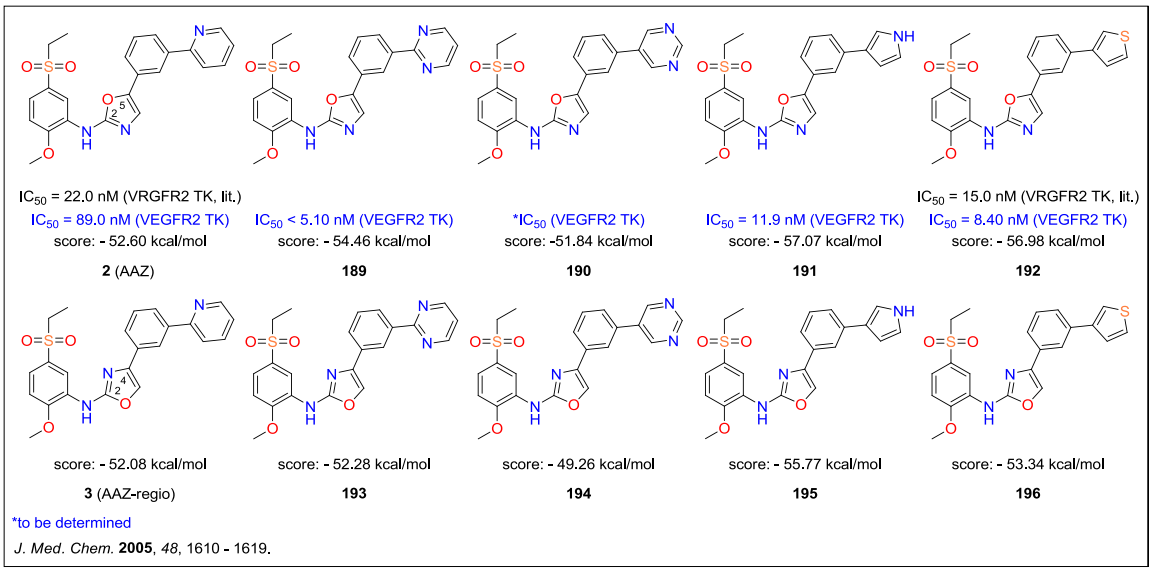

Figure 69. Vue d'ensemble des *N*,5-diaryloxazol-2-amines **2** (AAZ), **189** – **192** et des *N*,4-diaryloxazol-2-amines **3** (AAZ-regio), **193** – **196** conçues *in silico***,** synthétisées ou en cours de synthèse ainsi que leur activité inhibitrice (si disponible).

Les composés **189** et **191** ont montré une acitivité inhibitrice VEGFR2 TK importante, et tout spécialement **189** qui atteint le niveau sub-nanomolaire. (Figure 51)

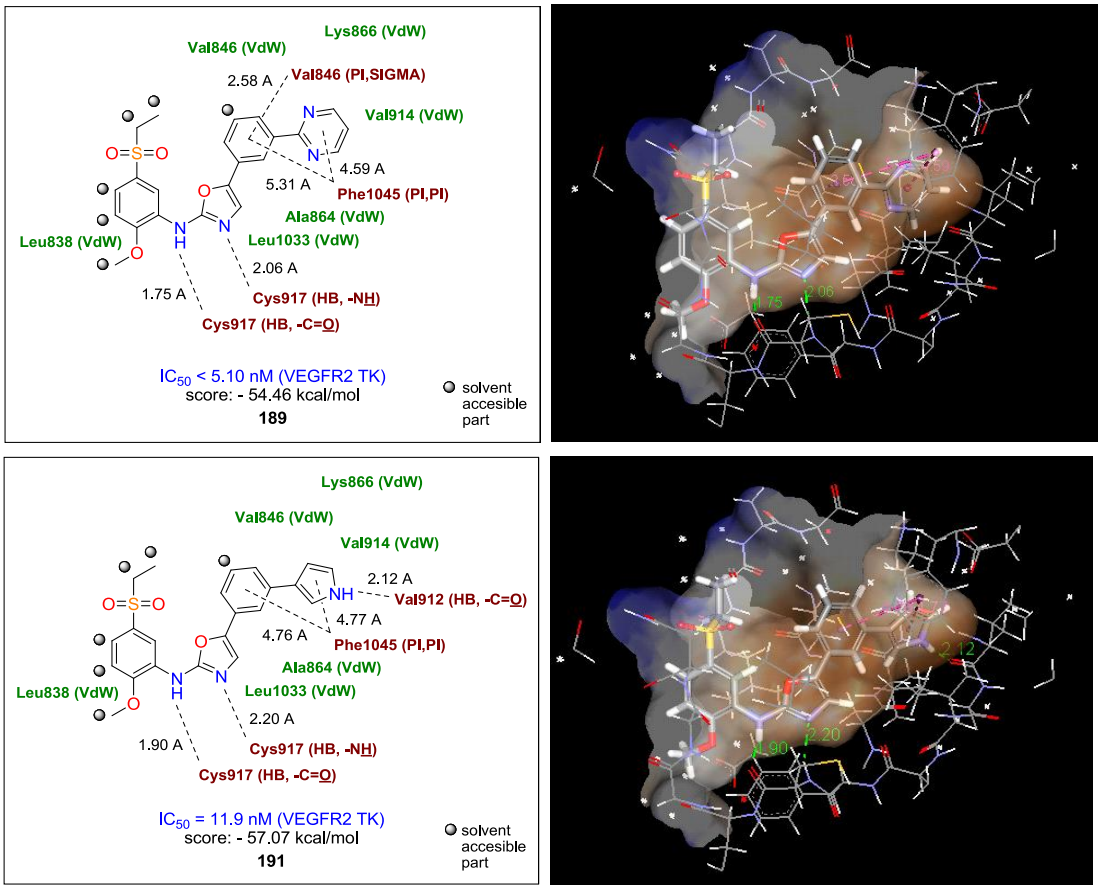

Figure 51. Analyse d'interaction, activité et position de liaison prédite de **189** et **191** dans le site actif de VEGFR2 TK.

Sur la base des informations provenant des bases de données (Reaxys, SciFinder) et de la littérature scientifique primaire, nous avons conçu des procédures de synthèse des *N*,5-diaryloxazol-2-amines **2** (AAZ), **189** – **192**.

Dans la première partie de la synthèse, un précurseur **107** d'oxazole important a été préparé. Sa préparation provient de l'aniline **122** qui a été développée dans notre groupe scientifique. Le composé **122** a été transformé en isothiocyanate **105** par $CSCl_2$ et ensuite utilisé dans une réaction de cyclisation thermique médiée par PPh_3 avec de l'α-azidoacétophénone **106** fournissant le précurseur cible d'oxazole **107**. (Schème 23)

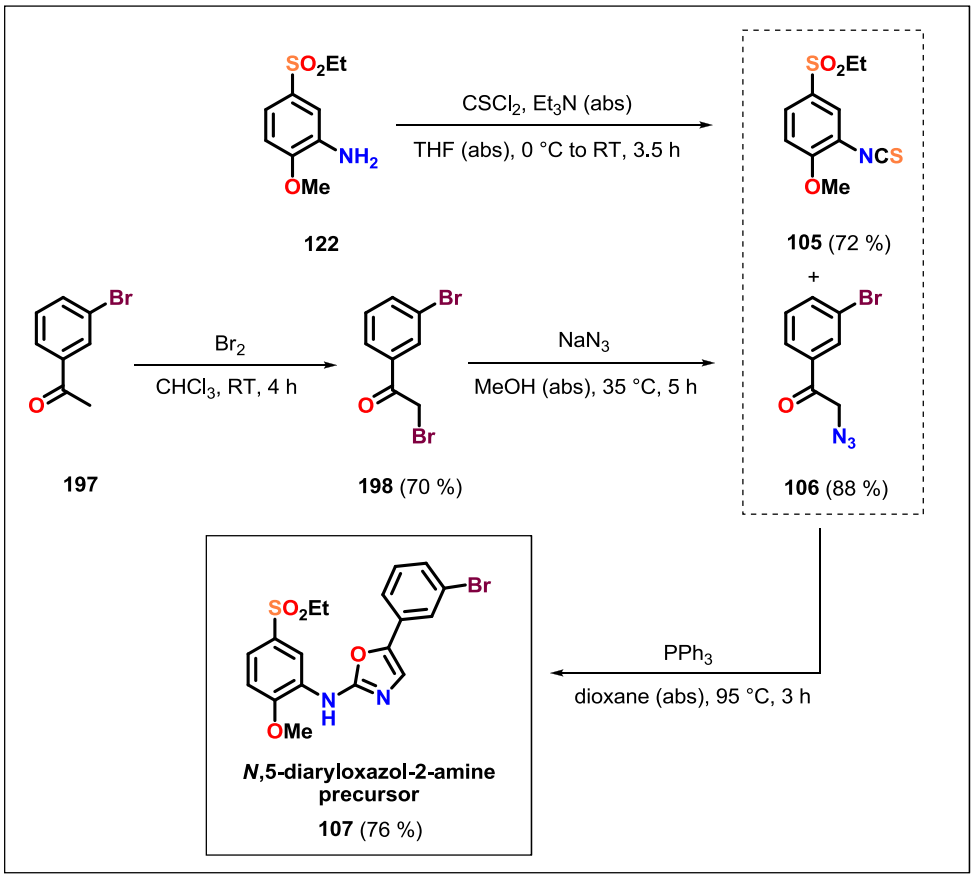

Schème 23. Synthèse du précurseur de *N*,5-diaryloxazol-2-amine **107**.

La réaction d'hétérocyclisation a été optimisée dans notre groupe et utilisée efficacement pour la synthèse de plusieurs dérivés différents de *N*,5-diaryloxazol-2-amines. Le mécanisme de réaction proposé a déjà été publié et il est représenté sur le schème ci-dessous.[82] (Schème 24)

Dans le mécanisme proposé de formation d'oxazol **M6**, PPh_3 réagit avec l'α-azidoacétophénone **M1** pour former un azaylide organique **M3** analogiquement à la réaction de Staudinger. L'azaylide **M3** formé attaque l'isothiocyanate organique **M2** fournissant carbodiimide **M5-1**. Le composé **M5-1** forme ensuite sa forme énol **M5-2**, qui subit une cyclisation menant au produit oxazol **M6**.

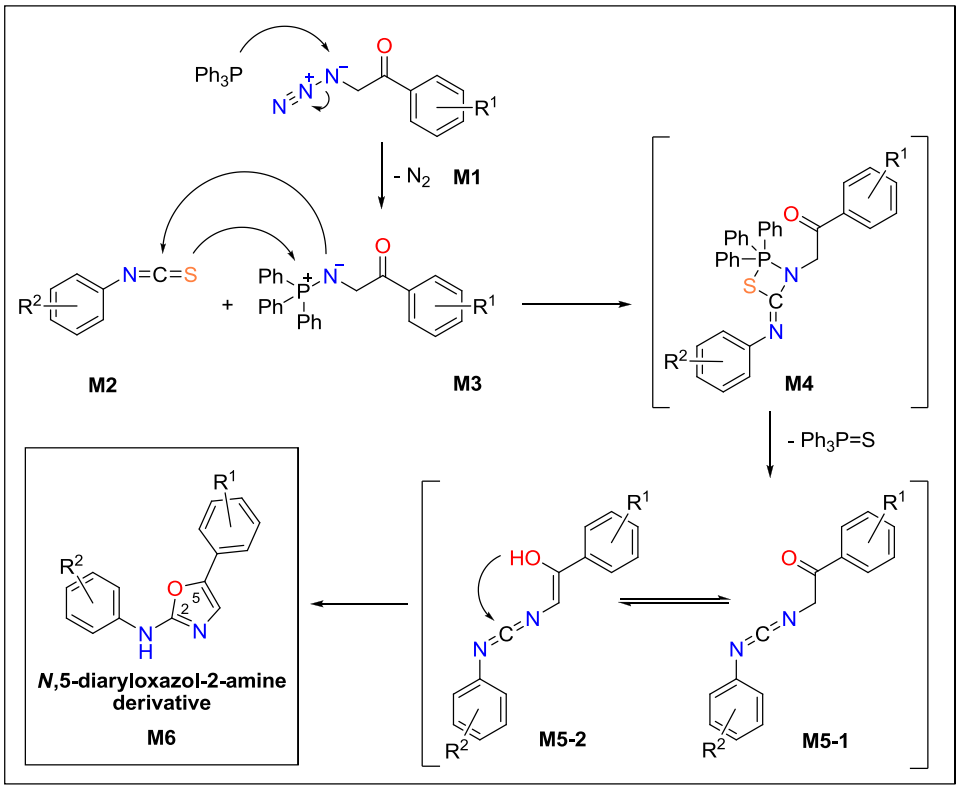

Schème 24. Proposed mechanism of the reaction providing *N*,5-diaryloxazol-2-amine derivative **M6**.

La deuxième partie de la synthèse menant aux *N*,5-diaryloxazol-2-amines **2** (AAZ), **189** – **192** a été réalisée avec succès par une réaction de couplage du précurseur **107** avec un réactif de couplage hétérocyclique approprié.

Les composés **2** (AAZ), **189** et **190** ont été préparés par la réaction de couplage de Stille de **107** avec les organostannanes **154**, **199** et **200** en présence de $Pd(PPh_3)_4$ et Bu_4NBr dans CH_3CN (abs). (Schème 25) En raison de l'utilisation ultérieure d'organostannanes hautement toxiques, d'une bonne disponibilité commerciale de réactifs de couplage boronique appropriés et de notre tentative de finalisation de la synthèse dans le plus court délai possible, nous avons décidé d'utiliser la réaction de couplage de Suzuki pour la préparation de **191** et **192**. Le composé **191** a été préparé par la réaction de couplage de **107** avec le borate de pinacol **201** en présence de $Pd(PPh_3)_4$ et de Na_2CO_3. Le composé **192** a été préparé par la réaction de couplage de **107** avec le borate de MIDA **202** en présence de $Pd(OAc)_2$, SPhos et K_3PO_4. (Schème 25 cont.)

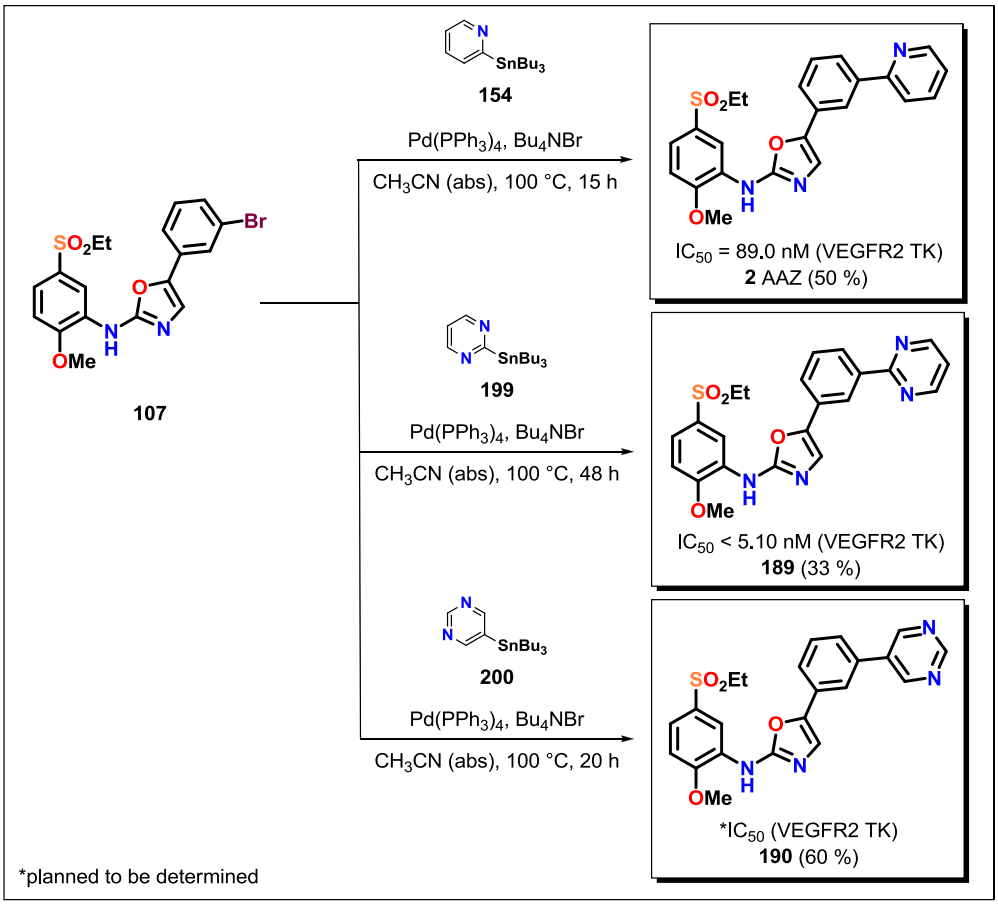

Schème 25. Synthèse des *N*,5-diaryloxazol-2-amines **2** (AAZ), **189** et **190**.

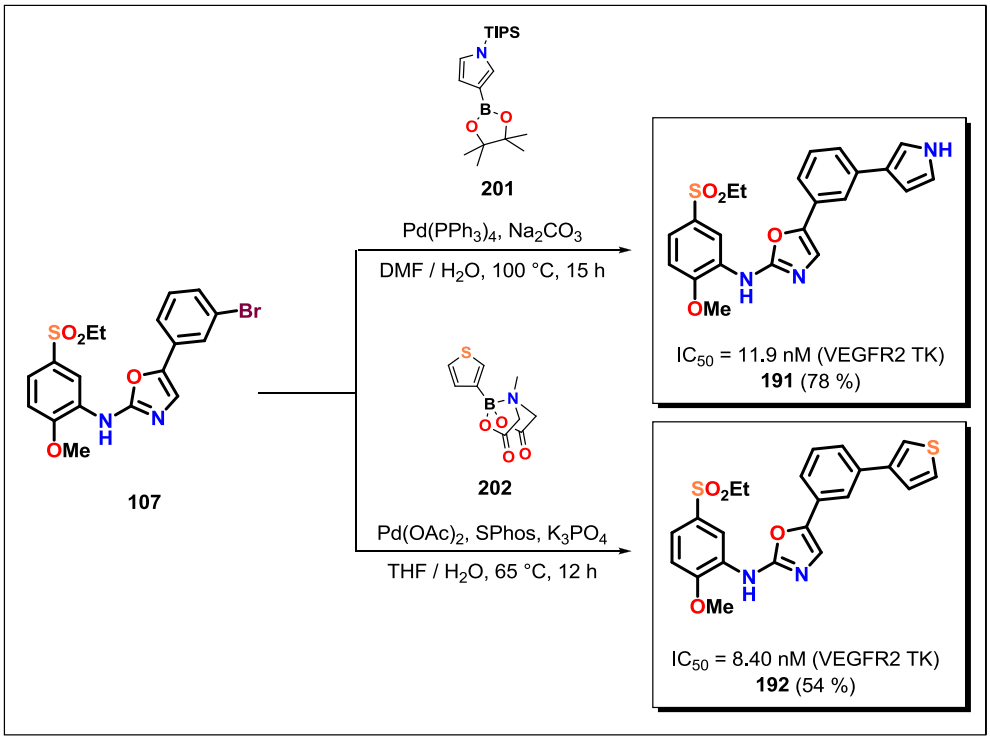

Schème 25 cont. Synthèse des *N*,5-diaryloxazol-2-amines **191** et **192**.

Au cours de la synthèse des dérivés **3** (AAZ-regio), **193 – 196**, nous avons découvert que l'hétérocyclisation, publiée dans la littérature,[89] d'acylurées avec des α-bromo-acétophénones donne sur notre substrat, non pas sur la *N*,4-diaryloxazol-2-amine **205** escomptée mais sur la 1,5-diarylimidazolidine-2,4-dione **204**. (Schème 26)

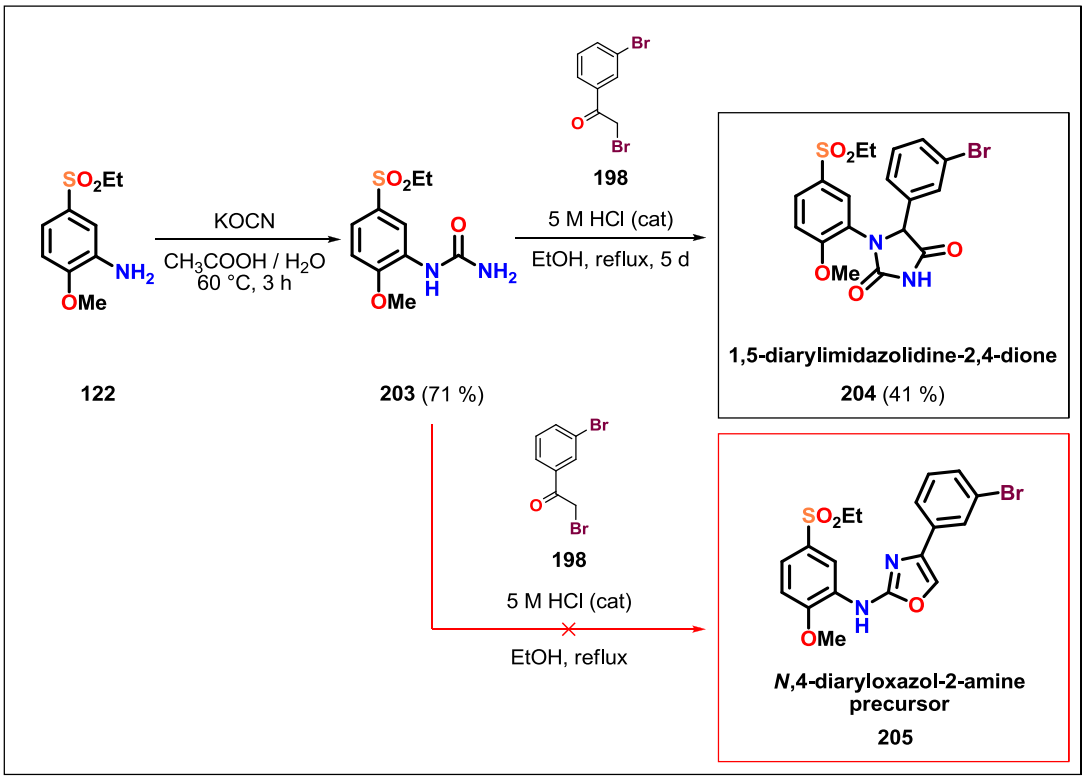

Schème 26. Synthèse inattendue du précurseur 1,5-diarylimidazolidine-2,4-dione **204**.

La structure de **204** a été confirmée par les méthodologies analytiques standards (^{1}H-RMN, ^{13}C-RMN, IR, MS, analyse élément.) et aussi par la spectroscopie à rayons X. (Figure 49)

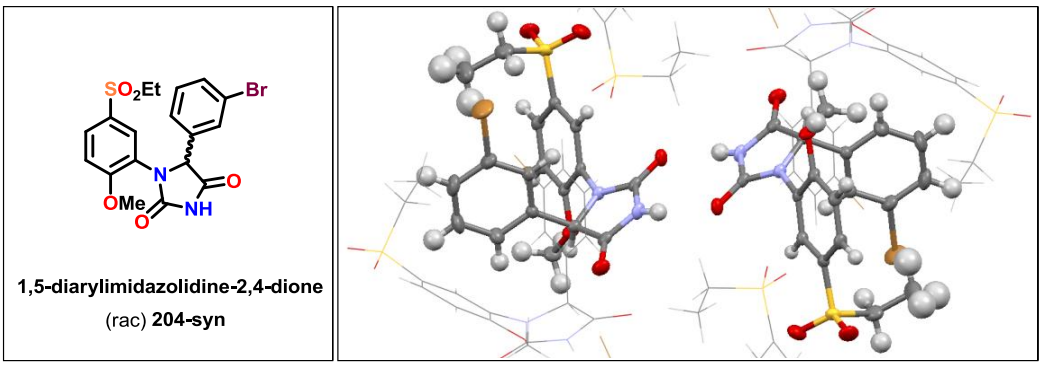

Figure 49. La structure et l'agencement moléculaire du (rac) **204-syn** prouvé par la spectroscopie à rayons X.

Le mécanisme proposé de la cyclisation conduisant à des dérivés de 1,5-diarylimidazolidine-2,4-dione est représenté sur le schème ci-dessous. (Schème 27)

L'α-bromoacétophénone **M7** est dans la réaction de dismutation catalytique thermodifiée par le HCl transformée en acétophénone **M8** et α, α-dibromoacétophénone **M9**. Une présence significative de **M8** et **M9** dans un mélange réactionnel après plusieurs heures de chauffage a été prouvée par des analyses de CCM et de ^{1}H-RMN. Le composé **M9** réagit par la suite avec le dérivé d'urée **M10** fournissant un intermédiaire **M12** qui subit la réaction de cyclisation menant à la formation du dérivé 1,5-diarylimidazolidine-2,4-dione (rac) **M15-syn**.

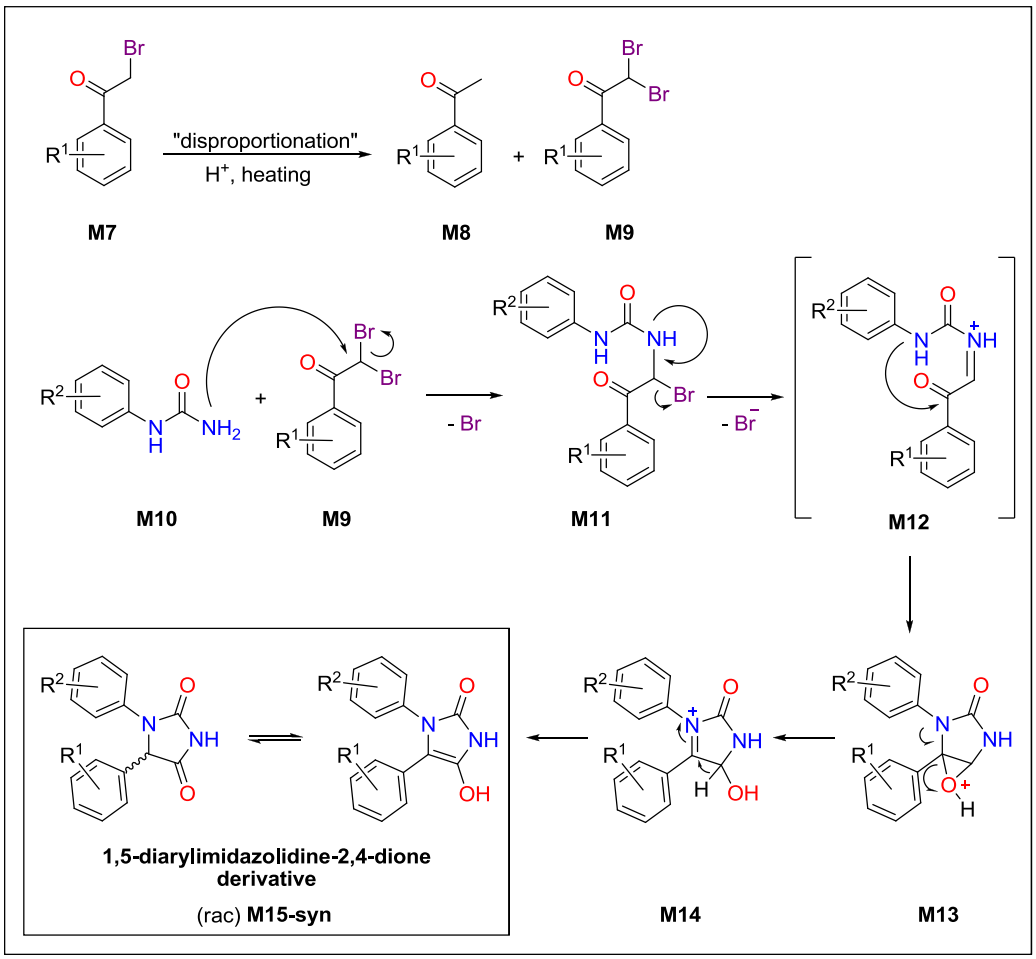

Schème 27. Mécanisme proposé de la réaction conduisant au dérivé 1,5-diarylimidazolidine-2,4-dione (rac) **M15-syn.**

Etant donné la structure intéressante de **204** et son potentiel d'activité biologique, les dérivés **206** et **207** ont été synthétisés par une réaction de couplage de **204** avec les réactifs hétérocycliques **154** et **201**. Le composé **206** a été préparé dans des conditions de réaction de couplage de Stille de **204** avec du stannane **154** et le composé **207** a été préparé en utilisant le couplage de Suzuki de **204** avec le borate de pinacol **201**. (Schème 26 cont.)

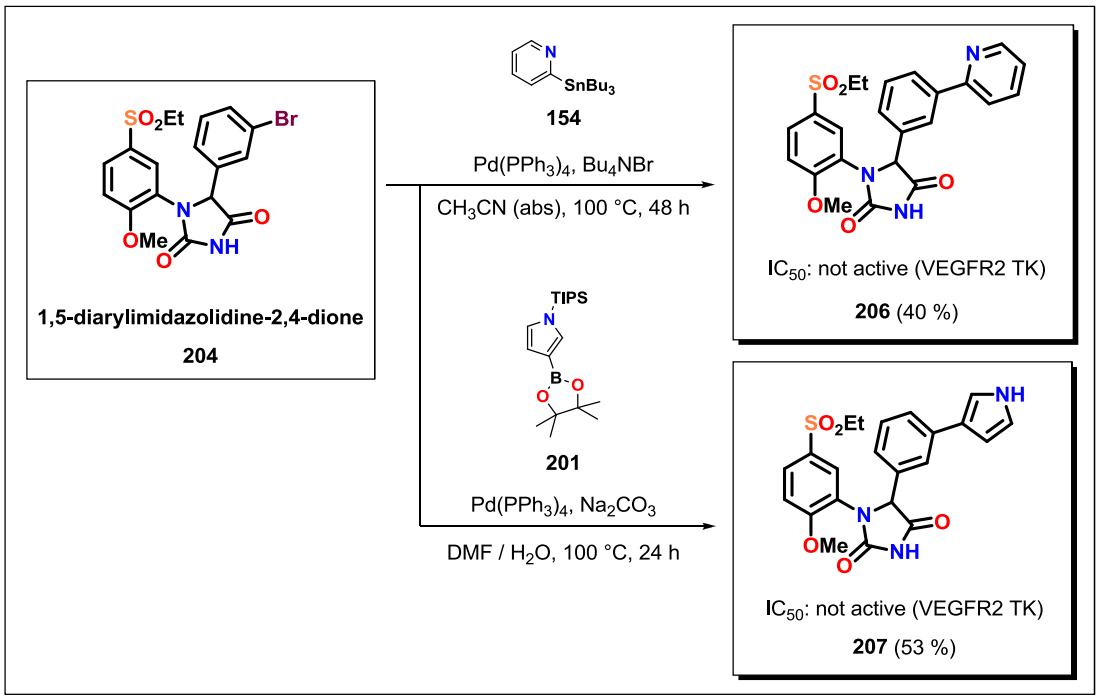

Schème 26 cont. Synthèse non planifiée du précurseur 1,5-diarylimidazolidine-2,4-dione **204** et de ses dérivés **206** et **207**.

Après nos tentatives infructueuses de suivre les procédures de la littérature et de synthétiser le précurseur de *N*,4-diaryloxazol-2-amine **205** pour la préparation des dérivés prédits **3** (AAZ-regio), **193** – **196**, nous avons dû repenser notre approche synthétique et développer notre propre synthèse.

Le précurseur de la *N*,4-diaryloxazol-2-amine **205** a été finalement préparé avec 10% de rendement isolé en catalysant la condensation de l'arylurée **203** avec l'α-bromo-acétophénone **198** avec du triflate d'argent.[129] Nous essayons actuellement d'optimiser cette réaction. (Schème 28) Le mécanisme proposé de la cyclisation menant aux dérivés de *N*,4-diaryloxazol-2-amine est représenté sur le schème ci-dessous. (Schème 29) Le dérivé d'urée **M10** attaque nucléophilement le groupe carbonyle de l'α-bromoacétophénone **M7** qui conduit à la formation d'un **M16** intermédiaire. Après la cyclisation thermique médiée

par Ag et l'élimination subséquente de l'eau, on forme le dérivé final *N*,4-diaryloxazol-2-amine **M18**.

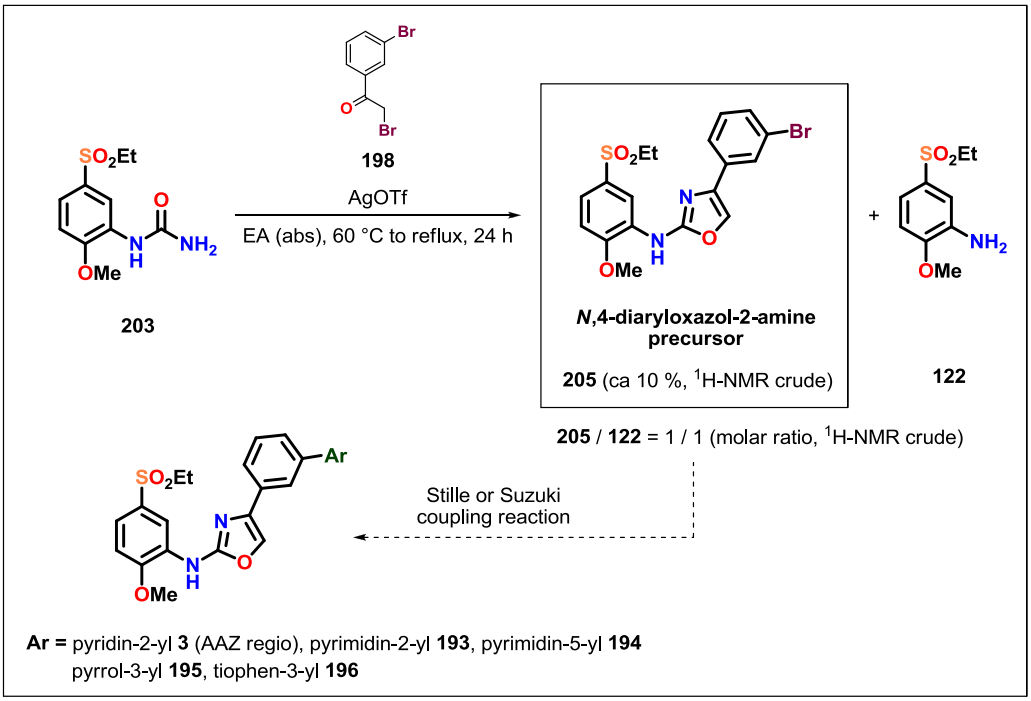

Schème 28. Synthèse du précurseur de *N*,4-diaryloxazol-2-amine **205**.

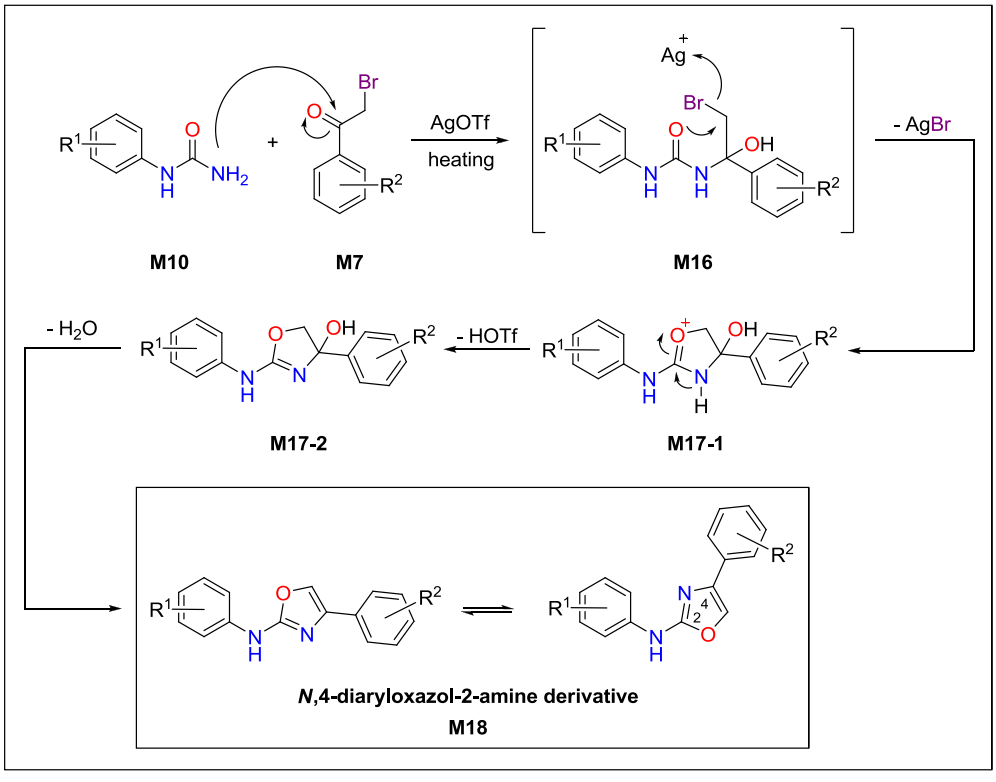

Schème 29. Mécanisme proposé de la réaction menant au dérivé *N*,4-diaryloxazol-2-amine **M18**.

La synthèse des *N*,4-diaryloxazol-2-amines **3** (AAZ-regio), **193** – **196** conçues *in silico* n'étant pas terminée, nous ne disposons pas encore des données biologiques nous permettant de valider notre hypothèse *RegBio*. Néanmoins, des progrès synthétiques réalisés récemment au laboratoire nous permettrons de finir ce projet à court terme.

11.2. Projet – "Salt bridge containing pocket" (SBCP)

Dans le cadre du deuxième projet "Salt bridge containing pocket" (SBCP), nous avons découvert une conformation intermédiaire spécifique DFG-IN / OUT de VEGFR2 TK qui peut être stabilisée par des interactions avec des ligands *N*,5-diaryloxazol-2-amines. Dans cette conformation, une nouvelle région de binding dans le VEGFR2 TK est créée. Nous avons nommé ce domaine Salt bridge containing pocket (SBCP) parce que les résidus Lys866 et Glu833 présents peuvent participer à des interactions supplémentaires. Conformément à nos observations et aux informations de la littérature, nous avons proposé que des dérivés de *N*,5-diaryloxazol-2-amine *p*-substitués judicieusement sélectionnés devraient posséder une activité inhibitrice accrue.[6]

Ainsi, nous nous sommes concentrés sur le développement des dérivés *p*-substitués de *N*,5-diaryloxazol-2-amine **208** – **212** ainsi que de leur analogues *m*-substitués **213** – **217** afin de comparer leur activité inhibitrice. Les deux séries de dérivés *p*-substitués et leurs équivalents *m*-substitués ont été préparées. Les activités inhibitrices (IC_{50}, VEGFR2 TK) de **208**, **209**, **210**, **211**, **213**, **214** et **216** ont été déterminées. Celle des dérivés *m*-substitués **215** et des acides hydroxamiques **212**, **217** est en cours d'évaluation. (Figure 70)

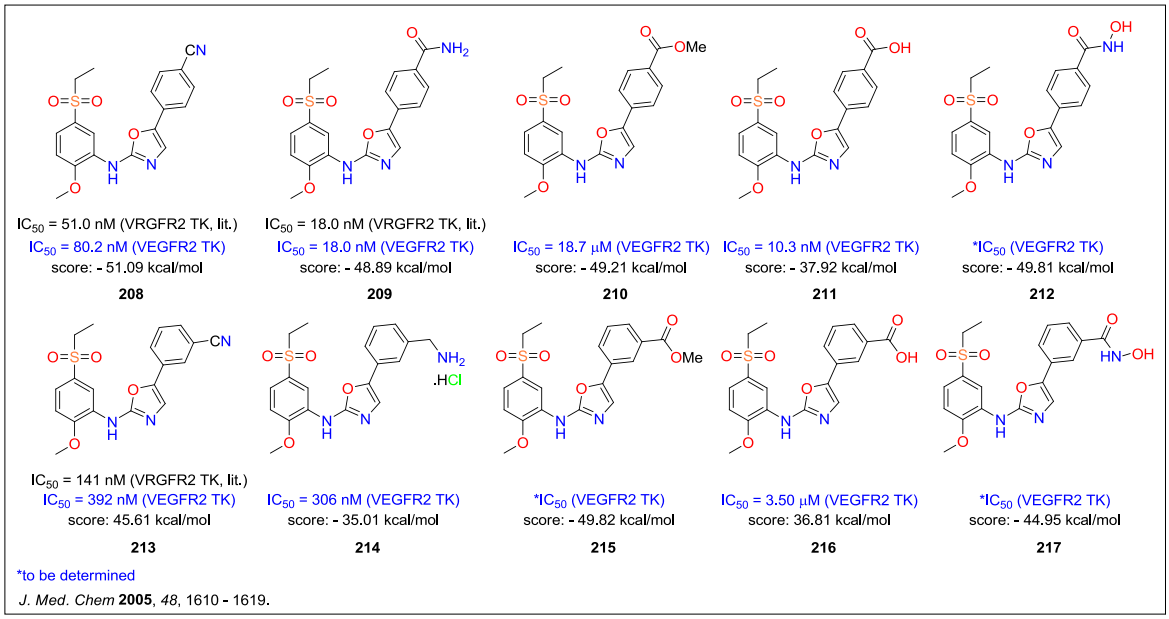

Figure 70. Vue d'ensemble des *N*,5-diaryloxazol-2-amines *p*-substituées **208** – **212** et de leurs analogues *m*-substitués **213** – **217** conçus *in silico* avec leur activité inhibitrice (si disponible).

Les résultats obtenus jusqu'à présent suggèrent que notre hypothèse est juste. En effet les dérivés *p*-substitués par un benzonitrile **208** ou un acide carboxylique **211** montrent de bien meilleures activités que leur analogues *m*-substitués **213** et **216**. En particulier, l'acide carboxylique **211** s'avère très actif. (Figure 71)

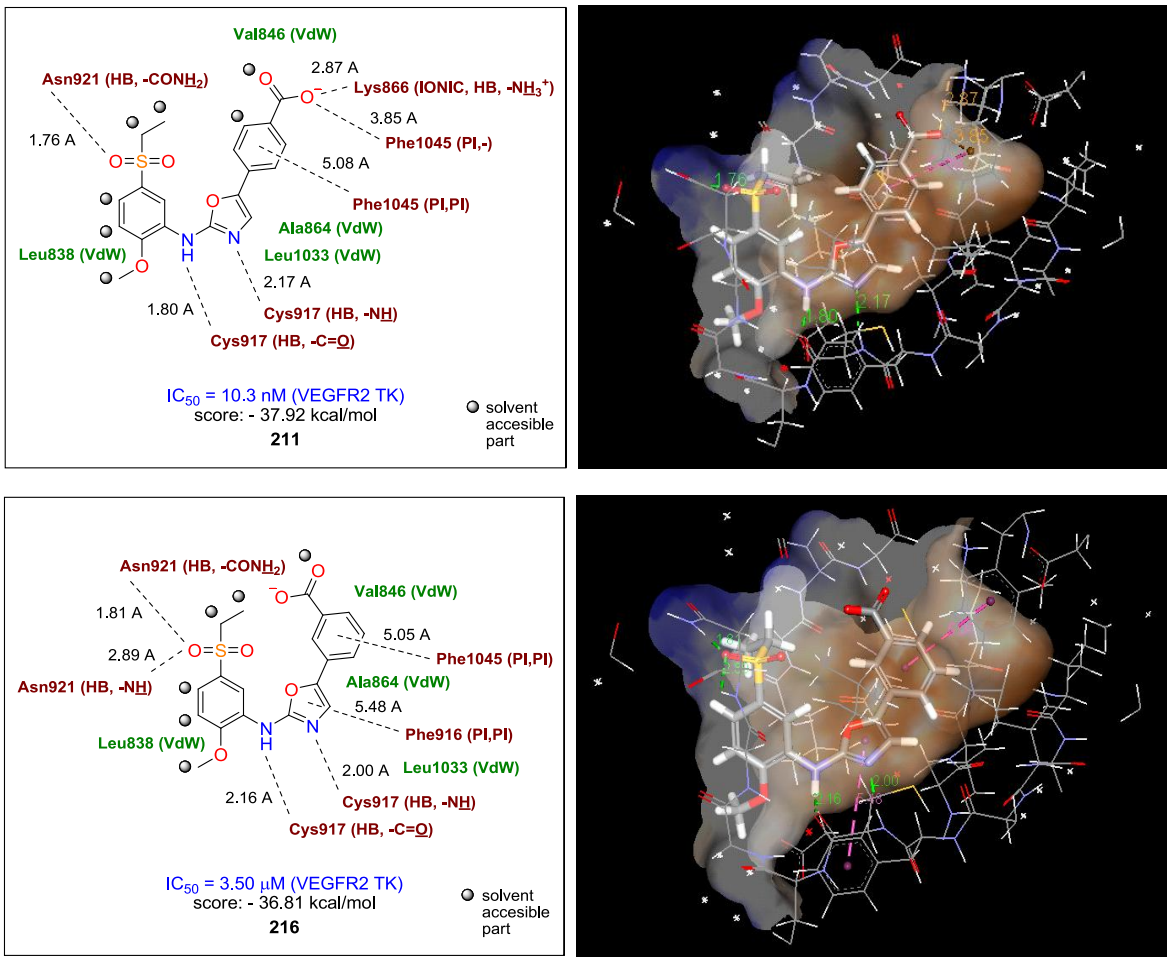

Figure 71. Analyse d'interaction, activité et position de liaison prédite des dérivés d'acide carboxylique **211** et **216** dans le site actif de VEGFR2 TK.

Sur la base des informations provenant des bases de données (Reaxys, SciFinder) et de la littérature scientifique primaire, nous avons conçu une préparation des dérivés *p*-substitués de *N*,5-diaryloxazol-2-amine **208** – **212**.

La synthèse de **208** provient du carbonitrile **225** disponible dans le commence qui a été transformé en son dérivé d'azide **226**. Une cyclisation thermique médiée par PPh_3 de **226** avec l'isothiocyanate **105** a fourni le dérivé oxazol cible **208**. Une procédure pour la préparation de l'oxazole **209** a commencé à partir du nitrile **225** qui a été transformé en

amide **227** par une hydrolyse d'acide thermique. Une réaction de **227** avec NaN_3 avait conduit à l'azide **228** qui a ensuite été utilisé dans la réaction d'oxazolation avec l'isothiocyanate **105** fournissant l'oxazole cible **209**. (Schème 30)

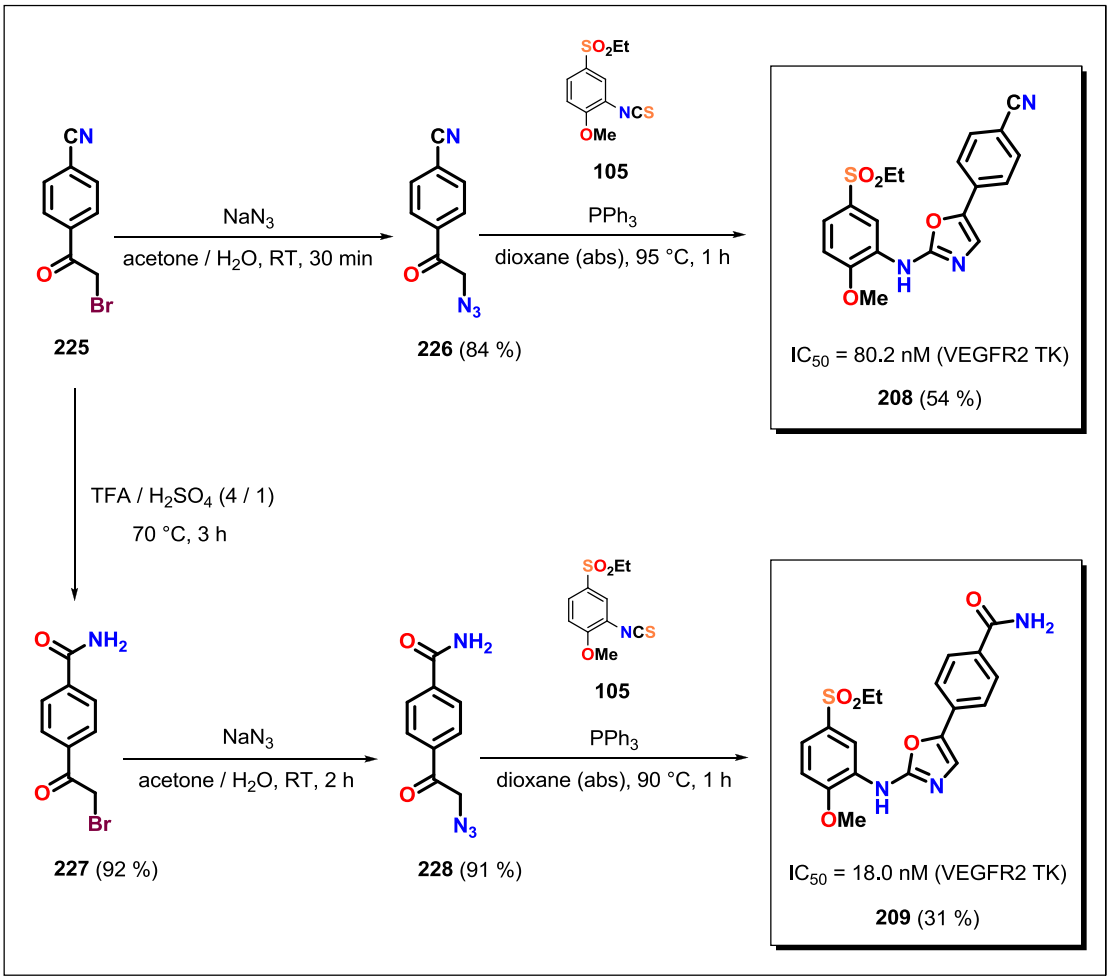

Schème 30. Synthèse des *N*,5-diaryloxazol-2-amines *p*-substituées **208** et **209**.

La synthèse de **210**, **211** et **212** a commencé à partir d'un 4-acétylbenzoate de méthyle commercialisé (**229**) qui a été transformé en son dérivé bromo **230**. Le composé **230** a ensuite été utilisé dans une réaction avec NaN_3 fournissant l'azide **231**. L'oxazolester cible **210** a été préparé par l'oxazolation thermique à médiation par PPh_3 de **231** avec l'isothiocyanate **105**. Le oxazolester **210** a été transformé en acide oxazolecarboxylique cible **211** par une hydrolyse thermique avec $LiOH.H_2O$. Finalement, nous avons effectué un couplage amide de l'acide oxazolecarboxylique **211** avec $BnONH_2.HCl$, HOBt, EDC.HCl et Et_3N fournissant de l'acide oxazolehydroxamique protégé en benzyle **232**.

L'intermédiaire **232** a été déprotégé par hydrogénolyse conduisant à l'acide oxazolehydroxamique cible **212**. (Schéme 31)

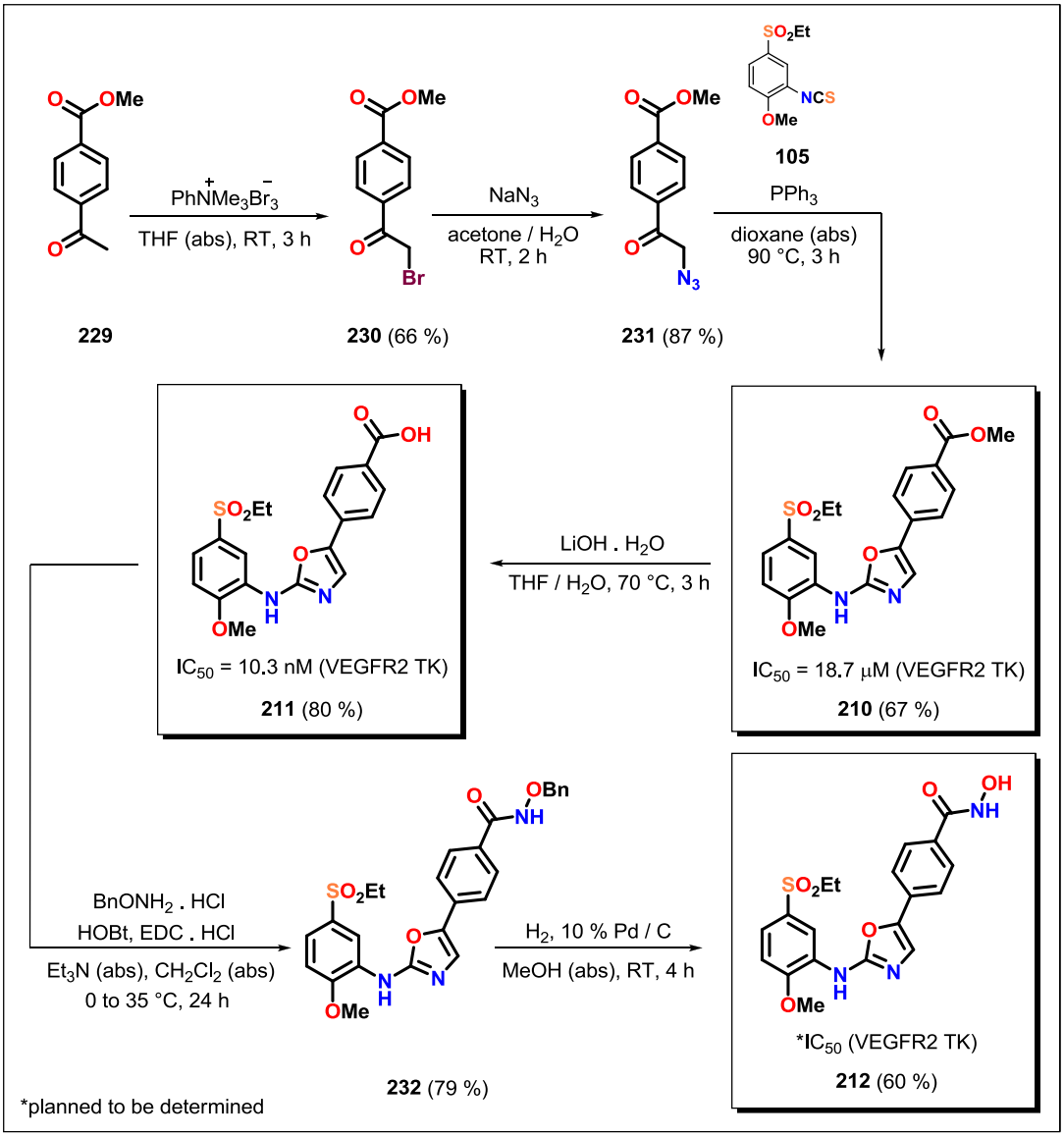

Schème 31. Synthèse des *N*,5-diaryloxazol-2-amines *p*-substituées **210**, **211** et **212**.

Une approche synthétique menant à la préparation de *N*,5-diaryloxazol-2-amines **213**, **215**, **216** et **217** *m*-substituées a été inspirée par la synthèse de leurs analogues *p*-substitués. Une synthèse du dérivé **214** a été plus spécifique et a nécessité de nouvelles recherches dans la littérature.

La synthèse de **213** a commencé à partir d'une 1-(3-bromophényl)éthanone (**197**) disponible dans le commerce qui a été transformée en benzonitrile **233** en utilisant une cyanation catalysée par Pd. Le composé **233** a été traité avec du tribromure de

triméthylphényl ammonium dans du THF (abs) en fournissant son dérivé bromo **234**. Le composé **234** a ensuite été utilisé dans une réaction avec du NaN_3 fournissant de l'azide **235**. L'oxazole benzonitrile **213** cible a été préparé par l'hétérocyclisation thermique à médiation par PPh_3 de **235** avec l'isothiocyanate **105**. La synthèse réussie du chlorhydrate d'oxazoleamine **214** a été réalisée par une hydrosilylation activée par un fluor de **213** avec $PhSiH_3$ et TBAF suivie d'une hydrolyse avec du 1M HCl dans du MeOH. (Schème 32)

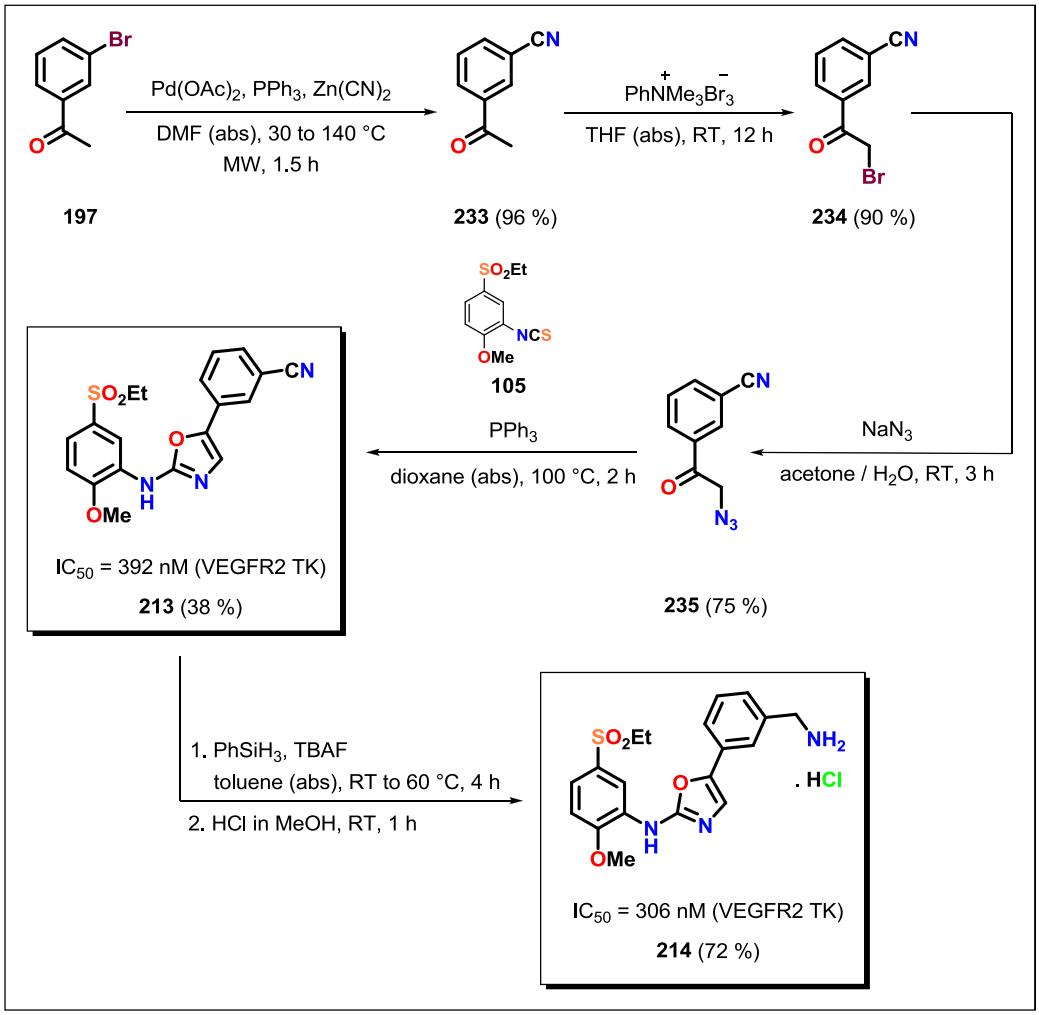

Schème 32. Synthèse des *N*,5-diaryloxazol-2-amines *m*-substituées **213** et **214**.

La synthèse de **215**, **216** et **217** a commencé à partir d'un 3-acétylbenzoate de méthyle commercialisé (**236**) qui a été transformé en son dérivé bromo **237** par du tribromide de triméthylphénylammonium dans du THF (abs). Le composé **237** a ensuite été utilisé dans une réaction avec NaN_3 dans un mélange d'acétone / H_2O fournissant de l'azide **238**. L'oxazolester cible **215** a été préparé par l'hétérocyclisation thermique à base de PPh_3 de

238 avec l'isothiocyanate **105**. L'oxazolester **215** a ensuite été transformé en acide oxazolecarboxylique cible **216** par une hydrolyse thermique avec $LiOH.H_2O$ dans un mélange de THF / H_2O. Le composé **216** a été converti par la réaction de couplage amide avec $BnONH_2.HCl$, HOBt, EDC.HCl et Et_3N dans CH_2Cl_2 (abs) en acide oxazolehydroxamique protégé par un benzyle **239**.

L'intermédiaire **239** a été purifié par FLC et le produit isolé a été déprotégé par hydrogénolyse en présence de 10 % de Pd / C dans MeOH (abs) fournissant l'acide oxazolehydroxamique cible **217**. (Schème 33)

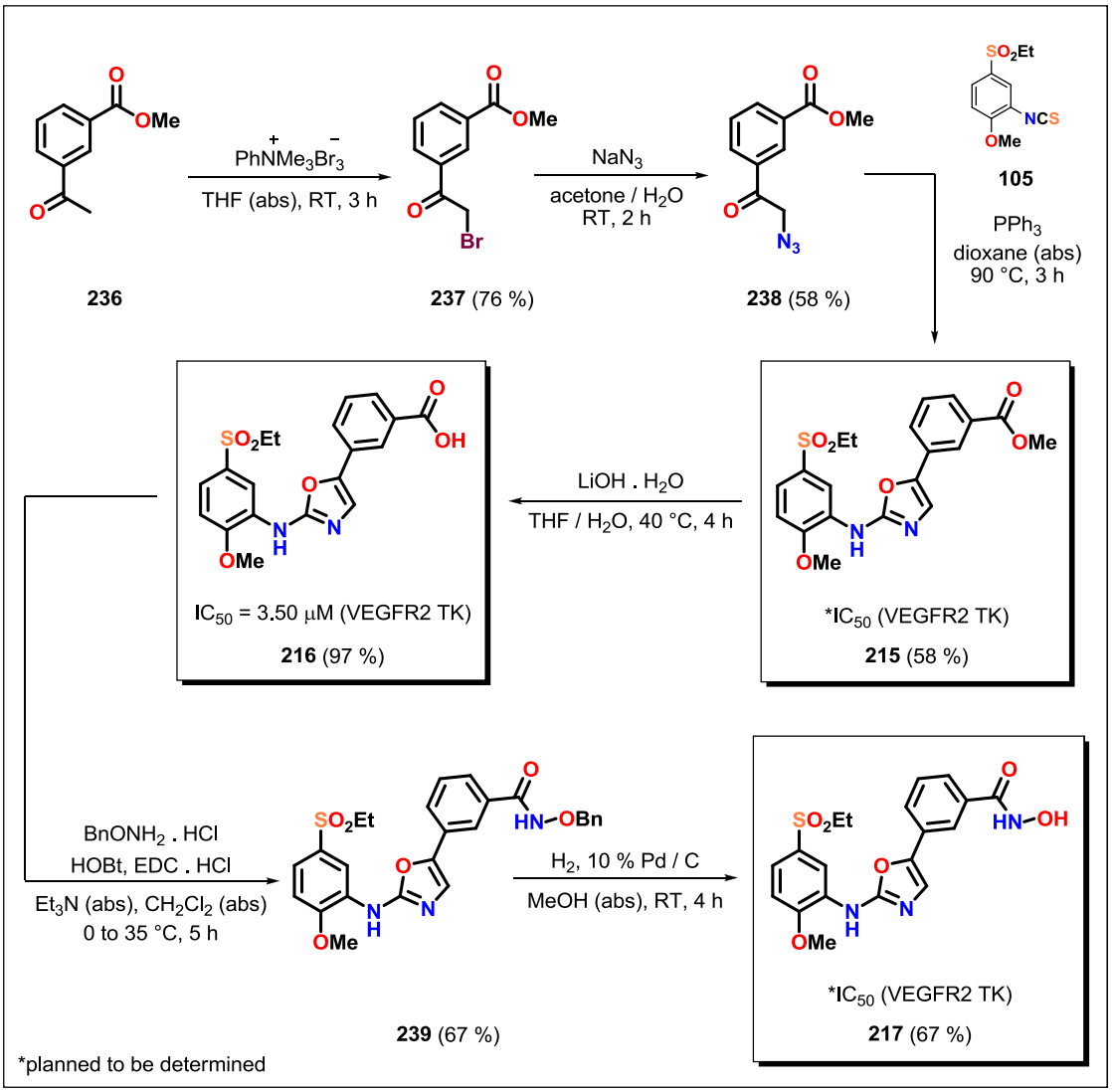

Schème 33. Synthèse des *N*,5-diaryloxazol-2-amines *m*-substituées **215**, **216** et **217**.

Dans le même ordre d'idées, nous avons développé une série de six *N*,5-diaryloxazol-2-amine *m*-substituées par un hétérocycle **218** – **223** pouvant établir à la fois une interaction

hydrophobe connue pour **2** (AAZ) et les interactions ioniques dans la SBCP. Nous avons également préparé la paire de *N*,5-diaryloxazol-2-amines **4**, **224** contenant à la fois un substituant polaire en *para* et un hétérocyclique en *meta* pouvant donner un binding synergique. Les séries de *N*,5-diaryloxazol-2-amines *m*-substituées par un hétérocycle **218**, **219**, **220**, **221**, **223** et *m*,*p*-disubstituées **4**, **224** ont été synthétisées et l'activité biologique des dérivés **220**, **221**, **223**, **4**, **224** a été déterminée. La préparation de **222** et l'évaluation biologique de **218** et **219** sont en cours au laboratoire. (Figure 72)

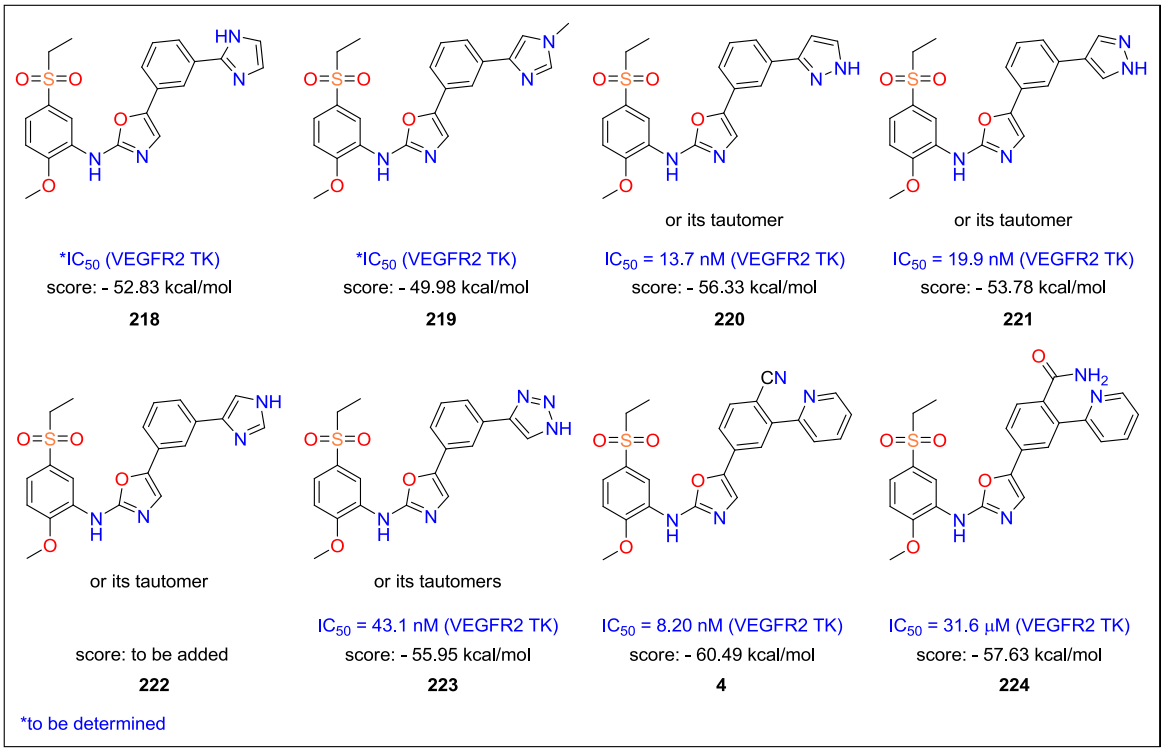

Figure 72. Vue d'ensemble des *N*,5-diaryloxazol-2-amines *m*-substituées par des hétérocycles **218** – **223** et de leurs analogues *p*,*m*-disubstitués **4** et **224** conçus *in silico* avec leur activité inhibitrice (si disponible).

Les dérivés *m*-substitués par un pyrazole **220**, **221** ou un triazole **223** étaient suspectés d'interagir dans la poche hydrophobe et de montrer une interaction supplémentaire avec le Glu833 de la SBCP, ou encore avec la Val912. Compte tenu des excellentes activités inhibitrices observées pour les trois dérivés, cette hypothèse a été vérifiée. (Figure 62 et 63)

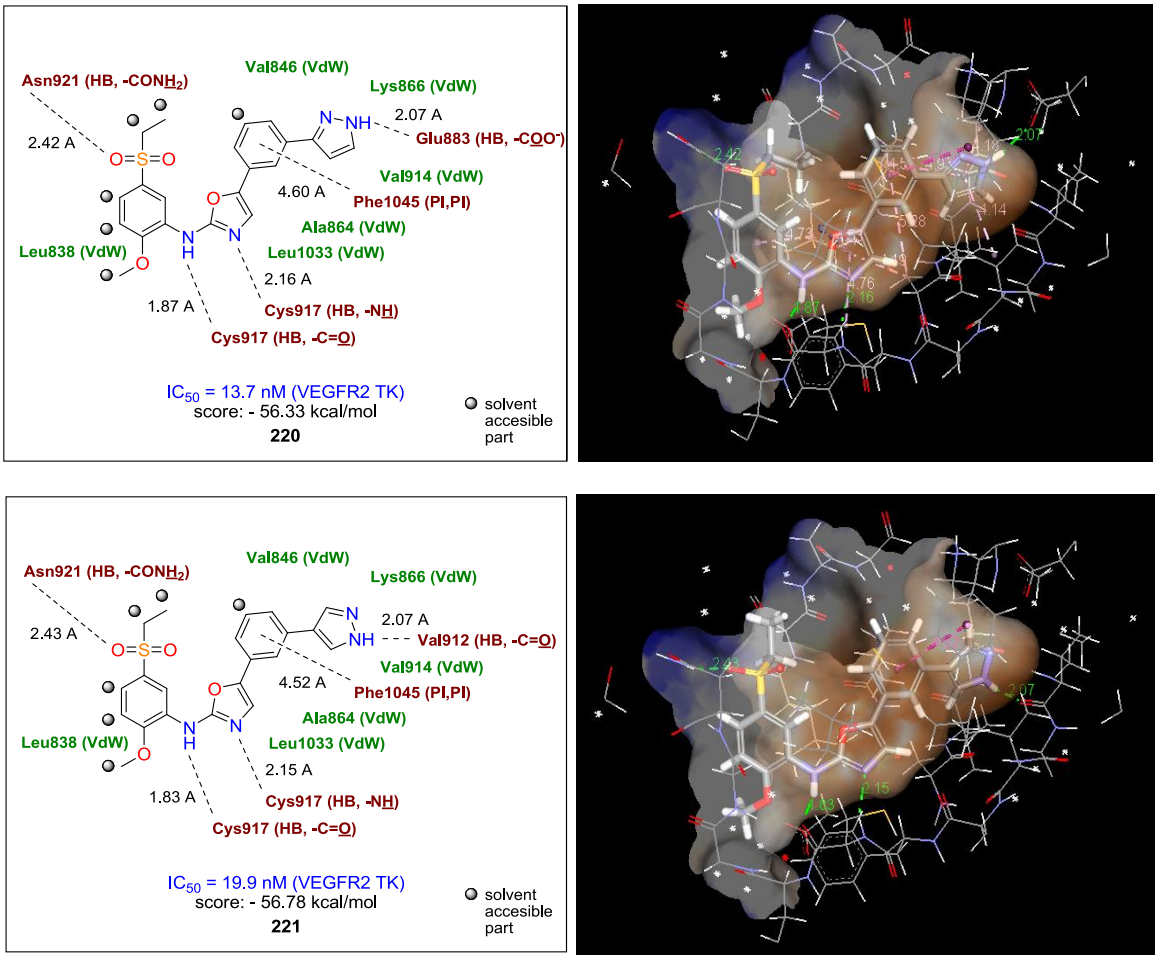

Figure 62. Analyse d'interaction, activité et position de liaison prédite des dérivés hétérocycliques **220** et **221** dans le site actif de VEGFR2 TK.

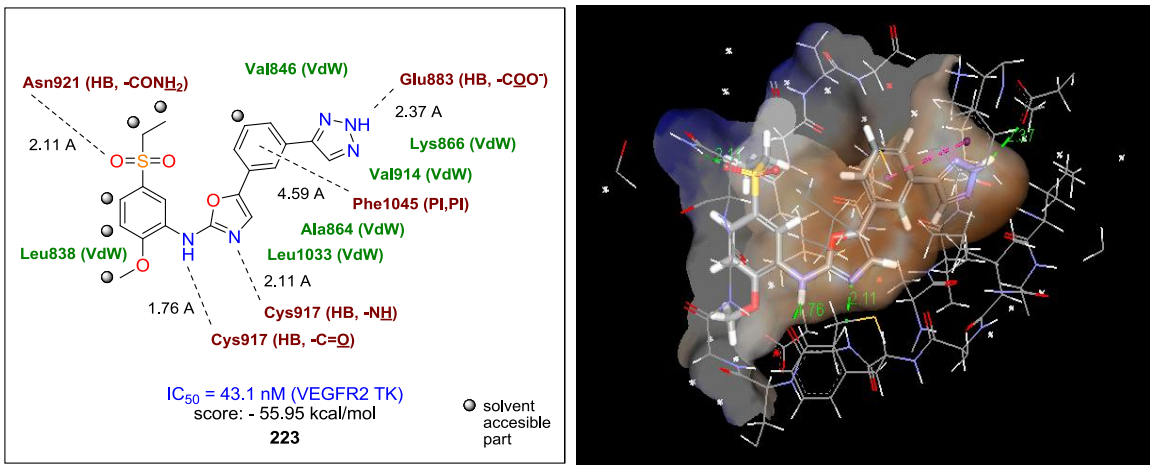

Figure 63. Analyse d'interaction, activité et position de liaison prédite de dérivé hétérocyclique **223** dans le site actif de VEGFR2 TK.

Les dérivés *m,p*-disubstitués **4** et **224** ont été conçus pour leur interaction synergique potentielle combinant les interactions hydrophobes de la pyridine en position *meta* et

l'interaction ionique dans la SBCP provoquée par le substituant en *p*ara. Cet effet synergique est bien observé dans le cas du dérivé **4** possédant un carbonitrile, puisqu'il présente une excellente activité. Par contre, l'activité du dérive **224** possédant un amide primaire chute considérablement. Nous pensons que cette chute d'activité est due à des interactions défavorables entre les substituants amide et pyridine de **224** (interaction stérique défavorable ou liaison hydrogène intramoléculaire…) rompant la conformation active idéale dans le site actif du VEGFR2 TK. (Figure 64 et 65)

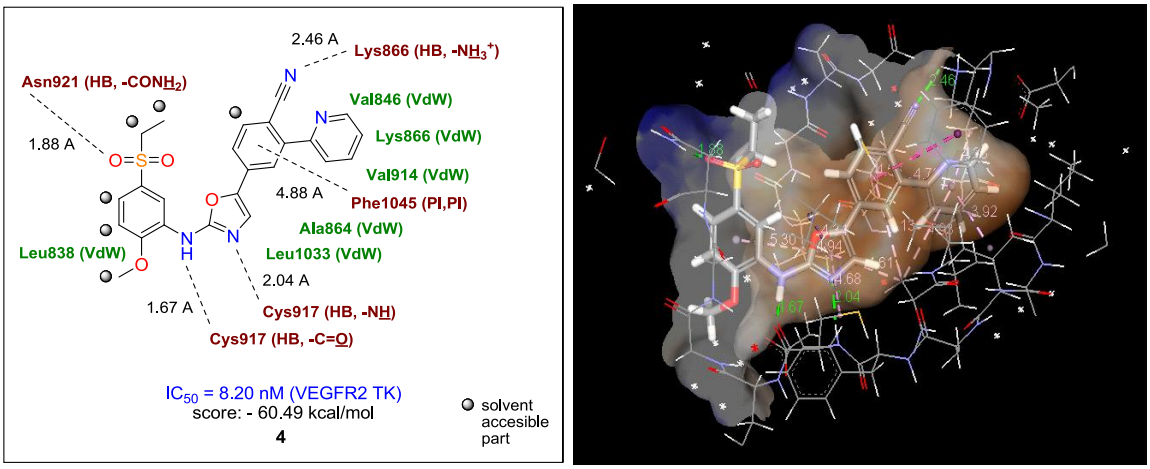

Figure 64. Analyse d'interaction, activité et position de liaison prédite de dérivé hétérocyclique **4** dans le site actif de VEGFR2 TK.

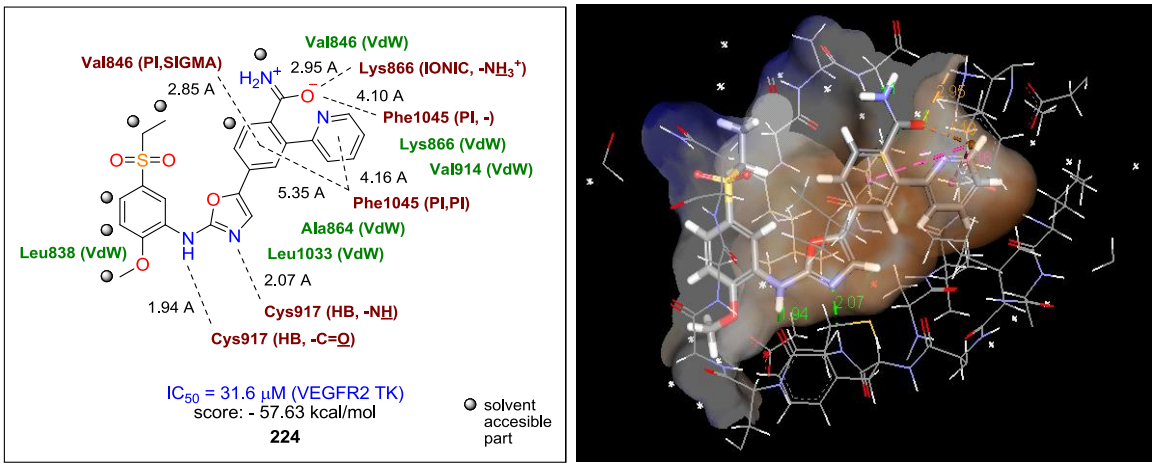

Figure 65. Analyse d'interaction, activité et position de liaison prédite de dérivé hétérocyclique **224** dans le site actif de VEGFR2 TK.

Une préparation des *N*,5-diaryloxazol-2-amines hétérocycliques *m*-substituées **218** – **221** a commencé à partir du précurseur de couplage **107** précédemment utilisé pour la préparation des composés **2** (AAZ), **189** – **192** (Figure 69) dans le cadre du projet *RegBio*.

Le composé **218** a été préparé par une réaction de couplage direct non conventionnelle de **107** avec de l'imidazole (**240**). La réaction a été effectuée en présence de $Pd(OAc)_2$ et de CuI dans du DMF (abs). Le mécanisme de cette réaction est probablement très similaire au couplage de Sonogashira. Le composé **219** a été préparé par la réaction de couplage de Stille de **107** avec organostannane **241** en présence de $Pd(PPh_3)_4$ et Bu_4NBr dans CH_3CN (abs). (Schème 34)

Les composés **220** et **221** ont été préparés par la réaction de couplage de Suzuki de **107** avec l'acide boronique **242**, resp. ester de pinacol d'acide boronique **243** en présence de $Pd(PPh_3)_4$ et Na_2CO_3 dans un mélange de DMF / H_2O. Tous les réactifs de couplage hétérocyclique utilisés ont été obtenus à partir des sources commerciales. (Schème 34 cont.)

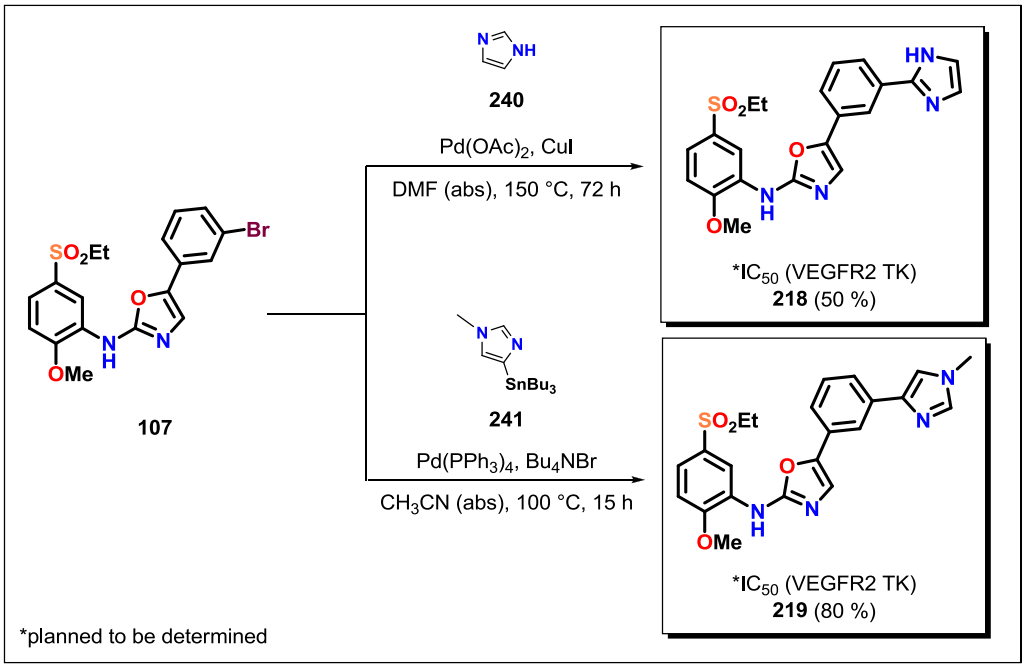

Schème 34. Synthèse des *N*,5-diaryloxazol-2-amines hétérocycliques *m*-substituées **218** et **219**.

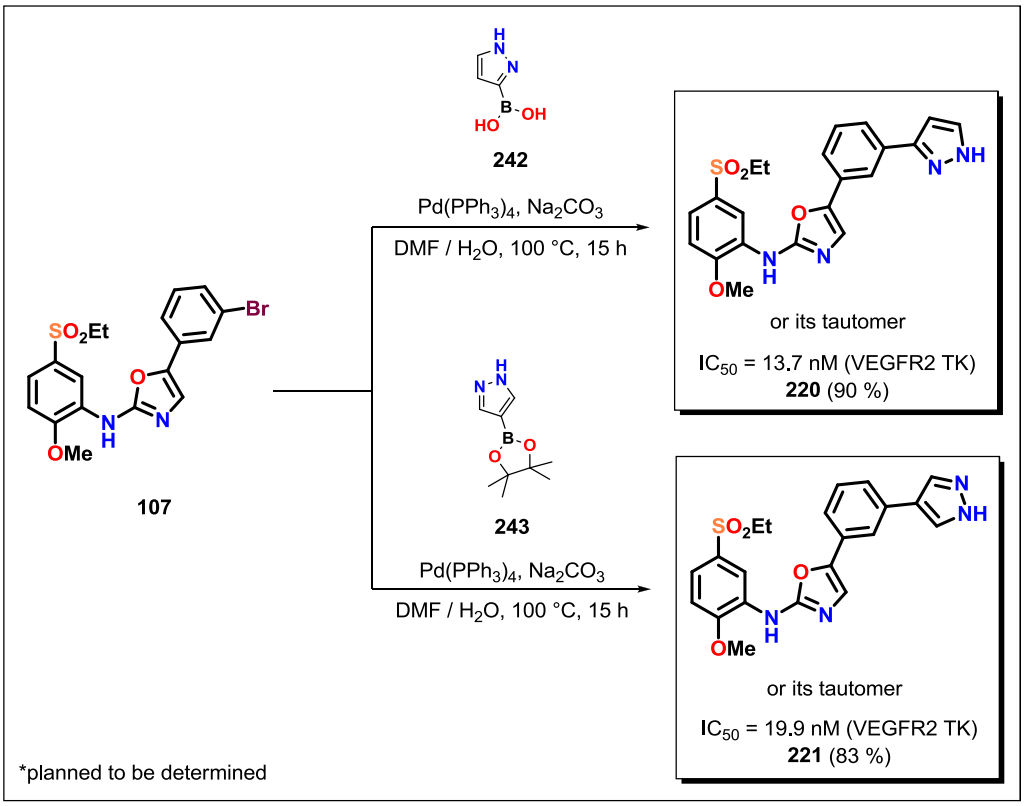

Schème 34 cont. Synthèse des *N*,5-diaryloxazol-2-amines hétérocycliques *m*-substituées **220** et **221**.

En raison de la disponibilité limitée de tout réactif de couplage de Stille ou de Suzuki de 1*H*-imidazol-4-yle et nos tentatives infructueuses d'effectuer la borylation de Miyaura sur le 4-bromo-1*H*-imidazole ou son dérivé protégé par Boc (seul le matériel de départ a été isolé), nous avons décidé de choisir une approche opposée.

Nous avons préparé un précurseur de couplage de Suzuki **245** par une réaction de **107** avec bis(pinacolato)diboron (**244**) en présence de $PdCl_2$(dppf) et de KOAc dans du toluène (abs). La préparation de **222** est actuellement en cours. (Schéme 35)

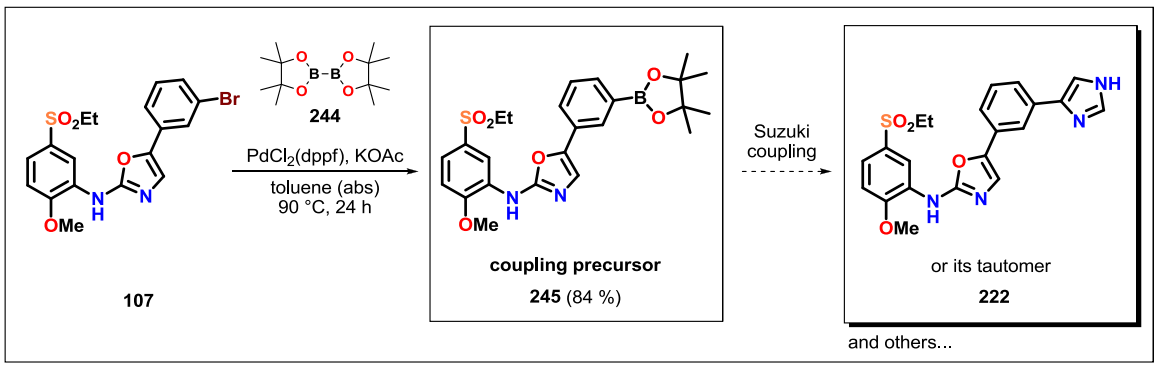

Schème 35. Synthèse du précurseur de couplage *N*,5-diaryloxazol-2-amine **245**.

Une synthèse conçue à l'origine pour la préparation du triazole **223** provient du composé **107**. Le composé **107** a ensuite été transformé par le couplage de Sonogashira avec son dérivé d'acétylène qui devait être transformé en produit final **223** par une réaction de clic médiée par CuI avec de l'azoture de triméthylsilyle. La synthèse a échoué dans la dernière étape en raison de la faible stabilité thermique du dérivé d'acétylène.

Selon les informations de la littérature, nous avons conçu une nouvelle procédure de synthèse à partir de la bromoacétophénone **197** qui a été transformée en acétylène **248** par la réaction de couplage de Sonogashira suivie d'une déprotection TMS. Une réaction de clic de **248** avec le dérivé d'azide **187** en présence de $CuSO_4.5H_2O$ et d'ascorbate de sodium dans un mélange de CH_2Cl_2 / H_2O a fourni le triazole **251** protégé par *p*-méthoxybenzyle. (Schéme 36) Un produit **252** a ensuite été synthétisé par une réaction de **251** avec du tribromure de triméthylphénylammonium dans du THF (abs). Le composé **252** a été utilisé dans une réaction avec du NaN_3 dans un mélange d'acétone / H_2O fournissant de l'azide **253**. Le triazole cible **223** a été préparé par l'hétérocyclisation thermique à médiation par PPh_3 de **253** avec l'isothiocyanate **105** suivi d'une déprotection de *p*-méthoxybenzyle dans TFA au reflux. (Schéme 36 cont.)

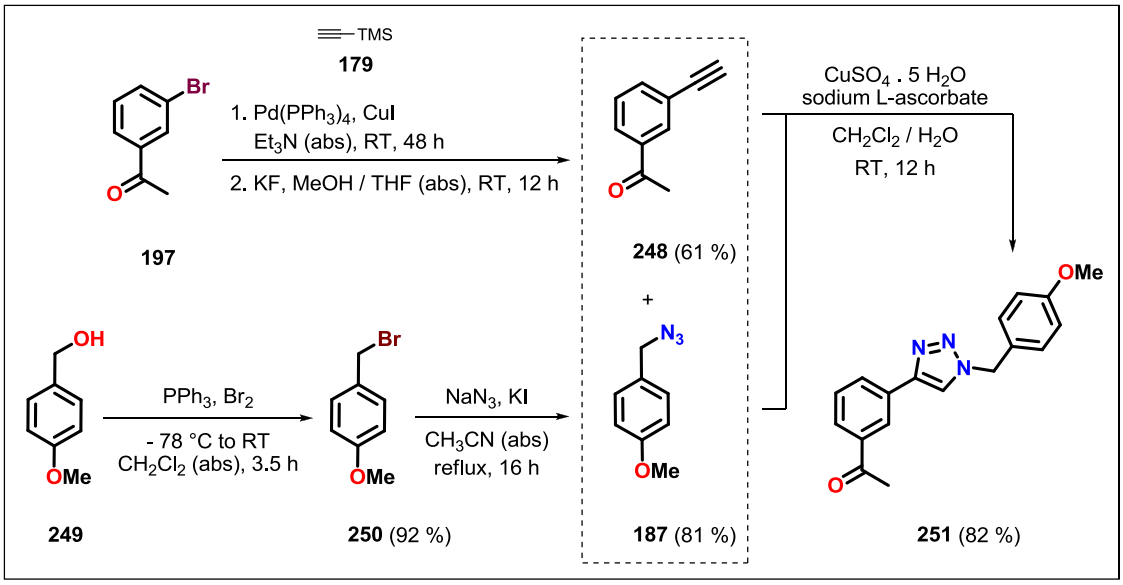

Scheme 36. Synthèse du triazole protégé par le *p*-méthoxybenzyle **251**.

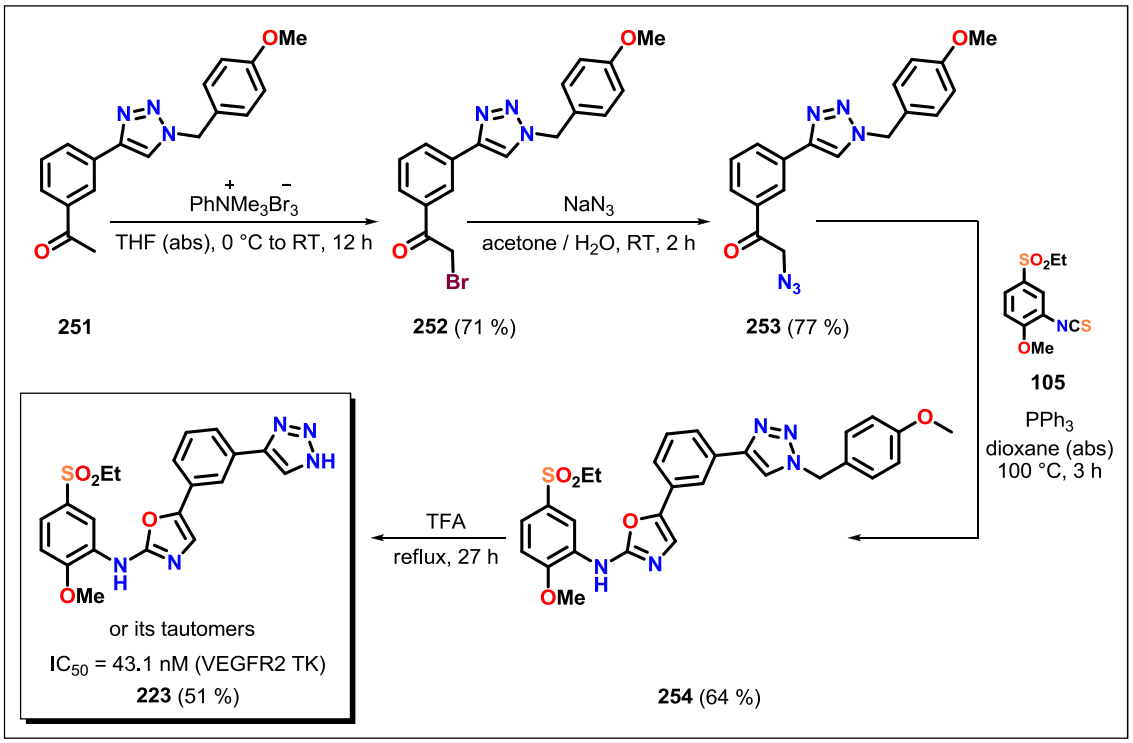

Schème 36 cont. Synthèse de *N*,5-diaryloxazol-2-amine hétérocyclique *m*-substituée **223**.

Une synthèse de *N*,5-diaryloxazol-2-amines hétérocycliques *p*,*m*-disubstituées **4** et **224** a été réalisée uniquement à petite échelle en raison des problèmes de stabilité, de purification et de caractérisation de certains intermédiaires et, par conséquent, elle doit encore être optimisée. C'est la raison pour laquelle cette synthèse n'est pas régulièrement présentée dans la partie expérimentale de la thèse.

La procédure de synthèse a commencé avec une transformation de l'aminoéthanone **255** en benzonitrile **256** par une réaction de diazotation en deux étapes en présence de ^{t}BuONO, $BF_3.Et_2O$ dans CH_2Cl_2 et CuCN, NaCN dans H_2O. Une bromation suivante de **256** utilisant Br_2 dans $CHCl_3$ a fourni le composé **257**. Le dérivé d'azide **258** a été préparé à partir de **257** par une réaction avec NaN_3 dans du MeOH. L'intermédiaire oxazole **259** a été préparé par l'hétérocyclisation thermique à médiation PPh_3 de **258** avec l'isothiocyanate **105**. Une réaction de couplage de Stille de **259** avec organostannane **154** en présence de $Pd(PPh_3)_4$ et LiCl dans du dioxane (abs) a fourni l'oxazole cible **4**. L'oxazole **224** cible a été préparé par une hydrolyse acide de **4** dans un mélange de TFA / H_2SO_4. Les produits cibles **4** et **224** ont été préparés uniquement en petite quantité (environ 10 mg chacun). Ils ont été caractérisés par des analyses ^{1}H-RMN et MS et utilisés directement dans l'analyse biologique (IC_{50}, VEGFR2 TK). (Schème 37)

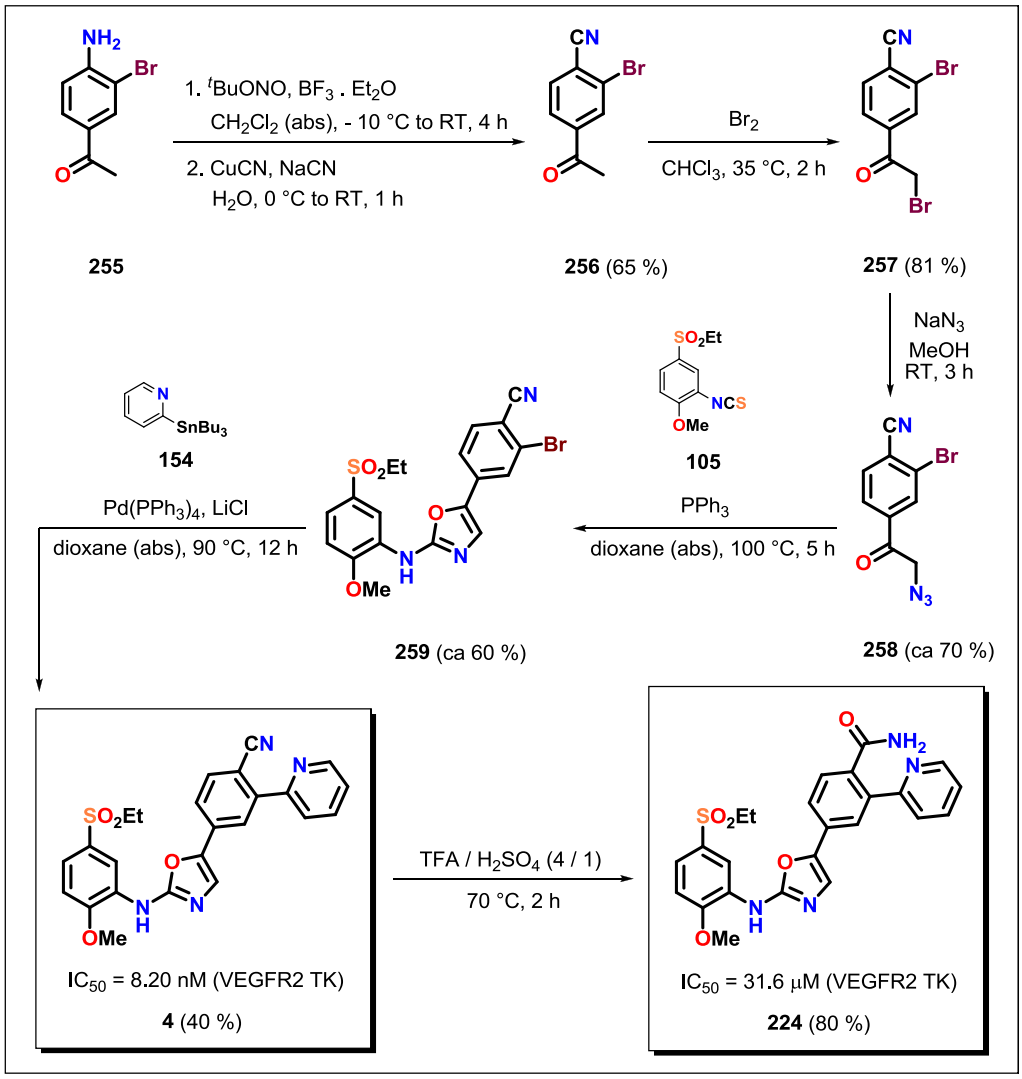

Schème 37. Synthèse des *N*,5-diaryloxazol-2-amines hétérocycliques *p*,*m*-disubstituées **4** et **224**.

11.3. Projet – Inhibition CLK1

Le troisième projet s'articule autour de l'inhibition des CLK1 et la découverte de quatre nouveaux inhibiteurs **97**, **260**, **261** et **98** possédant le squelette *N*,5-diaryloxazol-2-amine. (Figure 66) Nous avons montré que l'un de nos inhibiteurs développés possède une bonne activité à la fois sur les enzymes CLK1 et VEGFR2 TK et montre pour la première fois une activité inhibitrice duale sur ces récepteurs. Dans ce travail de thèse, nous avons développé une méthodologie pour la préparation d'un aldéhyde clef, précurseur utilisé pour la synthèse de **261** possédant une activité inhibitrice de CLK1 très importante. Ces résultats ont été publiés en 2017.[77]

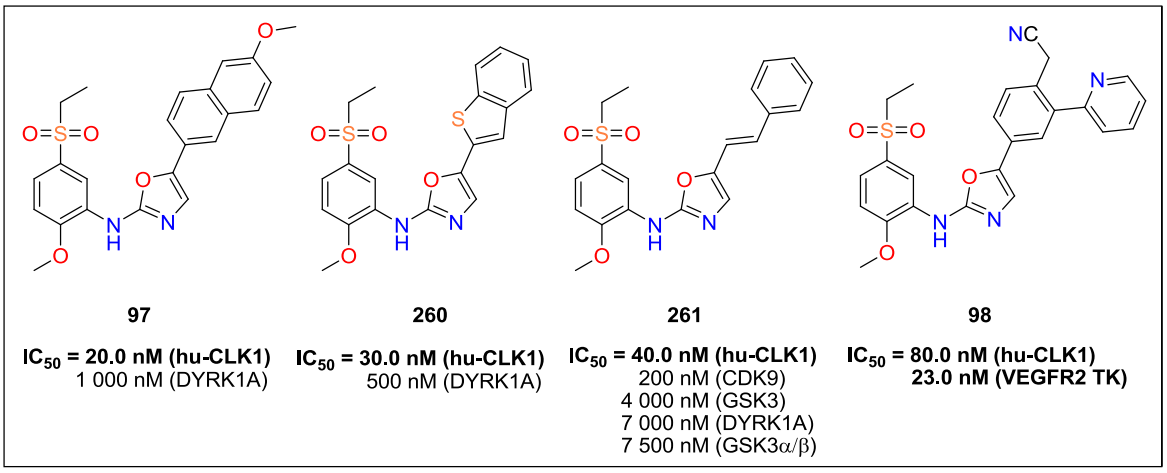

Figure 66. Inhibiteurs de CLK1 **97**, **260**, **261** et **98** développés avec leur activité biologique déterminée contre quelques CMGC protein kinases ou/et VEGFR2 TK.

Au cours de cette thèse, nous avons développé une méthodologie pour la préparation d'un important précurseur d'aldéhyde **269** qui a été utilisé dans la synthèse de l'inhibiteur hautement actif de CLK1 **261**. La synthèse a commencé par une réaction de 2-chloracétate d'éthyle (**262**) commercialisé avec du formiate d'éthyle (**263**) en présence de ^{t}BuOK dans du THF (abs) qui a fourni (*E*)-éthyl-2-chloro-3-hydroxyacrylate (**264**). Le composé **264** a ensuite été transformé en 2-aminooxazole **265** par la réaction de cyclisation avec de l'urée dans de l'H_2O. Une réaction de diazotation de **265** en présence de ^{t}BuONO, $CuCl_2$ (abs) dans CH_3CN a fourni le 2-chlorooxazole **266**. Une réaction d'addition-élimination de **266** avec l'aniline **122** dans ^{i}PrOH (abs) a fourni le dérivé de *N*-aryloxazol-2-amine **267**. Un groupe esterique de **267** a ensuite été réduit par $LiAlH_4$ dans du THF (abs) fournissant le

dérivé d'alcool **268**. Le précurseur d'aldéhyde final **269** a été préparé par une oxydation de **268** par MnO_2 dans CH_2Cl_2 (abs). (Schème 38)

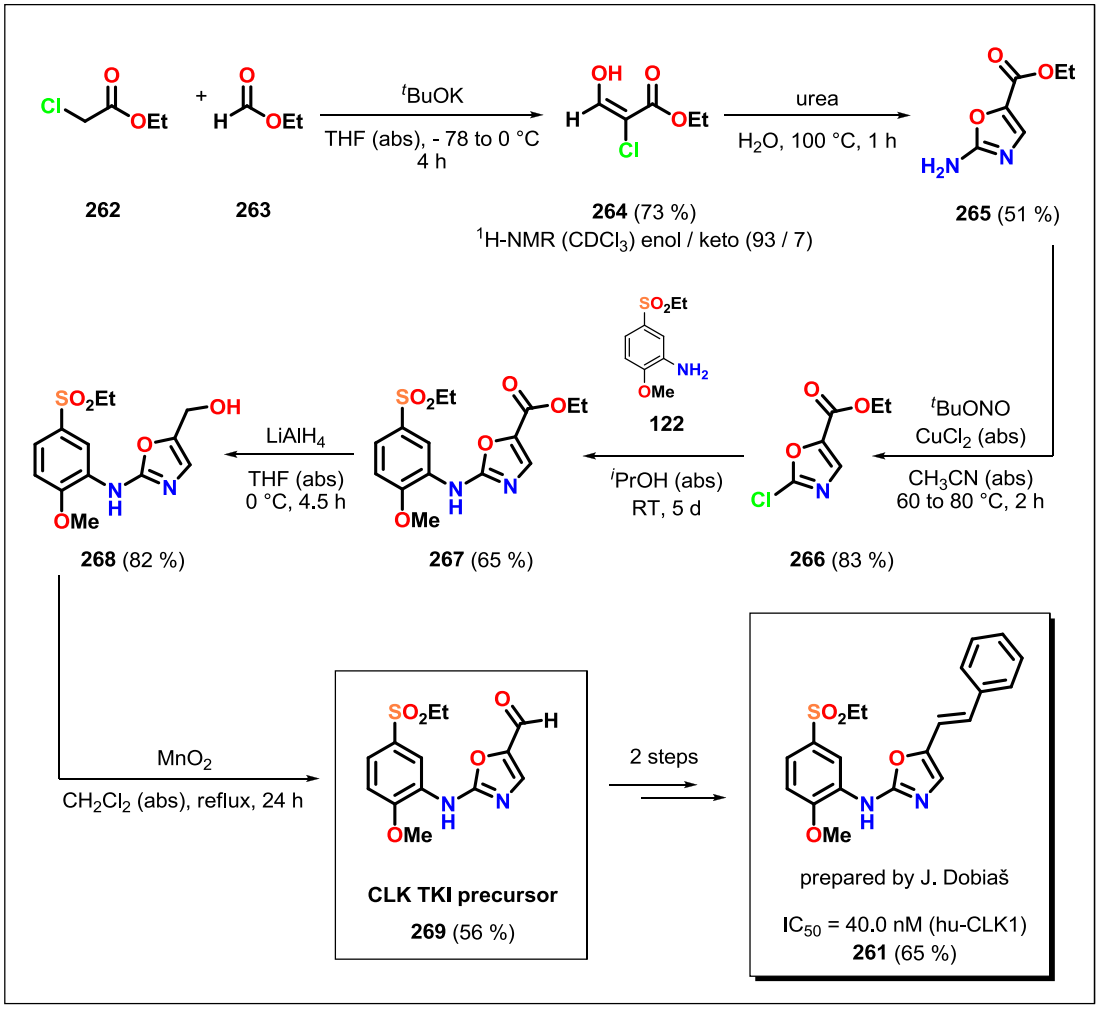

Schème 38. Synthèse du précurseur inhibiteur de CLK1 **269**.

11.4. Projet – HCC et HCSC influencés par les inhibiteurs de la tyrosine kinase (TKIs)

Enfin, dans le cadre du dernier projet, l'activité biologique des dérivés quinoides **270** – **274** (Figure 67) et des VEGFR2 TKIs **275**, **2** (AAZ), **191**, **15** (Figure 68) a été évaluée sur des lignées de cancers hépatocellulaires (HCC) et sur leurs cancer de cellule souche (HCSC). Les composés testés ont montré des valeurs IC_{50} µM contre les cellules HCC.

Le quinoide **272** a été capable d'éradiquer le cancer des cellules souches de manière identique à des HCSCs killer standards – DAPT. De plus, les VEFGR2 TKIs **275**, **2** (AAZ) et **191** cytotoxiques comprenant le sorafenib (Nexavar™) **15** qui est le produit approuvé par la FDA pour le traitement des HCC, enrichissent les populations de CSCs hépatocellulaire 2 à 3 fois après traitement. Un facteur d'agressivité (AF) caractéristique a été proposé pour estimer la qualité de nouveaux candidats pour leur capacité à éradiquer les sous-populations de CSCs. Pendant ces travaux de thèse, nous avons préparé la série de VEGFR2 TKIs **275**, **2** (AAZ) et **191** (le sorafenib **15** est disponible commercialement) et proposé un facteur d'agressivité caractéristique. Ces résultats ont été consignés dans un article en 2017.[79]

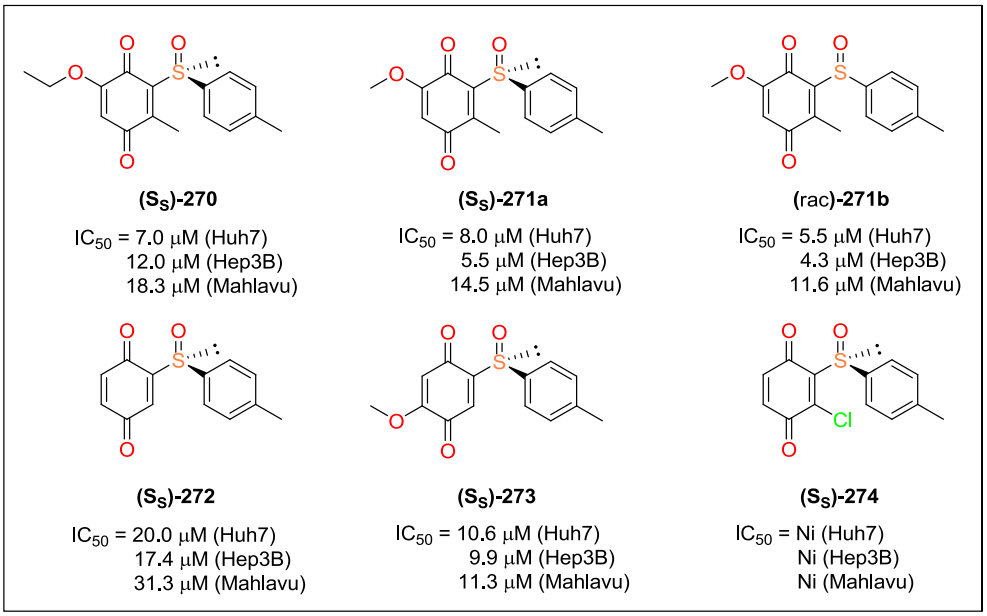

Figure 67. Structure chimique des quinoides **270** – **274** avec leur activité inhibitrices sur HCC et VEGFR2 TK.

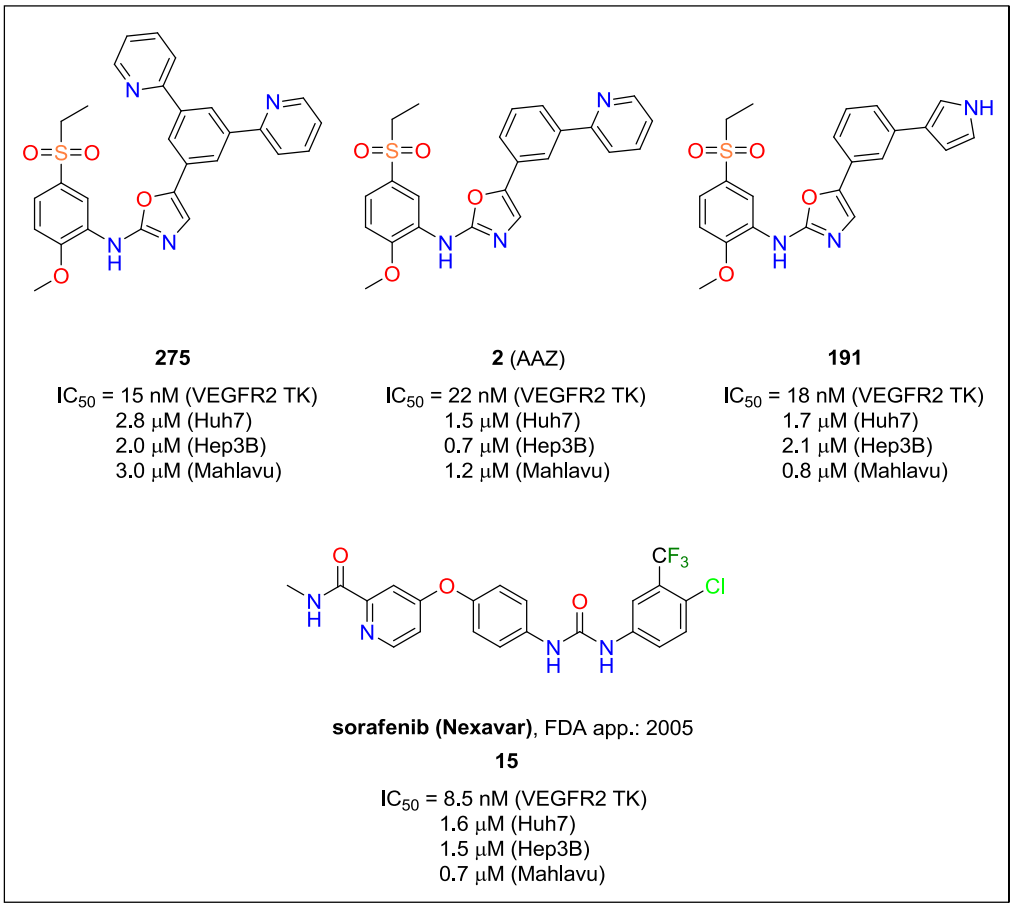

Figure 68. Structure chimique des VEGFR2 TKIs **275**, **2** (AAZ), **191** et **15** avec leur activité inhibitrices sur HCC et VEGFR2 TK.

11.5. Conclusions

Pendant les travaux de thèse, nous avons préparé 61 composés parmi lesquels 36 sont nouveaux. De 28 composés finaux conçus *in silico*, nous en avons testé 22 et 16 d'entre eux ont été évalués biologiquement (IC_{50}, VEGFR2 TK) avec pour certains des activités spectaculaires. Les composés **189**, **191**, **211**, **214**, **220**, **221**, **223** et **4** ont montré une activité nM. Les résultats ont été publiés dans deux revues à comité de lecture[77,79] (une troisième est en cours de rédaction) et présentés à cinq conférences scientifiques sous forme de communication orale ou de posters.

Chapter 12. **Future perspectives**

12. Future perspectives

The finalization of the *RegBio* project is dependent on our ability to effectively prepare the *N*,4-diaryloxazol-2-amine precursor **205** and subsequently the corresponding series of its predicted derivatives **3**, **193**, **194**, **195** and **196**.

As it was mentioned in the previous chapters, (Chapter 6.3 and 10) our attempts to prepare the precursor **205** by the AgOTf-mediated thermal heterocyclization of the arylurea **203** and α-bromoacetophenone **198** were partially successful. We managed to prepare the target compound **205** in ca 10 % yield (^{1}H-NMR, crude) but we also observed an intensive degradation of the utilized arylurea derivative **203** to aniline **122** and the problematic product purification.

After consideration of the known facts and further study of the available literature, we rethought our synthetic approach and decided to substitute the previously used α-bromoacetophenone **198** by its α-OTf-substituted analogue **276**. Because of higher reactivity of the α-OTf-derivative **276** (–OTf is better leaving group than –Br), we assumed the heterocyclization could be performed without AgOTf and at lower temperature.

Our most current results suggest that our attempts were finally successful. The optimized heterocyclization of the arylurea **203** with α-OTf-acetophenone **276** in CH_3CN (abs) at 45 °C yielded 67 % of the target *N*,4-diaryloxazol-2-amine precursor **205**. (Scheme 39) The compound **205** was purified by FLC (SiO_2) and its structure was proved by ^{1}H-NMR, ^{13}C-NMR and MS analysis.

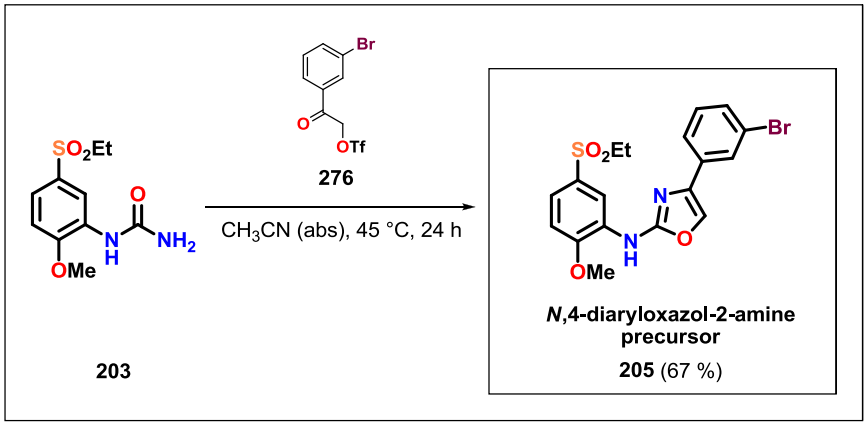

Scheme 39. Novel synthesis of *N*,4-diaryloxazol-2-amine precursor **205**.

Future perspectives

In the near future we are going to finish the synthesis of the predicted series of final compounds **3**, **193**, **194**, **195** and **196** using suitable palladium-catalyzed coupling reactions. A biological activity (IC_{50}, VEGFR2 TK) of the compounds will be subsequently determined and the *RegBio* hypothesis evaluated. Obtained results will be published as soon as possible.

Considering the finalization of the SBCP project, we are currently working on the synthesis of the imidazole derivative **222**. As it was explained in one of the previous chapters, (Chapter 7.3) our attempts to prepare the compound **222**, by the Suzuki coupling reaction, resulted in dominant formation of the homocoupling product of **245**. The utilization of the unprotected 4-bromo-1*H*-imidazole (**246**) and also its Boc-protected derivative **247** provided to the same result. The Boc-protected derivative **247** was proved to be deprotected during the reaction.

It is known fact that many of the standard protocols for palladium catalyzed C-C bond forming cross-coupling reactions fail in the presence of halo-substrates bearing acidic, nitrogen-rich heterocycles. In 2013 Düfert *et al.* published an interesting article dealing with the Suzuki coupling reactions of the unprotected, nitrogen-rich heterocycles. In the publication, possible inhibitory effects were well explained and a new methodology for the Suzuki coupling of a wide range of unprotected azoles, such as indazoles, benzimidazoles, pyrazoles, indoles, oxindoles and azaindoles was reported. Based on the reaction scope, the system using XPhos Pd G2 (**282**, **283**), K_3PO_4 in dioxane / H_2O at 100 °C provided the best results. On the following scheme is depicted a model reaction of bromopyrazoles (slightly more reactive than bromoimidazoles) to various boronic acids together with corresponding yields. [136] (Scheme 40)

[136] Düfert, M. A.; Billingsley, K. L.; Buchwald, S. L. *J. Am. Chem. Soc.* **2013**, *135*, 12877 – 12885.

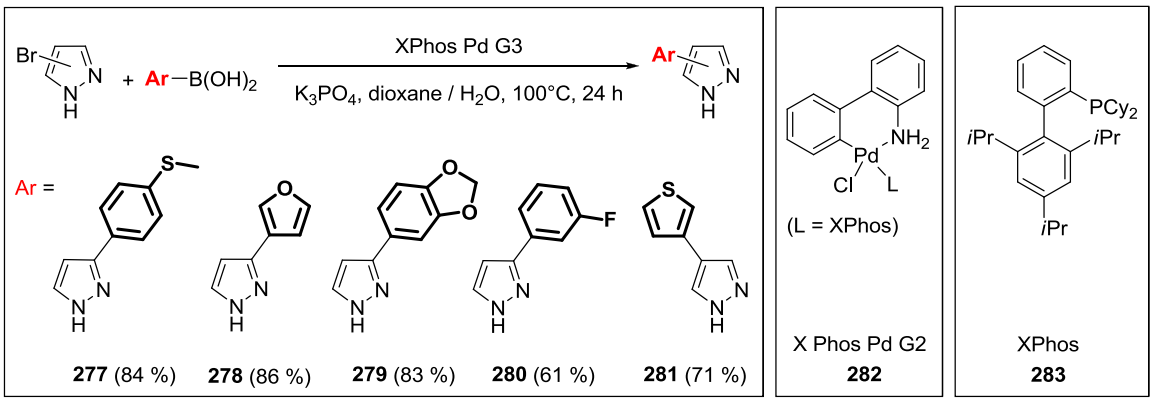

Scheme 40. Suzuki coupling of bromopyrazole to various boronic acids.

We expect that utilization the discussed methodology could possibly lead to our target imidazole derivative **222**. In the case of a failure, there is still possible to use a different coupling conditions, more stable protecting group (Bn, PMB, Tr, Ts etc.) on the bromoimidazole substrate or alternatively build the imidazol-4-yl substituent directly on the *N*,5-diaryloxazol-2-amine scaffold.

At present, we are working also on the synthesis of *p*,*m*-disubstituted heterocyclic *N*,5-diaryloxazol-2-amines **4** and **224**, which should be optimized and performed in a bigger scale. Hopefully, our optimization will be successful despite the partial instability of some intermediate products. More detailed analysis of this synthesis was discussed in the dedicated chapter. (Chapter 7.4) After finalized preparation of the compounds **222**, **4**, **224** and evaluation the corresponding biological data (IC_{50}, VEGFR2 TK), the complete SBCP project results will be published as soon as possible.

Chapter 13. **Experimental part**

13. Experimental part

13.1. Introduction

Commercially available compounds were purchased from Sigma-Aldrich, Fluorochem, Alfa Aesar, Acros Organics or TCI Europe vendors. Solvents were purchased from Sigma-Aldrich or Mikrochem in a technical grade, reagent grade or an analytical grade quality. When specified, anhydrous solvents were used; acetonitrile (CH_3CN), dichloromethane (CH_2Cl_2), 1,4-dioxane, toluene ($PhCH_3$) and triethylamine (Et_3N) were dried and distilled from CaH_2 under Ar. Tetrahydrofuran (THF) was distilled over sodium / benzophenone under Ar. Dimethylformamide (DMF), dimethylsulfoxide (DMSO) and methanol (MeOH) were purchased anhydrous from Sigma-Aldrich.

A progress of the reactions was monitored using Thin Layer Chromatography (TLC) analysis (Merck Millipore Silica gel 60 F254). UV lamp (254 nm) and iodine vapors were used for the visualization of TLC spots. Crude mixtures were purified by crystallization, trituration or Flash Liquid Chromatography (FLC) on the silica gel 60 (230-400 mesh, 0.040-0.063 mm) purchased from Merck Millipore or Sigma-Aldrich.

The prepared compounds were characterized by their M.p., NMR (NMR diagram and textual assignment), IR and MS spectroscopy and elemental, resp. X-Ray analysis. The NMR diagrams represent compendious and condensed information about assigned ^{1}H and ^{13}C-NMR data of a particular chemical structure. ^{1}H-NMR diagrams allow a smart and fast check of both chemical shifts and coupling constants. Numbers used on the diagrams mean chemical shift in δ ppm and numbers in parenthesis represent corresponding coupling constants in Hz. The reason why the NMR diagrams were used is to read and compare the NMR data more conveniently.

Nuclear Magnetic Resonance (NMR) spectra were measured on Bruker AC 400, Varian Gemini 300 or Varian Gemini 600 machines with the solvent peak as a reference. In the NMR diagrams and assignments, coupling constants (*J*) are expressed in Hertz (Hz), multiplicity is described with (s) as singlet, (br s) as broad singlet, (d) as doublet, (dd) as doublet of doublets, (ddd) as doublet of doublets of doublets, (dm) as doublet of multiplets, (t) as triplet and (q) as quadruplet.

Melting points were measured on Büchi Melting Point M-565 instrument and are given uncorrected. Infrared (IR) spectra were obtained neat using Agilent Technologies Cary 630

FTIR with diamond probe and MTS detector. Liquid Chromatography-Mass Spectrometry (LC-MS) analysis was performed on an Agilent Technologies 1200 Series instrument equipped with Mass spectrometer Agilent Technologies 6100 Quadrupole using electrospray ionization (ESI). Elemental and X-Ray analysis were obtained from the science analytical service at University of Strasbourg or Comenius University in Bratislava.

13.2. Project – Regioisomeric bioisostery (*RegBio*)

13.2.1. Synthesis of *N*,5-diaryloxazol-2-amine precursor 107

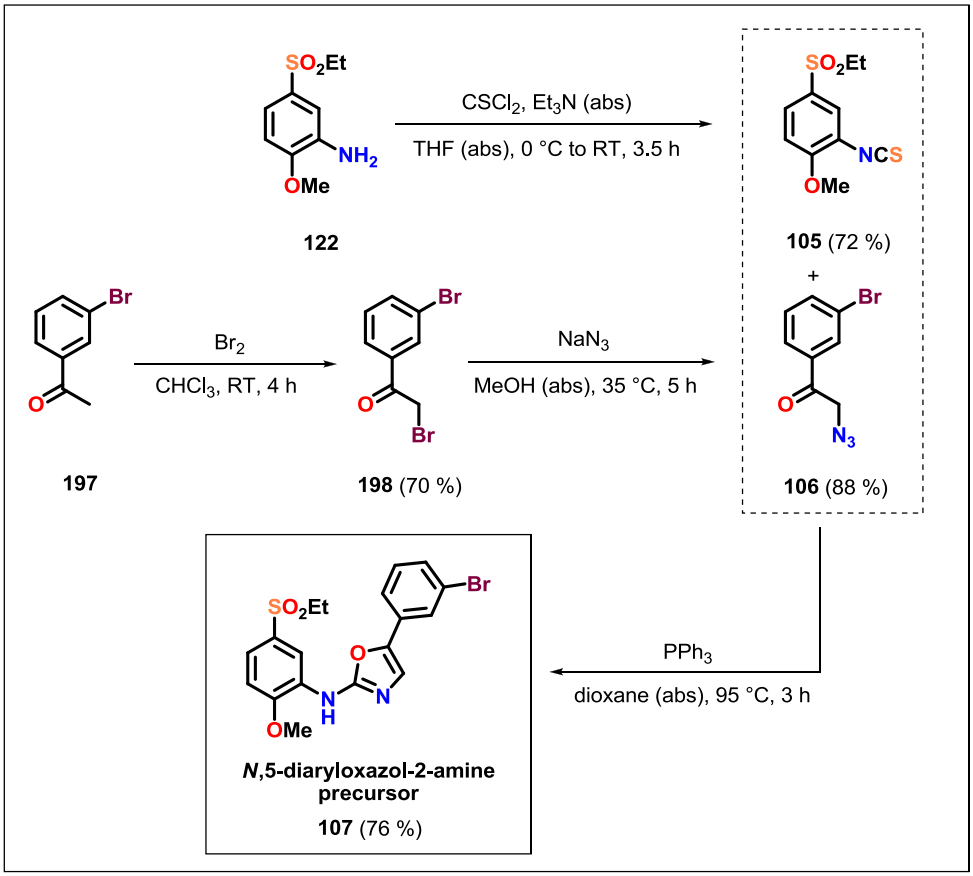

Scheme 23. Synthesis of *N*,5-diaryloxazol-2-amine precursor **107**.

Synthesis of 4-(ethylsulfonyl)-2-isothiocyanato-1-methoxybenzene (105)

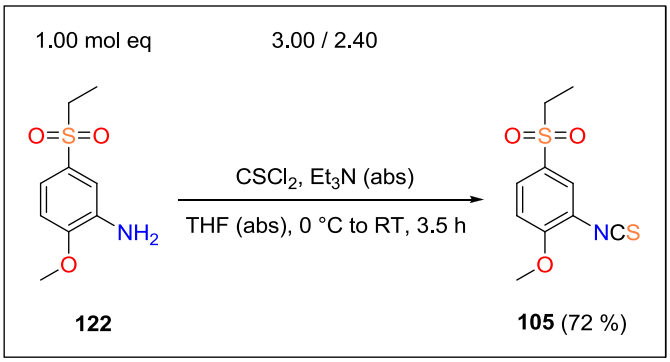

To a solution of 500 mg (2.32 mmol, 1.00 mol eq) aniline **122** in 15 ml THF (abs), 780 µL (5.57 mmol, 2.40 mol eq) of Et_3N (abs) was added under Ar. The mixture was cooled down to 0 °C and 530 µl (6.96 mmol, 3.00 mol eq) of thiophosgene was added dropwise within 30 min. Then the reaction was stirred 3.5 h at RT. After complete consumption of starting material **122** (TLC analysis), volatile parts were evaporated and a solid residue was stirred with 15 ml of EA. The obtained suspension was extracted with 15 ml of H_2O and 3 x 5 ml of $NaHCO_3$ (saturated aq solution). The organic layer was separated, dried over Na_2SO_4, filtered and concentrated under reduced pressure. The crude product was purified by FLC (Hex / EA = 2 / 1) yielding 427 mg (1.66 mmol, 72 %) of 4-(ethylsulfonyl)-2-isothiocyanato-1-methoxybenzene (**105**).

Novelty: The synthesis of **105** was described in the literature with the yield of 100 % together with its ^{1}H-NMR spectra and elemental analysis.[6]

M.p.: 108 – 110 °C [Hex / EA]. Off-white crystalline solid material.

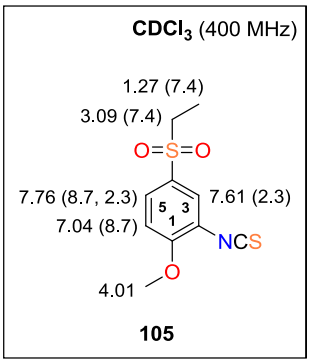

^{1}H-NMR (400 MHz, $CDCl_3$): δ 7.76 (dd, 1H, J(5,6) = 8.7 Hz, J(3,5) = 2.3 Hz, H-C(5)), 7.61 (d, 1H, J(3,5) = 2.3 Hz, H-C(3)), 7.04 (d, 1H, J(5,6) = 8.7 Hz, H-C(6)), 4.01 (s, 3H, -OCH_3), 3.09 (q, 2H, $J(CH_2CH_3)$ = 7.4 Hz, -$COOC\underline{H}_2CH_3$), 1.27 (t, 3H, $J(CH_2,CH_3)$ = 7.4 Hz, -$COOCH_2C\underline{H}_3$).

Synthesis of 2-bromo-1-(3-bromophenyl)ethanone (198)

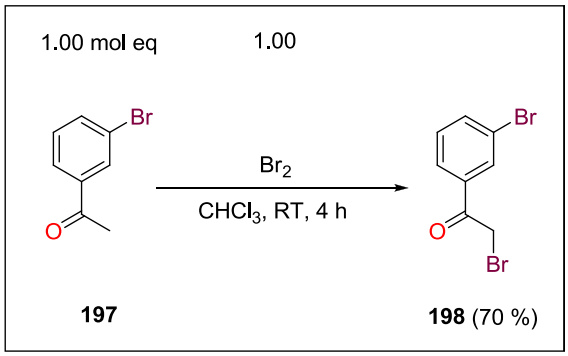

To a solution of 3.60 g (18.1 mmol, 1.00 mol eq) 1-(3-bromophenyl)ethanone (**197**) in 30 ml of $CHCl_3$, 2.89 g (18.1 mmol, 1.00 mol eq) of Br_2 in 10 ml of $CHCl_3$ was added dropwise at RT within 1 h. At the beginning of the addition, the reaction mixture was slightly heated (ca 50 – 60 °C) to start the bromination reaction indicated by decolorizing of the mixture. After completed addition the reaction mixture was stirred at RT for 3 h. When complete consumption the starting material **197** was confirmed (TLC analyze), the mixture was extracted with 2 x 10 ml of $NaHCO_3$ (aq saturated solution) and 10 ml of H_2O. Combined organic layers were dried over Na_2SO_4, filtered and evaporated under reduced pressure. The crude product was purified by crystallization from EtOH yielding 3.50 g (12.6 mmol, 70 %) of 2-bromo-1-(3-bromophenyl)ethanone (**198**).

Novelty: The synthesis of **198** was described in the literature with 78 % yield.[137] Its ^{1}H-NMR, ^{13}C-NMR, IR and HRMS spectra were also published.[138]

M.p.: 49.0 – 51.0 °C [EtOH] (lit. M.p.: 51 – 52 °C).[138] White crystalline solid material.

[137] Sanath Kumar T.S.S.P.N.S.; Prasant A.; Krupadanam D.G.L.; Kumar K.A. *Indian J. Chem. Sec B* **2012**, *51B*, 658 – 662.
[138] Xie L.; Wu Y.; Yi W.; Zhu L.; Xiang J.; He W. *J. Org. Chem.* **2013**, *78*, 9190 – 9195.

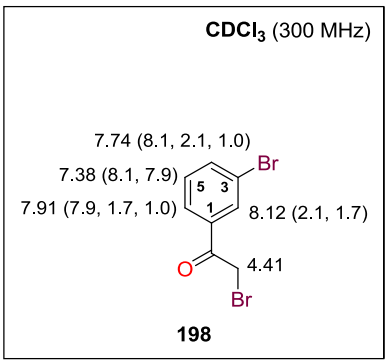

^{1}H-NMR (300 MHz, $CDCl_3$) δ 8.12 (dd, 1H, *J*(2,4) = 2.1 Hz, *J*(2,6) = 1.7 Hz, H-C(2)), 7.91 (ddd, 1H, *J*(5,6) = 7.9 Hz, *J*(2,6) = 1.7 Hz, *J*(4,6) = 1.0 Hz, H-C(6)), 7.74 (ddd, 1H, *J*(4,5) = 8.1 Hz, *J*(2,4) = 2.1 Hz, *J*(4,6) = 1.0 Hz, H-C(4)), 7.38 (dd, 1H, *J*(4,5) = 8.1 Hz, *J*(5,6) = 7.9 Hz, H-C(5)), 4.41 (s, 2H, -$COCH_2Br$).

Synthesis of 2-azido-1-(3-bromophenyl)ethanone (106)

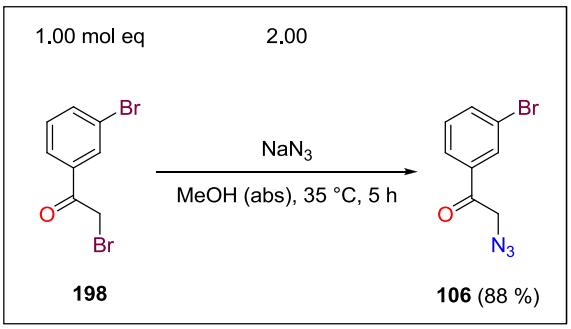

To a solution of 500 mg (1.80 mmol, 1.00 mol eq) 2-bromo-1-(3-bromophenyl)ethanone (**198**) in 5.0 ml of MeOH (abs), 234 mg (3.60 mmol, 2.00 mol eq) NaN_3 was added portionwise and the reaction mixture was stirred for 5 h at 35 °C under Ar. After consumption of starting material **198** (TLC analysis) the mixture was cooled down to RT and the solvent evaporated. A solid residue was partitioned between 30 ml of EA and 30 ml of H_2O, organic layer separated and aq layer extracted with 3 x 5 ml of EA. The combined organic layer was dried over Na_2SO_4, filtered and concentrated under reduced pressure. The crude product was purified by crystallization from a mixture of pentane / EtOH to yield 380 mg (1.58 mmol, 88 %) of 2-azido-1-(3-bromophenyl)ethanone (**106**).

Novelty: Synthesis of **106** was described in the literature with 91 % yield. Its ^{1}H-NMR, ^{13}C-NMR, IR and HRMS spectra were also published.[139]

M.p.: 71.0 – 74.0 °C [pentane / EtOH] (lit. M.p.: 51 – 53 °C [Hex / EA]).[139] Yellow crystalline solid material.

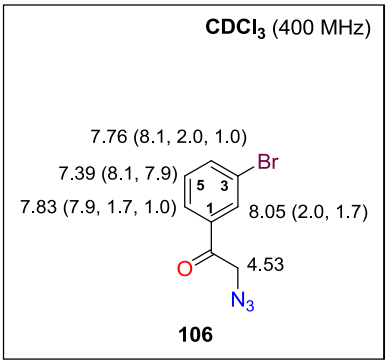

^{1}H-NMR (400 MHz, $CDCl_3$): δ 8.05 (dd, 1H, *J*(2,4) = 2.0 Hz, *J*(2,6) = 1.7 Hz, H-C(2)), 7.83 (ddd, 1H, *J*(5,6) = 7.9 Hz, *J*(2,6) = 1.7 Hz, *J*(4,6) = 1.0 Hz, H-C(6)), 7.76 (ddd, 1H, *J*(4,5) = 8.1 Hz, *J*(2,4) = 2.0 Hz, *J*(4,6) = 1.0 Hz, H-C(4)), 7.39 (dd, 1H, *J*(4,5) = 8.1 Hz, *J*(5,6) = 7.9 Hz, H-C(5)), 4.53 (s, 2H, -$COCH_2N_3$).

Synthesis of 5-(3-bromophenyl)-*N*-(5-(ethylsulfonyl)-2-methoxyphenyl) oxazol-2-amine (107)

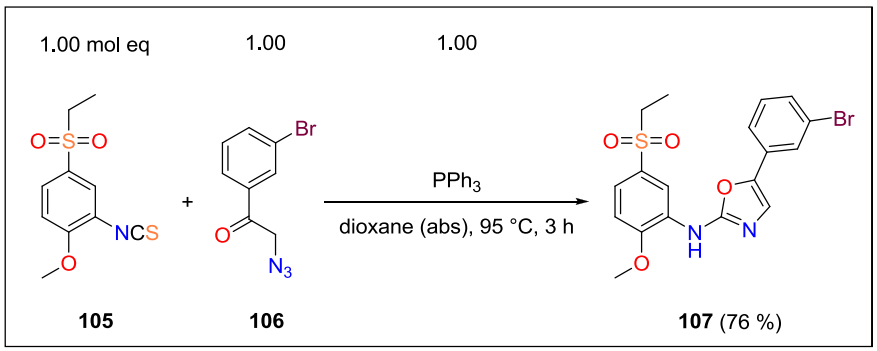

A mixture of 1.00 g (3.89 mmol, 1.00 mol eq) isothiocyanate **105**, 933 mg (3.89 mmol, 1.00 mol eq) of azide **106** and 1.00 g (3.89 mmol, 1.00 mol eq) of PPh_3 were dissolved in 25 ml of dioxane (abs) under Ar. The obtained solution was placed into the preheated 95

[139] Okumus S.; Tanyeli C.; Demir A.C. *Tetrahedron Lett.* **2014**, *55*, 4302 – 4305.

°C oil bath for 3 h. After consumption of the starting material **105** and **106** (TLC analysis), the reaction mixture was evaporated and an obtained solid material was dissolved in 25 ml of EA and extracted by 4 x 5 ml of brine. The organic layer was dried over Na_2SO_4, filtered and evaporated under reduced pressure. The crude product was purified by FLC (Hex / EA, 1 / 3) and crystallized from Hex / EA yielding 1.30 g (2.97 mmol, 76 %) of 5-(3-bromophenyl)-*N*-(5-(ethylsulfonyl)-2-methoxyphenyl)oxazol-2-amine (**107**).

Novelty: Synthesis of **107** was published in the literature with 35 % yield.[82] Also its ^{1}H-NMR, ^{13}C-NMR, IR, MS spectra and elemental analysis were published.[6,82]

M.p.: 177 – 178 °C [Hex / EA]. (lit. M.p.: 182 – 183 °C [Hex / EA]).[82] Pale yellow solid material.

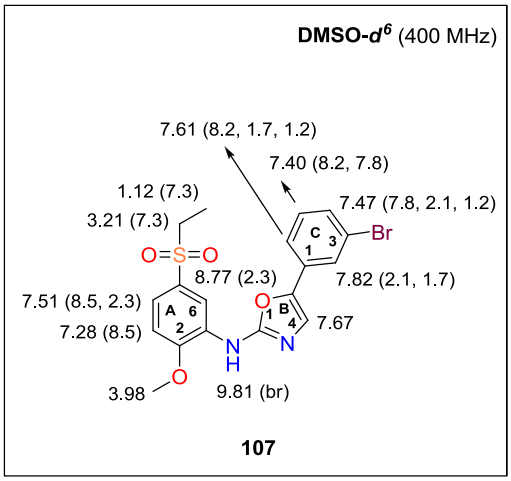

^{1}H-NMR (400 MHz, DMSO-d^6): δ 9.81 (br s, 1H, -NH-), 8.77 (d, 1H, $J(A_4,A_6)$ = 2.3 Hz, H-C_A(6)), 7.82 (dd, 1H, $J(C_2,C_4)$ = 2.1 Hz, $J(C_2,C_6)$ = 1.7 Hz, H-C_C(2)), 7.67 (s, 1H, H-C_B(4)), 7.61 (ddd, 1H, $J(C_5,C_6)$ = 8.2 Hz, $J(C_2,C_6)$ = 1.7 Hz, $J(C_4,C_6)$ = 1.2 Hz, H-C_C(6)), 7.51 (dd, 1H, $J(A_3,A_4)$ = 8.5 Hz, $J(A_4,A_6)$ = 2.3 Hz, H-C_A(4)), 7.47 (ddd, 1H, $J(C_4,C_5)$ = 7.8 Hz, $J(C_2,C_4)$ = 2.1 Hz, $J(C_4,C_6)$ = 1.2 Hz, H-C_C(4)), 7.40 (dd, 1H, $J(C_5,C_6)$ = 8.2 Hz, $J(C_4,C_5)$ = 7.8 Hz, H-C_C(5)), 7.28 (d, 1H, $J(A_3,A_4)$ = 8.5 Hz, H-C_A(3)), 3.98 (s, 3H, -OCH_3), 3.21 (q, 2H, $J(CH_2,CH_3)$ = 7.3 Hz, -$SO_2C\underline{H}_2CH_3$), 1.12 (t, 3H, $J(CH_2,CH_3)$ = 7.3 Hz, -$SO_2CH_2C\underline{H}_3$).

13.2.2. Synthesis of *N*,5-diaryloxazol-2-amines 2, 189, 190, 191, 192

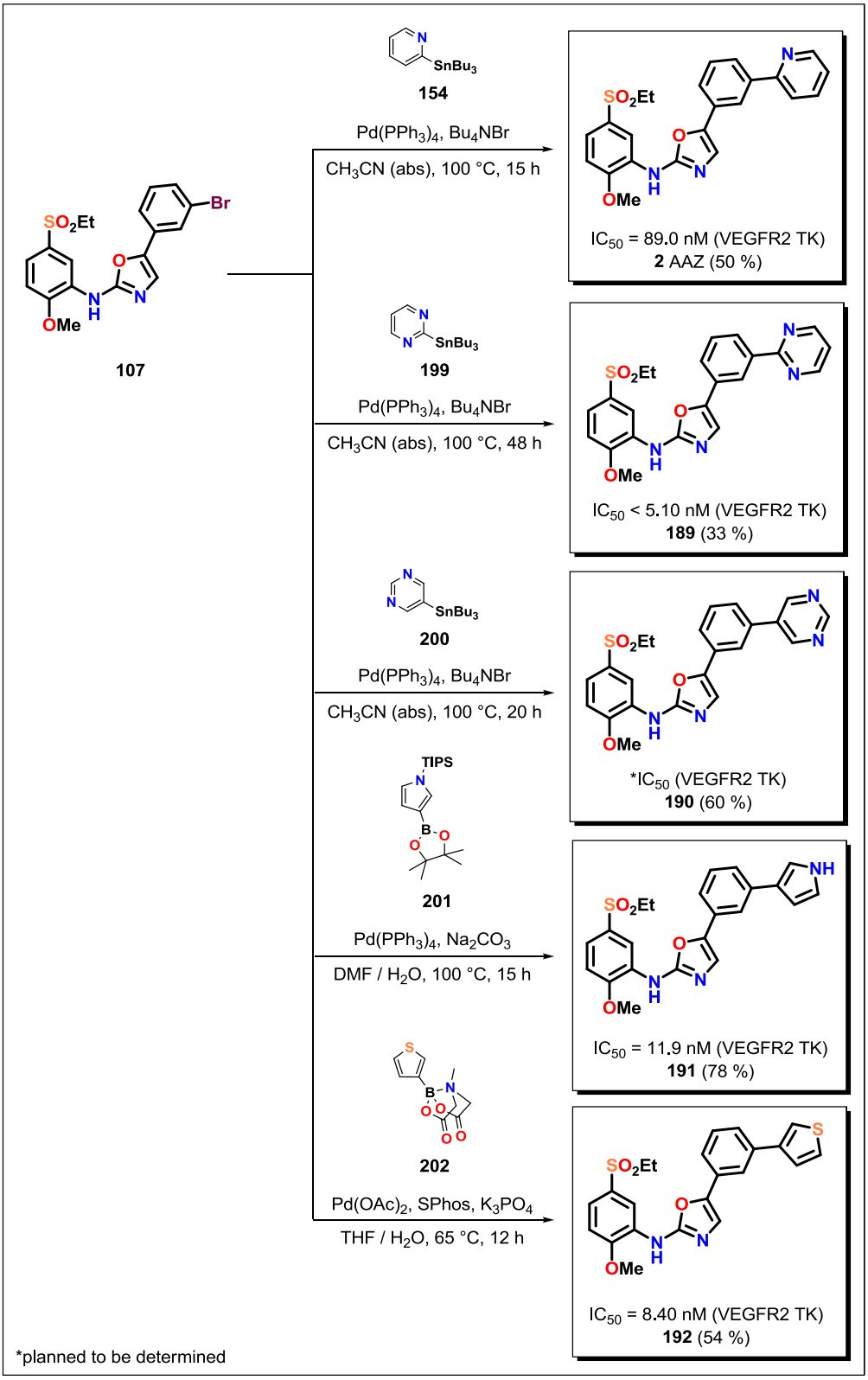

Scheme 25. Synthesis of *N*,5-diaryloxazol-2-amines **2**, **189**, **190**, **191**, **192**.

Synthesis of *N*-(5-(ethylsulfonyl)-2-methoxyphenyl)-5-(3-(pyridin-2-yl) phenyl)oxazol-2-amine (2)

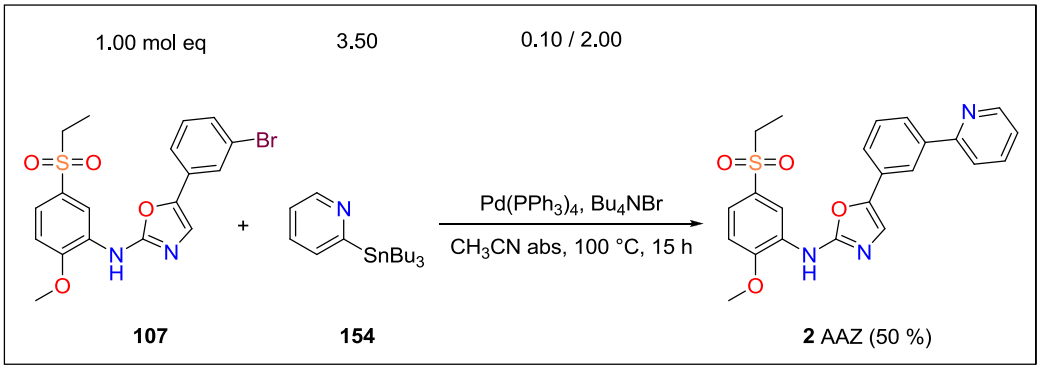

A suspension of 100 mg (0.23 mmol, 1.00 mol eq) starting material **107**, 26.4 mg (0.02 mmol, 0.10 mol eq) of $Pd(PPh_3)_4$ and 148 mg (0.46 mmol, 2.00 mol eq) of Bu_4NBr in 5 ml of CH_3CN (abs) prepared in a sealed tube was bubbled by Ar for 10 min. Afterwards 295 mg (0.80, 3.50 mol eq) of tributylstannane **154** was added and the mixture was stirred at 100 °C for 15 h. The reaction was cooled down to RT, diluted with 10 ml of EA, quenched with 10 ml of KF (saturated aq solution) and stirred for 3 h. The organic layer was separated, washed with 10 ml of H_2O, dried by Na_2SO_4, filtered and concentrated under reduced pressure. The crude product was purified by FLC (Hex / EA = 1 / 4) and triturated with Hex / EA yielding 50.0 mg (0.11 mmol, 50 %) of *N*-(5-(ethylsulfonyl)-2-methoxyphenyl)-5-(3-(pyridin-2-yl)phenyl)oxazol-2-amine (**2**).

Novelty: Synthesis of **2** was described in the literature with 51 % yield. Its ^{1}H-NMR, MS spectra and elemental analysis were also published.[6]

M. p.: 206 – 207 °C [Hex / EA]. Off white solid material.

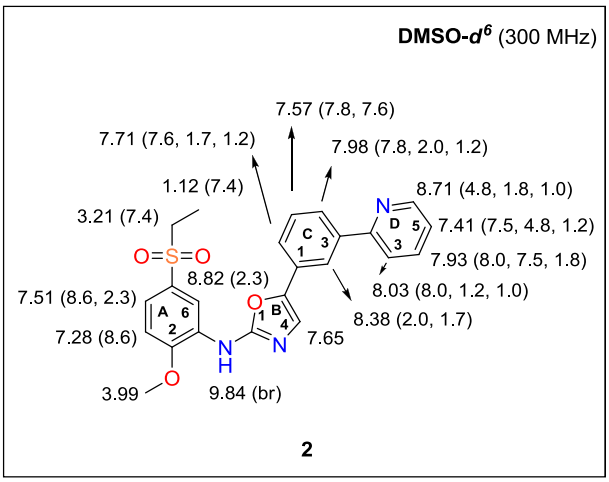

^{1}H-NMR (300 MHz, DMSO-d^6): δ 9.84 (br s, 1H, -NH-), 8.82 (d, 1H, $J(A_4,A_6)$ = 2.3 Hz, H-C_A(6)), 8.71 (ddd, 1H, $J(D_5,D_6)$ = 4.8 Hz, $J(D_4,D_6)$ = 1.8 Hz, $J(D_3,D_6)$ = 1.0 Hz, H-C_D(6)), 8.38 (dd, 1H, $J(C_2,C_4)$ = 2.0 Hz, $J(C_2,C_6)$ = 1.7 Hz, H-C_C(2)), 8.03 (ddd, 1H, $J(D_3,D_4)$ = 8.0 Hz, $J(D_3,D_5)$ = 1.2 Hz, $J(D_3,D_6)$ = 1.0 Hz, H-C_D(3)), 7.98 (ddd, 1H, $J(C_4,C_5)$ = 7.8 Hz, $J(C_2,C_4)$ = 2.0 Hz, $J(C_4,C_6)$ = 1.2 Hz, H-C_C(4)), 7.93 (ddd, 1H, $J(D_3,D_4)$ = 8.0 Hz, $J(D_4,D_5)$ = 7.5 Hz, $J(D_4,D_6)$ = 1.8 Hz, H-C_D(4)), 7.71 (ddd, 1H, $J(C_5,C_6)$ = 7.6 Hz, $J(C_2,C_6)$ = 1.7 Hz, $J(C_4,C_6)$ = 1.2 Hz, H-C_C(6)), 7.65 (s, 1H, H-C_B(4)), 7.57 (dd, 1H, $J(C_4,C_5)$ = 7.8 Hz, $J(C_5,C_6)$ = 7.6 Hz, H-C_C(5)), 7.51 (dd, 1H, $J(A_3,A_4)$ = 8.6 Hz, $J(A_4,A_6)$ = 2.3 Hz, H-C_A(4)), 7.41 (ddd, 1H, $J(D_4,D_5)$ = 7.5 Hz, $J(D_5,D_6)$ = 4.8 Hz, $J(D_3,D_5)$ = 1.2 Hz, H-C_D(5)), 7.28 (d, 1H, $J(A_3,A_4)$ = 8.6 Hz, H-C_A(3)), 3.99 (s, 3H, -OCH_3), 3.21 (q, 2H, $J(CH_2,CH_3)$ = 7.4 Hz, -$SO_2C\underline{H}_2CH_3$), 1.12 (t, 3H, $J(CH_2,CH_3)$ = 7.4 Hz, -$SO_2CH_2C\underline{H}_3$).

Synthesis of *N*-(5-(ethylsulfonyl)-2-methoxyphenyl)-5-(3-(pyrimidin-2-yl)phenyl)oxazol-2-amine (189)

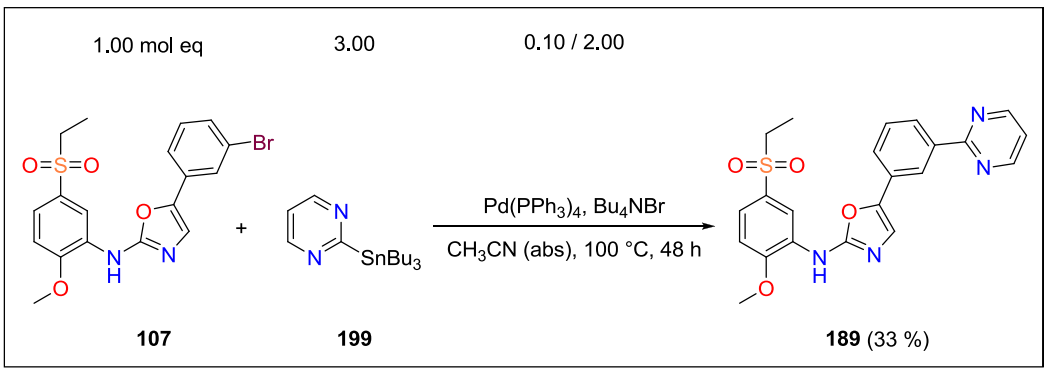

A suspension of 150 mg (0.34 mmol, 1.00 mol eq) starting material **107**, 39.6 mg (0.03 mmol, 0.10 mol eq) of $Pd(PPh_3)_4$ and 221 mg (0.69 mmol, 2.00 mol eq) of Bu_4NBr in 5 ml of CH_3CN (abs) prepared in a sealed tube was bubbled by Ar for 10 min. Afterwards 295 mg (1.03 mmol, 3.00 mol eq) of tributylstannane **199** was added and the mixture was stirred at 100 °C for 48 h. The reaction was cooled down to RT, diluted with 10 ml of EA, quenched with 10 ml of KF (saturated aq solution) and stirred for 3 h. The organic layer was separated, washed with 10 ml of H_2O, dried by Na_2SO_4, filtrated and concentrated under reduced pressure. The crude product was purified by FLC (Hex / EA = 1 / 2) and triturated with Hex / EA yielding 50.0 mg (0.11 mmol, 33 %) of *N*-(5-(ethylsulfonyl)-2-methoxyphenyl)-5-(3-(pyrimidin-2-yl)phenyl)oxazol-2-amine (**189**).

Novelty: Preparation or characterization of compound **189** has not been described in the literature.

M. p.: 220 – 223 °C [Hex / EA]. Pale yellow solid material.

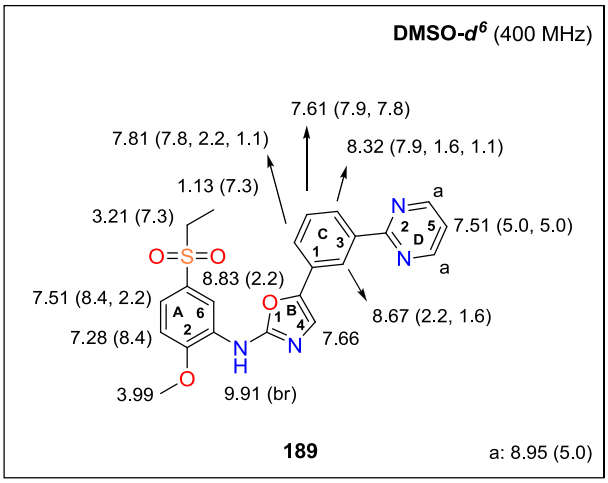

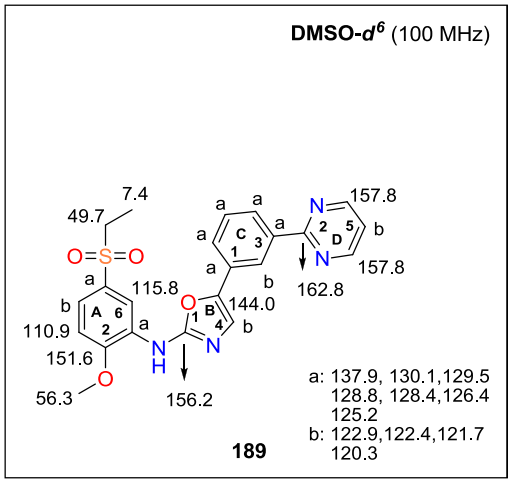

^{1}H-NMR (400 MHz, DMSO-d^6): δ 9.91 (br s, 1H, -NH-), 8.95 (d, 2H, $J(D_4,D_5)$ = 5.0 Hz, 2 x H-C_D(4)), 8.83 (d, 1H, $J(A_4,A_6)$ = 2.2 Hz, H-C_A(6)), 8.67 (dd, 1H, $J(C_2,C_6)$ = 2.2 Hz, $J(C_2,C_4)$ = 1.6 Hz, H-C_C(2)), 8.32 (ddd, 1H, $J(C_4,C_5)$ = 7.9 Hz, $J(C_2,C_4)$ = 1.6 Hz, $J(C_4,C_6)$ = 1.1 Hz, H-C_C(4)), 7.81 (ddd, 1H, $J(C_5,C_6)$ = 7.8 Hz, $J(C_2,C_6)$ = 2.2 Hz, $J(C_4,C_6)$ = 1.1 Hz, H-C_C(6)), 7.66 (s, 1H, H-C_B(4)), 7.61 (dd, 1H, $J(C_4,C_5)$ = 7.9 Hz, $J(C_5,C_6)$ = 7.8 Hz, H-C_C(5)), 7.51 (dd, 1H, $J(A_3,A_4)$ = 8.4 Hz, $J(A_4,A_6)$ = 2.2 Hz, H-C_A(4)), 7.51 (t, 1H, $J(D_4,D_5)$ = $J(D_5,D_6)$ = 5.0 Hz, H-C_D(5)), 7.28 (d, 1H, $J(A_3,A_4)$ = 8.4 Hz, H-C_A(3)), 3.99 (s,

3H, -OCH_3), 3.21 (q, 2H, $J(CH_2,CH_3)$ = 7.3 Hz, -$SO_2C\underline{H}_2CH_3$), 1.13 (t, 3H, $J(CH_2,CH_3)$ = 7.3 Hz, -$SO_2CH_2C\underline{H}_3$).

^{13}C-NMR (100 MHz, DMSO-d^6): δ 162.8 (C_D(2)), 157.8 (C_D(4) and C_D(6)), 156.2 (C_B(2)), 151.6 (C_A(2)), 144.0 (C_B(5)), 137.9, 130.1, 129.5, 128.8, 128.4, 126.4, 125.2, 122.9, 122.4, 121.7, 120.3, 115.8 (C_A(6)), 110.9 (C_A(3)), 56.3 (-OCH_3), 49.7 (-$SO_2\underline{C}H_2CH_3$), 7.4 (-$SO_2CH_2\underline{C}H_3$).

FT IR (solid, cm^{-1}): 3423 (w), 3029 (w), 2961 (w), 2323 (w), 2114 (w), 2079 (w), 1723 (w), 1613 (s), 1580 (s), 1529 (s), 1486 (m), 1453 (m), 1403 (s), 1351 (w), 1302 (s), 1264 (s), 1234 (m), 1123 (s), 1087 (s), 1049 (w), 1017 (m), 958 (w), 913 (w), 892 (w), 827 (w), 793 (m), 775 (s), 736 (s), 724 (s), 690 (m), 634 (w), 605 (m), 579 (w), 554 (m), 528 (s), 489 (s), 469 (s).

MS (ESI m/z): 437.1 $[M + H]^+$, 459.1 $[M + Na]^+$; in negative mode 435.0 $[M - H]^-$.

Anal. calcd for $C_{22}H_{20}N_4O_4S$ (436.48): C, 60.54; H, 4.62; N, 12.84; Found: C, 60.72; H, 4.51; N, 12.79.

Synthesis of *N*-(5-(ethylsulfonyl)-2-methoxyphenyl)-5-(3-(pyrimidin-5-yl)phenyl)oxazol-2-amine (190)

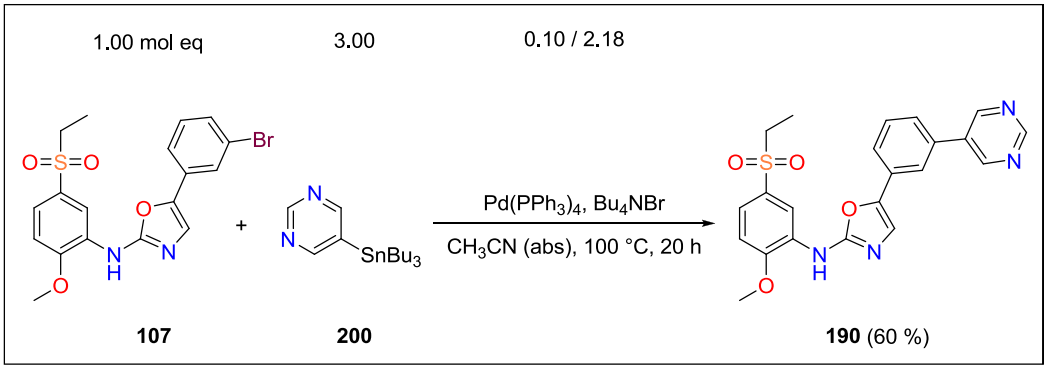

A suspension of 100 mg (0.23 mmol, 1.00 mol eq) starting material **107**, 26.4 mg (0.02 mmol, 0.10 mol eq) of $Pd(PPh_3)_4$ and 161 mg (0.50 mmol, 2.18 mol eq) of Bu_4NBr in 7 ml of CH_3CN (abs) prepared in a sealed tube was bubbled by Ar for 10 min. Afterwards 253

mg (0.69 mmol, 3.00 mol eq) of tributylstannane **200** was added and the mixture was stirred at 100 °C for 20 h. The reaction was cooled down to RT, diluted with 10 ml of EA, quenched with 10 ml of KF (saturated aq solution) and stirred for 3 h. The organic layer was separated, washed with 10 ml of H_2O, dried by Na_2SO_4, filtrated and concentrated under reduced pressure. The crude product was purified by FLC (Hex / EA = 1 / 2) and triturated with Hex / EA yielding 60.0 mg (0.14 mmol, 60 %) of *N*-(5-(ethylsulfonyl)-2-methoxyphenyl)-5-(3-(pyrimidin-5-yl)phenyl)oxazol-2-amine (**190**).

Novelty: Preparation or characterization of compound **190** has not been described in the literature.

M. p.: 220 – 223 °C [Hex / EA]. Pale red solid material.

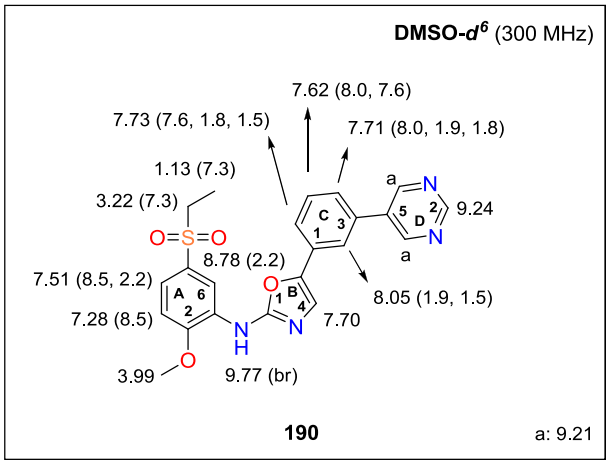

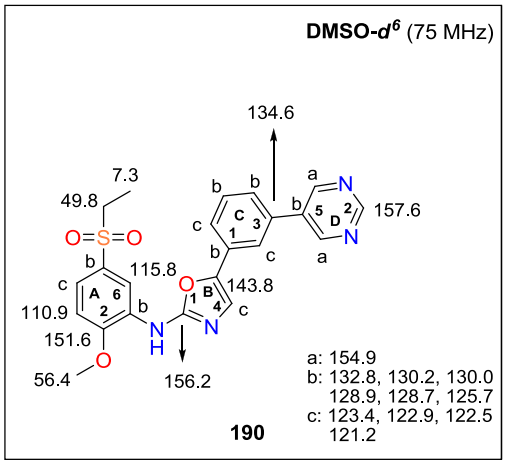

^{1}H-NMR (300 MHz, DMSO-d^6): δ 9.77 (br s, 1H, -NH-), 9.24 (s, 1H, H-C_D(2)), 9.21 (s, 2H, 2 x H-C_D(4)), 8.78 (d, 1H, J(A_4,A_6) = 2.2 Hz, H-C_A(6)), 8.05 (dd, 1H, J(C_2,C_4) = 1.9 Hz, J(C_2,C_6) = 1.5 Hz, H-C_C(2)), 7.73 (ddd, 1H, J(C_5,C_6) = 7.6 Hz, J(C_4,C_6) = 1.8 Hz, J(C_2,C_6) = 1.5 Hz, H-C_C(6)), 7.71 (ddd, 1H, J(C_4,C_5) = 8.0 Hz, J(C_2,C_4) = 1.9 Hz, J(C_4,C_6) = 1.8 Hz, H-C_C(4)), 7.70 (s, 1H, H-C_B(4)), 7.62 (dd, 1H, J(C_4,C_5) = 8.0 Hz, J(C_5,C_6) = 7.6 Hz, H-C_C(5)), 7.51 (dd, 1H, J(A_3,A_4) = 8.5 Hz, J(A_4,A_6) = 2.2 Hz, H-C_A(4)), 7.28 (d, 1H, J(A_3,A_4) = 8.5 Hz, H-C_A(3)), 3.99 (s, 3H, -OCH_3), 3.22 (q, 2H, J(CH_2,CH_3) = 7.3 Hz, -$SO_2C\underline{H}_2CH_3$), 1.13 (t, 3H, J(CH_2,CH_3) = 7.3 Hz, -$SO_2CH_2C\underline{H}_3$).

^{13}C-NMR (75 MHz, DMSO-d^6): δ157.8 (C_D(2)), 156.2 (C_B(2)), 154.9 (2 x C_D(4)), 151.6 (C_A(2)), 143.8 (C_B(5)), 134.6 (C_C(3)), 132.8, 130.2, 130.0, 128.9, 128.7, 125.7, 123.4,

122.9, 122.5, 121.2, 115.8 (C_A(6)), 110.9 (C_A(3)), 56.4 (-OCH_3), 49.8 (-$SO_2\underline{C}H_2CH_3$), 7.3 (-$SO_2CH_2\underline{C}H_3$).

FT IR (solid, cm^{-1}): 3420 (w), 2942 (w), 2207 (w), 1610 (s), 1577 (s), 1526 (m), 1489 (w), 1419 (m), 1347 (w), 1301 (m), 1263 (m), 1142 (s), 1121 (s), 1080 (m), 1050 (w), 1020 (m), 957 (w), 918 (w), 886 (w), 792 (m), 717 (s), 693 (m), 659 (w), 630 (w), 597 (w), 576 (m), 534 (w), 495 (s), 453 (m), 422 (w).

MS (ESI m/z): 437.3 $[M + H]^+$, 459.3 $[M + Na]^+$; in negative mode 435.4 $[M - H]^-$.

Anal. calcd for $C_{22}H_{20}N_4O_4S$ (436.48): C, 60.54; H, 4.62; N, 12.84; Found: C, 61.01; H, 4.82; N, 12.77.

Synthesis of 5-(3-(1*H*-pyrrol-3-yl)phenyl)-*N*-(5-(ethylsulfonyl)-2-methoxyphenyl)oxazol-2-amine (191)

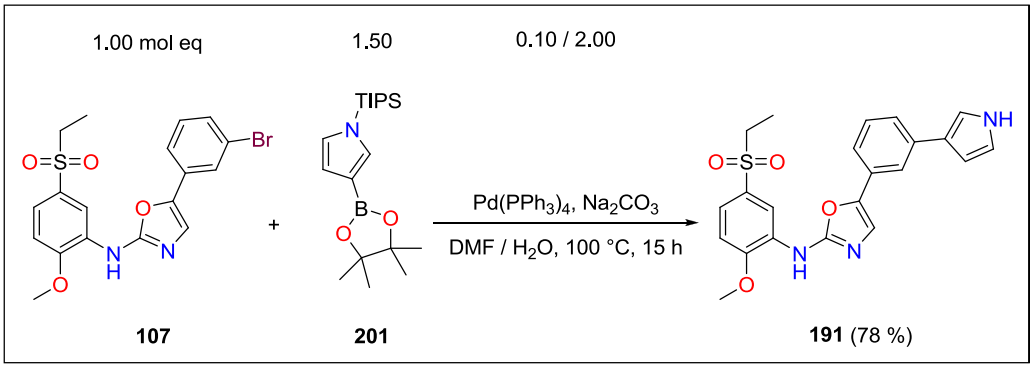

A suspension of 60.0 mg (0.14 mmol, 1.00 mol eq) starting material **107**, 71.8 mg (0.21, 1.50 mol eq) of pinacolboronate **201** and 15.8 mg (0.01 mmol, 0.10 mol eq) of $Pd(PPh_3)_4$ in 5 ml of DMF placed in a sealed tube was bubbled by Ar for 10 min. Afterwards a solution of 29.0 mg (0.27 mmol, 2.00 mol eq) Na_2CO_3 in 2 ml of H_2O was added and the reaction mixture was stirred at 100 °C for 15 h. Then the reaction was cooled to RT, diluted with 10 ml of EA and extracted with 3 x 5 ml of brine. The organic layer was separated, dried by Na_2SO_4, filtrated and concentrated under reduced pressure. The crude product was purified by FLC (Hex / EA = 1 / 9) and triturated with Hex / EA yielding 45.0

mg (0.11 mmol, 78 %) of 5-(3-(1*H*-pyrrol-3-yl)phenyl)-*N*-(5-(ethylsulfonyl)-2-methoxyphenyl)oxazol-2-amine (**191**).

Novelty: Preparation or characterization of **191** has not been described in the literature.

M. p.: 230 – 250 °C (dec) [Hex / EA]. Pale yellow solid material.

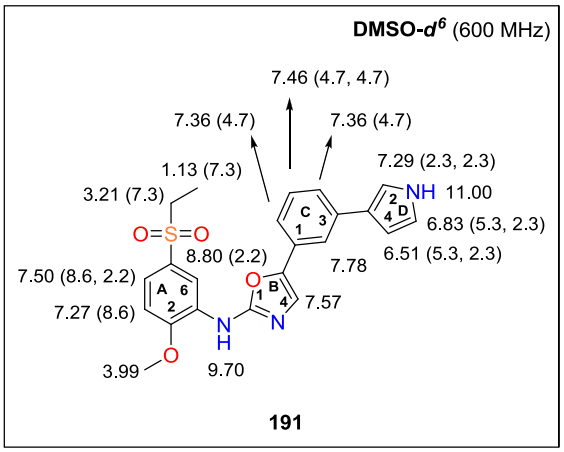

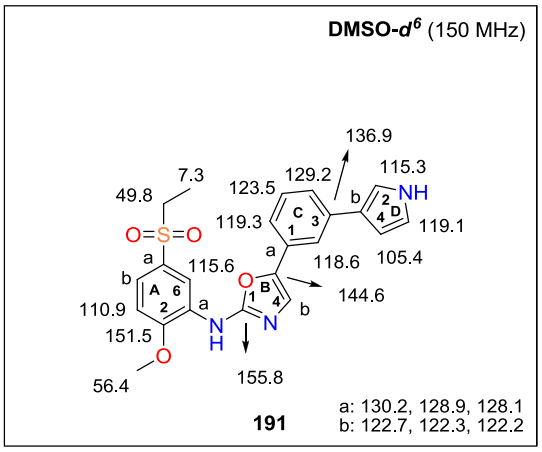

^{1}H-NMR (600 MHz, DMSO-d^6): δ 11.00 (s, 1H, -NH- pyrrol), 9.70 (s, 1H, -NH-), 8.80 (d, 1H, $J(A_4,A_6)$ = 2.2 Hz, H-C_A(6)), 7.78 (s, 1H, H-C_C(2)), 7.57 (s, 1H, H-C_B(4)), 7.50 (dd, 1H, $J(A_3,A_4)$ = 8.6 Hz, $J(A_4,A_6)$ = 2.2 Hz, H-C_A(4)), 7.46 (dd, 1H, $J(C_4, C_5)$ = $J(C_5, C_6)$ = 4.7 Hz, H-C_C(5)), 7.36 (d, 2H, $J(C_4, C_5)$ = $J(C_5, C_6)$ = 4.7 Hz, H-C_C(4) and H-C_C(6)), 7.29 (dd, 1H, $J(D_2,D_5)$ = $J(D_2,D_4)$ = 2.3 Hz, H-C_D(2)), 7.27 (d, 1H, $J(A_3,A_4)$ = 8.6 Hz, H-C_A(3)), 6.83 (dd, 1H, $J(D_4,D_5)$ = 5.3 Hz, $J(D_2,D_5)$ = 2.3 Hz, H-C_D(5)), 6.51 (dd, 1H, $J(D_4,D_5)$ = 5.3 Hz, $J(D_2,D_4)$ = 2.3 Hz, H-C_D(4)), 3.99 (s, 3H, -OCH_3), 3.21 (q, 2H, $J(CH_2,CH_3)$ = 7.3 Hz, -$SO_2C\underline{H}_2CH_3$), 1.13 (t, 3H, $J(CH_2,CH_3)$ = 7.3 Hz, -$SO_2CH_2C\underline{H}_3$).

^{13}C-NMR (150 MHz, DMSO-d^6): δ 155.8 (C_B(2)), 151.5 (C_A(2)), 144.6 (C_B(5)), 136.9 (C_C(3)), 130.2, 129.2 (C_C(4)), 128.9, 128.1, 123.5 (C_C(5)), 122.7, 122.3, 122.2, 119.3 (C_C(6)), 119.1 (C_D(5)), 118.6 (C_C(2)), 115.6 (C_A(6)), 155.3 (C_D(2)), 110.9 (C_A(3)), 105.4 (C_D(4)), 56.4 (-OCH_3), 49.8 (-$SO_2\underline{C}H_2CH_3$), 7.3 (-$SO_2CH_2\underline{C}H_3$).

^{1}H- and ^{13}C-NMR shift assignments were determined using COSY and HSQC experiments.

FT IR (solid, cm^{-1}): 3415 (w), 3348 (w), 1613 (m), 1577 (s), 1529 (m), 1501 (w), 1488 (w), 1433 (m), 1347 (w), 1294 (m), 1259 (m), 1227 (w), 1185 (w), 1171 (w), 1137 (m), 1122 (s), 1074 (m), 1047 (m), 1018 (m), 968 (w), 925 (w), 888 (w), 880 (w), 813 (m), 794 (w), 779 (s), 732 (s), 713 (s), 684 (s), 656 (m), 635 (w).

MS (ESI m/z): 424.1 $[M + H]^+$; in negative mode 422.1 $[M - H]^-$.

Anal. calcd for $C_{22}H_{21}N_3O_4S$ (423.48): C, 62.40; H, 5.00; N, 9.92; found: C, 62.13; H, 5.11; N, 9.62.

Synthesis of *N*-(5-(ethylsulfonyl)-2-methoxyphenyl)-5-(3-(thiophen-3-yl) phenyl)oxazol-2-amine (192)

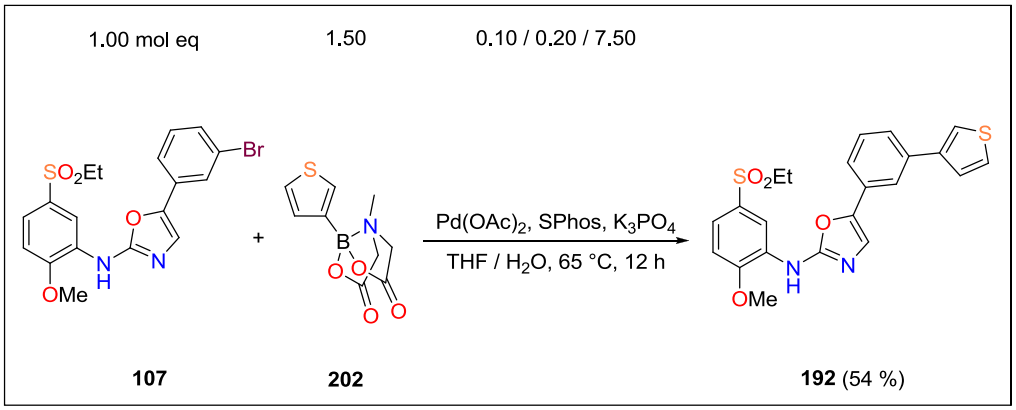

A suspension of 150 mg (0.34 mmol, 1.00 mol eq) starting material **107**, 123 mg (0.51, 1.50 mol eq) of MIDA boronate **202**, 7.70 mg (0.03 mmol, 0.10 mol eq) of $Pd(OAc)_2$ and 28.2 mg (0.07 mmol, 0.20 mol eq) of SPhos in 12 ml of THF placed in a sealed tube was bubbled by Ar for 10 min. Afterwards a solution of 546 mg (2.57 mmol, 7.50 mol eq) K_3PO_4 in 2.5 ml of H_2O was added and the mixture was stirred at 65 °C for 12 h. The reaction was cooled down to RT, diluted with 15 ml EA and extracted with 3 x 5 ml of brine. The organic layer was separated, dried by Na_2SO_4, filtered and concentrated under reduced pressure. The crude product was purified by FLC (Hex / EA = 1 / 1) and triturated with Hex / EA yielding 81.0 mg (0.18 mmol, 54 %) of *N*-(5-(ethylsulfonyl)-2-methoxyphenyl)-5-(3-(thiophen-3-yl)phenyl)oxazol-2-amine (**192**).

Novelty: Synthesis of **192** was described in the literature with 52 % yield. Its ^{1}H-NMR and HRMS spectra were also published.[6]

M. p.: 220 – 222 °C [Hex / EA]. Pale brown solid material.

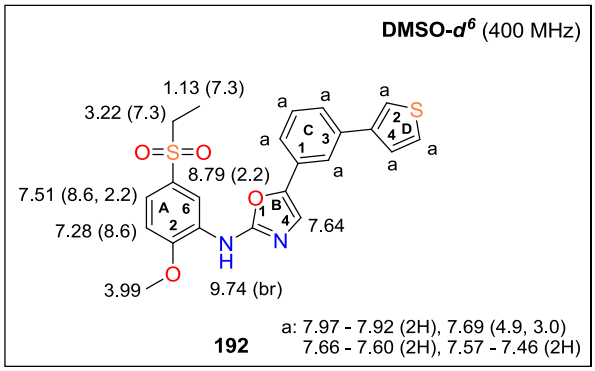

^{1}H-NMR (400 MHz, DMSO-d^6): δ 9.74 (br s, 1H, -NH-), 8.79 (d, 1H, $J(A_4,A_6)$ = 2.2 Hz, H-C_A(6)), 7.97 – 7.92 (m, 2H), 7.69 (dd, 1H, J = 4.9 Hz, J = 3.0 Hz), 7.66 – 7.60 (m, 2H), 7.64 (s, 1H, H-C_B(4)), 7.57 – 7.46 (m, 2H), 7.51 (dd, 1H, $J(A_3,A_4)$ = 8.6 Hz, $J(A_4,A_6)$ = 2.2 Hz, H-C_A(4)), 7.28 (d, 1H, $J(A_3,A_4)$ = 8.6 Hz, H-C_A(3)), 3.99 (s, 3H, -OCH_3), 3.22 (q, 2H, $J(CH_2,CH_3)$ = 7.3 Hz, -$SO_2C\underline{H}_2CH_3$), 1.13 (t, 3H, $J(CH_2,CH_3)$ = 7.3 Hz, -$SO_2CH_2C\underline{H}_3$).

13.2.3. Unexpected synthesis of 1,5-diarylimidazolidine-2,4-diones 206, 207

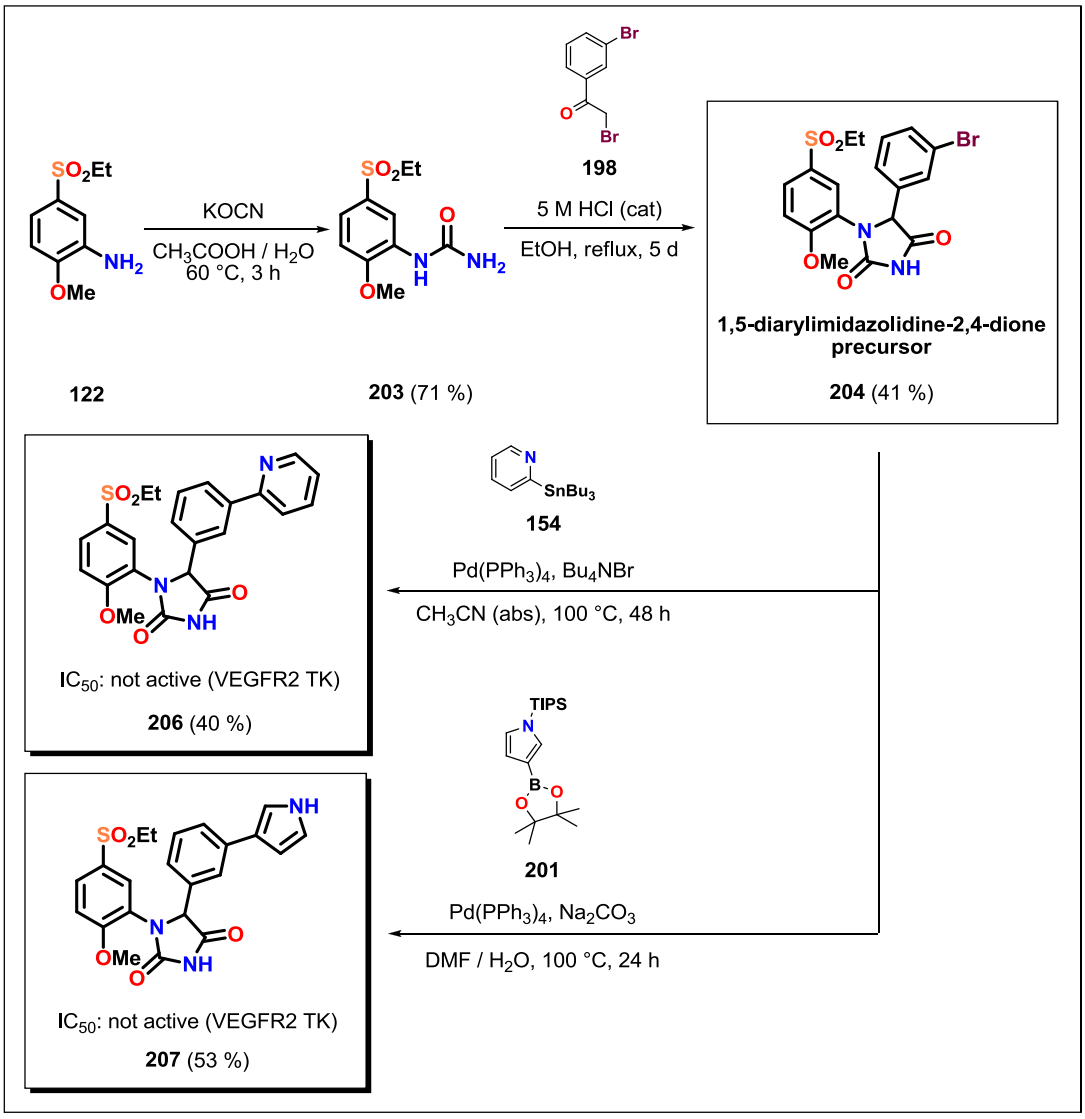

Scheme 26. Unexpected synthesis of 1,5-diarylimidazolidine-2,4-diones **206**, **207**.

Synthesis of 1-(5-(ethylsulfonyl)-2-methoxyphenyl)urea (203)

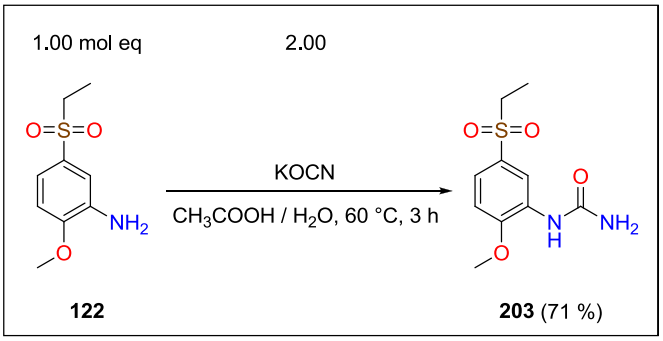

To 100 mg (0.46 mmol, 1.00 mol eq) of aniline **122** in a mixture of 2 ml CH_3COOH and 4 ml of H_2O, a solution of 75.4 mg (0.93, 2.00 mol eq) KOCN in 1 ml of H_2O was slowly added and the mixture was heated at 60 °C for 3 h. The reaction was diluted with H_2O, placed into an ice bath, neutralized using saturated aq solution of $NaHCO_3$ and extracted with 3 x 10 ml of EA. The organic layer was separated, dried with Na_2SO_4, filtered and concentrated under reduced pressure. The crude product was purified by crystallization from H_2O / EtOH yielding 85.0 mg (0.33 mmol, 71 %) of 1-(5-(ethylsulfonyl)-2-methoxyphenyl)urea (**203**).

Novelty: Synthesis of **203** was described in the literature with 58 % yield. Also its ^{1}H-NMR, ^{13}C-NMR, IR spectra and elemental analysis were previously published.[82]

M. p.: 196 – 197 °C [H_2O / EtOH]. (lit. M. p.: 198 – 199 °C [EA]).[82] Light brown solid material.

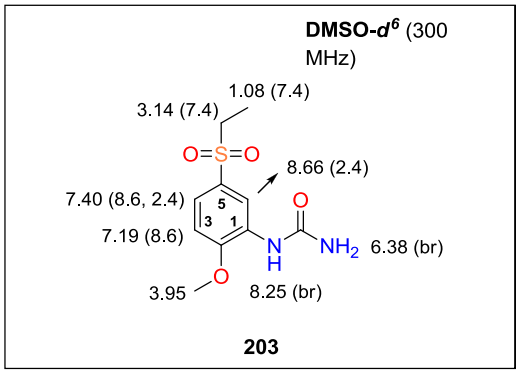

^{1}H-NMR (300 MHz, DMSO-d^6): δ 8.66 (d, 1H, J(4,6) = 2.4 Hz, H-C(6)), 8.25 (br s, 1H, -NHCONH$_2$), 7.40 (dd, 1H, J(3,4) = 8.6 Hz, J(4,6) = 2.4 Hz, H-C(4)), 7.19 (d, 1H, J(3,4) = 8.6 Hz, H-C(3)), 6.38 (br s, 2H, -NHCONH$_2$), 3.95 (s, 3H, -OCH$_3$), 3.14 (q, 2H, J(CH$_2$CH$_3$) = 7.4 Hz, -COOCH$_2$CH$_3$), 1.08 (t, 3H, J(CH$_2$,CH$_3$) = 7.4 Hz, -COOCH$_2$CH$_3$).

Synthesis of 5-(3-bromophenyl)-1-(5-(ethylsulfonyl)-2-methoxyphenyl) imidazolidine-2,4-dione (204)

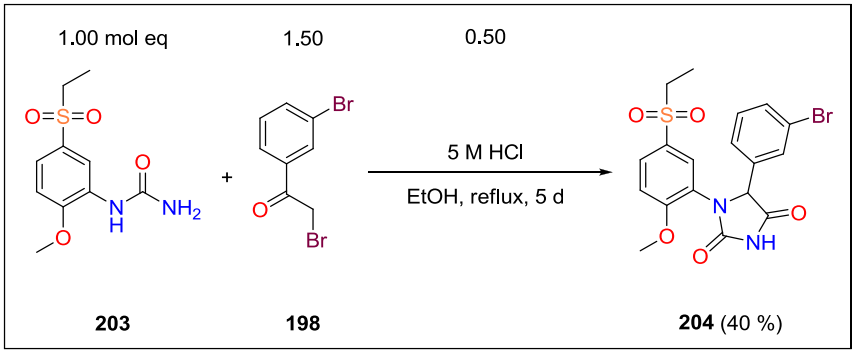

To a suspension of 1.86 g (7.20 mmol, 1.00 mol eq) urea **203** and 2.00 g (7.20 mmol, 1.00 mol eq) of acetophenone **198** in 30 ml EtOH, 1.5 ml (3.60 mmol, 0.5 mol eq) of 5 M HCl was added. The reaction mixture was refluxed for 3 d. Afterwards another 1.00 g (3.60 mmol, 0.50 mol eq) of acetophenone **198** was added and the mixture was refluxed for another 2 d. The solvent was evaporated, an obtained solid residue dissolved in 30 ml of EA and washed with 2 x 10 ml of saturated aq solution of $NaHCO_3$ and 10 ml of H_2O. Combined organic layers were dried by Na_2SO_4, filtered and concentrated under reduced pressure. The crude product was purified by FLC (Hex / EA = 1 / 3) yielding 1.30 g (2.87 mmol, 40 %) of 5-(3-bromophenyl)-1-(5-(ethylsulfonyl)-2-methoxyphenyl) imidazolidine-2,4-dione (**204**).

Novelty: Preparation or characterization of **204** has not been described in the literature.

M. p.: 217 – 218 °C [Hex / EA]. Off white solid material.

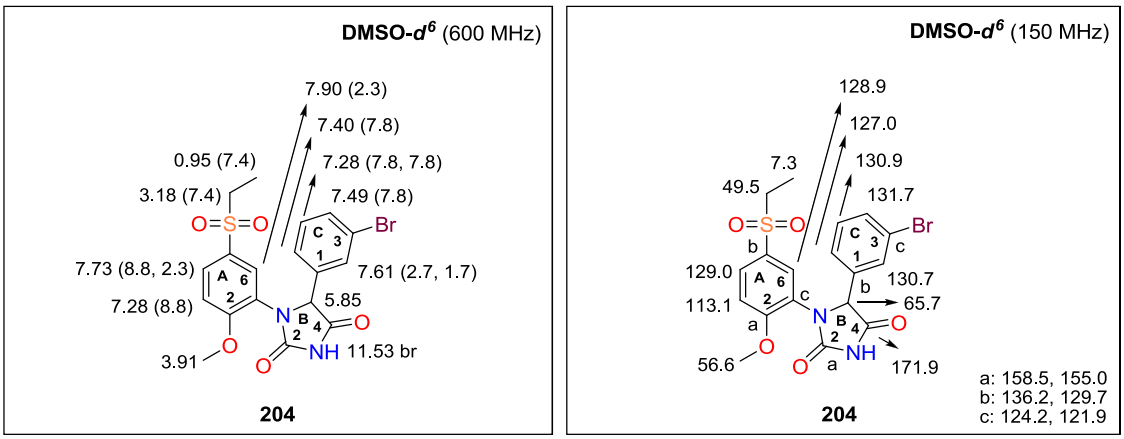

^{1}H-NMR (600 MHz, DMSO-d^6): δ 11.53 (br s, 1H, -NH-), 7.90 (d, 1H, $J(A_4,A_6)$ = 2.3 Hz, H-C_A(6)), 7.73 (dd, 1H, $J(A_3,A_4)$ = 8.8 Hz, $J(A_4,A_6)$ = 2.3 Hz, H-C_A(4)), 7.61 (dd, 1H, $J(C_2,C_4)$ = 2.7 Hz or 1.7 Hz, $J(C_2,C_6)$ = 2.7 Hz or 1.7 Hz, H-C_C(2)), 7.49 (d, 1H, $J(C_4,C_5)$ = 7.8 Hz, H-C_C(4)), 7.40 (d, 1H, $J(C_5,C_6)$ = 7.8 Hz, H-C_C(6)), 7.28 (d, 1H, $J(A_3,A_4)$ = 8.8 Hz, H-C_A(3)), 7.28 (dd, 1H, $J(C_4,C_5)$ = $J(C_5,C_6)$ = 7.8 Hz, H-C_C(5)), 5.85 (s, 1H, H-C_B(5)), 3.91 (s, 3H, -OCH_3), 3.18 (q, 2H, $J(CH_2,CH_3)$ = 7.4 Hz, -$SO_2C\underline{H}_2CH_3$), 0.95 (t, 3H, $J(CH_2,CH_3)$ = 7.4 Hz, -$SO_2CH_2C\underline{H}_3$).

^{13}C-NMR (75 MHz, DMSO-d^6): δ 171.9 (C_B(4)), 158.5, 155.0, 136.2, 131.7 (C_C(4)), 130.9 (C_C(5)), 130.7 (C_C(2)), 129.7, 129.0 (C_A(4)), 128.9 (C_A(6)), 127.0 (C_C(6)), 124.2, 121.9, 113.1 (C_A(3)), 65.7 (C_B(5)), 56.6 (-OCH_3), 49.5 (-$SO_2\underline{C}H_2CH_3$), 7.3 (-$SO_2CH_2\underline{C}H_3$). **^{1}H- and ^{13}C-NMR shift assignments were determined using COSY and HSQC experiments.**

FT IR (solid, cm^{-1}): 3171 (w), 3060 (w), 2747 (w), 2114 (w), 2052 (w), 1778 (m), 1707 (s), 1598 (m), 1507 (m), 1450 (m), 1426 (s), 1405 (m), 1301 (s), 1269 (s), 1232 (w), 1197 (w), 1189 (w), 1138 (s), 1099 (w), 1075 (s), 1009 (m), 941 (w), 864 (w), 885 (w), 819 (m), 787 (s), 737 (s), 668 (m), 667 (w), 594 (w), 538 (s), 488 (s), 462 (s), 436 (m).

MS (ESI m/z): 476.9 (100 %), 474.9 (98 %) $[M + Na]^+$; in negative mode 453.0 (100 %), 451.0 (98 %) $[M - H]^-$.

Anal. calcd for $C_{18}H_{17}BrN_2O_5S$ (453.31): C, 47.69; H, 3.78; N, 6.18; found: C, 48.56; H, 3.92; N, 6.24.

Synthesis of 1-(5-(ethylsulfonyl)-2-methoxyphenyl)-5-(3-(pyridin-2-yl) phenyl)imidazolidine-2,4-dione (206)

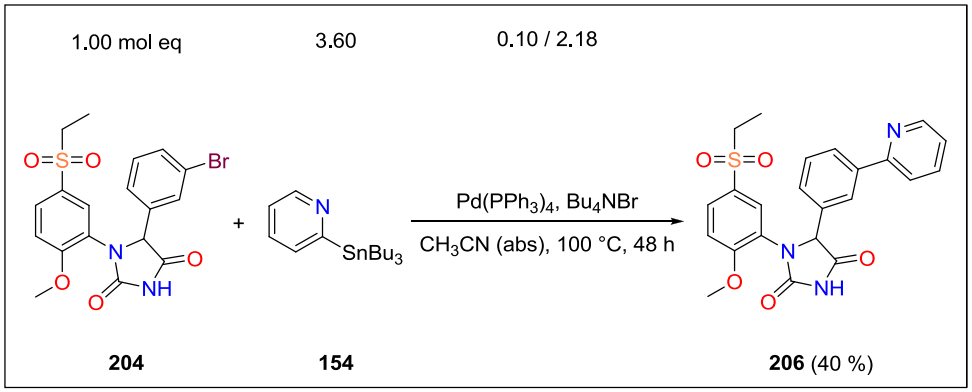

A suspension of 50.0 mg (0.11 mmol, 1.00 mol eq) starting material **204**, 13.2 mg (0.01 mmol, 0.10 mol eq) of $Pd(PPh_3)_4$ and 80.1 mg (0.25 mmol, 2.18 mol eq) of Bu_4NBr in 3.5 ml of CH_3CN (abs) in a glass tube was bubbled by Ar during 10 min. Afterwards 151 mg (0.41, 3.60 mol eq) of tributylstannane **154** was added, the glass tube was sealed and the mixture was stirred at 100 °C for 48 h. The reaction was cooled down to RT, diluted with 10 ml of EA, quenched with 10 ml of 1 M KF aq solution and stirred for 3 h. The organic layer was separated, dried by Na_2SO_4, filtrated and concentrated under reduced pressure. The crude product was purified by FLC (Hex / EA = 1 / 3) and trituration with Hex / EA yielding 20.0 mg (0.04 mmol, 40 %) of 1-(5-(ethylsulfonyl)-2-methoxyphenyl)-5-(3-(pyridin-2-yl)phenyl)imidazolidine-2,4-dione (**206**).

Novelty: Preparation or characterization of **206** has not been described in the literature.

M. p.: 138 – 140 °C [Hex / EA]. White solid material.

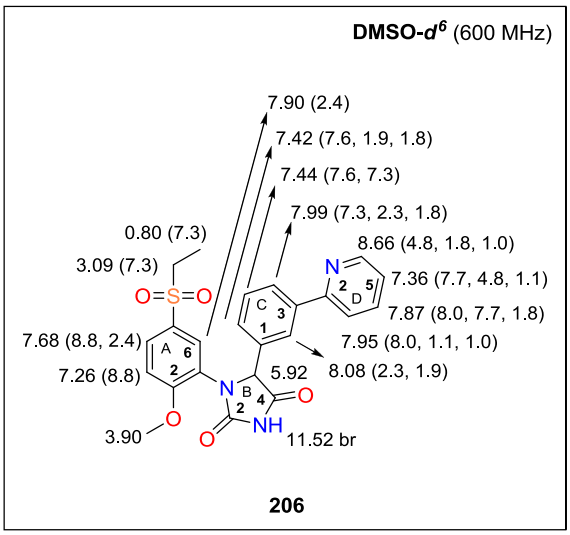

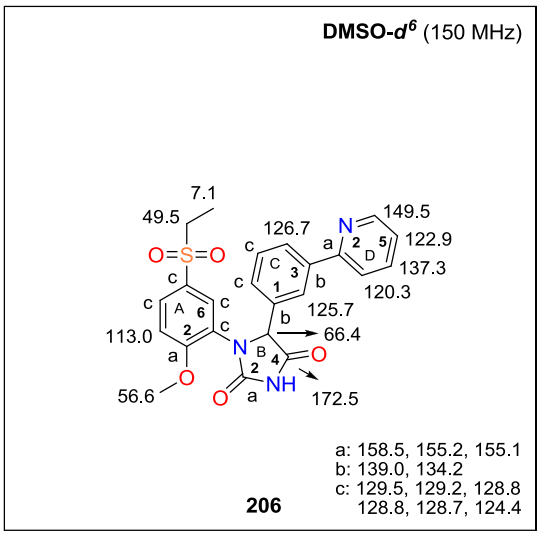

^{1}H-NMR (600 MHz, DMSO-d^6): δ 11.52 (br s, 1H, -NH-), 8.66 (ddd, 1H, $J(D_5,D_6)$ = 4.8 Hz, $J(D_4,D_6)$ = 1.8 Hz, $J(D_3,D_6)$ = 1.0 Hz, H-C_D(6)), 8.08 (dd, 1H, $J(C_2,C_4)$ = 2.3 Hz, $J(C_2,C_6)$ = 1.9 Hz, H-C_C(2)), 7.99 (ddd, 1H, $J(C_4,C_5)$ = 7.3 Hz, $J(C_2,C_4)$ = 2.3 Hz, $J(C_4,C_6)$ = 1.8 Hz, H-C_C(4)), 7.95 (ddd, 1H, $J(D_3,D_4)$ = 8.0 Hz, $J(D_3,D_5)$ = 1.1 Hz, $J(D_3,D_6)$ = 1.0 Hz, H-C_D(3)), 7.90 (d, 1H, $J(A_4,A_6)$ = 2.4 Hz, H-C_A(6)), 7.87 (ddd, 1H, $J(D_3,D_4)$ = 8.0 Hz, $J(D_4,D_5)$ = 7.7 Hz, $J(D_4,D_6)$ = 1.8 Hz, H-C_D(4)), 7.68 (dd, 1H, $J(A_3,A_4)$ = 8.8 Hz, $J(A_4,A_6)$ = 2.4 Hz, H-C_A(4)), 7.44 (dd, 1H, $J(C_5,C_6)$ = 7.6 Hz, $J(C_4,C_5)$ = 7.3 Hz, H-C_C(5)), 7.42 (ddd, 1H, $J(C_5,C_6)$ = 7.6 Hz, $J(C_2,C_6)$ = 1.9 Hz, $J(C_4,C_6)$ = 1.8 Hz, H-C_C(6)), 7.36 (ddd, 1H, $J(D_4,D_5)$ = 7.7 Hz, $J(D_5,D_6)$ = 4.8 Hz, $J(D_3,D_5)$ = 1.1 Hz, H-C_D(5)), 7.26 (d, 1H, $J(A_3,A_4)$ = 8.8 Hz, H-C_A(3)), 5.92 (s, 1H, H-C_B(5)), 3.90 (s, 3H, -OCH_3), 3.09 (q, 2H, $J(CH_2,CH_3)$ = 7.3 Hz, -$SO_2C\underline{H}_2CH_3$), 0.80 (t, 3H, $J(CH_2,CH_3)$ = 7.3 Hz, -$SO_2CH_2C\underline{H}_3$).

^{13}C-NMR (150 MHz, DMSO-d^6): δ 172.5 (C_B(4)), 158.5, 155.2, 155.1, 149.5 (C_D(6)), 139.0, 137.3 (C_D(4)), 134.2, 129.5, 129.2, 2 x 128.8, 128.7, 126.7 (C_C(4)), 125.7 (C_C(2)), 124.4, 122.9 (C_D(5)), 120.3 (C_D(3)), 113.0 (C_A(3)), 66.4 (C_B(5)), 56.6 (-OCH_3), 49.5 (-$SO_2\underline{C}H_2CH_3$), 7.1 (-$SO_2CH_2\underline{C}H_3$).

^{1}H- and ^{13}C-NMR shift assignments were determined using COSY and HSQC experiments.

FT IR (solid, cm^{-1}): 2925, (w), 2704 (w), 1771 (w), 1721 (s), 1593 (w), 1567 (w), 1504 (m), 1477 (w), 1438 (m), 1415 (m), 1388 (m), 1307 (m), 1262 (m), 1182 (w), 1136 (s),

1091 (w), 1040 (w), 1018 (m), 1005 (w), 923 (w), 864 (w), 824 (w), 800 (w), 782 (m), 766 (m), 757 (m), 731 (s), 716 (m), 696 (m), 631 (m).

MS (ESI m/z): 452.1 $[M + H]^+$; in negative mode 450.1 $[M - H]^-$.

Anal. calcd for $C_{23}H_{21}N_3O_5S$ (451.49): C, 61.18; H, 4.69; N, 9.31; found: C, 63.13; H, 4.68; N, 9.59.

Synthesis of 5-(3-(1*H*-pyrrol-3-yl)phenyl)-1-(5-(ethylsulfonyl)-2-methoxy phenyl)imidazolidine-2,4-dione (207)

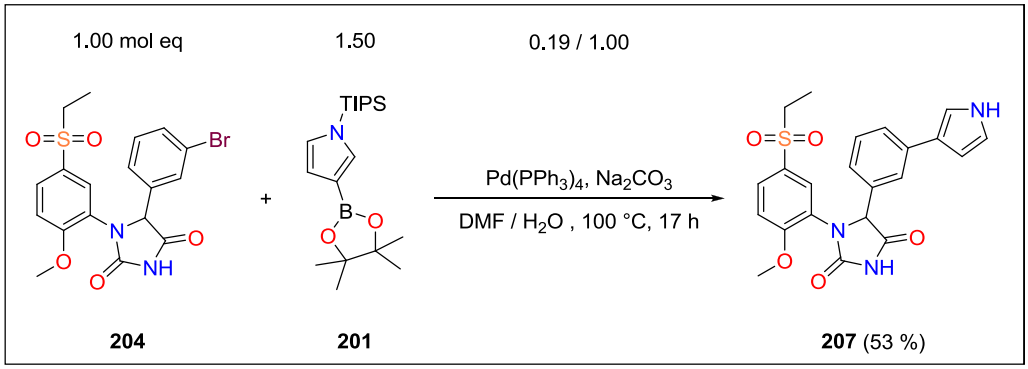

A suspension of 60.0 mg (0.13 mmol, 1.00 mol eq) starting material **204**, 71.8 mg (0.21 mmol, 1.50 mol eq) of pinacolboronate **201** and 30.1 mg (0.03 mmol, 0.19 mol eq) of $Pd(PPh_3)_4$ in 3 ml of DMF placed in a sealed tube was bubbled by Ar for 10 min. Afterwards, a solution of 14.5 mg (0.14 mmol, 1.00 mol eq) Na_2CO_3 in 1 ml of H_2O was added and the mixture was stirred at 100 °C for 17 h. The reaction was cooled down to RT, diluted with 10 ml of EA and extracted 3 x 5 ml of brine. The organic layer was separated, dried by Na_2SO_4, filtrated and concentrated under reduced pressure. The crude product was purified by FLC (Hex / EA = 1 / 2) and triturated with Hex / EA yielding 30.0 mg (0.07 mmol, 53 %) of 5-(3-(1*H*-pyrrol-3-yl)phenyl)-1-(5-(ethylsulfonyl)-2-methoxyphenyl) imidazolidine-2,4-dione (**207**).

Novelty: Preparation or characterization of **207** has not been described in the literature.

M. p.: 190 – 193 °C [Hex / EA]. Light brown solid material.

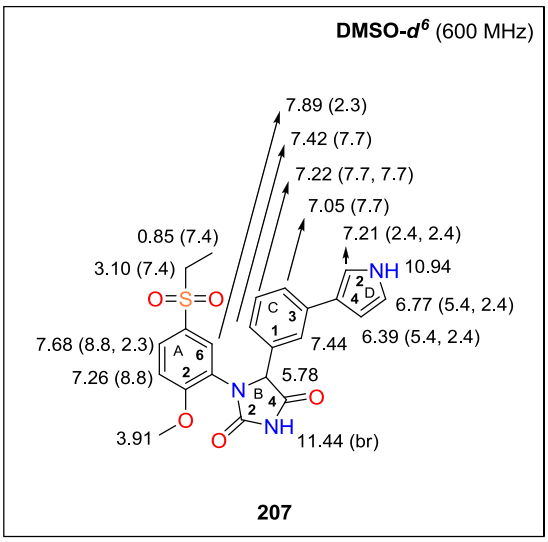

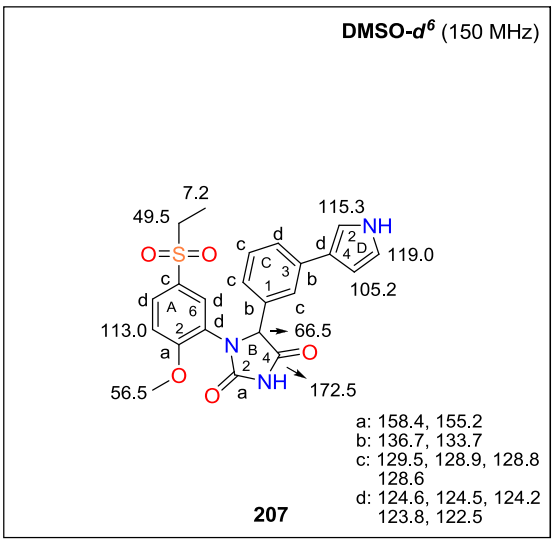

^{1}H-NMR (600 MHz, DMSO-d^6): δ 11.44 (br s, 1H, -NH-), 10.94 (s, 1H, -NH- pyrrol), 7.89 (d, 1H, $J(A_4,A_6)$ = 2.3 Hz, H-C_A(6)), 7.68 (dd, 1H, $J(A_3,A_4)$ = 8.8 Hz, $J(A_4,A_6)$ = 2.3 Hz, H-C_A(4)), 7.44 (s, 1H, H-C_C(2)), 7.42 (d, 1H, $J(C_5,C_6)$ = 7.7 Hz, H-C_C(6)), 7.26 (d, 1H, $J(A_3,A_4)$ = 8.8 Hz, H-C_A(3)), 7.22 (dd, 1H, $J(C_4,C_5)$ = $J(C_5,C_6)$ = 7.7 Hz, C_C(5)), 7.21 (dd, 1H, $J(D_2,D_4)$ = $J(D_2,D_5)$ = 2.4 Hz, H-C_D(2)), 6.77 (dd, 1H, $J(D_4,D_5)$ = 5.4 Hz, $J(D_2,D_5)$ = 2.4 Hz, H-C_D(5)), 6.39 (dd, 1H, $J(D_4,D_5)$ = 5.4 Hz, $J(D_2,D_4)$ = 2.4 Hz, H-C_D(4)), 5.78 (s, 1H, H-C_B(5)), 3.91 (s, 3H, -OCH_3), 3.10 (q, 2H, $J(CH_2,CH_3)$ = 7.4 Hz, -$SO_2C\underline{H}_2CH_3$), 0.85 (t, 3H, $J(CH_2,CH_3)$ = 7.4 Hz, -$SO_2CH_2C\underline{H}_3$).

^{13}C-NMR (150 MHz, DMSO-d_6): δ 172.5 (C_B(4)), 158.4, 155.2, 136.7, 133.7, 129.5, 128.9, 128.8, 128.6, 124.6, 124.5, 124.2, 123.8, 122.5, 119.0 (C_D(5)), 115.3 (C_D(2)), 113.0 (C_A(3)), 105.2 (C_D(4)), 66.5 (C_B(5)), 56.5 (-OCH_3), 49.5 (-$SO_2\underline{C}H_2CH_3$), 7.2 (-$SO_2CH_2\underline{C}H_3$).

^{1}H- and ^{13}C-NMR shift assignments were determined using COSY and HSQC experiments.

FT IR (solid, cm^{-1}): 3367 (w), 3060 (w), 2932 (w), 1773 (m), 1723 (s), 1595 (w), 1581 (w), 1552 (w), 1502 (m), 1437 (m), 1390 (m), 1302 (m), 1276 (m), 1267 (w), 1230 (w), 1188 (m), 1160 (w), 1152 (w), 1136 (s), 1087 (m), 1043 (w), 1028 (w), 1013 (m), 954 (w), 937 (w), 910 (w), 877 (w), 862 (w), 825 (w), 811 (w), 794 (m -SO_2-), 778 (w), 738 (m), 727 (m), 698 (m), 674 (m), 668 (m), 634 (m).

MS (ESI m/z): 440.1 $[M + H]^+$; in negative mode 438.1$[M - H]^-$.

Anal. calcd for $C_{22}H_{21}N_3O_5S$ (439.48): C, 60.12; H, 4.82; N, 9.56; found: C, 60.94; H, 5.01; N, 9.42.

13.2.4. Synthesis of *N*,4-diaryloxazol-2-amine precursor 205

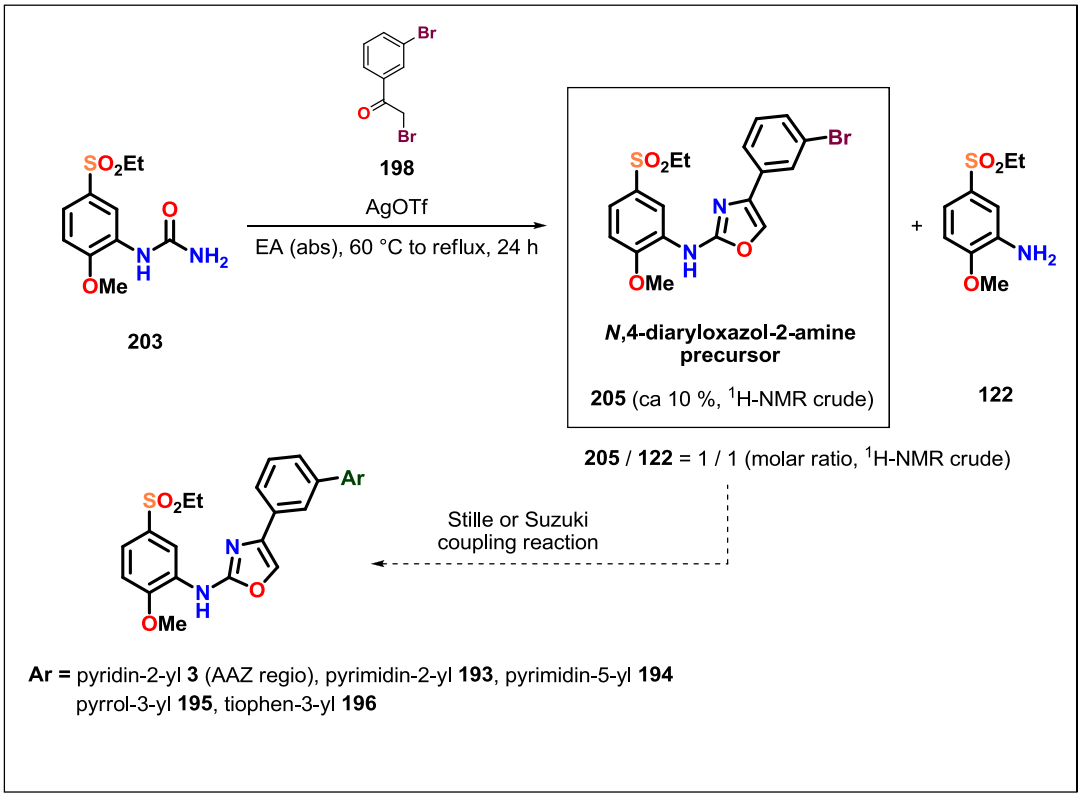

Scheme 28. Synthesis of *N*,4-diaryloxazol-2-amine precursor **205**.

Synthesis of 4-(3-bromophenyl)-*N*-(5-(ethylsulfonyl)-2-methoxyphenyl) oxazol-2-amine (205)

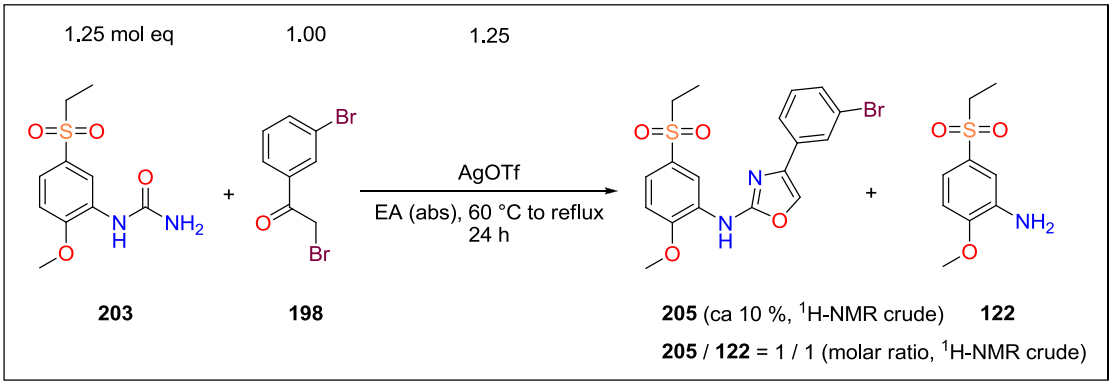

A solution of 50.0 mg (0.18 mmol, 1.00 mol eq) acetophenone **198** and 57.8 mg (0.22 mmol, 1.25 mol eq) of AgOTf in 5 ml of EA (abs) was stirred under Ar at 60 °C for 1 h. Afterwards 58.1 mg (0.22 mmol, 1.25 mol eq) of urea **203** was added and the reaction mixture was refluxed under Ar for 23 h. The TLC analysis showed one dominant new spot and much less intensive spots belonging to the starting material **198** and **203**. The mixture was then cooled down to RT, diluted with 10 ml of EA, filtered through a silica pad and extracted with 5 ml of 1 % aq solution of $NaHCO_3$ and 2 x 5 ml of brine. The separated organic layer was dried over Na_2SO_4, filtered and evaporated under reduced pressure. The crude product was isolated as brown viscous oil (40.0 mg). ^{1}H-NMR analysis of the crude showed a dominant presence of 4-(3-bromophenyl)-*N*-(5-(ethylsulfonyl)-2-methoxy phenyl)oxazol-2-amine (**205**) and aniline **122** in a molar ratio of 1 / 1. The starting material **198**, **203** and a significant amount of unidentified products were also detected. The estimated yield of the target product **205** is ca 10 %. A subsequent purification using FLC (cyclohexane / EA = 1 / 1) provided 15.0 mg of yellow oil. ^{1}H-NMR analysis of the oil showed a presence of **205** and **122** in a molar ratio of 1 / 1. A composition of the analyzed sample was confirmed also by the MS spectrometry.

Note: The compounds **205** and **122** share a very similar polarity and therefore the separation on SiO_2 could be difficult.

Novelty: Preparation or characterization of **205** has not been described in the literature. Synthesis and characterization of **122** was described and published in our group.[140]

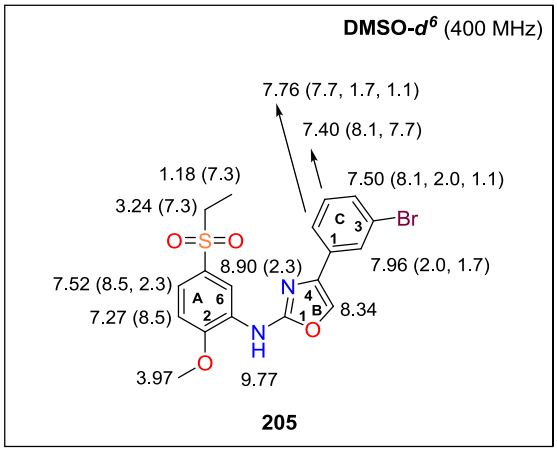

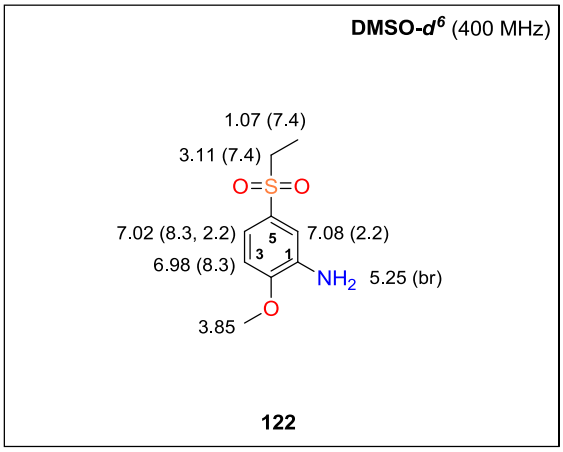

^{1}H-NMR (400 MHz, DMSO-d^6) **205**: δ 9.77 (s, 1H, -NH-), 8.90 (d, 1H, $J(A_4,A_6)$ = 2.3 Hz, H-C_A(6)), 8.34 (s, 1H, H-C_B(5)), 7.96 (dd, 1H, $J(C_2,C_4)$ = 2.0 Hz, $J(C_2,C_6)$ = 1.7 Hz, H-C_C(2)), 7.76 (ddd, 1H, $J(C_5,C_6)$ = 7.7 Hz, $J(C_2,C_6)$ = 1.7 Hz, $J(C_4,C_6)$ = 1.1 Hz, H-C_C(6)), 7.52 (dd, 1H, $J(A_3,A_4)$ = 8.5 Hz, $J(A_4,A_6)$ = 2.3 Hz, H-C_A(4)), 7.50 (ddd, 1H, $J(C_4,C_5)$ = 8.1 Hz, $J(C_2,C_4)$ = 2.0 Hz, $J(C_4,C_6)$ = 1.1 Hz, H-C_C(4)), 7.40 (dd, 1H, $J(C_4,C_5)$ = 8.1 Hz, $J(C_5,C_6)$ = 7.7 Hz, H-C_C(5)), 7.27 (d, 1H, $J(A_3,A_4)$ = 8.5 Hz, H-C_A(3)), 3.97 (s, 3H, -OCH_3), 3.24 (q, 2H, $J(CH_2,CH_3)$ = 7.3 Hz, -$SO_2C\underline{H}_2CH_3$), 1.18 (t, 3H, $J(CH_2,CH_3)$ = 7.3 Hz, -$SO_2CH_2C\underline{H}_3$).

^{1}H-NMR (400 MHz, DMSO-d^6) **122**: δ 7.08 (d, 1H, J(4,6) = 2.2 Hz, H-C(6)), 7.02 (dd, 1H, J(3,4) = 8.3 Hz, J(4,6) = 2.2 Hz, H-C(4)), 6.98 (d, 1H, J(3,4) = 8.3 Hz, H-C(3)), 5.25 (br s, 2H, -NH_2), 3.85 (s, 3H, -OCH_3), 3.11 (q, 2H, $J(CH_2,CH_3)$ = 7.4 Hz, -$SO_2C\underline{H}_2CH_3$), 1.07 (t, 3H, $J(CH_2,CH_3)$ = 7.4 Hz, -$SO_2CH_2C\underline{H}_3$).

MS (ESI m/z) **205**: 437.0 (95 %), 439.0 (100 %) $[M + H]^+$.

MS (ESI m/z) **122**: 216.1 $[M + H]^+$.

[140] Murár, M.; Addová, G.; Boháč, A. *Beilstein J. Org. Chem.* **2013**, *9*, 173 – 179.

13.3. Project – Salt bridge containing pocket (SBCP)

13.3.1. Synthesis of *p*-substituted *N*,5-diaryloxazol-2-amines 208, 209

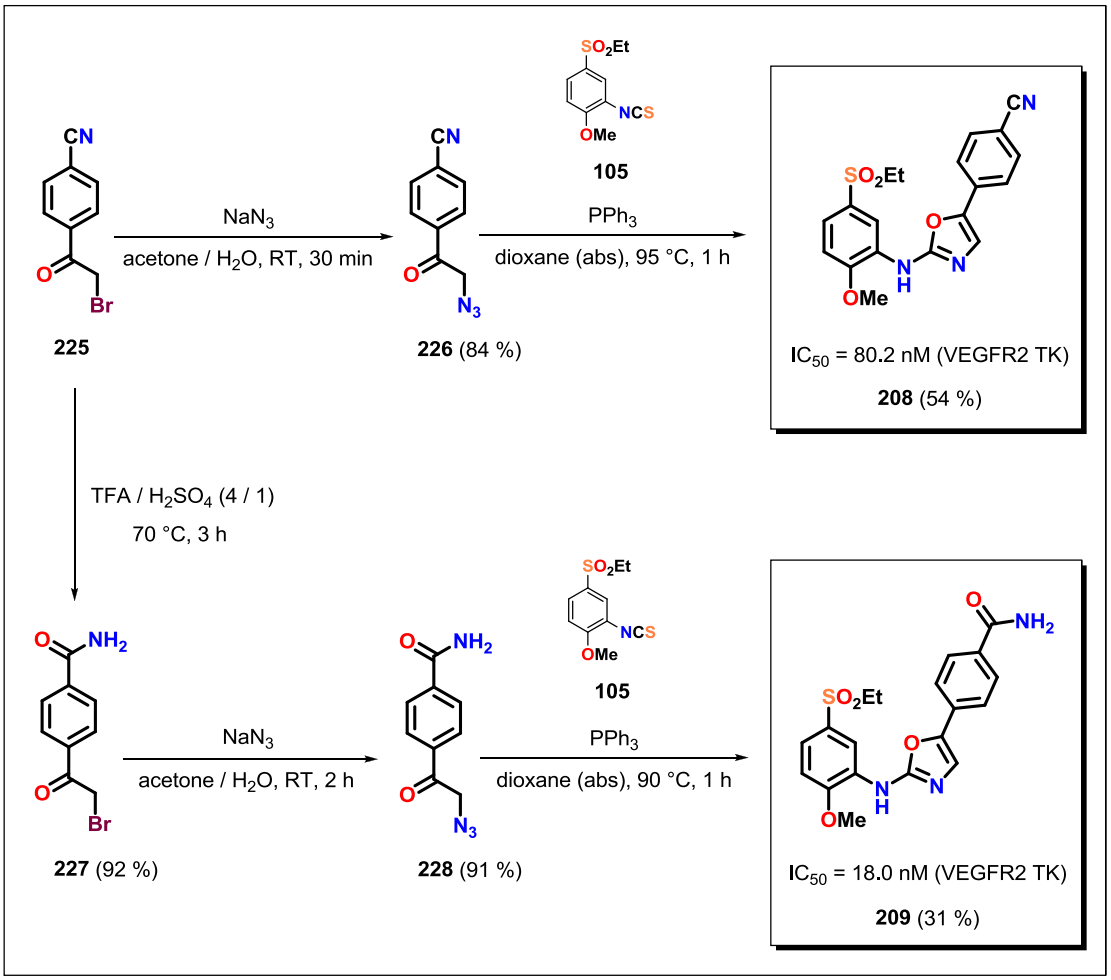

Scheme 30. Synthesis of *p*-substituted *N*,5-diaryloxazol-2-amines **208**, **209**.

Synthesis of 4-(2-azidoacetyl)benzonitrile (226)

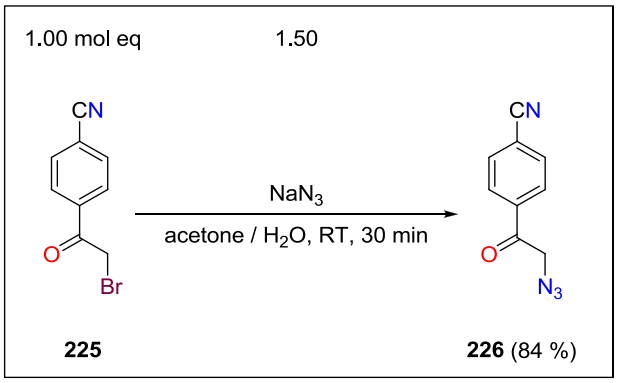

To a solution of 500 mg (2.23 mmol, 1.00 mol eq) bromoacetophenone **225** in 15 ml of acetone, 218 mg (3.35 mmol, 1.50 mol eq) of NaN_3 dissolved in 5 ml of H_2O was added dropwise. The reaction mixture was subsequently stirred at RT for 30 min. After complete consumption of the staring material **225** (TLC analysis), the mixture was evaporated. A remaining oily material was diluted with 15 ml of EA and extracted with 3 x 5 ml of brine. The organic layer was separated, dried by Na_2SO_4, filtrated and concentrated under reduced pressure. The crude product was purified by FLC (cyclohexane / EA = 2 / 1) yielding 350 mg (1.88 mmol, 84 %) of 4-(2-azidoacetyl)benzonitrile (**226**).

Novelty: Synthesis of **226** was described in the literature with 80 % yield. Also its ^{1}H-NMR, ^{13}C-NMR, IR and HRMS spectra were published.[141]

M. p.: 129 – 130 °C [cyclohexane / EA]. (lit. M. p.: 127 – 130 °C [Hex / EA]).[141] Yellow crystalline solid material.

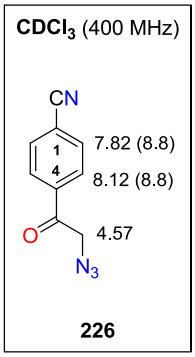

[141] Singh, P. N. D.; Mandel, S. M.; Robinson, R. M.; Zhu, Z.; Franz, R.; Ault, B. S.; Gudmundsdottir, A. D. *J. Org. Chem.* **2003**, *68*, 7951 – 7960.

^{1}H-NMR (400 MHz, $CDCl_3$): δ 8.12 (d, 2H, J(2,3) = 8.8 Hz, 2 x H-C(3)), 7.82 (d, 2H, J(2,3) = 8.8 Hz, 2 x H-C(2)), 4.57 (s, 2H, -$COCH_2N3$).

Synthesis of 4-(2-(5-(ethylsulfonyl)-2-methoxyphenylamino)oxazol-5-yl) benzonitrile (208)

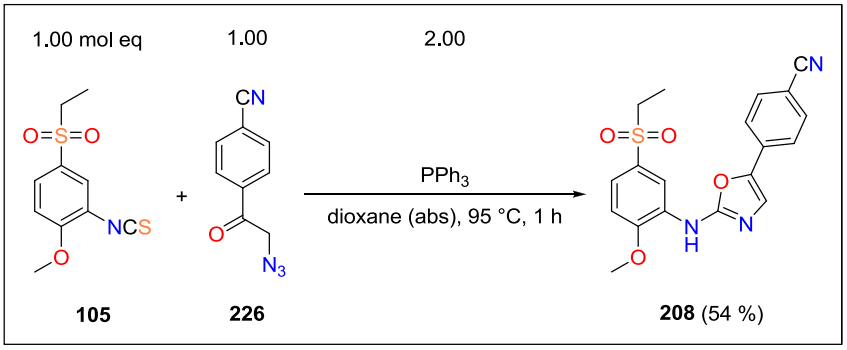

A mixture of 100 mg (0.39 mmol, 1.00 mol eq) isothiocyanate **105**, 72.4 mg (0.39 mmol, 1.00 mol eq) of azide **226** and 204 mg (0.78 mmol, 2.00 mol eq) of PPh_3 was dissolved in 10 ml of dioxane (abs) under Ar. The prepared solution was placed into a preheated 95 °C oil bath for 1 h. After consumption of the starting material **105** and **226** (TLC analysis), the reaction mixture was evaporated and a remaining solid material was dissolved in 15 ml of EA and washed with 3 x 5 ml of brine. The organic layer was dried over Na_2SO_4, filtered and evaporated under reduced pressure. The crude product was purified by FLC (Hex / EA = 1 / 7) and crystallized from Hex / EA yielding 80.0 mg (0.21 mmol, 54 %) of 4-(2-(5-(ethylsulfonyl)-2-methoxyphenylamino)oxazol-5-yl)benzonitrile (**208**).

Novelty: Synthesis of **208** was described in the literature with 6 % yield. Also its ^{1}H-NMR and HRMS spectra were published.[6]

M.p.: 240 – 243 °C [Hex / EA]. Pale orange solid material.

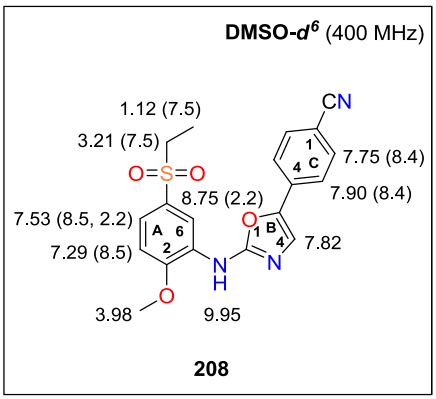

^{1}H-NMR (400 MHz, DMSO-d^6): δ 9.95 (s, 1H, -NH-), 8.75 (d, 1H, $J(A_4,A_6)$ = 2.2 Hz, H-C_A(6)), 7.90 (d, 2H, J(2,3) = 8.4 Hz, 2 x H-C(3)), 7.82 (s, 1H, C_B(4)), 7.75 (d, 2H, J(2,3) = 8.4 Hz, 2 x H-C(2)), 7.53 (dd, 1H, $J(A_3,A_4)$ = 8.5 Hz, $J(A_4,A_6)$ = 2.2 Hz, H-C_A(4)), 7.29 (d, 1H, $J(A_3,A_4)$ = 8.5 Hz, H-C_A(3)), 3.98 (s, 3H, -OCH_3), 3.21 (q, 2H, $J(CH_2,CH_3)$ = 7.5 Hz, -$SO_2C\underline{H_2}CH_3$), 1.12 (t, 3H, $J(CH_2,CH_3)$ = 7.5 Hz, -$SO_2CH_2C\underline{H_3}$).

Synthesis of 4-(2-bromoacetyl)benzamide (227)

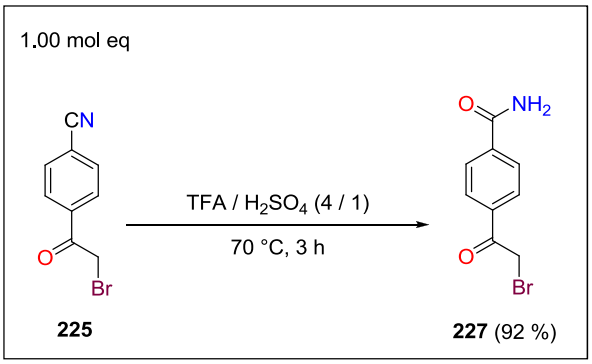

A solution of 100 mg (0.45 mmol, 1.00 mol eq) benzonitrile **225** in 2 ml of CF_3COOH (TFA) and H_2SO_4 (conc) mixture (4 / 1) was stirred at 70 °C for 3 h. After complete consumption of the starting material **225** (TLC analysis), the reaction was cooled to RT, an ice-cold H_2O was added and the aq mixture was placed into a freezer for 1 h. A formed precipitate was filtered and the obtained solid material dried under reduced pressure (HV) yielding 99.0 mg (0.41 mmol, 92 %) of 4-(2-bromoacetyl)benzamide (**227**).

Novelty: Synthesis of **227** was described in the literature with 83 % yield together with its MS spectral analysis.[142]

M.p.: 175 – 176 °C [TFA / H_2SO_4 / H_2O]. White crystalline solid material.

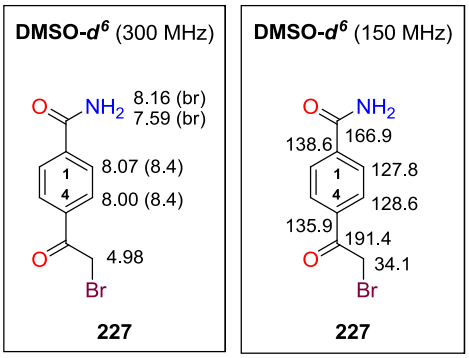

^{1}H-NMR (300 MHz, $CDCl_3$): δ 8.16 (br s, 1H, -$CONH_2$), 8.07 (d, 2H, J(2,3) = 8.4 Hz, 2 x H-C(2)), 8.00 (d, 2H, J(2,3) = 8.4 Hz, 2 x H-C(3)), 7.59 (br s, 1H, -$CONH_2$), 4.98 (s, 2H, -$COCH_2Br$).

^{13}C-NMR (150 MHz, DMSO-d_6): δ 191.4 (-$\underline{C}OCH_2Br$), 166.9 (-$CONH_2$), 138.6 (C(1)), 135.9 (C(4)), 128.6 (2 x C(3)), 127.8 (2 x C(2)), 34.1 (-$CO\underline{C}H_2Br$).

FT IR (solid, cm^{-1}): 3364 (m), 3162 (m), 2992 (w), 2943 (w), 2115 (w), 2097 (w), 1949 (w), 1817 (w), 1692 (s), 1655 (s), 1619 (s), 1567 (m), 1504 (m), 1407 (s), 1386 (s), 1302 (m), 1279 (s), 1195 (s), 1180 (s), 1144 (s), 1127 (m), 997 (s), 840 (s), 796 (s), 758 (s), 690 (s), 651 (s), 617 (s), 557 (s), 520 (s), 496 (s), 419 (m).

MS (ESI m/z): 242.0 (75 %), 244.0 (70 %) $[M + H]^+$.

Anal. calcd for $C_9H_8BrNO_2$ (242.07): C, 44.66; H, 3.33; N, 5.79; found: C, 44.83; H, 3.51; N, 5.23.

[142] Courtney, S.; Yarnold, C.; Flanagan, S.; Brace, G.; Barker, J.; Ichinara, O.; Gadoleau, E.; Richardson, A.; Kondo, T.; Imagawa, A.; Nakatani, S.; Suzuki, R.; Kouyama, S. *Ono Pharmaceutical CO., LTD.* **2013**, WO2013/93484, A1.

Synthesis of 4-(2-azidoacetyl)benzamide (228)

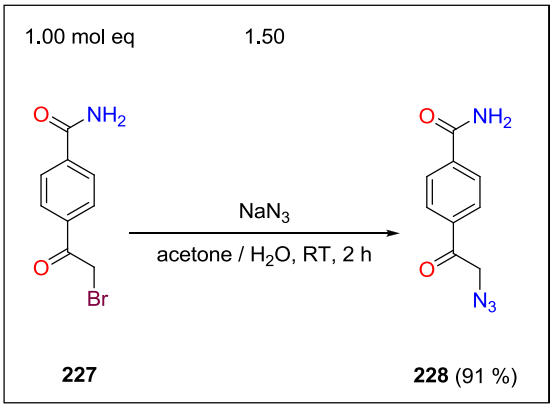

To a solution of 60.0 mg (0.25 mmol, 1.00 mol eq) benzamide **227** in 3 ml of acetone, 24.2 mg (0.37 mmol, 1.50 mol eq) of NaN_3 dissolved in 0.5 ml of H_2O was added dropwise. The reaction mixture was stirred at RT for 2 h. After the complete consumption of the staring material **227** (TLC analysis), the mixture was evaporated. A remaining material was dissolved with 10 ml of EA and extracted with 2 x 5 ml of brine. The organic layer was separated, dried by Na_2SO_4, filtered and concentrated under reduced pressure yielding 46.0 mg (0.23 mmol, 91 %) of 4-(2-azidoacetyl)benzamide (**228**).

Novelty: Preparation or characterization of **228** has not been described in the literature.

M. p.: 162 – 164 °C (dec) [EA]. Light yellow crystalline solid material.

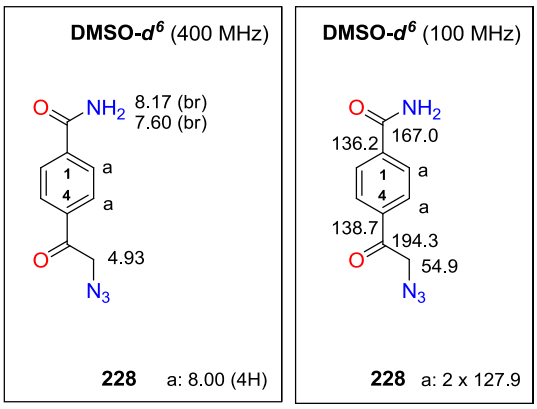

^{1}H-NMR (400 MHz, $CDCl_3$): δ 8.17 (br s, 1H, -$CONH_2$), 8.00 (s, 4H, 2 x H-C(2), 2 x H-C(3)), 7.60 (br s, 1H, -$CONH_2$), 4.93 (s, 2H, -$COCH_2N_3$).

^{13}C-NMR (100 MHz, DMSO-d_6): δ 194.3 (-$\underline{C}OCH_2N_3$), 167.0 (-$CONH_2$), 138.7 (C(4)), 136.2 (C(1)), 2 x 127.9 (2 x C(2) and 2 x C(3)), 54.9 (-$CO\underline{C}H_2N_3$).

FT IR (solid, cm^{-1}): 3366 (m), 3166 (m), 2973 (w), 2895 (w), 2196 (w), 2095 (s), 1989 (w), 1827 (w), 1688 (s), 1655 (s), 1621 (s), 1569 (m), 1506 (w), 1407 (s), 1352 (m), 1302 (m), 1284 (m), 1216 (s), 1184 (s), 1145 (m), 1128 (m), 1005 (s), 960 (w), 905 (s), 855 (s), 646 (s), 624 (s), 566 (s), 551 (s), 502 (s).

MS (ESI m/z): not detectable in positive / negative mode.

Anal. calcd for $C_9H_8N_4O_2$ (204.19): C, 52.94; H, 3.95; N, 27.44; found: C, 53.22; H, 4.06; N, 27.32.

Synthesis of 4-(2-(5-(ethylsulfonyl)-2-methoxyphenylamino)oxazol-5-yl)benzamide (209)

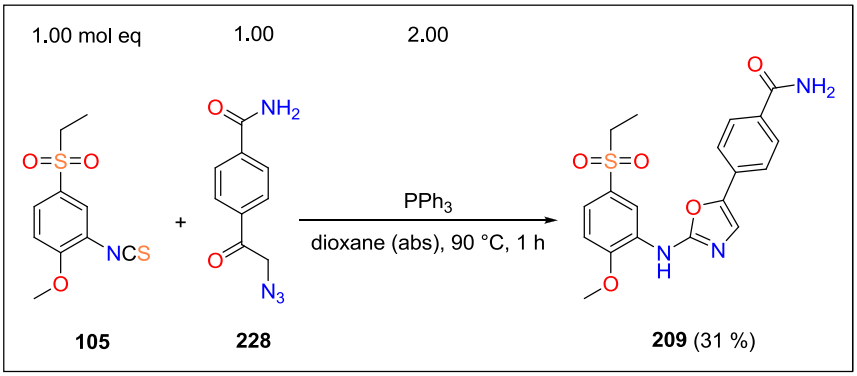

A solution of 290 mg (1.13 mmol, 1.00 mol eq) isothiocyanate **105**, 230 mg (1.13 mmol, 1.00 mol eq) of azide **228** and 591 mg (2.25 mmol, 2.00 mol eq) of PPh_3 in 10 ml of dioxane (abs) was stirred under Ar in the preheated 90°C oil bath for 1 h. After consumption of the starting material **105** and **228** (TLC analysis), the reaction mixture was evaporated. A remaining solid material was dissolved in the mixture of 10 ml of DMSO and 50 ml of EA and washed with 3 x 20 ml of brine. The organic layer was dried over Na_2SO_4, filtered and concentrated under reduced pressure. An obtained solid was purified by FLC (gradient: cyclohexane / EA = 1 / 7 to EA to EA / MeOH = 1 / 2) and crystallized

from hot acetone yielding 140 mg (0.35 mmol, 31 %) of 4-(2-(5-(ethylsulfonyl)-2-methoxyphenylamino)oxazol-5-yl)benzamide (**209**).

Note: The synthesis of **209** could be also performed by hydrolysis of the benzonitrile **208** using THF / H_2SO_4, 70 °C, 2 h in the yield of ca 90 %.

Novelty: Synthesis of **209** was described in the literature with 97 % yield (by hydrolysis of **208**) together with its ^{1}H-NMR and HRMS spectral analysis.[6]

M.p.: 259 – 261 °C [acetone]. Off-white solid material.

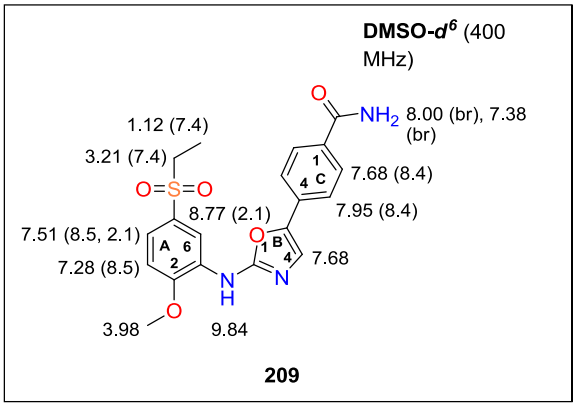

^{1}H-NMR (400 MHz, DMSO-d^6): δ 9.84 (s, 1H, -NH-), 8.77 (d, 1H, $J(A_4,A_6)$ = 2.1 Hz, H-C_A(6)), 8.00 (br s, 1H, -$CONH_2$), 7.95 (d, 2H, J(2,3) = 8.4 Hz, 2 x H-C(3)), 7.68 (d, 2H, J(2,3) = 8.4 Hz, 2 x H-C(2)), 7.68 (s, 1H, C_B(4)), 7.51 (dd, 1H, $J(A_3,A_4)$ = 8.5 Hz, $J(A_4,A_6)$ = 2.1 Hz, H-C_A(4)), 7.38 (br s, 1H, -$CONH_2$), 7.28 (d, 1H, $J(A_3,A_4)$ = 8.5 Hz, H-C_A(3)), 3.98 (s, 3H, -OCH_3), 3.21 (q, 2H, $J(CH_2,CH_3)$ = 7.4 Hz, -$SO_2C\underline{H}_2CH_3$), 1.12 (t, 3H, $J(CH_2,CH_3)$ = 7.4 Hz, -$SO_2CH_2C\underline{H}_3$).

13.3.2. Synthesis of *p*-substituted *N*,5-diaryloxazol-2-amines 210, 211, 212

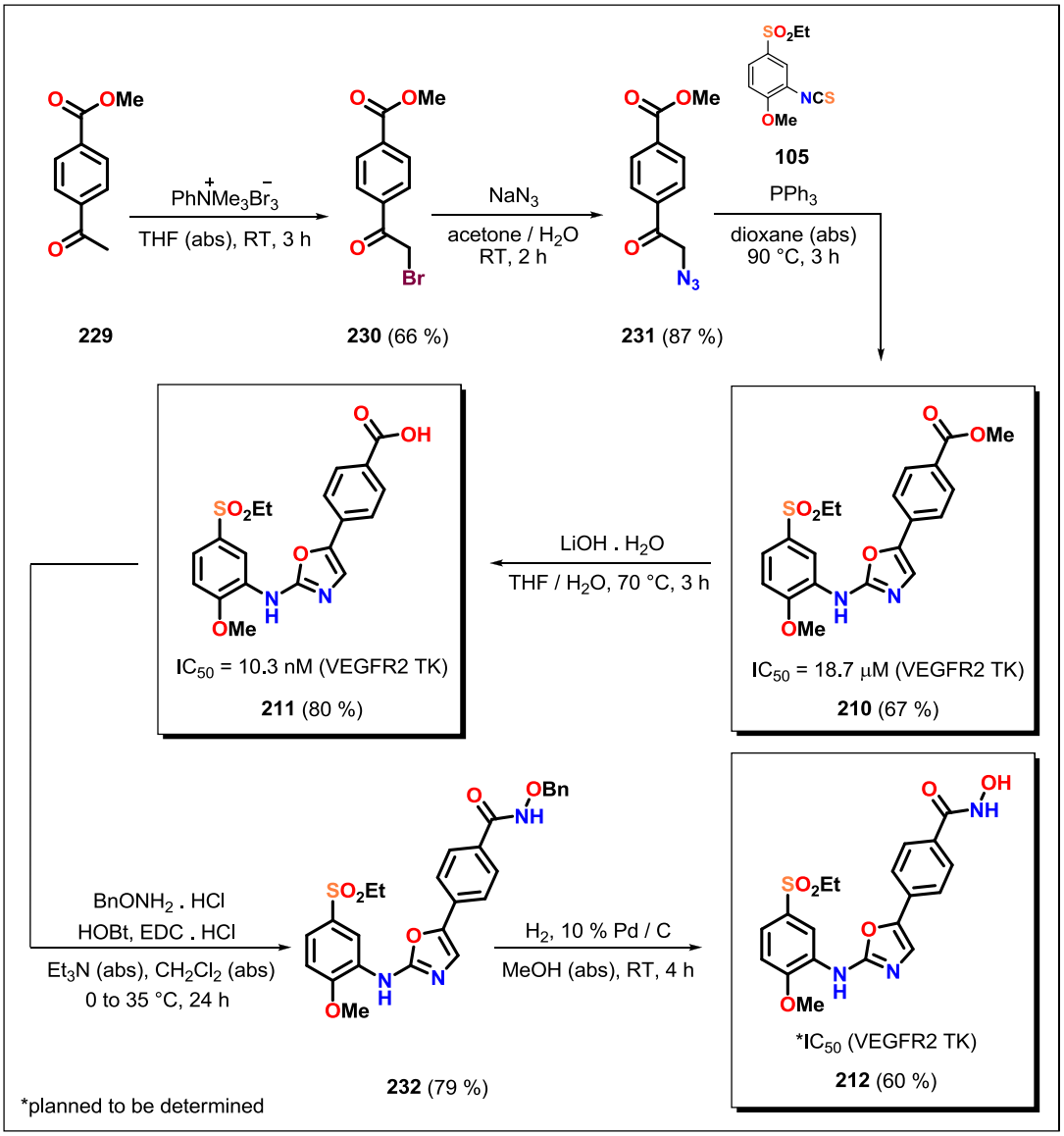

Scheme 31. Synthesis of *p*-substituted *N*,5-diaryloxazol-2-amines **210**, **211** and **212**.

Synthesis of methyl 4-(2-bromoacetyl)benzoate (230)

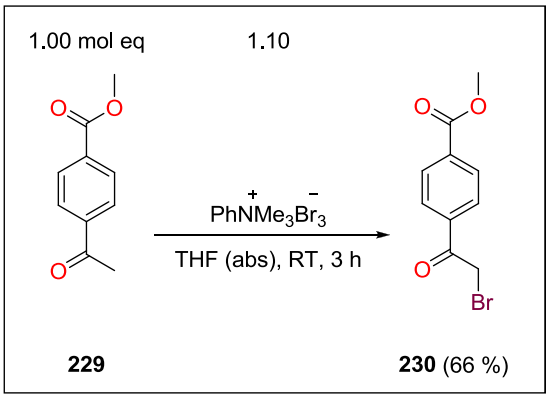

To a solution of 1.00 g (5.61 mmol, 1.00 mol eq) acetophenone **229** in 40 ml of THF (abs), 2.32 g (6.17 mmol, 1.10 mol eq) of trimethylphenylammonium tribromide dissolved in 20 ml of THF (abs) was added dropwise. The reaction mixture was stirred under Ar at RT for 3 h. After complete consumption of the starting material **229** (TLC analysis), the reaction mixture was concentrated. An obtained solid material was dissolved in 60 ml of EA and extracted with 3 x 20 ml of brine. The organic layer was dried over Na_2SO_4, filtered and evaporated under reduced pressure. The crude product was purified by crystallization from EtOH yielding 952 mg (3.70 mmol, 66 %) of methyl 4-(2-bromoacetyl)benzoate (**230**).

Novelty: Synthesis of **230** was described in the literature with 75 % yield together with its ^{1}H-NMR, ^{13}C-NMR, IR and HRMS spectra.[143]

M.p.: 132 – 135 °C [EtOH]. (lit. M. p.: 124 °C [pentane / CH_2Cl_2])[143] White crystalline solid material.

[143] Hou, Z.; Nakanishi, I.; Kinoshita, T.; Takei, Y.; Yasue, M.; Misu, R.; Suzuki, Y.; Nakamura, S.; Kure, T.; Ohno, H.; Murata, K.; Kitaura, K.; Hirasawa, A.; Tsujimoto, G.; Oishi, S.; Fujii, N. *J. Med. Chem.* **2012**, *55*, 2899 – 2903.

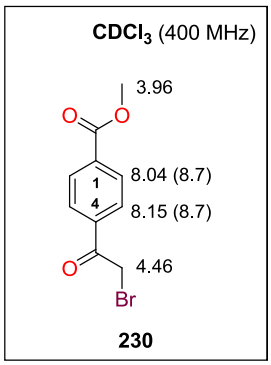

^{1}H-NMR (400 MHz, $CDCl_3$): δ 8.15 (d, 2H, J(2,3) = 8.7 Hz, 2 x H-C(3)), 8.04 (d, 2H, J(2,3) = 8.7 Hz, 2 x H-C(2)), 4.46 (s, 2H, -$COCH_2Br$), 3.96 (s, 3H, -$COOCH_3$).

Synthesis of methyl 4-(2-azidoacetyl)benzoate (231)

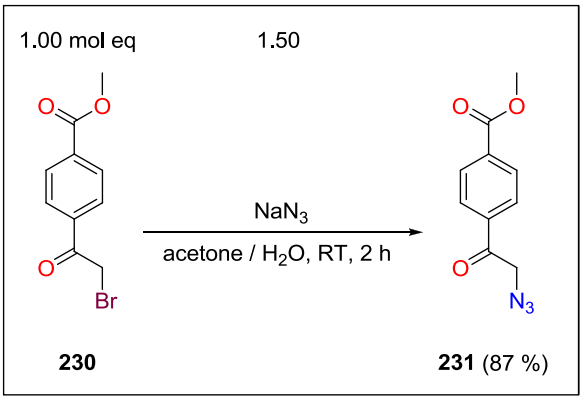

To a solution of 1.00 g (3.89 mmol, 1.00 mol eq) starting material **230** in 20 ml of acetone, 379 mg (5.83 mmol, 1.50 mol eq) of NaN_3 dissolved in 5 ml of H_2O was added. The reaction mixture was stirred for 2 h at RT. After consumption of the starting material **230** (TLC analysis), the reaction mixture was evaporated. A remaining material was dissolved in 30 ml of EA and washed with 2 x 10 ml of brine and 1 x 10 ml of H_2O. The organic layer was dried over Na_2SO_4, filtered and concentrated under reduced pressure giving 742 mg (3.39 mmol, 87 %) of crude 4-(2-azidoacetyl)benzoate (**231**) which was used in the next step without further purification.

Novelty: Synthesis of **231** was described in the literature with 76 % yield.[144] ^{1}H-NMR[145] and IR[146] spectra were also published.

M.p.: 94 – 96 °C (dec) [EA]. (lit. M. p.: 98 – 101 °C decomp. [petroleum ether])[146] Light yellow crystalline solid material.

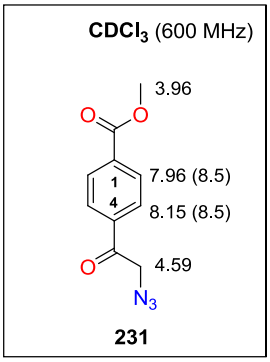

^{1}H-NMR (600 MHz, $CDCl_3$): δ 8.15 (d, 2H, J(2,3) = 8.5 Hz, 2 x H-C(3)), 7.96 (d, 2H, J(2,3) = 8.5 Hz, 2 x H-C(2)), 4.59 (s, 2H, -$COCH_2N_3$), 3.96 (s, 3H, -$COOCH_3$).

Synthesis of methyl 4-(2-(5-(ethylsulfonyl)-2-methoxyphenylamino) oxazol-5-yl)benzoate (210)

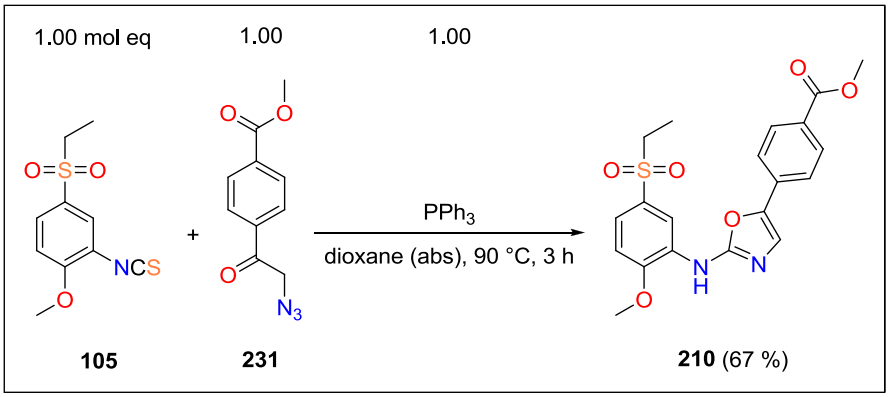

[144] Nilsson, M.; Zhou, X. X.; Oden, L.; Classon, B.; Noren, R.; Grabowska, U.; Jackson, P.; Fallon, P.; Carr, A.; Liley, M;. Tozer, M.; Johnson, T.; Diaz, V.; Crespo, L.; Kangasmetsa, J.; Bonnaud, T. *Medavir AB* **2005**, WO2005/066180, A1.
[145] Su, Y.; Petersen, J. L.; Gregg, T. L.; Shi, X. *Org. Lett.* **2015**, *17*, 1208 – 1211.
[146] Ehrenfreund, J.; Zbiral, E. *Tetrahedron* **1972**, *28*, 1697 – 1704.

A mixture of 836 mg (3.25 mmol, 1.00 mol eq) isothiocyanate **105**, 712 mg (3.25 mmol, 1.00 mol eq) of azide **231** and 852 mg (3.25 mmol, 1.00 mol eq) of PPh_3 in 40 ml of dioxane (abs) was stirred under Ar at 90 °C for 3 h. After consumption of the starting material **105** and **231** (TLC analysis), the reaction mixture was evaporated. A remaining material was dissolved in 40 ml of EA and washed with 2 x 15 ml of brine and 1 x 10 ml of H_2O. The separated organic layer was dried over Na_2SO_4, filtered and concentrated under reduced pressure. The crude product was purified by FLC (EA + 10 % MeOH) and subsequently crystallized from Hex / EA yielding 900 mg (2.16 mmol, 67 %) of methyl 4-(2-(5-(ethylsulfonyl)-2-methoxyphenylamino)oxazol-5-yl)benzoate (**210**).

Novelty: Preparation or characterization of **210** has not been described in the literature.

M. p.: 219 – 222 °C [EA / MeOH]. Light yellow solid material.

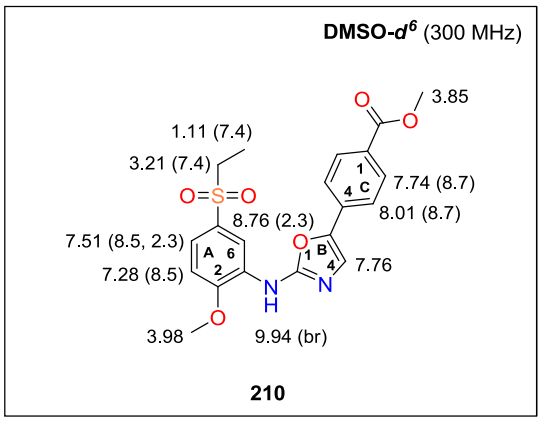

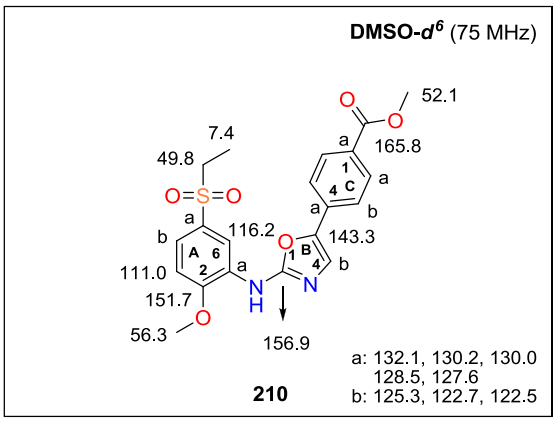

^{1}H-NMR (300 MHz, DMSO-d^6): δ 9.94 (br s, 1H, -NH-), 8.76 (d, 1H, $J(A_4,A_6)$ = 2.3 Hz, H-C_A(6)), 8.01 (d, 2H, J(2,3) = 8.7 Hz, 2 x H-C(3)), 7.76 (s, 1H, C_B(4)), 7.74 (d, 2H, J(2,3) = 8.7 Hz, 2 x H-C(2)), 7.51 (dd, 1H, $J(A_3,A_4)$ = 8.5 Hz, $J(A_4,A_6)$ = 2.3 Hz, H-C_A(4)), 7.28 (d, 1H, $J(A_3,A_4)$ = 8.5 Hz, H-C_A(3)), 3.98 (s, 3H, -OCH_3), 3.85 (s, 3H, -$COOCH_3$), 3.21 (q, 2H, $J(CH_2,CH_3)$ = 7.4 Hz, -$SO_2C\underline{H}_2CH_3$), 1.11 (t, 3H, $J(CH_2,CH_3)$ = 7.4 Hz, -$SO_2CH_2C\underline{H}_3$).

^{13}C-NMR (75 MHz, DMSO-d_6): δ 165.8 (-$\underline{C}OOCH_3$), 156.9 (C_B(2)), 151.7 (C_A(2)), 143.3 (C_B(5)), 132.1, 130.2, 130.0, 128.5, 127.6, 125.3, 122.7, 122.5, 116.2 (C_A(6)), 111.0 (C_A(3)), 56.3 (-OCH_3), 52.1 (-$COO\underline{C}H_3$), 49.8 (-$SO_2\underline{C}H_2CH_3$), 7.4 (-$SO_2CH_2\underline{C}H_3$).

FT IR (solid, cm^{-1}): 3419 (w), 2114 (w), 2064 (w), 1714 (m), 1605 (m), 1576 (s), 1523 (m), 1483 (m), 1459 (w), 1427 (m), 1345 (w), 1302 (m), 1258 (s), 1230 (m), 1179 (m), 1142 (s), 1122 (s), 1084 (s), 1045 (m), 1020 (m), 965 (m), 947 (m), 912 (w), 894 (w), 854 (m), 805 (s), 770 (s), 734 (s), 718 (s), 641 (w), 622 (w), 600 (m), 555 (m), 531 (s), 488 (s), 454 (m).

MS (ESI m/z): 417.0 $[M + H]^+$; in negative mode: 415.0 $[M - H]^-$.

Anal. calcd for $C_{20}H_{20}N_2O_6S$ (416.45): C, 57.68; H, 4.84; N, 6.73; found: C, 57.98; H, 4.43; N, 6.68.

Synthesis of 4-(2-(5-(ethylsulfonyl)-2-methoxyphenylamino)oxazol-5-yl) benzoic acid (211)

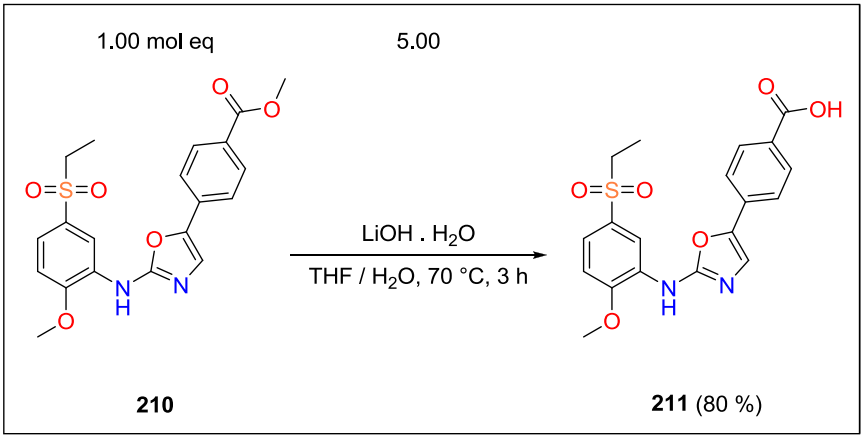

To a suspension of 150 mg (0.36 mmol, 1.00 mol eq) ester **210** in 4 ml of THF, 75.6 mg (1.80 mmol, 5.00 mol eq) of $LiOH.H_2O$ dissolved in 2 ml of H_2O was added. The reaction mixture was stirred at 70 °C for 3 h. After complete consumption of the starting material **210** (TLC analysis), the mixture was concentrated. Obtained aq solution was placed into ice bath, acidified to pH = 2 using 2M HCl solution and moved to a fridge for 5 h. A precipitated solid material was separated on a Büchner funnel, washed with water and Et_2O and dried by HV yielding 116 mg (0.29 mmol, 80 %) of 4-(2-(5-(ethylsulfonyl)-2-methoxyphenylamino)oxazol-5-yl)benzoic acid (**211**).

Novelty: Preparation or characterization of **211** has not been described in the literature.

M. p.: 273 – 278 °C (dec) [H_2O]. Grey solid material.

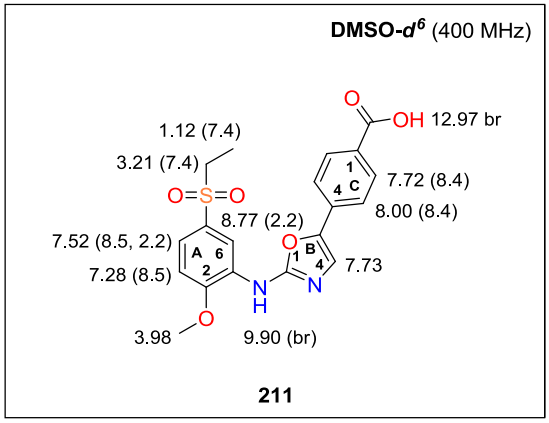

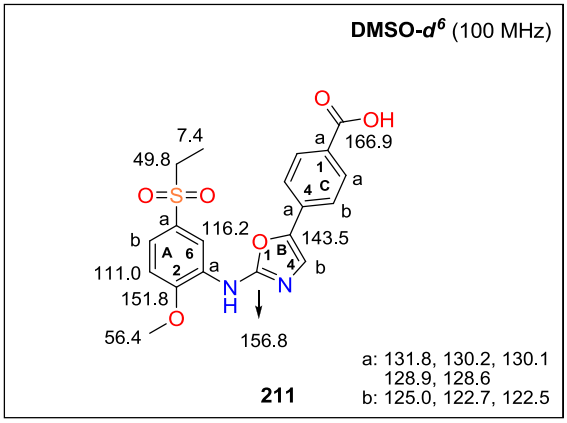

^{1}H-NMR (400 MHz, DMSO-d^6): δ 12.97 (br s, 1H, -COOH), 9.90 (s, 1H, -NH-), 8.77 (d, 1H, $J(A_4,A_6)$ = 2.2 Hz, H-C_A(6)), 8.00 (d, 2H, J(2,3) = 8.4 Hz, 2 x H-C(3)), 7.73 (s, 1H, C_B(4)), 7.72 (d, 2H, J(2,3) = 8.4 Hz, 2 x H-C(2)), 7.52 (dd, 1H, $J(A_3,A_4)$ = 8.5 Hz, $J(A_4,A_6)$ = 2.2 Hz, H-C_A(4)), 7.28 (d, 1H, $J(A_3,A_4)$ = 8.5 Hz, H-C_A(3)), 3.98 (s, 3H, -OCH_3), 3.21 (q, 2H, $J(CH_2,CH_3)$ = 7.4 Hz, -$SO_2C\underline{H}_2CH_3$), 1.12 (t, 3H, $J(CH_2,CH_3)$ = 7.4 Hz, -$SO_2CH_2C\underline{H}_3$).

^{13}C-NMR (100 MHz, DMSO-d_6): δ 166.9 (-COOH), 156.8 (C_B(2)), 151.8 (C_A(2)), 143.5 (C_B(5)), 131.8, 130.2, 130.1, 128.9, 128.6, 125.0, 122.7, 122.5, 116.2 (C_A(6)), 111.0 (C_A(3)), 56.4 (-OCH_3), 49.8 (-$SO_2\underline{C}H_2CH_3$), 7.4 (-$SO_2CH_2\underline{C}H_3$).

FT IR (solid, cm^{-1}): 3411 (w), 3070 (w), 2656 (w), 2323 (w), 2124 (w), 2086 (w), 1919 (w), 1685 (s), 1601 (s), 1575 (s), 1524 (m), 1483 (m), 1418 (m), 1356 (w), 1330 (m), 1264 (s), 1177 (m), 1141 (s), 1121 (s), 1080 (m), 1047 (m), 1014 (m), 950 (w), 917 (w), 893 (w), 858 (w), 825 (w), 796 (m), 772 (m), 736 (s), 717 (s), 662 (w), 624 (w), 597 (m), 576 (s), 532 (m), 496 (s), 456 (m).

MS (ESI m/z): 403.0 $[M + H]^+$; in negative mode: 401.0 $[M - H]^-$.

Anal. calcd for $C_{19}H_{18}N_2O_6S$ (402.42): C, 56.71; H, 4.51; N, 6.96; found: C, 56.65; H, 4.55; N, 6.82.

Synthesis of *N*-(benzyloxy)-4-(2-(5-(ethylsulfonyl)-2-methoxyphenyl amino)oxazol-5-yl)benzamide (232)

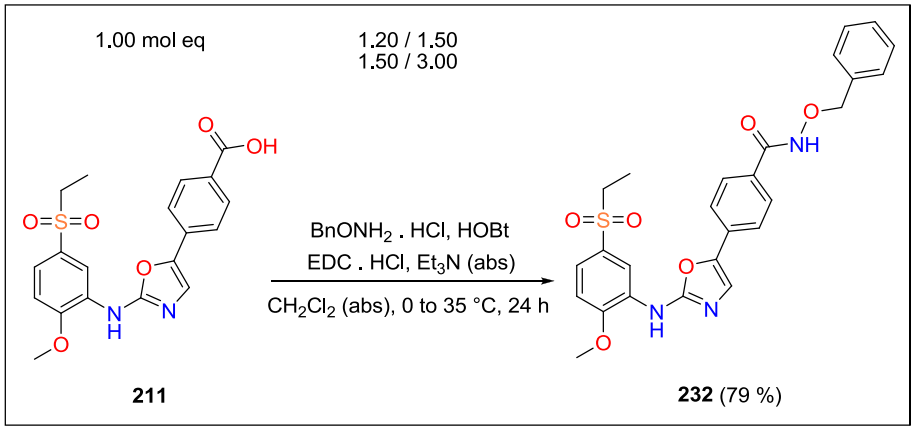

To a suspension of 100 mg (0.25 mmol, 1.00 mol eq) carboxylic acid **211** in 5 ml of CH_2Cl_2 (abs) at 0 °C, 50.4 mg (0.37 mmol, 1.50 mol eq) of HOBt, 71.5 mg (0.37 mmol, 1.50 mol eq) of EDC . HCl, 0.1 ml (75.4 mg, 0.75 mmol, 3.00 mol eq) of Et_3N (abs) and 47.6 mg (0.30 mmol, 1.20 mol eq) of $BnONH_2$. HCl were added gradually. Afterwards the reaction mixture was stirred under Ar for 10 min at RT and 24 h at 35 °C. After complete consumption of the starting material **211** (TLC analysis), the mixture was concentrated. Obtained solid residue was dissolved in 20 ml of CH_2Cl_2 and extracted with 2 x 5 ml of 10 % aq solution of citric acid and 2 x 5 ml of saturated aq solution of $NaHCO_3$. The organic layer was dried over Na_2SO_4, filtered and concentrated under reduced pressure. The crude product was purified by recrystalization from cyclohexane / EA yielding 100 mg (0.20 mmol, 79 %) of *N*-(benzyloxy)-4-(2-(5-(ethylsulfonyl)-2-methoxyphenylamino)oxazol-5-yl)benzamide (**232**).

Novelty: Preparation or characterization of **232** has not been described in the literature.

M. p.: 195 – 197 °C [cyclohexane / EA]. Light grey solid material.

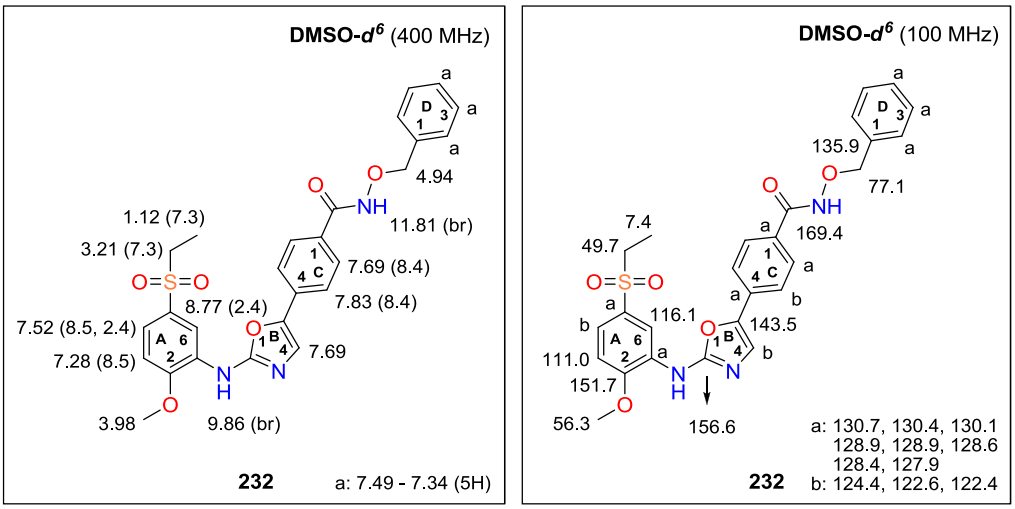

^{1}H-NMR (400 MHz, DMSO-d^6): δ 11.81 (br s, 1H, -CONHO-), 9.86 (s, 1H, -NH-), 8.77 (d, 1H, $J(A_4,A_6)$ = 2.4 Hz, H-C_A(6)), 7.83 (d, 2H, J(2,3) = 8.4 Hz, 2 x H-C(3)), 7.69 (s, 1H, C_B(4)), 7.69 (d, 2H, J(2,3) = 8.4 Hz, 2 x H-C(2)), 7.52 (dd, 1H, $J(A_3,A_4)$ = 8.5 Hz, $J(A_4,A_6)$ = 2.4 Hz, H-C_A(4)), 7.49 – 7.34 (m, 5H, -$CH_2C_6\underline{H}_5$), 7.28 (d, 1H, $J(A_3,A_4)$ = 8.5 Hz, H-C_A(3)), 4.94 (s, 2H, -$C\underline{H}_2C_6H_5$), 3.98 (s, 3H, -OCH_3), 3.21 (q, 2H, $J(CH_2,CH_3)$ = 7.3 Hz, -$SO_2C\underline{H}_2CH_3$), 1.12 (t, 3H, $J(CH_2,CH_3)$ = 7.3 Hz, -$SO_2CH_2C\underline{H}_3$).

^{13}C-NMR (100 MHz, DMSO-d_6): δ 169.4 (-CONHO-), 156.6 (C_B(2)), 151.7 (C_A(2)), 143.5 (C_B(5)), 135.9 (C_D(1)), 130.7, 130.4, 130.1, 2 x 128.9, 128.6, 128.4, 127.9, 124.4, 122.6, 122.4, 116.1 (C_A(6)), 111.0 (C_A(3)), 77.1 (-$\underline{C}H_2C_6H_5$), 56.3 (-OCH_3), 49.7 (-$SO_2\underline{C}H_2CH_3$), 7.4 (-$SO_2CH_2\underline{C}H_3$).

FT IR (solid, cm^{-1}): 3418 (w), 3220 (w), 2986 (w), 2942 (w), 2123 (w), 1737 (w), 1625 (s), 1577 (s), 1528 (m), 1482 (m), 1458 (w), 1429 (m), 1308 (s), 1260 (s), 1223 (w), 1198 (w), 1138 (s), 1122 (s), 1081 (m), 1048 (w), 1020 (s), 969 (w), 950 (w), 915 (w), 892 (w), 857 (w), 835 (w), 798 (m) , 770 (w), 735 (s), 717 (s), 597 (m), 574 (m), 556 (m), 519 (m), 482 (s), 451 (m).

MS (ESI m/z): 508.0 $[M + H]^+$; in negative mode: 506.0 $[M - H]^-$.

Anal. calcd for $C_{26}H_{25}N_3O_6S$ (507.56): C, 61.53; H, 4.96; N, 8.28; found: C, 61.55; H, 5.00; N, 8.17.

Synthesis of 4-(2-(5-(ethylsulfonyl)-2-methoxyphenylamino)oxazol-5-yl)-*N*-hydroxybenzamide (212)

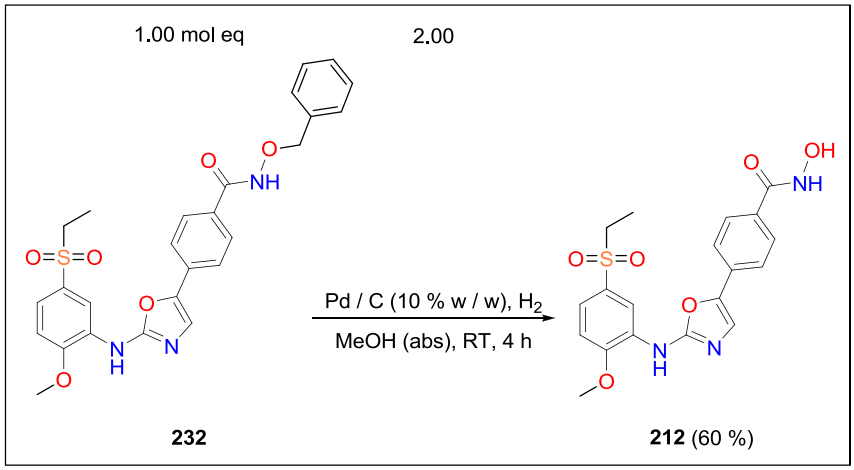

A solution of 81.0 mg (0.16 mmol. 1.00 mol eq) benzyl ester **232**, 16.9 mg (0.16 mmol, 1.00 mol eq) of Pd / C (10 % w / w) in 10 ml of MeOH (abs) was stirred under H_2 atmosphere at RT. After 2 h 16.9 mg (0.16 mmol, 1.00 mol eq) of Pd / C (10 % w / w) was added and the reaction mixture was stirred for another 2 h. After complete consumption of the starting material **232** (TLC analysis), the mixture was filtered. A MeOH filtrate was put aside and a solid residue was transferred from a filtration paper to a flask with 20 ml of THF (abs). The prepared mixture was stirred under Ar for 20 min at 50 °C and immediately filtered. The MeOH filtrate was then combined with THF filtrate and evaporated under reduced pressure. The crude product was purified by crystallization from cyclohexane / THF yielding 40.0 mg (0.10 mmol, 60 %) of 4-(2-(5-(ethylsulfonyl)-2-methoxyphenylamino)oxazol-5-yl)-*N*-hydroxybenzamide (**212**).

Novelty: Preparation or characterization of **212** has not been described in the literature.

M. p.: 187 – 189 °C (dec) [cyclohexane / THF]. White solid material.

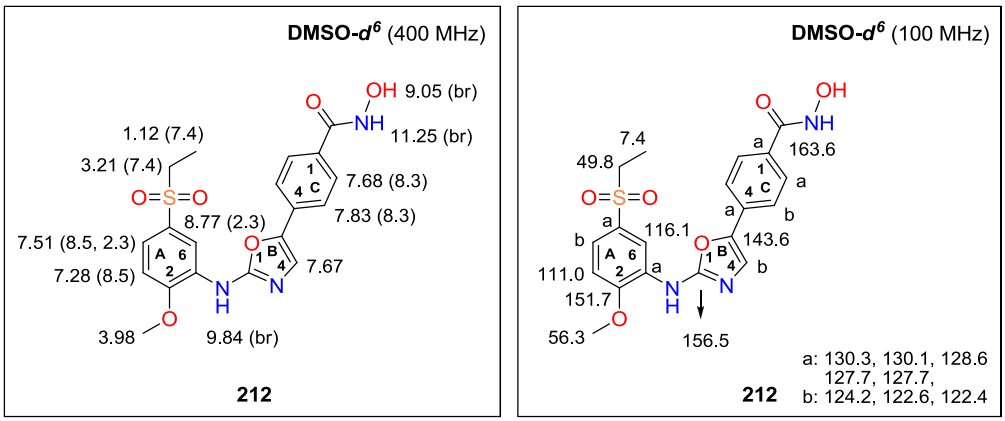

^{1}H-NMR (400 MHz, DMSO-d^6): δ 11.25 (br s, 1H, -CONHOH), 9.84 (s, 1H, -NH-), 9.05 (s br, 1H, -CONHOH), 8.77 (d, 1H, $J(A_4,A_6)$ = 2.3 Hz, H-C_A(6)), 7.83 (d, 2H, J(2,3) = 8.3 Hz, 2 x H-C(3)), 7.68 (d, 2H, J(2,3) = 8.3 Hz, 2 x H-C(2)), 7.67 (s, 1H, C_B(4)), 7.51 (dd, 1H, $J(A_3,A_4)$ = 8.5 Hz, $J(A_4,A_6)$ = 2.3 Hz, H-C_A(4)), 7.28 (d, 1H, $J(A_3,A_4)$ = 8.5 Hz, H-C_A(3)), 3.98 (s, 3H, -OCH_3), 3.21 (q, 2H, $J(CH_2,CH_3)$ = 7.4 Hz, -$SO_2CH_2CH_3$), 1.12 (t, 3H, $J(CH_2,CH_3)$ = 7.4 Hz, -$SO_2CH_2CH_3$).

^{13}C-NMR (100 MHz, DMSO-d_6): δ 163.6 (-CONHOH), 156.5 (C_B(2)), 151.7 (C_A(2)), 143.6 (C_B(5)), 130.3, 130.1, 128.6, 2 x 127.7, 124.2, 122.6, 122.4, 116.1 (C_A(6)), 111.0 (C_A(3)), 56.3 (-OCH_3), 49.8 (-$SO_2CH_2CH_3$), 7.4 (-$SO_2CH_2CH_3$).

FT IR (solid, cm^{-1}): 3335 (w), 3216 (w), 2938 (w), 2083 (w), 1577 (s), 1541 (m), 1486 (m), 1458 (m), 1419 (m), 1348 (w), 1230 (s), 1265 (s), 1226 (w), 1178 (w), 1141 (s), 1123 (s), 1085 (w), 1044 (w), 1020 (m), 926 (w), 895 (w), 841 (w), 796 (w), 775 (w), 735 (s), 719 (s), 598 (m), 575 (m), 558 (m), 527 (m), 493 (s), 446 (w).

MS (ESI m/z): 418.0 $[M + H]^+$; in negative mode: 416.0 $[M - H]^-$.

Anal. calcd for $C_{19}H_{19}N_3O_6S$ (417.44): C, 54.67; H, 4.59; N, 10.07; found: C, 55.12; H, 4.91; N, 9.24.

13.3.3. Synthesis of *m*-substituted *N*,5-diaryloxazol-2-amines 213, 214

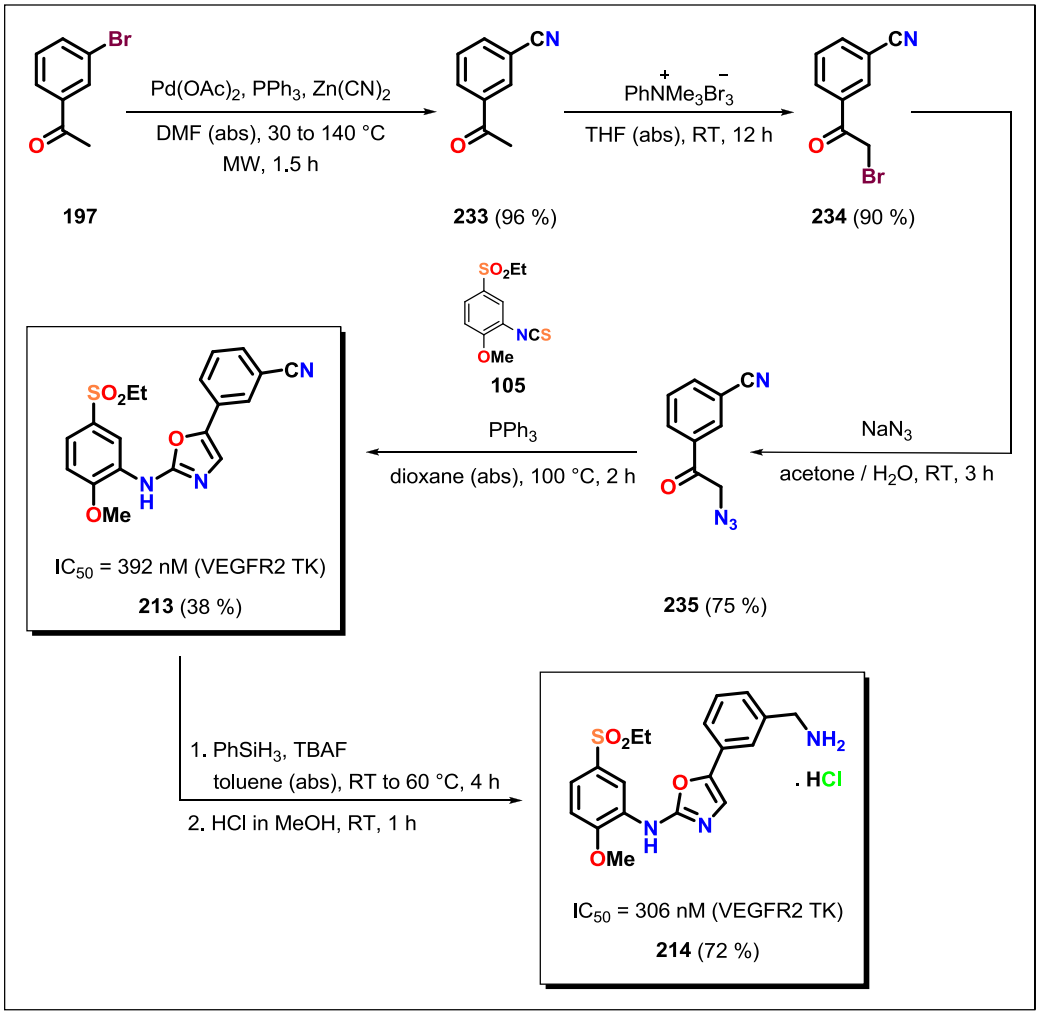

Scheme 32. Synthesis of *m*-substituted *N*,5-diaryloxazol-2-amines **213**, **214**.

Synthesis of 3-acetylbenzonitrile (233)

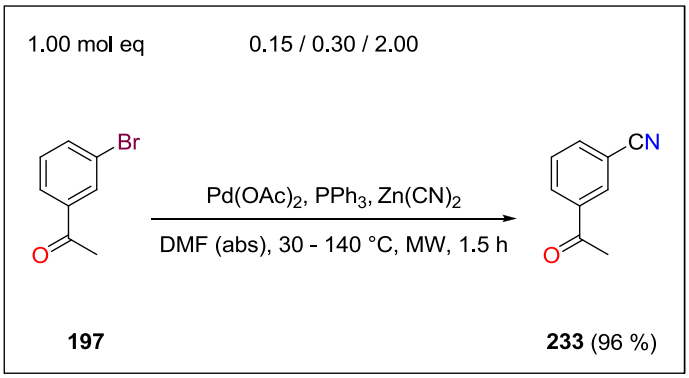

A solution of 254 mg (1.13 mmol, 0.15 mol eq) $Pd(OAc)_2$ and 593 mg (2.26 mmol, 0.30 mol eq) of PPh_3 in 30 ml of DMF (abs) was prepared in a MW tube and stirred at 30 °C for 1 h. When color of the solution changed from brown to dark red, 1.50 g (7.54 mmol, 1.00 mol eq) of bromoacetophenone **197** and 1.80 g (15.1 mmol, 2.00 mol eq) of $Zn(CN)_2$ were added. The reaction mixture was sealed, placed into a MW reactor and stirred at 140 °C for 1.5 h. After consumption of the starting material **197** (TLC analysis), the mixture was diluted with 50 ml of EA, filtered through a silica pad and extracted with 2 x 20 ml of brine and 20 ml of H_2O. The organic layer was dried over Na_2SO_4, filtered and concentrated under reduced pressure. The crude product was purified by FLC (Hex / EA = 2 / 1) yielding 1.05 g (7.23 mmol, 96 %) of 3-acetylbenzonitrile (**233**).

Novelty: Synthesis of **233** was described in the literature with 89 % yield.[147] ^{1}H-NMR ^{13}C-NMR, IR and MS spectra were also published.[148]

M.p.: 94 – 96 °C [Hex / EA]. (lit. M. p.: 95 – 97 °C [petroleum ether / EA])[148] White crystalline solid material.

[147] Srivastava, R. R.; Collibee, S. E. *Tetrahedron Lett.* **2004**, *45*, 8895 – 8897.
[148] Dutta, U.; Lupton, D. W.; Maiti, D. *Org. Lett.* **2016**, *18*, 860 – 863.

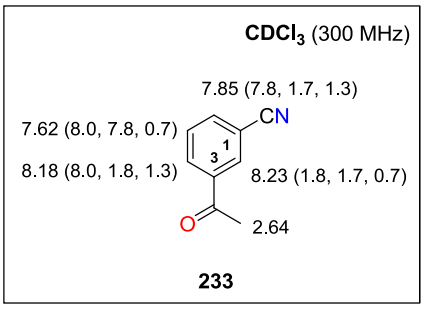

^{1}H-NMR (300 MHz, $CDCl_3$): δ 8.23 (ddd, 1H, *J*(2,4) = 1.8 Hz, *J*(2,6) = 1.7 Hz, *J*(2,5) = 0.7 Hz, H-C(2)), 8.18 (ddd, 1H, *J*(4,5) = 8.0 Hz, *J*(2,4) = 1.8 Hz, *J*(4,6) = 1.3 Hz, H-C(4)), 7.85 (ddd, 1H, *J*(5,6) = 7.8 Hz, *J*(2,6) = 1.7 Hz, *J*(4,6) = 1.3 Hz, H-C(6)), 7.62 (ddd, 1H, *J*(4,5) = 8.0 Hz, *J*(5,6) = 7.8 Hz, *J*(2,5) = 0.7 Hz, H-C(5)), 2.64 (s, 3H, -$COCH_3$).

Synthesis of 3-(2-bromoacetyl)benzonitrile (234)

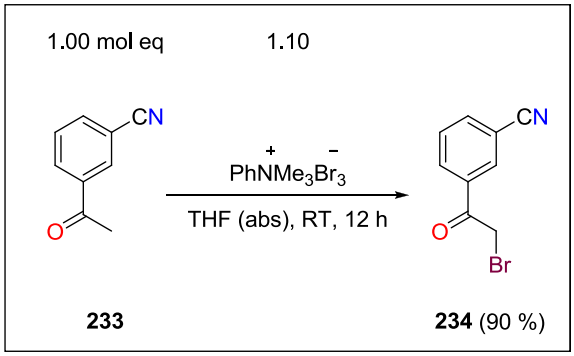

To a solution of 500 mg (3.44 mmol, 1.00 mol eq) benzonitrile **233** in 15 ml of THF (abs), 1.42 g (3.79 mmol, 1.10 mol eq) of trimethylphenylammonium tribromide dissolved in 10 ml of THF (abs) was added dropwise. The reaction mixture was stirred at RT under Ar for 12 h. After consumption of the starting material **233** (TLC analysis), the reaction mixture was concentrated, an obtained residual material was dissolved in 30 ml of EA and extracted with 2 x 10 ml of brine and 10 ml of H_2O. The organic layer was dried over Na_2SO_4, filtered and evaporated under reduced pressure. The crude product was purified by crystallization from EtOH yielding 690 mg (3.08 mmol, 90 %) of 3-(2-bromoacetyl)benzonitrile (**234**).

Novelty: Synthesis of **234** was described in the literature with 78 % yield.[149] ^{1}H-NMR ^{13}C-NMR, IR and MS spectra were also published.[149,150]

M.p.: 68 – 70 °C [EtOH]. (lit. M. p.: 70 – 71 °C [Hex / EA])[149] White crystalline solid material.

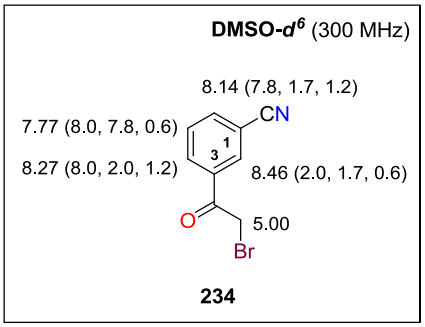

^{1}H-NMR (300 MHz, DMSO-d_6): δ 8.46 (ddd, 1H, J(2,4) = 2.0 Hz, J(2,6) = 1.7 Hz, J(2,5) = 0.6 Hz, H-C(2)), 8.27 (ddd, 1H, J(4,5) = 8.0 Hz, J(2,4) = 2.0 Hz, J(4,6) = 1.2 Hz, H-C(4)), 8.14 (ddd, 1H, J(5,6) = 7.8 Hz, J(2,6) = 1.7 Hz, J(4,6) = 1.2 Hz, H-C(6)), 7.77 (ddd, 1H, J(4,5) = 8.0 Hz, J(5,6) = 7.8 Hz, J(2,5) = 0.6 Hz, H-C(5)), 5.00 (s, 2H, -COCH$_2$Br).

Synthesis of 3-(2-azidoacetyl)benzonitrile (235)

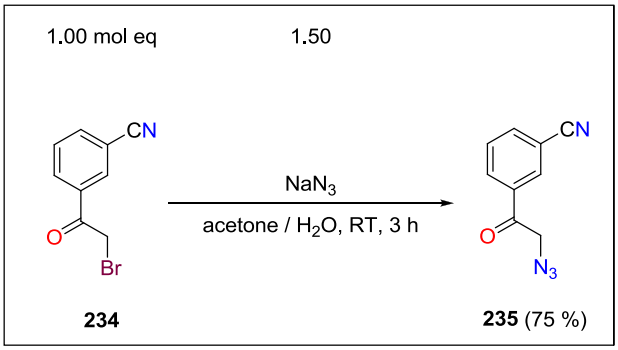

To a solution of 1.50 g (6.69 mmol, 1.00 mol eq) nitrile **234** in 20 ml of acetone, 653 mg (10.0 mmol, 1.50 mol eq) of NaN_3 dissolved in 5 ml of H_2O was added dropwise. The reaction mixture was stirred for 3 h at RT. After consumption of the starting material **234**

[149] Watson, C. Y.; Whish, W. J. D.; Threadgill, M. D. *Bioorg. Med. Chem.* **1998**, *6*, 721 – 734.
[150] Perez, D. I.; Palomo, V.; Perez, C.; Gil, C.; Dans, P. D.; Luque, F. J.; Conde, S.; Martinez, A. *J. Med. Chem.* **2011**, *54*, 4042 – 4056.

(TLC analysis), the mixture was evaporated. A remaining material was dissolved in 30 ml of EA and washed with 2 x 10 ml of brine and 1 x 10 ml of H_2O. The organic layer was dried over Na_2SO_4, filtered and concentrated under reduced pressure giving 930 mg (5.00 mmol, 75 %) of crude 3-(2-azidoacetyl)benzonitrile (**235**) which was used in the next step without further purification.

Novelty: Synthesis of **235** was described in the literature.[6] The reaction yield and spectra of **235** have not been published.

M.p.: 93 – 95 °C (dec) [EA]. (lit. M. p.: 99 – 101 °C [EtOH])[151] Orange crystalline solid material.

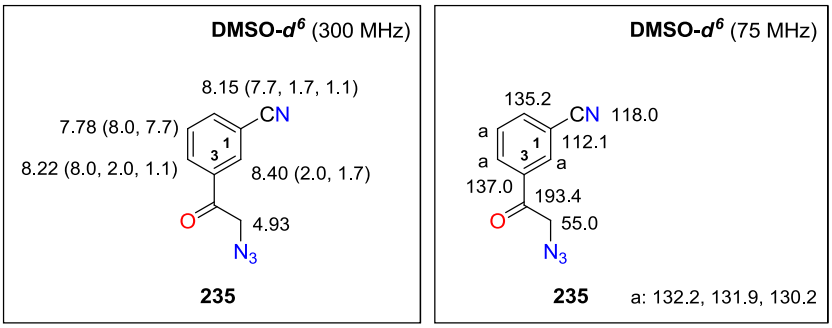

^{1}H-NMR (300 MHz, DMSO-d_6): δ 8.40 (dd, 1H, J(2,4) = 2.0 Hz, J(2,6) = 1.7 Hz, H-C(2)), 8.22 (ddd, 1H, J(4,5) = 8.0 Hz, J(2,4) = 2.0 Hz, J(4,6) = 1.1 Hz, H-C(4)), 8.15 (ddd, 1H, J(5,6) = 7.7 Hz, J(2,6) = 1.7 Hz, J(4,6) = 1.1 Hz, H-C(6)), 7.78 (dd, 1H, J(4,5) = 8.0 Hz, J(5,6) = 7.7 Hz, H-C(5)), 4.93 (s, 2H, -$COCH_2N_3$).

^{13}C-NMR (75 MHz, DMSO-d_6): δ 193.4 (-$\underline{C}OCH_2N_3$), 137.0 (C(3)), 135.2 (C(6)), 132.2, 131.9, 130.2, 118.0 (-CN), 112.1 (C(1)), 55.0 (-CO$\underline{C}H_2N_3$).

FT IR (solid, cm^{-1}): 3385 (w), 3074 (w), 2965 (w), 2892 (w), 2581 (w), 2376 (w), 2343 (w), 2281 (w), 2231 (m), 2111 (s), 1996 (w), 1734 (w), 1701 (s), 1597 (m), 1474 (w), 1417 (m), 1348 (m), 1301 (m), 1240 (s), 1174 (w), 1147 (s), 1102 (m), 1035 (s), 984 (m), 837 (w), 810 (s), 773 (m), 678 (s), 628 (m), 607 (m), 553 (m), 527 (s), 483 (w), 441 (w).

[151] Brown, D.; Dowell, R.; Hargreaves, R. B.; Main, B. *Imperial Chemical Industries PLC* **1983**, US4423045, A1.

MS (ESI m/z): not detectable in positive / negative mode.

Anal. calcd for $C_9H_6N_4O$ (186.17): C, 58.06; H, 3.25; N, 30.09; found: C, 58.23; H, 3.32; N, 29.95.

Synthesis of 3-(2-(5-(ethylsulfonyl)-2-methoxyphenylamino)oxazol-5-yl) benzonitrile (213)

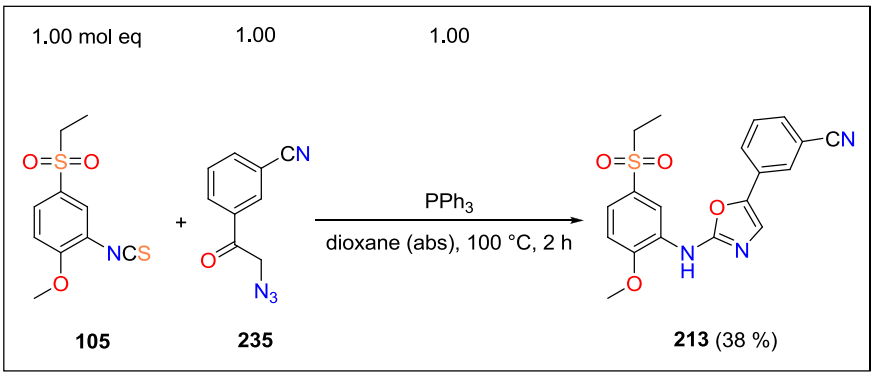

A mixture of 809 mg (3.14 mmol, 1.00 mol eq) isothiocyanate **105**, 585 mg (3.14 mmol, 1.00 mol eq) of azide **235** and 824 mg (3.14 mmol, 1.00 mol eq) of PPh_3 in 20 ml of dioxane (abs) was stirred under Ar at 100 °C for 2 h. After consumption of the starting material **105** and **235** (TLC analysis), the reaction mixture was evaporated. A remaining solid was dissolved in 30 ml of EA and washed with 2 x 10 ml of brine and 1 x 10 ml of H_2O. The organic layer was dried over Na_2SO_4, filtered and concentrated under reduced pressure. The crude product was purified by FLC (Hex / EA = 1 / 2) and triturated with Hex / EA yielding 450 mg (1.17 mmol, 38 %) of 3-(2-(5-(ethylsulfonyl)-2-methoxyphenylamino)oxazol-5-yl)benzonitrile (**213**).

Novelty: Synthesis of **213** was described in the literature in 1 % yield together with its ^{1}H-NMR and HRMS spectral analyses.[6]

M.p.: 156 – 159 °C (dec) [Hex / EA]. Pale yellow solid material.

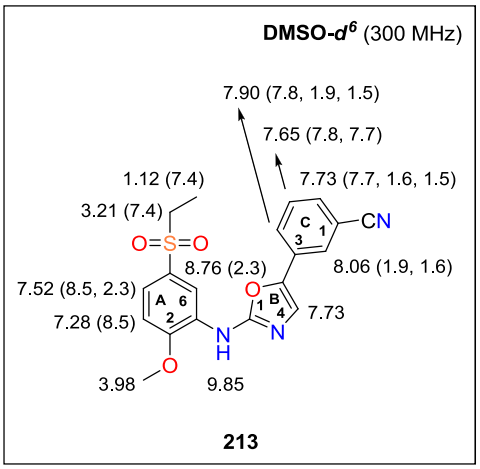

^{1}H-NMR (300 MHz, DMSO-d^6): δ 9.85 (s, 1H, -NH-), 8.76 (d, 1H, $J(A_4,A_6)$ = 2.3 Hz, H-C_A(6)), 8.06 (dd, 1H, $J(C_2,C_4)$ = 1.9 Hz, $J(C_2,C_6)$ = 1.6 Hz, C_C(2)), 7.90 (ddd, 1H, $J(C_4,C_5)$ = 7.8 Hz, $J(C_2,C_4)$ = 1.9 Hz, $J(C_4,C_6)$ = 1.5 Hz, H-C_C(4)), 7.73 (ddd, 1H, $J(C_5,C_6)$ = 7.7 Hz, $J(C_2,C_6)$ = 1.6 Hz, $J(C_4,C_6)$ = 1.5 Hz, H-C_C(6)), 7.73 (s, 1H, C_B(4)), 7.65 (dd, 1H, $J(C_4,C_5)$ = 7.8 Hz, $J(C_5,C_6)$ = 7.7 Hz, H-C_C(5)), 7.52 (dd, 1H, $J(A_3,A_4)$ = 8.5 Hz, $J(A_4,A_6)$ = 2.3 Hz, H-C_A(4)), 7.28 (d, 1H, $J(A_3,A_4)$ = 8.5 Hz, H-C_A(3)), 3.98 (s, 3H, -OCH_3), 3.21 (q, 2H, $J(CH_2,CH_3)$ = 7.4 Hz, -$SO_2C\underline{H}_2CH_3$), 1.12 (t, 3H, $J(CH_2,CH_3)$ = 7.4 Hz, -$SO_2CH_2C\underline{H}_3$).

Synthesis of 5-(3-(aminomethyl)phenyl)-*N*-(5-(ethylsulfonyl)-2-methoxy phenyl)oxazol-2-amine hydrochloride (214)

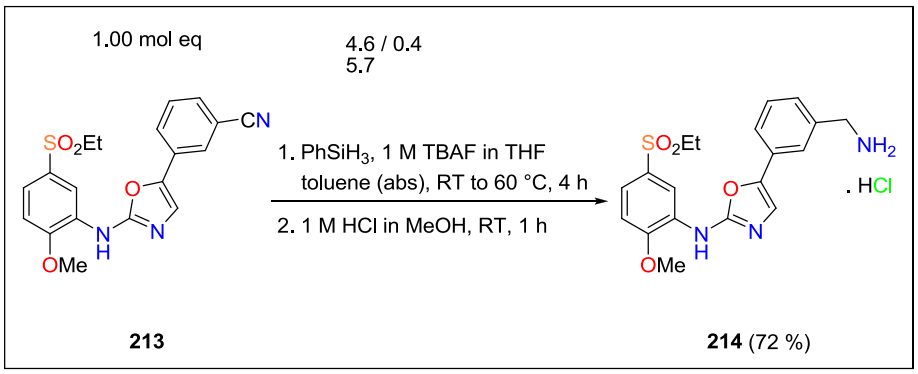

A solution of 100 mg (0.26 mmol, 1.00 mol eq) nitrile **213** and 45.2 mg (0.05 ml) (0.41 mmol, 1.60 mol eq) of $PhSiH_3$ in 3 ml of toluene (abs) was stirred at RT for 10 min. Subsequently 0.05 ml (0.05 mmol, 0.20 mol eq) of 1 M TBAF in THF was added and the

reaction mixture was stirred under Ar at 60 °C for 2 h. Afterwards the reaction was cooled down to RT, additional 84.7 mg (0.10 ml) (0.78 mmol, 3.00 mol eq) of $PhSiH_3$ and 0.05 ml (0.05 mmol, 0.20 mol eq) of 1 M TBAF in THF were added and the reaction was stirred under Ar at 60 °C for 2 h. After consumption of the starting material **213** (TLC analysis), the reaction mixture was cooled to RT, 1.5 ml (1.50 mmol, 5.70 mol eq) of 1 M HCl in MeOH was added and the stirring continued for 1 h. Later the reaction mixture was concentrated, 2 ml of 1 M HCl in MeOH and 2 ml of CH_2Cl_2 were added, for precipitation of the product **214**, and the mixture was concentrated again. The crude product was purified by trituration with acetone yielding 80.0 mg (0.19 mmol, 72 %) of amine **214**.

Novelty: Preparation or characterization of **214** has not been described in the literature.

M. p.: 162 – 170 °C (dec) [HCl / MeOH / CH_2Cl_2]. Pale brown solid material.

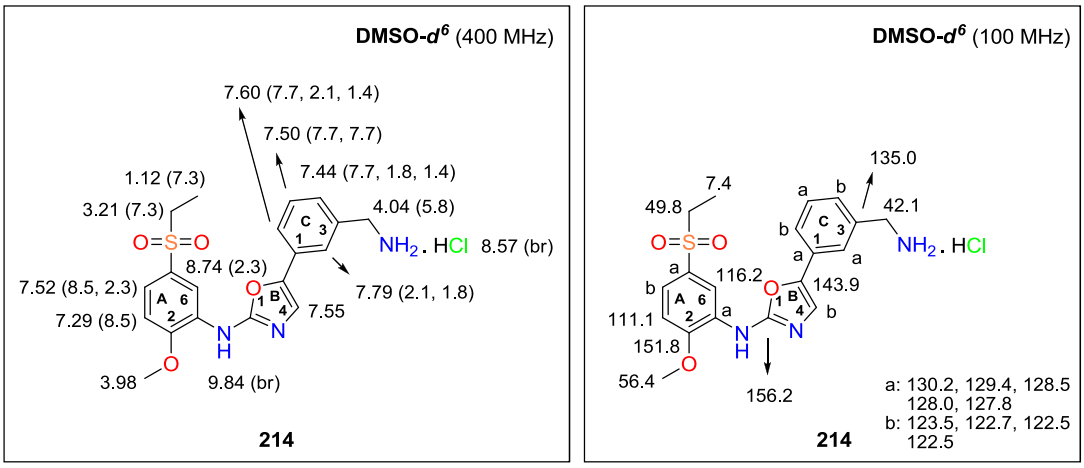

^{1}H-NMR (400 MHz, DMSO-d^6): δ 9.84 (br s, 1H, -NH-), 8.74 (d, 1H, $J(A_4,A_6)$ = 2.3 Hz, H-C_A(6)), 8.57 (br s, 3H, -$CH_2N\underline{H}_2.\underline{H}Cl$), 7.79 (dd, 1H, $J(C_2,C_6)$ = 2.1 Hz, $J(C_2,C_4)$ = 1.8 Hz, H-C_C(2)), 7.60 (ddd, 1H, $J(C_5,C_6)$ = 7.7 Hz, $J(C_2,C_6)$ = 2.1 Hz, $J(C_4,C_6)$ = 1.4 Hz, H-C_C(6)), 7.55 (s, 1H, H-C_B(4)), 7.52 (dd, 1H, $J(A_3,A_4)$ = 8.5 Hz, $J(A_4,A_6)$ = 2.3 Hz, H-C_A(4)), 7.50 (dd, 1H, $J(C_4,C_5)$ and $J(C_5,C_6)$ = 7.7 Hz, H-C_C(5)), 7.44 (ddd, 1H, $J(C_4,C_5)$ = 7.7 Hz, $J(C_2,C_4)$ = 1.8 Hz, $J(C_4,C_6)$ = 1.4 Hz, H-C_C(4)), 7.29, (d, 1H, $J(A_3,A_4)$ = 8.5 Hz, H-C_A(3)), 4.04 (q, 2H, $J(CH_2,NH_2.HCl)$ = 5.8 Hz, -$C\underline{H}_2NH_2.HCl$), 3.98 (s, 3H, -OCH_3), 3.21 (q, 2H, $J(CH_2,CH_3)$ = 7.3 Hz, -$SO_2C\underline{H}_2CH_3$), 1.12 (t, 3H, $J(CH_2,CH_3)$ = 7.3 Hz, -$SO_2CH_2C\underline{H}_3$).

^{13}C-NMR (100 MHz, DMSO-d^6): δ 156.2 (C_B(2)), 151.8 (C_A(2)), 143.9 (C_B(5)), 135.0 (C_C(3)), 130.2, 129.4, 128.5, 128.0, 127.8, 123.5, 122.7, 2 x 122.5, 116.2 (C_A(6)), 111.1 (C_A(3)), 56.4 (-OCH_3), 49.8 (-$SO_2\underline{C}H_2CH_3$), 42.1 (-CH_2NH_2 . HCl), 7.4 (-$SO_2CH_2\underline{C}H_3$).

FT IR (solid, cm^{-1}): 2940 (m), 2617 (w), 2109 (w), 2061 (w), 1999 (w), 1676 (s), 1597 (m), 1576 (m), 1505 (m), 1457 (w), 1425 (w), 1381 (w), 1302 (m), 1268 (m), 1230 (w), 1197 (w), 1123 (s), 1087 (m), 1047 (w), 1015 (m), 918 (w), 792 (m), 734 (m), 697 (m), 593 (w), 557 (w), 520 (m), 490 (s), 443 (m).

MS (ESI m/z): 388.1 $[M + H]^+$; in negative mode: 386.0 $[M - H]^-$.

Anal. calcd for $C_{19}H_{21}N_3O_4S$ (387.45): C, 58.90; H, 5.46; N, 10.85; found: C, 60.01; H, 6.21; N, 9.87.

13.3.4. Synthesis of *m*-substituted *N*,5-diaryloxazol-2-amines 215, 216, 217

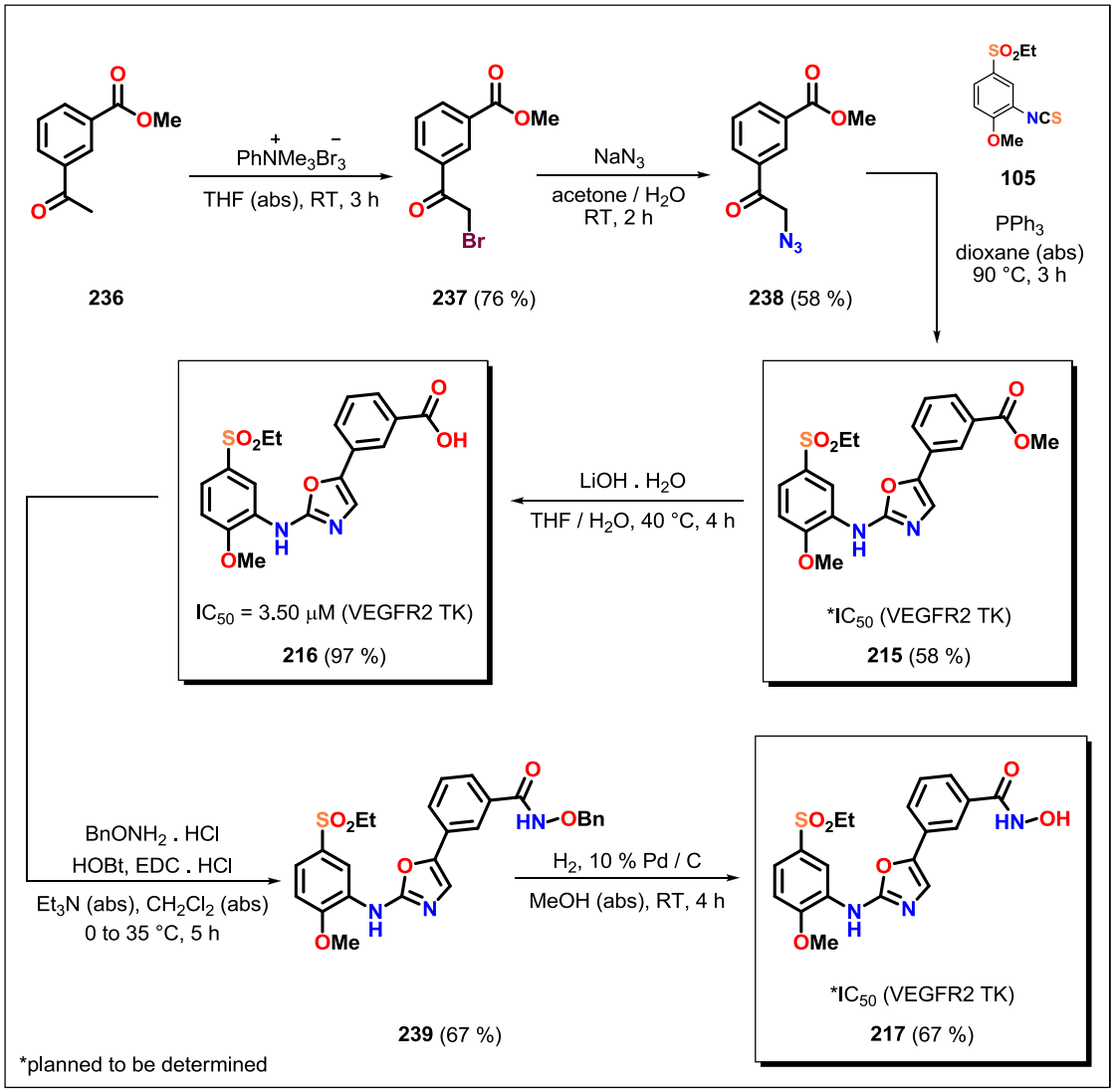

Scheme 33. Synthesis of *m*-substituted *N*,5-diaryloxazol-2-amines **215**, **216** and **217**.

Synthesis of methyl 3-(2-bromoacetyl)benzoate (237)

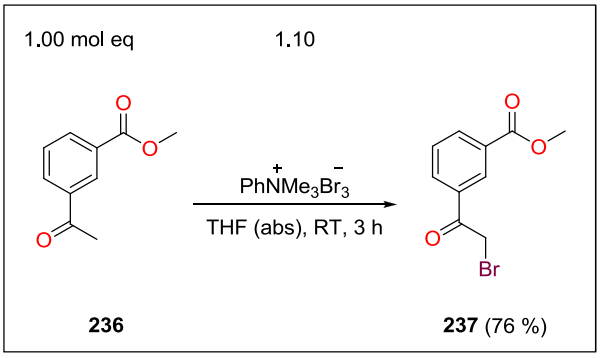

To a solution of 500 mg (2.81 mmol, 1.00 mol eq) benzoate **236** in 20 ml of THF (abs), 1.16 g (3.09 mmol, 1.10 mol eq) of trimethylphenylammonium tribromide dissolved in 10 ml of THF (abs) was added dropwise. The reaction mixture was stirred at RT under Ar for 3 h. After consumption of the starting material **236** (TLC analysis), the reaction mixture was concentrated. An obtained residual material was dissolved in 30 ml of EA and extracted with 2 x 10 ml of brine and 10 ml of H_2O. The organic layer was dried over Na_2SO_4, filtered and evaporated under reduced pressure. The crude product was purified by crystallization from EtOH yielding 550 mg (2.14 mmol, 76 %) of 3-(2-bromoacetyl)benzoate (**237**).

Novelty: Synthesis of **237** was described in the literature with 100 % yield.[152] Its ^{1}H-NMR and MS spectra were also published.[153]

M.p.: 66 – 67 °C [EtOH]. (lit. M. p.: 68 – 70 °C [MeOH])[154] White crystalline solid material.

[152] Suzuki, T.; Muto, N.; Bando, M.; Itoh, Y.; Masaki, A.; Ri, M.; Ota, Y.; Nakagawa, H.; Iida, S.; Shirahige, K.; Miyata, N. *ChemMedChem* **2014**, *9*, 657 – 664.
[153] Jones, P.; Muraglia, E.; Ontoria, J. M. *Instituto di Ricerche di Biologia Molecolare P. Angeletti S.p.A.* **2007**, WO2007/144669, A1.
[154] Collin, D. T.; Hartley, D.; Jack, D.; Lunts, L. H. C.; Press, J. C.; Ritchie, A. C.; Toon, P. *J. Med. Chem.* **1970**, *13*, 674 – 680.

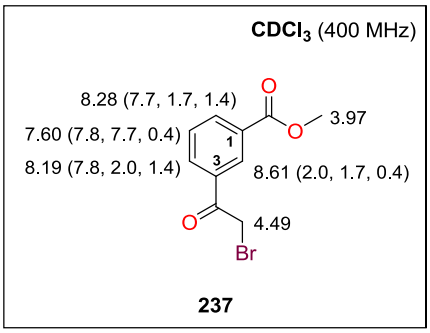

^{1}H-NMR (400 MHz, $CDCl_3$): δ 8.61 (ddd, 1H, *J*(2,4) = 2.0 Hz, *J*(2,6) = 1.7 Hz, *J*(2,5) = 0.4 Hz, H-C(2)), 8.28 (ddd, 1H, *J*(5,6) = 7.7 Hz, *J*(2,6) = 1.7 Hz, *J*(4,6) = 1.4 Hz, H-C(6)), 8.19 (ddd, 1H, *J*(4,5) = 7.8 Hz, *J*(2,4) = 2.0 Hz, *J*(4,6) = 1.4 Hz, H-C(4)), 7.60 (ddd, 1H, *J*(4,5) = 7.8 Hz, *J*(5,6) = 7.7 Hz, *J*(2,5) = 0.4 Hz, H-C(5)), 4.49 (s, 2H, -$COCH_2Br$), 3.97 (s, 3H, -$COOCH_3$).

Synthesis of methyl 3-(2-azidoacetyl)benzoate (238)

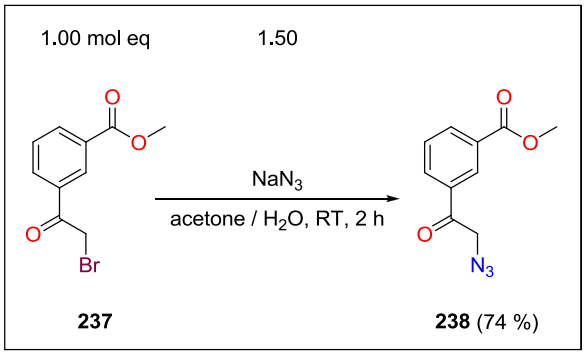

To a solution of 550 mg (2.14 mmol, 1.00 mol eq) bromide **237** in 10 ml of acetone, 209 mg (3.21 mmol, 1.50 mol eq) of NaN_3 dissolved in 2 ml of H_2O was added. The reaction mixture was stirred for 2 h at RT. After consumption of the starting material **237** (TLC analysis), the mixture was evaporated. A remaining material was dissolved in 15 ml of EA and washed with 2 x 5 ml of brine and 5 ml of H_2O. The organic layer was dried over Na_2SO_4, filtered and concentrated under reduced pressure giving 340 mg (1.55 mmol, 74 %) of crude 3-(2-azidoacetyl)benzoate (**238**) which was used in the next step without further purification.

Novelty: Synthesis or characterization of **238** has not been described in the literature.

M.p.: 63 – 66 °C [EA]. Yellow crystalline solid material.

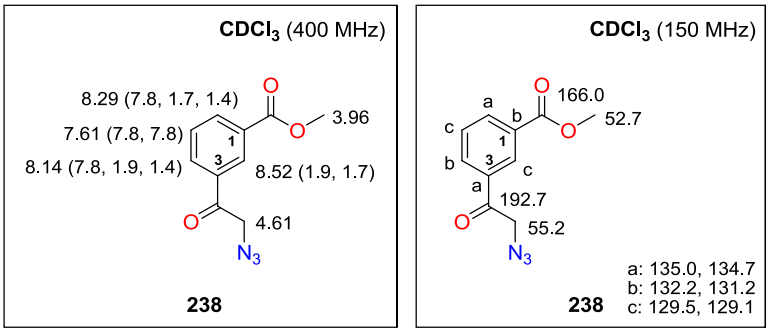

^{1}H-NMR (400 MHz, $CDCl_3$): δ 8.52 (dd, 1H, J(2,4) = 1.9 Hz, J(2,6) = 1.7 Hz, H-C(2)), 8.29 (ddd, 1H, J(5,6) = 7.8 Hz, J(2,6) = 1.7 Hz, J(4,6) = 1.4 Hz, H-C(6)), 8.14 (ddd, 1H, J(4,5) = 7.8 Hz, J(2,4) = 1.9 Hz, J(4,6) = 1.4 Hz, H-C(4)), 7.61 (dd, 1H, J(4,5) = J(5,6) = 7.8 Hz, H-C(5)), 4.61 (s, 2H, -$COCH_2N_3$), 3.96 (s, 3H, -$COOCH_3$).

^{13}C-NMR (150 MHz, $CDCl_3$): δ 192.7 (-$\underline{C}OCH_2N_3$), 166.0 (-$\underline{C}OOCH_3$), 135.0, 134.7, 132.2, 131.2, 129.5, 129.1, 55.2 (-CO$\underline{C}H_2N_3$), 52.7 (-COO$\underline{C}H_3$).

FT IR (solid, cm^{-1}): 3070 (w), 2982 (w), 2951 (w), 2908 (w), 2266 (w), 2211 (w), 2150 (w), 2092 (s), 1929 (w), 1861 (w), 1722 (s), 1692 (s), 1601 (m), 1483 (w), 1465 (w), 1428 (s), 1345 (w), 1298 (s), 1274 (s), 1206 (s), 1105 (s), 1075 (s), 1037 (s), 973 (s), 917 (s), 850 (w), 820 (w), 746 (s), 720 (s), 681 (s), 617 (s), 553 (s), 520 (w), 471 (m), 439 (w).

MS (ESI m/z): not detectable in positive / negative mode.

Anal. calcd for $C_{10}H_9N_3O_3$ (219.20): C, 54.79; H, 4.14; N, 19.17; found: C, 54.90; H, 4.32; N, 19.15.

Synthesis of methyl 3-(2-(5-(ethylsulfonyl)-2-methoxyphenylamino) oxazol-5-yl)benzoate (215)

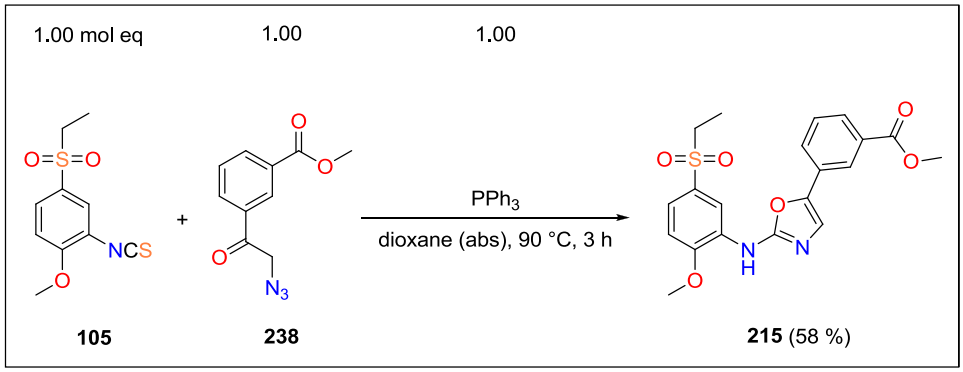

A solution of 235 mg (0.91 mmol, 1.00 mol eq) isothiocyanate **105**, 200 mg (0.91 mmol, 1.00 mol eq) of azide **238** and 239 mg (0.91 mmol, 1.00 mol eq) of PPh_3 in 15 ml of dioxane (abs) under Ar was placed into preheated 90 °C oil bath for 3 h. After consumption of the starting material **105** and **238** (TLC analysis), the reaction mixture was evaporated and an obtained solid material was dissolved in 15 ml of EA and extracted with 2 x 5 ml of brine and 5 ml of H_2O. The organic layer was separated, dried over Na_2SO_4, filtered and evaporated under reduced pressure. The crude product was purified by FLC (gradient: Hex / EA = 1 / 3 to 1 / 4 to 1 / 5) and triturated with Hex / EA yielding 220 mg (0.53 mmol, 58 %) of methyl 3-(2-(5-(ethylsulfonyl)-2-methoxyphenylamino)oxazol-5-yl)benzoate (**215**).

Novelty: Synthesis or characterization of **215** has not been described in the literature.

M.p.: 204 – 205 °C [Hex / EA]. Off-white solid material.

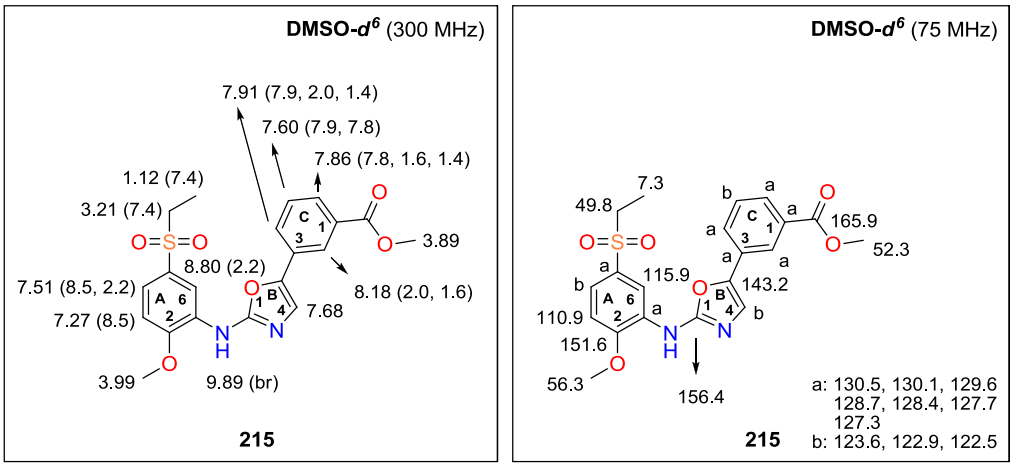

^{1}H-NMR (300 MHz, DMSO-*d*^{6}): δ 9.89 (br s, 1H, -NH-), 8.80 (d, 1H, $J(A_4,A_6)$ = 2.2 Hz, H-C_A(6)), 8.18 (dd, 1H, $J(C_2,C_4)$ = 2.0 Hz, $J(C_2,C_6)$ = 1.6 Hz, C_C(2)), 7.91 (ddd, 1H, $J(C_4,C_5)$ = 7.9 Hz, $J(C_2,C_4)$ = 2.0 Hz, $J(C_4,C_6)$ = 1.4 Hz, H-C_C(4)), 7.86 (ddd, 1H, $J(C_5,C_6)$ = 7.8 Hz, $J(C_2,C_6)$ = 1.6 Hz, $J(C_4,C_6)$ = 1.4 Hz, H-C_C(6)), 7.68 (s, 1H, C_B(4)), 7.60 (dd, 1H, $J(C_4,C_5)$ = 7.9 Hz, $J(C_5,C_6)$ = 7.8 Hz, H-C_C(5)), 7.51 (dd, 1H, $J(A_3,A_4)$ = 8.5 Hz, $J(A_4,A_6)$ = 2.2 Hz, H-C_A(4)), 7.27 (d, 1H, $J(A_3,A_4)$ = 8.5 Hz, H-C_A(3)), 3.99 (s, 3H, -OCH_3), 3.89 (s, 3H, -$COOCH_3$), 3.21 (q, 2H, $J(CH_2,CH_3)$ = 7.4 Hz, -$SO_2C\underline{H}_2CH_3$), 1.12 (t, 3H, $J(CH_2,CH_3)$ = 7.4 Hz, -$SO_2CH_2C\underline{H}_3$).

^{13}C-NMR (75 MHz, DMSO-*d*^{6}): δ 165.9 (-$\underline{C}OOCH_3$), 156.4 (C_B(2)), 151.6 (C_A(2)), 143.2 (C_B(5)), 130.5, 130.1, 129.6, 128.7, 128.4, 127.7, 127.3, 123.6, 122.9, 122.5, 115.9 (C_A(6)), 110.9 (C_A(3)), 56.3 (-OCH_3), 52.3 (-$COO\underline{C}H_3$), 49.8 (-$SO_2\underline{C}H_2CH_3$), 7.3 (-$SO_2CH_2\underline{C}H_3$).

FT IR (solid, cm^{-1}): 3418 (w), 3089 (w), 2840 (w), 2211 (w), 2077 (w), 1925 (w), 1723 (s), 1615 (s), 1579 (s), 1523 (m), 1482 (m), 1459 (m), 1421 (m), 1346 (w), 1302 (m), 1247 (s), 1221 (m), 1184 (w), 1140 (s), 1122 (s), 1086 (s), 1054 (w), 1039 (w), 1016 (s), 988 (w), 950 (w), 918 (w), 890 (w), 832 (w), 809 (m), 794 (m), 779 (w), 753 (s), 733 (s), 716 (s), 681 (m), 657 (w), 623 (w), 600 (w), 553 (m), 529 (s), 511 (w), 488 (s), 470 (s).

MS (ESI m/z): 439.0 $[M + Na]^+$; in negative mode: 415.0 $[M - H]^-$.

Anal. calcd for $C_{20}H_{20}N_2O_6S$ (416.45): C, 57.68; H, 4.84; N, 6.73; found: C, 57.45, H, 4.81; N, 6.68.

Synthesis of 3-(2-(5-(ethylsulfonyl)-2-methoxyphenylamino)oxazol-5-yl) benzoic acid (216)

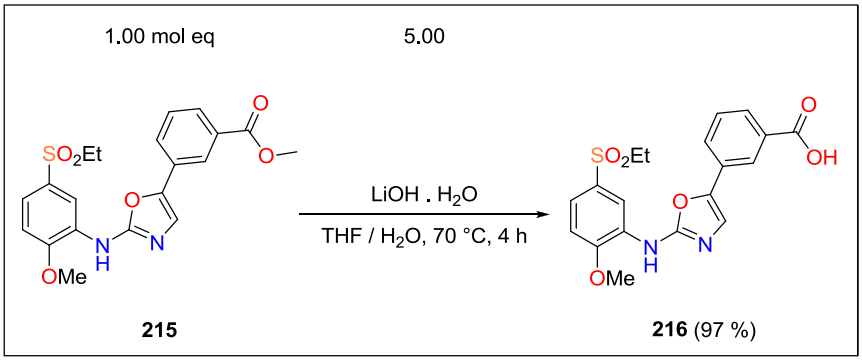

To a suspension of 100 mg (0.24 mmol, 1.00 mol eq) ester **215** in 2 ml THF, 50.3 mg (1.20 mmol, 5.00 mol eq) of LiOH.H_2O dissolved in 0.5 ml of H_2O was added. The reaction mixture was stirred at 70 °C for 4 h. After consumption of the starting material **215** (TLC analysis), the mixture was concentrated. A residual material was cooled in an ice bath, acidified to pH = 2 by 2 M HCl and moved to a fridge for 5 h. A precipitated solid material was filtered, washed with water and Et_2O and dried by HV yielding 65.0 mg (0.16 mmol, 97 %) of 3-(2-(5-(ethylsulfonyl)-2-methoxyphenylamino)oxazol-5-yl)benzoic acid (**216**).

Novelty: Preparation or characterization of **216** has not been described in the literature.

M. p.: 285 – 288 °C (dec) [H_2O]. Light yellow solid material.

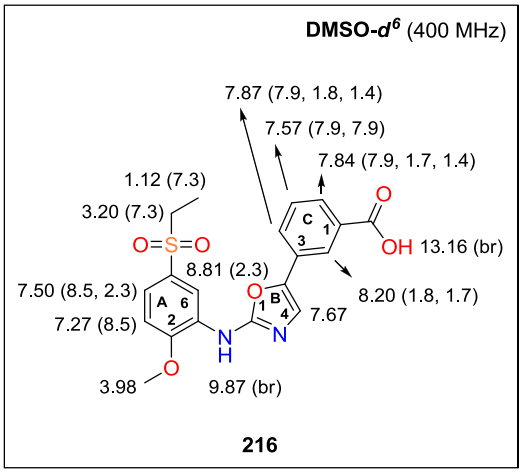

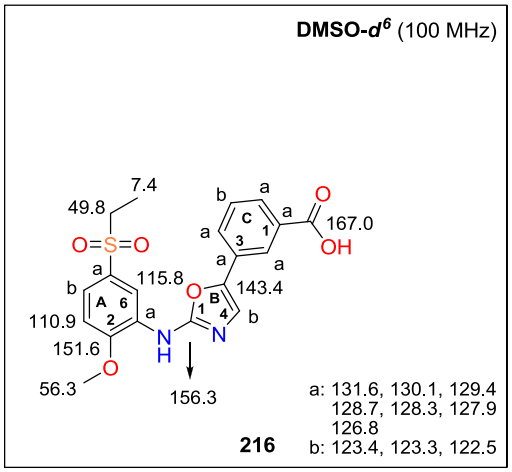

^{1}H-NMR (400 MHz, DMSO-d^6): δ 13.16 (br s, 1H, -COOH), 9.87 (br s, 1H, -NH-), 8.81 (d, 1H, $J(A_4,A_6)$ = 2.3 Hz, H-C_A(6)), 8.20 (dd, 1H, $J(C_2,C_4)$ = 1.8 Hz, $J(C_2,C_6)$ = 1.7 Hz, C_C(2)), 7.87 (ddd, 1H, $J(C_4,C_5)$ = 7.9 Hz, $J(C_2,C_4)$ = 1.8 Hz, $J(C_4,C_6)$ = 1.4 Hz, H-C_C(4)), 7.84 (ddd, 1H, $J(C_5,C_6)$ = 7.9 Hz, $J(C_2,C_6)$ = 1.7 Hz, $J(C_4,C_6)$ = 1.4 Hz, H-C_C(6)), 7.67 (s, 1H, C_B(4)), 7.57 (dd, 1H, $J(C_4,C_5)$ = $J(C_5,C_6)$ = 7.9 Hz, H-C_C(5)), 7.50 (dd, 1H, $J(A_3,A_4)$ = 8.5 Hz, $J(A_4,A_6)$ = 2.3 Hz, H-C_A(4)), 7.27 (d, 1H, $J(A_3,A_4)$ = 8.5 Hz, H-C_A(3)), 3.98 (s, 3H, -OCH_3), 3.20 (q, 2H, $J(CH_2,CH_3)$ = 7.3 Hz, -$SO_2C\underline{H}_2CH_3$), 1.12 (t, 3H, $J(CH_2,CH_3)$ = 7.3 Hz, -$SO_2CH_2C\underline{H}_3$).

^{13}C-NMR (100 MHz, DMSO-d^6): δ 167.0 (-COOH), 156.3 (C_B(2)), 151.6 (C_A(2)), 143.4 (C_B(5)), 131.6, 130.1, 129.4, 128.7, 128.3, 127.9, 126.8, 123.4, 123.3, 122.5, 115.8 (C_A(6)), 110.9 (C_A(3)), 56.3 (-OCH_3), 49.8 (-$SO_2\underline{C}H_2CH_3$), 7.4 (-$SO_2CH_2\underline{C}H_3$).

FT IR (solid, cm^{-1}): 3161 (w), 2986 (w), 2936 (w), 2843 (w), 2604 (w), 2488 (w), 2115 (w), 1882 (w), 1691 (m), 1625 (m), 1579 (m), 1506 (m), 1455 (w), 1381 (w), 1333 (w), 1305 (s), 1268 (s), 1233 (m), 1207 (w), 1141 (s), 1122 (s), 1088 (m), 1019 (m), 960 (w), 926 (w), 844 (w), 809 (m), 755 (m), 718 (s), 699 (m), 678 (m), 622 (w), 596 (w), 574 (w), 522 (m), 493 (s), 457 (w).

MS (ESI m/z): not detectable in positive mode; in negative mode: 401.0 $[M - H]^-$.

Anal. calcd for $C_{19}H_{18}N_2O_6S$ (402.42): C, 56.71; H, 4.51; N, 6.96; found: C, 57.11; H, 4.60; N, 6.75.

Synthesis of *N*-(benzyloxy)-3-(2-(5-(ethylsulfonyl)-2-methoxyphenyl amino)oxazol-5-yl)benzamide (239)

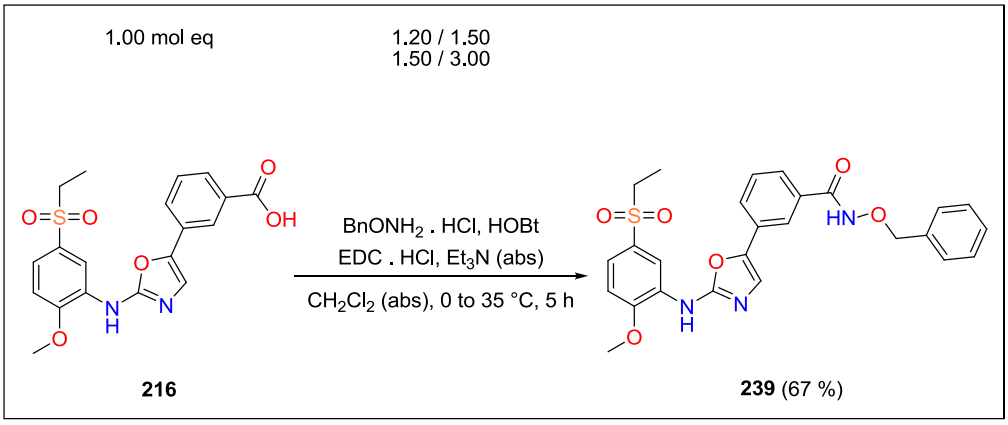

To a suspension of 230 mg (0.57 mmol, 1.00 mol eq) carboxylic acid **216** in 15 ml of CH_2Cl_2 (abs) at 0 °C, 116 mg (0.86 mmol, 1.50 mol eq) of HOBt, 192 mg (0.86 mmol, 1.50 mol eq) of EDC.HCl, 0.2 ml (174 mg, 1.71 mmol, 3.00 mol eq) of Et_3N (abs) and 109 mg (0.69 mmol, 1.20 mol eq) of $BnONH_2$.HCl were added gradually. Afterwards the reaction mixture was stirred under Ar for 10 min at RT and 5 h at 35 °C. After complete consumption of the starting material **216** (TLC analysis), the mixture was concentrated. An obtained solid residue was dissolved in 40 ml of CH_2Cl_2 and extracted with 2 x 10 ml of citric acid (10 % aq solution) and 2 x 10 ml of $NaHCO_3$ (saturated aq solution). The organic layer was dried over Na_2SO_4, filtered and concentrated under reduced pressure. The crude product was purified by FLC (EA) yielding 194 mg (0.38 mmol, 67 %) of *N*-(benzyloxy)-3-(2-(5-(ethylsulfonyl)-2-methoxyphenylamino)oxazol-5-yl)benzamide (**239**).

Novelty: Preparation or characterization of **239** has not been described in the literature.

M. p.: 130 – 133 °C [EA]. Pale grey solid material.

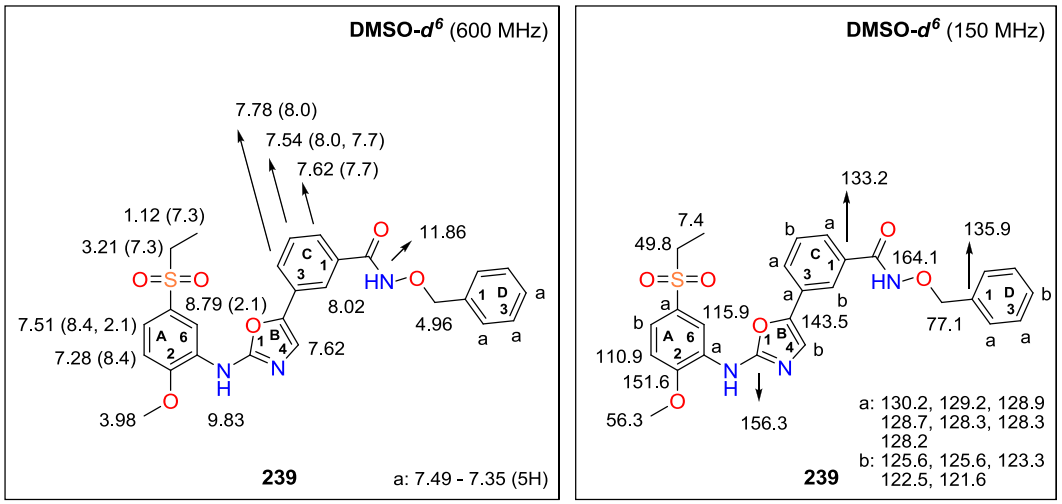

^{1}H-NMR (600 MHz, DMSO-d^6): δ 11.86 (s, 1H, -CONH-), 9.83 (s, 1H, -NH-), 8.79 (d, 1H, $J(A_4,A_6)$ = 2.1 Hz, H-C_A(6)), 8.02 (s, 1H, C_C(2)), 7.78 (d, 1H, $J(C_4,C_5)$ = 8.0 Hz, H-C_C(4)), 7.62 (d, 1H, $J(C_5,C_6)$ = 7.7 Hz, H-C_C(6)), 7.62 (s, 1H, C_B(4)), 7.54 (dd, 1H, $J(C_4,C_5)$ = 8.0 Hz, $J(C_5,C_6)$ = 7.7 Hz, H-C_C(5)), 7.51 (dd, 1H, $J(A_3,A_4)$ = 8.4 Hz, $J(A_4,A_6)$ = 2.1 Hz, H-C_A(4)), 7.49 – 7.35 (m, 5H, -$CH_2C_6\underline{H}_5$), 7.28 (d, 1H, $J(A_3,A_4)$ = 8.4 Hz, H-C_A(3)), 4.96 (s, 1H, -$C\underline{H}_2C_6H_5$), 3.98 (s, 3H, -OCH_3), 3.21 (q, 2H, $J(CH_2,CH_3)$ = 7.3 Hz, -$SO_2C\underline{H}_2CH_3$), 1.12 (t, 3H, $J(CH_2,CH_3)$ = 7.3 Hz, -$SO_2CH_2C\underline{H}_3$).

^{13}C-NMR (150 MHz, DMSO-d^6): δ 164.1 (-CONH-), 156.3 (C_B(2)), 151.6 (C_A(2)), 143.5 (C_B(5)), 135.9 (C_D(1)), 133.2 (C_C(1)), 130.2, 129.2, 128.9, 128.7, 2 x 128.3, 128.2, 2 x 125.6, 123.3, 122.5, 121.6, 115.9 (C_A(6)), 110.9 (C_A(3)), 77.1 (-$\underline{C}H_2C_6H_5$), 56.3 (-OCH_3), 49.8 (-$SO_2\underline{C}H_2CH_3$), 7.4 (-$SO_2CH_2\underline{C}H_3$).

FT IR (solid, cm^{-1}): 3417 (w), 3256 (w), 3079 (w), 2981 (w), 2936 (w), 2282 (w), 2205 (w), 2118 (w), 2086 (w), 1987 (w), 1736 (w), 1642 (m), 1616 (s), 1577 (s), 1526 (m), 1480 (m), 1458 (w), 1430 (m), 1371 (w), 1347 (m), 1301 (s), 1264 (s), 1144 (s), 1123 (s), 1082 (m), 1038 (m), 1017 (s), 919 (w), 900 (w), 808 (m), 754 (s), 734 (s), 716 (s), 701 (s), 660 (w), 623 (w), 596 (m), 576 (s), 536 (m), 495 (s), 452 (m).

MS (ESI m/z): 530.0 $[M + Na]^+$; in negative mode: 506.0 $[M - H]^-$.

Anal. calcd for $C_{26}H_{25}N_3O_6S$ (507.56): C, 61.53; H, 4.96; N, 8.28; found: C, 62.01; H, 4.72; N, 7.92.

Synthesis of 3-(2-(5-(ethylsulfonyl)-2-methoxyphenylamino)oxazol-5-yl)-*N*-hydroxybenzamide (217)

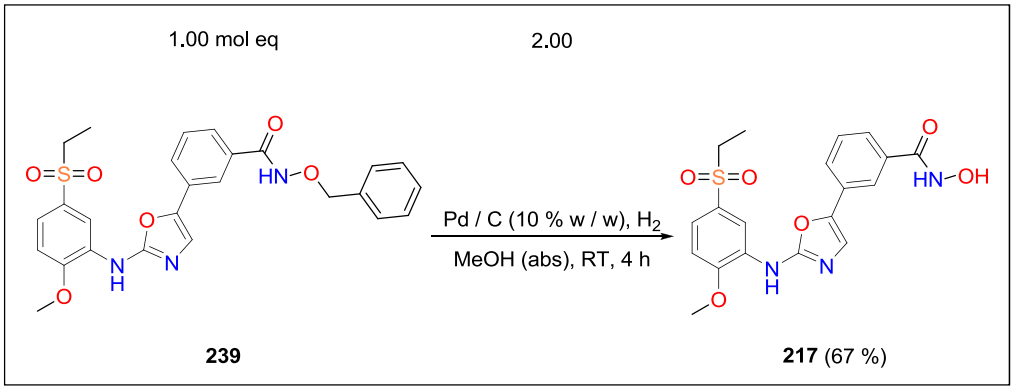

A suspension of 90.0 mg (0.18 mmol. 1.00 mol eq) hydroxamic ester **239**, 18.9 mg (0.18 mmol, 1.00 mol eq) of Pd / C (10 % w / w) in 10 ml of MeOH (abs) was stirred under H_2 atmosphere at RT for 2 h. Afterwards 18.9 mg (0.18 mmol, 1.00 mol eq) of Pd / C (10 % w / w) was added and the reaction mixture was stirred for another 2 h. After consumption of the starting material **239** (TLC analysis), the mixture was filtered, a filtrate was put aside and a solid residue was washed with 2 x 10 ml of 50 °C THF (abs). The filtrates were combined and evaporated under reduced pressure. The crude product was purified by crystallization from cyclohexane / THF yielding 50.0 mg (0.12 mmol, 67 %) of 3-(2-(5-(ethylsulfonyl)-2-methoxy phenylamino)oxazol-5-yl)-*N*-hydroxybenzamide (**217**).

Novelty: Preparation or characterization of **217** has not been described in the literature.

M. p.: 90 – 110 °C (dec) [cyclohexane / THF]. White solid material.

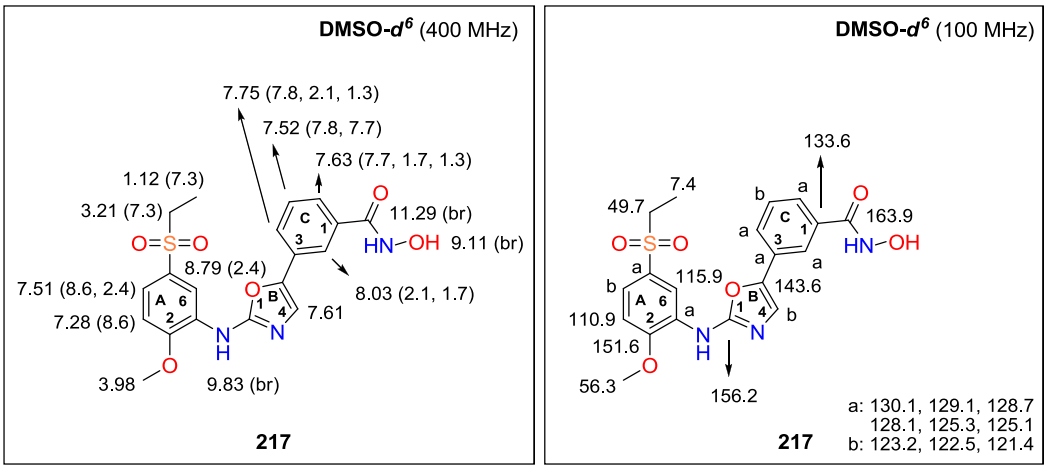

^{1}H-NMR (400 MHz, DMSO-d^6): δ 11.29 (br s, 1H, -CONHOH), 9.83 (br s, 1H, -NH-), 9.11 (br s, 1H, -CONHOH), 8.79 (d, 1H, $J(A_4,A_6)$ = 2.4 Hz, H-C_A(6)), 8.03 (dd, 1H, $J(C_2,C_4)$ = 2.1 Hz, $J(C_2,C_6)$ = 1.7 Hz, C_C(2)), 7.75 (ddd, 1H, $J(C_4,C_5)$ = 7.8 Hz, $J(C_2,C_4)$ = 2.1 Hz, $J(C_4,C_6)$ = 1.3 Hz, H-C_C(4)), 7.63 (ddd, 1H, $J(C_5,C_6)$ = 7.7 Hz, $J(C_2,C_6)$ = 1.7 Hz, $J(C_4,C_6)$ = 1.3 Hz, H-C_C(6)), 7.61 (s, 1H, C_B(4)), 7.52 (dd, 1H, $J(C_4,C_5)$ = 7.8 Hz, $J(C_5,C_6)$ = 7.7 Hz, H-C_C(5)), 7.51 (dd, 1H, $J(A_3,A_4)$ = 8.6 Hz, $J(A_4,A_6)$ = 2.4 Hz, H-C_A(4)), 7.28 (d, 1H, $J(A_3,A_4)$ = 8.6 Hz, H-C_A(3)), 3.98 (s, 3H, -OCH_3), 3.21 (q, 2H, $J(CH_2,CH_3)$ = 7.3 Hz, -$SO_2CH_2CH_3$), 1.12 (t, 3H, $J(CH_2,CH_3)$ = 7.3 Hz, -$SO_2CH_2CH_3$).

^{13}C-NMR (100 MHz, DMSO-d^6): δ 163.9 (-CONHOH), 156.2 (C_B(2)), 151.6 (C_A(2)), 143.6 (C_B(5)), 133.6 (C_C(1)), 130.1, 129.1, 128.7, 128.1, 125.3, 125.1, 123.2, 122.5, 121.4, 115.9 (C_A(6)), 110.9 (C_A(3)), 56.3 (-OCH_3), 49.7 (-$SO_2CH_2CH_3$), 7.4 (-$SO_2CH_2CH_3$).

FT IR (solid, cm^{-1}): 3240 (w), 3089 (w), 2979 (w), 2941 (w), 2115, 2088 (w), 1613 (s), 1573 (s), 1527 (m), 1483 (m), 1458 (w), 1426 (m), 1346 (w), 1301 (m), 1264 (s), 1228 (w), 1141 (s), 1121 (s), 1084 (m), 1018 (m), 969 (w), 901 (m), 807 (m), 718 (s), 687 (m), 658 (m), 596 (m), 576 (m), 519 (m), 492 (m).

MS (ESI m/z): 440.0 $[M + Na]^+$; in negative mode: 415.9 $[M - H]^-$.

Anal. calcd for $C_{19}H_{19}N_3O_6S$ (417.44): C, 54.67; H, 4.59; N, 10.07; found: C, 54.75; H, 4.66; N, 9.98.

13.3.5. Synthesis of *m*-substituted *N*,5-diaryloxazol-2-amines 218, 219, 220, 221

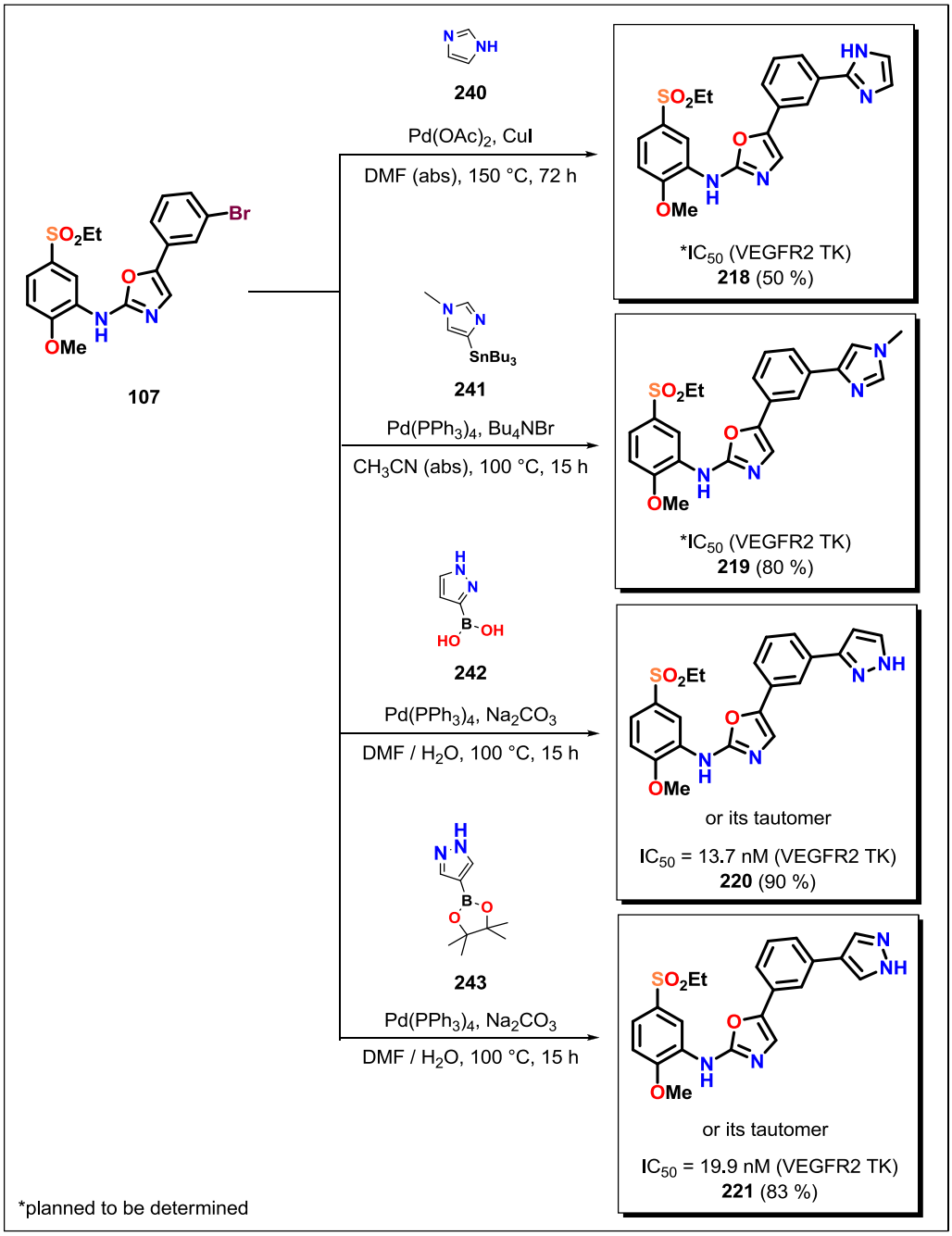

Scheme 34. Synthesis of *m*-substituted *N*,5-diaryloxazol-2-amines **218**, **219**, **220** and **221**.

Synthesis of 5-(3-(1*H*-imidazol-2-yl)phenyl)-*N*-(5-(ethylsulfonyl)-2-methoxyphenyl)oxazol-2-amine (218)

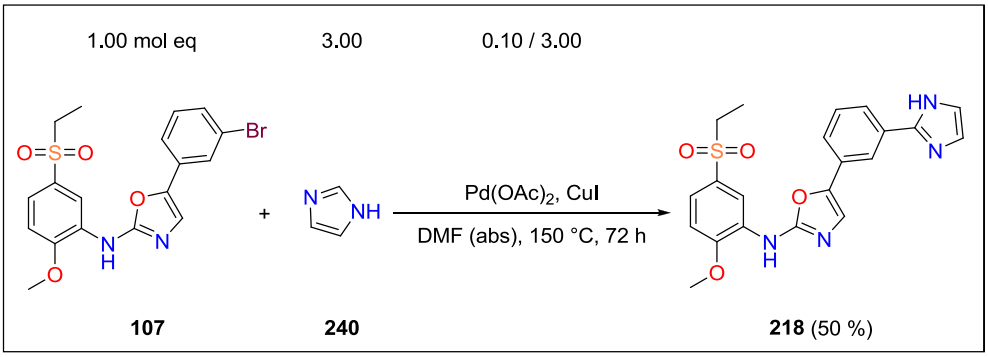

A suspension of 175 mg (0.40 mmol, 1.00 mol eq) oxazole **107**, 54.5 mg (0.80 mmol, 2.00 mol eq) of imidazole (**240**), 4.49 mg (0.02 mmol, 0.05 mol eq) of $Pd(OAc)_2$ and 152 mg (0.80 mmol, 2.00 mol eq) of CuI in 8 ml of DMF (abs) was bubbled with Ar for 10 min. The reaction mixture was stirred under Ar at 150 °C for 48 h. Afterwards 27.2 mg (0.40 mmol, 1.00 mol eq) of imidazole (**240**), 4.49 mg (0.02 mmol, 0.05 mol eq) of $Pd(OAc)_2$ and 76.2 mg (0.40 mmol, 1.00 mol eq) of CuI was added and the mixture was stirred under Ar at 150 °C for another 24 h. After consumption of the starting material **107** (TLC analysis), the reaction was diluted with 15 ml of EA, 15 ml of NH_4Cl (saturated aq solution) adjusted to pH = 8 with NH_4OH (aq) was added and the mixture was stirred for 45 min. Then the layers were separated and the aqueous phase was extracted with 3 x 5 ml of EA. The combined organic layer was washed with 3 x 10 ml of brine, dried over Na_2SO_4, filtered and evaporated under reduced pressure. The crude product was purified by trituration with Hex / EA yielding 85.0 mg (0.20 mmol, 50 %) of 5-(3-(1*H*-imidazol-2-yl)phenyl)-N-(5-(ethylsulfonyl)-2-methoxyphenyl)oxazol-2-amine (**218**).

Novelty: Preparation or characterization of **218** has not been described in the literature.

M. p.: 136 – 143 °C (dec) [Hex / EA]. Light brown solid material.

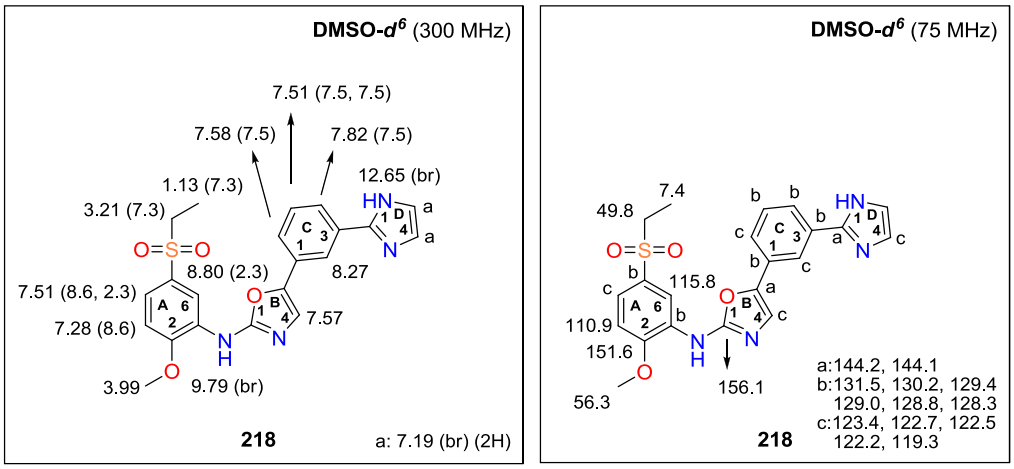

^{1}H-NMR (300 MHz, DMSO-d^6): δ 12.65 (br s, 1H, -NH- imidazole), 9.79 (br s, 1H, -NH-), 8.80 (d, 1H, $J(A_4,A_6)$ = 2.3 Hz, H-C_A(6)), 8.27 (s, 1H, H-C_C(2)), 7.82 (d, 1H, $J(C_4,C_5)$ = 7.5 Hz, H-C_C(4)), 7.58 (d, 1H, $J(C_5,C_6)$ = 7.5 Hz, H-C_C(6)), 7.57 (s, 1H, H-C_B(4)), 7.51 (dd, 1H, $J(C_4,C_5)$ = $J(C_5,C_6)$ = 7.5 Hz, H-C_C(5)), 7.51 (dd, 1H, $J(A_3,A_4)$ = 8.6 Hz, $J(A_4,A_6)$ = 2.3 Hz, H-C_A(4)), 7.28 (d, 1H, $J(A_3,A_4)$ = 8.6 Hz, H-C_A(3)), 7.19 (br s, 2H, H-C_D(4) and H-C_D(5)), 3.99 (s, 3H, -OCH_3), 3.21 (q, 2H, $J(CH_2,CH_3)$ = 7.3 Hz, -$SO_2C\underline{H}_2CH_3$), 1.13 (t, 3H, $J(CH_2,CH_3)$ = 7.3 Hz, -$SO_2CH_2C\underline{H}_3$).

^{13}C-NMR (75 MHz, DMSO-d^6): δ 156.1 (C_B(2)), 151.6 (C_A(2)), 144.2, 144.1, 131.5 130.2, 129.4, 129.0, 128.8, 128.3, 123.4, 122.7, 122.5, 122.2, 119.3, 115.8 (C_A(6)), 110.9 (C_A(3)), 56.3 (-OCH_3), 49.8 (-$SO_2\underline{C}H_2CH_3$), 7.4 (-$SO_2CH_2\underline{C}H_3$).

FT IR (solid, cm^{-1}): 3423 (w), 3308 (w), 3070 (w), 2986 (w), 2926 (w), 2812 (w), 2325 (w), 2221 (w), 2114 (w), 2082 (w), 1920 (w), 1731 (w), 1677 (w), 1602 (s), 1572 (s), 1524 (m), 1490 (m), 1458 (m), 1426 (m), 1375 (w), 1348 (w), 1298 (s), 1265 (s), 1143 (s), 1123 (s), 1085 (m), 1045 (m), 1015 (m), 976 (w), 917 (w), 890 (w), 793 (m), 751 (m), 733 (s), 716 (s), 688 (m), 658 (m), 622 (w), 595 (m), 577 (m), 536 (m), 492 (s), 458 (m), 415 (w).

MS (ESI m/z): 425.1 $[M + H]^+$; in negative mode 423.0 $[M - H]^-$.

Anal. calcd for $C_{21}H_{20}N_4O_4S$ (424.47): C, 59.42; H, 4.75; N, 13.20; found: C, 59.68; H, 4.89; N, 12.99.

Synthesis of *N*-(5-(ethylsulfonyl)-2-methoxyphenyl)-5-(3-(1-methyl-1*H*-imidazol-4-yl)phenyl)oxazol-2-amine (219)

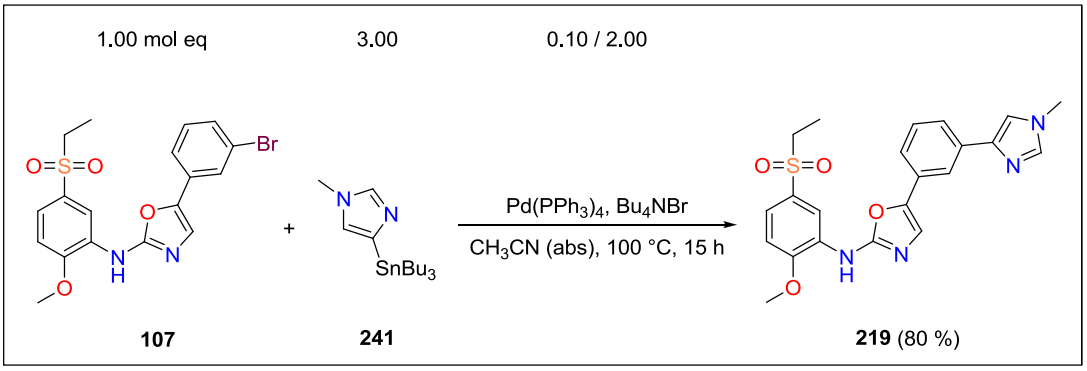

A suspension of 50.0 mg (0.11 mmol, 1.00 mol eq) oxazole **107**, 13.2 mg (0.01 mmol, 0.10 mol eq) of $Pd(PPh_3)_4$ and 73.7 mg (0.23 mmol, 2.00 mol eq) of Bu_4NBr in 5 ml of CH_3CN (abs) prepared in a sealed tube was bubbled by Ar for 10 min. Afterwards 127 mg (0.34, 3.00 mol eq) of tributylstannane **241** was added and the mixture was stirred at 100 °C for 15 h. After consumption of the starting material **107** (TLC analysis), the reaction was cooled down to RT and diluted with 10 ml of EA. Then 10 ml of KF (saturated aq solution) was added and the mixture was stirred for 3 h. The organic layer was separated, washed with 10 ml of H_2O, dried by Na_2SO_4, filtered and concentrated under reduced pressure. The crude product was purified by trituration with Hex / EA yielding 40.0 mg (0.09 mmol, 80 %) of *N*-(5-(ethylsulfonyl)-2-methoxyphenyl)-5-(3-(1-methyl-1*H*-imidazol-4-yl)phenyl) oxazol-2-amine (**219**).

Novelty: Preparation or characterization of **219** has not been described in the literature.

M. p.: 235 – 236 °C [Hex / EA]. Yellow solid material.

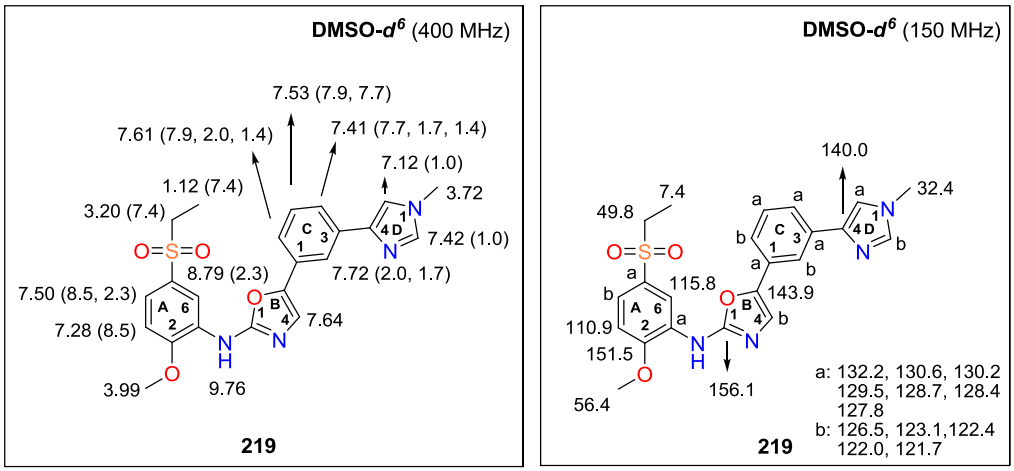

^{1}H-NMR (400 MHz, DMSO-d^6): δ 9.76 (s, 1H, -NH-), 8.79 (d, 1H, $J(A_4,A_6)$ = 2.3 Hz, H-C_A(6)), 7.72 (d, 1H, $J(C_2,C_6)$ = 2.0 Hz, $J(C_2,C_4)$ = 1.7 Hz, H-C_C(2)), 7.64 (s, 1H, H-C_B(4)), 7.61 (ddd, 1H, $J(C_5,C_6)$ = 7.9 Hz, $J(C_2,C_6)$ = 2.0 Hz, $J(C_4,C_6)$ = 1.4 Hz, H-C_C(6)), 7.53 (d, 1H, $J(C_5,C_6)$ = 7.9 Hz, $J(C_4,C_5)$ = 7.7 Hz, H-C_C(5)), 7.50 (dd, 1H, $J(A_3,A_4)$ = 8.5 Hz, $J(A_4,A_6)$ = 2.3 Hz, H-C_A(4)), 7.42 (d, 1H, $J(D_2,D_5)$ = 1.0 Hz, H-C_D(2)), 7.41 (ddd, 1H, $J(C_4,C_5)$ = 7.7 Hz, $J(C_2,C_4)$ = 1.7 Hz, $J(C_4,C_6)$ = 1.4 Hz, H-C_C(4)), 7.28 (d, 1H, $J(A_3,A_4)$ = 8.5 Hz, H-C_A(3)), 7.12 (d, 1H, $J(D_2,D_5)$ = 1.0 Hz, H-C_D(5)), 3.99 (s, 3H, -OCH_3), 3.72 (s, 3H, -CH_3 imidazole), 3.20 (q, 2H, $J(CH_2,CH_3)$ = 7.4 Hz, -$SO_2C\underline{H}_2CH_3$), 1.12 (t, 3H, $J(CH_2,CH_3)$ = 7.4 Hz, -$SO_2CH_2C\underline{H}_3$).

^{13}C-NMR (150 MHz, DMSO-d^6): δ 156.1 (C_B(2)), 151.5 (C_A(2)), 143.9 (C_B(5)), 140.0 (C_D(4)), 132.2, 130.6, 130.2, 129.5, 128.7, 128.4, 127.8, 126.5, 123.1, 122.4, 122.0, 121.7, 115.8 (C_A(6)), 110.9 (C_A(3)), 56.4 (-OCH_3), 49.8 (-$SO_2\underline{C}H_2CH_3$), 32.4 (-CH_3 imidazole), 7.4 (-$SO_2CH_2\underline{C}H_3$).

FT IR (solid, cm^{-1}): 2945 (w), 2114 (w), 1734 (w), 1611 (m), 1567 (s), 1500 (m), 1458 (w), 1418 (m), 1376 (w), 1346 (w), 1305 (m), 1267 (m), 1228 (w), 1139 (s), 1123 (s), 1089 (m), 1046 (m), 1027 (m), 979 (w), 920 (w), 834 (w), 797 (s), 759 (m), 735 (s), 716 (s), 655 (m), 618 (w), 595 (m), 575 (s), 535 (m), 494 (s), 468 (w), 425 (w).

MS (ESI m/z): not detectable in positive mode; in negative mode 437.0 $[M - H]^-$.

Anal. calcd for $C_{22}H_{22}N_4O_4S$ (438.50): C, 60.26; H, 5.06; N, 12.78; found: C, 60.65; H, 5.21; N, 12.39.

Synthesis of 5-(3-(1*H*-pyrazol-3-yl)phenyl)-*N*-(5-(ethylsulfonyl)-2-methoxyphenyl)oxazol-2-amine (220)

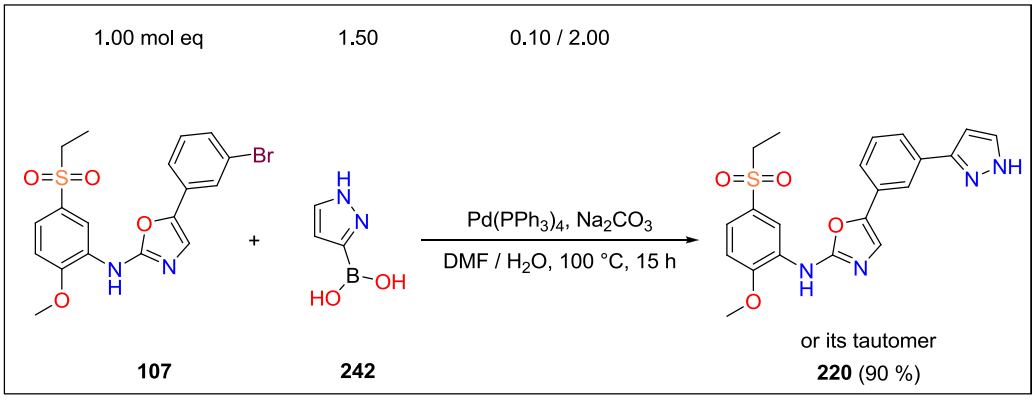

A suspension of 60.0 mg (0.14 mmol, 1.00 mol eq) oxazole **107**, 23.0 mg (0.21, 1.50 mol eq) of boronic acid **242** and 15.8 mg (0.01 mmol, 0.10 mol eq) of $Pd(PPh_3)_4$ in 5 ml of DMF placed in a sealed tube was bubbled by Ar for 10 min. Afterwards a solution of 29.0 mg (0.27 mmol, 2.00 mol eq) Na_2CO_3 in 2 ml of H_2O was added and the reaction mixture was stirred at 100 °C for 15 h. Then the reaction was cooled down to RT, diluted with 10 ml of EA and extracted with 3 x 5 ml of brine. The organic layer was separated, dried by Na_2SO_4, filtered and concentrated under reduced pressure. The crude product was purified by trituration with Hex / EA yielding 52.0 mg (0.12 mmol, 90 %) of 5-(3-(1*H*-pyrazol-3-yl)phenyl)-*N*-(5-(ethylsulfonyl)-2-methoxyphenyl)oxazol-2-amine (**220**).

Novelty: Preparation or characterization of **220** has not been described in the literature.

M. p.: 220 – 223 °C [Hex / EA]. Off-white solid material.

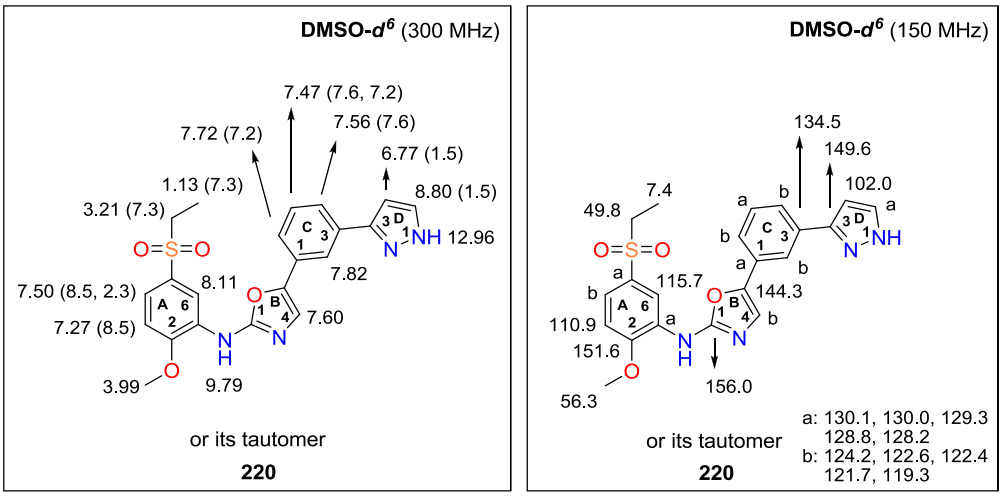

^{1}H-NMR (300 MHz, DMSO-d^6): δ 12.96 (s, 1H, -NH- pyrazole), 9.79 (s, 1H, -NH-), 8.80 (d, 1H, $J(D_4,D_5)$ = 1.5 Hz, H-C_D(5)), 8.11 (s, 1H, H-C_A(6)), 7.82 (s, 1H, H-C_C(2)), 7.72 (d, 1H, $J(C_5,C_6)$ = 7.2 Hz, H-C_C(6)), 7.60 (s, 1H, H-C_B(4)), 7.56 (d, 1H, $J(C_4,C_5)$ = 7.6 Hz, H-C_C(4)), 7.50 (dd, 1H, $J(A_3,A_4)$ = 8.5 Hz, $J(A_4,A_6)$ = 2.3 Hz, H-C_A(4)), 7.47 (dd, 1H, $J(C_4,C_5)$ = 7.6 Hz, $J(C_5,C_6)$ = 7.2 Hz, H-C_C(5)), 7.27 (d, 1H, $J(A_3,A_4)$ = 8.5 Hz, H-C_A(3)), 6.77 (d, 1H, $J(D_4,D_5)$ = 1.5 Hz, H-C_D(4)), 3.99 (s, 3H, -OCH_3), 3.21 (q, 2H, $J(CH_2,CH_3)$ = 7.3 Hz, -$SO_2C\underline{H}_2CH_3$), 1.13 (t, 3H, $J(CH_2,CH_3)$ = 7.3 Hz, -$SO_2CH_2C\underline{H}_3$).

^{13}C-NMR (150 MHz, DMSO-d^6): δ 156.0 (C_B(2)), 151.6 (C_A(2)), 149.6 (C_D(3)), 144.3 (C_B(5)), 134.5 (C_C(3)), 130.1, 130.0, 129.3, 128.8, 128.2, 124.2, 122.6, 122.4, 121.7, 119.3, 115.7 (C_A(6)), 110.9 (C_A(3)), 102.0 (C_D(4)), 56.3 (-OCH_3), 49.8 (-$SO_2\underline{C}H_2CH_3$), 7.4 (-$SO_2CH_2\underline{C}H_3$).

FT IR (solid, cm^{-1}): 3414 (w), 3241 (w), 2976 (w), 2936 (w), 2617 (w), 2215 (w), 2116 (w), 1921 (w), 1734 (w), 1618 (s), 1578 (s), 1526 (m), 1486 (m), 1434 (m), 1346 (w), 1301 (s), 1265 (s), 1225 (w), 1186 (w), 1142 (s), 1122 (s), 1079 (m), 1044 (m), 1019 (m), 978 (w), 931 (w), 884 (w), 801 (m), 765 (m), 735 (s), 717 (s), 687 (m), 658 (w), 626 (w), 596 (w), 576 (m), 533 (m), 492 (s), 454 (m).

MS (ESI m/z): 447.0 $[M + Na]^+$; in negative mode 423.0 $[M - H]^-$.

Anal. calcd for $C_{21}H_{20}N_4O_4S$ (424.47): C, 59.42; H, 4.75; N, 13.20; found: C, 60.13; H, 4.86; N, 13.23.

Synthesis of 5-(3-(1*H*-pyrazol-4-yl)phenyl)-*N*-(5-(ethylsulfonyl)-2-methoxyphenyl)oxazol-2-amine (221)

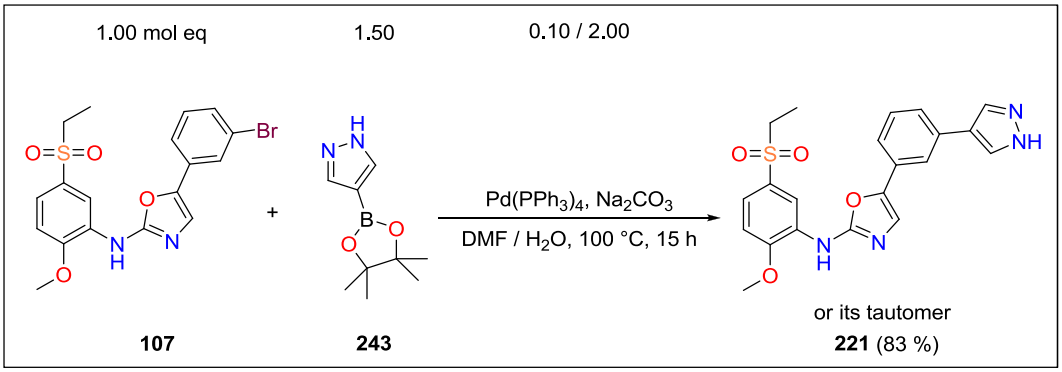

A suspension of 60.0 mg (0.14 mmol, 1.00 mol eq) oxazole **107**, 40.0 mg (0.21, 1.50 mol eq) of pinacolboronate **243** and 15.8 mg (0.01 mmol, 0.10 mol eq) of $Pd(PPh_3)_4$ in 5 ml of DMF placed in a sealed tube was bubbled by Ar for 10 min. Afterwards a solution of 29.0 mg (0.27 mmol, 2.00 mol eq) Na_2CO_3 in 2 ml of H_2O was added and the reaction mixture was stirred at 100 °C for 15 h. Then the reaction was cooled to RT, diluted with 10 ml of EA and extracted with 3 x 5 ml of brine. The organic layer was separated, dried by Na_2SO_4, filtered and concentrated under reduced pressure. The crude product was purified by trituration with EA yielding 48.0 mg (0.11 mmol, 83 %) of 5-(3-(1*H*-pyrazol-4-yl)phenyl)-*N*-(5-(ethylsulfonyl)-2-methoxy phenyl)oxazol-2-amine (**221**).

Novelty: Preparation or characterization of **221** has not been described in the literature.

M. p.: 264 – 267 °C [EA]. Pale yellow solid material.

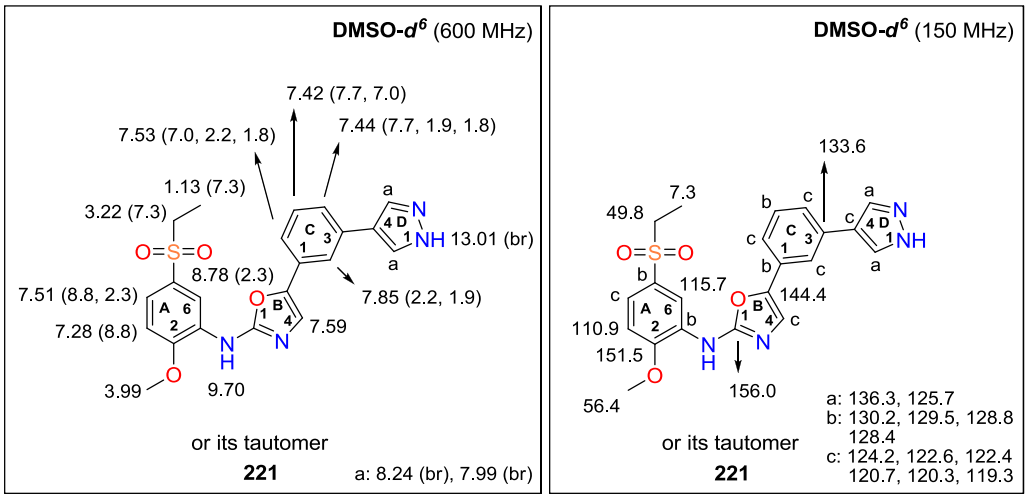

^{1}H-NMR (600 MHz, DMSO-d^6): δ 13.01 (br s, 1H, -NH- pyrazole), 9.70 (s, 1H, -NH-), 8.78 (d, 1H, $J(A_4,A_6)$ = 2.3 Hz, H-C_A(6)), 8.24 (br s, 1H, H-C_D(3) or H-C_D(5)), 7.99 (br s, 1H, H-C_D(3) or H-C_D(5)), 7.85 (dd, 1H, $J(C_2,C_6)$ = 2.0 Hz, $J(C_2,C_4)$ = 1.9 Hz, H-C_C(2)), 7.59 (s, 1H, H-C_B(4)), 7.53 (ddd, 1H, $J(C_5,C_6)$ = 7.0 Hz, $J(C_2,C_6)$ = 2.2 Hz, $J(C_4,C_6)$ = 1.8 Hz, H-C_C(6)), 7.51 (dd, 1H, $J(A_3,A_4)$ = 8.8 Hz, $J(A_4,A_6)$ = 2.3 Hz, H-C_A(4)), 7.44 (ddd, 1H, $J(C_4,C_5)$ = 7.7 Hz, $J(C_2,C_4)$ = 1.9 Hz, $J(C_4,C_6)$ = 1.8 Hz, H-C_C(4)), 7.42 (dd, 1H, $J(C_4,C_5)$ = 7.7 Hz, $J(C_5,C_6)$ = 7.0 Hz, H-C_C(5)), 7.28 (d, 1H, $J(A_3,A_4)$ = 8.8 Hz, H-C_A(3)), 3.99 (s, 1H, -OCH_3), 3.22 (q, 2H, $J(CH_2,CH_3)$ = 7.3 Hz, -$SO_2C\underline{H}_2CH_3$), 1.13 (t, 3H, $J(CH_2,CH_3)$ = 7.3 Hz, -$SO_2CH_2C\underline{H}_3$).

^{13}C-NMR (150 MHz, DMSO-d^6): δ 156.0 (C_B(2)), 151.5 (C_A(2)), 144.4 (C_B(5)), 136.3 (C_D(3) or C_D(5)), 133.6 (C_C(3)), 130.2, 129.5, 128.8, 128.4, 125.7 (C_D(3) or C_D(5)), 124.2, 122.6, 122.4, 120.7, 120.3, 119.3, 115.7 (C_A(6)), 110.9 (C_A(3)), 56.4 (-OCH_3), 49.8 (-$SO_2\underline{C}H_2CH_3$), 7.3 (-$SO_2CH_2\underline{C}H_3$).

FT IR (solid, cm^{-1}): 3413 (w), 3102 (w), 3055 (w), 2964 (w), 2323 (w), 2111 (w), 1919 (w), 1719 (w), 1617 (m), 1576 (s), 1527 (m), 1484 (w), 1430 (m), 1349 (w), 1301 (s), 1262 (s), 1227 (w), 1141 (s), 1120 (s), 1080 (m), 1047 (m), 1012 (m), 979 (w), 933 (w), 862 (w), 786 (s), 737 (s), 716 (s), 685 (m), 658 (w), 622 (w), 597 (m), 572 (s), 535 (m), 492 (s), 452 (m).

MS (ESI m/z): 447.0 $[M + Na]^+$; in negative mode 423.0 $[M - H]^-$.

Anal. calcd for $C_{21}H_{20}N_4O_4S$ (424.47): C, 59.42; H, 4.75; N, 13.20; found: C, 59.48; H, 4.87; N, 13.11.

13.3.6. Synthesis of *m*-substituted *N*,5-diaryloxazol-2-amine coupling precursor 245

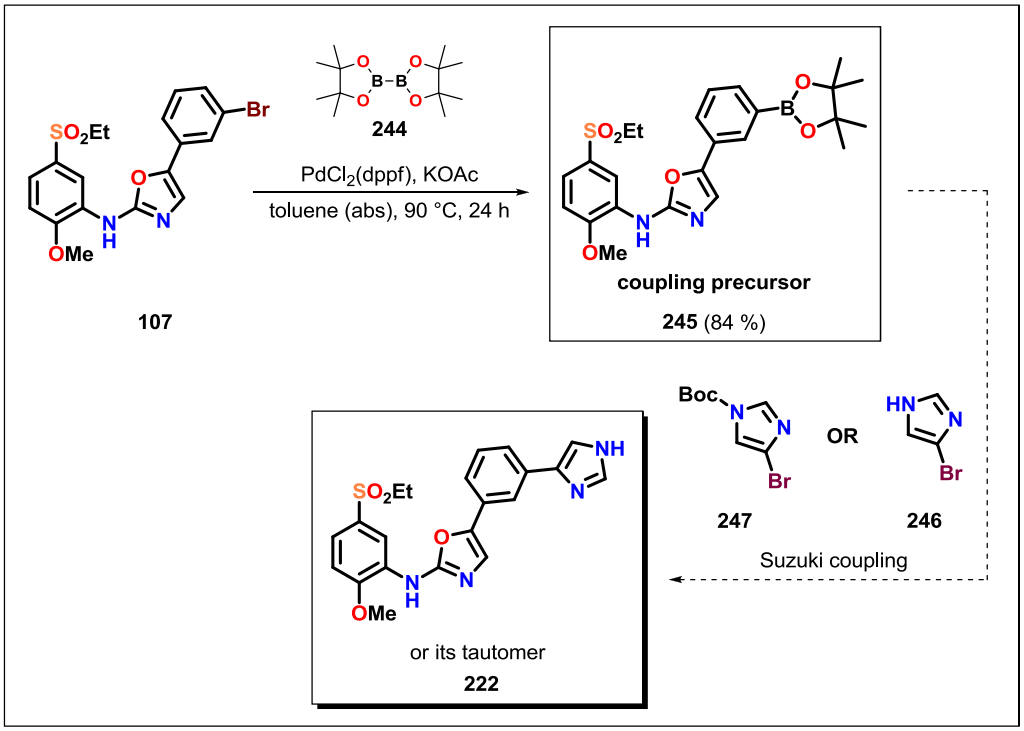

Scheme 35. Synthesis of *m*-substituted *N*,5-diaryloxazol-2-amine coupling precursor **245**.

Synthesis of *N*-(5-(ethylsulfonyl)-2-methoxyphenyl)-5-(3-(4,4,5,5-tetra methyl-1,3,2-dioxaborolan-2-yl)phenyl)oxazol-2-amine (245)

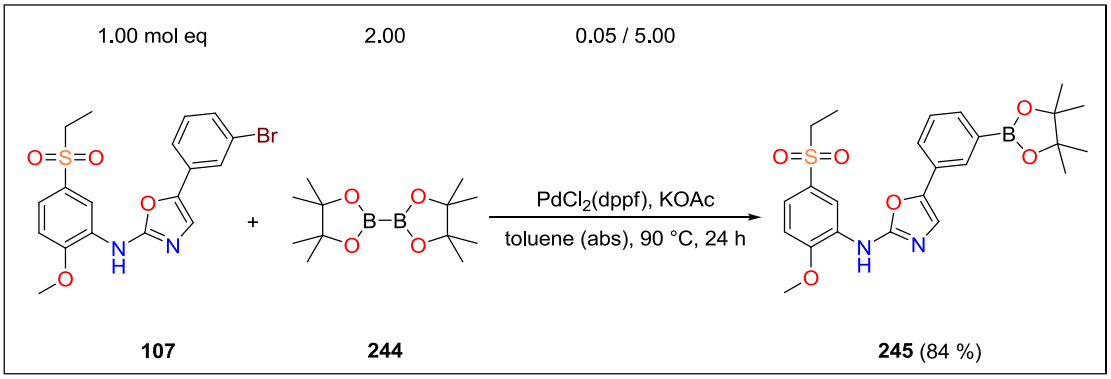

A suspension of 50.0 mg (0.11 mmol, 1.00 mol eq) starting material **107**, 58.0 mg (0.23, 2.00 mol eq) of bis(pinacolato)diboron (**244**) and 56.1 mg (0.57 mmol, 5.00 mol eq) of KOAc in 5 ml of toluene (abs) placed in a sealed tube was bubbled by Ar for 10 min. Afterwards 4.18 mg (5.72 μmol, 0.05 mol eq) of $PdCl_2$(dppf) was added and the reaction mixture was stirred at 90 °C for 24 h. After complete consumption of **107** (TLC analysis), the reaction was cooled to RT and evaporated under reduced pressure. A residual solid material was purified using FLC (cyclohexane / EA = 2 / 1) yielding 46.0 mg (0.09 mmol, 84 %) of pinacolboronate **245**.

Note: Because of possible sensitivity of **245** it is recommended to place it on a chromatographic column dissolved in suitable solvent, not immobilized on SiO_2.
For the removal of traces of the starting material **244** in FLC purified product **245**, it is recommended to dissolve it in $CHCl_3$ and extract with larger amount of water.

Novelty: Preparation or characterization of **245** has not been described in the literature.

M. p.: 175 – 177 °C [$CHCl_3$]. Off white crystalline solid material.

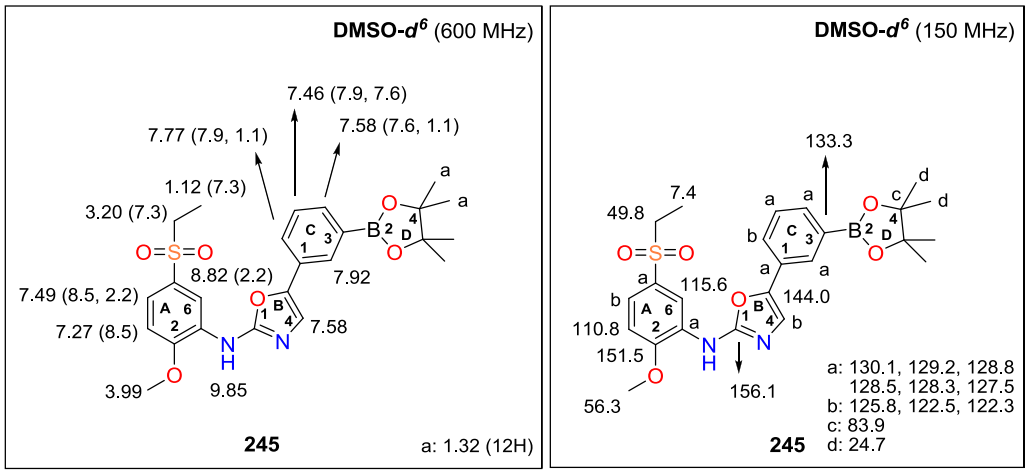

^{1}H-NMR (600 MHz, DMSO-d^6): δ 9.85 (s, 1H, -NH-), 8.82 (d, 1H, $J(A_4,A_6)$ = 2.2 Hz, H-C_A(6)), 7.92 (s, 1H, H-C_C(2)), 7.77 (dd, 1H, $J(C_5,C_6)$ = 7.9 Hz, $J(C_4,C_6)$ = 1.1 Hz, H-C_C(6)), 7.58 (dd, 1H, $J(C_4,C_5)$ = 7.6 Hz, $J(C_4,C_6)$ = 1.1 Hz, H-C_C(4)), 7.58 (s, 1H, H-C_B(4)), 7.49 (dd, 1H, $J(A_3,A_4)$ = 8.5 Hz, $J(A_4,A_6)$ = 2.2 Hz, H-C_A(4)), 7.46 (dd, 1H, $J(C_5,C_6)$ = 7.9 Hz, $J(C_4,C_5)$ = 7.6 Hz, H-C_C(5)), 7.27 (d, 1H, $J(A_3,A_4)$ = 8.5 Hz, H-C_A(3)), 3.99 (s, 3H, -OCH_3), 3.20 (q, 2H, -$SO_2C\underline{H}_2CH_3$), 1.32 (s, 12H, 4 x -CH_3 pinacol), 1.12 (t, 3H, -$SO_2CH_2C\underline{H}_3$).

^{13}C-NMR (150 MHz, DMSO-d^6): δ156.1 (C_B(2)), 151.5 (C_A(2)), 144.0 (C_B(5)), 133.3 (C_C(3)), 130.1, 129.2, 128.8, 128.5, 128.3, 127.5, 125.8, 122.5, 122.3, 115.6 (C_A(6)), 110.8 (C_A(3)), 83.9 (2 x C_D(4)), 56.3 (-OCH_3), 49.8 (-$SO_2\underline{C}H_2CH_3$), 24.7 (4 x –CH_3 pinacol), 7.4 (-$SO_2CH_2\underline{C}H_3$).

FT IR (solid, cm^{-1}): 3426 (m), 3115 (w), 2973 (m), 2938 (w), 2613 (w), 2376 (w), 2121 (w), 2088 (w), 1880 (w), 1614 (s), 1571 (s), 1523 (m), 1485 (w), 1466 (w), 1430 (m), 1409 (m), 1381 (w), 1358 (s), 1316 (m), 1296 (s), 1264 (s), 1211 (m), 1139 (s), 1119 (s), 1081 (m), 1047 (m), 1025 (m), 923 (w), 897 (w), 859 (m), 818 (m), 794 (m), 700 (s), 622 (w), 580 (m), 529 (m), 490 (m), 467 (m), 427 (s).

MS (ESI m/z): 507.1 $[M + Na]^+$; in negative mode 483.0 $[M - H]^-$.

Anal. calcd for $C_{24}H_{29}BN_2O_6S$ (484.37): C, 59.51; H, 6.03; N, 5.78; found: C, 59.60; H, 6.10; N, 5.80.

13.3.7. Synthesis of *m*-substituted *N*,5-diaryloxazol-2-amine 223

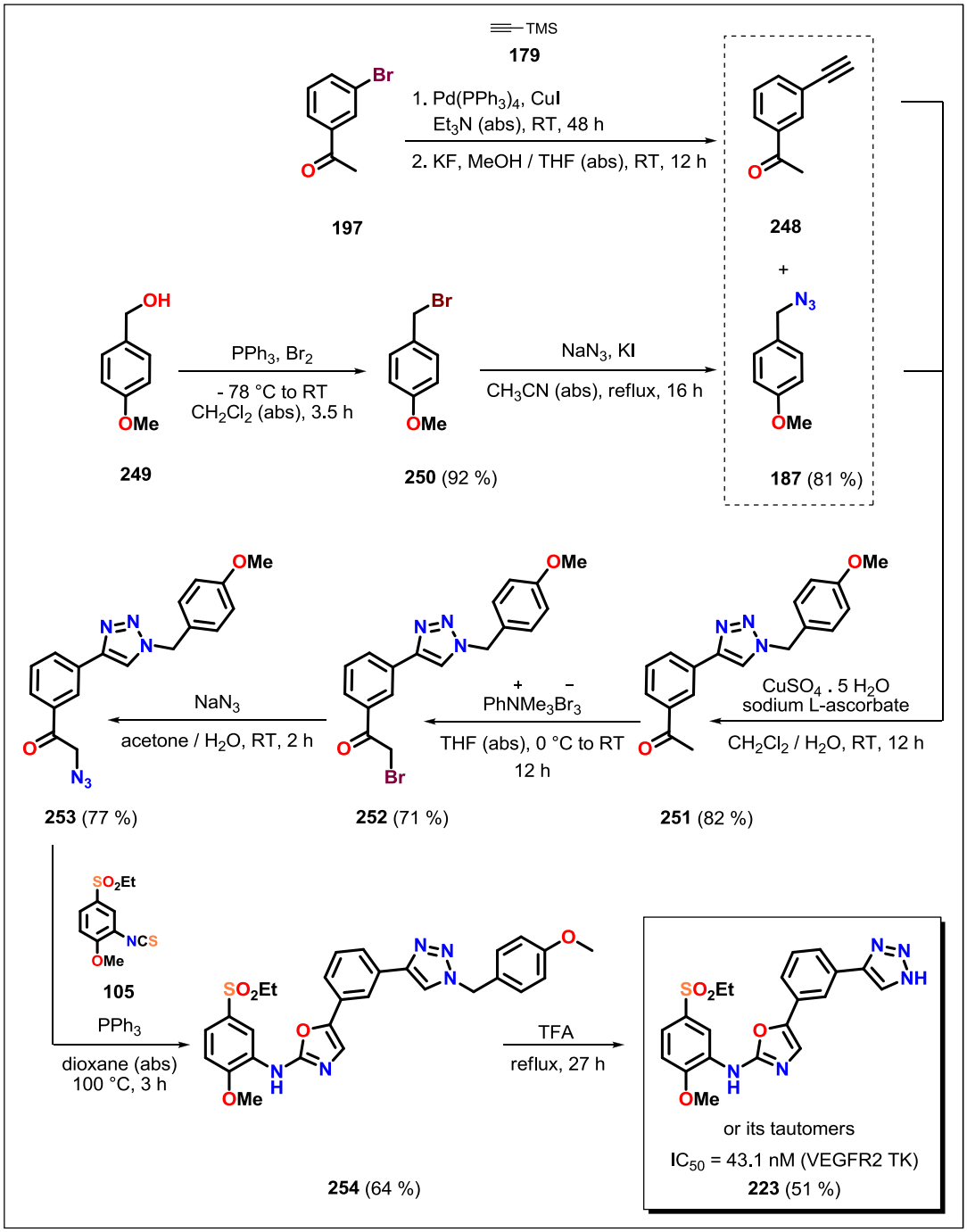

Scheme 36. Synthesis of *m*-substituted *N*,5-diaryloxazol-2-amine **223**.

Synthesis of 1-(3-ethynylphenyl)ethanone (248)

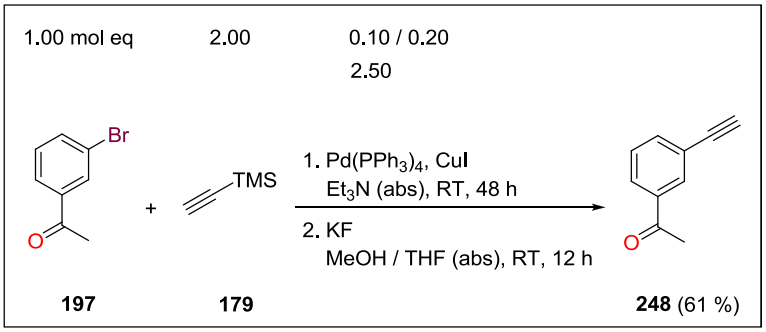

A mixture of 1.00 g (5.02 mmol, 1.00 mol eq) acetophenone **197**, 987 mg (10.0 mmol, 2.00 mol eq) of trimethylsilylacetylene (**179**) and 191 mg (1.00 mmol, 0.20 mol eq) of CuI in 15 ml of Et_3N (abs) was bubbled with Ar for 10 min. Afterwards (0.50 mmol, 0.10 mol eq) of $Pd(PPh_3)_4$ was added and the reaction mixture was stirred under Ar at RT for 48 h. After complete consumption of the starting material **197** (TLC analysis), the mixture was evaporated under reduced pressure. A remaining solid material was dissolved in 15 ml of EA and extracted with 3 x 5 ml of H_2O. An organic layer was separated, dried over Na_2CO_3, filtered and concentrated. An obtained solid was dissolved in a mixture of 20 ml of MeOH (abs) and 10 ml of THF (abs), 730 mg (12.6 mmol, 2.50 mol eq) of KF was added and the mixture was stirred under Ar at RT overnight. After complete consumption of TMS-protected product (TLC analysis), the mixture was evaporated, a remaining material was dissolved in 30 ml of EA and extracted with 3 x 10 ml of saturated aq solution of NH_4Cl. A separated organic layer was dried over Na_2SO_4, filtered and concentrated again. The crude product was purified by FLC (Hex / EA = 9 / 1) yielding 440 mg (2.98 mmol, 61 %) of 1-(3-ethynylphenyl)ethanone (**248**).

Novelty: The synthesis of **248** was described in the literature with 93 % yield.[155] Its ^{1}H-NMR, ^{13}C-NMR[156] and MS[157] spectra were published.

M. p.: 54 – 55 °C [EA]. (lit. M. p.: 53 – 54 °C [Et_2O])[158] Yellow crystalline solid material.

[155] Bernardon, J. M. *Galderma Research and Development S.N.C.* **2001**, US6689922, B1.
[156] Dutta, U.; Lupton, D. W.; Maiti, D. *Org. Lett.* **2016**, *18*, 860 – 863.
[157] Fujimura, O.; Fukunaga, K.; Honma, T.; Machida, T. *Ube Industries* **2009**, EP2042506, A1.
[158] Zimmer, O.; Vollenberg, W.; Seipp, U.; Englberger, W.; Haurand, M.; Bosman, B. J.; Schneider, J. *Gruenenthal GMBH* **1993**, US5202349, A1.

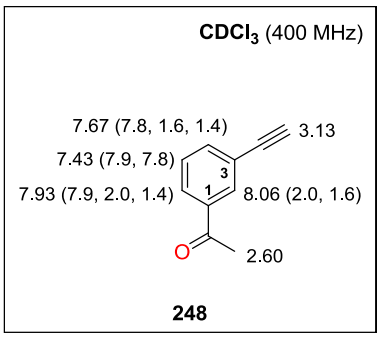

^{1}H-NMR (400 MHz, $CDCl_3$): δ 8.06 (dd, 1H, *J*(2,6) = 2.0 Hz, *J*(2,4) = 1.6 Hz, H-C(2)), 7.93 (ddd, 1H, *J*(5,6) = 7.9 Hz, *J*(2,6) = 2.0 Hz, *J*(4,6) = 1.4 Hz, H-C(6)), 7.67 (ddd, 1H, *J*(4,5) = 7.8 Hz, *J*(2,4) = 1.6 Hz, *J*(4,6) = 1.4 Hz, H-C(4)), 7.43 (dd, 1H, *J*(5,6) = 7.9 Hz, *J*(4,5) = 7.8 Hz, H-C(5)), 3.13 (s, 1H, -C≡CH), 2.60 (s, 3H, $-COCH_3$).

Synthesis of 1-(bromomethyl)-4-methoxybenzene (250)

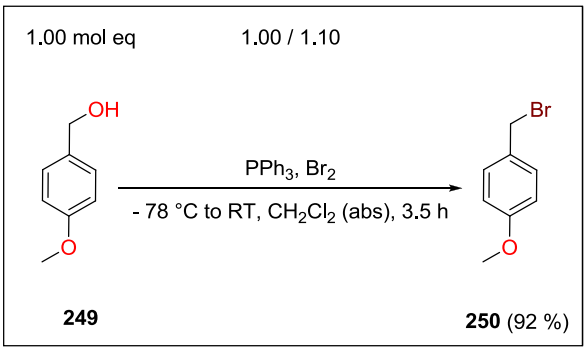

To a solution of 2.85 g (10.9 mmol, 1.00 mol eq) PPh_3 in 20 ml of CH_2Cl_2 (abs) under Ar at 0 °C, 1.91 g (11.9 mmol, 1.10 mol eq) of Br_2 was added dropwise. The reaction mixture was stirred at RT for 30 min. Afterwards it was cooled to - 75 °C, a solution of 1.50 g (10.9 mmol, 1.00 mol eq) **249** in 15 ml of CH_2Cl_2 was slowly added and the mixture was stirred at RT for 3 h. After consumption of the starting material **249** (TLC analysis), 50 ml of 0.1 M solution of $Na_2S_2O_3$ was added and the mixture was stirred for 10 min. Then 50 ml of 1 M solution of $NaHCO_3$ was added, an aqueous layer was separated and extracted with 2 x 50 ml of CH_2Cl_2. Organic layers were combined, dried over Na_2SO_4, filtered and concentrated under reduced pressure. The crude product was purified by trituration to hexane. After filtration of a remaining solid and complete evaporation of a filtrate (rotavap,

HV), 2.00 g (9.95 mmol, 92 %) of 1-(bromomethyl)-4-methoxybenzene (**250**) was obtained.

Novelty: The synthesis of **250** was described in the literature with 100 % yield.[159] Its ^{1}H-NMR, ^{13}C-NMR,[160] IR and MS[161] spectra were also published.

Colorless oily material.

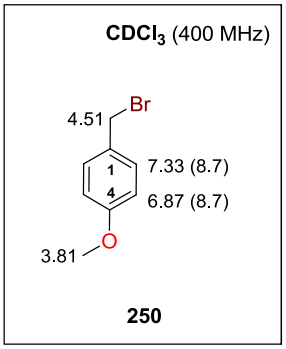

^{1}H-NMR (400 MHz, $CDCl_3$): δ 7.33 (d, 2H, J(2,3) = 8.7 Hz, 2 x H-C(2)), 6.87 (d, 2H, J(2,3) = 8.7 Hz, 2 x H-C(3)), 4.51 (s, 2H, -CH_2Br), 3.81 (s, 3H, -OCH_3).

Synthesis of 1-(azidomethyl)-4-methoxybenzene (187)

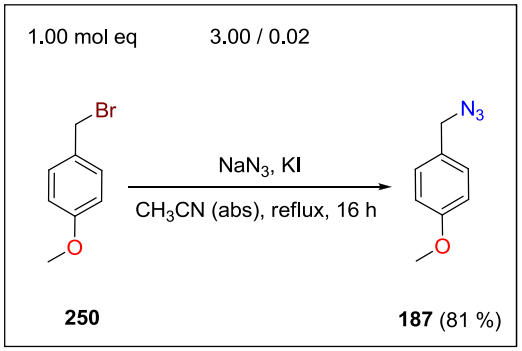

A suspension of 1.00 g (4.97 mmol, 1.00 mol eq) starting material **250**, 647 mg (9.95 mmol, 2.00 mol eq) of NaN_3 and 17.0 mg (0.10 mmol, 0.02 mol eq) of KI in 20 ml of

[159] Champagne, P. A.; Benhassine, Y.; Desroches, J.; Paquin, J. F. *Angew. Chem. Int. Ed.* **2014**, *53*, 13835 – 13839.
[160] Louafi, F.; Hurvois, J. P.; Chibani, A.; Roisnel, T. *J. Org. Chem.* **2010**, *75*, 5721 – 5724.
[161] Shen, Z. L.; Zhuo, G. L.; Jiang, X. Z. *Ind. J. Chem., Sect. B* **2002**, *41*, 2395 – 2398.

CH_3CN (abs) was refluxed under Ar for 16 h. After consumption of the starting material **250** (TLC analysis), the reaction mixture was concentrated by rotavap. The temperature of the water bath was kept below 30 °C. A residual material was then portioned between 20 ml of CH_2Cl_2 and 20 ml of 0.1 M aq solution of Na_2SO_3 and thoroughly shaken. The organic layer was separated, dried over Na_2SO_4, filtered and evaporated under reduced pressure giving 660 mg (1.55 mmol, 74 %) of 1-(azidomethyl)-4-methoxybenzene (**187**) which was used in the next step without further purification.

Novelty: The synthesis of **187** was described in the literature with 100 % yield.[162] Its ^{1}H-NMR, ^{13}C-NMR,[162] IR and HRMS[163] spectra were also published.

Pale yellow oily material.

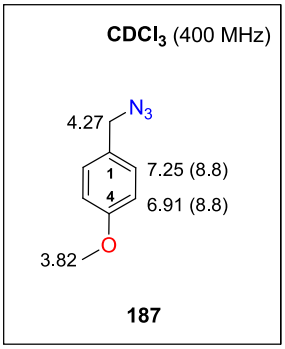

^{1}H-NMR (400 MHz, $CDCl_3$): δ 7.25 (d, 2H, J(2,3) = 8.8 Hz, 2 x H-C(2)), 6.91 (d, 2H, J(2,3) = 8.8 Hz, 2 x H-C(3)), 4.27 (s, 2H, -CH_2N_3), 3.82 (s, 3H, -OCH_3).

[162] Wünsch, S.; Breit, B. *Chem. Eur. J.* **2015**, *21*, 2358 – 2363.
[163] Suzuki, T.; Ota, Y.; Kasuya, Y.; Mutsuga, M.; Kawamura, Y.; Tsumoto, H.; Nakagawa, H.; Finn, M. G.; Miyata, N. *Angew. Chem. Int. Ed.* **2010**, *49*, 6817 – 6820.

Synthesis of 1-(3-(1-(4-methoxybenzyl)-1*H*-1,2,3-triazol-4-yl)phenyl) ethanone (251)

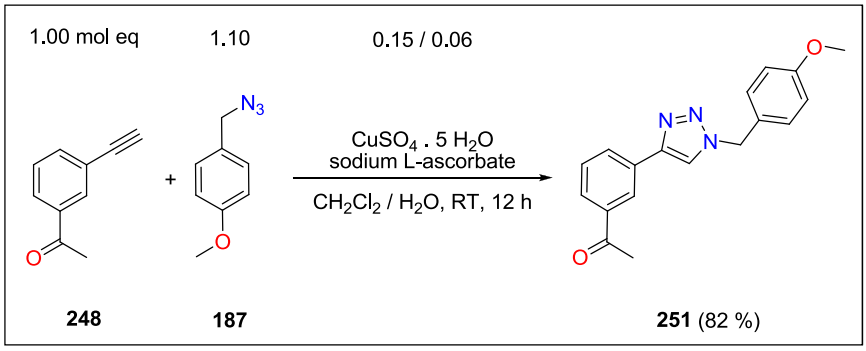

To a stirred suspension of 200 mg (1.39 mmol, 1.00 mol eq) acetophenone **248** and 249 mg (1.53 mmol, 1.10 mol eq) of benzyl azide **187** in 2 ml of CH_2Cl_2 and 2 ml of H_2O, 21.0 mg (0.08 mmol, 0.06 mol eq) of $CuSO_4.5H_2O$ and 41.2 mg (0.21 mmol, 0.15 mol eq) of sodium L-ascorbate was added gradually. The reaction mixture was then stirred at RT for 12 h. After consumption of starting material **248** and **187** (TLC analysis), 10 ml of CH_2Cl_2 was added and the mixture was extracted with 2 x 4 ml of brine and 4 ml of H_2O. An organic layer was separated, dried over Na_2SO_4, filtered and concentrated under reduced pressure. The crude product was purified by FLC (Hex / EA = 1 / 1) yielding 352 mg (1.15 mmol, 82 %) of 1-(3-(1-(4-methoxybenzyl)-1*H*-1,2,3-triazol-4-yl)phenyl)ethanone (**251**).

Novelty: Preparation or characterization of **251** has not been described in the literature.
M. p.: 97 – 98 °C [Hex / EA]. Off white crystalline solid material.

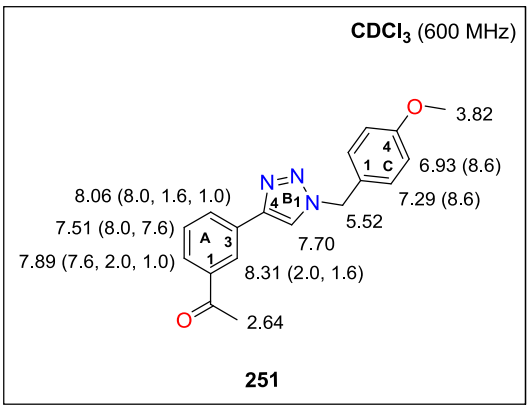

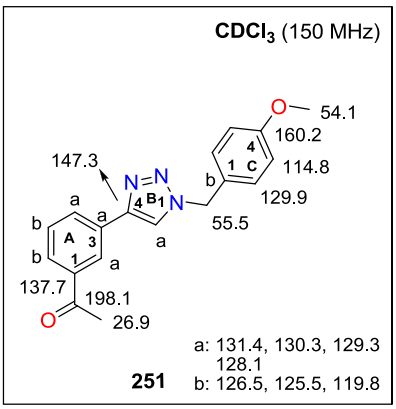

^{1}H-NMR (600 MHz, $CDCl_3$): δ 8.31 (dd, $J(A_2,A_6)$ = 2.0 Hz, $J(A_2,A_4)$ = 1.6 Hz, 1H, H-C_A(2)), 8.06 (ddd, 1H, $J(A_4,A_5)$ = 8.0 Hz, $J(A_2,A_4)$ = 1.6 Hz, $J(A_4,A_6)$ = 1.0 Hz, H-C_A(4)), 7.89 (ddd, 1H, $J(A_5,A_6)$ = 7.6 Hz, $J(A_2,A_6)$ = 2.0 Hz, $J(A_4,A_6)$ = 1.0 Hz, H-C_A(6)), 7.70 (s, 1H, H-C_B(5)), 7.51 (dd, 1H, $J(A_4,A_5)$ = 8.0 Hz, $J(A_5,A_6)$ = 7.6 Hz, H-C_A(5)), 7.29 (d, 1H, $J(C_2,C_3)$ = 8.6 Hz, 2 x H-C_C(2)), 6.93 (d, 1H, $J(C_2,C_3)$ = 8.6 Hz, 2 x H-C_C(3)), 5.52 (s, 2H, -CH_2-), 3.82 (s, 3H, -OCH_3), 2.64 (s, 3H, -$COCH_3$).

^{13}C-NMR (150 MHz, $CDCl_3$): δ 198.1 (-$\underline{C}OCH_3$), 160.2 (C_C(4)), 147.3 (C_B(4)), 137.7 (C_A(1)), 131.4, 130.3, 129.9 (2 x C_C(2)), 129.3, 128.1, 126.5, 125.5, 119.8, 114.8 (2 x C_C(3)), 55.5 (-CH_2-), 54.1 (-OCH_3), 26.9 (-CO$\underline{C}H_3$).

FT IR (solid, cm^{-1}): 3352 (w), 3114 (w), 3075 (w), 3002 (w), 2964 (w), 2840 (w), 2286 (w), 2119 (w), 2082 (w), 1985 (w), 1680 (s), 1609 (s), 1584 (m), 1513 (s), 1431 (m), 1358 (m), 1306 (w), 1245 (s), 1223 (s), 1179 (s), 1094 (w), 1074 (m), 1050 (m), 1023 (s), 997 (w), 965 (w), 934 (w), 911 (m), 836 (m), 806 (s), 788 (s), 764 (s), 738 (w), 693 (s), 671 (m), 626 (w), 588 (s), 555 (s), 518 (s), 443 (w).

MS (ESI m/z): 308.0 $[M + H]^+$; in negative mode 386.0 $[M + Br]^-$.

Anal. calcd for $C_{18}H_{17}N_3O_2$ (307.35): C, 70.34; H, 5.58; N, 13.67; found: C, 70.55; H, 5.50; N, 13.72.

Synthesis of 2-bromo-1-(3-(1-(4-methoxybenzyl)-1*H*-1,2,3-triazol-4-yl) phenyl)ethanone (252)

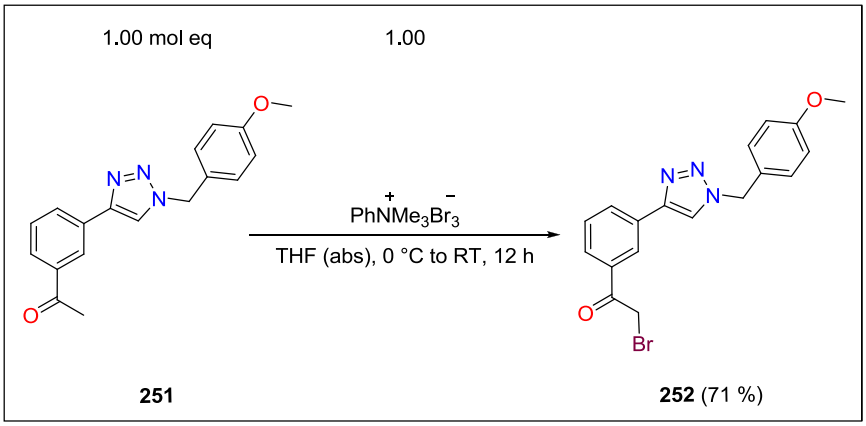

To a solution of 100 mg (0.33 mmol, 1.00 mol eq) starting material **251** in 5 ml of THF (abs), 123 mg (0.33 mmol, 1.00 mol eq) of trimethylphenylammonium tribromide dissolved in 5 ml of THF (abs) was added dropwise. The reaction mixture was subsequently stirred at RT under Ar for 12 h. After complete consumption of the starting material **251** (TLC analysis), the reaction mixture was concentrated. An obtained residual material was dissolved in 30 ml of EA and extracted with 2 x 5 ml of brine and 5 ml of H_2O. The organic layer was dried over Na_2SO_4, filtered and evaporated under reduced pressure. The crude product was purified by trituration with Hex / EA yielding 90.0 mg (0.18 mmol, 71 %) of 2-bromo-1-(3-(1-(4-methoxybenzyl)-1*H*-1,2,3-triazol-4-yl)phenyl) ethanone (**252**).

Novelty: Preparation or characterization of **252** has not been described in the literature.

M. p.: 109 – 112 °C [Hex / EA]. White crystalline solid material.

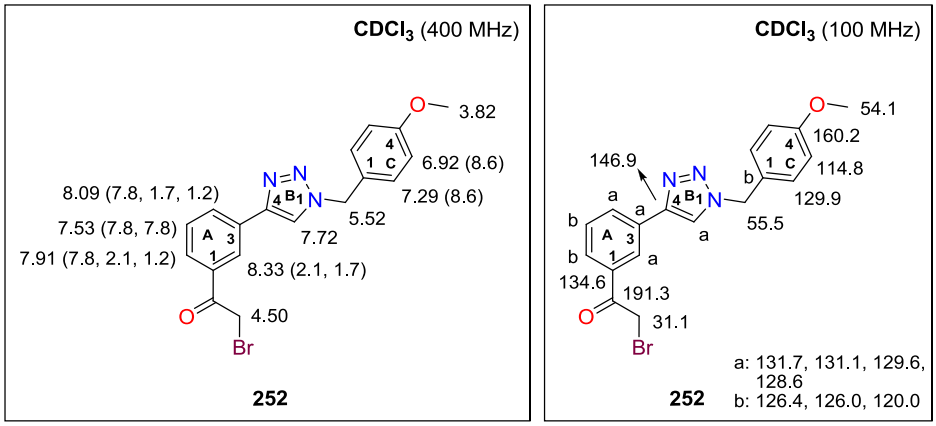

^{1}H-NMR (400 MHz, $CDCl_3$): δ 8.33 (dd, 1H, $J(A_2,A_4)$ = 1.7 Hz, $J(A_2,A_6)$ = 2.1 Hz, H-C_A(2)), 8.09 (ddd, 1H, $J(A_4,A_5)$ = 7.8 Hz, $J(A_2,A_4)$ = 1.7 Hz, $J(A_4,A_6)$ = 1.2 Hz, H-C_A(4)), 7.91 (ddd, 1H, $J(A_5,A_6)$ = 7.8 Hz, $J(A_2,A_6)$ = 2.1 Hz, $J(A_4,A_6)$ = 1.2 Hz, H-C_A(6)), 7.72 (s, 1H, H-C_B(5)), 7.53 (dd, 1H, $J(A_4,A_5)$ = 7.8 Hz, $J(A_5,A_6)$ = 7.8 Hz, H-C_A(5)), 7.29 (d, 1H, $J(C_2,C_3)$ = 8.6 Hz, 2 x H-C_C(2)), 6.92 (d, 1H, $J(C_2,C_3)$ = 8.6 Hz, 2 x H-C_C(3)), 5.52 (s, 2H, -CH_2-), 4.50 (s, 2H, -$COCH_2Br$), 3.81 (s, 3H, -OCH_3).

^{13}C-NMR (100 MHz, $CDCl_3$): δ191.3 (-$\underline{C}OCH_2Br$), 160.2 (C_C(4)), 146.9 (C_B(4)), 134.6 (C_A(1)), 131.7, 131.1, 129.9 (2 x C_C(2)), 129.6, 128.6, 126.4, 126.0, 120.0, 114.8 (2 x C_C(3)), 55.5 (-CH_2-), 54.1 (-OCH_3), 31.1 (-$CO\underline{C}H_2Br$).

FT IR (solid, cm^{-1}): 3121 (w), 3071 (w), 3000 (w), 2952 (w), 2836 (w), 2374 (w), 2194 (w), 2114 (w), 2082 (w), 1989 (w), 1908 (w), 1698 (s), 1610 (m), 1584 (w), 1549 (w), 1513 (s), 1459 (w), 1436 (w), 1416 (m), 1386 (w), 1337 (w), 1293 (w), 1247 (s), 1204 (s), 1172 (s), 1128 (w), 1102 (w), 1077 (m), 1045 (m), 1023 (s), 915 (w), 878 (w), 824 (m), 794 (s), 765 (s), 725 (w), 682 (s), 618 (s), 550 (s), 517 (m), 494 (w), 456 (w).

MS (ESI m/z): 385.9 (49 %), 388.0 (51 %) $[M + H]^+$; in negative mode 385.1 $[M - H]^-$.

Anal. calcd for $C_{18}H_{16}N_3O_2$ (386.24): C, 55.97; H, 4.18; N, 10.88; found: C, 60.05; H, 4.24; N, 10.76.

Synthesis of 2-azido-1-(3-(1-(4-methoxybenzyl)-1*H*-1,2,3-triazol-4-yl) phenyl)ethanone (253)

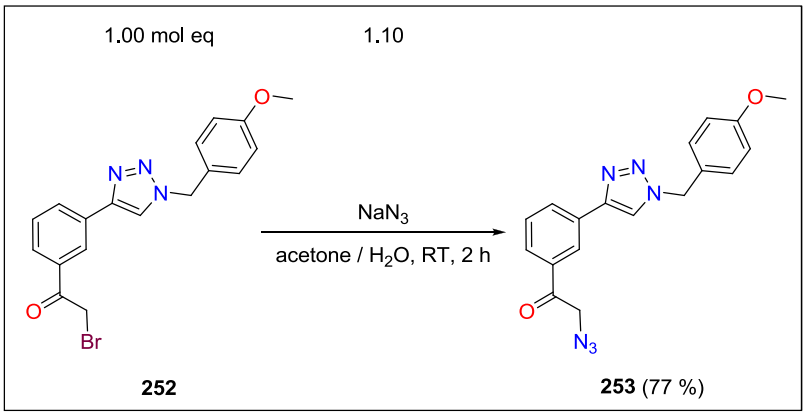

To a solution of 310 mg (0.80 mmol, 1.00 mol eq) starting material **252** in 10 ml of acetone, 57.4 mg (0.88 mmol, 1.10 mol eq) of NaN_3 dissolved in 1.5 ml of H_2O was added. The reaction mixture was stirred for 2 h at RT. After consumption of the starting material **252** (TLC analysis), the mixture was evaporated. A remaining material was dissolved in 15 ml of EA and washed with 2 x 5 ml of brine and 5 ml of H_2O. The organic layer was dried over Na_2SO_4, filtered and concentrated under reduced pressure. The crude product was

purified by FLC (gradient: Hex /EA = 2 / 1 to 1 / 1 to EA) yielding 216 mg (0.62 mmol, 77 %) of 2-azido-1-(3-(1-(4-methoxybenzyl)-1*H*-1,2,3-triazol-4-yl)phenyl)ethanone (**253**).

Novelty: Synthesis or characterization of **253** has not been described in the literature.

M.p.: 95 – 97 °C [Hex / EA]. White solid material.

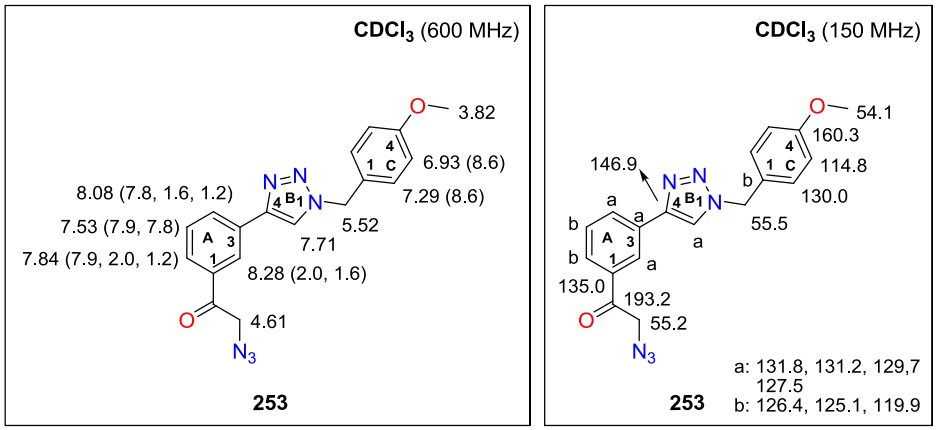

^{1}H-NMR (600 MHz, $CDCl_3$): δ 8.28 (dd, 1H, $J(A_2,A_4)$ = 1.6 Hz, $J(A_2,A_6)$ = 2.0 Hz, H-C_A(2)), 8.08 (ddd, 1H, $J(A_4,A_5)$ = 7.8 Hz, $J(A_2,A_4)$ = 1.6 Hz, $J(A_4,A_6)$ = 1.2 Hz, H-C_A(4)), 7.84 (ddd, 1H, $J(A_5,A_6)$ = 7.9 Hz, $J(A_2,A_6)$ = 2.0 Hz, $J(A_4,A_6)$ = 1.2 Hz, H-C_A(6)), 7.71 (s, 1H, H-C_B(5)), 7.53 (dd, 1H, $J(A_5,A_6)$ = 7.9 Hz, $J(A_4,A_5)$ = 7.8 Hz, H-C_A(5)), 7.29 (d, 1H, $J(C_2,C_3)$ = 8.6 Hz, 2 x H-C_C(2)), 6.93 (d, 1H, $J(C_2,C_3)$ = 8.6 Hz, 2 x H-C_C(3)), 5.52 (s, 2H, -CH_2-), 4.61 (s, 2H, -$COCH_2N_3$), 3.82 (s, 3H, -OCH_3).

^{13}C-NMR (150 MHz, $CDCl_3$): δ193.2 (-$\underline{C}OCH_2N_3$), 160.3 (C_C(4)), 146.9 (C_B(4)), 135.0 (C_A(1)), 131.8, 131.2, 130.0 (2 x C_C(2)), 129.7, 127.5, 126.4, 125.1, 119.9, 114.8 (2 x C_C(3)), 55.5 (-CH_2-), 55.2 (-$CO\underline{C}H_2N_3$), 54.1 (-OCH_3).

FT IR (solid, cm^{-1}): 3128 (w), 3067 (w), 2984 (w), 2950 (w), 2883 (w), 2837 (w), 2375 (w), 2269 (w), 2211 (w), 2142 (w), 2101 (s), 1927 (w), 1890 (w), 1698 (s), 1610 (m), 1585 (w), 1545 (w), 1513 (m), 1459 (w), 1413 (m), 1336 (w), 1287 (w), 1253 (s), 1216 (s), 1177 (s), 1130 (w), 1112 (w), 1073 (w), 1046 (w), 1015 (s), 909 (m), 823 (w), 791 (s), 766 (s), 750 (m), 726 (w), 683 (s), 621 (m), 548 (s), 523 (m), 495 (w), 459 (w).

MS (ESI m/z): 349.0 $[M + H]^+$; not detectable in negative mode.

Anal. calcd for $C_{18}H_{16}N_6O_2$ (348.36): C, 62.06; H, 4.63; N, 24.12; found: C, 62.24; H, 4.70; N, 24.10.

Synthesis of *N*-(5-(ethylsulfonyl)-2-methoxyphenyl)-5-(3-(1-(4-methoxy benzyl)-1*H*-1,2,3-triazol-4-yl)phenyl)oxazol-2-amine (254)

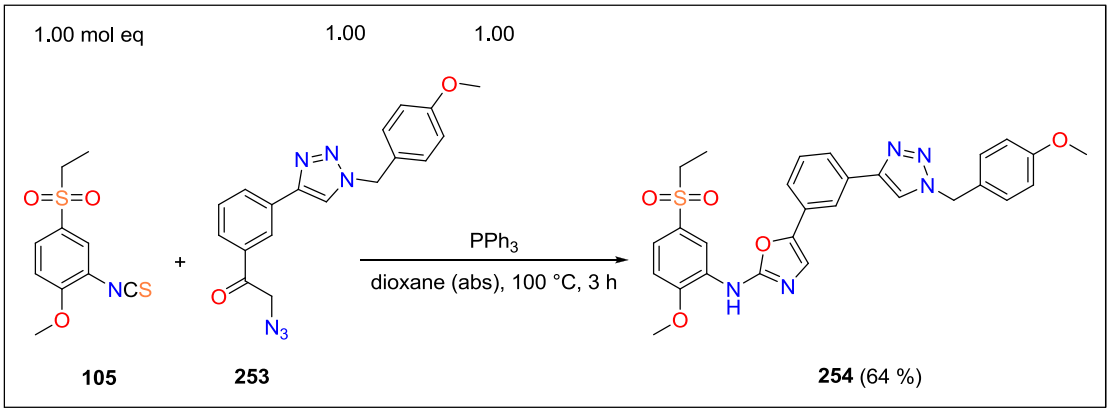

A solution of 74.0 mg (0.29 mmol, 1.00 mol eq) isothiocyanate **105**, 100 mg (0.29 mmol, 1.00 mol eq) of azide **253** and 75.4 mg (0.29 mmol, 1.00 mol eq) of PPh_3 in 5 ml of dioxane (abs) under Ar was placed into the preheated 100 °C oil bath for 3 h. After consumption of the starting material **105** and **253** (TLC analysis), the reaction mixture was evaporated and an obtained solid material was dissolved in 15 ml of EA and extracted with 2 x 5 ml of brine and 5 ml of H_2O. The organic layer was separated, dried over Na_2SO_4, filtered and evaporated under reduced pressure. The crude product was purified by trituration with Hex / EA yielding 100 mg (0.18 mmol, 64 %) of *N*-(5-(ethylsulfonyl)-2-methoxyphenyl)-5-(3-(1-(4-methoxybenzyl)-1*H*-1,2,3-triazol-4-yl) phenyl)oxazol-2-amine (**254**).

Novelty: Synthesis or characterization of **254** has not been described in the literature.

M.p.: 200 – 202 °C [Hex / EA]. Pale brown solid material.

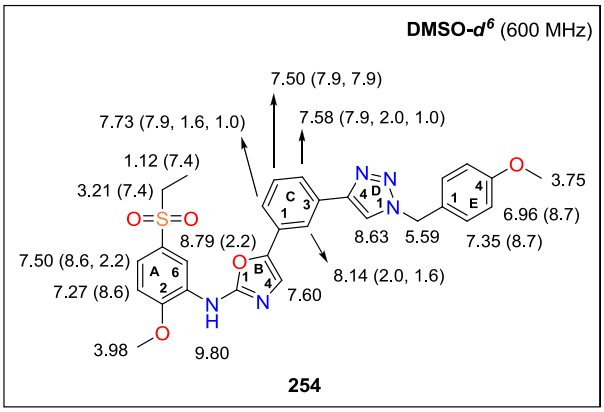

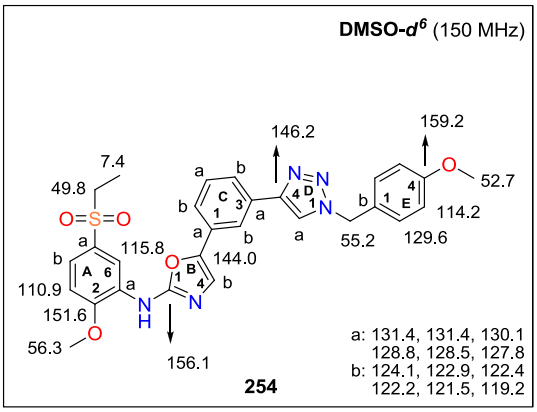

^{1}H-NMR (600 MHz, DMSO-d^6): δ 9.80 (s, 1H, -NH-), 8.79 (d, 1H, $J(A_4,A_6)$ = 2.2 Hz, H-C_A(6)), 8.63 (s, 1H, H-C_D(5)), 8.14 (dd, 1H, $J(C_2,C_4)$ = 2.0 Hz, $J(C_2,C_6)$ = 1.6 Hz, H-C_C(2)), 7.73 (ddd, 1H, $J(C_5,C_6)$ = 7.9 Hz, $J(C_2,C_6)$ = 1.6 Hz, $J(C_4,C_6)$ = 1.0 Hz, H-C_C(6)), 7.60 (s, 1H, H-C_B(4)), 7.58 (ddd, 1H, $J(C_4,C_5)$ = 7.9 Hz, $J(C_2,C_4)$ = 2.0 Hz, $J(C_4,C_6)$ = 1.0 Hz, H-C_C(4)), 7.50 (dd, 1H, $J(A_3,A_4)$ = 8.6 Hz, $J(A_4,A_6)$ = 2.2 Hz, H-C_A(4)), 7.50 (dd, 1H, $J(C_4,C_5)$ = 7.9 Hz, $J(C_5,C_6)$ = 7.9 Hz, H-C_C(5)), 7.35 (d, 2H, $J(E_2,E_3)$ = 8.7 Hz, 2 x H-C_E(2)), 7.27 (d, 1H, $J(A_3,A_4)$ = 8.6 Hz, H-C_A(3)), 6.96 (d, 2H, $J(E_2,E_3)$ = 8.7 Hz, 2 x H-C_E(3)), 5.59 (s, 2H, -CH_2-), 3.98 (s, 3H, -OCH_3 phenyl), 3.75 (s, 3H, -OCH_3 benzyl), 3.21 (q, 2H, $J(CH_2,CH_3)$ = 7.4 Hz, -$SO_2C\underline{H}_2CH_3$), 1.12 (t, 3H, $J(CH_2,CH_3)$ = 7.4 Hz, -$SO_2CH_2C\underline{H}_3$).

^{13}C-NMR (150 MHz, DMSO-d^6): δ 159.2 (C_E(4)), 156.1 (C_B(2)), 151.6 (C_A(2)), 146.2 (C_D(4)), 144.0 (C_B(5)), 2 x 131.4, 130.1, 129.6 (2 x C_E(2)), 128.8, 128.5, 127.8, 124.1, 122.9, 122.4, 122.2, 121.5, 119.2, 115.8 (C_A(6)), 114.2 (2 x C_E(3)), 110.9 (C_A(3)), 56.3 (-OCH_3 phenyl), 55.2 (-CH_2-), 52.7 (-OCH_3 benzyl), 49.8 (-$SO_2\underline{C}H_2CH_3$), 7.4 (-$SO_2CH_2\underline{C}H_3$).

FT IR (solid, cm^{-1}): 3429 (w), 3128 (w), 2976 (w), 2937 (w), 2842 (w), 2240 (w), 2106 (w), 2085 (w), 1735 (w), 1613 (s), 1580 (s), 1513 (s), 1482 (w), 1456 (w), 1430 (m), 1402 (w), 1345 (w), 1302 (m), 1250 (s), 1176 (m), 1139 (s), 1121 (s), 1082 (m), 1045 (w), 1024 (m), 920 (w), 892 (w), 826 (m), 794 (s), 769 (s), 753 (s), 718 (m), 686 (m), 657 (w), 639 (w), 603 (w), 557 (m), 522 (m), 493 (s), 474 (s), 452 (m).

MS (ESI m/z): 546.0 $[M + H]^+$, 568.0 $[M + Na]^+$; in negative mode 544.1 $[M - H]^-$.

Anal. calcd for $C_{28}H_{27}N_5O_5S$ (545.61): C, 61.64; H, 4.99; N, 12.84; found: C, 61.60; H, 5.10; N, 12.71.

Synthesis of 5-(3-(1*H*-1,2,3-triazol-4-yl)phenyl)-*N*-(5-(ethylsulfonyl)-2-methoxyphenyl)oxazol-2-amine (223)

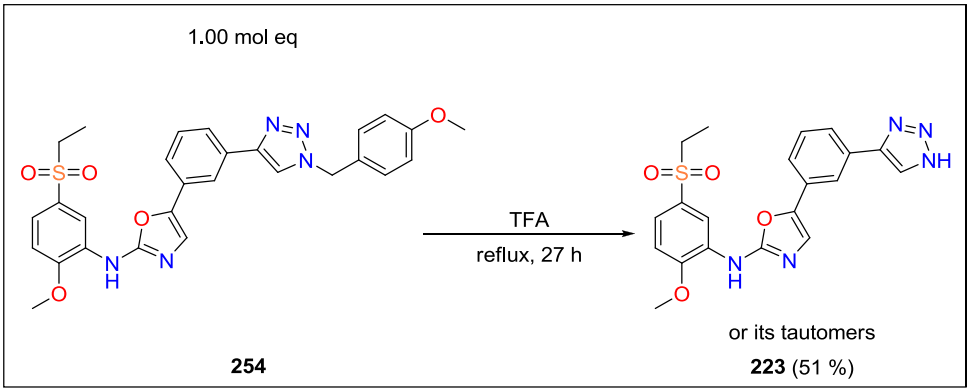

A solution of 100 mg (0.18 mmol, 1.00 mol eq) starting material **254** in 6 ml of CF_3COOH (TFA) was refluxed under Ar for 27 h. After complete consumption of starting material **254** (TLC analysis), the reaction mixture was diluted with 3 ml of H_2O, placed into an ice bath and neutralized using a saturated solution of Na_2CO_3. The aqueous mixture was then extracted with 3 x 10 ml of EA. The separated organic layers were combined, dried over Na_2SO_4, filtered and evaporated under reduced pressure. The crude product was purified by trituration with EA or by FLC (CH_2Cl_2 / EA = 2 / 1) yielding 40.0 mg (0.07 mmol, 51 %) of 5-(3-(1*H*-1,2,3-triazol-4-yl)phenyl)-*N*-(5-(ethylsulfonyl)-2-methoxyphenyl)oxazol-2-amine (**223**).

Novelty: Synthesis or characterization of **223** has not been described in the literature.

M.p.: 270 – 273 (dec) °C [EA]. Off white solid material.

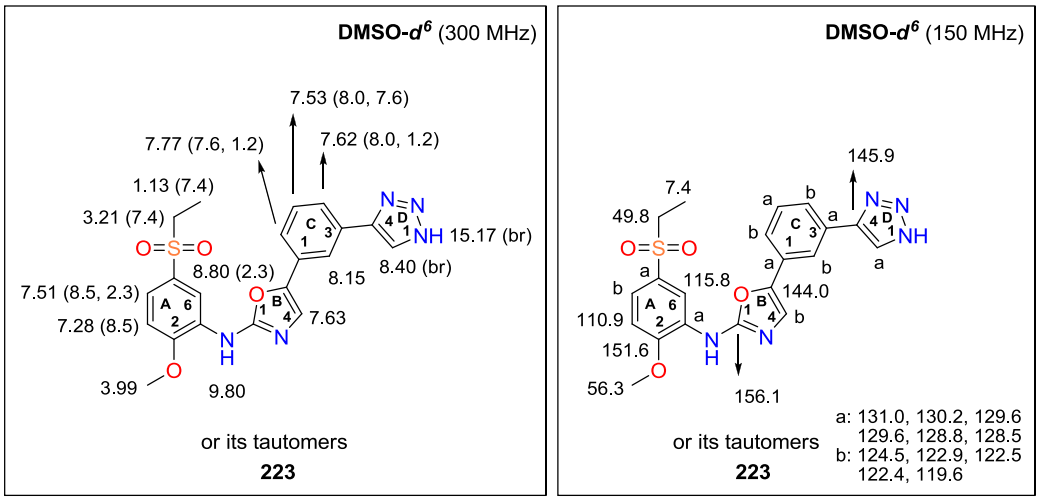

^{1}H-NMR (300 MHz, DMSO-d^6): δ 15.17 (br s, 1H, -NH- triazole), 9.80 (br s, 1H, -NH-), 8.80 (d, 1H, $J(A_4,A_6)$ = 2.3 Hz, H-C_A(6)), 8.40 (br s, 1H, H-C_D(5)), 8.15 (s, 1H, H-C_C(2)), 7.77 (dd, 1H, $J(C_5,C_6)$ = 7.6 Hz, $J(C_4,C_6)$ = 1.2 Hz, H-C_C(6)), 7.63 (s, 1H, H-C_B(4)), 7.62 (dd, 1H, $J(C_4,C_5)$ = 8.0 Hz, $J(C_4,C_6)$ = 1.2 Hz, H-C_C(4)), 7.53 (dd, 1H, $J(C_4,C_5)$ = 8.0 Hz, $J(C_5,C_6)$ = 7.6 Hz, H-C_C(5)), 7.51 (dd, 1H, $J(A_3,A_4)$ = 8.5 Hz, $J(A_4,A_6)$ = 2.3 Hz, H-C_A(4)), 7.28 (d, 1H, $J(A_3,A_4)$ = 8.5 Hz, H-C_A(3)), 3.99 (s, 3H, -OCH_3), 3.21 (q, 2H, $J(CH_2,CH_3)$ = 7.4 Hz, -$SO_2C\underline{H}_2CH_3$), 1.13 (t, 3H, $J(CH_2,CH_3)$ = 7.4 Hz, -$SO_2CH_2C\underline{H}_3$).

^{13}C-NMR (150 MHz, DMSO-d^6): δ 156.1 (C_B(2)), 151.6 (C_A(2)), 145.9 (C_D(4)), 144.0 (C_B(5)), 131.0, 130.2, 2 x 129.6, 128.8, 128.5, 124.5, 122.9, 122.5, 122.4, 119.6, 115.8 (C_A(6)), 110.9 (C_A(3)), 56.3 (-OCH_3), 49.8 (-$SO_2\underline{C}H_2CH_3$), 7.4 (-$SO_2CH_2\underline{C}H_3$).

FT IR (solid, cm^{-1}): 3403 (w), 3118 (w), 2827 (w), 2137 (w), 1686 (w), 1618 (s), 1577 (s), 1523 (m), 1486 (m), 1433 (m), 1351 (w), 1300 (m), 1262 (m), 1225 (w), 1141 (s), 1121 (s), 1081 (m), 1047 (m), 1008 (m), 974 (m), 922 (w), 894 (w), 847 (w), 796 (m), 747 (s), 718 (s), 685 (m), 658 (w), 627 (w), 597 (m), 571 (s), 518 (m), 494 (s), 454 (m), 421 (w).

MS (ESI m/z): 426.0 $[M + H]^+$, 448.0 $[M + Na]^+$; in negative mode 424.1 $[M - H]^-$.

Anal. calcd for $C_{20}H_{19}N_5O_4S$ (425.46): C, 56.46; H, 4.50; N, 16.46; found: C, 56.83; H, 4.86; N, 16.50.

13.4. Project – CLK1 inhibition

13.4.1. Synthesis of CLK1 inhibitor precursor 269

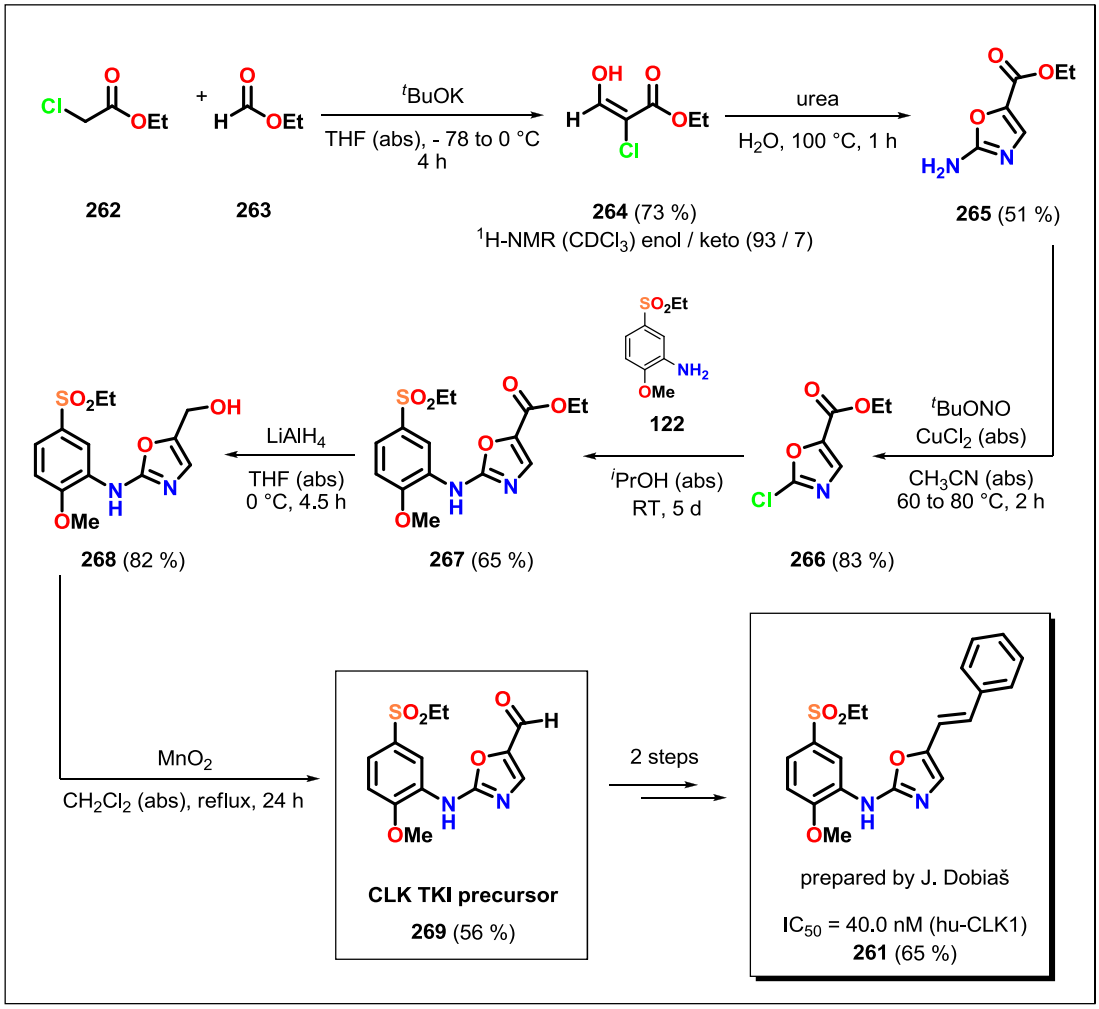

Scheme 38. Synthesis of CLK1 inhibitor precursor **269**.

Synthesis of (*E*)-ethyl 2-chloro-3-hydroxyacrylate (264)

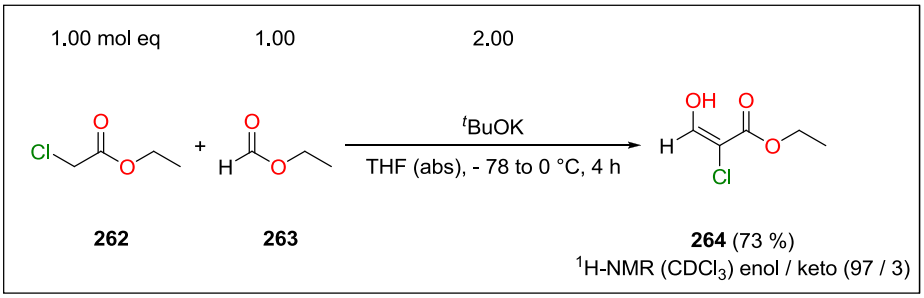

A stirred solution of 5.00 g (40.7 mmol, 1.00 mol ekv) ethyl 2-chloroacetate (**262**) and 3.02 g (40.7 mmol, 1.00 mol ekv) of ethyl formate (**263**) in 80 ml of THF (abs) was cooled down to – 78 °C under Ar. Subsequently 9.13 g (81.4 mmol, 2.00 mol ekv) of ^{t}BuOK in 80 ml of THF (abs) was added dropwise during 1 h. After the completed addition the reaction mixture was stirred at – 78 °C for 1 h and then at 0 °C for additional 3 h. Afterwards at the same temperature the pH was adjusted to 2 using 2 M HCl, 30 ml of brine was added and the mixture was extracted with 3 x 150 ml of Et_2O. The combined organic layers were dried with Na_2SO_4, filtered and concentrated under reduced pressure. Isolated crystals were purified using trituration with hexane yielding 4.50 g (29.9 mmol, 73 %) of (*E*)-ethyl 2-chloro-3-hydroxyacrylate (**264**).

Novelty: The synthesis of **264** was described in the literature with 71 % yield.[164] Its ^{1}H-NMR,[165] IR[166] and MS[167] spectra were also published.

M. p.: 71 – 72 °C [Hex]. (lit. M. p.: 83 – 84 °C [benzene])[165] Off-white crystalline solid material.

[164] Hartz, R. A.; Ahuja, V. T.; Rajamani, R.; Dzierba, C. D.; Bronson, J. J.; Macor, J. E. *Bristol-Myers Squibb Company* **2015**, WO2015/26574, A1.
[165] Yoffe, S.T.; Petrovsky, P.V.; Goryunov, Y.I.; Yershova, T.V.; Kabachnik, M.I. *Tetrahedron* **1972**, *28*, 2783 – 2789.
[166] Noi, R. S. *et al. J. Org. Chem. USSR (Eng. Trans.)* **1976**, *12*, 2188 – 2189.
[167] Turner, W. W.; Arnold, L. D.; Maag, H.; Zlotnick, A. *Indiana University Research and Technology Corporation; Assembly Biosciences, Inc.* **2015**, WO2015/138895, A1.

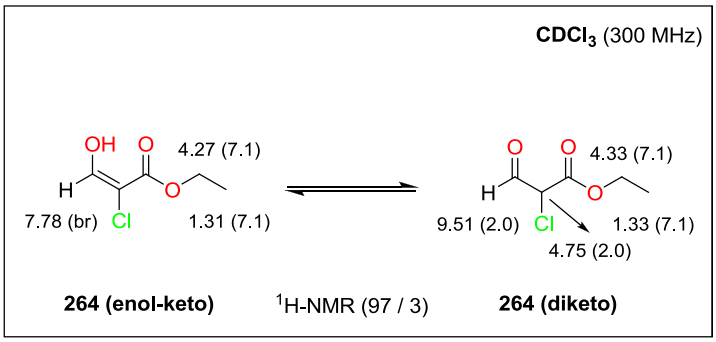

^{1}H-NMR (300 MHz, $CDCl_3$) (**enol-keto**): δ 7.78 (br s, 1H, C<u>H</u>(OH)=), 4.27 (q, 2H, $J(CH_2,CH_3)$ = 7.1 Hz, -COOC<u>H</u>$_2$CH$_3$), 1.31 (t, 3H, $J(CH_2,CH_3)$ = 7.1 Hz, -COOCH$_2$C<u>H</u>$_3$). (**diketo**): δ 9.51 (d, 1H, J(1,2) = 2.0 Hz, -CHO), 4.75 (d, 1H, J(1,2) = 2.0 Hz, -CH(Cl)-), 4.33 (q, 2H, $J(CH_2,CH_3)$ = 7.1 Hz, -COOC<u>H</u>$_2$CH$_3$), 1.33 (t, 3H, $J(CH_2,CH_3)$ = 7.1 Hz, -COOCH$_2$C<u>H</u>$_3$).

Synthesis of ethyl 2-aminooxazole-5-carboxylate (265)

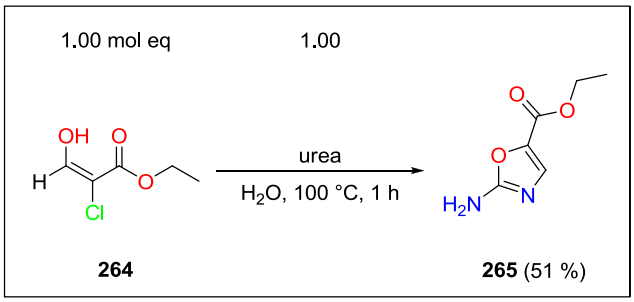

A suspension of 4.48 g (29.8 mmol, 1.00 mol eq) (*E*)-ethyl 2-chloro-3-hydroxyacrylate (**264**) and 1.79 g (29.8 mmol, 1.00 mol eq) of urea in 40 ml of H_2O was stirred at 100 °C for 1 h. Then the reaction mixture was cooled down to RT, neutralized by a saturated aq. solution of $NaHCO_3$ and extracted with 3 x 50 ml of EA. The combined organic layers were dried over Na_2SO_4, filtered and concentrated under reduced pressure. The crude product was purified by FLC (Hex / EA = 1 / 2) yielding 2.40 g (15.4 mmol, 51 %) of ethyl 2-aminooxazole-5-carboxylate (**265**).

Novelty: The synthesis of **265** was described in the literature with 64 % yield together with its ^{1}H-NMR, ^{13}C-NMR and IR spectra were also published.[82]

M. p.: 154 – 155 °C [Hex / EA]. (lit. M. p.: 153 – 154 °C [EA])[82] Off-white solid material.

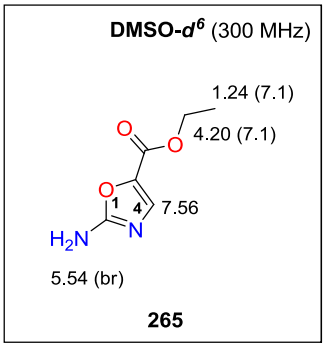

^{1}H-NMR (300 MHz, DMSO-d^6): δ 7.56 (s, 1H, H-C(4)), 5.54 (br s, 2H, -NH_2), 4.20 (q, 2H, $J(CH_2,CH_3)$ = 7.1 Hz, -COOC$\underline{H}_2$CH$_3$), 1.24 (t, 3H, $J(CH_2,CH_3)$ = 7.1 Hz, -COOCH$_2$C$\underline{H}_3$).

Synthesis of ethyl 2-chlorooxazole-5-carboxylate (266)

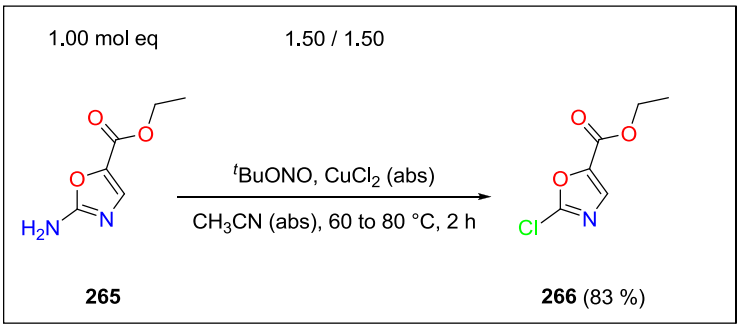

A mixture of 1.19 g (8.80 mmol, 1.50 mol eq) $CuCl_2$ (abs) and 1.05 ml (8.80 mmol, 1.50 mol eq) ^{t}BuONO in 30 ml of CH_3CN (abs) under Ar was heated to 60 °C. By this temperature 920 mg (5.90 mmol, 1.00 mol eq) of ethyl 2-aminooxazole-5-carboxylate (**265**) was added portion wise. Then the temperature was raised to 80 °C and the reaction mixture was stirred for 2 h. After the consumption of starting material **265** (TLC analysis) the reaction mixture was cooled down to RT and 15 ml of H_2O and 8 ml of 2 M HCl was added. The mixture was extracted with 3 x 20 ml of EA and the combined organic layers were washed with brine, dried over Na_2SO_4, filtered and concentrated under reduced pressure yielding 850 mg (4.80 mmol, 83 %) of ethyl 2-chlorooxazole-5-carboxylate (**266**).

Note: The crude product **266** was prepared in a sufficient purity to be possibly used in the next reaction step. More precious purification of **266** can be done using FLC (Hex / EA = 1 / 1), however because of its instability, the yield is lowered to approximately 40 %.

Novelty: The synthesis of **266** was described in the literature with 74 % crude yield together with its ^{1}H-NMR, ^{13}C-NMR and IR spectra were also published.[82]

Light yellow oily material.

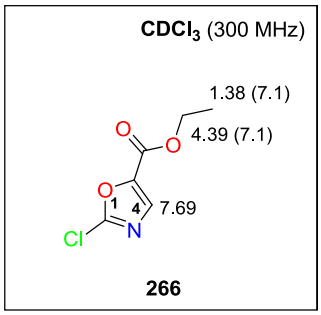

^{1}H-NMR (300 MHz, $CDCl_3$): δ 7.69 (s, 1H, H-C(4)), 4.39 (q, 2H, $J(CH_2,CH_3)$ = 7.1 Hz, -COOC$\underline{H}_2$CH$_3$), 1.38 (t, 3H, $J(CH_2,CH_3)$ = 7.1 Hz, -COOCH$_2$C$\underline{H}_3$).

Synthesis of ethyl 2-(5-(ethylsulfonyl)-2-methoxyphenylamino)oxazole-5-carboxylate (267)

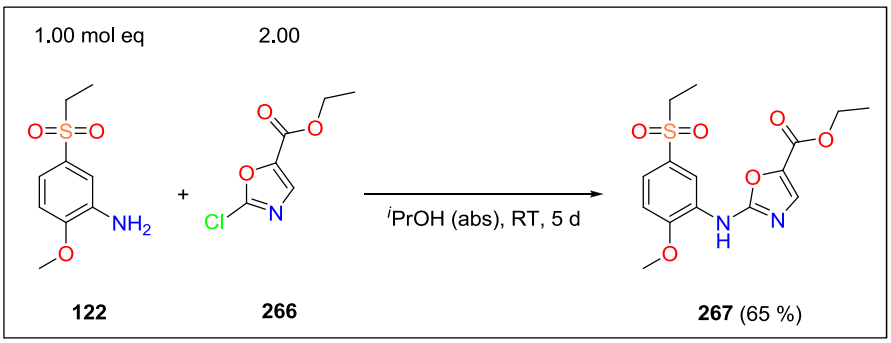

To a suspension of 1.41 g (6.50 mmol, 1.00 mol eq) aniline **122** in 40 ml of ^{i}PrOH (abs), 2.29 g (13.1 mmol, 2.00 mol ekv) of ethyl 2-chlorooxazole-5-carboxylate (**266**) in 20 ml of ^{i}PrOH (abs) was added dropwise and the reaction mixture was stirred under Ar for 5 d at RT. After complete consumption of the starting material **122** (TLC analysis), the solvent

was evaporated under reduced pressure. The obtained solid material was dissolved in 80 ml of EA and extracted with 2 x 20 ml of $NaHCO_3$ (saturated aq solution) and 2 x 20 ml of H_2O. The separated organic layer was dried by Na_2SO_4, filtered and concentrated under reduced pressure. The crude product was purified by FLC (gradient: Hex / EA = 1 / 2 to 1 / 3) yielding 1.50 g (4.20 mmol, 65 %) of ethyl 2-(5-(ethylsulfonyl)-2-methoxy phenyl amino)oxazole-5-carboxylate (**267**).

Novelty: The synthesis of **267** was described in the literature with 77 % yield together with its ^{1}H-NMR, ^{13}C-NMR and IR spectra were also published.[82]

M. p.: 107 – 109 °C [Hex / EA]. (lit. M. p.: 141 – 143 °C [Hex / EA])[82] Pale brown solid material.

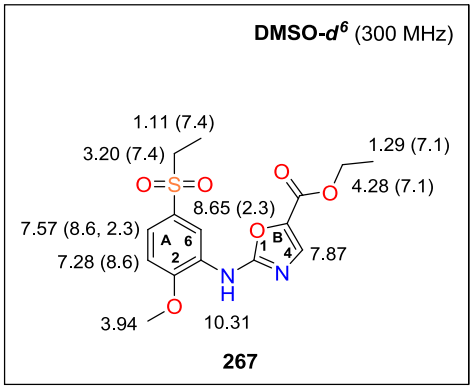

^{1}H-NMR (300 MHz, DMSO-d^6): δ 10.31 (s, 1H, -NH-), 8.65 (d, 1H, $J(A_4,A_6)$ = 2.3 Hz, H-C_A(6)), 7.87 (s, 1H, H-C_B(4)), 7.57 (dd, 1H, $J(A_3,A_4)$ = 8.6 Hz, $J(A_4,A_6)$ = 2.3 Hz, H-C_A(4)), 7.28 (d, 1H, $J(A_3,A_4)$ = 8.6 Hz, H-C_A(3)), 4.28 (q, 2H, $J(CH_2,CH_3)$ = 7.1 Hz, -COOC$\underline{H}_2$CH$_3$), 3.94 (s, 3H, -OCH$_3$), 3.20 (q, 2H, $J(CH_2,CH_3)$ = 7.4 Hz, -SO$_2$C$\underline{H}_2$CH$_3$), 1.29 (t, 3H, $J(CH_2,CH_3)$ = 7.1 Hz, -COOCH$_2$C$\underline{H}_3$), 1.11 (t, 3H, $J(CH_2,CH_3)$ = 7.4 Hz, -SO$_2$CH$_2$C$\underline{H}_3$).

Synthesis of (2-(5-(ethylsulfonyl)-2-methoxyphenylamino)oxazol-5-yl)methanol (268)

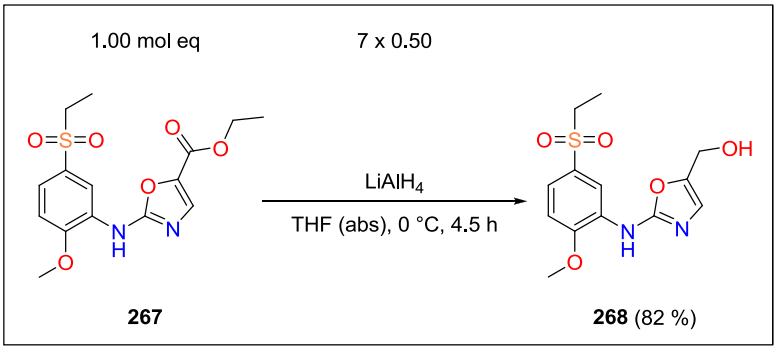

A solution of 470 mg (1.30 mmol, 1.00 mol eq) ester **267** in of 15 ml of THF (abs) was placed into an ice bath. Then 176 mg (4.60 mmol, 3.50 mol eq) of $LiAlH_4$ was added into the reaction mixture in seven portions (25.2 mg, 0.70 mmol, 0.50 mol eq) gradually in the period of 30 min. After the complete addition of $LiAlH_4$, the reaction mixture was stirred under Ar at 0 °C for another 1 h. The reaction was quenched with 15 ml of ice cold NH_4Cl (saturated aq solution) and stirred for 10 min. The solution was extracted with 3 x 15 ml of EA. The combined organic layers were dried over Na_2SO_4, filtered and concentrated under reduced pressure yielding 341 mg (1.10 mmol, 82 %) of (2-(5-(ethylsulfonyl)-2-methoxyphenylamino)oxazol-5-yl)methanol (**268**). The crude product **268** was prepared in a sufficient purity to be used in the next reaction step.

Note: More precious purification of **268** can be done using FLC (EA + 10 % MeOH). Probably because of high polarity of **268** the yield is usually lowered to approximately 60 %.

Novelty: Synthesis or characterization of **268** has not been described in the literature.

M.p.: 155 – 156 (dec) °C [EA]. Pale yellow solid material.

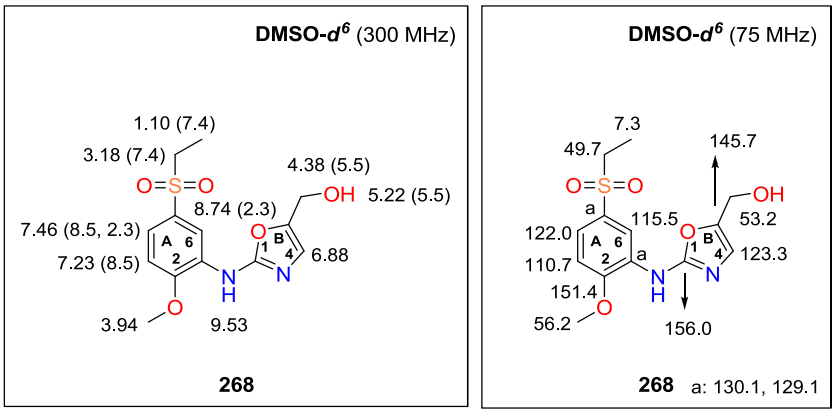

^{1}H-NMR (300 MHz, DMSO-*d*^{6}): δ 9.53 (s, 1H, -NH-), 8.74 (d, 1H, $J(A_4,A_6)$ = 2.3 Hz, H-C_A(6)), 7.46 (dd, 1H, $J(A_3,A_4)$ = 8.5 Hz, $J(A_4,A_6)$ = 2.3 Hz, H-C_A(4)), 7.23 (d, 1H, $J(A_3,A_4)$ = 8.5 Hz, H-C_A(3)), 6.88 (s, 1H, H-C_B(4)), 5.22 (t, 1H, $J(CH_2,OH)$ = 5.5 Hz, -$CH_2O\underline{H}$), 4.38 (d, 2H, $J(CH_2,OH)$ = 5.5 Hz, -$C\underline{H}_2OH$), 3.94 (s, 3H, -OCH_3), 3.18 (q, 2H, $J(CH_2,CH_3)$ = 7.4 Hz, -$SO_2C\underline{H}_2CH_3$), 1.10 (t, 3H, $J(CH_2,CH_3)$ = 7.4 Hz, -$SO_2CH_2C\underline{H}_3$).

^{13}C-NMR (75 MHz, DMSO-*d*^{6}): δ 156.0 (C_B(2)), 151.4 (C_A(2)), 145.7 (C_B(5)), 130.1, 129.1, 123.3 (C_B(4)), 122.0 (C_A(4)), 115.5 (C_A(6)), 110.7 (C_A(3)), 56.2 (-OCH_3), 53.2 (-CH_2OH), 49.7 (-$SO_2\underline{C}H_2CH_3$), 7.3 (-$SO_2CH_2\underline{C}H_3$).

FT IR (solid, cm^{-1}): 3457 (m), 3205 (w), 2943 (w), 2839 (w), 1621 (m), 1595 (m), 1574 (s), 1543 (m), 1488 (m), 1461 (s), 1421 (m), 1364 (w), 1291 (s), 1266 (s), 1230 (m), 1220 (m), 1183 (w), 1148 (m), 1135 (s), 1114 (s), 1084 (s), 1044 (m), 1022 (m), 1009 (s), 992 (m), 981 (m), 926 (m), 912 (m), 895 (m), 830 (m), 813 (s), 736 (s), 716 (s), 661 (m), 630 (m).

MS (ESI m/z): 313.1 $[M + H]^+$, 335.1 $[M + Na]^+$; in negative mode 311.2 $[M - H]^-$.

Anal. calcd for $C_{13}H_{16}N_2O_5S$ (312.34): C, 49.99; H, 5.16; N, 8.97; found: C, 50.19; H, 5.04; N, 9.15.

Synthesis of 2-(5-(ethylsulfonyl)-2-methoxyphenylamino)oxazole-5-carbaldehyde (269)

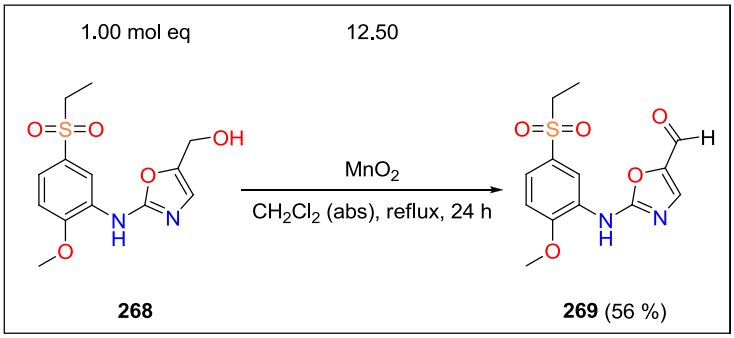

Into a solution of 180 mg (0.60 mmol, 1.00 mol eq) alcohol **268** in 12 ml of CH_2Cl_2 (abs), 251 mg (2.90 mmol, 5.00 mol eq) of MnO_2 (activated, Merck) was added and the reaction mixture was refluxed under Ar for 12 h. Afterwards another 376 mg (4.30 mmol, 7.50 mol eq) of MnO_2 was added into the reaction mixture in three portions (125 mg, 1.50 mmol, 2.50 mol eq) gradually in the period of 4 h. After complete consumption of the starting material **268** (TLC analysis), the reaction mixture was cooled down to RT, filtered through a silica pad and concentrated under reduced pressure. The crude product was purified by FLC (EA) yielding 100 mg (0.30 mmol, 56 %) of 2-(5-(ethylsulfonyl)-2-methoxyphenyl amino)oxazole-5-carbaldehyde (**269**).

Novelty: Synthesis or characterization of **269** has not been described in the literature.

M.p.: 138 – 139 °C [EA]. Pale yellow solid material.

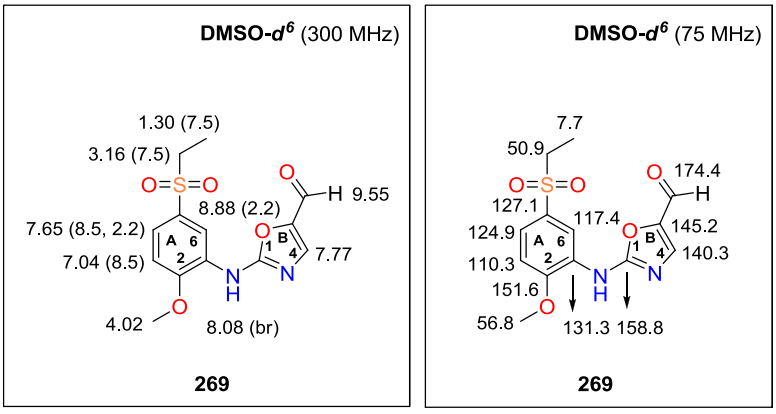

^{1}H-NMR (300 MHz, $CDCl_3$): δ 9.55 (s, 1H, -CHO), 8.88 (d, 1H, $J(A_4,A_6)$ = 2.2 Hz, H-C_A(6)), 8.08 (br s, 1H, -NH-), 7.77 (s, 1H, H-C_B(4)), 7.65 (dd, 1H, $J(A_3,A_4)$ = 8.5 Hz, $J(A_4,A_6)$ = 2.2 Hz, H-C_A(4)), 7.04 (d, 1H, $J(A_3,A_4)$ = 8.5 Hz, H-C_A(3)), 4.02 (s, 3H, -OCH_3), 3.16 (q, 2H, $J(CH_2,CH_3)$ = 7.5 Hz, -$SO_2C\underline{H}_2CH_3$), 1.30 (t, 3H, $J(CH_2,CH_3)$ = 7.5 Hz, -$SO_2CH_2C\underline{H}_3$).

^{13}C-NMR (75 MHz, $CDCl_3$): δ 174.4 (-CHO), 158.8 (C_B(2)), 151.6 (C_A(2)), 145.2 (C_B(5)), 140.3 (C_B(4)), 131.3 (C_A(1)), 127.1 (C_A(5)), 124.9 (C_A(4)), 117.4 (C_A(6)), 110.3 (C_A(3)), 56.8 (-OCH_3), 50.9 (-$SO_2\underline{C}H_2CH_3$), 7.7 (-$SO_2CH_2\underline{C}H_3$).

FT IR (solid, cm^{-1}): 3563 (w), 3399 (w), 3096 (w), 2944 (w), 2846 (w), 1656 (s), 1606 (s), 1567 (s), 1519 (m), 1493 (m), 1448 (w), 1426 (m), 1305 (m), 1383 (m), 1348 (w), 1318 (w), 1292 (m), 1265 (s), 1228 (w), 1198 (m), 1158 (m), 1144 (s), 1120 (s), 1084 (s), 1048 (m), 1024 (s), 978 (m), 916 (m), 891 (w), 817 (m), 802 (m), 762 (s), 735 (s), 720 (s), 661 (m).

MS (ESI m/z): 311.1 $[M + H]^+$, 333.0 $[M + Na]^+$; in negative mode 309.2 $[M - H]^-$.

Anal. calcd for $C_{13}H_{14}N_2O_5S$ (310.33): C, 50.31; H, 4.55; N, 9.03; found: C, 50.51; H, 4.27; N, 9.22.

Chapter 14. **Characterization of the prepared compounds**

14. Characterization of the prepared compounds

Compound			Identity										Purity						
Code	New	Known	M.p.	^{1}H NMR	^{13}C NMR	Different NMR	IR	ESI-MS	Elemental analysis	UV-VIS	X-ray analysis (ORTEP)	e.r. / d.r.	Chiroptical data [α] / CD	fig. ^{1}H NMR spectra	fig. ^{13}C NMR spectra	fig. IR	fig. ESI-MS	fig. Elemental analysis	fig. Chromatogram	Quant. data GC / HPLC
105		√	√	√										√						
198		√	√	√										√						
106		√	√	√										√						
107		√	√	√										√						
2		√	√	√										√						
189	√		√	√	√		√	√	√					√	√	√				
190	√		√	√	√		√	√	√					√	√	√				
191	√		√	√	√	*A*	√	√	√					√	√	√				
192		√	√	√										√						
203		√	√	√										√						
204	√		√	√	√	*A*	√	√	√		√			√	√	√				
206	√		√	√	√	*A*	√	√	√					√	√	√				
207	√		√	√	√	*A*	√	√	√					√	√	√				
205	√		√	√				√						√						
226	√		√	√										√						
208	√		√	√										√						
227	√		√	√	√		√	√	√					√	√	√				
228		√	√	√	√		√		√					√	√	√				

A – COSY, HSQC

Characterization of the prepared compounds

Compound			Identity											Purity						
Code	New	Known	M.p.	^{1}H NMR	^{13}C NMR	Different NMR	IR	ESI-MS	Elemental analysis	UV-VIS	X-ray analysis (ORTEP)	e.r. / d.r.	Chiroptical data [α] / CD	fig. ^{1}H NMR spectra	fig. ^{13}C NMR spectra	fig. IR	fig. ESI-MS	fig. Elemental analysis	fig. Chromatogram	Quant. data GC / HPLC
209		√	√	√										√						
230		√	√	√										√						
231		√	√	√										√						
210	√		√	√	√		√	√	√					√	√	√				
211	√		√	√	√		√	√	√					√	√	√				
232	√		√	√	√		√	√	√					√	√	√				
212	√		√	√	√		√	√	√					√	√	√				
233		√	√	√										√						
234		√	√	√										√						
235		√	√	√	√		√		√					√	√	√				
213		√	√	√										√						
214	√		√	√	√		√	√	√					√	√	√				
237		√	√	√										√						
238	√		√	√	√		√		√					√	√	√				
215	√		√	√	√		√	√	√					√	√	√				
216	√		√	√	√		√	√	√					√	√	√				
239	√		√	√	√		√	√	√					√	√	√				
217	√		√	√	√		√	√	√					√	√	√				
218	√		√	√	√		√	√	√					√	√	√				
219	√		√	√	√		√	√	√					√	√	√				

Compound			Identity										Purity						
Code	New	Known	M.p.	^{1}H NMR	^{13}C NMR	Different NMR	IR	ESI-MS	Elemental analysis	UV-VIS	X-ray analysis (ORTEP)	e.r. / d.r.	Chiroptical data [α] / CD	fig. ^{1}H NMR spectra	fig. ^{13}C NMR spectra	fig. IR	fig. ESI-MS	fig. Elemental analysis	fig. Chromatogram	Quant. data GC / HPLC
220	√		√	√	√		√	√	√					√	√	√				
221	√		√	√	√		√	√	√					√	√	√				
245	√		√	√	√		√	√	√					√	√	√				
248		√	√	√										√						
250		√		√										√						
187		√		√										√						
251	√		√	√	√		√	√	√					√	√	√				
252	√		√	√	√		√	√	√					√	√	√				
253	√		√	√	√		√	√	√					√	√	√				
254	√		√	√	√		√	√	√					√	√	√				
223	√		√	√	√		√	√	√					√	√	√				
264		√	√	√										√						
265		√	√	√										√						
266		√		√										√						
267		√	√	√										√						
268	√		√	√	√		√	√	√					√	√	√				
269	√		√	√	√		√	√	√					√	√	√				

Chapter 15. **Annex – Published papers**

European Journal of Medicinal Chemistry 126 (2017) 754–761

Contents lists available at ScienceDirect

European Journal of Medicinal Chemistry

journal homepage: http://www.elsevier.com/locate/ejmech

Research paper

Novel CLK1 inhibitors based on *N*-aryloxazol-2-amine skeleton - A possible way to dual VEGFR2 TK/CLK ligands

Miroslav Murár [a], Juraj Dobiaš [a], Peter Šramel [a, c], Gabriela Addová [b], Gilles Hanquet [c], Andrej Boháč [a, d, *]

[a] Department of Organic Chemistry, Faculty of Natural Sciences, Comenius University in Bratislava, Mlynská Dolina, Ilkovičova 6, 842 15 Bratislava, Slovakia
[b] Institute of Chemistry, Faculty of Natural Sciences, Comenius University in Bratislava, Mlynská Dolina, Ilkovičova 6, 842 15 Bratislava, Slovakia
[c] Université de Strasbourg, Ecole Européenne de Chimie, Polyméres et Matériaux (ECPM) Laboratoire de Synthése et Catalyse (UMR CNRS 7509), 25, Rue Becquerel, F-67087 Strasbourg, France
[d] Biomagi, Ltd., Mamateyova 26, 851 04 Bratislava, Slovakia

ARTICLE INFO

Article history:
Received 4 July 2016
Received in revised form
29 October 2016
Accepted 2 November 2016
Available online 18 November 2016

Keywords:
Dual CLK1/VEGFR2 kinase ligands
CDK9
GSK3
DYRK1A
GSK3α/β
Muti-targeted kinase inhibitors

InChIKeys:
XQSZOOXIJIGDLV-UHFFFAOYSA-N
ZIKVYDDNZDVYHF-UHFFFAOYSA-N
YIEXHVPVWYOPCC-MDZDMXLPSA-N
IPHOJHHAZPKUQW-UHFFFAOYSA-N

ABSTRACT

Background: Inhibitors of CLK protein kinases suppress cell growth and induce apoptosis by modulating pre-mRNA splicing in cancer. CLK family kinases are also involved in alternative splicing and RNA processing in *Duchenne muscular dystrophy*, *Alzheimer's disease*, *HIV-1*, and *influenza virus*. Small inhibitors are valuable tools for better understanding the molecular mechanisms of splicing and may serve as seeds for a novel class of therapeutics.

Achievements: Here we describe a discovery of four novel CLK1 inhibitors possessing *N*-aryloxazol-2-amine skeleton. Their activity against CLK1 (IC_{50}: 20, 30, 40 and 80 nM) and some other CMGC kinases, predicted CLK binding poses, synthesis and physico-chemical characteristics are also stated. Additionally analysis of all PDB available CLK structures and interactions of their ligands was performed. There are only few powerful dual CLK/VEGFR inhibitors known in the literature. We proposed that our inhibitors have similar binding places and interactions in CLK1, 3 and VEGFR2 TK mostly due to the joint *N*-aryloxazol-2-amine pharmacophoric fragment. One of our *N*-aryloxazol-2-amines already proved a good activity against both VEGFR2 and CLK1 enzymes (23/80 nM, resp). We proposed that the presented class of compounds has a potential to be developed in dual VEGFR2/CLK clinical compounds with prospective synergy to treat cancer.

1. Introduction

Alternative splicing is a regulated process during the gene expression that greatly increases the biodiversity of proteins and allows the human genome to direct the synthesis of many more proteins (50–100 000) than would be expected from human 20 000 protein-coding genes [1]. There is a growing recognition of the importance of protein kinases in the control of alternative splicing. Splicing requires reversible phosphorylation of serine/arginine-rich (SR) proteins in eukaryotic mRNA. These phosphorylation events are dependent on SR proteins and cdc2-like kinase (CLK) families [2]. The CLKs are an evolutionarily conserved group belonging to the CMGC Ser/Thr protein kinase family from Human Kinome [3,4] (for CMGC part see supplementary material (chapter: *CLKs in the Human Kinome*). CLKs are primarily localized to the cytoplasm and nucleus [5]. CLKs are part of LAMMER PK family possessing identity of the motif "EHLAMMERILG" in their kinase subdomain (see supplementary material: chapter *Superimposed CLKs with marked LAMMER subdomain*). This motif was reported to be essential for kinase activity [6]. CLKs (CDC2-like or LAMMER kinases) are dual specific kinases that have been shown to autophosphorylate on serine, threonine and tyrosine residues and phosphorylate exogenous substrates on serine and threonine residues. The CLK family kinases are found in diverse species, from yeast to human. A critical role of the CLK family kinases is the regulation of mRNA splicing. CLK have shown to interact with, and phosphorylate, serine- and arginine-rich (SR) proteins [7,8]. SR

* Corresponding author. Biomagi, Ltd., Mamateyova 26, 851 04 Bratislava, Slovakia.
E-mail address: andrej.bohac@fns.uniba.sk (A. Boháč).

http://dx.doi.org/10.1016/j.ejmech.2016.11.003
0223-5234/

proteins are splicing factors that regulate the assembly of the spliceosome, a macromolecular complex where RNA splicing occurs in nucleus [9]. CLKs can co-exist as full-length catalytically active and alternatively-spliced truncated inactive forms [10]. The CLK family consists of four isoforms CLK1-4 exhibiting the typical protein kinase fold (see supplementary material: chapter *Graphical abstract*). CLK1-4 isoforms possess different length of amino acids (AAs) chain: Clk1 (484 AAs), Clk2 (499 AAs), Clk3 (638 AAs), Clk4 (481 AAs) [11]. CLK1 regulates its own splicing [12]. CLKs inhibitors suppress cell growth and induce apoptosis by modulating pre-mRNA splicing in cancer [13]. CLK family kinases are also involved in alternative splicing and RNA processing in *Duchenne muscular dystrophy, Alzheimer's disease, HIV-1*, and *influenza virus* [14]. CLK1 is involved in the pathophysiology of *Alzheimer's* disease, hence the inhibition of CLK1 can be used as a therapeutic strategy for it [9]. CLK1 in the host cells is responsible for alternative splicing of the M2 gene of influenza virus during influenza infection and replication. Therefore CLK1 inhibitors may have potential in anti-influenza drug screening [15]. CLK1 has been shown to interact and phosphorylate other protein kinases as well as protein phosphatases [12]. Human CLK2 links cell cycle progression, apoptosis and telomere length regulation [16]. CLK2 acts as a suppressor of hepatic gluconeogenesis and glucose output [17]. CLK2 is overexpressed in breast tumours. Downregulation of CLK2 inhibits breast cancer growth [18]. CLK3 is a protein kinase with a non-conserved *N*-terminal domain.

CLK small molecule inhibitors are valuable tools for better understanding the molecular mechanisms of splicing and may serve as seeds for a novel class of therapeutics [2,14].

The limitations of many mono-kinase inhibitors can be overcome by agents with multi-target action by increasing their potency, due to the synergistic effect. A review was published in 2015 about the most recent examples of multi-kinase inhibitors [19]. Some dual inhibitors for distanced kinases CLK1 and CK1 were developed recently based on pyrido[3′, 2′:4, 5]thieno[3, 2-*d*]pyrimidin-4-amine skeleton [20].

Table 1
hu-CLK structures published in PDB database.

	Protein structure[a]	Kinase/ligand complex structure[a]
hu-CLK1[b]	none	PDB: 2VAG (**V25**; IC_{50} = 19.7 nM; 2007, 1.80 Å, diphosphorylated kinase) [22] PDB: 1Z57 (**DBQ**;[c] 2005, 1.70 Å) [2]
hu-CLK2[b]	none	PDB: 3NR9 (**NR9**; 2010, 2.89 Å) [23]
hu-CLK3[b]	PDB: 2EU9 (2005, 1.53 Å) [2] PDB: 2EXE (2005, 2.35 Å, phosphorylated) [24][e]	PDB: 3RAW (**3RA**;[d] 2011, 2.09 Å) [25] PDB: 2WU6 (**DKI**; IC_{50} = 29.2 nM; 2009, 1.92 Å) [22] PDB: 2WU7 (**V25**; IC_{50} = 530 nM; 2009, 2.25 Å) [22]
hu-CLK4	none	none

[a] The data are described in the following order: PDB: code (**ligand code,** it's activity; year of deposition in PDB DB; X-ray resolution; notes, if any).
[b] All CLK kinase structures in PDB are in an active DFG-IN conformation: DFG fragment (Asp-Phe-Gly triade and their isoform specific primary sequence numbers: 325–327 (hu-CLK1), 327–329 (hu-CLK2), 320–322 (hu-CLK3).
[c] Also known as 10*Z*-Hymenialdisine.
[d] Also known as leucettine (L41).
[e] This is an incomplete structure of CLK3.

2. Results and discussion

2.1. Analysis of hu-CLKs structures in PDB

With the aim to perform docking experiments we analysed CLKs structures in the PDB database [21]. Currently, there are 8 X-ray structures of human CLK1-3: two hu-CLK3 proteins and six CLK1-3/ligand complexes. No structure of hu-CLK4 was published. According to our analysis, all CLK structures in PDB are in an active DFG-IN kinase conformation (Table 1).

2.2. Analysis of hu-CLKs PDB ligand interactions

To understand the ligand/CLK bindings, interactions diagrams of all inhibitors (2×**V25**, **DBQ**, **DKI**, **NR9** and **3RA**) from PDB hu-CLK complexes were composed. The ligand structures on diagrams are drawn uniformly according their positions in an *Africa*-like kinase perspective [26]. Some biological activities of CLK PDB inhibitors are listed too [27]. The data for all CLKs PDB ligands can be found in supplementary material (chapter: *Analysis of hu-CLKs PDB ligand interactions*). Here we present an example of analysis for ligand **V25** from both complexes CLK1 (PDB: 2VAG) and CLK3 (PDB: 2WU7). (Fig. 1**).**

2.2.1. (*E*)-Ethyl 3-(2-amino-1-cyanovinyl)-6,7-dichloro-1-methyl-1*H*-indole-2-carboxylate (***V25***) in complex with hu-CLK1 and ***3***

For compound **V25** [SciFinder CAS: 1354037-26-5; Reaxys RRN: 21739116] the following IC_{50} activities were described in the literature: hu-CLK1 (19.7 nM), hu-CLK3 (530 nM) and hu-DYRK1A (55.2 nM) [27].

2.3. Interaction diagrams

See Fig. 1.

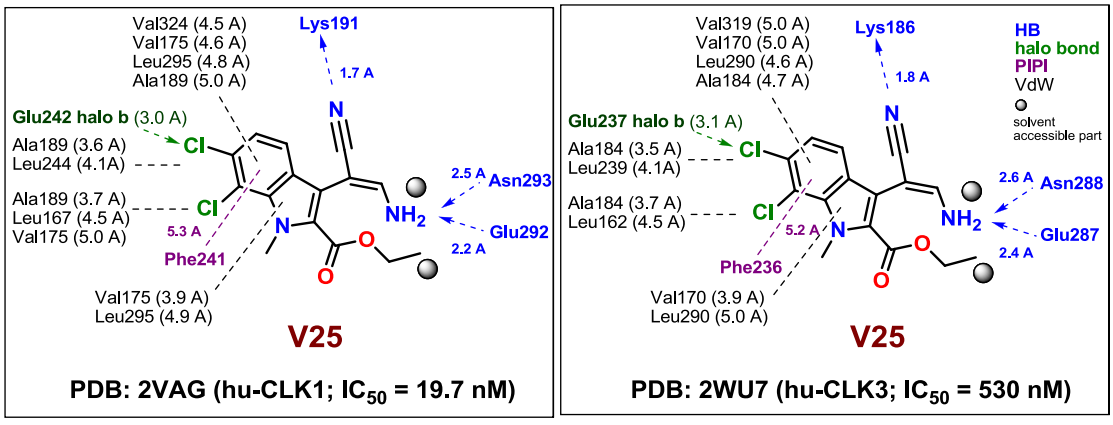

Fig. 1. The structure and intermolecular interactions of **V25** determined in hu-CLK1 and 3 complexes.

2.4. CLKs inhibitors

In order to know how many inhibitors exist, CLKs abbreviations and synonyms [28] were collected and used to search biological active CLK compounds in the Reaxys DB [27]. The search resulted in the amount of inhibitors depicted for each kinase in parenthesis: CLK1 (176), CLK2 (108), CLK3 (84), CLK4 (261). By combining the above hit sets, we found 388 known compounds connected with CLKs activities.

2.5. Clinical drugs as CLKs inhibitors

There are only few clinical drugs able to inhibit CLK kinases. The drugs CLK activities were mostly determined by searching their side effects [29] by screening pharmaceutical compounds against 456 human kinases (*Kinome scan*). The determined drug CLK affinities are as follows: CLK1 (sunitinib K_D = 22 nM, bosutinib K_D = 600 nM, nilotinib K_D = 2100 nM); CLK2 (sunitinib K_D = 20 nM, ruxolitinib K_D = 460 nM, bosutinib K_D = 1700 nM); CLK3 (bosutinib K_D = 300 nM); CLK4 (sunitinib K_D = 29 nM, ruxolitinib K_D = 1700 nM, imatinib K_D = 2100 nM). The above drugs were developed for different primary target(s) as CLKs. From them only sunitinib was developed against VEGFR2 TK. The dual CLK and VEGFR2 activities of sunitnib are interesting because both CLKs and VEGFR2 inhibitors are important as potential anticancer drugs.

2.6. VEGFR2 TK drugs

VEGFR2 TK (also named as KDR kinase) is an important receptor for VEGF signalling. VEGF is a key mediator of angiogenesis in cancer [30]. Similarly as for CLKs above we identified 6299 active compounds against VEGFR1-3 in Reaxys DB. Within recent ten years pharmaceutical companies produced nine approved anticancer drugs inhibiting VEGFR2 TK [31]. Their structures, year of approval and name of owning pharma company are published in supplementary material (chapter: *A list of VEGFR2 approved drugs*).

2.7. Synthesis of CLK1 inhibitors **6**, **10**, **21** and **29**

CLK1 inhibitors **6**, **10**, **21** and **29** and their intermediates were prepared according the procedures depicted on Schemes 1–4. Synthetic details, characterisation and figures of spectra of all compounds are stated in supplementary material (chapter: *Supplementary Experimental*).

2.8. Biological screening

Compounds **6**, **10**, **21** and **29** previously developed to inhibit VEGFR2 TK were screened on eleventh protein kinases by radiometric protein kinase assay in 10 semi-logarithmic concentrations on a panel of eleventh protein kinases: CDK2/CyclinA (cyclin-dependant kinase); CDK5/p25; CDK9/CyclinT; PIM1 (proto-oncogene serine/threonine-protein kinase); DYRK1A (dual specificity tyrosine-phosphorylation-regulated kinase); GSK3α/β (glycogen synthase kinase); GSK3; CLK1 (CDC2-like or LAMMER family dual specificity protein kinase); CK1δ/ε (caseine kinase 1); CK1; HASPIN (haploid germ cell-specific nuclear protein kinase); AURKB (Aurora kinase B); RIPK3 (receptor-interacting serine/threonine-protein

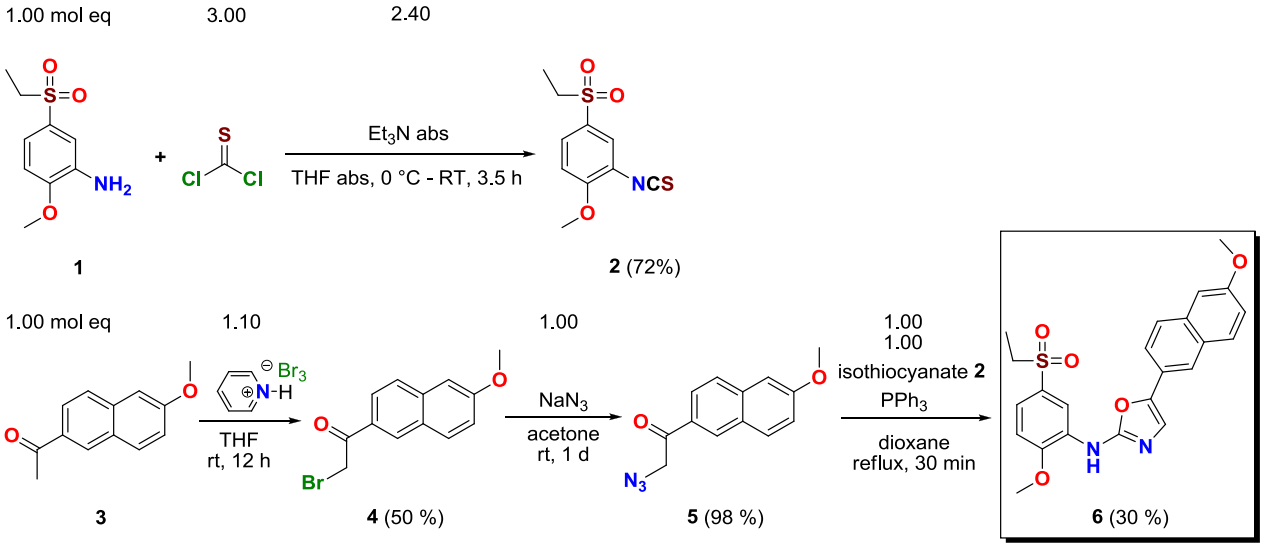

Scheme 1. Synthetic pathway to final naphthalenyloxazolamine **6**.

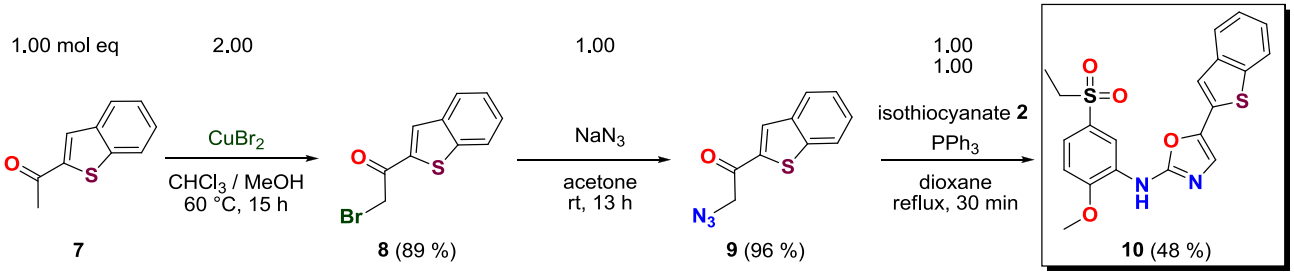

Scheme 2. Synthetic pathway to required benzothiophenyloxazolamine **10**.

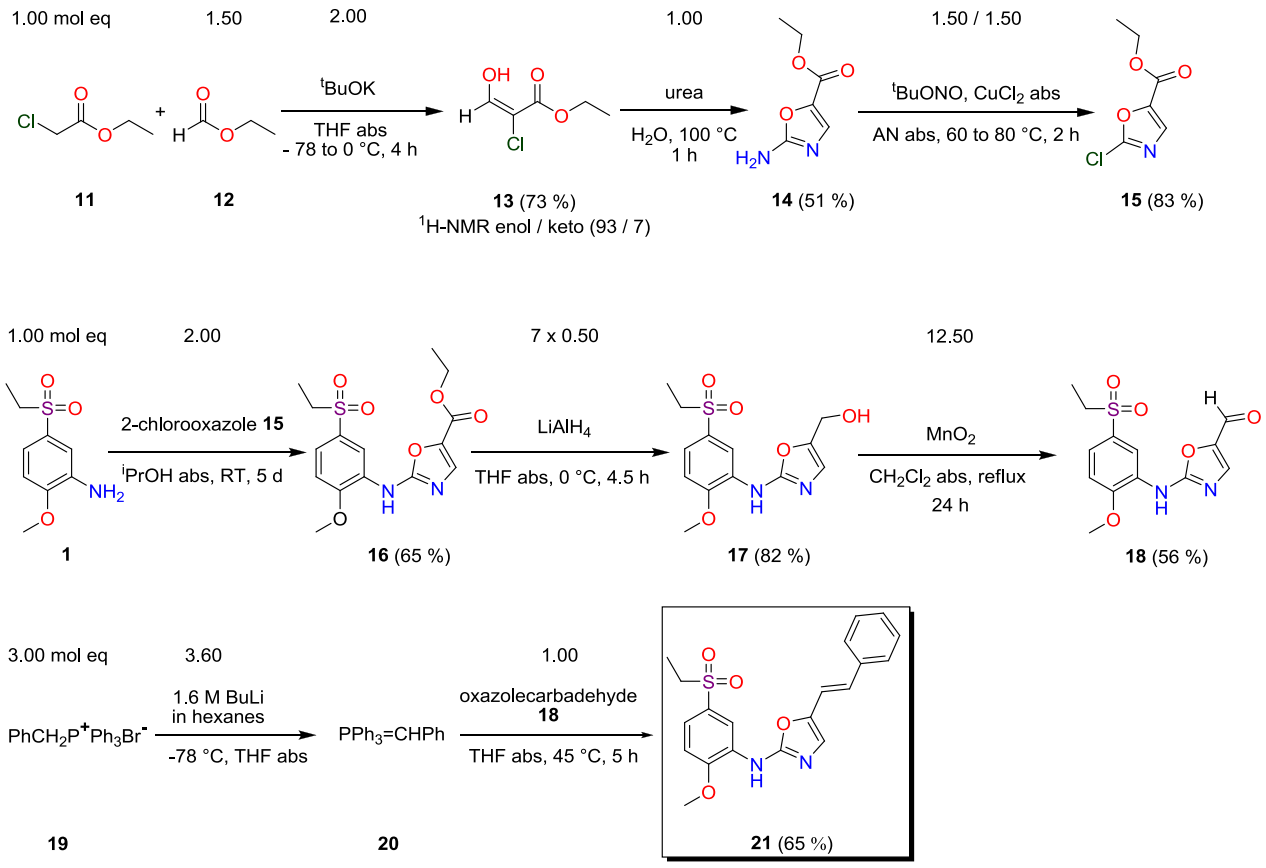

Scheme 3. Synthesis of final styryloxazolamine **21**.

kinase) and TLK (tousled-like kinase). The IC_{50} activities were obtained by Dr. Stéphane Bach and Thomas Robert (Station Biologique de Roscoff, Place Georges Teissier, CS 90074, 29688 Roscoff cedex, France). All compounds **6**, **10**, **21** and **29** were showed to be powerful CLK1 inhibitors. The results are given in Fig. 2. (see also the Supplementary material chapter *Biological activity assay*) Compound **29** was screened likewise on VEGFR2 TK activity. Surprisingly, this compound performed dual VEGFR2/CLK1 kinase activity even though VEGFR2 is not relative kinase to CLKs and belongs to distant TK subgroup in the Human Kinome [4].

2.9. Predicted CLK1 inhibitors binding poses

In order to find binding poses for CLK1 inhibitors (**6**, **10**, **21** and

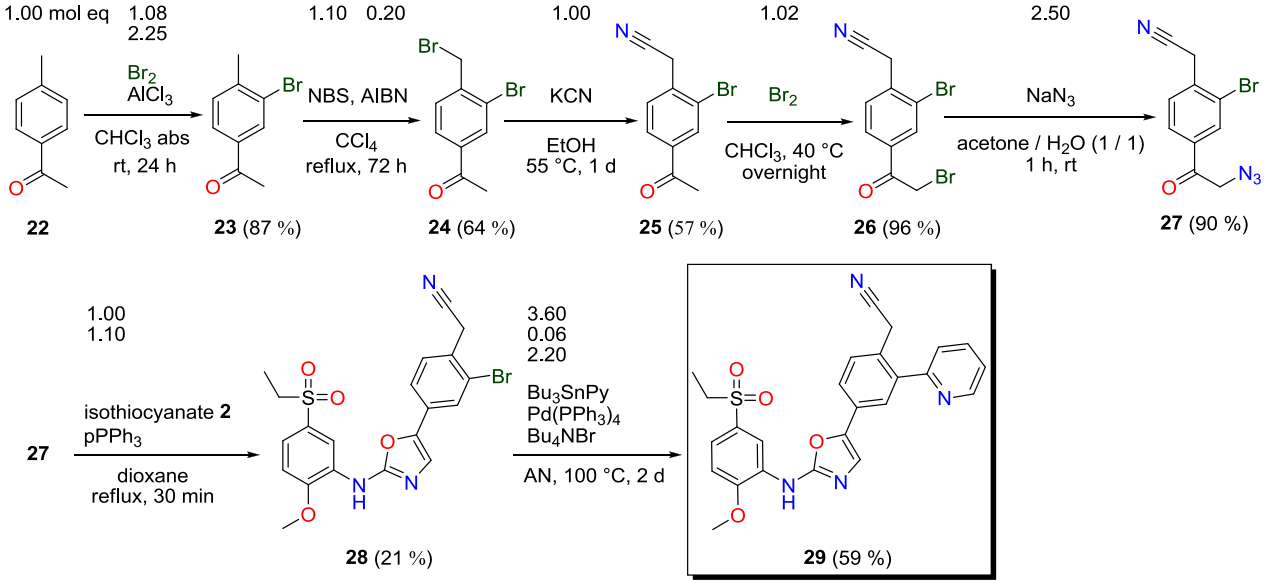

Scheme 4. Synthetic pathway to aminooxazolephenylacetonitrile **29**.

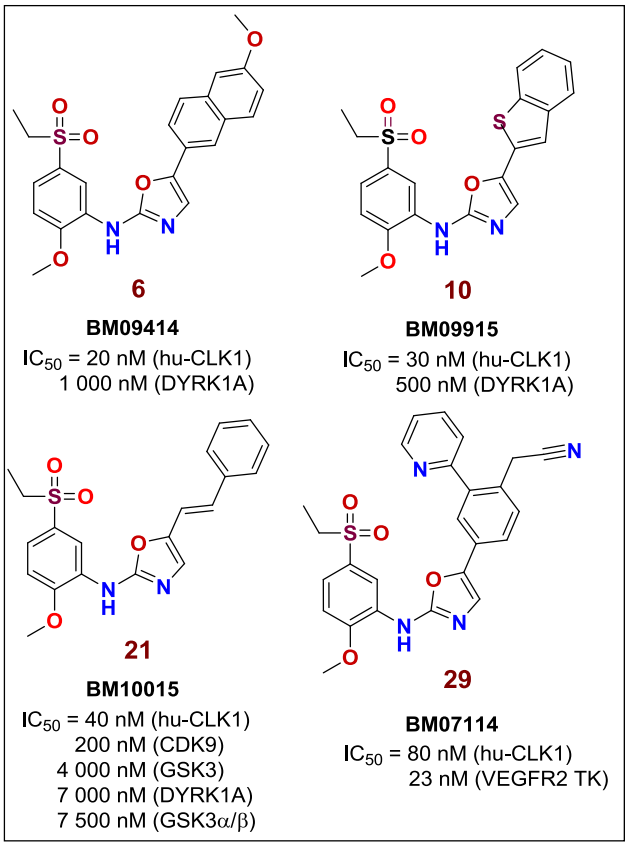

Fig. 2. Novel hu-CLK1 inhibitors **6**, **10**, **21**, **29** and their biological activities determined against some CMGC protein kinases together with VEGFR2 TK activity for **29**.

29), docking experiments [32] on seven CLK proteins from PDB DB were performed. An incomplete 2EXE structure of CLK3 was excluded (Table 1). Most of the PDB CLK proteins showed to be unfavourable for docking experiments due to their inappropriate kinase conformation. Only the kinase variant from hu-CLK3 (2WU6) significantly outperformed the other models by docking scores and predicted poses for all ligands (**6**, **10**, **21** and **29**). As can be seen from ligands superimpositions especially the poses of their joint *N*-aryloxazole-2-amine parts were almost identical (Fig. 3).

The most active inhibitor **6** (IC_{50} = 20 nM) was predicted to form three hydrogen bonds (HBs) with two amino acids Leu239 and Asn242 (both from a kinase hinge region) and one ligand specific HB between -OMe group and Lys186. Moreover, *N*-aryloxazole-2-amine ligands showed their poses and binding interactions to be similar in both hu-CLK3 (2WU6) and VEGFR-2 TK (1Y6A) (Figs. 4 and 7).

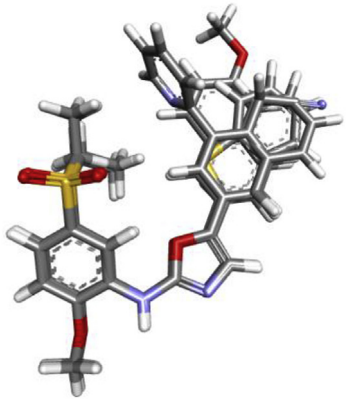

Fig. 3. The superimposed poses of inhibitors **6**, **10**, **21** and **29** from aligned complexes obtained after ligands docking in CLK3 (2WU6) protein conformer.

As mentioned above, both available CLK1 (1Z57, 2VAG) were not suitable for docking of our CLK1 inhibitors. In order to investigate problematic amino acid residues predicted CLK3 (2WU6)/(**6, 10, 21** and **29**) complexes were aligned with both CLK1 protein conformers. Then we could recognise that the most important unfavourable ligand interactions in CLK1 (2VAG) were between an amino group of *N*-aryloxazol-2-amines and too closely located carbonyl group of Leu244 from a hinge region. Due to the above repulsion the structures (**6**, **10**, **21** and **29**) could not be stabilized in good position in CLK1 (2VAG) (Fig. 5). In cases of **6** and **29** also some steric clashes with Phe172 were seen but they disappeared after a problematic ligand group rotation.

In the other CLK1 (1Z57) conformer, the most important unfavourable interactions were identified between the oxygen from -SO_2Et group of the ligand and too close positioned carboxylate oxygen from a hinge Asp250. This interaction could not be eliminated by simple changing the conformation of -SO_2Et group. The problematic Asp250 in CLK1 (1Z57) is replaced by Glu245 in CLK3 (2WU6). Even though positions of Asp250 and Glu245 are similar, the problematic carboxylate in larger Glu245 is folded out of the -SO_2Et ligand group excluding so unfavourable interactions in CLK3 compared to CLK1 (Fig. 6). Similarly as in CLK1 (2VAG) also in CLK1 (1Z57) the inhibitors **6** and **29** possess some clashes also with Phe172. (see Table 2).

To conclude the above observation, a different conformation of CLK1 kinase will be required to find the correct binding poses for *N*-aryloxazole-2-amine ligands with respect to their CLK1 activity. Therefore we aligned CLK1 proteins (1Z57, 2VAG) with **6**/CLK3 (2WU6) complex. In order to enable improved ligand docking to CLK1 the geometry minimization was carried out on both CLK1 (1Z57, 2VAG) conformers with ligand **6** from CLK3 (2WU6) complex. This approach resulted in CLK1 optimized protein models (1Z57opt, 2VAGopt) with significantly improved performance to give docked CLK1 inhibitors (**6**, **10**, **21** and **29**) positioned to keep essential hinge hydrogen bonds and docking scores that followed their IC_{50} values. These models will be used for further CLK1 ligands development. (see supplementary material, chapter: *Predicted inhibitors binding poses in CLK1 optimized protein*).

2.10. *N*-aryloxazole-2-amines in VEGFR2 and CLK

Compound **29** inhibits both kinases VEGFR2 (IC_{50} = 23 nM) and CLK1 (IC_{50} = 80 nM). The reason for a dual kinase activity of **29** can be explained by its similar binding pose and interactions in each kinase where the pair of hinge amino acid residues (Cys917/Asn921 in VEGFR2; Leu239/Asn242 in CLK3 or Leu244/Ser247 in CLK1) fixes a pharmacophoric *N*-arylooxazole-2-amine group in an ATP binding pocket. The interaction diagrams for ligands **AAZ**/VEGFR2 and **6**/CLK3 were composed. (Fig. 7).

2.11. Dual VEGFR/CLK active compounds

With aim to determine the amount of dual VEGFR/CLK inhibitors an intersection between previously found 388 CLKs inhibitors and 6299 VEGFRs TKIs in Reaxys DB was performed. This experiment resulted in 85 dual modulators with activities mostly determined between 1 and 10 μM concentrations. Many of duals were uncovered by searching target-off activities through Kinome scan for another biomacromolecule against that compounds were primarily developed. As we have seen, the activities of many of them were not very important or they were unbalanced for both

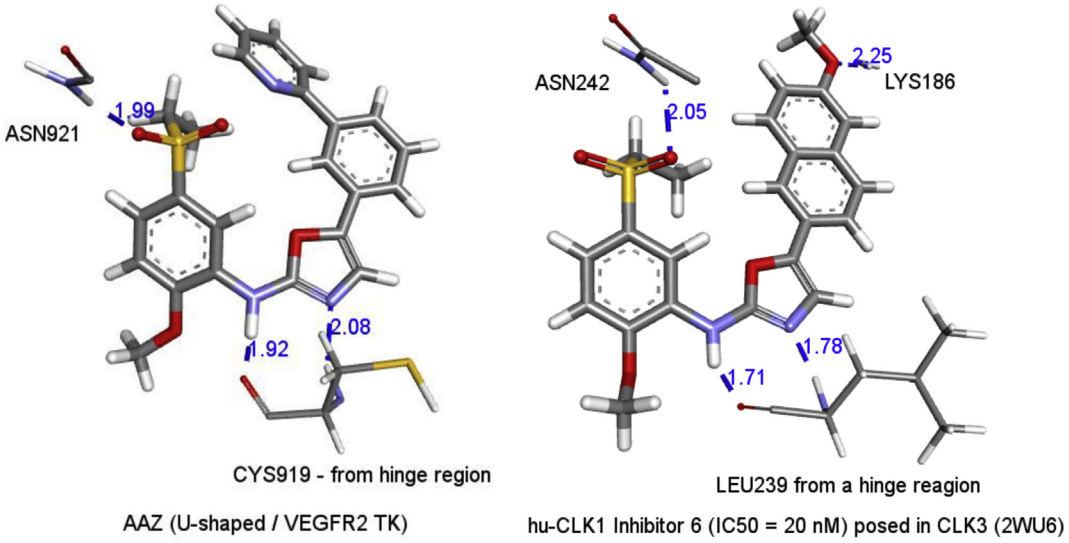

Fig. 4. Interactions of **AAZ** in VEGFR2 TK (1Y6A) and **6** in CLK3 (2WU6) to demonstrate similar binding interactions of *N*-aryloxazol-2-amine in both kinases.

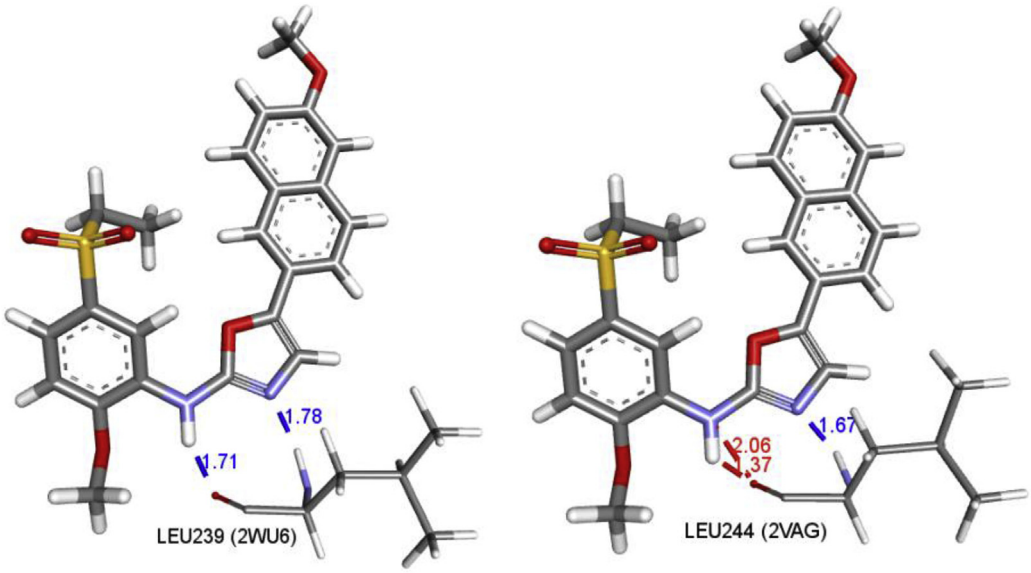

Fig. 5. In the left: the predicted pose of inhibitor **6** in CLK3 (2WU6) showing two hydrogen bonds (1.7 and 1.8 Å, in blue) with a hinge Leu239. In the right: Inhibitor **6** positioned in CLK-1 (2VAG) possessing unfavourable interactions with Leu244 (2.06 Å electrostatic repulsion, 1.4 Å steric clash, both in red). (For interpretation of the references to colour in this figure legend, the reader is referred to the web version of this article.)

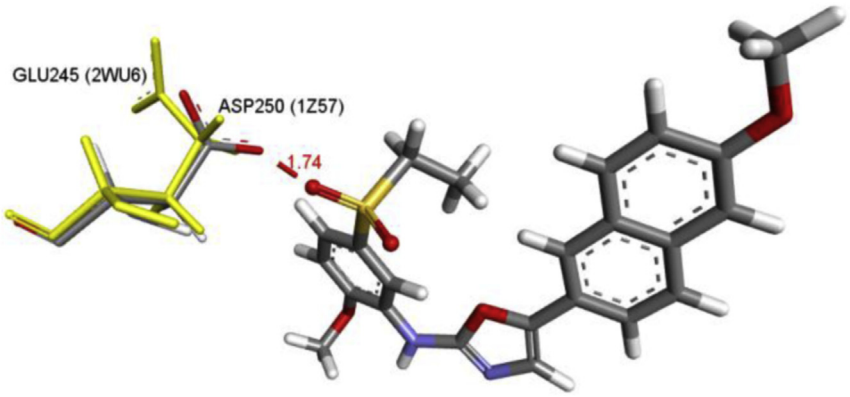

Fig. 6. A complex **6**/CLK3 (2WU6), obtained after docking, was aligned with CLK1 (1Z57) kinase. A hinge Glu245 from CLK3 (2WU6) is replaced by Asp250 (yellow) in CLK1 (1Z57) and forms unfavourable interaction with oxygen from -SO_2Et group of **6**. Observed strong electrostatic repulsion (1.7 Å, red) is hindering ligand **6** to be docked in CLK1 (1Z57) in an appropriate position. (For interpretation of the references to colour in this figure legend, the reader is referred to the web version of this article.)

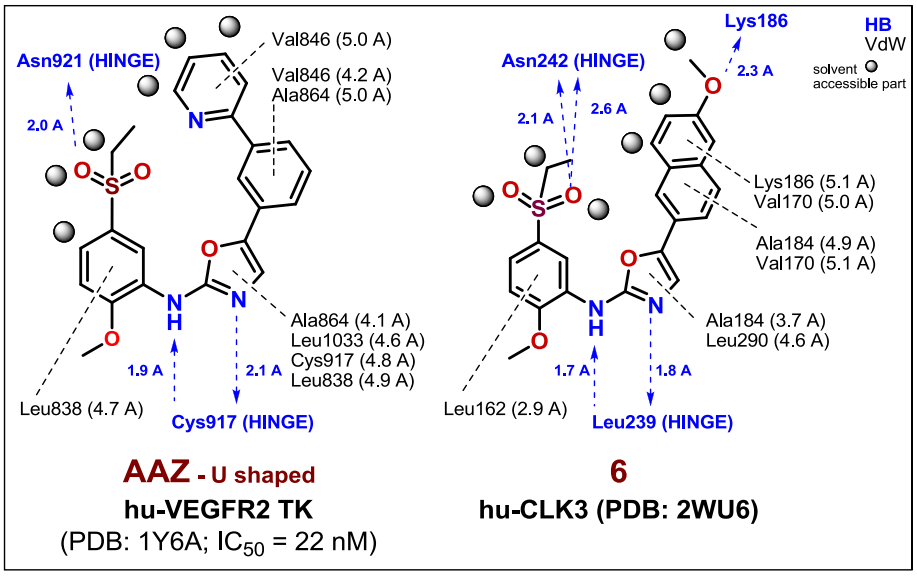

Fig. 7. The interactions of **AAZ** ligand with VEGFR2 TK and **6** in CLK3 are very similar especially for their joint *N*-aryloxazole-2-amine part.

Table 2
A summary for *N*-aryloxazole2-amine **6** interactions favourable for CLK3 (2WU6) kinase and problematic for both CLK1s (2VAG, 1Z57) proteins.

	oxazole-2-amine of **6**	-SO_2Et of **6**
CLK3 (2WU6)	hinge-Leu239 (CO, NH: 1.7, 1.8 Å)	hinge-Asn242 ($CONH_2$: 2.1 Å)
CLK1 (2VAG)	hinge-Leu244 (NH: 1.7 Å) UI: Leu244 (CO) (1.4, 2.1 Å)	hinge-Ser247 (NH: 2.5 Å)
CLK1 (1Z57)	hinge-Leu244 (CO, NH) (2 × 1.8 Å)	hinge-Ser247 (NH: 2.5 Å) UI Asp250 (COO^-: 1.7 Å)

UI: unfavourable interactions in CLK3, CLK1 isoforms possessing some replaced AAs residues (Leu239 to Leu244 and Asn242 to Ser 247, resp.).

kinases. A list of Reaxys codes (RRN) for 85 dual inhibitors are given in supplementary material (chapter: *Reaxys RRN codes of 85 compounds possessing dual VEGFR/CLK activities*). Among 85 structures there are about 7 with more balanced CLKs/VEGFRs activities (RRN: 18647647, 20385666, 20278959, 22546881, 20385602, 21237166 and 22449988.). One structure, a triazole-staurosporine like compound (RRN: 18647647, CAS: [1359754-81-6]) possess submicromolar bivalent activities to VEGFR2 and CLK2 (200/350 nM, resp.) [33]. We found also that sunitinib (RRN: 15426924, [CAS: 341031-54-7]) a multi-targeted tyrosine kinase ligand (PDGF, VEGFR2 TK) has strong ability to inhibit CLKs. K_D affinities for sunitinib are listed here: CLK1 (22 nM) CLK2 (20 nM), CLK4 (29 nM) [29]. There are only few powerful and activity balanced dual VEGFR2/CLKs inhibitors described in the literature. Such compounds could be advantageous for the development of clinical drugs treating tumours by two VEGFR2 and CLKs independent pathways. From this point of view *N*-aryloxazol-2-amine CLK1 inhibitors (**6**, **10**, **21** and **29**) previously designed as VEGFR2 TKIs seem to be a good starting point for such development.

3. Conclusions

Four novel *N*-aryloxazol-2-amine CLK1 inhibitors (**6**, **10**, **21** and **29**) were identified and their ATP binding poses in CLK kinase were predicted. Compound **29** has comparable activity for CLK1 and VEGFR2 TK. The observed dual inhibition of **29** was explained by similar binding interactions of its pharmacophoric *N*-(5-(ethylsulfonyl)-2-methoxyphenyl)oxazol-2-amine fragment that has joint affinities to CLK1 and VEGFR2 kinases *via* hinge amino acid residues HBs. We found that there are only few dual VEGFR/CLK inhibitors with comparable and strong activities on both targets. Such dual kinase compounds could be advantageous for development of clinical compounds targeting tumours by two independent and synergy pathways. Therefore presented *N*-aryloxazole-2-amine CLK1 inhibitors (**6**, **10**, **21** and **29**) can be used in the further study of the molecular mechanisms of splicing and seem to be also good seeds for development a novel class of VEGFR2/CLKs dual kinase therapeutics.

4. Experimental

The syntheses of biologically active compounds **6, 10, 21** and **29** and their intermediates are described in the Supplementary material *(chapter: Supplementary Experimental)*.

Acknowledgements

The research was supported by Biomagi, Ltd. (development of kinase research, compounds design and selection), VEGA 1/0634/13 (organic synthesis), bilateral project APV SK-FR-2015-0014 (researchers and student exchange), program Cotutelle and Collège Doctoral Européen - Université de Strasbourg (support for joint PhD student PŠ), ITMS 26240220007 (HPLC MS), Comenius University Science Park - 2.phase. Our big thanks belong to Dr. Nadine Martinet (Consultant in Cosmetics and Medicinal Chemistry, Nice, France, nadine.martinet1@free.fr) for chemistry/biology networking and Dr. Stéphane Bach (bach@sb-roscoff.fr) from Station Biologique de Roscoff, France for biological screening. Our

acknowledgement is addressed also to European cooperation in science and technology COST Actions: StemChem CM1106 and MuTaLig CA15135 for research networking. This paper is dedicated to our teachers and enthusiastic colleagues prof. Marta Sališová and prof. Margita Lácová from Comenius University in Bratislava, Slovakia. We appreciate their research knowledge, management and personal behaviour that we and our students could and still can learn from them.

Appendix A. Supplementary data

Supplementary data associated with this article can be found in the online version, at http://dx.doi.org/10.1016/j.ejmech.2016.11.003. These data include MOL files and InChiKeys of the most important compounds described in this article.

References

[1] D.L. Black, Mechanisms of alternative pre-messenger RNA splicing, Annu. Rev. Biochem. 72 (2003) 291–336, http://dx.doi.org/10.1146/annurev.biochem.72.121801.161720.
[2] A.N. Bullock, S. Das, J.E. Debreczeni, P. Rellos, O. Fedorov, F.H. Niesen, K. Guo, E. Papagrigoriou, A.L. Amos, S. Cho, B.E. Turk, G. Ghosh, S. Knapp, Kinase domain insertions define distinct roles of CLK kinases in SR protein phosphorylation, Structure 17 (2009) 352–362, http://dx.doi.org/10.1016/j.str.2008.12.023.
[3] G. Manning, D.B. Whyte, R. Martinez, T. Hunter, S. Sudarsanam, The protein kinase complement of the human genome, Science 298 (2002) 1912–1934, http://dx.doi.org/10.1126/science.1075762.
[4] Cell Signaling Technology Interactive Human Kinome Tree. http://www.cellsignal.com/contents/science-protein-kinases/protein-kinases-interactive-human-kinome/kinases-human-kinome (accessed 22.06.16).
[5] G. Sessa, V. Raz, S. Savaldi, R. Fluhr, PK12, a plant dual specificity protein kinase of the LAMMER family, is regulated by the hormone ethylene, Plant Cell 8 (1996) 2223–2234.
[6] S. Savaldi-Goldstein, G. Sessa, R. Fluhr, The ethylene inducible PK12 kinase mediates the phosphorylation of SR splicing factors, Plant J. 21 (2000) 91–96.
[7] O. Nayler, S. Stamm, A. Ullrich, Characterization and comparison of four serine- and arginine-rich (SR) protein kinases, Biochem. J. 326 (1997) 693–700.
[8] (a) K. Colwill, T. Pawson, B. Andrews, J. Prasad, J.L. Manley, J.C. Bell, P.I. Duncan, The Clk/Sty protein kinase phosphorylates SR splicing factors and regulates their intranuclear distribution, EMBO J. 15 (1996) 265–275;
(b) J. Prasad, J.L. Manley, Mol. Cell Biol. 23 (2003) 4139–4149;
(c) M. Muraki, B. Ohkawara, T. Hosoya, H. Onogi, J. Koizumi, T. Koizumi, K. Sumi, J.-I. Yomoda, M.V. Murray, H. Kimura, K. Furuichi, H. Shibuya, A.R. Krainer, M. Suzuki, M. Hagiwara, Manipulation of alternative splicing by a newly developed inhibitor of clks, J. Biol. Chem. 279 (2004) 24246–24254, http://dx.doi.org/10.1074/jbc.M314298200.
[9] P. Jain, C. Karthikeyan, N.S. Moorthy, D.K. Waiker, A.K. Jain, P. Trivedi, Human CDC2-like kinase 1 (CLK1): a novel target for Alzheimer's disease, Curr. Drug Targets 15 (2014) 539–550.
[10] J. Hanes, H. von der Kammer, J. Klaudiny, K.H. Scheit, Characterization by cDNA cloning of two new human protein kinases: evidence by sequence comparison of a new family of mammalian protein kinases, J. Mol. Biol. 244 (1994) 665–672, http://dx.doi.org/10.1006/jmbi.1994.1763.
[11] The UniProt Database. http://www.uniprot.org/ (assessed 03.04.16).
[12] A. García-Sacristán, M.J. Fernández-Nestosa, P. Hernández, J.B. Schvartzman, D.B. Krimer, Protein kinase clk/STY is differentially regulated during erythroleukemia cell differentiation: a bias toward the skipped splice variant characterizes postcommitment stages, Cell Res. 15 (2005) 495–503, http://dx.doi.org/10.1038/sj.cr.7290319.
[13] S. Araki, R. Dairiki, Y. Nakayama, A. Murai, R. Miyashita, M. Iwatani, T. Nomura, O. Nakanishi, Inhibitors of CLK protein kinases suppress cell growth and induce apoptosis by modulating pre-mRNA splicing, PLoS One 10 (2015) e0116929, http://dx.doi.org/10.1371/journal.pone.0116929 eCollection 2015.
[14] Shinsuke Araki, Ryo Dairiki, Yusuke Nakayama, Aiko Murai, Risa Miyashita, Misa Iwatani, Toshiyuki Nomura, Osamu nakanishi inhibitors of CLK protein kinases suppress cell growth and induce apoptosis by modulating pre-mRNA splicing, PLoS One 10 (2015) e0116929, http://dx.doi.org/10.1371/journal.pone.0116929.
[15] B.Z. Mian, L. Chao, F. Jian-Song, L. Wen-Wen, L. Ai-Lin, Z. Li-Shu, D. Guan-Hua, Drug discovery of host CLK1 inhibitors for Influenza treatment, Molecules 20 (2015) 19735–19747.
[16] N. Jiang, C.Y. Bénard, H. Kébir, E.A. Shoubridge, S. Hekimi, CLK2 may serve as a link between cell cycle progression, apoptosis, and telomere length regulation, J. Biol. Chem. 278 (2003) 21678–21684.
[17] PhosphoSitePlus Cell Signaling Technology. http://www.phosphosite.org/proteinAction.do?id=810&showAllSites=true (assessed 26.06.2016).
[18] T. Yoshida, J.H. Kim, K. Carver, Y. Su, S. Weremowicz, L. Mulvey, S. Yamamoto, C. Brennan, S. Mei, H. Long, J. Yao, K. Polyak, CLK2 is an oncogenic kinase and splicing regulator in breast Cancer, Cancer Res. 75 (2015) 1516–1526, http://dx.doi.org/10.1158/0008-5472.CAN-14-2443.
[19] L. Garuti, M. Roberti, G. Bottegoni, Multi-kinase inhibitors, Curr. Med. Chem. 22 (2015) 695–712, http://dx.doi.org/10.2174/0929867321666141216125528.
[20] Y. Loidreau, E. Deau, P. Marchand, M.-R. Nourrisson, C. Logé, G. Coadou, N. Loaëc, L. Meijer, T. Besson, Synthesis and molecular modelling studies of 8-arylpyrido[3′,2′:4,5]thieno[3,2-*d*]pyrimidin-4-amines as multitarget Ser/Thr kinases inhibitors, Eur. J. Med. Chem. 92 (2015) 124–134, http://dx.doi.org/10.1016/j.ejmech.2014.12.038.
[21] RCSB Protein Data Bank. http://www.rcsb.org (accessed 22.06.16).
[22] O. Fedorov, K. Huber, A. Eisenreich, P. Filippakopoulos, O. King, A.N. Bullock, D. Szklarczyk, L.J. Jensen, D. Fabbro, J. Trappe, U. Rauch, F. Bracher, S. Knapp, Specific clk inhibitors from a novel chemotype for regulation of alternative splicing, Chem. Biol. 18 (2011) 67–76, http://dx.doi.org/10.1016/j.chembiol.2010.11.009.
[23] A. Chaikuad, P. Savitsky, T. Krojer, J. Muniz, P. Filippakopoulos, P. Rellos, T. Keates, O. Fedorov, A. Pike, J. Eswaran, G. Berridge, C. Phillips, Y. Zhang, F. von Delft, J. Weigelt, C. Arrowsmith, A. Edwards, C. Bountra, S. Knapp, (Structural Genomics Consortium) S to be published, http://dx.doi.org/10.2210/pdb3nr9/pdb.
[24] E. Papagrigoriou, P. Rellos, S. Das, A. Bullock, L.J. Ball, A. Turnbull, O. Fedorov, C. Johansson, E. Ugochukwu, F. Sobott, F. von Delft, A. Edwards, M. Sundstrom, J. Weigelt, C. Arrowsmith, S. Knapp, Crystal structure of the phosphorylated CLK3 to be published, http://dx.doi.org/10.2210/pdb2exe/pdb.
[25] P. Filippakopoulos, O. Fedorov, O. King, A. Bullock, J.R.C. Muniz, F. von Delft, C.H. Arrowsmith, A.M. Edwards, J. Weigelt, C. Bountra, S. Knapp, Crystal Structure of human CDC-like kinase 3 isoform with a benzo-dioxol ligand (Structural Genomics Consortium) to be published, http://dx.doi.org/10.2210/pdb3raw/pdb.
[26] L. Lintnerová, M. García-Caballero, F. Gregáň, M. Melicherčík, A.R. Quesada, J. Dobiaš, J. Lác, M. Sališová, A. Boháč, A development of chimeric VEGFR2 TK inhibitor based on two ligand conformers from PDB: 1Y6A complex - Medicinal chemistry consequences of a TKs analysis, Eur. J. Med. Chem. 72 (2014) 146–159, http://dx.doi.org/10.1016/j.ejmech.2013.11.023.
[27] Reaxys Database. https://www.reaxys.com (accessed 22.06.16).
[28] The UniProt Database. http://www.uniprot.org/ (accessed 26.06.16).
[29] The Targets and their Inhibitors. http://www.guidetopharmacology.org/GRAC/searchPage.jsp (accessed 26.06.16).
[30] P. Carmeliet, VEGF as a key mediator of angiogenesis in cancer, Oncology 69 (Suppl. 3) (2005) 4–10, http://dx.doi.org/10.1159/000088478.
[31] IUPHAR/BPS Guide to Pharmacology. http://www.guidetopharmacology.org/GRAC/ObjectDisplayForward?objectId=1813 (accessed 31.01.16).
[32] J.J. Irwin, B.K. Shoichet, M.M. Mysinger, N. Huang, F. Colizzi, P. Wassam, Y. Cao, Automated docking screens: a feasibility study, J. Med. Chem. 52 (2009) 5712–5720, http://dx.doi.org/10.1021/jm9006966. Software Dock Blaster, http://blaster.docking.org/ (assessed 26.06.16).
[33] G. Gu, H. Wang, P. Liu, C. Fu, Z. Li, X. Cao, Y. Li, Q. Fang, F. Xu, J. Shen, P.G. Wang, Discovery and structural insight of a highly selective protein kinase inhibitor hit through click chemistry, Chem. Commun. 48 (2012) 2788–2790, http://dx.doi.org/10.1039/c1cc15851a.

MedChemComm

RESEARCH ARTICLE

View Article Online
View Journal

Cite this: DOI: 10.1039/c6md00392c

Quinoides and VEGFR2 TKIs influence the fate of hepatocellular carcinoma and its cancer stem cells†‡

Deniz Cansen Kahraman,[a] Gilles Hanquet,[b] Loïc Jeanmart,[c] Steve Lanners,[c] Peter Šramel,[de] Andrej Boháč*[de] and Rengul Cetin-Atalay*[f]

Received 15th July 2016,
Accepted 27th September 2016

DOI: 10.1039/c6md00392c

www.rsc.org/medchemcomm

Bioactivities of quinoides **1–5** and VEGFR2 TKIs **6–10** in hepatocellular cancer (HCC) and cancer stem cells (HCSCs) were studied. The compounds exhibited IC_{50} values in μM concentrations in HCC cells. Quinoide **3** was able to eradicate cancer stem cells, similar to the action of the stem cell inhibitor **DAPT**. However, the more cytotoxic VEFGR TKIs (IC_{50}: 0.4–3.0 μM) including sorafenib, which is the only FDA approved drug for the treatment of HCC, enriched the hepatocellular cancer stem cell population by 2–3 fold after treatment. An aggressiveness factor (A_F) was proposed to quantify the characteristics of drug candidates for their ability to eradicate the CSC subpopulation. Considering the tumour heterogeneity and marker positive cancer stem cell like subpopulation enrichment upon treatments in patients, this study emphasises the importance of the chemotherapeutic agent choice acting differentially on all the subpopulations including marker-positive CSCs.

Introduction

Hepatocellular carcinoma (HCC) is the sixth most frequent and second most deadly cancer worldwide.[1] HCC patients are resistant to chemotherapy and radiotherapy, because conventional therapies can only reduce the bulk of the tumour mass but are unable to restrain tumour regrowth and relapse. HCC is a highly heterogeneous tumour in terms of morphology and clinical outcome.[2] The enrichment of cancer stem cells is one of the main reasons behind failure in treatment of HCC patients. Sorafenib (**6**), a multi-kinase inhibitor acting on VEGFR2-TK and also the only FDA approved drug for the treatment of HCC patients, inhibits proliferation and migration of tumour cells and angiogenesis. Recently, it has been reported that many patients develop resistance to sorafenib. This was explained by the enrichment of cancer stem cells that have the capacity to self-renew, differentiate into cancer cells and acquire resistance to chemotherapy in most of the cancer types.[3,4] Hence, it is crucial to develop novel drugs against the differentiated cancer cells as well as liver cancer stem cells in order to successfully eradicate liver cancer. Liver cancer stem cells could be identified and isolated by several surface markers including CD133, CD90, CD44, CD13, EpCAM, OV-6, CD24, DLK1 and ICAM-1.[5] Cells that carry one or two of these markers were shown to possess CSC features.

The epithelial–mesenchymal transition (EMT) is a critical step for stemness. In this study, we have selected liver cancer cell lines with different phenotypic properties based on their genotypes. Huh7 and Hep3B cells are known to have epithelial features (well-differentiated), whereas Mahlavu and SNU-475 cells were characterized as mesenchymal-like (poorly-differentiated) cells.[6] Huh7 and Hep3B cells express genes associated with epithelial like properties. These cells express the HCC marker AFP along with the epithelial marker E-cadherin, while Mahlavu and SNU-475 cells don't express AFP and E-cadherin genes while they express high levels of vimentin protein.[6] Furthermore, Huh7 and Hep3B cells have normal migratory properties, but Mahlavu and SNU-475 cells have high migratory properties which may be due to their differential PI3K/Akt pathway activities. It was shown that Mahlavu and SNU-475 cells have constitutively active Akt protein due to loss of the PTEN tumor suppressor.[7] Current studies and clinical trials focus on the anti-CSC compounds targeting extracellular mediators or cell surface molecules as well as molecules involved in EMT and metastasis.[8] Thus, it is crucial to define which marker is efficient to detect and

[a] Dept. of Mol. Biol. and Gen., Bilkent University, Ankara, 06800, Turkey
[b] Laboratoire Syncat, UMR CNRS 7509, ECPM, Université de Strasbourg, 25 rue Becquerel, 67087 Strasbourg, France
[c] Department of Chemistry and Namur Medicine & Drug Innovation Center (NAMEDIC), University of Namur, 61 rue de Bruxelles, 5000 Namur, Belgium
[d] Faculty of Natural Sciences, Comenius University, Ilkovičova 6, Mlynskádolina842 15 Bratislava (PŠ, AB), Slovakia
[e] Biomagi Ltd., Mamateyova 26, 851 04 Bratislava, Slovakia
[f] Cancer Systems Biology Laboratory, Graduate School of Informatics, ODTU, Ankara, 06800, Turkey. E-mail: rengul@metu.edu.tr

† The authors declare no competing interests.

‡ Electronic supplementary information (ESI) available. See DOI: 10.1039/c6md00392c

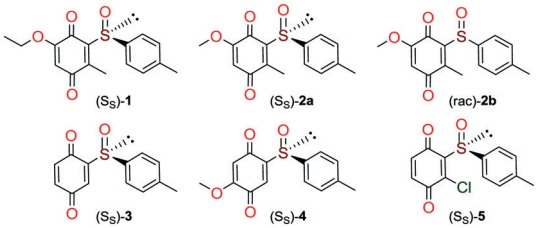

Fig. 1 The structures of tested quinoides **1–5**.

analyse cancer stem cell markers in each cell line, which we studied by flow cytometry.

Quinones and quinone-like compounds seem to be promising candidates against cancer stem cells; however, they are mainly organotoxic. It has been reported that minor changes in the side chains of the quinone structure can lead to a strong variation in the biological toxicity;[9–11] thus, modelization of various quinoid derivatives with strong inhibitory activity and low toxicity is conceivable. Therefore, we prepared a series of quinoides, **1–5** (Fig. 1), and evaluated their activities in different HCC cell lines and their cancer stem cell (HCSC) population (Tables 1, 2A and B and Fig. 5). Furthermore, VEGFR2 TKIs **6–10** (Fig. 2) were also screened in HCC cell lines (Tables 1 and 2A). Compound **6** is sorafenib tosylate (Nexavar®), and compound **9** was developed by GlaxoSmithKline as a drug candidate to inhibit VEGFR2 TK. Compounds **7**, **8** and **10** were designed by Biomagi, Ltd. to modulate VEGFR2 TK activity.

Results and discussion

Chemistry

Compounds **1**, **2a** and **2b** were prepared according to our previous work starting from commercially available 2-methylhydroquinone (**S1**) (Scheme 1).[12]

Compounds **3** and **5** were prepared (Scheme 2) according to Carreño's procedure with slight modifications (see the ESI‡).[13–15]

Table 1 Screening of quinoides **1–5** and VEGFR2-TKIs **6–10** in HCC cell lines

Compound	IC$_{50}$ (μM)[a]		
	Huh7	Hep3B	Mahlavu
1	7.0 ± 0.8	12.0 ± 1.7	18.3 ± 0.8
2a	8.0 ± 0.9	5.5 ± 1.8	14.5 ± 1.3
2b	5.5 ± 0.4	4.3 ± 0.7	11.6 ± 0.2
3	20.0 ± 1.7	17.4 ± 2.1	31.3 ± 0.3
4	10.6 ± 2.0	9.9 ± 2.3	11.3 ± 0.6
5	Ni	Ni	Ni
6	1.6 ± 0.8	1.5 ± 0.3	0.7 ± 0.4
7	2.8 ± 1.3	2.0 ± 0.9	3.0 ± 0.5
8	1.7 ± 0.7	2.1 ± 0.3	0.8 ± 0.5
9	1.5 ± 0.7	0.7 ± 0.1	1.2 ± 0.4
10	0.4 ± 0.3	0.9 ± 0.3	1.1 ± 0.7
DAPT	5.0 ± 1.2	5.0 ± 2.0	5.0 ± 1.5

[a] Experiments were performed in triplicate; Ni: no growth inhibition.

Table 2 IC$_{50}$ values and A_F factors of quinoides **1–5** and VEGFR2-TKIs **6–10** in (A) Huh7 and Hep3B epithelial cells and of quinoides **1–5** in (B) Mahlavu (MV) and SNU-475 (S-475) mesenchymal cells

A	IC$_{50}$		A_F	
	Huh7	Hep3B	Huh7	Hep3B
1	7.0	12.0	1.2	1.0
2a	8.0	5.5	1.1	1.1
2b	5.5	4.3	1.3	1.1
3	20.0	17.4	0.9	1.1
4	10.6	9.9	0.9	1.1
5	Ni	Ni	0.7	1.0
6	1.6	1.5	2.3	2.3
7	2.8	2.0	2.3	2.9
8	1.7	2.1	2.3	2.1
9	1.5	0.7	1.7	1.7
10	0.4	0.9	1.7	2.6
DAPT	5.0	5.0	0.8	0.7

B	IC$_{50}$		A_F	
	MV	S-475	MV	S-475
1	18.3	5.5	1.7	0.5
2a	14.5	10.5	1.3	0.5
2b	11.6	6.1	2.2	2.0
3	31.3	0.3	0.3	0.0
4	11.3	9.0	2.3	2.0
5	Ni	Ni	0.8	1.5
DAPT	5.0	0.6	0.2	0.5

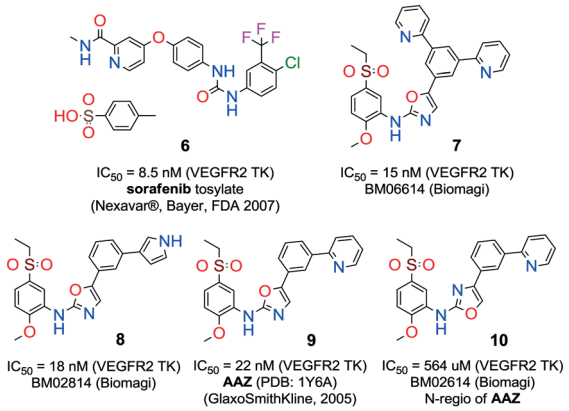

Fig. 2 VEGFR2 TKIs **6–10** used in this study and their origin and VEGFR2 IC$_{50}$ activities that were obtained through a commercial service in Germany (www.proqinase.com).

The new quinoide **4** was obtained from vanillin (**S7**) in very good overall yield using the sequence depicted in Scheme 3.

VEGFR2 TKI **6** was obtained from Bayer Inc. Synthesis of **7** was described by Lintnerová *et al.*[16] Compound **9** was prepared according the procedure described by Harris *et al.*[17] Novel compounds **8** and **10** were synthesized using the sequence depicted in Scheme 4 (see also the ESI‡).

Biological evaluation

Bioactivities of quinoides and VEGFR2-TKs in HCC cells. NCI-SRB assay was initially performed to define the inhibitory concentrations (IC$_{50}$ values) of compounds in HCC cell lines Huh7, Hep3B, and Mahlavu. Results have shown that almost all compounds (except for **5**) had IC$_{50}$ values in μM concentrations for all cell lines (Table 1). **DAPT** (γ-secretase inhibitor) was used as a control for CSC inhibition.

Expression of cancer stem cell markers in HCC cell lines. CSC marker expression varies among cell lines of HCC, since

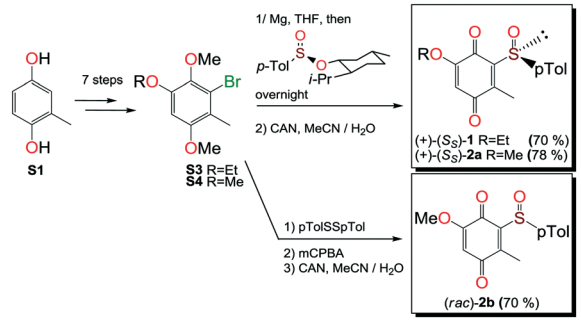

Scheme 1 Preparation of quinones **1**, **2a** and **2b** from 2-methylhydroquinone (**S1**).

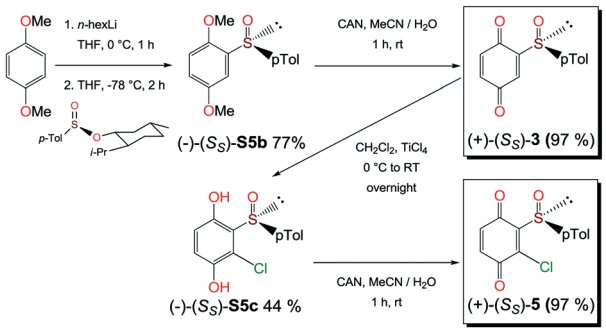

Scheme 2 Syntheses of quinones **3** and **5** from 1,4-dimethoxybenzene.

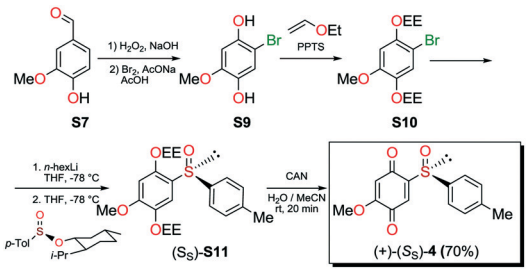

Scheme 3 Synthesis of compound **4**.

liver CSCs exist heterogeneously and these features determine the characteristics of the cancer (tumourigenicity and metastatic tendency). It has previously been reported that the epithelial cell adhesion molecule (EpCAM) and CD133 expressing cells are more likely to execute epithelial features, whereas CD90 expressing cells are more likely to be mesenchymal.[18,19] Expression of these markers in HCC cell lines was analyzed using flow cytometry. It was shown that CSCs of Huh7 cells could be identified by CD133 and EpCAM positivity (20–30%). CSCs of Mahlavu and SNU-475 could be identified by CD90 positivity (0.2–0.6%) (Fig. 3).

As stated above, the EMT is critical for cancer cell stemness. Huh7 and Hep3B cells carry epithelial features, whereas Mahlavu and SNU-475 cells carry migratory mesenchymal-like properties.[6,7] Furthermore, Huh7 and Hep3B cells differ in their p53 gene status: Huh7 cells express p53(Y220S), but Hep3B cells are null for the TP53 gene. Therefore, the expression of mutant p53 causes differential activation of the β-catenin protein and its downstream mesenchymal proteins such as E-cadherin, vimentin, snail and slug. The significantly higher expression of β-catenin[20] due to the lack of p53 protein in Hep3B cells correlates with the higher expression of EpCAM and CD133 markers in this cell (Fig. 3).

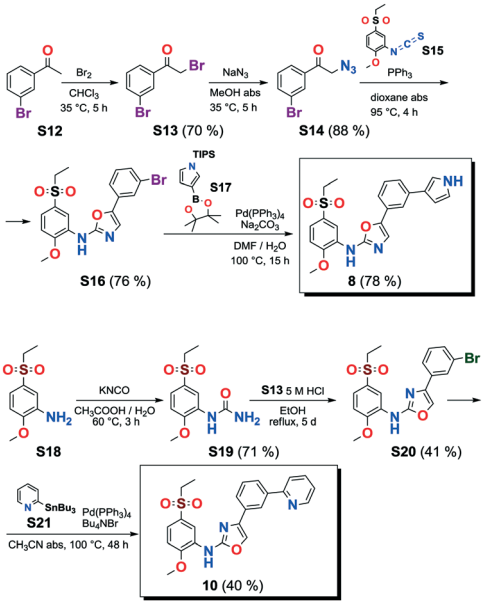

Scheme 4 Syntheses of **8** and **10**.

Effects of quinoides and VEGFR2-TKIs on hepatocellular cancer stem cells (HCSCs). It is essential to discover novel compounds that were able to alter the enrichment of the CSC

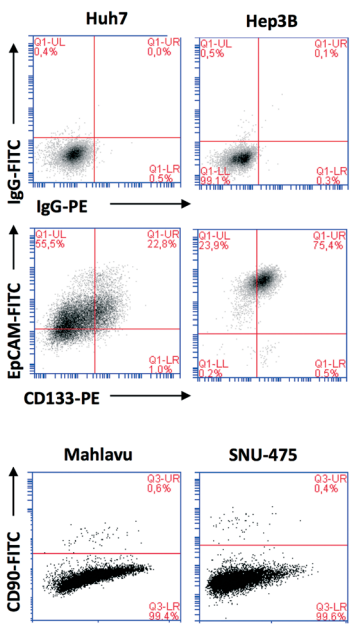

Fig. 3 Flow cytometry analysis of HCC cell lines indicating the positivity of HCC cell lines for cancer stem cell markers CD133, EpCAM and CD90. Top row: IgG isotype controls, middle row: cells stained for CD133 and EpCAM markers, bottom row: cells stained for CD90.

population as well as the cancer cells. For this reason, compounds **1–10** that were initially tested against HCC cell lines were further studied to determine the changes in the CSC marker positivity of Huh7 cells. Cells that were killed by the treatment were discarded, and the remaining cells were used in flow cytometry analyses. Interestingly, some of the compounds were able to reduce the percentage of CSC population, while some had the adverse effect on Huh7 cells that enriched the CSC subpopulation (Fig. 4). It was observed that unlike VEGFR2-TKIs, some of the quinoides were able to attenuate the CSC side population in Huh7 cells.

Due to the distinct dispersion of CD90 cells, we decided to include SNU-475 cells for testing the anti-HCSC activities of quinoides. Therefore, we also determined the bioactivities of quinoides in SNU475 cells. The IC_{50} values were 5.5 ± 1.4, 10.5 ± 1.5, 6.1 ± 2.0, 0.3 ± 1.2, 9.0 ± 2.1, and 0.6 ± 1.1 μM for compounds **1**, **2a**, **2b**, **3**, **4**, and **DAPT**, respectively. No growth inhibition was observed for compound **5** (Fig. 5 and Table 2B).

Although compounds **6–10** were stronger HCC inhibiting agents as quinoides **1–5**, they caused enrichment of Huh7 HCSCs in the rest of the HCC after treatment. Therefore, the positive cytotoxic effect of **6–10** was discredited by their ability to leave the HCC residue fraction after treatment enriched with aggressive HCSC cells that are highly susceptible to disease relapse and that acquired drug resistance frequently observed after HCC treatment in clinics.

Further analyses were carried out on Hep3B, Mahlavu and SNU-475 cells to test whether the same effect could be observed in other HCC cell lines as well. Among all compounds tested, **3** was able to attenuate the CSCs especially in mesenchymal-like cells, surpassing the efficacy of the stem cell inhibitor, **DAPT** (Fig. 5). Altogether, the results have shown that compound **3** is potentially capable of impairing the cancer stem cells in HCC cells with a mechanism not yet discovered.

On the other hand, treatments of cells with VEGFR2-TKIs **6–10** were shown to enrich the cancer stem cell population of Huh7 and Hep3B cells at about 1.7–2.9 times as opposed to the effect of **DAPT** (Fig. 4 and Table 2A).

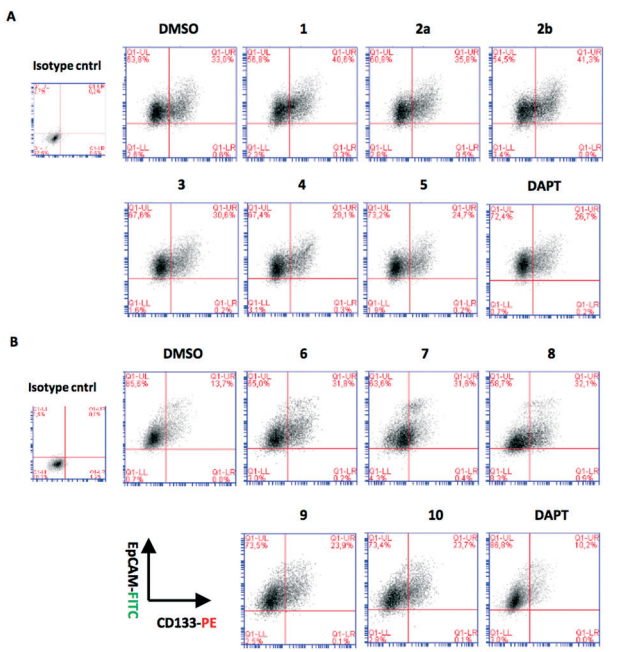

Fig. 4 Expression of stem cell markers CD133 and EpCAM in Huh7 cells treated with (A) quinoides **1–5** and (B) VEGFR2-TKIs **6–10** as shown by flow cytometry analysis.

Conclusions

There is only one literature report describing macrocyclic benzoquinone herbimycin A [CAS: 70563-58-5, BRN: 4834067] that inhibits (61–78%) human bone marrow mesenchymal stem cells at 1–5 μM concentration.[21] We present here for the first time the screening of benzoquinone compounds in CSCs. One of the achievements of our pivotal study is identification of quinoide **3** as an exceptional compound to treat HCSCs. Although its mechanism is not yet known, we hypothesize different behaviours of screened quinoides **1–5** based on their structural differences, benzoquinone reactivity and general medicinal chemistry knowledge. All quinoides **1–5** possess a chemically reactive benzoquinone fragment that can likely be an irreversible inhibitor binding to a biological target *e.g.* by the Michael reaction with a cysteine amino acid residue. The most active quinoide **3** in Mahlavu and SNU-475 is the one that misses most of substitutions on its benzoquinone skeleton compared to the other tested quinoides. The steric and electronic properties of **3** could be a reason why quinoide **3** is the most active one included (Fig. 5). In the case of the SNU-475 tumour, there are three active quinoides (**1**, **2a** and **3**); therefore, other mechanism(s) can also be included. As could be seen, all VEGFR2 TKIs **6–10** are cytotoxic to HCC cell lines (IC_{50} = 3.0–0.4 μM, Table 1), and at the same time, they are less toxic towards HCSCs since it was observed that cancer stem cells were enriched up to 3 times after treatment (Fig. 5 and Table 2A). The most synergic case would be to identify cytotoxic compounds for both HCCs and HCSCs. The results obtained by screening of VEGFR2 TKIs can deliver two positive consequences: i) VEGFR2 TKIs can be used to enrich the % of stem cells in the final fraction before stem cell isolation for research purposes. Moreover, such stem cells can remember VEGFR2 TKI treatment and can be used for the development of the next generation of inhibitors. ii) It is obvious that experimental compounds can be differently cytotoxic towards heterogeneous tumour cells. Their different influence on CSCs should be quantified separately because of its practical meaning.

In cancer therapeutics, it is important to identify treatment regimens against cancer stem cells as well as tumor cells, because patients suffer from relapse or incomplete recovery after treatment if it fails to eliminate CSCs. The percentage of DMSO treated cells in flow cytometry analysis represents the initial CSC marker positivity of the cells before treatment (Fig. 4) Thus, we suggest that once the cells were treated with a compound, the number of cells with marker

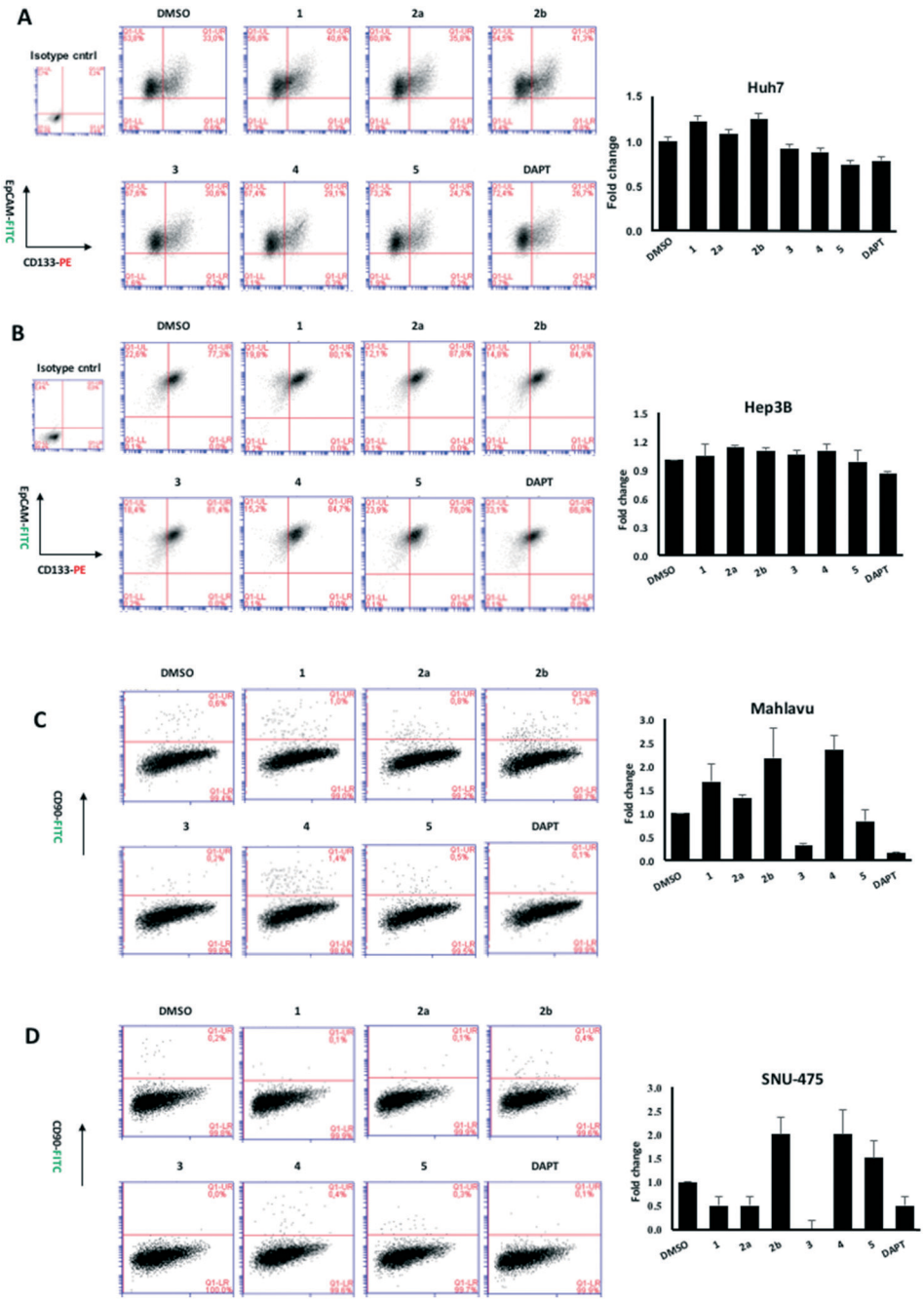

Fig. 5 Flow cytometry analysis of HCC cell lines after 72 hours of treatment with quinoides **1**–**5**. (A) Huh7, (B) Hep3B, (C) Mahlavu, and (D) SNU-475. Cancer stem cells were defined by their positivity for CSC markers, CD133 together with EpCAM, or CD90. Each treatment was compared to its corresponding DMSO control to define the changes in percentage of double positive population. **DAPT** is used as positive control for CSC inhibition. The bar graphs indicate the fold change in positivity for markers between DMSO control and experimental groups.

positivity can be compared with the DMSO control in order to define the fold change in the percentage of cancer stem cells. Since only the cells that stay alive after treatment are analyzed (see methods), it is important to emphasize the density of the cancer stem cells before and after treatment. Therefore, the compounds that cause a decrease or enrichment in cancer stem cell population can be quantified simply by normalizing the treated cell population by DMSO controls.

Here, we suggest the aggressiveness factor (A_F), a new characteristic quantifying the risk for certain compounds to be able to develop a more aggressive disease: A_F (exp. cmpd.) = [(total number of CSCs after exp. cmpd. treatment)/(total number of CSCs before treatment)].

The low A_F value is an indication for the quality of a drug candidate toward cancer cells. Such molecules don't possess drug resistance or induce more aggressive tumours (Table 2). A_F

reflects the fold increase of CSCs that survived the compound treatment independently of the shrinkage of the tumour itself.

The compounds with A_F values below 1 can be regarded as molecules which reduce the cancer stem cell population, whereas A_F values above 1 signify molecules that enrich the cancer stem cell population. Thus, the usage of A_F values defines the success or failure of the compounds in affecting cancer cells toward cancer stem cell population.

Cancer stem cell-like subpopulations carry behaviors such as higher tumor-forming and metastasis capacities along with resistance to antitumor drugs which allows tumors to survive and relapse.[8] The analysis of the action of the chemotherapeutics that deplete the CSC-like population by the following surface markers may enumerate the qualities of the compounds and may allow one to assess their differential action. Our results represent parallel findings with sorafenib (**6**) and other compounds and allow comparative analysis of the compounds toward cancer stem cell marker positive cell populations. The A_F concept introduced in this study clearly demonstrates the differential action of the compounds.

It is known that patients used to develop resistance towards sorafenib (**6**). This is consistent with our data with sorafenib (**6**) having an A_F value that is 2 fold higher compared to that of the DMSO control while maintaining good cytotoxicity through the low IC_{50} values (Table 2A). However, the known CSC inhibitor (**DAPT**) has low A_F values and its IC_{50} is much higher than that for sorafenib (**6**). Furthermore, while quinoide **5** does not possess cytotoxic actions (for each HCC line) and **3** has high IC_{50} values against Huh7, Hep3B or MV (Mahlavu) cells, they both significantly reduce the CSC marker positive subpopulations in mesenchymal Mahlavu and SNU-475 cells (Tables 2A and B).

The normalized aggressiveness factor allows selection of promising experimental compounds possessing lower probability to form aggressive tumours in comparison to a particular drug with known clinical behaviour. The methodology can serve as a simple and valuable tool for pre-clinical screening.

Experimental section

Syntheses of compounds 1–10

The syntheses and physicochemical properties of prepared organic compounds **1–10** can be found in the ESI.‡

Cell culture

Huh7 and Mahlavu, human hepatocellular carcinoma (HCC) cell lines, were maintained in Dulbecco's modified Eagle's medium (DMEM) (Invitrogen/GIBCO), supplemented with 10% fetal bovine serum (FBS) (Invitrogen/GIBCO) and 0.1 mM nonessential amino acid, whereas SNU-475 cells were maintained in RPMI (Invitrogen/GIBCO), supplemented 10% fetal bovine serum (FBS) and 2 mM L-glutamine. Both media contained 100 units per mL penicillin and 100 units per mL streptomycin. Cells were grown at 37 °C in a humidified incubator under 5% CO_2.

NCI-60 sulforhodamine B (SRB) cytotoxicity assay

Huh7 and Hep3B (2000 cells per well), SNU-475 (1000 cells per well) and Mahlavu (1000 cells per well) cells were inoculated into 96-well plates (150 μl per well). After 24 hours, molecules of interest and DMSO control were applied in concentrations of 40 μM to 2.5 μM in serial dilutions. After 72 h of treatment, cells were fixed with cold 10% (w/v) trichloroacetic acid (MERCK) for an hour. Then, the wells were washed with ddH_2O and dried. 50 μl of 0.4% SRB dye (Sigma-Aldrich) was applied to each well and incubated at room temperature for 10 min. Each well was washed with 1% acetic acid and left for air-drying. SRB dye was solubilised using 100 μl per well 10 mM Tris-Base solution, and the absorbance was measured at 515 nm. The experiment was performed in triplicate, and the absorbance values were normalized to DMSO controls.

Flow cytometry

HCC cells are inoculated into 100 mm^2 culture dishes (100 000–200 000 cells). 24 hours later, cells were treated with the compounds (IC_{100} conc.) for 72 hours. Dead cells that no longer remained attached to the surface of the culture plates were discarded through vacuum aspiration and cells that remained attached were collected to be fixed with 4% paraformaldehyde for 30 minutes. Huh7 and Hep3B cells were stained for cancer stem cell markers using anti-CD133/1 (AC133)–biotin (Miltenyi, 130-090-664), anti-biotin–PE (Miltenyi, 130-090-756), and anti-EpCAM–FITC (Miltenyi, 130-080-301), whereas Mahlavu and SNU-475 cells were stained using anti-CD90–FITC (Miltenyi, 130-095-403). For isotype controls, mouse IgG1 isotype control–FITC conjugate (Miltenyi, 130-092-213) and mouse IgG1 isotype control antibody–biotin conjugate (Miltenyi, 130-093-018) were used. Staining of cells was performed according to the manufacturer's protocol. Cells were analyzed using the BD Accuri C6 Flow Cytometer and Software (BD Biosciences). The same staining procedure was applied for the analysis of HCC cells in order to determine the CSC marker positivity.

Acknowledgements

Liver cancer stem cell studies and DCK supported by TUBITAK grant #113S540. COST Actions: CM1106, CA15135, VEGA 1/0634/13, APV SK-FR-2015-0014 and Biomagi, Ltd. are acknowledged for chemistry. Sorafenib tosylate (**6**) was obtained as a gift from Bayer, Inc.

References

1 B. W. Stewart and C. P. Wild, *World Cancer Report 2014*, 2014.
2 T. Yamashita and X. W. Wang, *J. Clin. Invest.*, 2013, **123**(5), 1911–1918.
3 H.-W. Xin, C. M. Ambe, D. M. Hari, G. W. Wiegand, T. C. Miller, J. Q. Chen, A. J. Anderson, S. Ray, J. E. Mullinax, T. Koizumi, R. C. Langan, D. Burka, M. A. Herrmann, P. K. Goldsmith, A. Stojadinovic, U. Rudloff, S. S. Thorgeirsson and I. Avital, *Gut*, 2013, **62**, 1777–1786.

4 A. K.-M. Chow, L. Ng, C. S.-C. Lam, S. K.-M. Wong, T. M.-H. Wan, N. S.-M. Cheng, T. C.-C. Yau, R. T.-P. Poon and R. W.-C. Pang, *PLoS One*, 2013, **8**, e78675.
5 J.-H. Sun, Q. Luo, L.-L. Liu and G.-B. Song, *World J. Gastroenterol.*, 2016, **22**, 3547–3557.
6 H. Yuzugullu, K. Benhaj, N. Ozturk, S. Senturk, E. Celik, A. Toylu, N. Tasdemir, M. Yilmaz, E. Erdal, K. C. Akcali, N. Atabey and M. Ozturk, *Mol. Cancer Ther.*, 2009, **8**, 90.
7 I. Durmaz, E. B. Guven, T. Ersahin, M. Ozturk, I. Calis and R. Cetin-Atalay, *Phytomedicine*, 2016, **23**, 42–51.
8 F. Marcucci, C. Rumio and F. Lefoulon, *Front. Radiat. Oncol.*, 2016, **6**, 115.
9 T. J. Monks, R. P. Hanzlik, G. M. Cohen, D. Ross and D. G. Graham, *Toxicol. Appl. Pharmacol.*, 1992, **112**, 2–16.
10 T. J. Monks and D. C. Jones, *Curr. Drug Metab.*, 2002, **3**, 425–438.
11 K. Ollinger and A. Brunmark, *J. Biolumin. Chemilumin.*, 1991, **266**, 21496–21503.
12 D. A. Lanfranchi and G. Hanquet, *J. Organomet. Chem.*, 2006, **71**, 4854–4861.
13 M. C. Carreño and J. L. García Ruano, *Synthesis*, 1992, **1992**, 651–653.
14 M. C. Carreño, J. L. G. Ruano, M. A. Toledo and A. Urbano, *Tetrahedron Lett.*, 1994, **35**, 9759–9762.
15 M. A. Brimble, L. J. Duncalf and D. C. W. Reid, *Tetrahedron: Asymmetry*, 1995, **6**, 263–269.
16 L. Lintnerová, M. García-Caballero, F. Gregáň, M. Melicherčík, A. R. Quesada, J. Dobiaš, J. Lác, M. Sališová and A. Boháč, *Eur. J. Med. Chem.*, 2014, **72**, 146–159.
17 P. A. Harris, M. Cheung, R. N. Hunter, M. L. Brown, J. M. Veal, R. T. Nolte, L. Wang, W. Liu, R. M. Crosby, J. H. Johnson, A. H. Epperly, R. Kumar, D. K. Luttrell and J. A. Stafford, *J. Med. Chem.*, 2005, **48**, 1610–1619.
18 T. Yamashita and S. Kaneko, *J. Gastroenterol.*, 2014, **49**, 1105–1110.
19 Z. F. Yang, D. W. Ho, M. N. Ng, C. K. Lau, W. C. Yu, P. Ngai, P. W. K. Chu, C. T. Lam, R. T. P. Poon and S. T. Fan, *Cancer Cell*, 2008, **13**, 153–166.
20 T. Cagatay and M. Ozturk, *Oncogene*, 2002, **21**, 7971–7980.
21 S. Mruthyunjaya, R. Manchanda, R. Godbole, R. Pujari, A. Shiras and P. Shastry, *Biochem. Biophys. Res. Commun.*, 2010, **391**, 43–48.